DOCTOR OF PHILOSOPHY

An integrated geotechnical-geophysical procedure for the prediction of liquefaction in uncemented sands.

Pyrah, J R.

Award date:
1996

Awarding institution:
Bangor University

AN INTEGRATED GEOTECHNICAL - GEOPHYSICAL PROCEDURE FOR THE PREDICTION OF LIQUEFACTION IN UNCEMENTED SANDS.

BY J. R. PYRAH.

A thesis presented for

the degree of Philosophiae Doctor,

University of Wales.

School of Ocean Sciences,
University of Wales, Bangor,
Menai Bridge,
Gwynedd,
LL59 5EY,
U.K.

Ysgol Gwyddorau Eigion,
Prifysgol Cymru, Bangor,
Porthaethwy,
Gwynedd,
LL59 5EY,
U.K.

January, 1996.

Ionawr, 1996.

ABSTRACT.

This project represents an in depth study into the inter-relationships between the seismic shear wave velocity of uncemented sands and their liquefaction potential. This was achieved by combining the concepts of steady / critical state soil mechanics with the measurement of shear wave velocity. In the laboratory this was facilitated with the use of a modified triaxial cell, allowing both the shear wave velocity behaviour and liquefaction susceptibility of a particular sand to be quantified. Use of this equipment illustrated that for a specific sand, a 'critical shear wave velocity line' may be defined, dividing sand states of potentially contractive or dilative behaviour. Further, these studies also show that a shear wave velocity derived state index, ψ_s, may be statistically correlated with other more conventional indices of sand consolidation state.

The results of the laboratory study are then applied to a real field situation, the Fraser River Delta, located in earthquake prone south-western British Columbia. Currently, many of the sub-aerial sediments have been identified as being potentially liquefiable. Offshore, the difficulties associated with sampling seabed sediments *in-situ* have limited past attempts to quantify liquefaction potential. Laboratory shear wave data, based upon laboratory analysis of sediment samples from the Fraser Delta and *in-situ* shear wave velocity field data, have been used in an attempt to quantify the risk of liquefaction for part of the offshore delta, namely Roberts Bank. The data presented in this study, based upon both conventional and proposed shear wave methods of analysis, suggest that there is a significant risk of liquefaction on the offshore Fraser Delta, particularly around Roberts Bank.

ACKNOWLEDGEMENTS.

I would like to express my gratitude to Dr. Angela Davis, who initiated this project and who supervised and supported me throughout. Many other people were also actively involved in different aspects of the presented work, the main parties being:

Dr Jim Bennell, who provided a wealth of practical and academic advice throughout the project.

Dr Dei Huws, who assisted in the collection of the Fraser Delta shear wave data, and who has been a constant source of advice for the past three years.

Mr Sinclair Buchan, who assisted in the early stages of the triaxial testing, and who provided constructive criticism for parts of this thesis.

Mr Dave Gill, Mr Elwyn Jones, Mr Mike Roberts and Mr Geraint Williams, whose patience and high standards of technical ability made the life of the author a little easier.

Mr Nick Harrop, who successfully fielded a flying triaxial cell at the beginning of the laboratory experiments.

Special thanks must be also made to all those at the Pacific & Atlantic Geoscience Centres who made me feel very welcome during my two visits to Canada, including Harold Christian, for releasing much of the field geotechnical data presented herein, Pat Monahan, who provided copies of much of the SCPT data, Ivan Frydecky, who provided some useful software, Ralph Currie, for the loan of his push-bike, Vaughn Barrie & Kim Conway, who patiently answered many of my questions about the Fraser Delta.

Thanks also go to my Parents, who made it possible for me to be here in the first place, Sharon, for emotionally (and occasionally physically) supporting me, Kris, Ben and the rest of my friends and house mates, who have put up with me over the past 3 or so years.

This project was funded by EPSRC, through the provision of a research studentship (No:- 92000956), and the Geological Survey of Canada (GSC) who funded the University of Wales' (UWB) involvement in the Fraser Delta project. Particular thanks go to Dr David Prior of the GSC for helping setup UWB's involvement in the project.

LIST OF CONTENTS.

CHAPTER 1.

INTRODUCTION.

CHAPTER 2.

A REVIEW OF EXISTING LABORATORY AND *IN-SITU* TESTING METHODS.

CHAPTER 3.

CONVENTIONAL APPROACHES TO THE PREDICTION OF LIQUEFACTION POTENTIAL.

CHAPTER 4.

A BREIF BACKGROUND TO SHEAR WAVE VELOCITY STUDIES, WITH PARTICULAR REFERENCE TO LIQUEFACTION PREDICTION.

CHAPTER 5.

MATERIALS AND METHODS.

CHAPTER 8.

CASE STUDY: THE FRASER RIVER DELTA, BRITISH COLUMBIA.

OVERVIEW AND FIELD RESULTS.

CHAPTER 9.

DISCUSSION.

CHAPTER 10.

CONCLUSIONS.

LIST OF FIGURES.

CHAPTER 2.

CHAPTER 3.

CHAPTER 4.

CHAPTER 5.

CHAPTER 6.

CHAPTER 7.

CHAPTER 8.

CHAPTER 9.

LIST OF PLATES.

CHAPTER 1.

CHAPTER 5.

LIST OF ABBREVIATIONS.

a = constant.
a_{max} = maximum acceleration at the ground surface.
a_t = surface threshold ground acceleration.
a_p = peak ground surface acceleration.
b = constant.
c_u = unit cohesion.
c = sample constant.
d = sample constant.
d_s = depth to sand layer (m).
d_w = depth of water table below ground level (m).
e = void ratio = $Volume\ of\ voids / Volume\ of\ solids$
e_{con} = void ratio after consolidation.
e_{pred} = predicted void ratio.
e_{ss} = void ratio at steady state.
e_1 = intercept of steady state line at 1kPa.
f = sample constant.
f_s = cone side friction.
g = acceleration due to gravity.
g' = sample constant.
k = permeability.
k' = constant.
m = constant.
m_1, m_2 = material constants.
n = constant.
n_a, n_b = material constants.
p = total mean stress (overburden pressure).
p_o = reference pressure, usually 100 kPa.
p' = effective mean stress (effective confining stress) = $(\sigma'_1+2\sigma'_3)/3$.
p'_c = effective confining stress after consolidation.
p'_{ss} = effective confining stress at steady state.
$\Delta p'$ = change in effective confining stress occuring during triaxial test.
q = deviator stress = $(\sigma'_1-\sigma'_3)$
q_c = cone penetration resistance.
q_{c1} = normalised cone penetration resistance.
q_{co} = function of shaking intensity.
q_{crit} = critical cone penetration resistance, dividing liquefiable & non-liquefiable soils.
q_{max} = maximum value of devaitor stress during triaxial test.
q'_{ss} = deviator stress at steady state.
r_c = constant.
r_d = stress reduction factor or flexibility coefficient.
u = pore-pressure.
Δu = excess pore-pressure.
z = depth to sand layer.

A = $m_1(P_a)^{na+nb}$
B' = $m_1(P_a)^{na+nb}$
B = Skempton's 'B' value.
C = dimensionless factor accounting for grain shape.
C_N = standard penetration resistance correction factor.
C_Q = cone penetration correction factor similar to C_N.
C_{ss} = slope of steady state line in e-log p' plane.
Df = degrees of freedom.
D_r = relative density.
D_{50} = median grain size.

F = F-value.
F = $(2.17-e_{min})^2/(1+e_{min})$
F_L = factor of safety against liquefaction.
G = shear modulus.
G_N = normailised shear modulus.
G_o = dynamic shear modulus.
G_{max} = dynamic shear modulus.
G_s = particle specific gravity.
H_o = depth to sand layer (m).
H_w = depth of water below ground level (m).
K = bulk modulus.
K_n = $\left[(\sigma_1/\sigma_3-1)\right]/\left[(\sigma_1/\sigma_3)_{max}-1\right]$
M = mean sqaure value.
M = slope of steady state line in q - p' plane.
M_s = mass of solid particles.
N = standard penetration resistance.
N_1 = normalised penetration resistance.
$N_{1(60)}$ = N_1 value standardised to 60% of the free fall energy.
N_{crit} = critical N value separating liquefiable from non-liquefiable soils.
N_E = equivalent SPT blow count.
N_s = function of shaking intensity.
P_a = reference pressure, usually 100 kPa.
Q_C = modified cone penetration resistance.
S_{su} = undrained steady-state shear strength.
V_p = compressional wave velocity (m/s).
V_s = shear wave velocity (m/s).
$V_{s'c}$ = shear wave velocity after consolidation (m/s).
$V_{s'crit}$ = critical shear wave velocity (m/s).
V_{smax} = maximum recorded shear wave velocity, at a specific confining stress.
V_{smin} = minimum recorded shear wave velocity, at a specific confining stress.
$V_{s'ss}$ = shear wave velocity at steady state.
V_{s1} = normalised shear wave velocity.
V_{s100} = shear wave velocity normailised to 100kPa.
V_{s300} = shear wave velocity normailised to 300kPa.
V_T = total volume.

ϕ'_{ss} = effective friction angle at steady state.
$\tan\phi$ = angle of shearing resistance.
γ = strain.
γ_t = threshold strain.
ρ = bulk density.
ρ_W = denisty of water.
σ'_a = effective stress in the direction of wave propagation.
σ = effective stress in the direction of particle motion.
σ_1 = major principle stress.
σ_2 = intermediate principle stress.
σ_3 = minor principle stress.
σ'_1 = major principle effective stress.
σ'_2 = intermediate principle effective stress.
σ'_3 = minor principle effective stress.
$(\sigma_1/\sigma_3)_{max}$ = stress ratio at failure.
σ_h' = *in-situ* horizontal effective stress.
σ_o = total overburden pressure on sand layer.
σ_{vo}' = initial vertical effective stress.
τ = peak shear strength.
τ_{av} = average cyclic shear stress.

τ_{av}/σ_{vo}' = average stress ratio.
τ_d = *in-situ* driving shear stress.
ψ = state parameter.
ψ_s = shear wave state parameter (m/s).

'And every one that hereth these sayings of mine, and doeth them not shall be likened unto a foolish man, which built his house on sand:
And the rain descended, and the floods came, and the winds blew, and beat upon that house: and it fell: and great was the fall of it'.

Matthew, Ch 7., v 26-27.

For My Grandfather, Leslie Norman Pyrah, C.B.E., 1899 - 1995.

CHAPTER 1.

INTRODUCTION.

1.1. Background.

The term 'liquefaction' is derived from the Latin words *liquere* and *facere*, and means literally 'to change into a liquid'. For the soil engineer, liquefaction has a more specific meaning and may be more precisely defined as 'the loss of static shearing resistance of saturated, loose, non-cohesive sediments due to a tendency towards a closer packing of the constituent grains, driven by either static or cyclic loading' (Holzer *et al.*, 1989). Contemporary accounts of the phenomenon can be traced back for more than a century. In his classic report on the Indian Great Earthquake of 12th June 1897, R.D Oldham (Oldham, 1899) describes...

'...at about quarter past five in the afternoon of the 12th June 1897, there burst on the western portion of Assam an earthquake which, for violence and extent, has not been surpassed by any of which we have historic record. Lasting about two and a half minutes, it had not ceased at Shillong before an area of 150,000 square miles had been laid in ruins, all means of communication interrupted, the hills rent and cast down with landslips, and the plains fissured and riddled with vents, from which sand and water poured out in the most astounding quantities.....'.

Modern investigations into the phenomenon were initiated by the 1964 Niigata (Japan) and Anchorage (Alaska) earthquakes, which caused spectacular foundation failures, with many buildings suffering large scale tilting due simply to liquefaction of their foundations (Plate 1.1). More than 30 years of intensive study, towards the prediction and prevention of liquefaction have followed. However, reports from the 1995 Hyogo-ken Nambu (Kobe) earthquake describe widespread liquefaction around the port and harbour area, where quay walls collapsed and dock-side cranes were toppled (O'Rourke, 1995). Clearly then, there is a need for continued study and development of improved methods of liquefaction prediction, both on- and offshore.

The traditional land based field investigation technique for liquefaction assessment is the Standard Penetration Test (SPT), which is still widely used in many parts of the world despite its variety of well documented deficiencies (Schmertmann, 1978). More recently, the Cone Penetration Test (CPT) has been used for this type of investigation, offering the various advantages of simplicity of testing, continuous profiling and reproducibility of results (Robertson, 1982). More recently still, it has been recognised that shear wave velocity may represent a useful additional index to the liquefaction potential of a sediment. This use of shear wave velocity as an aid to the prediction of liquefaction susceptibility potentially offers certain advantages over conventional techniques, in terms of both undisturbed, *in-situ* testing and the application of the results of detailed laboratory testing on representative samples directly to the field.

Research at the University of Wales, Bangor (UWB) over the past decade has been directed towards the development of various techniques for the measurement of shear wave velocity onshore, offshore and in the laboratory. As a direct result of this research, a variety of standard laboratory instruments have been equipped with transducers allowing the measurement of shear wave velocity to be made prior to, and during standard geotechnical testing procedures (Schultheiss, 1983). In addition, a towed seafloor sledge, capable of making pseudo-underway shear wave velocity evaluations, has been successfully used in various seafloor mapping studies (Huws, 1993). These recently developed and proven techniques provide a sound basis for laboratory, and subsequent field investigation of liquefaction potential, using both geotechnical and geophysical methodologies.

Further opportunity for research has been provided by the Geological Survey of Canada (GSC), who are currently engaged in a project to quantify the effects of a major earthquake on the Fraser River Delta, British Columbia, Canada. This delta is an example of an economically vital, physically unstable site located in an area of high earthquake risk.

1.2 Thesis aims and objectives.

The principle aim of this thesis was to test the hypothesis, *'shear wave velocity may be used to provide a useful index to liquefaction potential'*.

It was proposed that this aim was to be achieved by using previously developed laboratory instrumentation (primarily an adapted triaxial cell) to combine the conceptual framework of critical / steady state soil mechanics and *in-situ* shear wave velocity measurements, enabling the prediction of liquefaction on the basis of a 'critical shear wave velocity'. In addition, a further objective was to use the data collected in the laboratory and apply them to the specific 'problem area' of the Fraser River Delta, in an attempt to quantify the seafloor sediment's potential behaviour under earthquake loading.

In the early stages of this project, and after a detailed literature review regarding the measurement of shear wave velocity and its use as an index to liquefaction potential had been performed, it was found that very few detailed laboratory investigations on the subject had been attempted. Most of the small amounts of literature that did exist either related to purely empirical field correlations, or were based on work using the cyclic triaxial apparatus. At the start of the research period no detailed laboratory studies appeared to have been undertaken into the possible combination of the concepts of critical / steady state soil mechanics and specific shear wave velocity propagation phenomenon.

1.3 Mechanism of soil liquefaction.

The property that enables a material to remain in equilibrium when its surface is not level is known as its shear strength (Smith, 1990). Non-cohesive granular soils (e.g. sands), derive much of their shear strength from inter-granular friction. When these soils are saturated with water any normal stress is carried by a combination of two components, the stress carried by the soil particles themselves and that carried by pressure of the fluid in the pore-spaces. In the relationship between normal stress and volume change (e.g. that occurring upon consolidation), the controlling factor is not the total normal stress, but the difference between the total normal stress (ie overburden stress) and the pressure of fluid within the pore-spaces. This difference between the total normal stress (due to the weight of the overburden) and the water pressure in the pore spaces is known as the effective mean stress (effective confining stress or simply the effective stress). Effective stress can be defined:-

$$p' = p - u \qquad (1.1).$$

where, p' = effective mean stress (or effective confining stress).
p = total mean stress.
u = pore-pressure.

The effective mean stress controls to a large degree the strength and deformation characteristics of all granular materials, as illustrated by the Mohr-Coulomb relation:-

$$\tau = c_u + (p - u)\tan\phi \qquad (1.2).$$

where, τ = peak shear strength.
c_u = unit cohesion.
$\tan\phi$ = angle of shearing resistance.

This relationship clearly illustrates that for non-cohesive sediments (where $c = 0$) an increase in the pore-pressure will lead to a direct reduction in the shear strength. If the pore-pressure reaches a magnitude equal to the total mean stress, the shear strength will drop to zero, and the sediment can be regarded as having liquefied. An additional feature of soil behaviour is that unlike metals, which only change in volume when the mean total stress p is changed, soils also change in volume upon shear. This phenomenon is generally known as dilatancy.

In more detail, under undrained monotonic or cyclic loading conditions, a loose sand, or one under sufficiently high confining pressures will tend to decrease in volume, or contract. If the soil is saturated, volume contraction cannot occur because water is virtually incompressible and cannot escape from the soil pores during the relatively short period of loading. In order to maintain an equilibrium, some change in the existing stress system must take place. This is achieved in the form of a reduction in the existing effective mean confining stress due to an increase in the pore-water pressure. Given continued loading, pore-water pressures continue to rise, until the pore-water pressure nearly equals the total stress; consequently the effective stress and peak shear strength reach values close to zero. In loose soils, once this condition is reached the soil skeleton collapses and large deformations will occur at a constant low residual stress known as the steady state or residual strength. This collapse of soil structure and consequent loss of strength is known as flow liquefaction. The residual or steady state shear strength, which occurs at high strains in loose soils, and unlike the peak shear strength, is solely a function of void ratio and soil structure. The excess pore-pressure gradients created

during undrained loading of loose sediments may in tum be vented upwards, causing further liquefaction of upper soil layers and the production of sand boils or vents on the soil surface.

In contrast, a dense soil, or one under an extremely low confining stress, under undrained loading will also initially build up positive pore-pressures, since even dense soils behave contractively under small shear strains. Continued loading will tend to cause the soil to dilate, pore-pressures will drop and the soil will 'strain-harden', displaying increased strength. Flow liquefaction, with its associated soil structure collapse, and subsequent large deformations, is impossible in dense soils. However, cyclic loading studies of dense sands in the laboratory have shown that after a period of sustained loading, peak pore-water pressures may momentarily equal the confining stress. This type of behaviour is known as 'initial liquefaction' and does not result in large deformations.

1.3.1 Definitions of liquefaction.

There has been a considerable amount of academic debate over the past few decades concerning soil liquefaction, with the root of these debates being poor definitions of the different types of earthquake induced liquefaction which can be observed. Seed (1979) defines three useful terms used to describe liquefaction behaviour:-

1. *Liquefaction (or flow liquefaction):* denotes a condition where a soil will undergo continued deformation at a constant low residual stress or with low residual resistance, due to the build-up and maintenance of high pore water pressures, which reduce the effective mean stress to a very low value; pore-pressure build-up leading to liquefaction may be due either to static or cyclic stress applications and the possibility of its occurrence will depend on the void ratio and the confining pressure; it may also be caused by a critical hydraulic gradient during an upward flow of water in a sand deposit.
2. *Peak Cyclic Pore Pressure Ratio of 100% (or 'initial' liquefaction):* denotes a condition where, during the course of cyclic stress applications, the residual pore-water pressure on completion of any full stress cycle becomes equal to the applied confining pressure; the development of a peak cyclic pore pressure of 100% has no implications concerning the subsequent magnitude of soil deformations, however, it defines a condition that is a useful basis for assessing various possible forms of subsequent soil behaviour.

3. *Peak Cyclic Pore Pressure Ratio of 100% with Limited Strain Potential (or Cyclic Mobility):* denotes a condition in which cyclic stress applications develop a peak cyclic pore pressure ratio of 100% and subsequent cyclic stress applications cause limited strains to develop either because of the remaining resistance of the soil to deformation or because the soil dilates, the pore-pressure drops, and the soil stabilises under the applied loads. Cyclic mobility may also be used in a broader sense to describe the cyclic straining that may occur even with pore pressure ratios less than 100%, in which case the actual peak value of pore pressure ratio may be simply stated.

1.3.2. Factors influencing soil liquefaction potential.

Based upon the results of a large number of (dominantly cyclic) laboratory tests and field observations, Seed & Idriss (1971) & Seed (1979) identified the following factors controlling the liquefaction potential of a soil:

1. soil type,
2. relative density or void ratio,
3. initial confining pressure,
4. method of soil formation (soil structure and microstructure),
5. period under sustained load (ageing or diagenetic effects),
6. previous strain history,
7. lateral earth pressure coefficient and overconsolidation,
8. intensity and nature of ground shaking,
9. duration of ground shaking.

1. Soil type. The most liquefiable soil types range from coarse/medium sands to medium silts, with fine to medium sands being particularly susceptible. Evidence also suggests that uniformly sorted materials are more susceptible than well graded materials (Ross, *et al.*, 1969; Lee & Fitton, 1968). Laboratory and field evidence also shows that small quantities of fine particles (>63μm) can dramatically increase the risk of flow liquefaction (Ishihara, 1993). Fine grained clayey soils under cyclic loading tend not to 'liquefy' as such but may develop increased pore pressures (Cao & Law, 1992), resulting in cyclic shear strains, especially if the cyclic stress is very large (Castro & Christian, 1976). Very sensitive clays, for example the well documented Norwegian 'quick clays' (Bjerrum & Landra, 1966), can display a dramatic loss of shearing strength upon loading, due to

freshwater leaching. This behaviour is not however regarded as true liquefaction as described in the context of this thesis. At the other grain size extreme, it is generally recognised that very coarse gravelly soils are immune to liquefaction, the very high permeability of these deposits preventing significant pore-pressure build-up during shaking. However, Stokoe II, *et al.* (1988a), describe the lateral spreading of (cyclic mobility) very loose gravelly soils in the 1983 Borah Peak, Idaho earthquake.

2. Void ratio. Since the classical work of Casagrande (1936), void ratio has been recognised as one of the most critical factors controlling liquefaction for a particular sediment. Casagrande recognised that for a given earthquake a loose sand may suffer flow liquefaction, but the same material in a denser condition may not, with a 'critical void ratio' dividing the two types of response. This conclusion is illustrated by the 1964 Niigata earthquake. Liquefaction was extensive where the relative density was around 50%, while it was not observed where the relative density exceeded 70% (Seed & Idriss, 1971).

3. Initial confining pressure. Laboratory testing (Casagrande, 1975; Been & Jefferies, 1985) demonstrates that the undrained response of a sand with a certain void ratio depends on the initial effective confining stress. However, the specific effects of confining pressure upon sand response illustrates an interesting paradox between the different approaches used to predict liquefaction potential. Seed & his co-workers from Berkeley suggest that, based upon cyclic triaxial testing, the risk of liquefaction decreases with increasing depth. In contrast, Casagrande and his co-workers illustrate that, based upon monotonic triaxial testing, liquefaction potential increases with increasing depth. This apparent paradox will be discussed in more detail in Chapter 3.

4. Method of soil formation (soil structure). Investigations by various workers have demonstrated that the liquefaction characteristics measured in the laboratory, under cyclic loading, are significantly influenced by the method of sample preparation and hence soil structure. Nemat-Nasser & Takahashi (1984) observed that for samples prepared by pluviating dry sand through air, grains are packed in the horizontal plane, while in samples prepared using moist tamping the orientation of the grains is essentially random; this inherent anisotropy affects both the densification and the liquefaction potential of the sample. In contrast, Been & Jefferies (1985) illustrate that liquefaction

characteristics derived from monotonic laboratory testing, are less significantly influenced by differing methods of sample preparation.

5. Period under sustained load (ageing effects). The age of the deposit tends to increase its resistance to liquefaction. This is due in part to cementation which may occur at contact points between sand particles, and in part to being associated with the secondary consolidation of the soil (Lee & Focht, 1975). Clough *et al.* (1989) conclude that 'cemented sands have unique characteristics relative to their uncemented cousins. When saturated and subjected to seismic loading, the cemented sand can liquefy, but its resistance to liquefaction is greater than that of the uncemented sand. Given that many natural sand deposits are cemented to some degree, the influence of cementation on liquefaction resistance is important, and should be considered in engineering deposits'.

6. Previous strain history. Studies by Finn *et al.* (1970) investigating the effects of previous strain history show that both cyclic (caused by small earthquake shocks) and static strains (imposed by large structures) drastically reduce the liquefaction resistance of a sand.

7. Lateral earth pressure coefficient and overconsolidation. Both theory and experimental data show that the stress ratios required to cause cyclic mobility are significantly influenced by the coefficient of earth pressure at rest, K_o (Seed, 1979). These data indicate that overconsolidated samples under cyclic loading are more resistant to liquefaction than normally consolidated samples.

8. Intensity and nature of ground shaking. The intensity of ground shaking has an important effect on the behaviour of a potentially liquefiable sediment. A more intense earthquake will tend to generate greater pore-pressures and at a faster rate, inducing liquefaction over greater areas, while weak events may not generate any significant pore-pressures and liquefaction will not occur. This type of effect is illustrated by the response of structures in the Japanese city of Niigata to earthquake shaking over the past 370 years. During this time the city has been shaken by around 25 significant earthquakes. However, historical records show that there have been only three occasions on which liquefaction has been reported; on these occasions the estimated accelerations were in excess of 0.13g. In the case of the other 22 earthquakes,

estimations were in the range 0.005 to 0.12g, and were clearly not great enough to induce liquefaction in this particular region (Seed & Idriss, 1971). The nature of ground shaking is also an important factor in determining liquefaction potential. Most cyclic laboratory testing only approximates the complex multi-directional shaking which occurs in an earthquake. Laboratory simulations usually simplify this 3-dimensional movement to a simple 1-D case in which the sample is loaded along the principle stress direction with a smooth wave form. This may be an adequate representation for water wave loading problems, but for earthquake studies Seed (1979), notes that under multi-directional shaking or stress conditions, pore water pressures build up faster than under unidirectional stress conditions, and that the stress ratio required to cause a peak cyclic pore-pressure ratio of 100% under multi-directional shaking conditions is about 10% less than that under uni-directional loading conditions.

9. The duration of ground shaking. The duration of ground shaking is a significant factor in determining liquefaction potential because it determines in a general way the number of significant stress cycles to which the soil is subjected. Many laboratory studies of soils under cyclic loading have shown that for a specific sample, the onset of liquefaction occurs after a certain number of cycles (Seed & Idriss, 1971). In the field, the significance of shaking duration was illustrated by the landslides and ground failures which were triggered by liquefaction in Anchorage (Alaska) during the 1964 earthquake. These slides did not occur until about 90 seconds after the shaking started. Seed & Idriss (1971) suggest that if the duration of ground shaking had only been 45 seconds, no liquefaction would have occurred.

1.4 Thesis layout.

Chapter 2 lists the most commonly used field and laboratory methods in liquefaction prediction. Chapter 3 contains a review of the current geotechnical techniques used in liquefaction evaluation. Chapter 4 presents a critical review of the current 'state of the art' in the measurement of shear wave velocity, onshore, offshore and in the laboratory, together with theoretical models and current engineering applications, with particular reference to liquefaction prediction. The laboratory and field methods used during this study are described in Chapter 5. Shear wave velocity and steady state results are presented in Chapter 6, while the integrated geophysical and geotechnical data are contained in Chapter 7. Chapter 8 presents the Fraser River Delta as a case study

consisting of a brief literature review followed by an attempt to quantify potential behaviour under earthquake loading using both the methods presented in this thesis and conventional techniques. Chapter 9 presents a discussion on the research findings as a whole, with the main conclusions drawn from the work presented in Chapter 10.

Plate 1.1. Tilting of apartment blocks in the Kawagishi - cho district in Niigata, as a result of liquefaction of the sandy soil on which they were supported (*after Seed & Idriss, 1967*).

CHAPTER 2.

A review of existing laboratory and *in-situ* test methods.

2.1. Introduction.

A wide variety of different testing methods have been used to both study and predict liquefaction potential over the past 30 years. The laboratory methods have been used to provide a fundamental understanding of the phenomenon, while field methods have generally been used to simply divide liquefiable and non-liquefiable soils, and also as an aid to the extrapolation of laboratory results to the field. Each of these techniques has its own set of individual advantages and disadvantages, and an understanding of these is necessary before any further discussion of the actual approaches used to predict liquefaction is attempted.

2.2. Laboratory methods used in the prediction of liquefaction potential.

Laboratory methods have been used for a number of years now to investigate the liquefaction behaviour of sands, under a variety of different loading conditions. The results of many investigations by different authors using different laboratory techniques have allowed the identification of the various factors which directly affect a soil's susceptibility to liquefaction (described in Section 1.2.2. above). Advantages of testing materials in the laboratory include, convenience, close control over boundary conditions, availability of standard apparatus, and modest cost when compared to *in-situ* methods.

Any method which relies upon the testing of representative 'undisturbed' samples in the laboratory will be highly sensitive to any changes which may occur to the sample prior to testing. Non-cohesive soils are particularly sensitive to changes in volume and soil particle arrangement (Sasitharan, *et al.* 1992), which may occur at any time during sampling, transportation to the laboratory and subsequent re-consolidation. In general, loose to medium sands will tend to densify as a result of sampling, while dense sands will tend to dilate, with all types of sample suffering from the possible loss of cementation, long-term loading, and seismic history effects. These changes occurring to the sample as a result of retrieval from the field are likely to have a significant effect on any subsequent laboratory evaluation of cyclic mobility potential (Seed, 1979).

Typical approaches to 'undisturbed' sampling are described in a review by Castro *et al.* (1992), and include the use of fixed piston sampling, tripod tube sampling, and hand carving techniques; field density techniques are employed to measure in-situ void ratios, allowing subsequent corrections to be applied once in the laboratory. Another alternative is that of ground freezing, described by Yoshimi *et al.* (1994); however, the cost involved with ground freezing limits this kind of investigation to those associated with large capital projects.

The collection of 'undisturbed' samples from offshore areas becomes even more difficult, due partly to the effects of pressure release on gas saturated pore-fluids and to the difficulties simply in collecting samples in the more hostile marine environment. Thus, mainly because of the experimental advantages, laboratory data on the liquefaction behaviour still provides the fundamental basis for our current understanding of the phenomenon.

2.2.1. The triaxial apparatus [1].

The triaxial (or more properly the 'confined uniaxial') apparatus is probably the most widely used apparatus for investigating the stress : strain behaviour of soils and, in various forms, it has provided the basis of laboratory liquefaction prediction work over the past 30 or so years. At its simplest, a cylindrical soil sample contained in a thin rubber membrane is placed in a testing cell. The sample itself sits in the cell between a rigid base and a rigid top cap, which may be loaded by means of a ram passing through the top of the cell (Figure 2.1). The testing cell is then filled with fluid (usually water) and pressurised, while the rubber membrane isolates the sample from the surrounding fluid, allowing back pressures to be applied to the sample, and hence accurate control of the effective stress. Both the top and bottom caps have pore-water drains leading from them, allowing the measurement of either volume change in drained tests, or pore-pressure change if drainage is prevented. Loads may then be applied to the cell via the ram, either by placing dead loads on a hanger (stress control), or by reaction against a loading frame (strain control). Under these conditions, the axial stress (that applied by the ram) is the major principal stress σ_1, while the intermediate and minor principal stresses (σ_2 and σ_3 respectively) are equal to the cell pressure.

[1] A more detailed description of the triaxial test as used in this study is given in Chapter 5.

The quantities usually measured during the course of a triaxial test include the cell pressure, the axial force (deviator stress) applied via the loading ram, the change in length of the sample, and for a test in which drainage is prevented, the pressure of the pore-fluid, while for a test in which drainage is allowed, the change in volume. Generally the application of the all-round cell pressure and of the load via the ram occur in two separate stages of the test. On the basis of these separate stages, Bishop & Henkel (1964) classified the test into three main types:

1. *Undrained tests.* No drainage, and hence no dissipation of pore-pressure, is permitted during the application of the all round stress. No drainage is allowed during the application of the deviator stress.
2. *Consolidated-undrained (or constant volume) tests.* Drainage is permitted during the application of the all round stress, so that the sample is fully consolidated under this pressure. No drainage is allowed during the application of the deviator stress.
3. *Drained tests.* Drainage is permitted throughout the test, so that full consolidation occurs under the all-round stress and no excess pore-pressure is set up during the application of the deviator stress.

In addition to the commonly performed triaxial compression test, in which deviator stress is gradually increased, if some provision is made for pulling the top cap (instead of pushing) it is possible for the ram force and deviator stress to be negative; these tests are known as triaxial extension tests (Wood, 1994).

The biggest advantage of the triaxial test is that it allows control of drainage conditions and the possibility of pore-pressure measurement during testing. However, some limitations can be recognised. These include (Bishop & Henkel, 1964):

1. *Influence of the value of intermediate principal stress.* Under normal triaxial loading conditions the intermediate principal stress, σ_2 is equal to the minor principal stress, σ_3. In many engineering problems approximating plane strain, this condition does not hold and the value of σ_2 is greater than σ_3.
2. *Change in principal stress directions.* In the cylindrical compression test the principal planes are fixed in relation to the axis of the specimen. In problems involving active or passive pressure in zones with a horizontal boundary, this restriction is relatively

unimportant, but in problems where the direction of σ_1 changes steadily under the applied stresses, this limits the accuracy with which pore-pressure can be predicted.

3. Influence of the end platens. The interaction of the rigid end caps, necessary to transmit the axial load, and the ends of the specimen, restricts lateral deformation adjacent to these surfaces. This leads to a departure from the condition of uniform stress and strain, and non-uniformities which can in turn affect the strength, volume and pore-pressure characteristics of the sample under test. This problem can be solved to some extent by either testing samples with a length/diameter ratio of 2, which generally ensures deformation is approximately uniform over the middle portion of the specimen, or using lubricated (or 'frictionless') end platens, so that lateral restraint is not developed (Green & Reades, 1975).

4. Duration of test. The duration of the triaxial compression test is usually determined by operator convenience, and for a typical undrained test (not including the consolidation stages) may be of the order of 10-20 minutes. The main criticism here is that no account is made of soil creep. While this may be negligible in sands, it can represent a significant error in the testing of clays.

5. Membrane effects. Kuberis & Vaid (1990) note that the rubber membrane used to enclose the sample can carry part of the axial load applied to the specimen in addition to affecting the magnitude of confining pressure. These strength effects can become a significant fraction of the overall applied stresses, especially those performed at low confining pressures and on loose sands that undergo liquefaction. Membrane penetration effects in granular media (especially those at low confining stresses) can also affect triaxial results and '....can lead to significant errors in the triaxial testing of granular soils....' (Sladen & Oswell, 1989).

Despite these limitations, the standard triaxial apparatus is possibly the best tool for investigating the mechanical properties of soils, and because of this remains an essential part of the modern soil mechanics laboratory. In the investigation of the phenomenon of liquefaction of sands, not all of the above criticisms listed above are valid and as such the triaxial apparatus has been used to give soil engineers throughout the world an important insight into the mechanism of flow liquefaction.

2.2.2. The cyclic triaxial apparatus.

An early adaptation of the standard triaxial test, allowed the application of cyclic loads to a soil sample. One of the earliest cyclic triaxial systems was developed in an attempt to model the stresses associated with wheel loads constituting vehicular traffic and the behaviour of soil under repeated application of these stresses (Grainger & Lister, 1962). Later studies used the apparatus to study the effects of cyclic loading on sands, with particular relevance to liquefaction studies (Seed & Lee, 1966).

The cyclic triaxial apparatus itself usually consists of a standard triaxial system in which the deviator stress (and sometimes cell pressure) can be varied in a cyclic (usually sine-wave) manner. This loading procedure creates stress conditions on a plane at 45° through the sample, analogous to those produced on a horizontal plane in the ground during an earthquake. This correspondence of the laboratory sample and *in-situ* soils is the basis on which the cyclic triaxial test is utilised as a useful procedure for producing meaningful data to assess the resistance of sands to liquefaction (Ishihara, 1993).

Early cyclic systems produced the desired stress wave mechanically, pneumatically, electrically or hydraulically (Cullingford *et al.*, 1972). These usually purpose-built machines however, tended to show an uncertainty of loading over long periods and a lack of flexibility of application. These problems were overcome by the incorporation of a servo-controlled hydraulic piston to apply the deviator load, which brought about a significant improvement both in the control of the waveform and frequency response (Cullingford, *et al.*, 1972). One of the most recent developments links the hydraulic piston of the stress path cell to a microprocessor based pressure controller, allowing precise control of the input waveform.

Seed (1979) recognised the various problems associated with the cyclic triaxial test, some of which are common with the standard triaxial test, and others which are unique to the cyclic test. They include:

1. the test does not reproduce the correct initial stress conditions in the ground since it must be performed with an initial ambient pressure condition (K_o) to produce the symmetrically reversing shear stress conditions representative of level ground condition,
2. stress concentrations at the cap and base of the specimen,

3. a 90° rotation of the direction of the major principal stress during the two halves of the loading cycle,
4. 'necking' of the sample around the end platens may develop and invalidate test data,
5. the intermediate principal stress does not have the same relative value during the two halves of the loading cycle,
6. difficulty in achieving a high degree of accuracy for stress ratios above 0.6.

In addition, Townsend (1978), in a detailed review of factors affecting cyclic triaxial tests, concluded that sample preparation methods, differences between intact and reconstituted specimens, and pre-straining, have a large effect on cyclic strength. Differing sample preparation methods caused a difference in the stress ratio required for failure by as much as 110%. Loading wave form and consolidation stress ratio have noticeable, but less significant effects, while loading frequency, specimen size, and frictionless caps and bases had relatively minor effects on cyclic triaxial strengths.

Partly because of the limitations described above, cyclic simple shear tests sometimes provide an alternative method with which to study liquefaction.

2.2.3. Cyclic simple shear tests.

During an earthquake, a soil element in the ground is subjected to a complex series of essentially random motions. In many cases these ground motions may be attributed to the upward propagation of shear waves from the underlying soil. If the ground surface is approximately horizontal, there is no shear stress on the horizontal plane. During the earthquake the normal stresses on this plane remain constant, while reversing cyclic shear stresses are induced by the shear waves propagating from below (Peacock & Seed, 1968). Cyclic triaxial tests approximate this condition, while cyclic simple shear conditions appear to represent a better correlation to field conditions (Seed, 1979).

Peacock & Seed (1968) describe a simple shear apparatus used in an early study of sand liquefaction under simple shear conditions. Essentially a square sand sample is contained in a rubber membrane inside a shear box, with two hinged walls and two fixed walls so that the samples can be subjected to deformations of the type shown in Figure 2.2.

These early studies suffered from problems in effecting a uniform shear stress condition on the sample and in preparing a sample that entirely filled the box. Later studies suffered from long recognised inherent difficulties with the shear box, including sample preparation, the development of uniform stress conditions throughout the test sample, the application of uniform stress conditions to the sample and the avoidance of stress concentrations at the ends of the sample. Despite improvements to the technique, including the use of very large samples, undesirable differences existed in reported simple shear data, due partly to problems with sample preparation and membrane compliance. In addition, Moussa (1975) notes that the undrained shearing resistance of sand to cyclic simple shear loading is greatly affected by the previous stress and strain history. However, Seed (1979) concludes '....that carefully conducted simple shear or torsional shear tests using good quality equipment can provide data comparable to that obtained with large scale test samples and presumably representative of simple shear field conditions if these could develop uni-directionally'.

2.2.4. Vibration table studies.

Studies of liquefaction for large saturated sand samples excited on a vibration table appear to offer a number of general advantages over both the small scale cyclic triaxial and cyclic simple shear tests (Finn, 1972). These include:

1. large homogeneous samples of saturated sand may be prepared, and since inertia effects of embedded instruments are negligible for such large samples, inertial strains and accelerations can be measured,
2. it is possible to use displacement, velocity or acceleration modes of control to provide a wide range of acceleration records and frequencies, including those recorded during real earthquakes,
3. uniform accelerations will be developed throughout the sample at low frequencies under plain strain conditions that correspond to the upward propagation of shear waves *in-situ*,
4. it is possible to trace the actual pore-water pressure distribution in a large mass of sand during liquefaction,
5. a visual examination of the sample during vibration is possible.

Finn (1972) describes an example of a typical vibration table. 'The sample measured approximately 9ft long by 6ft wide by 7inches high, and was mounted on a table which was constrained to allow movement in one direction. The desired motions were transmitted to the sample via a hydraulic ram mounted on a fixed frame, controlled by an earthquake simulator console. Pore-pressures during the test were monitored at five locations in the middle of the sample...'

Finn (1972) concludes that when compared with results obtained from the cyclic triaxial and cyclic simple shear tests (Seed & Lee, 1966; Peacock & Seed, 1968), shake table results show a general qualitative agreement. Vibration table studies may however, be regarded as more representative, due simply to their larger scale and better reproduction of true earthquake conditions.

2.2.5. Summary.

Laboratory testing of the type described above has produced a vast amount of data on both simple compression and cycling loading of non-cohesive (and cohesive) soils. These laboratory methods have the advantage that they all allow the careful control of boundary conditions, making the identification of individual influencing factors relatively simple. However, all the laboratory methods described above represent some sort of compromise, in terms of adequate simulation of field conditions, system compliance, membrane penetration and the development of uniform shear stresses. In addition, the difficulty in obtaining undisturbed sediment samples, in particular from the marine environment, has spurred the development of more applicable *in-situ* approaches.

2.3. *In-situ* methods used in the prediction of liquefaction potential.

A rapid development of *in-situ* methods for the measurement of a wide variety of soil properties has occurred over the past 30 years, partly in response to some of the limitations of laboratory tests described above. Robertson (1982), identified a number of distinct advantages *in-situ* methods have over laboratory techniques, including:

1. the ability to test 'difficult to sample' sediments, such as sands, and in harsher environments (e.g. offshore),
2. the ability to test a larger volume of soil,

3. avoidance of some of the difficulties of laboratory testing, including sample disturbance, simulation of *in-situ* stresses, temperature etc.,
4. increased cost-effectiveness.

These points clearly illustrate the advantages of *in-situ* testing in what are conventionally regarded as difficult to sample areas, where the recovery of undisturbed samples for subsequent laboratory may be impossible. However, *in-situ* testing methods also suffer a number of other limitations including lack of independent variation of stress path and stress direction, poor control on drainage conditions, and the possible effects of future changes in environmental conditions cannot be readily determined (Robertson, 1982). In most cases these limitations are far outweighed by the significance of the *in-situ* test results.

Despite these advantages, most of the descriptions below refer to generally land-based techniques, simply reflecting the relative ease of measurement. In shallow water areas some of these methods, particularly the Standard Penetration Test & Cone Penetration Test, may be 'marinised' by simply mounting them on a barge. In deeper water, this becomes more difficult and specially designed systems are required. Clearly any attempt at a 'standard' geotechnical site survey offshore, involves significant increases in cost. Because of this, many offshore site investigations are beginning to place a heavier reliance on geophysics, which offers significant advantages in terms of both data coverage and ease of measurement.

2.3.1. The Standard Penetration Test (SPT).

The Standard Penetration Test, originally developed to investigate the status of cohesionless deposits for pile installation (Bowles, 1992), is one of the most practised world-wide tests for determining *in-situ* soil conditions. The SPT, as standardised by the American Standards of Testing and Materials (ASTM) D1568, consists of a 63.5kg mass free-falling a height of 760mm onto an anvil connected to drill rods, which in turn drive a standard split barrel (also called 'split spoon') into soil at the bottom of a boring (Figure 2.3). Counting the blows required to drive the sampler 305mm (after a seating drive of 152mm) yields the blow count, N. The obtained N value can then be empirically correlated in sands to soil parameters such as overburden pressure, relative density, particle size, ageing, overconsolidation and liquefaction potential (Skempton, 1986). In

addition, (highly disturbed) sediment samples can also be collected from the borehole, allowing physical description and limited subsequent laboratory testing. Because of its highly dynamic nature, the SPT suffers greatly from the problems of a lack of repeatability and reliability. Schmertmann (1978) identifies various factors which account for the variability of the test (each factor capable of causing a change in N value of up to 100%):

1. use of drilling mud versus casing and water to support the boring,
2. differing borehole diameters,
3. number of rope turns on the cathead winch,
4. anvil size,
5. drill rod length,
6. variations in drop height,
7. depth range over which penetration resistance is measured.

In addition, since the hammer is usually controlled manually, an additional unquantifiable human error is added to the results. Schmertmann (1978) points out that '...the SPT as practised in the United States under ASTM Method D 1586, suffers from a perhaps fatal or near fatal flaw. Practising engineers know all too well that the test and its N-values have a poor reproducibility and great variability between different operators and equipment...'. Further, he concludes that '..the profession needs to establish and enforce an alternative ASTM Method D1586 standard test that requires a mechanised hammer drop, a calibrated energy content in the first compression wave in the rods, and the use of rotary drilling in a hole kept continuously full of drilling mud'. However, despite this rather damning conclusion the SPT remains one of the most commonly used world-wide site investigation methods in use today. The use of the SPT in liquefaction prediction work is further discussed in Section 3.2.1. below.

2.3.2. The Cone Penetration Test (CPT).

The Cone Penetration Test (also known as the 'Dutch Cone') is a method of site investigation in which no samples are taken (Figure 2.4). The test itself exists in various forms (including the static, dynamic, screw and inertial), however, the static method, in which the cone is advanced into the ground using a hydraulic jacking technique, is most commonly used in current engineering practice and is the type described here. A basic

electric cone system consists of a cone with a standard tip geometry (usually 60° tip and 10cm^2 area) which is pushed into the ground at a standard rate of 2cm/second. A friction sleeve is located above the conical tip, and has a standard area (usually of 150cm^2). Load cells mounted in the cone allow continuous recording of the end resistance (q_c) and side friction (f_s). These load cells can be made in a variety of capacities, depending on the strength of the soil to be penetrated; current developments (circa. 1995) are allowing the penetration of soft rocks for the first time, using a 40 ton cone truck (Robertson, *pers. comm.,* 1995). One of the more recent developments is the addition of a pore-pressure transducer, which allows measurement of excess pore-pressures (Δu); if penetration is halted, the coefficient of consolidation and (after all excess pressures have dissipated), the equilibrium pore-pressure value (q_o) may be interpolated (Robertson, 1982). A cone test in which the cone has been fitted with a pore-pressure transducer is known as the peizocone penetration test (CPTU); another variant is the resistivity cone penetration test (RCPTU) (Campanella & Kokan, 1992), which allows the measurement of continuous resistivity data; a further variant still is the Seismic Cone Penetrometer, which allows the measurement of the field shear wave velocity profile (see Section 4.3.2.1.).

Like all other mechanical *in-situ* penetration tests the CPT does not actually measure any specific soil property, rather it measures the soil response to an imposed deformation. Due to the lack of a suitable general theoretical solution allowing extraction of geotechnical information from the test (Been *et al.,* 1986), interpretation of the data collected is therefore generally achieved using empirical correlations. Typically the CPT is used to provide an accurate determination of the soil profile, based upon the Friction Ratio (f_s/q_c x 100) and the differential pore-pressure ($\Delta u/q_c$). Other empirical correlations have been made with relative density, shear strength, compressibility, modulus and consolidation state (liquefaction potential). All these correlations implicitly assume the cone bearing to represent the ultimate values from thick deposits, a soil layer only 10 - 20 cone diameters in thickness may not be correctly interpreted because of the close proximity of the adjacent surfaces. Fully instrumented electrical cones, despite their high initial cost and requirement for skilled operators, have the advantages of rapidity of testing, continuous recording but probably most significantly, a high degree of accuracy and repeatability.

2.3.3. Pressuremeter tests.

The Pressuremeter test involves the insertion of a tube into the ground, and the subsequent expansion of a membrane against the soil under controlled conditions, providing a very powerful technique for the determination of soil elastic parameters (Robertson, 1982). Although various types of pressuremeter exist (e.g. the Menard Pressuremeter and the Push-in Pressuremeter), the Self-boring Pressuremeter (Fahey & Randolph, 1984; Jewell *et al.,* 1980) offer, in cohesionless soils, the advantages of insertion with minimal disturbance and direct determination of soil parameters. Self boring pressuremeter data can be used to determine friction angle ϕ', dilation angle ν (Jewell, *et al.,* 1980), shear modulus G_o (Hepton, 1989), permeability k (Chandler *et al.,* 1990), state parameter ψ (Yu, 1994) and *in-situ* horizontal effective stress σ_h' (Schnaid & Houlsby, 1992). The greatest limitation of the self boring pressuremeter is the high cost associated with the equipment and installation, and the need for highly trained personnel (Robertson, 1982).

2.3.4. *In-situ* shear devices - the Piezovane.

A relatively new approach to the *in-situ* determination of liquefaction potential is to use an *in-situ* vane shear device, fitted with a transducer to allow the monitoring of pore-pressure during shear, called the Piezovane by the authors, Charlie *et al.* (1995) (Figure 2.5). The piezovane consists of a standard four-bladed field vane, 63.5mm in diameter by 127mm high, with a blade thickness of 3.2mm. Four ports provide a continuous fluid connection from the vane blade edges to a pressure transducer mounted in the top of the vane. The vane, when inserted in the soil, is rotated by hand with a torque wrench, while angular displacement, applied torque and pore-pressure changes are measured continuously. The authors argue that, during the test, an increase in the monitored pore-pressure (and consequent decrease in effective stress) indicates a contractive response and the risk of flow liquefaction. A decrease in pore-water pressure indicates a potentially dilative response and no consequent risk of large scale deformations.

2.3.5. Summary.

The use of *in-situ* field investigative techniques, such as those described above, are fundamental to the prediction of liquefaction potential at a particular field site. Early investigations merely compared sites which liquefied and sites which did not liquefy during the same earthquake, and generally utilised the SPT. Many of these early investigations were severely compromised by some of the limitations associated with the SPT (described above) and as a result, for this type of investigation the SPT is slowly being superseded by the CPT. However, a large amount of field SPT data exists, collected over many years and covering a wide variety of earthquake conditions. Many engineers still use SPT based correlations and because of this, the biggest current limitation of the CPT as a liquefaction prediction tool, is a result of the small size of the CPT data base when compared to the large volumes of SPT data collected over the past 30 years. In addition, all the *in-situ* techniques are either difficult or expensive to implement offshore. However there still appears to be a need for some index to liquefaction potential which may be used cheaply and reliably.

The prediction of liquefaction potential using the laboratory and *in-situ* methods described above is generally performed using two distinct approaches, which are described in the next chapter.

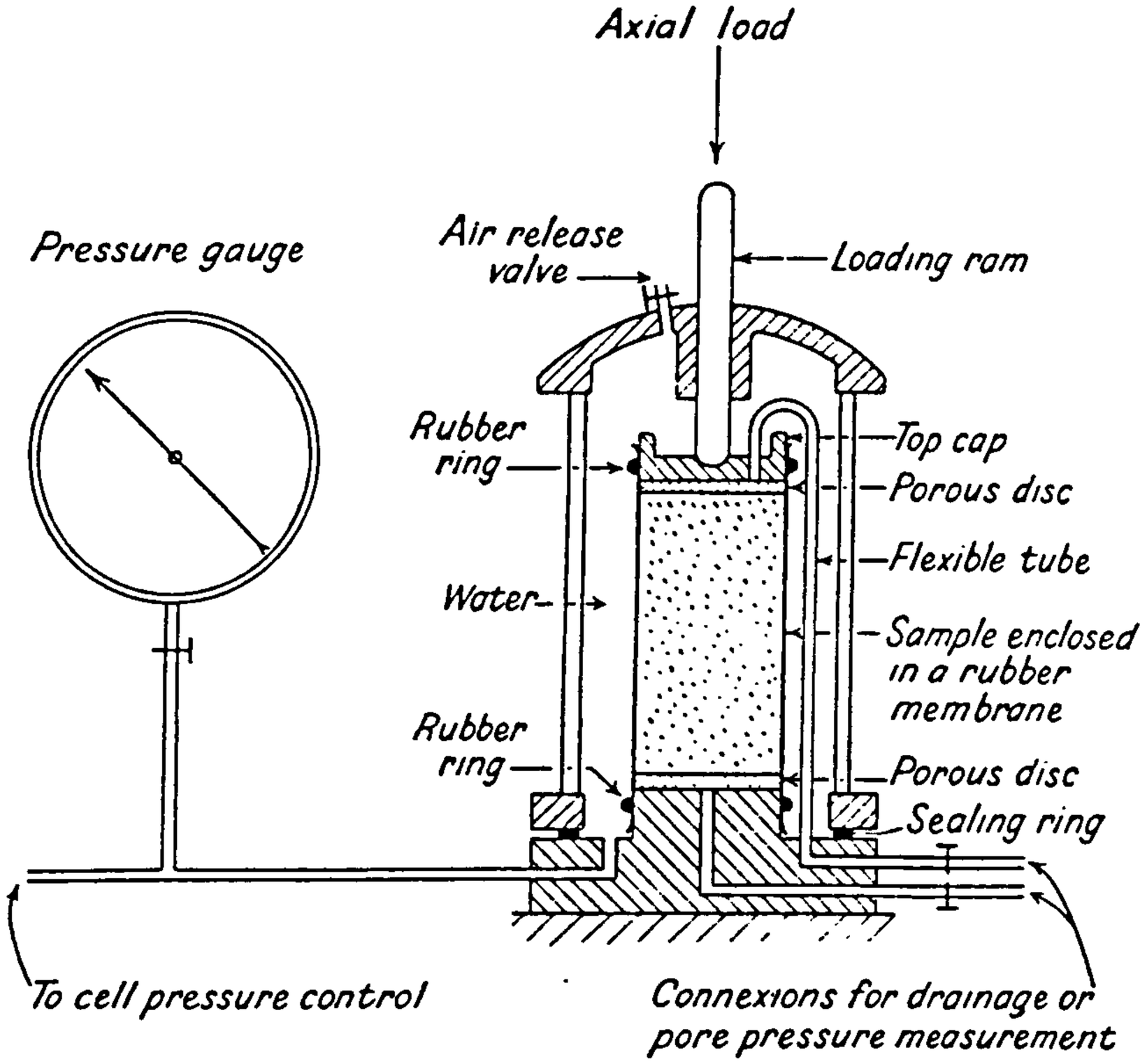

Figure 2.1. Diagrammatic layout of the triaxial cell (*after Bishop & Henkel, 1964*).

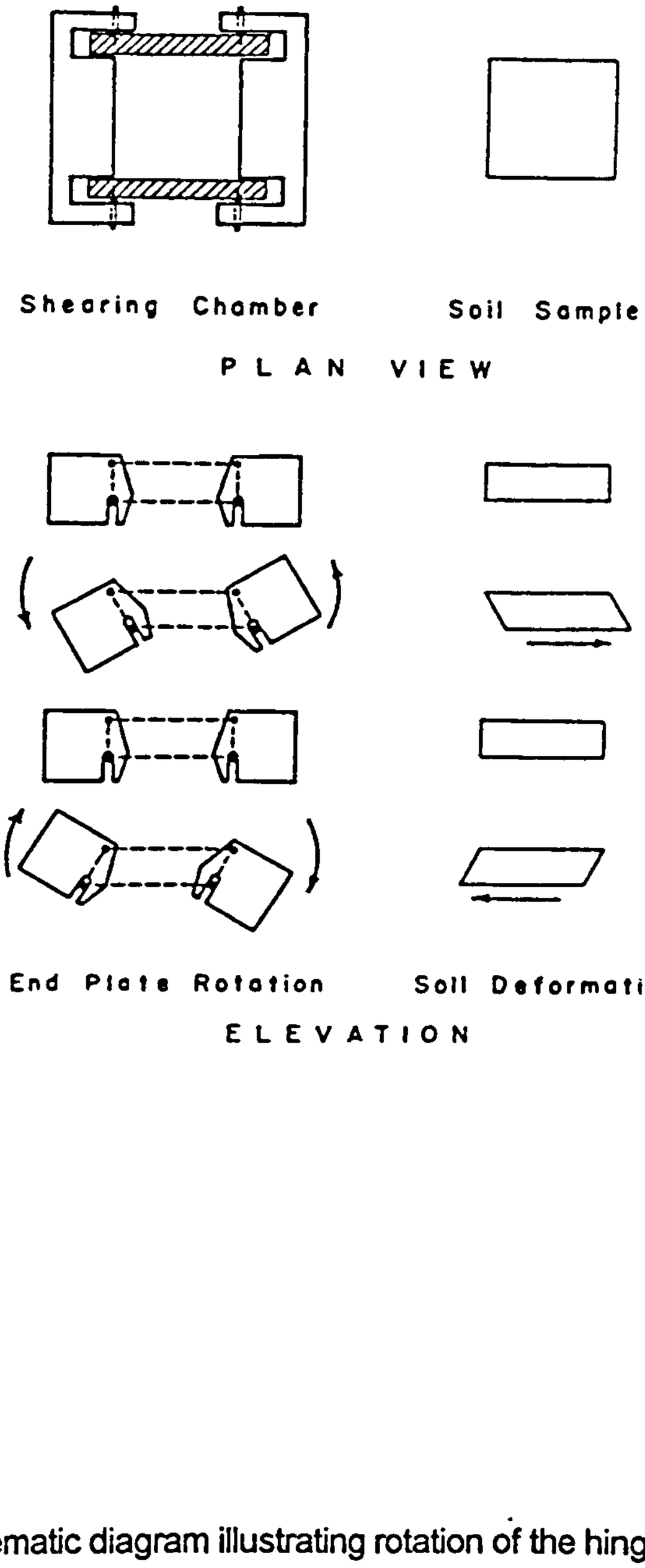

Figure 2.2. Schematic diagram illustrating rotation of the hinged ends of a cyclic shear box and associated soil deformation (*after Peacock & Seed, 1968*).

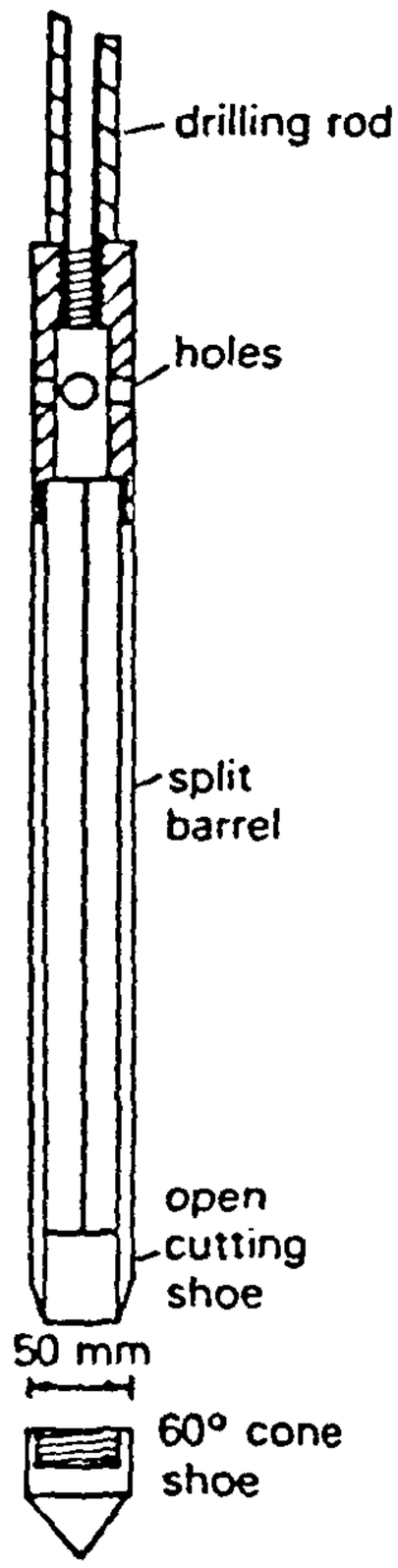

Figure 2.3. Spilt spoon sampler (*after Whitlow, 1990*).

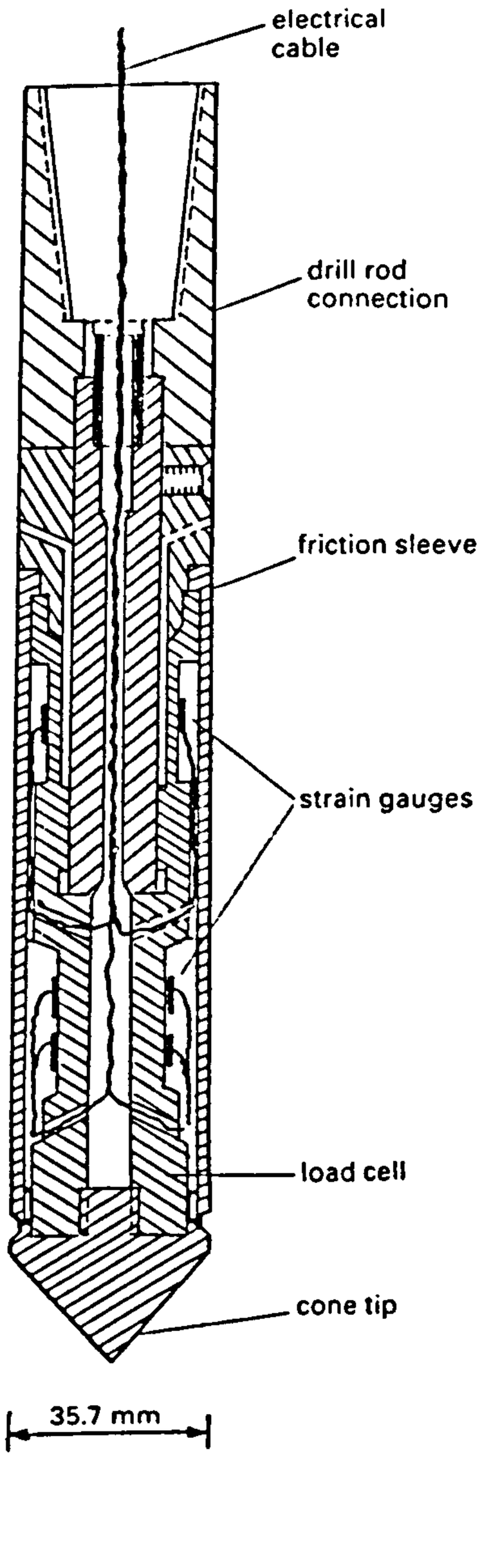

Figure 2.4. Electric cone penetrometer (*after Whitlow, 1990*).

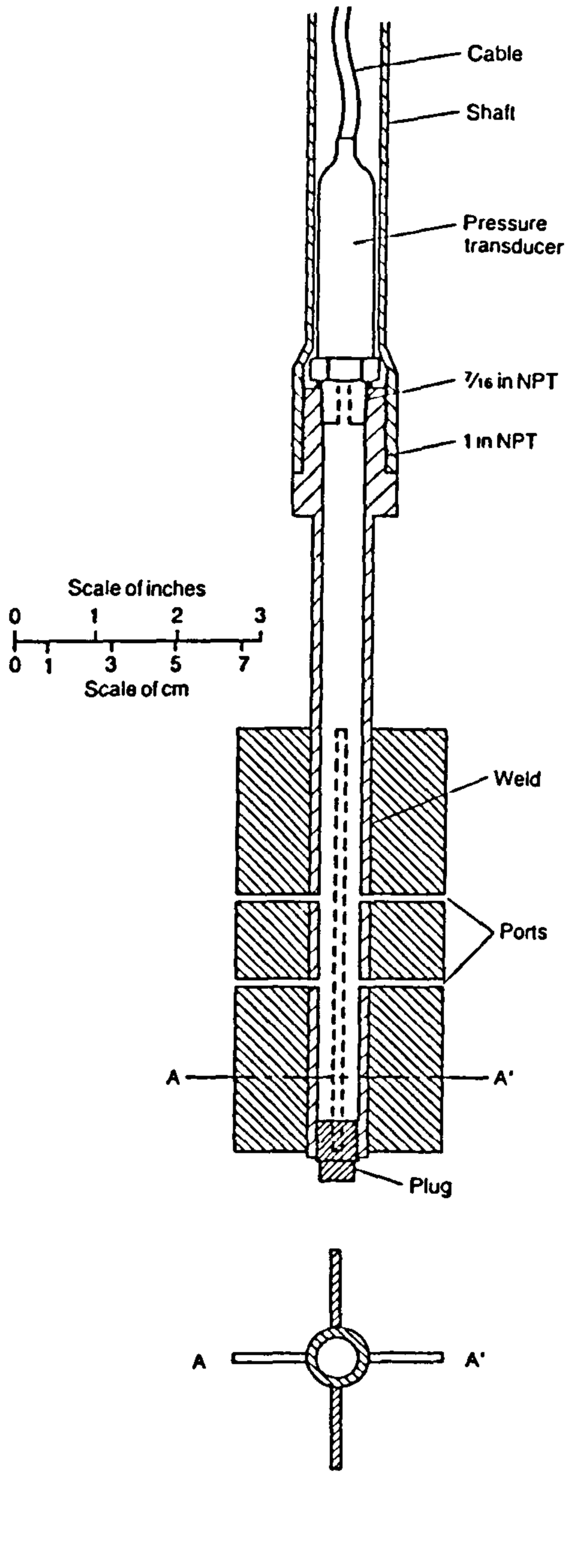

Figure 2.5. *In-situ* shear device - the Piezovane (*after Charlie et al., 1995*).

CHAPTER 3.

Conventional approaches to the prediction of liquefaction potential.

3.1. Background.

Over the past 30 years, a wide variety of different geotechnical techniques have been employed in attempts to predict the liquefaction potential of non-cohesive sediments. In the laboratory these efforts have been centred around the cyclic simple shear apparatus and the cyclic or monotonic triaxial compression test, while field techniques have often involved either the Standard Penetration Test (SPT) or the Cone Penetration Test (CPT). Two main approaches for the evaluation of liquefaction or cyclic mobility of sediments subjected to earthquake shaking have been developed. These are:

1. the 'Berkeley approach', based principally around the work of Professor H.B Seed at the University of California, Berkeley. This approach is based upon observations of performance of sand deposits in previous earthquakes, and methods based on evaluation of stress conditions in the field and laboratory causing cyclic mobility or liquefaction of soils (*e.g.* Seed, 1979),

2. the 'steady state', 'static', or 'Harvard approach', based principally around the work of Professor A. Casagrande and his co-workers at Harvard University. This approach is based upon a detailed laboratory examination of non-cohesive soils under monotonic shear, followed by subsequent correlation to the field (*e.g.* Casagrande, 1975).

Available literature is divided between these two differing approaches, and conclusions are often contrasting, making a review of the subject rather complex. The Berkeley approach tends to dominate much earlier literature, while the steady state approach appears to dominate the more recent literature.

For the case of earthquake loading, the basic assumption of both the approaches described above is that during a period of shaking the soil behaves in an essentially undrained manner. This allows the evaluation of subsequent behaviour on the basis of undrained laboratory techniques. An alternative approach is to use non-linear response analyses which allows a detailed assessment of the stress-deformation characteristics of

a sand stratum as a modelled design earthquake progresses. These methods of analysis can be divided into two different categories: total stress methods (*e.g.* Seed & Idriss, 1967) and effective stress methods (*e.g.* Dikmen & Ghaboussi, 1984). Total stress methods model the material as a one phase equivalent solid in which the pore-pressure effects during the response analysis are not considered. In effective stress analysis the pore-pressures are computed, and their effects during the dynamic response are taken into account. Use of effective stress analysis allows the modelling of pore-water build-up during the earthquake and subsequent dissipation once shaking ceases. These analyses are complex analytical models which require a large number of input variables many of which are extremely difficult to measure in practice with the required accuracy in the soil profile. Because of the highly complex nature of these models, they will not be considered further in this thesis; for further information the reader is directed towards Finn *et al.* (1977); Dikmen & Ghaboussi (1984) & Ghaboussi & Dikmen (1984).

3.2 The Berkeley or 'cyclic' approach.

Seed (1984) describes the Berkeley method, as presented for the last 20 years, as consisting of:

1. the acquisition of a comprehensive background concerning field case histories of soil liquefaction during earthquakes and all proposed methods for evaluating the liquefaction potential of soil deposits,
2. the development and use of methods for evaluating the liquefaction potential based on field observations and case studies,
3. the conduct of laboratory studies on soil samples to throw light on the physical mechanisms by which liquefaction occurs under idealised conditions in the laboratory and to evaluate the possible effects of earthquake shaking on representative samples taken from the field,
4. the conduct of analytical studies to explore the mechanisms leading to the generation of pore-pressures in idealised models of soil deposits, including where appropriate, consideration of soil softening and surface layer isolation,
5. the development of simplified procedures for evaluating the liquefaction potential in practice, based on a knowledge of all aspects of the problem listed but with special emphasis on the use of engineering judgement based on field performance data: where

analysis procedures are used they are checked against field performance data for applicability.

For simplicity this list may be amended to the include the following two points (Seed *et al.*, 1983):

1. methods based on field observations of the performance of sand deposits in previous earthquakes and involving the use of some *in-situ* characteristic of the deposits to determine the probable similarities or dissimilarities between these sites and a proposed new site with regard to their potential behaviour,
2. methods based on an evaluation of the cyclic stress or strain conditions likely to be developed in the field by a proposed design earthquake and comparing these stresses or strains with those observed to cause liquefaction of representative samples of the deposit in some appropriate laboratory test.

Use of this type of approach (described in more detail below) allowed Seed and his co-workers to conclude the following points (McRoberts & Sladen, 1992):

1. initial liquefaction (zero effective stress) is possible in medium to dense sand,
2. liquefaction potential decreases with increased confining pressure,
3. the liquefaction potential decreases with increasing initial (or *in-situ*) principal stress ratio, and therefore sand is less susceptible to liquefaction beneath a slope than beneath a horizontal surface.

These conclusions are significantly different to the conclusions obtained using the 'static approach', and the implications of this will be further discussed in Section 3.2.3 below.

3.2.1. Field performance methods.

This approach to liquefaction prediction represents possibly the oldest and simplest approach to the problem. The technique (and detailed study of liquefaction as a whole) is probably a direct result of the Magnitude 7.5 Niigata earthquake of 16th June, 1964. Detailed site investigations by various workers (*e.g.* Koizumi, 1966; Kawakami & Asada, 1966; Seed & Idriss, 1967), involved use of the SPT to differentiate between soils which did and those which did not liquefy during earthquake shaking. These

investigations, and others from other sites around the world, have allowed the production of relationships between SPT *N*-values and the possibility of liquefaction, based upon an estimation of the average cyclic shearing stress occurring during the earthquake. Despite the limitations of the SPT technique, the relative scarcity of data from other techniques has ensured the continued use of these correlations. In addition, many engineers prefer to use this style of approach as it avoids the problems associated both with laboratory testing and with obtaining undisturbed samples (Seed *et al.*, 1983). More recent investigations have used the CPT in the same manner.

Field liquefaction characteristics, for level ground conditions, are usually represented by the average stress ratio, τ_{av} / σ'_{vo} (the ratio of the average cyclic shear stress, τ_{av}, developed on horizontal planes in the soil as a result of the earthquake motions, to the initial vertical effective stress, σ'_{vo}) (Robertson & Campanella, 1985). This parameter allows the comparison of sites which have differing soil layer depths, water table depths, and intensities of earthquake shaking (Seed *et al.*, 1983).

3.2.1.1. Existing SPT based liquefaction assessment methods.

The SPT *N*-value, as mentioned above, was first used as a liquefaction prediction tool after the 1964 Niigata earthquake, based upon the concept of a 'critical *N*-value', separating liquefiable from non-liquefiable soils (Koizumi, 1966). Later investigations focused on the prediction of relative density, allowing correlation with laboratory test results (Seed & Idriss, 1971). Tokimatsu & Yoshimi (1983) suggest that the continued justifications for the use of the SPT specifically as a liquefaction prediction tool include:

1. the SPT is an *in-situ* test which (theoretically) reflects stress history and strain history effects, soil fabric, horizontal effective stress, relative density and vertical stress,
2. numerous case histories of soil liquefaction during past earthquakes are available for which SPT N-values before the earthquakes are known,
3. the SPT yields representative samples of soil, from which some index properties may be determined,
4. relatively low cost.

Seed & Idriss (1971) & Seed *et al.* (1983) present a method which evaluates liquefaction potential, based upon available field data; this method is summarised below:

1. calculate the stresses induced at different depths by the earthquake, for which the maximum ground acceleration is known, using:

$$\frac{\tau_{av}}{\sigma'_{vo}} \cong 0.65 \frac{a_{max}}{g} \cdot \frac{\sigma_o}{\sigma'_{vo}} \cdot r_d \qquad (3.1).$$

(Seed & Idriss, 1971)

where, a_{max} = maximum acceleration at the ground surface,
σ_o = total overburden pressure on sand layer under consolidation,
σ'_{vo} = initial vertical effective stress,
τ_{av} = average cyclic shear stress,
r_d = stress reduction factor generally varying between 1.0 & 0.9.

2. correlate the value of stress ratio obtained from Equation 3.1 above with sites that did and did not liquefy during earthquake shaking.

In later versions of this method penetration resistances were typically normalised to an effective overburden pressure of 1 ton/sq. ft (4.8 kPa) using:-

$$N_1 = C_N \cdot N \qquad (3.2).$$

where N_1 = normalised penetration resistance,
C_N = a function of the effective overburden pressure at the depth where the penetration test was conducted, and
N = field penetration resistance.

In addition, Skempton (1986), suggests that it is also essential to correct the blow count to the value which would have been measured using a specified rod energy. This correction typically standardises the N_1 value to 60% of the free fall energy of the standard hammer weight and drop, and is represented as $N_{1(60)}$

The use of Equations 3.1 & 3.2 has allowed the detailed evaluation of field performance, in terms of STP N_1 - value and estimated cyclic stress ratio for particular earthquakes (Figure 3.1). An early limitation of this particular technique was an initial lack of field data, although additional data from the subsequent earthquakes, including the Chinese Haicheng (1974) & Tangshan (1976) earthquakes, the Guatemala (1976) earthquake, the Argentina (1977) earthquake, the Japanese Miyagiken-Oki (1978) earthquake and others has much improved the situation.

Liquefaction studies in China, also using the SPT as the primary investigative tool, have allowed the production of a critical N value, N_{crit}, separating liquefiable from non-liquefiable conditions to a depth of around 50 ft (Seed *et al.*, 1983):-

$$N_{crit} = N_s[1 + 0.125(d_s - 3) - 0.05(d_w - 2)] \qquad (3.3).$$

where, N_s = a function of shaking intensity,
d_s = depth to sand layer under consideration (m),
d_w = depth of water table below ground level (m).

From a comparison of these two SPT based field methods, (Seed, 1979) notes 'a very high degree of agreement between the critical boundary' determined by the two different Standard Penetration Test based methods described above and also, 'that it is significant and remarkable that such a great similarity both in procedures and criteria should have evolved in countries with so little technical communication'. Further, for sands under level ground conditions, he concludes that '...if (use of this methodology) provides evidence of an amply large factor of safety, this might well be taken as a reliable indication that cyclic mobility or liquefaction could not develop under the design earthquake conditions. However, where the factor of safety is undesirably low, especially for critical structures, and because the empirical charts do not take into account other significant factors affecting liquefaction.....(the interpretation) may be open to question. It appears to be the general belief among most engineers that these results they provide should be supplemented by detailed studies, based on stress evaluations using ground response analyses and detailed soil testing programs in order to arrive at a meaningful evaluation of the cyclic mobility or liquefaction potential of a particular site'.

Because of the huge amount of SPT data of this type collected from sites around the world over the past 30 or so years, and in many cases both before and after the particular earthquake, this type of approach remains unique in terms of correlations with field performance.

3.2.1.2. Existing CPT based liquefaction assessment methods.

Because of the advantages offered by the CPT in terms of reliability and repeatability, attempts have been made more recently to correlate CPT data to liquefaction

resistance. A variety of different methods have been employed to this end; possibly one of the first of the approaches is reported by (Zhou, 1980) based upon data collected from the Tangshan (1976) earthquake, where the sand was primarily clean, with a low fines content:

$$q_{crit} = q_{co}[1-0.065(H_w-2)][1-0.05(H_o-2)] \qquad (3.4).$$

where, q_{crit} = critical cone penetration resistance,
q_{co} = function of shaking intensity,
H_w = depth of water table below ground (m),
H_o = depth to top of sand layer under consideration.

Another approach utilising the CPT is based upon relative density correlations, obtained using calibration chambers (Tanizawa *et al.,* 1988). These methods cannot be strictly classified as a true field correlation, and also tend to underestimate liquefaction resistance because of failure to recognise other important factors affecting liquefaction behaviour, such as ageing, cementation and stress history, all of which tend to increase resistance to liquefaction (Robertson & Campanella, 1985). However, based on calibration chamber testing of Toyoura sand (a uniform, clean sand, with a D_{50} of 0.16mm), Tanizawa *et al.* (1988) proposed the following relationship:-

$$D_r = -85.0 + 76.2 \log\left(q_c/\sigma_v{}^{0.5}\right) \qquad (3.5).$$

where, D_r = relative density (%),
q_c = Cone penetration resistance,
σ_v = Initial vertical effective stress.

The conversion of SPT to CPT data provides possibly a more logical method for deriving a CPT based liquefaction relation (Robertson & Campanella, 1985). This approach has the advantage that it provides access to the huge SPT database, and in addition correct conversion of SPT to CPT data better accounts for factors such as ageing and stress history than a simple relative density relationship. This conversion of data may be achieved in one of two main ways (Seed *et al.*, 1983):

1. conducting preliminary studies at each new site to establish a correlation between CPT data and *N* values for the sand at the site; and,

2. using available correlations between SPT test data and CPT test data based on test programmes conducted previously.

The former approach is useful in localised sites, but for commercial purposes is generally neglected because of the requirement for both a SPT and a CPT rig at the same site. Because of this principally commercial limitation, the former method will be ignored for the purposes of this discussion. However, a considerable amount of literature does exist on the correlation between the SPT & the CPT (*e.g.* Robertson *et al.*, 1983).

The first step in the correlation of SPT data with CPT data is to normalise cone resistance in a similar manner to the SPT, where cone bearing, q_c, is modified to an overburden stress level of 1 kg/cm^2 using:-

$$Q_c = C_Q \cdot q_c \qquad (3.6)$$

where, Q_c = modified cone penetration resistance,
C_Q = correction factor similar to that used for the SPT N_1 values.

A wide range of q_c/N ratios have been published; the range of values is due in part to variations in mean grain size, SPT hammer type and the amount of energy delivered to the SPT drill rods (Figure 3.2). However, despite these problems, Robertson & Campanella (1985) suggest, that the relationship shown in Figure 3.3, based predominately on field observations of liquefaction related phenomena for earthquakes of magnitude 7.5, and assuming a q_c/N of 4.5 (D_{50} ~0.25mm), may be used to classify liquefiable soils. Using the CPT soil classification system which is based upon an analysis of normalised cone resistance, friction ratio and pore-pressure ratio (Robertson & Campanella, 1983), and a knowledge of the effects of increasing fines content on both penetration resistance and liquefaction potential, silty sands may also be incorporated into the model.

Robertson & Campanella (1985) conclude, after a preliminary field evaluation of the technique, that...

> '....CPT data can provide information to identify potential critical areas where a detailed assessment may be required, which may include sampling or further *in-*

situ testing, or both. This is especially so for some fine grained soils that can be successfully sampled and tested in the laboratory..'.

3.2.2. Laboratory and field determinations of liquefaction potential.

These methods are based upon an evaluation of stress conditions in the field, and laboratory determinations of stress conditions causing cyclic mobility or liquefaction of soils. They involve two independent determinations (Seed, 1979):

1. an evaluation of the cyclic stresses induced at different levels in the deposit by the earthquake shaking, and,
2. a laboratory investigation to determine the cyclic stresses which, at given confining pressures representative of specific depths in the deposit, will cause the soil to develop a peak cyclic pore-pressure ratio of 100% or undergo various degrees of cyclic strain.

The advantages of a combined laboratory and field approach are that it provides a deeper insight into the nature of the problems involved, a greater and more versatile capability if properly applied, and the possibility of extension of existing field data to a wider variety of situations (Seed, 1979).

This type of stress analysis-property determination, even in its simplest form, requires five basic steps:

1. evaluation of the stresses developed in a potentially liquefiable soil during a given earthquake,
2. conversion of the irregular stress history produced by the earthquake to an equivalent uniform cyclic stress series,
3. testing of representative samples of soil under cyclic loading to evaluate the cyclic stresses required to cause a peak pore-pressure ratio of 100% or an intolerable level of strain,
4. an evaluation of all the factors influencing the cyclic mobility or liquefaction characteristics of soils,
5. determination of the effects of sample disturbance on the *in-situ* properties of natural deposits.

Methods for evaluating the stresses induced by earthquake loading include total and effective stress ground response analyses (*e.g.* Seed & Idriss, 1967; Dikmen & Ghaboussi, 1984; Finn *et al.* 1977). At the basis of the laboratory technique is the laboratory cyclic simple shear and cyclic triaxial methods. These techniques are used to evaluate the cyclic stresses required to cause 'initial liquefaction'. Subject to corrections allowing for sample disturbance, the laboratory data were then compared to the predicted field stresses (Figure 3.4). The factor of safety in evaluating cyclic mobility or liquefaction potential may then be expressed using:

$$Factor\ of\ safety = \frac{Uniform\ shear\ stress\ required\ to\ cause\ a\ peak\ cyclic\ pore\ pressure\ ratio\ of\ 100\%\ or\ an\ acceptable\ limit\ of\ strain\ in\ N\ cycles}{Average\ shear\ stress\ induced\ by\ earthquake\ for\ N\ cycles} \quad (3.7).$$

By definition, a factor of safety of less than unity denotes a significant risk of cyclic mobility or liquefaction. However, as Seed (1979) notes, the final acceptable level of safety will clearly depend on the accuracy with which each of the individual steps can be made.

3.2.3. Limitations of the Berkeley approach.

The main limitations of the Berkeley approach to the prediction of liquefaction potential appear to be centred around the use of either cyclic laboratory tests or, in the field Standard Penetration Testing. The conclusions, listed in Section 3.2. above, resulting from this approach, in the words of Casagrande (1975), '....appeared to contradict all my past experience...'.

In response to these conclusions, Casagrande (1975) & Castro (1975), performed a series of cyclic triaxial tests on dense sands. The results of these investigations indicated that during application of the stress cycles most of the axial strains developed in a horizontal zone at the top of the sample. Continued cyclic loading resulted in the development of alternate necking and bulging and in the most extreme cases a layer of free water developed at the top of the specimen. Subsequent analyses of the samples tested indicated the development of significant non-uniformities in terms of relative density; during the course of the test, the top zone become considerably looser, while the lower portion of the sample became considerably denser. Casagrande (1975)

concluded that the development of these non-uniformities during testing, resulted from a radical redistribution of water content, which in turn was due to three main factors, boundary effects, development of high pore-pressures and softening when the specimen is cycled through the state of hydrostatic stress, and a 'pumping action', which draws water to the top of the sample released in the moment when cycling through the hydrostatic state of stress.

The assumption that the stresses imposed by an earthquake can be adequately modelled in the laboratory using isotropic consolidation and subsequent positive and negative cyclic variation of the deviator stress (isotropically consolidated cyclic triaxial tests), may also represent somewhat of an oversimplification. *In-situ* stresses are rarely isotropic. McRoberts & Sladen (1992) and Casagrande (1975) raised the question as to why [the cyclic triaxial] tests were not carried out under more realistic *in-situ* stress conditions. McRoberts & Sladen (1992) quote from an unreferenced report by Professor K. L. Lee to the Waterways Experimental Station, on the history of the development of the cyclic triaxial test, which goes some way to answering this question. Lee describes how he first attempted cycling between two anisotropic states of stress, but failed to produce 'liquefaction' (pore-pressure rising to confining pressure). From this he concluded that '...as long as some shear stress remained, there would always be enough dilating tendency to keep the excess pore-pressure below the total confining pressure, and zero effective stress or liquefaction would not be achieved...'. He continues that '...complete stress reversal, to produce zero shear stresses in the sample, was essential to develop liquefaction'. This observation suggests that the laboratory technique was modified to allow agreement with established views.

Casagrande (1975), on the basis of static tests on sands (described below) also calls into question Professor Seed's conclusion that liquefaction is less likely under steep slopes or embankments on the basis of higher confining pressures. While noting that on the basis of cyclic laboratory tests higher confining stresses do act to reduce cyclic mobility, in reality, to argue that resistance to (flow) liquefaction is improved by increasing confining pressure is counter-intuitive, and could lead to potentially disastrous consequences.

McRoberts & Sladen (1992) note that for cyclic tests on sands, the volume of membrane penetration can be the same order of magnitude as the volume change that

would have occurred during drained conditions. These tests therefore do not impose a constant void ratio condition, and cannot therefore be truly compared to undrained conditions. Finally, Xia & Hu (1991) conclude, that for cyclic triaxial tests on sands, the back pressure method (used in ensuring high degrees of saturation) should not be used, and that Terzaghi's effective stress principle is not valid unless additional conditions are included to allow for the actions of interparticle forces in soils.

Casagrande (1975), in addition to noting the fundamental problems associated with the SPT, concluded that '...because of the basic differences between the mechanisms that produce cyclic pore-pressures and strains in the laboratory and *in-situ* ....it is virtually an impossible task to extrapolate or estimate from such laboratory tests, with the help of empirical relationships, how cyclic pore-pressures and strains will develop *in-situ*'.

3.2.4. Summary.

The Berkeley or cyclic approaches to liquefaction prediction as summarised by Seed (1984 & 1979) have been used in the prediction of liquefaction potential in the field for many years. However, they are often based upon either unrealistic laboratory test conditions or unreliable and un-repeatable field investigation techniques. An attempt to reconcile some of the more dangerous conclusions has resulted in the development of a large number of correction factors. These factors do not address the fundamental problems with the method, and as such, the Berkeley method as described above, remains essentially flawed. An alternative 'steady / critical state' or 'static' approach provides a different line of reasoning.

3.3. The steady / critical state approach to liquefaction prediction.

The steady state approach to liquefaction analysis of sands was described initially by Casagrande & his co-workers (*e.g.* Casagrande, 1975). This research was paralleled by investigations into general soil behaviour by Roscoe and his co-workers at the University of Cambridge, leading to the development of critical state soil mechanics (*e.g.* Roscoe *et al.*, 1958 & Wood, 1994). The steady state approach is essentially an empirical approach, developed from an experimental study of sand behaviour and applied to the prediction of flow liquefaction. In contrast, critical state soil mechanics attempts to model various aspects of soil behaviour, including strength, compression,

dilatancy, and the existence of critical states, in which unlimited deformations can occur without changes of stresses or volume, (Wood, 1994). Despite their different developmental histories, in the case of sands at least, there appears to be little conceptual difference between the two approaches (Been *et al.*, 1991). However, differences in the precise definition of the steady and critical state do exist, and this has given rise to a certain amount of academic debate (*e.g.* Poulos, 1981; Sladen *et al.*, 1985). Been *et al.* (1991) illustrate that for a sand these differences are insignificant, and that the critical state and steady state in sands may be considered to be coincident. This makes it possible to adopt some of the concepts derived from critical state theory, extending the steady state approach and improving the method of liquefaction analysis (Sladen *et al.*, 1985); for the purposes of this discussion, the terms critical and steady state will be regarded as synonymous. The only true differences between critical state and steady state workers (in sands at least) remain the methods of measurement: critical state workers tend to use drained triaxial, strain-rate-controlled tests on dilatant samples to determine critical state, while the steady state of deformation is usually measured using undrained triaxial tests on loose (contractive) samples. The advantages of undrained triaxial testing on loose sands, and hence its use in the determination of 'steady state' parameters include (Sladen & Oswell, 1989):

1. a wide availability of apparatus,
2. increasing pore-pressures during undrained shear tend to minimise the development of non-uniformities within the sample,
3. steady state techniques have been developed specifically in an attempt to explain flow liquefaction (which occurs only in soils in a loose state), rather than as a generalised model for soil behaviour.

3.3.1. Laboratory observations of monotonic, undrained shear on clean sands .

The origins of the 'steady state' approach date back to early investigations into the development of flow slides (*e.g.* Casagrande, 1936). Flow slides may occur in both natural (*e.g.* sub-aerial and sub-marine slopes) and man-made deposits (e.g., tailings dams and hydraulic fills). The collapse and flow of these deposits are usually associated with some sort of undrained loading. This loading may be what is generally regarded as cyclic, *e.g.* earthquakes, blasting, pile-driving, or static, (*e.g.* rapid construction or oversteepening of a slope). In addition, flow slides may be initiated under drained

conditions, such as those associated with a slow rise in a water table, although the subsequent deformations associated with the failure can be regarded as undrained (Sasitharan *et al.*, 1993). Casagrande's work on this type of failure led directly to the 'critical void ratio' concept, which is based upon some simple observations of sand behaviour under triaxial shear.

Under undrained monotonic loading such as found in an undrained triaxial test, a dense sand, or a sand under a sufficiently low confining stress will, after some initial small pore-pressure rise, tend to dilate. In the case of undrained testing, volume change is impossible and so the effective confining stress will increase. Deviator stress increases steadily and corresponding pore-pressures will drop steadily (Figure 3.5). In some cases, pore-pressure may drop below the ambient atmospheric pressure resulting in cavitation, subsequent loss of saturation and a deviation from the undrained constant volume assumption. For design purposes, Been & Jefferies (1985) consider that it is not acceptable to rely on static tests on dilative sands, because failure occurs along a discrete shear plane running at approximately 45° through the sample, upon which void ratio is unknown but may dominate sample behaviour (Sladen *et al.*, 1985); this also allows resultant excess pore-pressures to equalise relatively rapidly.

In contrast, a loose sand will tend to contract. Once again, under undrained conditions, volume change is prevented and therefore raised pore-pressures rapidly develop, and the deviator stress, after reaching a peak at a typically small strain (~2%), rapidly softens to a constant ('steady state') strength, due to a collapse of the grain structure. In load controlled tests this characteristic brittle or collapse behaviour resulting in a distinctive 'flow structure' and large strains (in excess of 20%) occurs in a fraction of a second (Figure 3.6). This condition, in which the sample is shearing at constant volume and effective stress, was defined by Poulos (1981) as....

'...the steady state of deformation for any mass of particles is that state in which the mass is continuously deforming at constant volume, constant normal effective stress, constant shear stress, and constant velocity. The steady state of deformation is achieved only after all particle orientation has reached a statistically steady state condition and after all particle breakage, if any, is complete, so that the shear stress needed to continue deformation and the velocity of deformation remain constant'.

For a given sand, the effective stress conditions after soil structure collapse are a reasonably unique function of void ratio (Sladen & Oswell, 1989). Conventionally the results of a series of tests, performed on sands of differing void ratio and initial effective stress are plotted in e- log p' space. The locus of these points is known as the critical void ratio, F (flow) line, or steady state line. This fundamental line is generally linear in nature and separates potentially liquefiable from non-liquefiable sand states (Figure 3.7).

Observations of sand behaviour under monotonic loading conditions of this type allowed Casagrande (*circa.* 1938) to draw the following conclusions (Casagrande, 1975):

1. all combinations of void ratio and effective normal stress which are located below, or to the left, of the critical line, represent states in which the sand would develop a dilative response and are safe against (flow or actual) liquefaction,
2. all points above or to the right of the critical line represent states that result in a contractive response. In order to produce a flow slide, and not merely a slump of limited dimensions, the starting point needs to be substantially to the right of the critical void ratio line so that in the liquefied state the effective stresses drop to a small fraction of those that existed at the start of shear,
3. the greater the effective confining pressure (i.e. greater depth), the lower is the critical void ratio, or more simply, at a large confining stress the sand must be denser to ensure prevention of (actual or flow) liquefaction. When heavily loaded, even a medium dense sand may be susceptible to (actual or flow) liquefaction.

In addition, Casagrande (1975), based upon observations of flow behaviour in the stress or load control triaxial test, concluded that when sand is liquefied and is actually flowing, it must have a different structure from when the sand is static. This postulated flow structure:

1. spreads by a chain reaction,
2. exists only during flow, and,
3. reverts into a static structure in the moment flow stops and the individual particles re-arrange themselves into a static structure which, after the excess water has drained, will be slightly denser than the static structure before liquefaction occurred.

Later analysis (Konrad, 1990a) showed that there is a third distinct type of sand behaviour as observed in the undrained triaxial test. A medium-loose sand, consolidated under a high confining pressure, may initially exhibit contractive behaviour under shear; pore-pressures rise and the deviator stress displays a distinctive drop to a lower value. However, further straining causes dilation, a gain in strength and a concurrent decrease in pore-pressure, and the specimen gains strength (strain hardens). This state of minimum strength, or point of phase transformation is termed the 'quasi-steady state' (Ishihara, 1993) and is governed by the void ratio and applied confining pressure at the time of consolidation (Figure 3.8). This quasi-steady state has been selected by many workers as a conservative estimate of steady state (Alarcon-Guzman *et al.*, 1987); however, only the final steady state which appears to continue indefinitely should be used to define the true steady state line.

Critical state soil mechanics demonstrates that the behaviour of soil under any loading condition is dominated by its initial state relative to the steady / critical state line (McRoberts & Sladen, 1992). This led Been & Jefferies (1985), in an effort to quantify the stability of artificial sand islands in the Canadian Beaufort sea, to further develop the steady / critical state hypotheses, defining a 'state parameter', ψ. This parameter is defined using:

$$\psi = e_{con} - e_{ss} \qquad (3.8).$$

where, e_{con} = void ratio after consolidation,
e_{ss} = void ratio at steady state.

Significant engineering design parameters may be related to samples with a positive initial ψ, including, angle of phase transformation, peak shear stress and pore-pressure at phase transformation. For sands with a negative ψ, significant relationships exist between ψ and the drained angle of shearing resistance and volumetric response (Been & Jefferies, 1985). The advantage of this parameter over more conventional measures of sand behaviour (e.g. relative density), is that ψ accommodates the effects of effective confining stress. Examination of Figure 3.7 clearly shows that a sand with a particular void ratio (or relative density) may exhibit either a dilative or contractive response, depending upon the effective confining stress. Relative density does not represent this dependency on *in-situ* stress conditions.

Sasitharan *et al.* (1993) note that, although the steady state line is most commonly expressed in e-log p' space, it may also be represented in three dimensional $e - q - p'$ space, as shown in Figure 3.9. This slightly complex three dimensional stress space may be reduced to a two dimensional plot by normalising stresses with respect to the corresponding stress conditions at steady state, at the same void ratio. This has the effect of collapsing the steady state line into a single point; any soils possessing an initial positive ψ will have a p'/p'_{ss} greater than unity (where p'_{ss} is the effective confining stress at steady state) (Sladen *et al.*, 1985). Figure 3.10 illustrates a typical series of normalised stress paths for sands tested in triaxial compression. Sladen *et al.* (1985), further suggest that a straight line may be drawn through the peak points of the normalised stress paths which passes through the steady state point. This line was named the 'collapse surface', and defines the trigger of collapse and strain softening of loose sands leading to steady state under undrained loading. The collapse surface does not represent a state boundary surface, as the postpeak soil state can pass slightly above it, but it represents the limit of stability if drainage is impeded under static loading conditions.

3.3.2. Field liquefaction prediction methods using the 'static' approach.

Laboratory analyses of the kind described above have greatly improved understanding of the basic mechanisms controlling flow liquefaction under undrained monotonic loading. Fundamentally this type of approach may be applied to liquefaction analyses using a conceptual flow chart, as described by Robertson *et al.* (1992a) (Figure 3.11). However, practical application of this design method is somewhat problematical, but may essentially be divided into two distinct groups: methods involving triaxial testing of 'undisturbed' samples recovered from the field, or correlation between reconstituted field samples and *in-situ* techniques (e.g. the CPT & Self-boring Pressuremeter). If 'undisturbed' samples are used, direct comparisons may be made with the deposit (assuming the samples were representative and that no disturbance occurred). More usually, because of the difficulties in obtaining 'undisturbed' samples, the latter approach is used.

3.3.2.1. Methods involving testing of 'undisturbed' samples.

Poulos *et al.* (1985) present a liquefaction evaluation procedure based upon the steady state testing of undisturbed samples obtained from the field. Essentially the procedure involves five basic steps:

1. determination of the *in-situ* void ratio, using a combination of fixed piston sampling, ground freezing or sampling in test pits,
2. determination of the steady-state void ratio, or density as a function of effective stress using compacted samples, involving undrained triaxial tests on laboratory prepared samples,
3. determination of the undrained steady state strengths for 'undisturbed' field specimens, using undrained triaxial tests,
4. correction of measured undrained steady-state strengths to *in-situ* void ratios. This allows corrections to be made for changes in void ratio occurring during laboratory consolidation,
5. calculation of the *in-situ* driving shear stress, τ_d, using conventional methods of stability analysis, and subsequently the factor of safety against liquefaction, F_L, using:

$$F_L = \frac{S_{su}}{\tau_d} \qquad (3.9).$$

S_{su}= undrained steady-state shear strength.

A factor of safety of significantly greater than 1 ($\tau_d < S_{su}$) indicates that the soil is in stable equilibrium and that a flow slide due to liquefaction cannot occur. The strains that occur during an earthquake do depend on the shaking intensity, however these strains stop when shaking stops and do not lead to liquefaction. A F_L of less than 1 ($\tau_d > S_{su}$) indicates that the soil mass is in a state of unstable equilibrium; erosion at the toe of the slope, a foundation movement, earthquake shaking, pile driving, or any other form of static or cyclic undrained loading, may then cause liquefaction and subsequent flow slides.

The advantage of this method (and indeed other steady state methods), is that the undrained steady state shear strength of the soil is solely a function of the *in-situ* void ratio, and is not therefore affected by soil structure, method or rate of loading, or pore-

pressures or strains induced by earthquake loading. However, as Poulos *et al.* (1985) note, the undrained steady state shear strength is very sensitive to minor void ratio changes, making direct comparisons with what may be regarded as 'undisturbed' samples extremely difficult.

3.3.2.2. Methods involving correlation with penetration resistances.

Conventionally, penetration resistances, obtained from either the SPT or CPT (as already described above), may be used to predict liquefaction potential, in terms of either field correlations or relative density correlations which are based upon calibration chamber tests on uniform sands. Use of calibration tests to correlate relative density with the CPT (as described above) suffer from the following problems (Sladen, 1989):

1. there is no direct evidence to prove that data obtained in a large chamber are directly relevant to field conditions, even for the sand studied in the chamber,
2. it is not known that if a relationship developed for one sand, is applicable to any other sand, particularly to a variable deposit, and,
3. there is considerable evidence to suggest that relative density is not a reliable index for comparison between different sands. In addition, relative density approaches suffer from the fundamental limitation that they fail to recognise the influence of mean effective confining stress has on sand behaviour.

An alternative method is provided by Been *et al.* (1986) & Been *et al.* (1987), who based upon undrained triaxial data and calibration chamber data, correlate ψ with CPT tip resistance. Essentially this method is based upon the hypothesis that normalised tip resistance is a unique function of state parameter, where normalised tip resistance is defined as:-

$$(q_c - p)/p' = k' \exp(-m\psi) \qquad (3.10).$$

where, $(q_c - p)/p'$ = normalised tip resistance, and
k' & m = constants.

Mean relationships for various sands are illustrated in Figure 3.12. Robertson & Campanella (1983) & Robertson *et al.* (1992a), further suggest that, based upon this approach, the following approximate normalised penetration resistance values may be used to identify sands with a contractive state:

$$q_c/\sigma'_o \leq 40-50 \qquad (3.11).$$

σ'_o = effective overburden pressure

However, from examination of the data upon which these q_c - ψ relationships are based, a considerable scatter in the data is evident (see Figure 3.13). Recognising that the vertical axis is a logarithmic scale, for a state parameter of -0.100, possible normalised cone penetration resistances range between 30-100. Sladen (1989), concludes that use of CPT interpretations of this type to evaluate susceptibility to liquefaction 'could be potentially catastrophic', unless the effect of other factors, such as stress level, are properly considered.

3.3.2.3. State parameter interpretations using the Self-boring Pressuremeter.

A relatively recent approach to liquefaction prediction is presented by Yu (1994), who suggests that, on the basis of both numerical analyses and calibration chamber testing, there is a unique linear correlation between the pressuremeter loading slope and the initial state parameter of the soil. The correlation can be determined as long as the critical state parameters of the material are known.

3.3.2.4. Estimations of sand state using the Piezovane.

This technique is described in section 2.3.5 above.

3.3.3. Limitations of the static approach.

Most of the limitations of this approach are related to uncertainties surrounding the determination of the *in-situ* void ratio and the relevant steady / critical state line. Kramer (1989) notes that the steady state line is usually obtained from a linear regression analysis of the results of a series of undrained triaxial compression tests. These data

usually display some degree of scatter, resulting from a number factors, including errors associated with void ratio calculation (Sladen & Handford, 1987), problems in determining the true steady state point, errors due to membrane penetration, etc. The resulting lines obtained vary widely both in position and inclination; these differences are generally a result of variations in grain size distribution and particle shape (Poulos *et al.*, 1985). However, for many soils, the steady state line is very flat, so that even small differences in void ratio can lead to large differences in steady state shear strength. This suggests that accurate measurements of the *in-situ* void ratio and the associated steady state shear strength are vital.

However, the accuracy with which the *in-situ* void ratio can actually be measured in the field is relatively low, which makes it exceptionally difficult to determine with confidence the soil state in a material that is close to critical (i.e. $F_L \approx 1$). McRoberts & Sladen (1992) consider that even under ideal circumstances it is not usually possible to determine void ratio to an accuracy of better than +/- 0.03-0.05. In addition, sands in the field are rarely homogeneous, varying both in terms of size gradation and fines content, both of which can dramatically affect large strain behaviour. The problem of which steady state line to adopt and how many different 'representative' samples are required may be solved by making a conservative estimate, and suffering the consequent economic penalties.

In addition, McRoberts & Sladen (1992), identify a number of theoretical criticisms surrounding the steady state approach, including:

1. questions relating to the uniqueness of the steady state line,
2. the problem of dense sands liquefying under laboratory cyclic loading,
3. no account made of damage due to cyclic mobility during earthquake shaking, even though no liquefaction occurs, and,
4. progressive failure potential in a brittle soil can invalidate conventional stability analyses.

There is also some evidence to suggest that the location of the steady state line may be influenced by strain rate, sample preparation procedures, stress path (extension, plane strain, or compression) and consolidation prior to shear. However, with the possible exception of triaxial extension tests, these factors may influence the behaviour of the

sample prior to failure and true steady state conditions remain unaffected (McRoberts & Sladen, 1992).

The criticisms surrounding progressive failure are simply a result of the slightly 'simplistic' approach applied to steady state methods, in that it does not attempt to explain certain observed features of liquefaction phenomena (Sladen *et al.*, 1985). Some of these features include the fact that failure actually occurs at shear stress levels very much higher than the steady state shear strength, and no comment is made upon the magnitude of disturbing force required to trigger liquefaction. However, the collapse surface as proposed by Sladen *et al.* (1985), does go some way to accounting for these limitations.

3.3.4. Summary.

The review of literature described above attempts to give the reader a brief account of the geotechnical methods and approaches that have been employed in order to predict liquefaction phenomena. As can be seen, a considerable variety of different techniques can, and have, been employed to this end. Partly as a result of this, a number of conflicting conclusions have been drawn by different workers. However, as evidenced by both the discussion above, and the recent liquefaction events during the Hyogo-ken Nambu (Kobe) earthquake (17th Jan, 1995), much work must be completed before liquefaction potential can be reliably determined in a routine and reasonably economical way. This argument is even more relevant for the marine environment, where the risks are potentially greater, and the conventional assessment methods described above significantly harder to apply.

Partly as a result of these criticisms, a number of workers have been examining the possible use of seismic shear wave velocity as a possible index property for liquefaction potential prediction, the subject which forms the basis of this thesis.

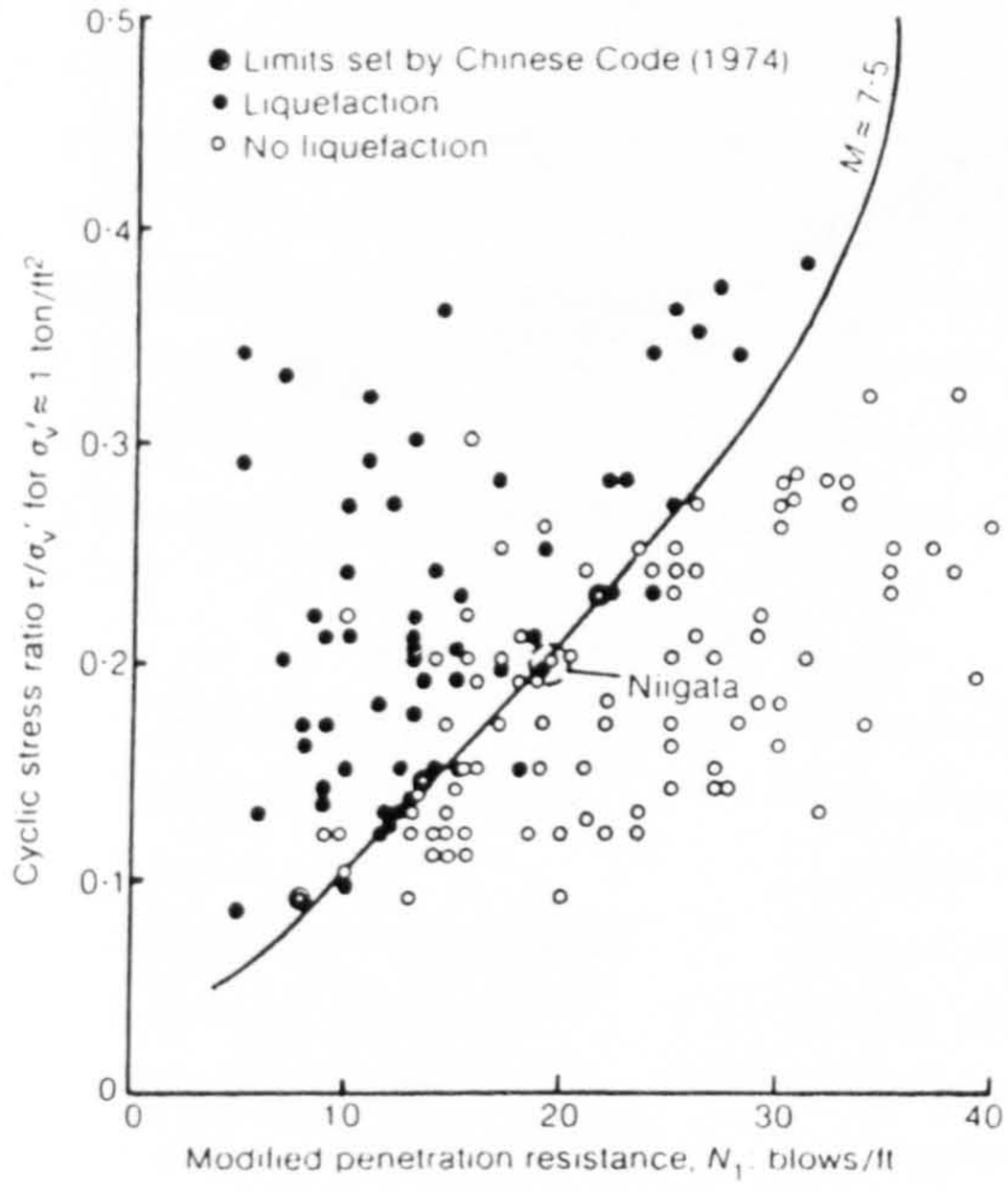

Figure 3.1. Correlation between field liquefaction behaviour under level ground conditions & Standard Penetration Resistance (*after Seed, 1984*).

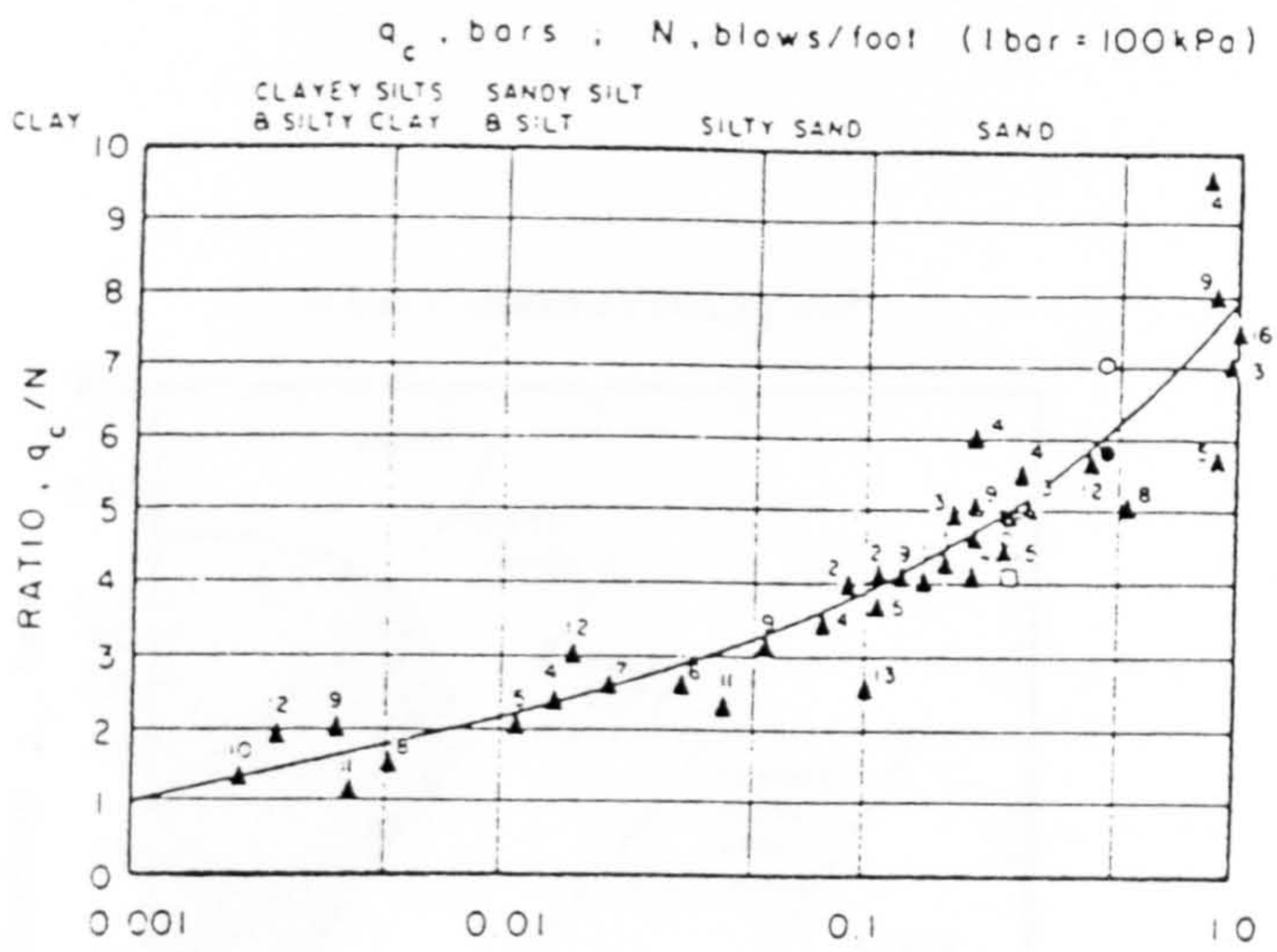

1. Meyerhof (1956)
2. Meigh and Nixon (1961)
3. Rodin (1961)
4. De Alencar Velloso (1959)
5. Schmertmann (1970)
6. Sutherland (1974)
7. Thornburn & MacVicar (1974)
8. Campanella et al. (1979)
9. Nixon (1982)
10. Kruizinga (1982)
11. Douglas (1982)
12. Muromachi & Kobayashi (1982)
13. Goel (1982)
14. Ishihara & Koga (1981)
15. Laing (1983)
16. Mitchell (1983)

TILBURY ISLAND SITE
□ SPT N , ER_i = 47%
■ SPT N_c , ER_i = 55%

UBC SITE, McDonald's Farm
○ SPT N , $ER_i \approx 65\%$
● SPT N_c , ER_i = 55%

Figure 3.2. Variation of q_c/N ratio with mean grain size (*after Robertson et al., 1983*).

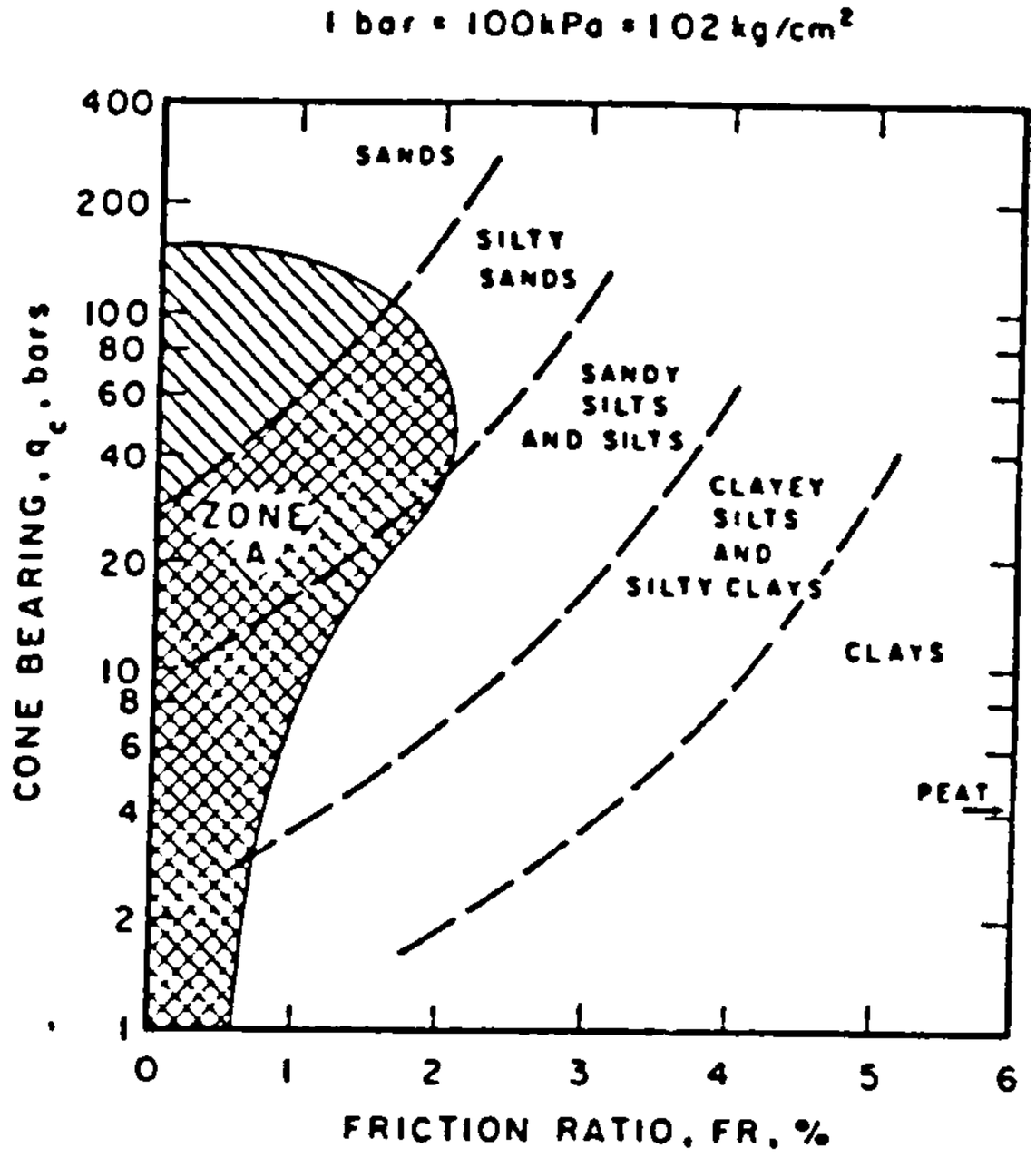

Figure 3.3. Soil classification chart for the electric cone showing zone of liquefiable soils (*after Robertson & Campanella, 1985*).

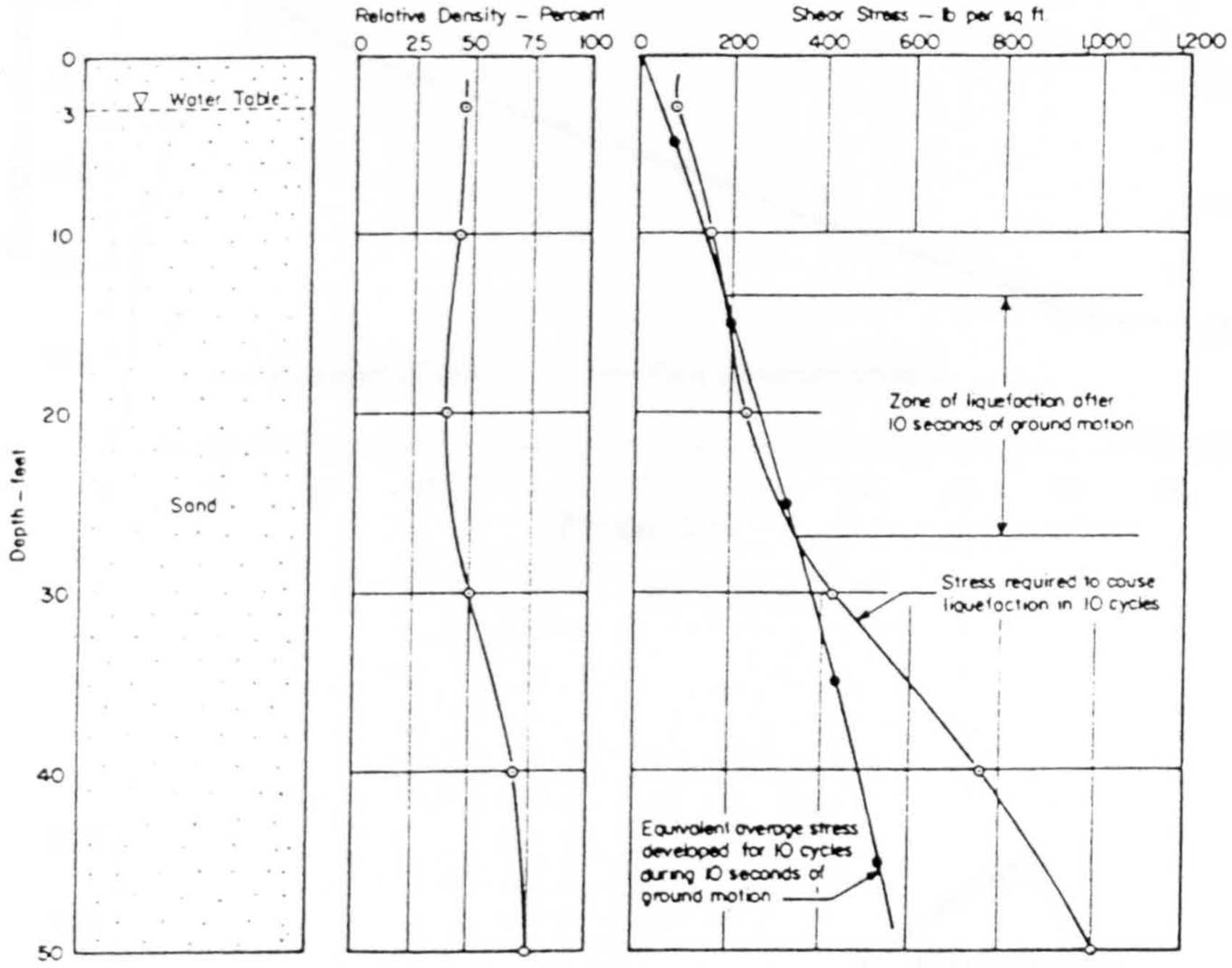

Figure 3.4. Analysis of liquefaction potential (*after Seed & Idriss, 1967*).

a.

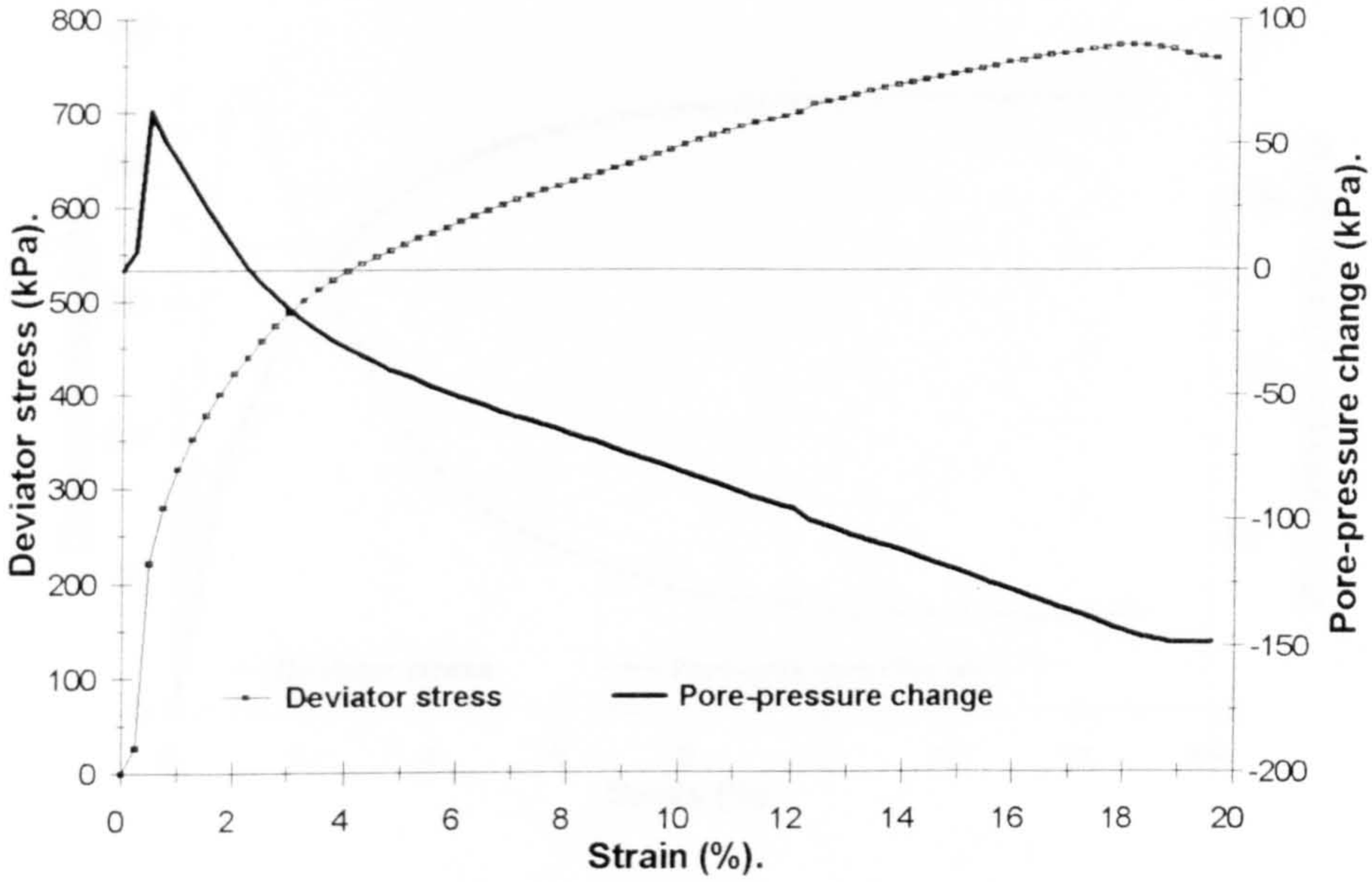

b.

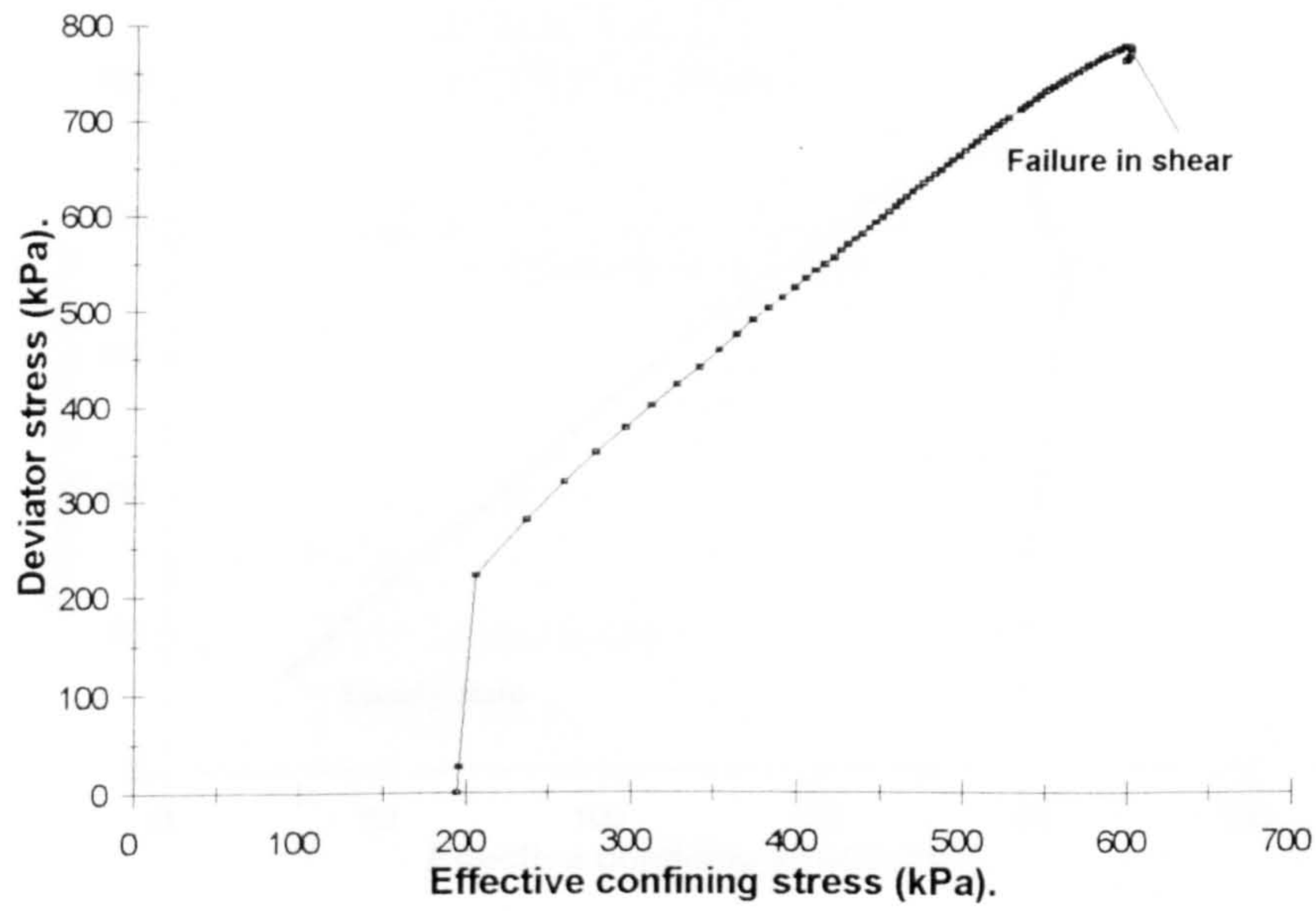

Figure 3.5. a & b. Typical undrained response of a dense sand, leading to failure in shear.

a.

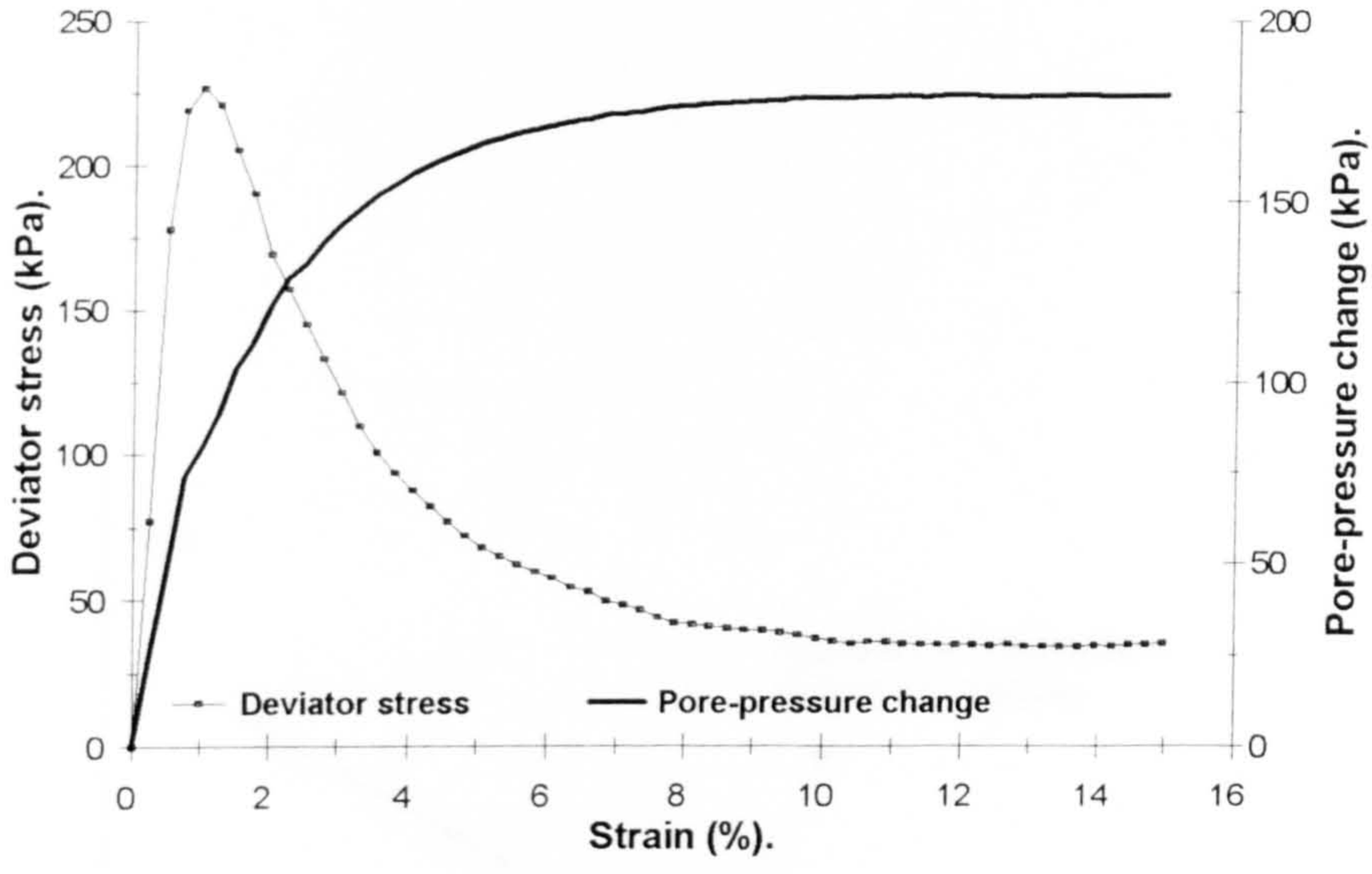

b.

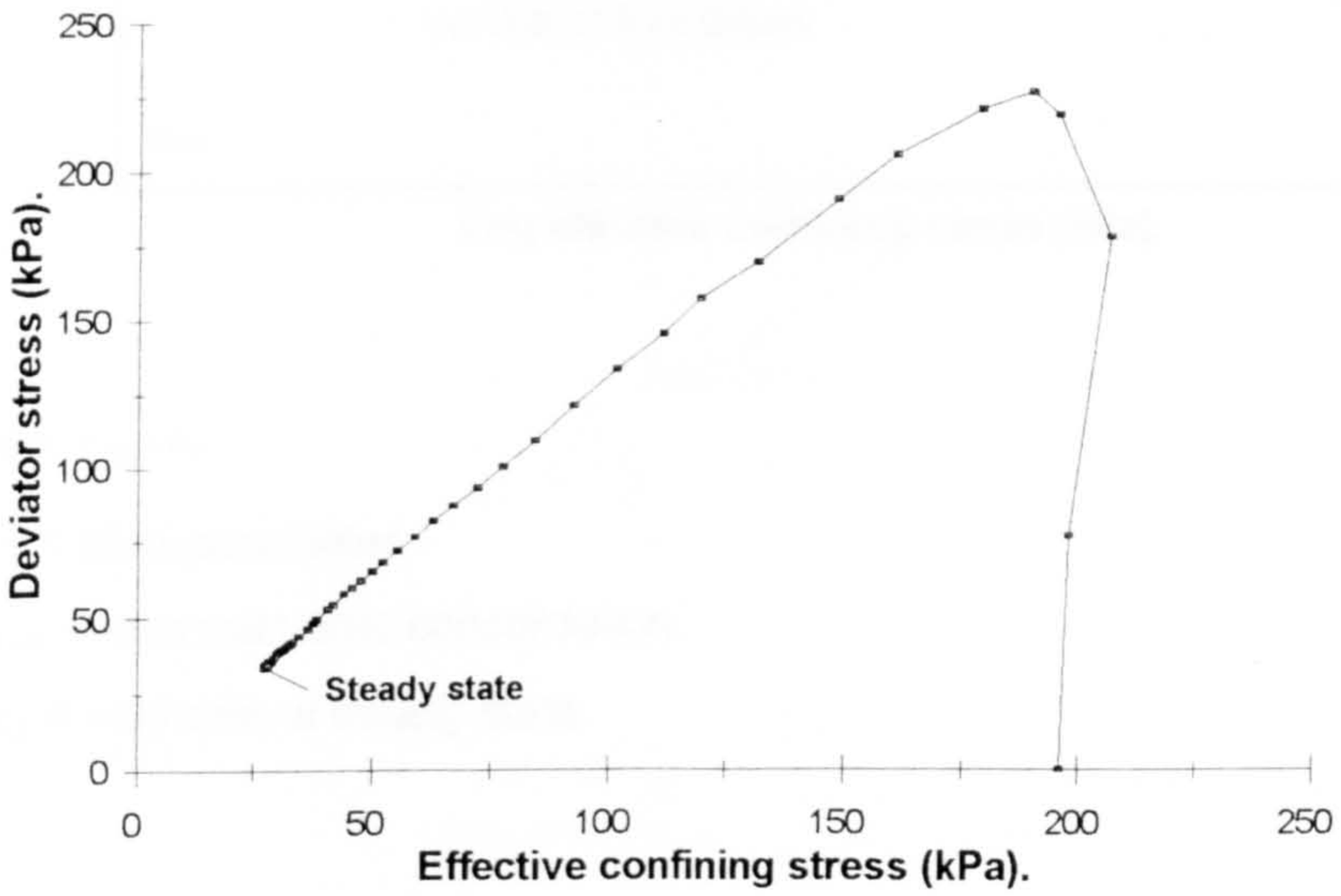

Figure 3.6. a & b. Typical undrained response of a loose sand, leading to failure at steady state.

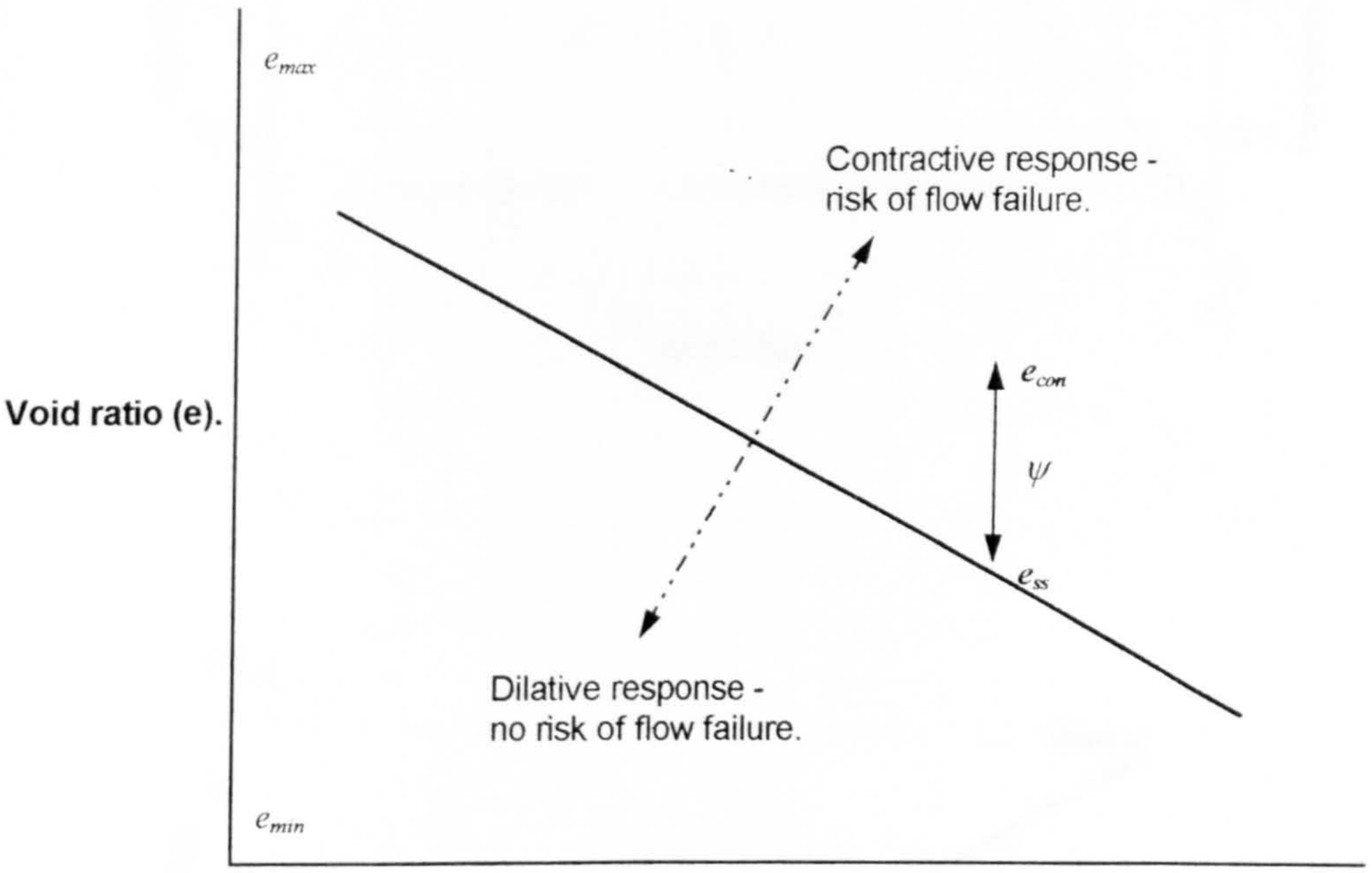

$$\psi = e_{con} - e_{ss}$$

where, ψ = state parameter.

e_{con} = void ratio after consolidation.

e_{ss} = void ratio at steady state.

Figure 3.7. Diagrammatic steady state line, and definition of the state parameter, ψ.

a.

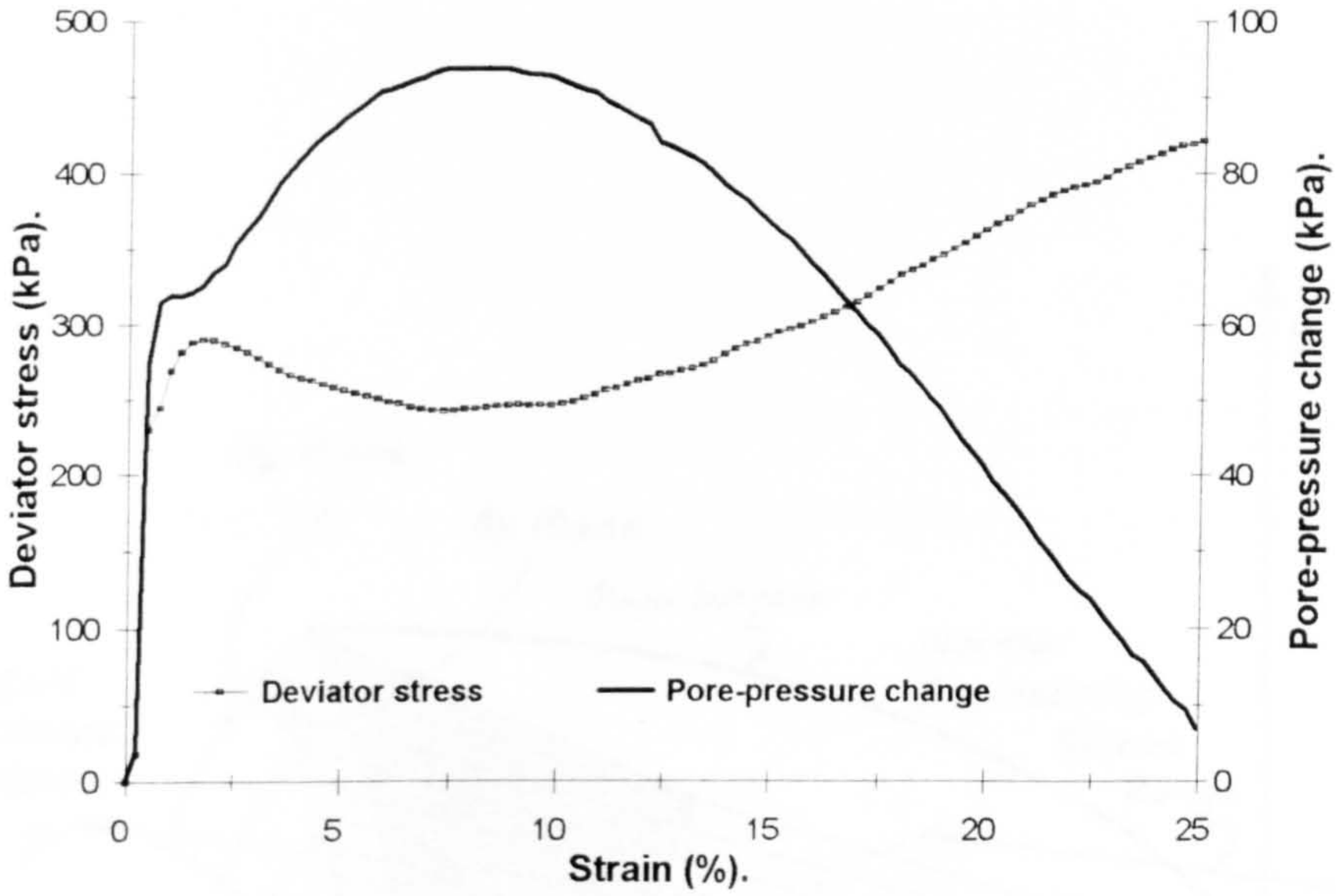

b.

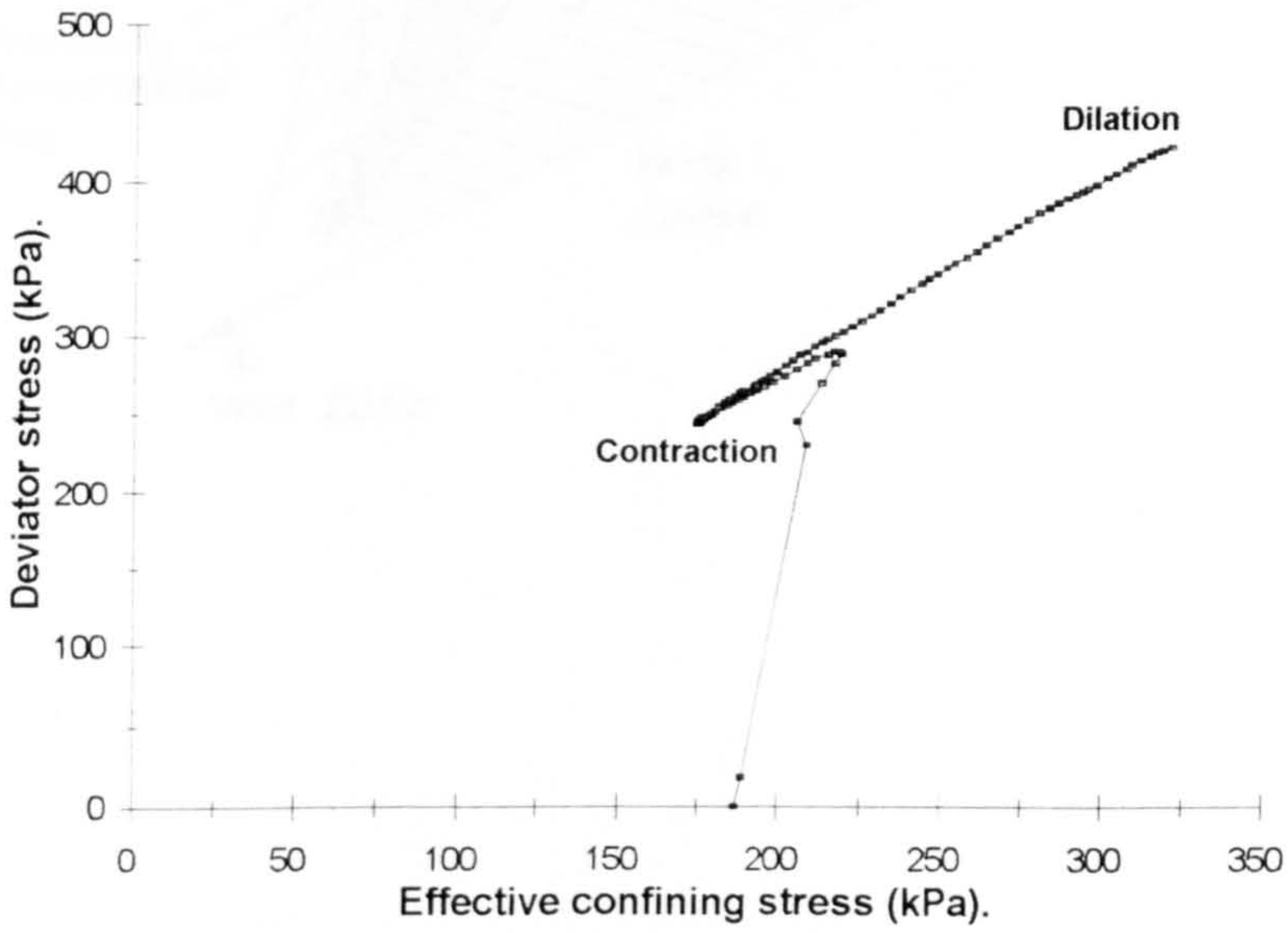

Figure 3.8. a & b. Undrained response of a medium dense sand.

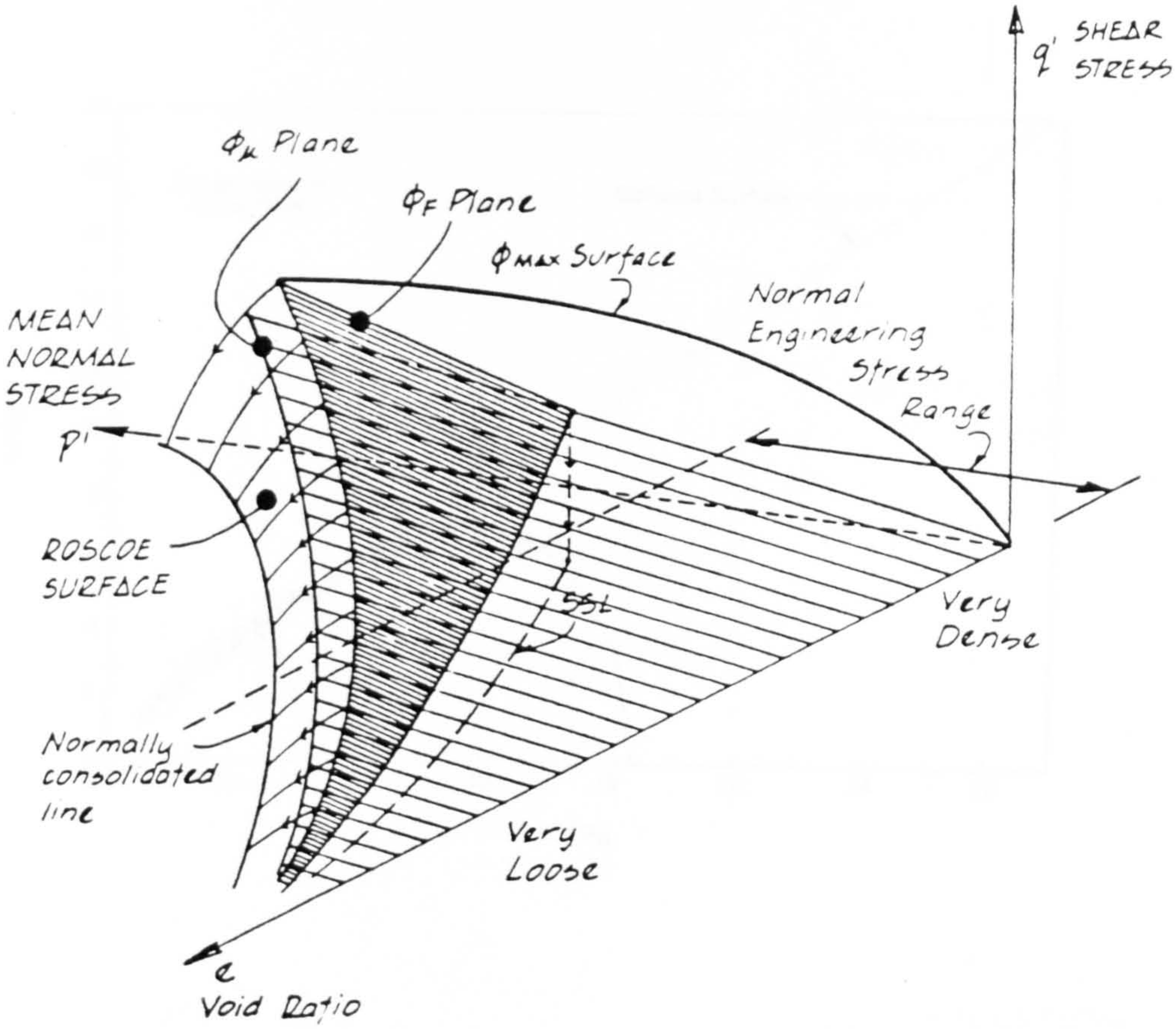

Figure 3.9. Idealised soil model showing surfaces that represent changes in behaviour for cohesionless soils (*after Robertson, 1982*).

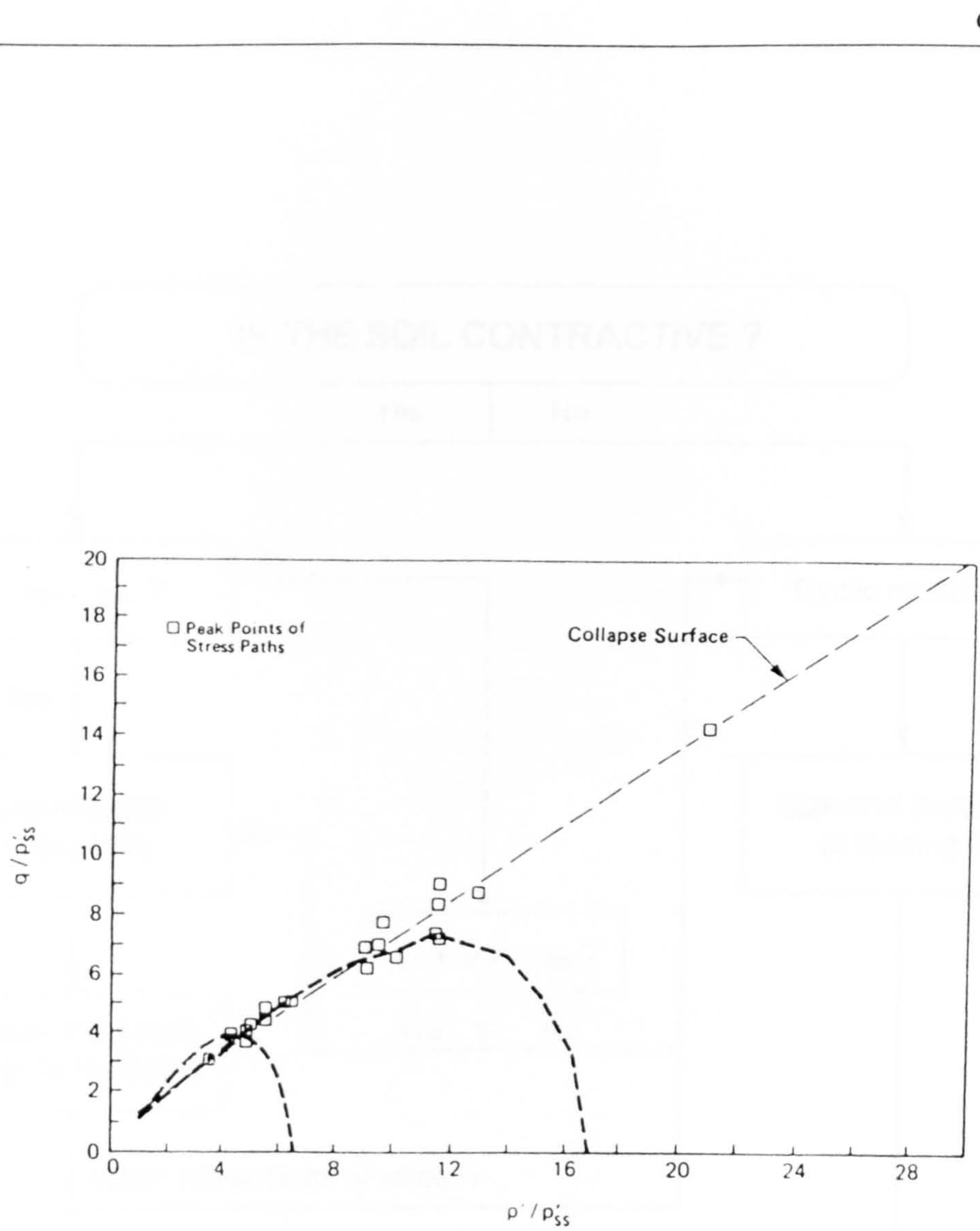

Figure 3.10. Normalised stress paths for a clean laboratory sand (for clarity, only two typical stress paths are shown, with additional peak points from other tests) (*after Sladen et al., 1985*).

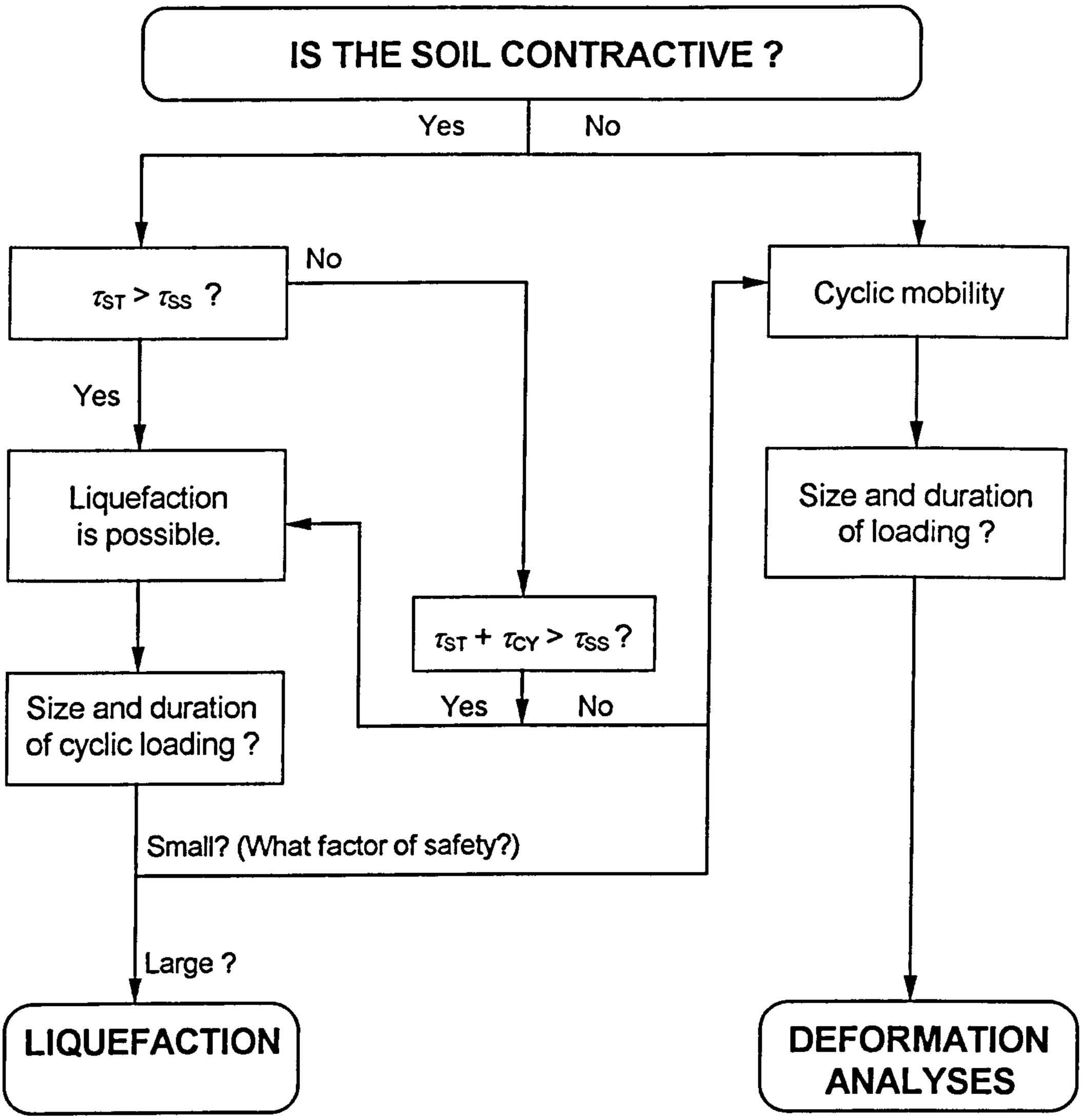

Figure 3.11. Flow chart for the analysis of liquefaction (*adapted from Robertson et al., 1992b*).

τ_{ST} = static shear stress.
τ_{CY} = cyclic shear stress.
τ_{SS} = undrained strength at steady state.

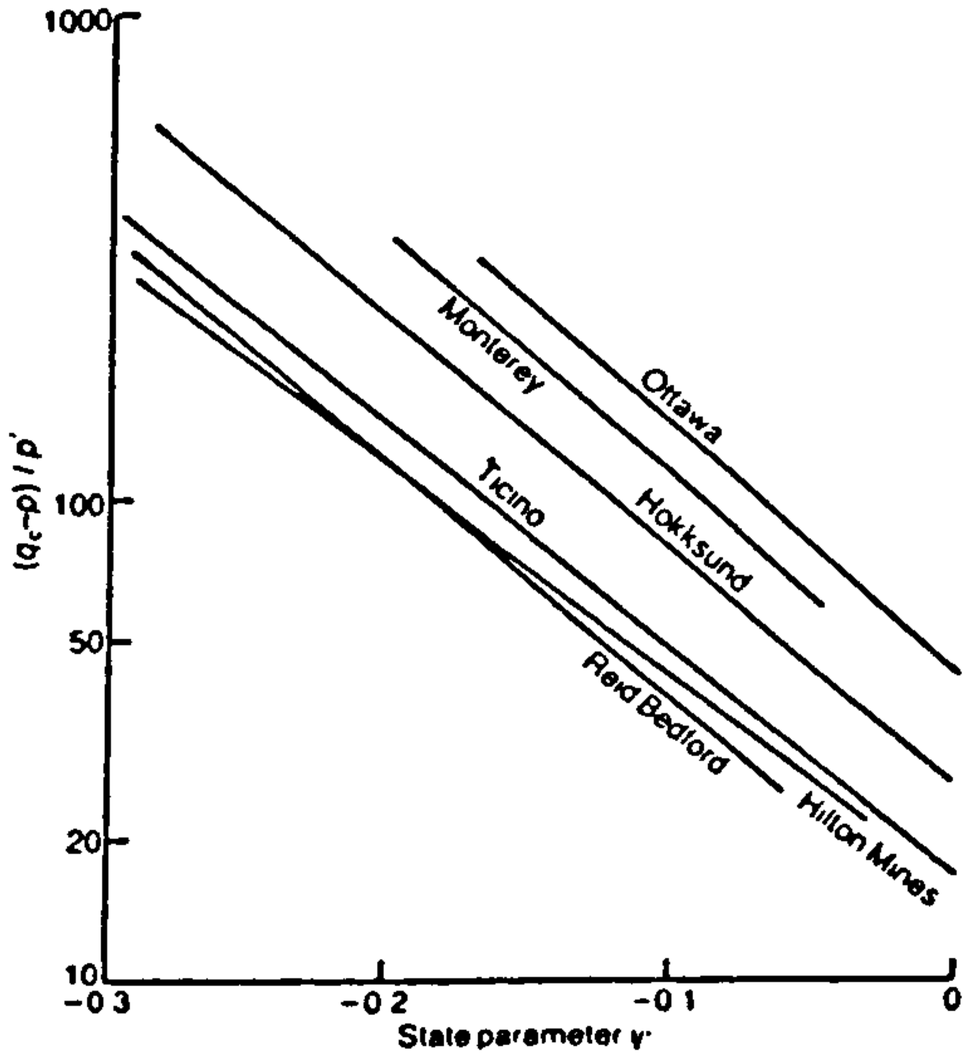

Figure 3.12. Summary of normalised cone resistance - ψ relationships, (*after Been et al., 1987*).

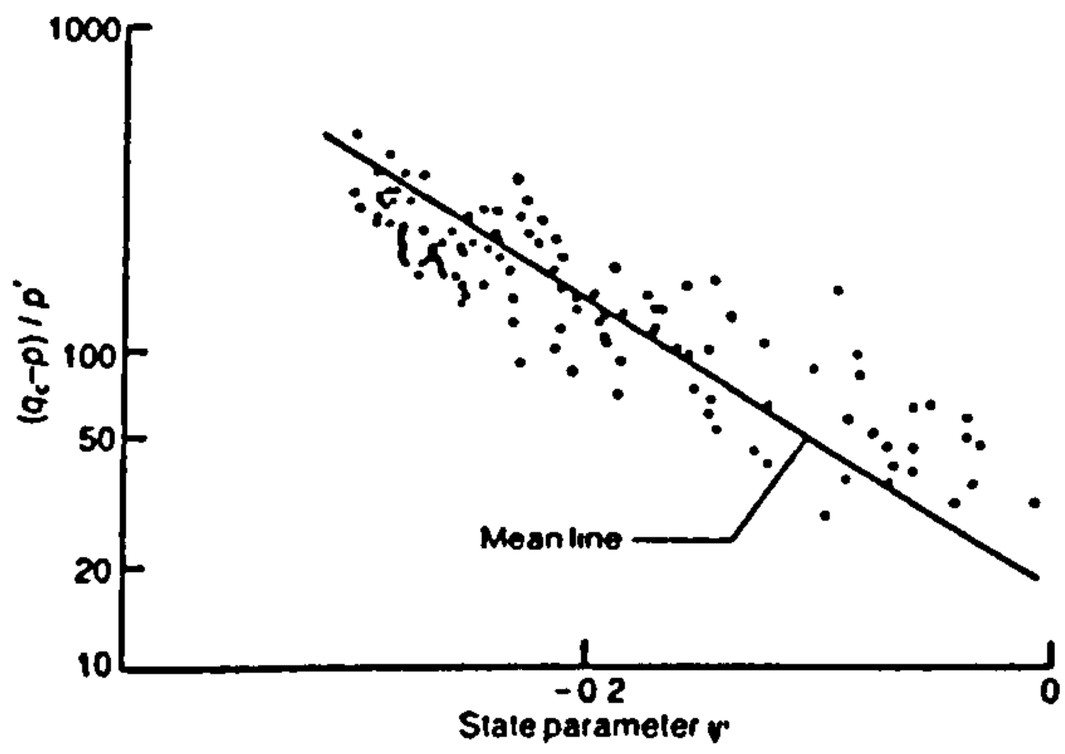

Figure 3.13. Typical scatter of data around the mean line of the cone resistance - ψ relationship for Ticino sand (*after Sladen, 1989*).

CHAPTER 4.

A brief background to shear wave velocity studies, with particular reference to liquefaction prediction.

4.1. Introduction.

Seismic shear waves (other names include transverse, or secondary waves) are body waves which propagate by a pure strain in a direction perpendicular to the direction of wave travel. Individual particle motions involve oscillation about a fixed point in a plane at right angles to the direction of wave propagation (Keary & Brooks, 1991). For measurements made near the surface, the direction of particle motion can be conveniently resolved into a component parallel to the surface (S_H), and a component in the vertical plane (S_V). The very small strains associated with the propagation of both shear waves and compressional waves means they may be regarded as essentially elastic in nature, allowing them to be described using Hooke's Law. This law essentially states that the strain induced in an elastic solid is linearly proportional to the applied stress. In its most generalised form, Hooke's Law requires 36 independent elastic constants (Schultheiss, 1983), however, in isotropic solids, these may be reduced to Lamé's constant, L & the shear (or rigidity) modulus, G. Derivation of the wave equations from Hooke's Law shows that the shear wave propagates at a speed given by:

$$V_s = \sqrt{G/\rho} \qquad (4.1).$$

where, V_s = Shear wave velocity.
ρ = bulk density.
G = Shear modulus = $Shear\ stress / Shear\ strain$

As can be seen from Equation (4.1) above, for the medium to transmit a shear wave it must exhibit a finite shear modulus. Because of this requirement for some element of rigidity, shear waves by definition must propagate through the individual sediment grains themselves and across grain to grain contacts. In contrast, compressional wave propagation may be more closely related to the fluid phase, rather than the solid phase, of the propagation medium, and propagates at a speed given by:

$$V_p = \sqrt{\frac{K + 4/3G}{\rho}} \qquad (4.2).$$

where, V_p = compressional wave velocity,
K = bulk modulus.

Various workers, on the basis of both land based field observations and laboratory testing (*e.g.* Dobry *et al.*, 1981; Seed *et al.*, 1983; De Alba *et al.*, 1984), have suggested that shear wave velocity may provide a useful index of liquefaction potential. The use of shear wave velocity as a field investigation tool, especially when combined with other *in-situ* methods, offers the potential of quantifying liquefaction potential in previously 'difficult to sample' areas, especially offshore. However, up until very recently no thorough systematic investigation of the inter-relationships between shear wave velocity and liquefaction potential had been undertaken.

This review will attempt to give a brief overview of the individual soil parameters controlling V_s, current practical shear wave measurement methodologies, and in particular how they may be applied in attempts to predict liquefaction potential.

4.2. Sediment characteristics influencing the propagation of seismic shear waves.

Various investigators (*e.g.* Hardin & Drnevich, 1972; Woods, 1991) have identified the sediment characteristics that directly affect the shear wave velocity for a particular material. These factors include:

1. void ratio,
2. effective confining pressure,
3. strain amplitude,
4. stress history,
5. degree of saturation,
6. grain characteristics (e.g. size, shape, grading, mineralogy),
7. overconsolidation ratio,
8. vibration frequency,
9. geological ageing effects, and,
10. temperature.

The individual effects on shear wave velocity of each of the individual parameters are discussed in more detail below.

4.2.1. Void ratio and effective stress.

Laboratory evidence shows clearly that for a sample of a specific void ratio, the shear wave velocity is primarily controlled by the mean effective stress (*e.g.* Bates, 1989) (Figure 4.1). Further testing also shows that for the range of void ratios commonly found in sands and at a specific confining stress, there is a linear relationship between shear wave velocity and void ratio (*e.g.* Hardin & Richart, 1963 & Robertson *et al.,* 1995) (Figure 4.2).

Based upon laboratory resonant column testing on sands, Hardin & Richart (1963) presented one of the first empirical relationships, relating void ratio, effective stress, and shear wave velocity:-

$$Vs = (m_1 - m_2 e)(p')^{0.25} \qquad (4.3).$$

where, e = void ratio,
p' = effective confining pressure
m_1 & m_2 = material constants.

Hardin & Richart (1963) & Hardin & Drnevich (1972), concluded that a knowledge of void ratio and effective confining pressure was adequate for the estimation of shear modulus. Based upon available laboratory results for sands, silts and clays over a pressure range of 24 - 700 kPa, and a void ratio range of 0.35 to 1.5, Bryan & Stoll (1988), suggest an alternative relationship:

$$G_o = 2526(p/p_o)^{0.45} \times \exp(-1.5\, e) \qquad (4.4).$$

where, G_o = dynamic shear modulus, (which may be related to V_s using Eqn. 4.1)
p = overburden pressure,
p_o = atmospheric pressure = 100 kPa.

Other workers have investigated the effects of stress ratio (i.e. σ_1/σ_3) on shear modulus. Tatsuoka *et al.* (1979), on the basis of torsional shear testing on sand, showed that the

stress ratio had a significant effect upon the shear modulus. However, under triaxial conditions the stress ratio effects on shear modulus could be considered to be almost insignificant. Roesler (1979), on the basis of tests on a cubic specimen in which individual stresses were applied independently, suggested that individual stresses play an important role in wave travel. In terms of shear wave velocity, Roesler (1979) proposed that:

$$V_s = (m_1 - m_2 e)(\sigma'_a)^{na}(\sigma'_p)^{nb} \qquad (4.5).$$

$$V_s = (A - B'e)\left(\sigma'_a / P_a\right)^{na}\left(\sigma'_p / P_a\right)^{nb} \qquad (4.6).$$

where, na & nb = material constants = 0.125,
σ'_a = effective stress in the direction of wave propagation,
σ'_p = effective stress in the direction of particle motion,
P_a = reference pressure, typically 100 kPa,
$A = m_1(P_a)^{na+nb}$
$B' = m_2(P_a)^{na+nb}$

In a comprehensive review of the subject, Yu & Richart (1984) noted that shear modulus tended to decrease with increasing stress ratio. However, they suggest that if the stress ratio is less than about 3.0, the effect on shear modulus is less than 10%, which they considered to be within the experimental error when evaluating shear modulus. Further, they suggest two forms of empirical equations may be derived for shear modulus (and hence shear wave velocity using Equation 3.1), having the general form:-

$$G_o = C P_a^{0.5}\left(\sigma_a + \sigma_p / 2\right)^{0.5}\left(1 - 0.3K_n^{1.5}\right) \qquad (4.7).$$

where, C = a dimensionless factor accounting for grain shape,
$K_n = \left[(\sigma_1/\sigma_3 - 1)\right] / \left[(\sigma_1/\sigma_3)_{max} - 1\right]$
$(\sigma_1 / \sigma_3)_{max}$ = stress ratio at failure,

$$G_o = C P_a^{0.49} \sigma_a^{0.26} \sigma_p^{0.25}\left(1 - 0.18K_n^{2}\right) \qquad (4.8).$$

With reference to applying these relationships from the laboratory to the field, Stoll (1991) stresses that other factors, such as sample disturbance, thixotropic effects due to ageing, differences in measurement frequency and changes on pore-pressure must be taken into account before direct predictions of *in-situ* response can be made from laboratory derived data. He further suggests that whilst the index constants remain approximately constant, it is necessary to multiply the final value of shear modulus by between 1.3 to 2.5, in order to properly compare laboratory and *in-situ* data.

4.2.2. Strain amplitude.

Strain amplitude is a fundamental factor controlling shear modulus in soils, and a good review is provided by Woods (1991). However, for the purposes of this particular study, which is specifically focused on shear wave velocity, the effects of strain amplitude will be disregarded as all the measurements will be based solely on shear waves which propagate at very low and constant strain levels (typically around 0.0001%). At these very low strains, the sediment may be regarded as being elastic in behaviour, and G is therefore the constant value, usually termed G_{max}, the dynamic shear modulus.

4.2.3. Stress history.

Stress history effects, caused by phenomena such as earthquakes or blasting, can cause a permanent reduction in the shear modulus. The amount of reduction and the degree of recovery depends on both the number of cycles and the amplitude of the high strain excursions (Figure 4.3).

4.2.4. Degree of saturation.

In sands, saturation effects on V_s may be regarded as practically negligible, since V_s is controlled dominantly by the grain to grain contacts making up the sediment framework. The small differences that do exist may be simply accounted for by changes occurring in the saturated bulk density of the material. Hardin & Richart (1963) & Woods (1991) note that as long as the minerals in the sediment do not react strongly to water (i.e. they are not clay minerals), saturation effects may be satisfactorily accounted for in this manner.

4.2.5. Grain characteristics.

The grain characteristics considered here, are partly as a result of the way the structure or fabric of the soil is defined. Conventionally, void ratio (or porosity) is taken as a bulk measure of soil structure, largely because it is in fact a reasonable indicator of soil structure, and is fairly easily measured. However, void ratio only provides an approximate description of the specific soil structure, which is in turn determined to a greater extent by grain shape and size distribution. Hardin & Richart (1963) were among the first investigators to provide direct experimental evidence on the effects of grain shape on shear wave velocities. Hardin & Richart (1963) illustrated that, all other factors being equal, a sediment composed of angular particles would exhibit a higher shear wave velocity that one composed of round particles.

4.2.6. Overconsolidation ratio.

The overconsolidation ratio is simply defined as the ratio of the maximum confining pressure experienced by the soil to the current confining pressure. In granular soils, consolidation effects of this type tend to be rather limited, although they become more significant in fine grained sands and silty sands. Hardin & Black (1968) suggest that the general effects of overconsolidation may be taken into account using the empirical equation:

$$G_{max} = 1230\left[(2.97-e)^2/(1+e)\right](OCR)^K(\sigma_o)^{0.5} \qquad (4.9).$$

where, G_{max} = dynamic shear modulus,

K ranges from 0 to 0.5 as the plasticity index ranges from 0 to 100.

4.2.7. Vibration frequency.

Various workers (*e.g.* Stoll, 1977; Stoll, 1989; Turgut & Yamamoto, 1991) using acoustic models, based on the classical theory of the mechanics of porous media developed by Maurice Biot, have shown that both shear waves and compressional waves display the phenomenon of velocity dispersion. As can be seen from Figure 4.4, the modelled shear wave velocity of a medium fine sand increases at greater frequencies, with the upward 'break' in phase velocity depending, to a large extent on

the permeability of the sediment. In the particular case of shear wave velocities in fine sands and sandy silts, this effect is of a generally small magnitude (5 - 10%) over a 1Hz - 1MHz frequency range.

4.2.8. Geological ageing effects.

The increase in stiffness and strength of soils as a function of time has been recognised for many years (Woods, 1991). This effect is a result of both primary and secondary consolidation resulting from an applied load and also cementation effects resulting from deposition of secondary minerals from the pore-fluids. The cementation of individual grains to each other intuitively suggests that in a condition of zero effective stress the sediment would retain some degree of stiffness; this is a condition which most common laboratory studies effectively ignore. These time effects have important implications when attempting to compare measurements made on disturbed or reconstituted sediments with field measurements, especially in sediments which may have remained undisturbed for potentially millions of years. In more recently deposited, normally consolidated sediments, which are those at most risk from flow liquefaction, these effects are likely to be less marked.

4.2.9. Temperature effects.

Woods (1991) notes that temperature effects on shear modulus are generally minor and totally recoverable.

4.2.10. Summary.

As can be seen from the brief discussion above, many of the factors which control shear wave propagation are similar to those controlling liquefaction potential. The individual effects of the variables described above on both shear wave velocity and cyclic strength are summarised below.

Factor	*Effect on cyclic strength of non-cohesive soils.*	*Effect on shear wave velocity.*
Increased confining stress	Increased	Increased
Increased density	Increased	Increased
Increased grain size[1]	Increased	Increased
Increased uniformity coefficient[1]	?	?
Increased angularity	Increased	Increased
Soil structure[2]	Increased	Increased
Vibration pre-straining	Increased	Increased
Overconsolidation	Increased	No effect[3]
Ageing effects/cementation	Increased	Increased
Static shear stress	Increased	No effect[3]
Decreased saturation	Increased	No effect
Temperature	Probably no effect.	No effect

Table 4.1. Summary of the factors affecting cyclic strength and shear wave velocity (*after Strachan, 1984*).

[1] for a constant relative density.
[2] moist tamped relative to dry pluviated.
[3] increased if mean effective confining pressure increased.

It is on this and similar bases (*i.e.* similar controlling factors) that research into the possible use of shear wave velocity as an index of liquefaction potential has been previously justified.

4.3. Shear wave measurement techniques.

Tokimatsu & Uchida (1990) note certain advantages that the use of shear wave velocity in liquefaction prediction has over conventional penetration resistance based techniques. These advantages include:

1. V_s is a dynamic soil property with a clear physical meaning and well defined controlling factors,
2. V_s may be measured non-destructively, and,
3. V_s is relatively easily measured in both the laboratory and the field.

As Tokimatsu & Uchida (1990) noted, V_s may be relatively easily measured both *in-situ* and in the laboratory, which is a significant advantage when attempting to apply laboratory results to the field situation. A brief review of the common techniques used to measure shear wave velocity is presented below.

4.3.1. Laboratory shear wave measurements.

In their review of laboratory shear wave techniques, Bennell & Taylor-Smith (1991) identify three main laboratory methods by which the shear wave propagation characteristics are commonly measured:

1. pulse excitation,
2. continuous vibration torsional resonance,
3. torsional cyclic loading.

4.3.1.1. Pulse measurements.

Pulse measurements generally utilise piezoelectric transducers to generate and detect low amplitude shear wave (and compressional) pulses. Three distinct types of pulse source and detector may be identified:

1. shear plates and radial expander transducers, which utilise either a Y-cut quartz crystal or a piezoelectric ceramic polarised perpendicular to an applied field. Application of an electrical field across the crystal, causes deformation and the generation of a shearing motion (Bennell & Taylor Smith, 1991);
2. pulse shearometers consist of a pair of parallel discs mounted in a glass cylinder containing the test material. Each disc is in contact with a piezoelectric crystal, which induces small amplitude torsional displacements relative to the other to initiate a shear wave pulse (Bennell & Taylor Smith, 1991);
3. bender transducers (described in more detail below), consist of two layers of piezoceramic bonded together. Alternate excitation of each layer produces a shearing motion and the generation of a shear wave pulse.

Possibly the most commonly used laboratory approach involves bimorph 'bender' transducers, and for this reason they are described in more detail below.

4.3.1.1.1. Bender transducers.

Bender transducers were originally developed by Shirley & Hampton (1978) & Shirley (1978). Essentially each transducer element consists of two thin piezoceramic expander

plates, composed of Lead Zirconate Titanate (PZT4), bonded together in a 'sandwich' arrangement. Between each element, and on their outer surfaces, are conducting electrodes (Figure 4.5). Polarisation of each individual plate ensures that when a driving voltage is applied (usually in the from of a step, spike or tone burst), one plate elongates, while the other shortens. The net result is a bending displacement which is greater in magnitude than the length change in either plate (Bennell & Taylor Smith, 1991). When suitably mounted and confined in a sediment, this motion results in the propagation of a shear wave, moving perpendicular to soil particle motion (Figure 4.6).

Bender elements are commercially available in two forms: series connected and parallel connected (Figure 4.7). Dyvik & Madshus (1985) suggest that a series connected element is twice as effective as a parallel connected when used as a receiver. In contrast, a parallel connected element is twice as effective as a series connected element when used as a transmitter.

By nature of their characteristically small size, bender elements have been installed in a variety of compression and triaxial cells, where they can be used to study the effects of different types of load on shear wave propagation (*e.g.* Schultheiss, 1983; Dyvik & Madshus, 1985; Bates, 1989). In addition, they may be also used as small scale *in-situ* probes (Jones & Jago, 1991) and in settling columns to study consolidation phenomena (McDermott, 1991).

4.3.1.2. Resonance techniques.

The resonant column test, as used for the determination of modulus and damping characteristics of soils, is based upon the theory of wave propagation in prismatic rods. In the United States, it has become the American Society of Testing and Materials (ASTM) standard method for determining the shear modulus and damping capacity of soils. The resonant column has also been used to determine the fundamental shear wave properties of samples of marine sediments (Davis & Bennell, 1985).

The resonant column, as described by Bennell & Taylor Smith (1991), essentially consists of a cylindrical sediment sample, mounted between two end platens, and contained in a pressure cell. The lower platen is usually the drive or active end, while the top platen may be either rigidly fixed or able to rotate (Figure 4.8). Vibration may be in

the first torsional mode and first longitudinal mode. Monitoring of the specimen's end displacements as a function of the resonant frequency for which the sinusoidal excitation force is in phase with the velocity of vibration, allows calculation of the dynamic shear modulus and dynamic compression modulus respectively.

One of the resonant column's biggest advantages is that it can test samples over a wide range of strain amplitudes (e.g. 0.0001% - 1%). This allows both low amplitude testing where the specimen behaves in a linearly elastic fashion, and higher amplitude testing, in which the sample behaves in an elastic-plastic fashion, which is more representative of earthquake strains (Bennell & Taylor Smith, 1991).

4.3.1.3. Torsional cyclic loading.

Torsional cyclic loading involves single torsional shear stress reversals at very low frequencies (0.01-0.1Hz) on a sample confined in a similar manner to the resonant column. Shear modulus (and hence shear wave velocity) is directly derived from the gradient of the line joining the end points of the hysteretic stress-strain loop (Bennell & Taylor Smith, 1991).

4.3.2. *In-situ* shear wave measurement techniques.

A variety of different techniques have been utilised in attempts to measure the *in-situ* shear wave properties of both surficial and deeper sediments. As with the *in-situ* geotechnical methods described previously (see Chapter 2), most *in-situ* shear wave techniques were originally developed for land based field use. Many of these techniques have, however been adapted to allow use offshore, despite the added complication that, unlike compressional waves, shear waves do not propagate through water. Examples of 'marinised' shear wave techniques include an underwater shear wave refraction sledge (*e.g.* Huws, 1993) and offshore Seismic Cone Penetrometers (*e.g.* Lange *et al.*, 1990), described below. These techniques bring about the real possibility of undisturbed, *in-situ* sampling in offshore areas previously regarded as being extremely hard to obtain 'undisturbed' samples.

Methods for determining the *in-situ* shear wave velocity of marine sediments can be essentially be divided into two distinct categories (Huws, 1993):

1. those which do not generate shear wave directly on the seafloor, but instead use mode converted shear waves, interface waves or background noise, and
2. those which generate and detect shear waves on the seafloor.

An excellent review of these various techniques is given in Huws (1993) and it is therefore not necessary to describe them in detail here. However, the attention of the reader is drawn to two main techniques which have a direct relevance to this research project: the University of Wales', seafloor refraction system (described in Chapter 5), and the offshore Seismic Cone Penetrometer, described below.

4.3.2.1. The Seismic Cone Penetrometer (SCPT).

The Seismic Cone Penetrometer has been described by various different workers (*e.g.* Robertson *et al.*, 1986; Hepton, 1989) and has been used in industry, both onshore and offshore, since around 1986 (Lange *et al.*, 1990). Essentially either a single or a pair of small geophones are incorporated into a standard Cone Penetrometer above the friction sleeve. The cone is steadily pushed into the ground generally ensuring a firm and continuous contact between the geophone and the soil, thus aiding signal response. Measurements are usually made at 1 metre intervals, as the cone is pushed into the ground. On land, polarised shear waves are generally produced using a hammer and beam arrangement, with coupling provided by the penetration truck's wheels (Robertson *et al.*, 1986). For inter-tidal work, the SCPT may be mounted on a barge, and measurements carried out at low tide when a rigid contact between the barge and the sediment exists.

For offshore work in significant depths of water, the generation of the shear wave is more problematical. Lange (1991) describes a fully offshore SCPT which has been in use with Fugro-McClelland engineers since 1987. Physically, the cone resembles a standard SCPT (described above). Offshore, the cone is pushed into the sediment from a heavy reaction frame anchored to the seabed. The shear wave source is located within the reaction frame, and consists of a horizontally orientated, hyrdaulically activated, spring hammer mounted in a steel box. The maximum penetration achieved using this system is around 60m, in soft normally consolidated clays.

Advantages of the system include (Robertson *et al.*, 1986; Lange, 1991):

1. shear wave data may be combined with other penetration data collected during the test, providing a wealth of data for a specific site,
2. resolution of thin high velocity layers, or velocity inversions that would otherwise be missed during a conventional surface refraction survey,
3. excellent coupling of the cone and sediment, ensuring an optimum sensitivity for shear waves.

4.3.3. Summary.

A variety of methodologies currently exist allowing the relatively simple measurement of shear wave velocity both *in-situ* and in the laboratory. In addition, a considerable amount of research and development work has been performed allowing the relatively simple collection of shear wave data offshore. The development of this apparatus over the past 10 to 20 years has directly led to both field and laboratory investigations of the inter-relationships between liquefaction potential and shear wave velocity.

4.4. A review of previous attempts to predict liquefaction potential using shear wave velocity.

Attempts to use shear wave velocity as an index to liquefaction may be divided into two main methods:

1. field correlations,
2. laboratory based correlations,

4.4.1. Field correlations.

Possibly the simplest approach to the use of shear wave velocity to predict liquefaction in some way is to compare shear wave velocity profiles (recorded prior to earthquake shaking) of sites which did and did not liquefy in the same earthquake. However, the main current limitation of this type of direct correlation is the extremely limited data base. This is due mainly to the somewhat unpredictable nature of earthquakes and the relatively short timescale of study, especially when compared to SPT based methods. In

an attempt to expand this data-base and thus further explore any possible link between shear wave velocity and liquefaction potential, additional correlations have been attempted between both shear wave velocity and SPT N values and CPT q_c values.

4.4.1.1. Direct field correlations.

Most of the evidence from this type of approach originates from a study by Youd & Wieczorek (1984), in the Imperial Valley, California. This site remains unique for direct field based correlations, comprising an area heavily instrumented with accelerometers and other seismological equipment, supplemented by data from numerous boreholes, all of which are often subject to earthquake activity. An analysis of data from the 1979 Imperial Valley and 1981 Westmorland earthquakes compared with previously obtained shear wave profiles suggests that all soils which liquefied during the earthquake had shear wave velocities below 140 m/s (460 ft/s). Stokoe II *et al.* (1988b) further extend this simple correlation to include the calculated maximum surface accelerations on adjacent firm ground (Figure 4.9). However, even data from this site are still extremely limited in nature, and the relationships presented remain somewhat questionable.

Based on data from the same site, Robertson *et al.* (1992a) present a correlation between V_s and cyclic stress ratio to cause liquefaction, based upon shear wave velocity normalised with respect to effective stress, using:-

$$V_{s1} = V_s \left(\frac{P_a}{\sigma'_o} \right)^{0.25} \qquad (4.10).$$

where, V_{s1} = normalised shear wave velocity,
P_a = reference stress, typically 100 kPa,
σ'_o = effective overburden stress.

This relationship is illustrated in Figure 4.10. Robertson *et al.* (1992a) note from a comparison of this relationship and data from the 1987 Superstition Hills earthquake that the minimum normalised shear wave velocity required to prevent the generation of excess pore-pressures and liquefaction is in the range 120-150m/s over a depth range of 3-6m.

4.4.1.2. V_s - N value correlations.

In a liquefaction potential mapping project, Wang (1992) attempts to correlate shear wave velocity with SPT N values producing the empirical relationship:-

$$N_E = \left(\frac{V_s}{53.91}\right)^{10/6} \qquad (4.11).$$

where, N_E = equivalent SPT blow count.

This type of empirical correlation, and others like it (*e.g.* Seed *et al.*, 1983), offer a possible route to the large SPT N value data base. The main disadvantage of this kind of approach however, is the fundamental unreliability surrounding the SPT test itself. This leads inevitably to a large scatter in experimental data, and associated uncertainties in interpretation.

4.4.1.3. V_s - q_c correlations.

Robertson *et al.* (1992b) suggest a correlation between normalised CPT q_c values and normalised V_s values, for young, uncemented, clean silica sands, having the form:-

$$V_{s1} = 60\left(q_{c1}\right)^{0.23} \qquad (4.12).$$

where, V_{sl} = normalised shear wave velocity,
q_{cl} = normalised cone penetration resistance.

Although this type of approach offers certain advantages over V_s - N correlations, a considerable scatter is still evident in the data (shown in Figure 4.11). Noting the logarithmic scales of both axes, and the scatter of data points, it is obvious that Equation 4.11 should be used with extreme caution when attempting to convert penetration test data into a shear wave equivalent.

4.4.2. Laboratory based correlations.

Laboratory approaches into the use of shear wave velocity in the prediction of liquefaction potential may be subdivided into:

1. cyclic strain approaches,
2. cyclic stress approaches,
3. monotonic or static approaches.

4.4.2.1. The cyclic strain approach.

The cyclic strain approach attempts to avoid some of the problems surrounding both conventional cyclic laboratory and SPT based liquefaction correlations. The method, originally proposed by Dobry *et al.* (1981), is based on laboratory evidence showing that cyclic shear strain is a more fundamental factor controlling pore-pressure build-up in saturated sands than cyclic stress. For laboratory saturated sands, a threshold strain, γ_t, of the order of 10^{-2}% exists. For strains below γ_t, there is no pore-pressure build-up when the saturated soil is subjected to undrained cyclic loading.

The cyclic strain approach, essentially involves determining whether or not excess pore-pressures can develop at a site for a given earthquake excitation, characterised by the peak ground surface acceleration, a_p. The surface threshold ground acceleration, a_t, required to initiate pore-pressure build-up is either measured or estimated, while the *in-situ* shear wave velocity is used to solve the equation:-

$$a_t/g = \frac{\gamma_t \left(G/G_{max}\right)_t}{g \cdot z \cdot r_d} \cdot Vs^2 \qquad (4.13).$$

where, $\gamma_t \sim 1 \times 10^{-2}\% - 3 \times 10^{-3}\%$.
$(G/G_{max})_t$ = modulus reduction factor
g = acceleration due to gravity
z = depth to sand layer
r_d = flexibility coefficient, typically ~1.0

At sand sites having relatively high shear wave velocities, the threshold accelerations are high and the ratio a_p/a_t will be < 1 for a given design earthquake. In this case γ_t is not

exceeded and excess pore-pressures will not be generated. In contrast if the threshold acceleration is exceeded ($a_p/a_t > 1$), excess pore-pressures will be generated. The excess pore-pressures themselves will be a function of a_p/a_t and duration of shaking.

The main advantage of this approach is that the effects of sample disturbance, common to cyclic triaxial techniques, are avoided. Possibly the biggest disadvantage is that only the possibility of raised pore-pressures are predicted, rather than the actual risk of liquefaction.

4.4.2.2. Cyclic stress approaches.

Cyclic stress approaches involving the cyclic triaxial test and monitoring of shear modulus or shear wave velocity have been described by Tokimatsu *et al.*, 1986; Tokimatsu *et al.*, 1988; Tokimatsu & Uchida, 1990; & De Alba *et al.*, 1984. These authors have two different approaches to the same problem.

Tokimatsu *et al.* (1986) studied the effects of differing sample density on both low strain shear modulus and the number of cycles required to cause a double amplitude axial strain (DA) of 5%. The laboratory method itself essentially involves a non-destructive cyclic test under undrained conditions to evaluate shear modulus at a 10^{-5} shear strain, followed by a standard undrained cyclic loading test at a frequency of 0.1 Hz.

The simplified procedure presented by Tokimatsu *et al.* (1986) consists of the following steps:

1. determination of the field elastic shear modulus, based upon *in-situ* shear wave velocities recorded at the site, using;

$$G_o = \rho Vs^2 \qquad (4.14).$$

2. evaluation of the normalised shear modulus (normalised with respect to effective stress σ_m' and minimum void ratio, e_{min}) of a laboratory sample, using;

$$G_N = \frac{G_o}{\left[F(e_{\min})(\sigma_m')^n\right]} \qquad (4.15).$$

where, G_N = normalised shear modulus
G_o = shear modulus of laboratory sample
$F = (2.17 - e_{max})^2 / (1+e_{max})$
$n \sim 0.5 - 0.67$

3. evaluation of the stress ratio ($\sigma_d / 2\sigma_o'$) to cause liquefaction in triaxial test conditions for a given number of loading conditions. A typical correlation between the number of cycles and earthquake magnitude is provided by Seed *et al.* (1985);

4. conversion of stress ratio to cause liquefaction for field K_o conditions, (τ_l / σ_v') using;

$$\left(\tau_l / \sigma_v'\right) = r_c \frac{1+2K_o}{3}\left(\sigma_d / 2\sigma_o'\right) \qquad (4.16).$$

where, rc = a constant reflecting multidirectional effects ~ 0.9 - 1.0
K_o = 0.4 - 1.0 typically.

This method then allows normalised shear modulus to be related to liquefaction resistance in terms of stress ratio (Figure 4.12). Tokimatsu & Uchida (1990) further evaluated current field performance data, which supported the effectiveness of the method described above. They further conclude that....

> '....the proposed method will play an important role in liquefaction evaluations, where full advantage can be taken of the usefulness of shear wave velocity'.

In contrast, De Alba *et al.* (1984) describe an alternative method in which both the shear wave velocity and compressional wave velocity of a sample were measured using piezoceramic transducers, prior to a conventional undrained cyclic triaxial test. The sample was considered to have liquefied once the cyclically induced pore-pressures reached the cell pressure; cyclic stress ratio was defined as the applied cyclic shear stress τ (one half of the cyclic deviator stress σ'_o), divided by the initial effective normal stress σ'_o. Shear wave and compressional wave velocities measured in each test were then plotted against the corresponding equivalent cyclic stress ratios for liquefaction in 10 cycles (see Figure 4.13).

De Alba *et al.* (1984) conclude that both shear wave velocity and compressional wave velocity may serve as an indictor of liquefaction resistance, although shear wave velocity is a more sensitive indicator, showing a larger percentage of variation for a given variation in stress ratio.

4.4.2.3. Monotonic or static approaches.

The combination of *in-situ* shear wave velocity measurements and the steady state approach to liquefaction prediction offers various fundamental advantages over the cyclic techniques described above. Firstly, as previously stated, definition of the state parameter requires a knowledge of both sample void ratio and effective stress; the same sediment characteristics control to a large extent the velocity of the shear wave. From this, it follows that just as the steady state line can be defined in void ratio - effective stress space dividing soils of contractive and dilative behaviour, a 'critical shear wave velocity line' could be defined in a similar manner. A knowledge of the critical V_s line could then be used to overcome some of the problems in determining the exact *in-situ* void ratio of a material in the field.

During the author's research period (1992 - early 1995), it appeared from the literature that no attempts had been made to combine the concepts of steady / critical state soil mechanics and the *in-situ* measurement of shear wave velocity, i.e. the research can be considered new and unique. However, shortly before the completion of this thesis, Robertson *et al.* (1995) published the results of a parallel study which used shear wave velocity to directly predict ψ in unconsolidated samples of Ottawa sand. This did cause a certain amount of disappointment, but can be regarded as further justification of the proposes technique. Because of the relevance of the study by Robertson *et al.* (1995) to the research presented in this project, close reference will be made to it throughout the remainder of this thesis.

4.5. Summary.

It is clear from the discussion above that shear wave velocity is controlled to a large extent by the same factors that control liquefaction potential. This fact alone suggests that V_s may be potentially used as an index for liquefaction potential in recent, uncemented non-cohesive sediments. In addition, shear wave based techniques appear

to have certain fundamental advantages over more conventional penetration based techniques including, ease of measurement, a clear physical meaning, and non-destructive test characteristics. Currently, a somewhat limited variety of different techniques have been developed in various attempts to identify some type of correlation between V_s and liquefaction potential. Published techniques range from direct field correlations to laboratory derived data, based upon cyclic stress, strain and monotonic approaches. All of these methods essentially arose from land based studies. Despite an exhaustive literature search it appears that no investigations have attempted to apply shear wave measurement approaches to a potentially liquefiable offshore area.

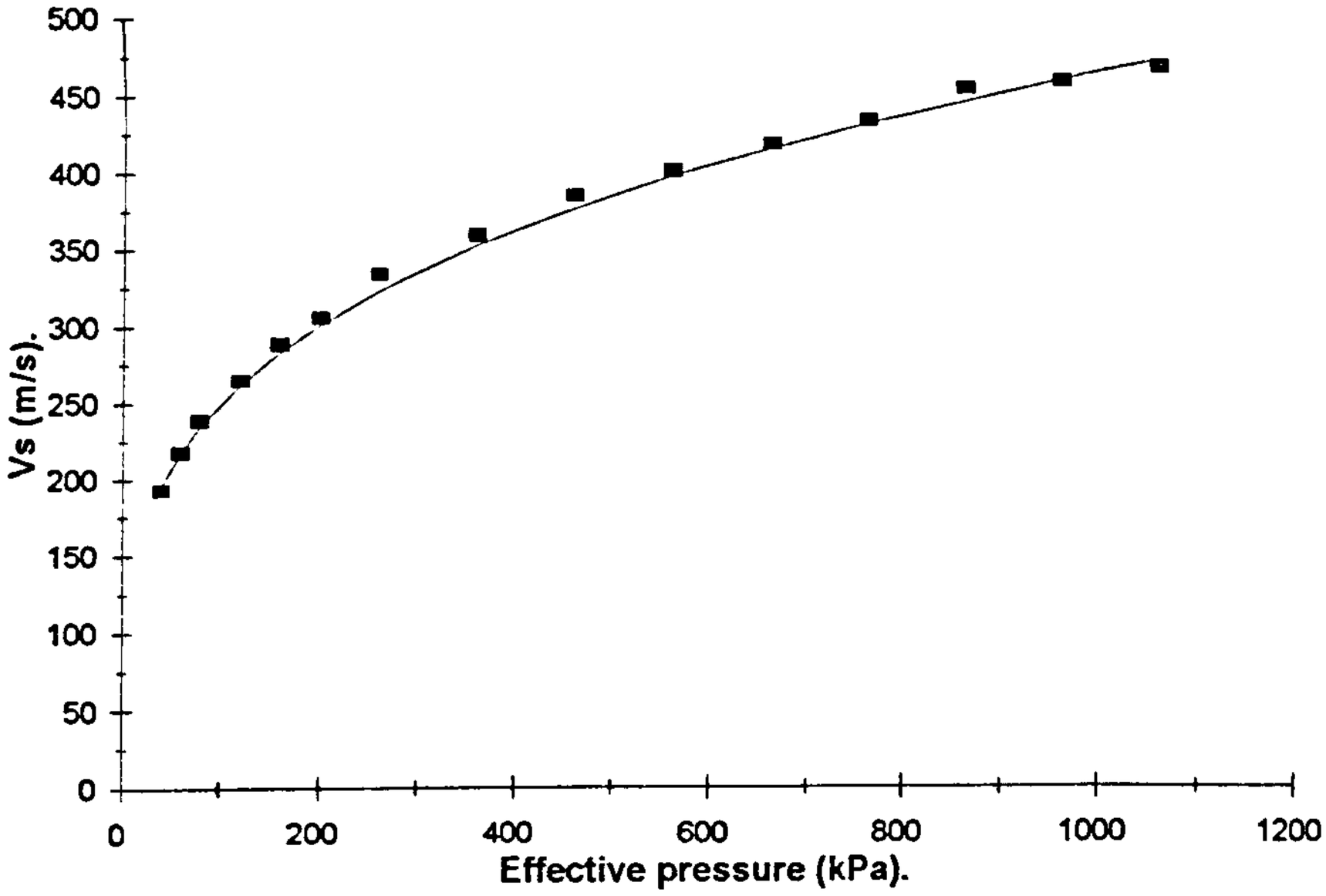

Figure 4.1. Typical relatonship between shear wave velocity and effective confining stress *(adapted from Bates, 1989).*

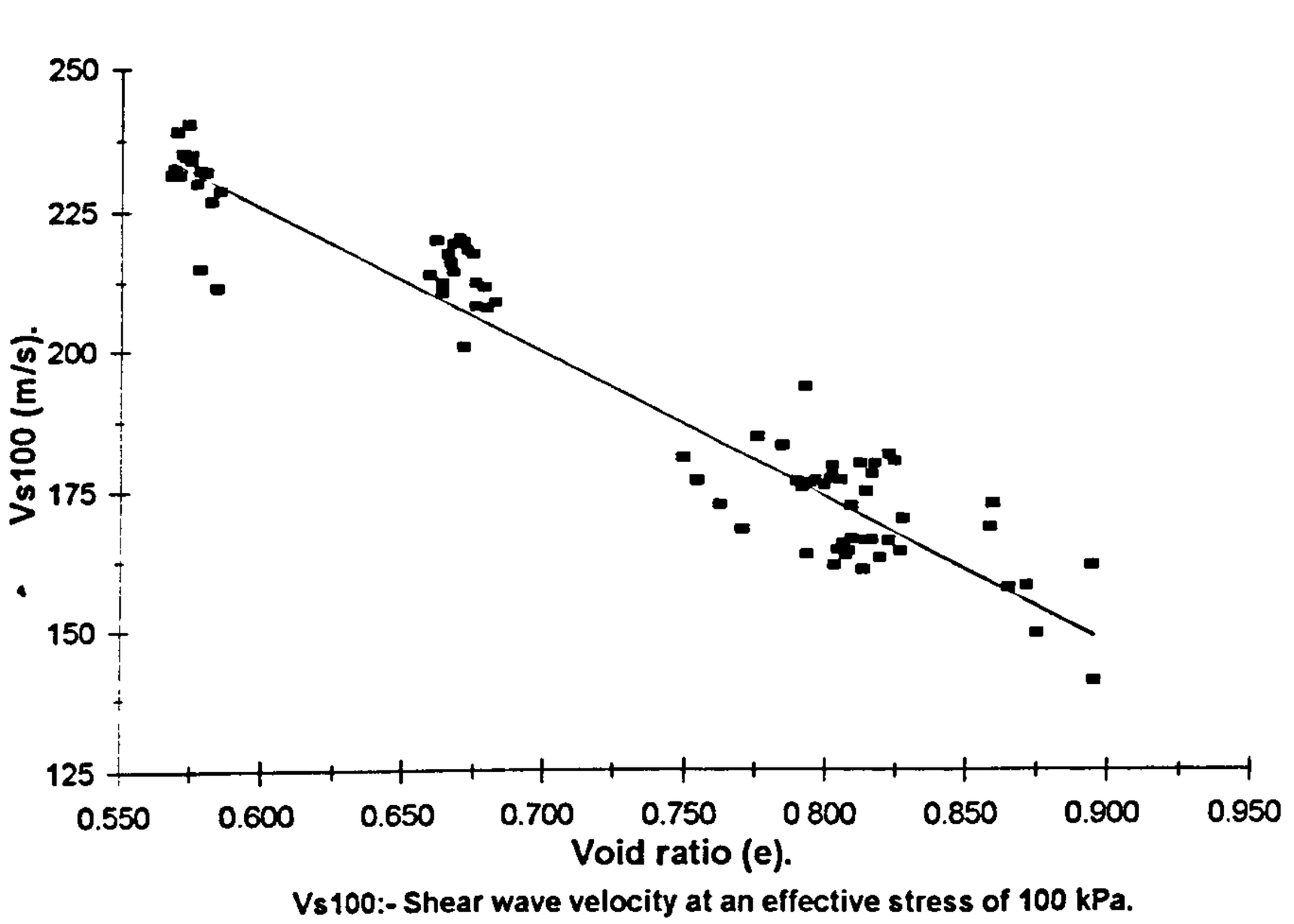

Figure 4.2. Typical relationship between shear wave velocity and void ratio *(adapted from Robertson et al., 1995).*

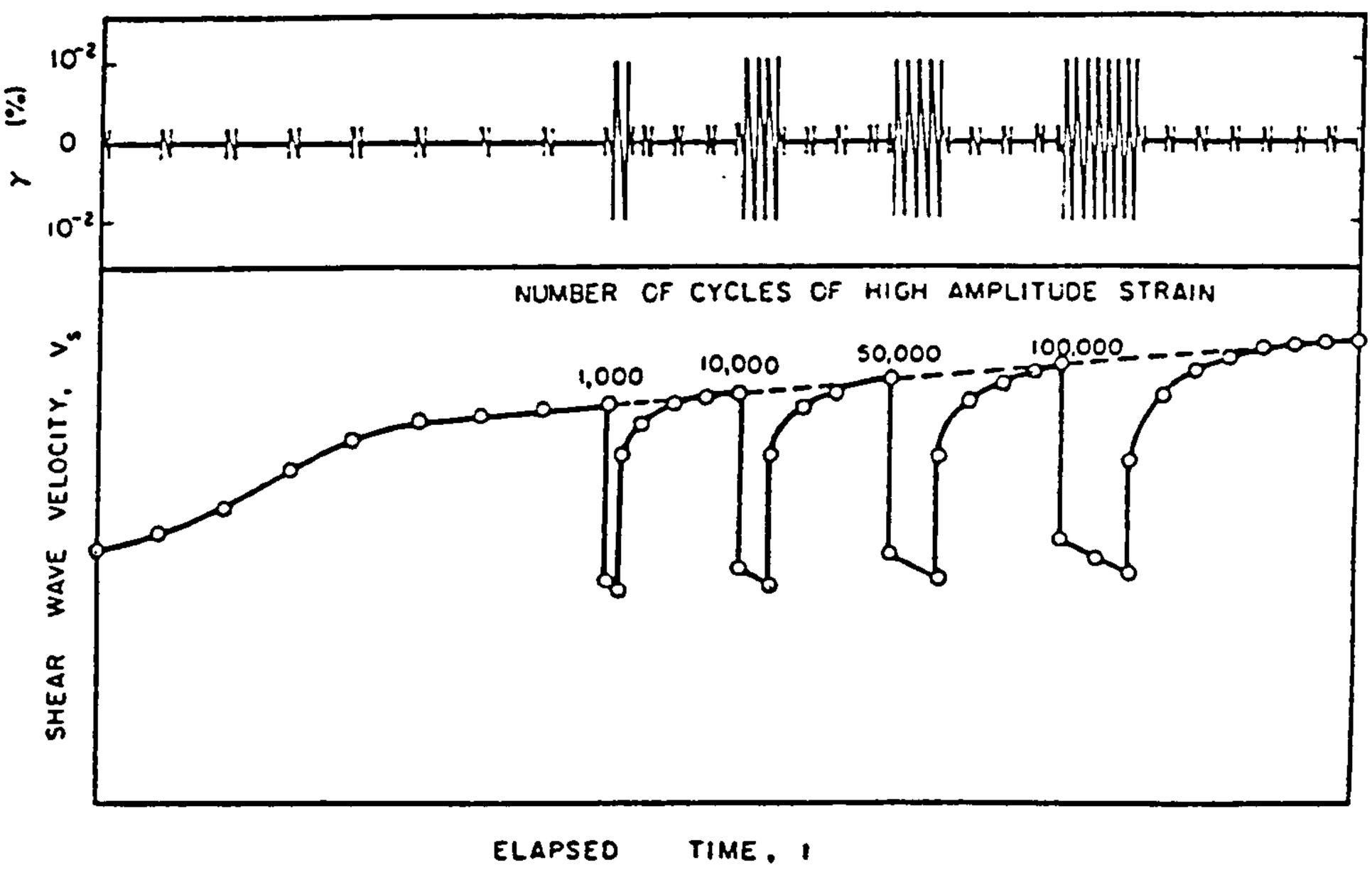

Figure 4.3. Effect of high shearing strain excursions upon shear wave velocity (*after Woods, 1991*).

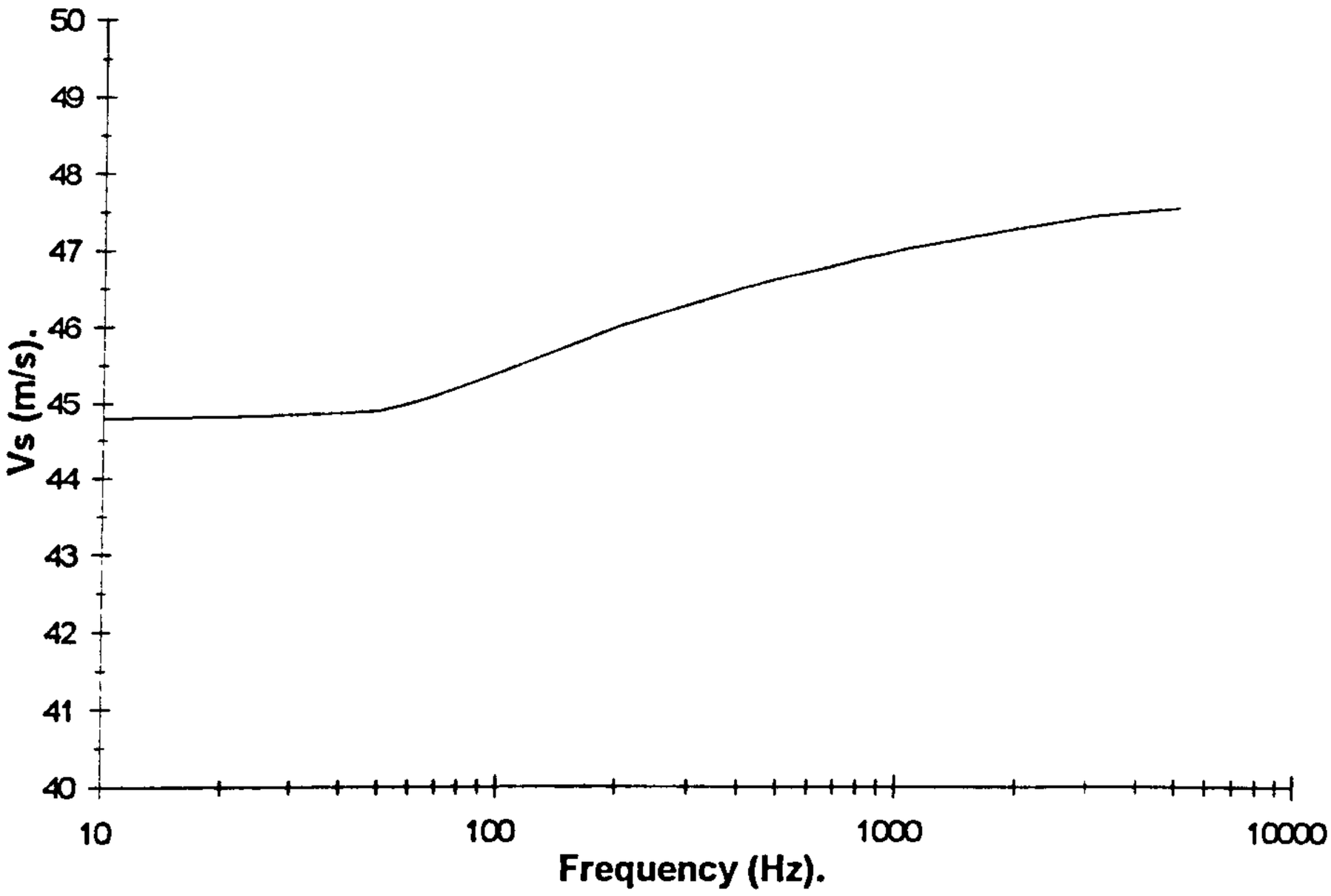

Biot-Stoll Model Parameters:-

Fluid density:- 1.00 gcm^{-3}
Fluid viscosity:- 0.01 dynsec/cm^3
Grain density:- 2.65 gcm^{-3}
Grain diameter:- 0.03 cm
Porosity:- 0.425
Bulk density:- 1.949 gcm^{-3}
Dry Vs:- 50 m/s
Dry log decrement:- 0.2
Permeability:- 0.1 x 10-5 cm^2
Pore size parameter:- 0.0074 cm
Structure constant:- 1.53

Figure 4.4. Predicted velocity dispersion for a well sorted, medium fine sand, due to fluid / solid coupling (*after Jones, 1990*).

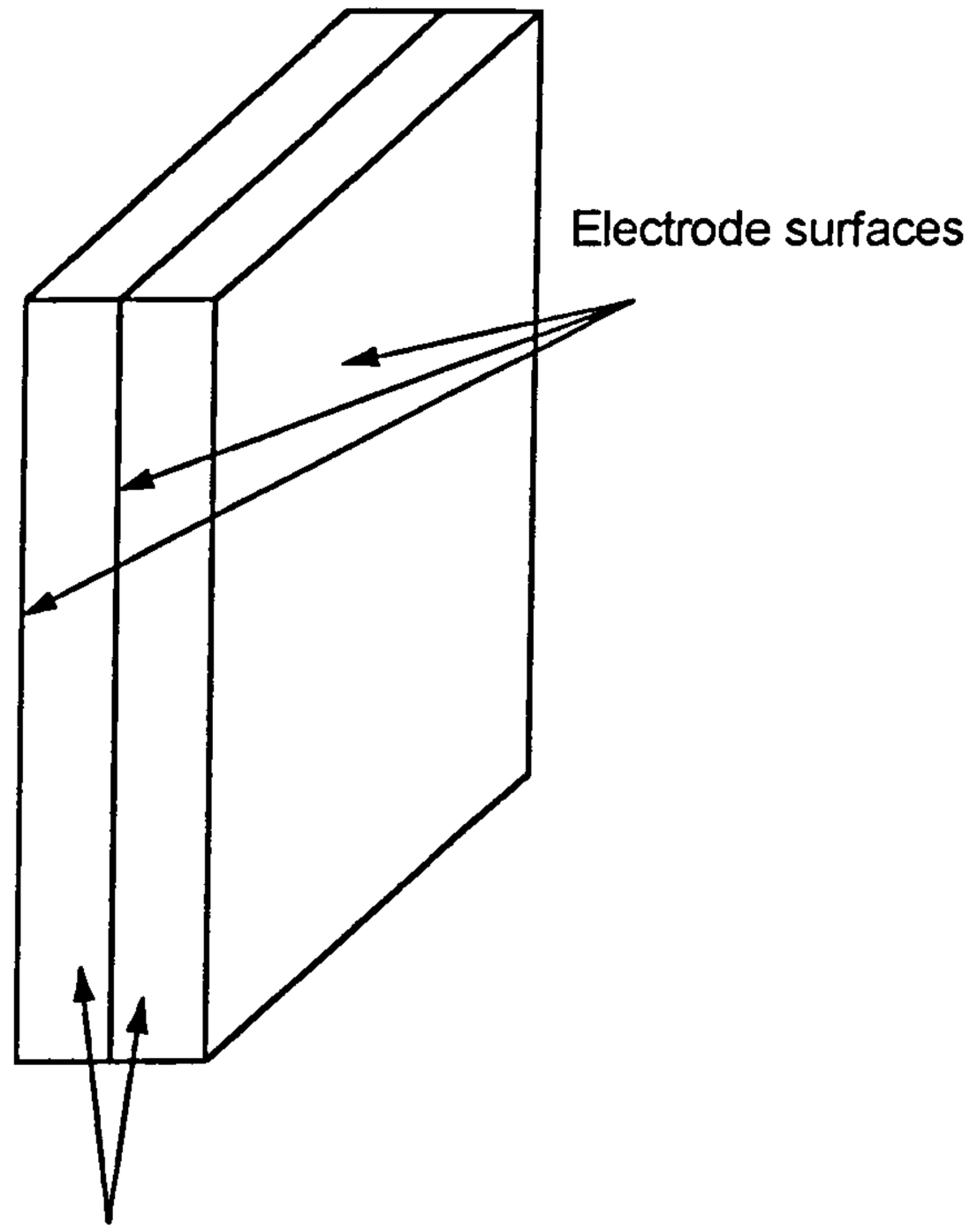

Figure 4.5. Bender transducer construction.

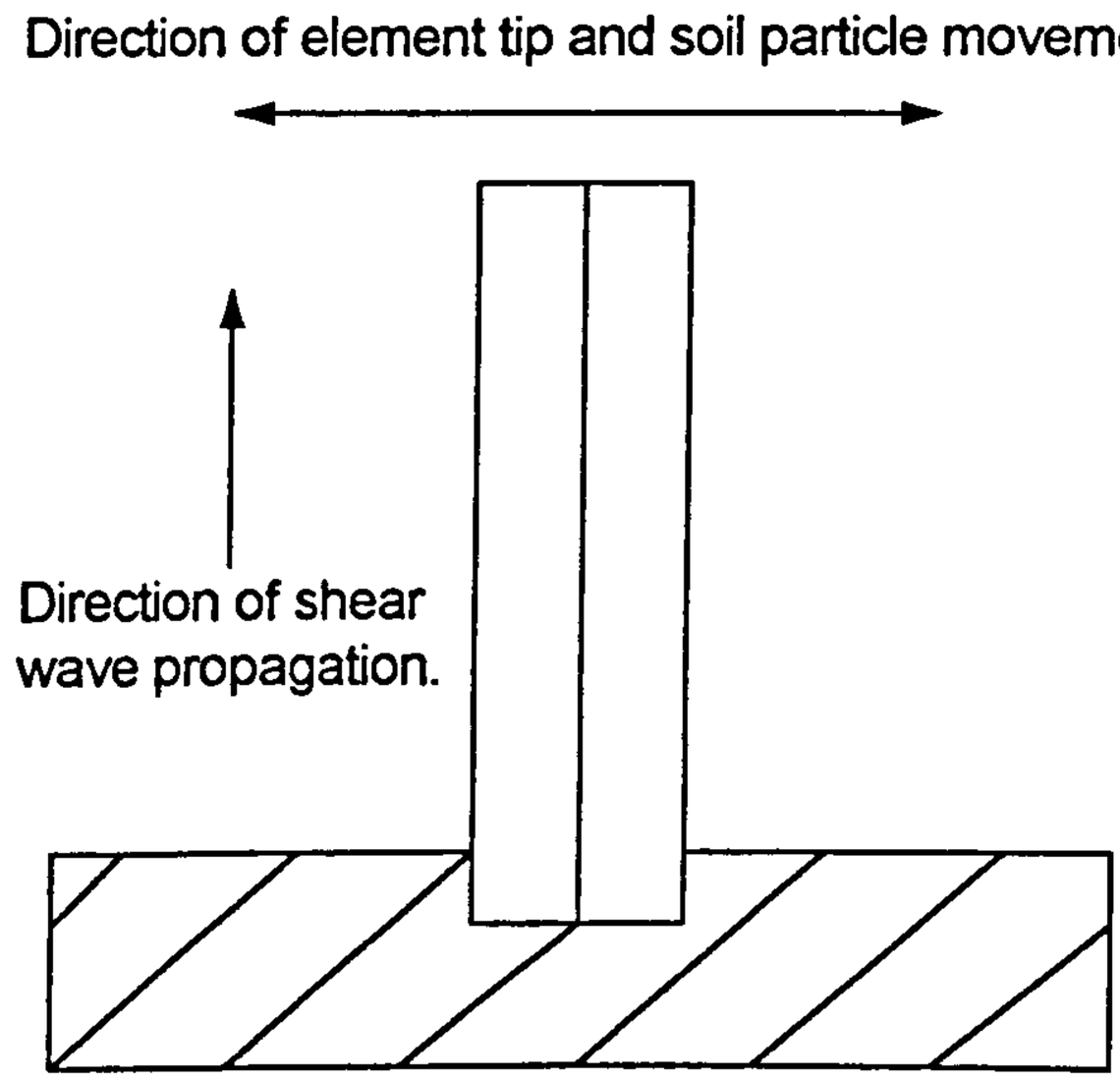

Figure 4.6. Bending motion induced in bimorph transducer.

a.

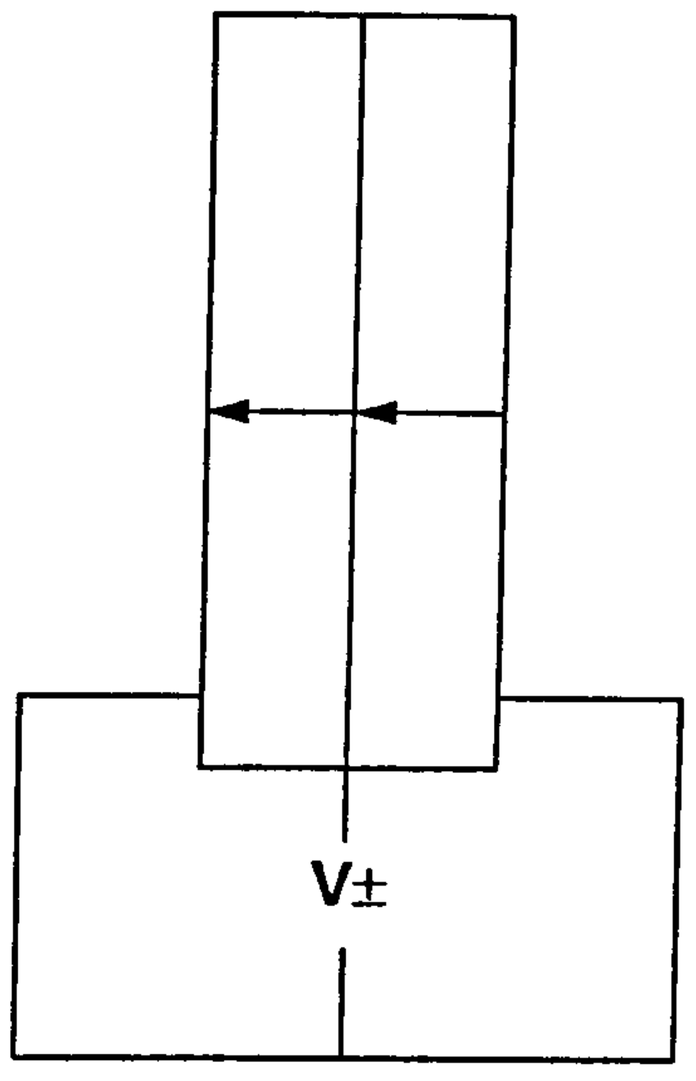

b.

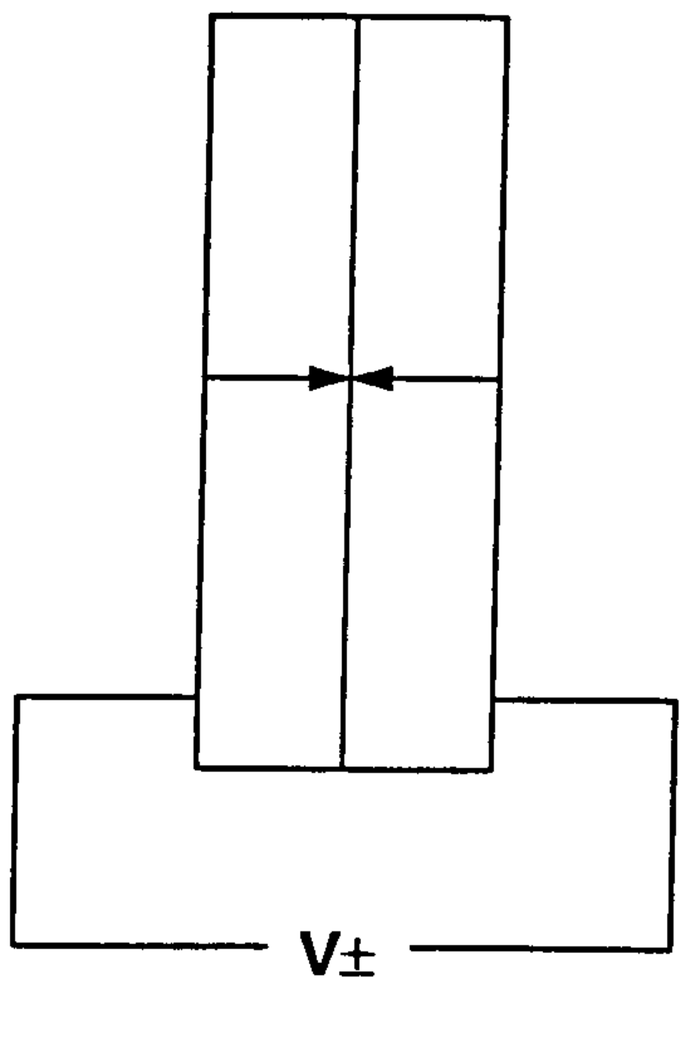

Indicates direction of polarisation.

Figure 4.7. a. Parallel connected piezoelectric bender element.

Figure 4.7. b. Series connected piezoelectric bender element.

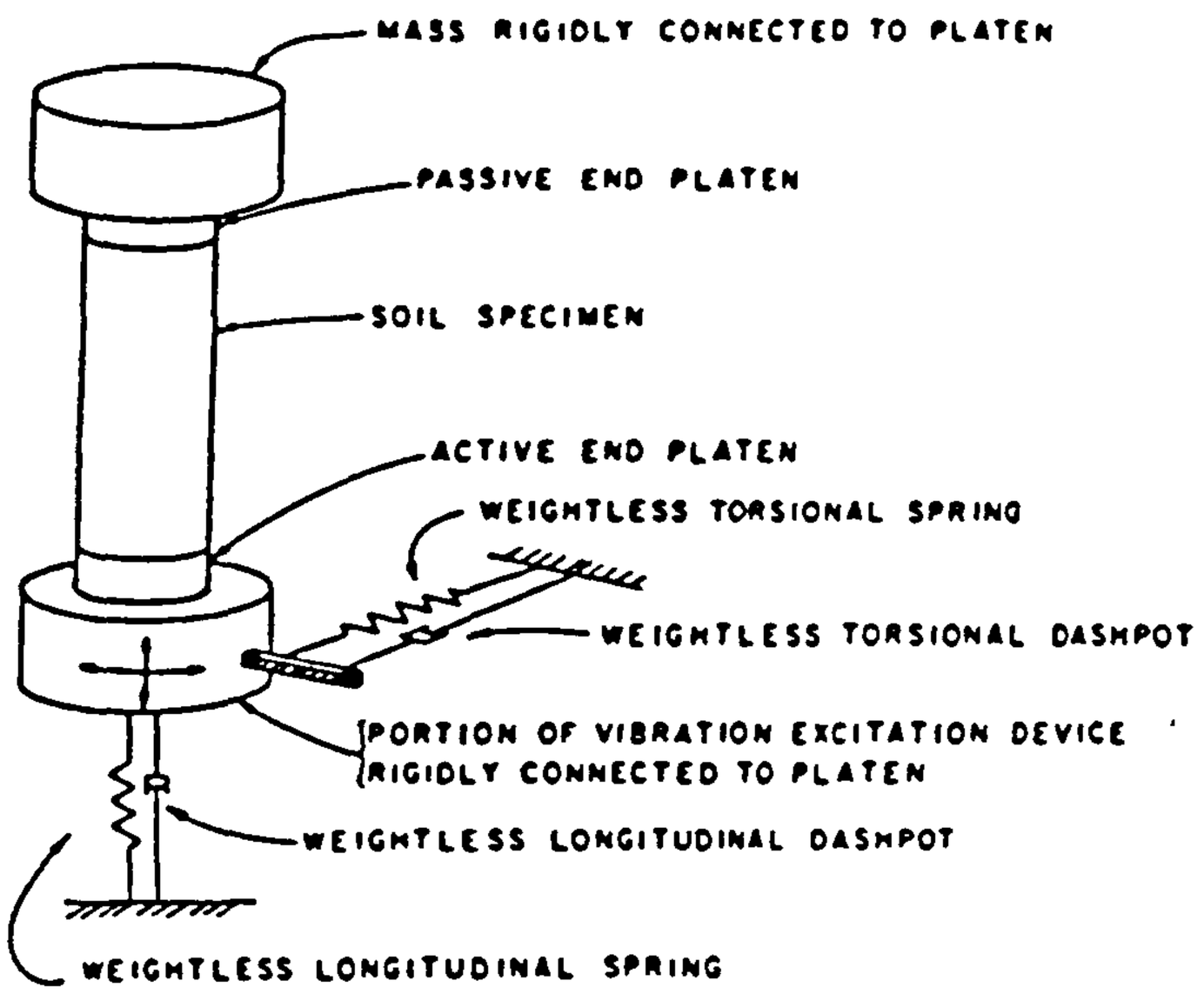

Figure 4.8. Schematic diagram of the resonant column apparatus (*after Dmevich, 1972*)

a.

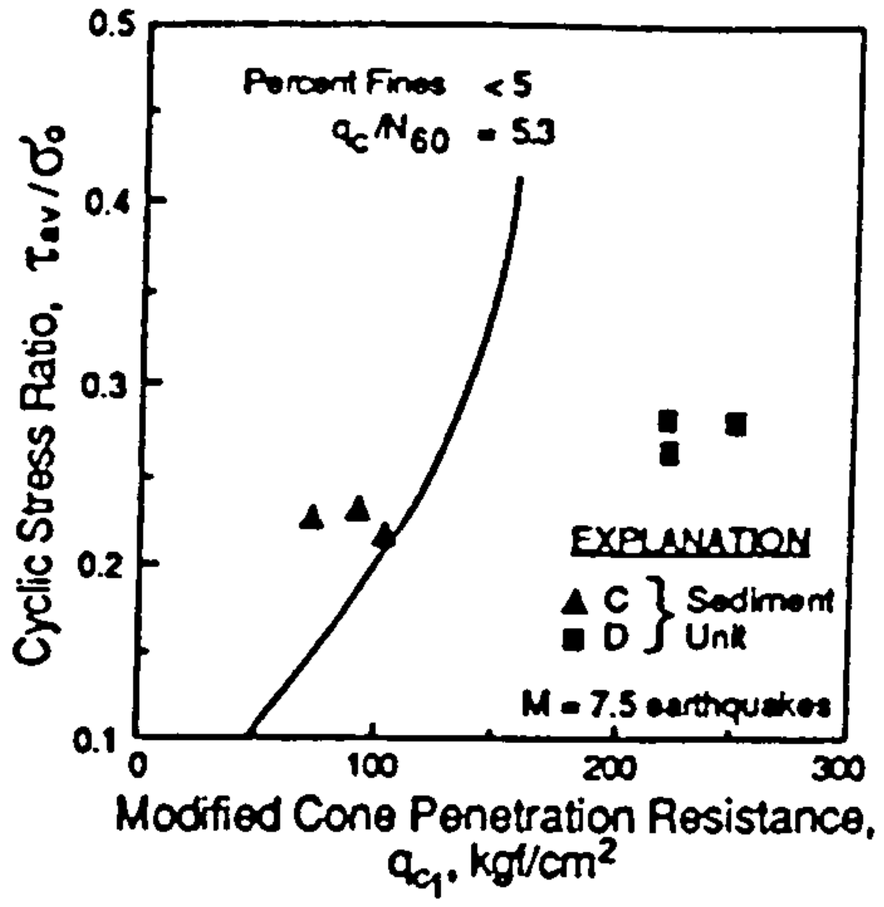

b.

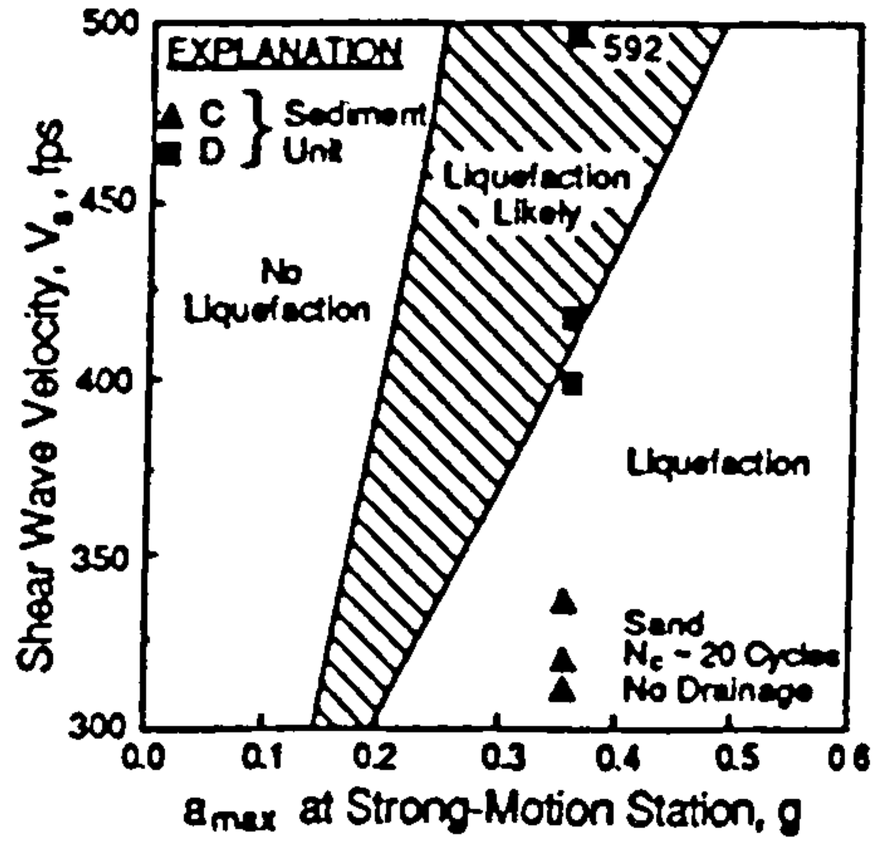

Figure 4.9. a. Liquefaction potential chart based upon modified penetration resistance *(after Stokoe II, et al., 1988b)*.

Figure 4.9. b. Liquefaction potential chart based upon shear wave velocity, *(after Stokoe II, et al., 1988b)*.

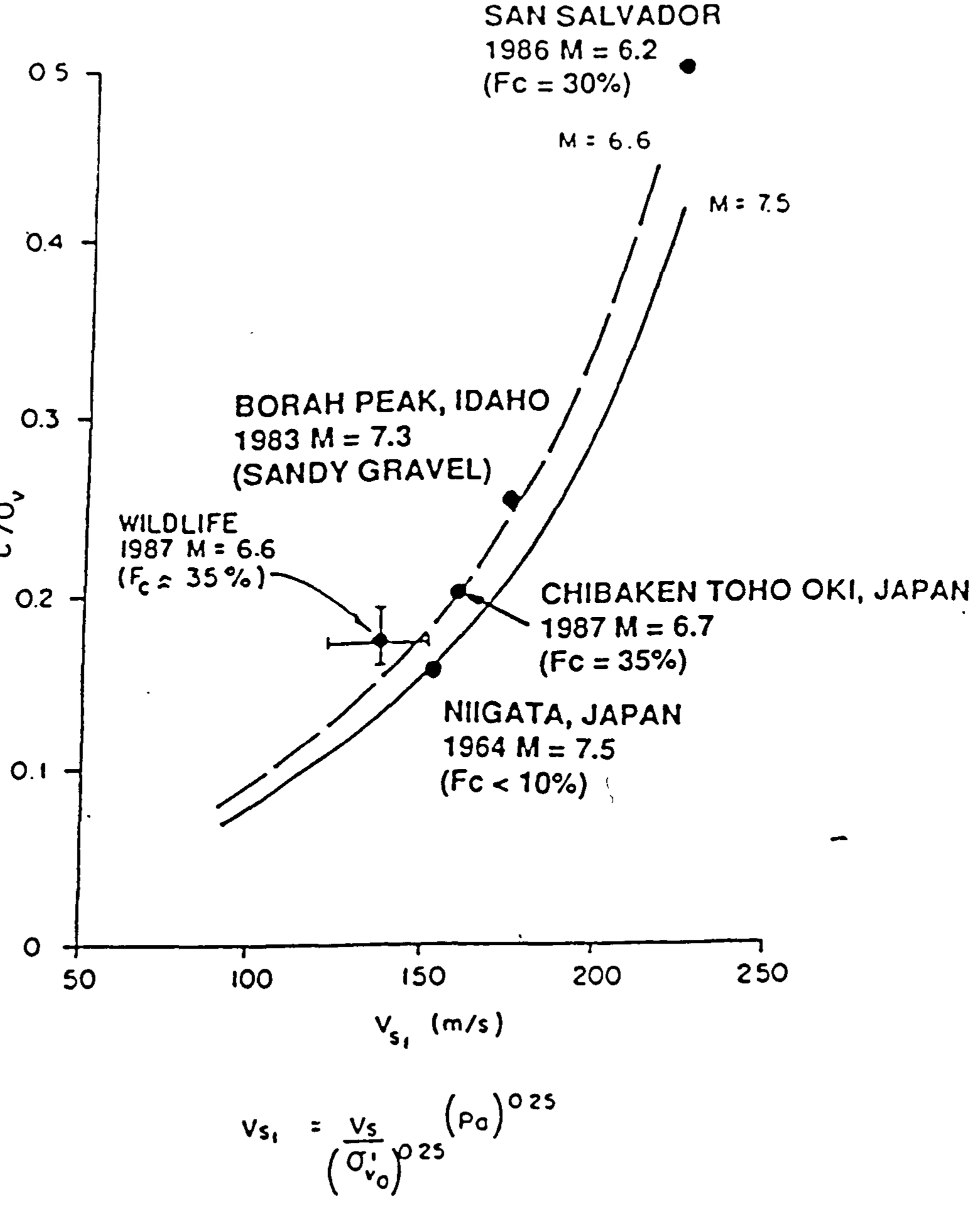

$$V_{s_1} = \frac{V_s}{\left(\sigma'_{v_0}\right)^{0.25}} \left(P_a\right)^{0.25}$$

V_s in m/s.

Figure 4.10. Correlation between normalised shear wave velocity and cyclic stress ratio to cause liquefaction (*after Robertson et al., 1992b*).

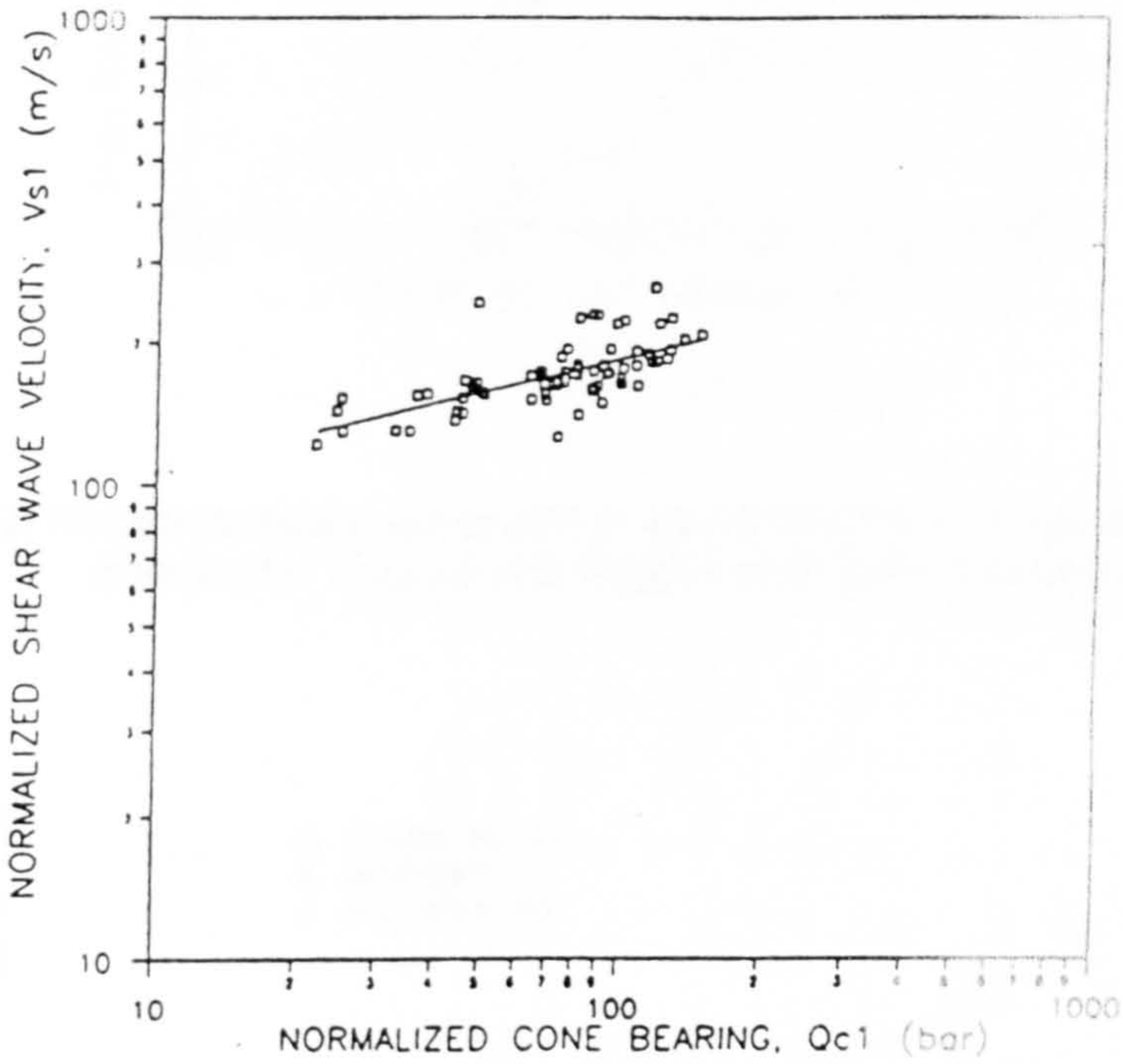

Figure 4.11. Correlation between normalised shear wave velocity and normalised CPT penetration resistance for a young, uncemented silica sand (*after Robertson et al., 1992a*).

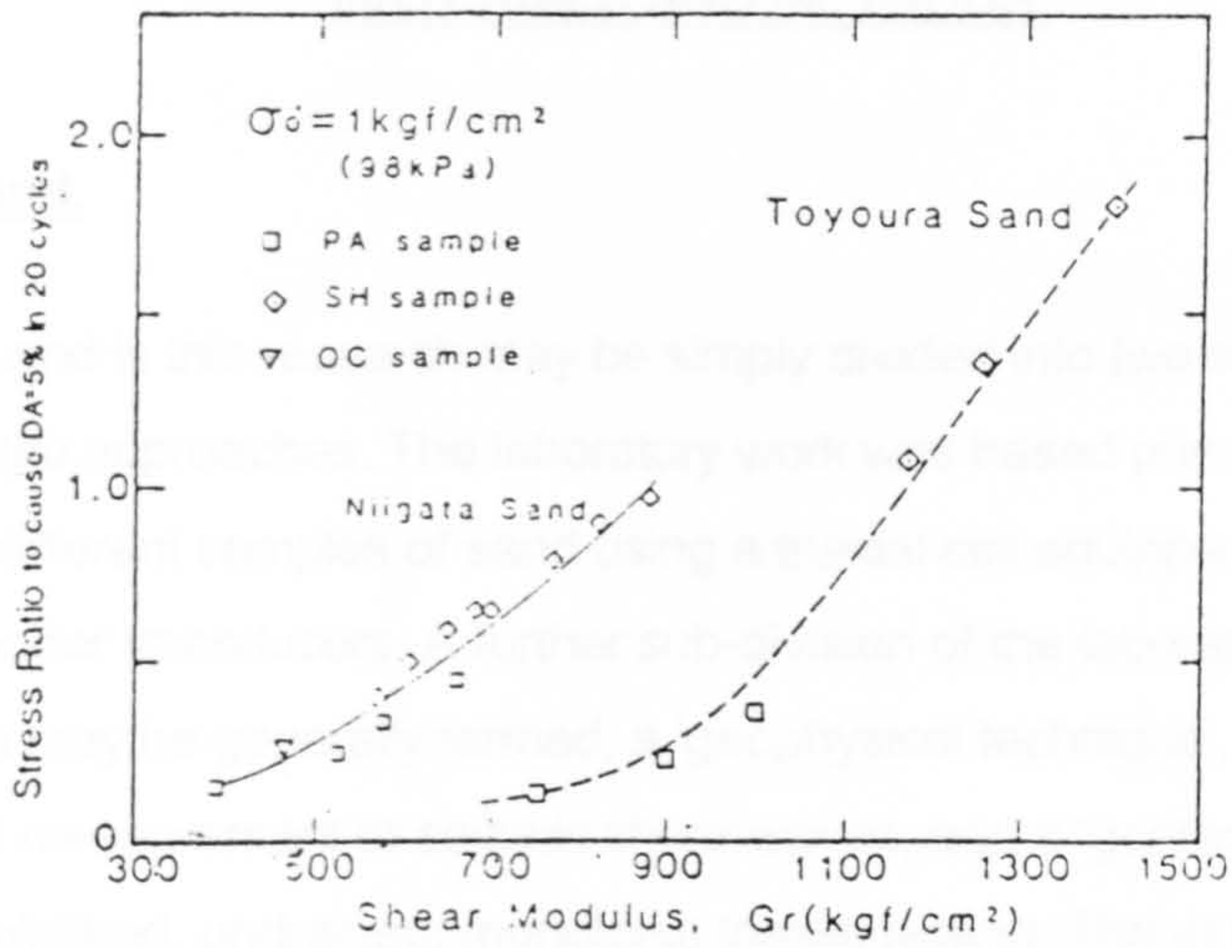

Figure 4.12. Relation between stress ratio to cause DA=5% in 20 cycles and shear modulus for Toyoura and Niigata sands (*after Tokimatsu et al., 1986*).

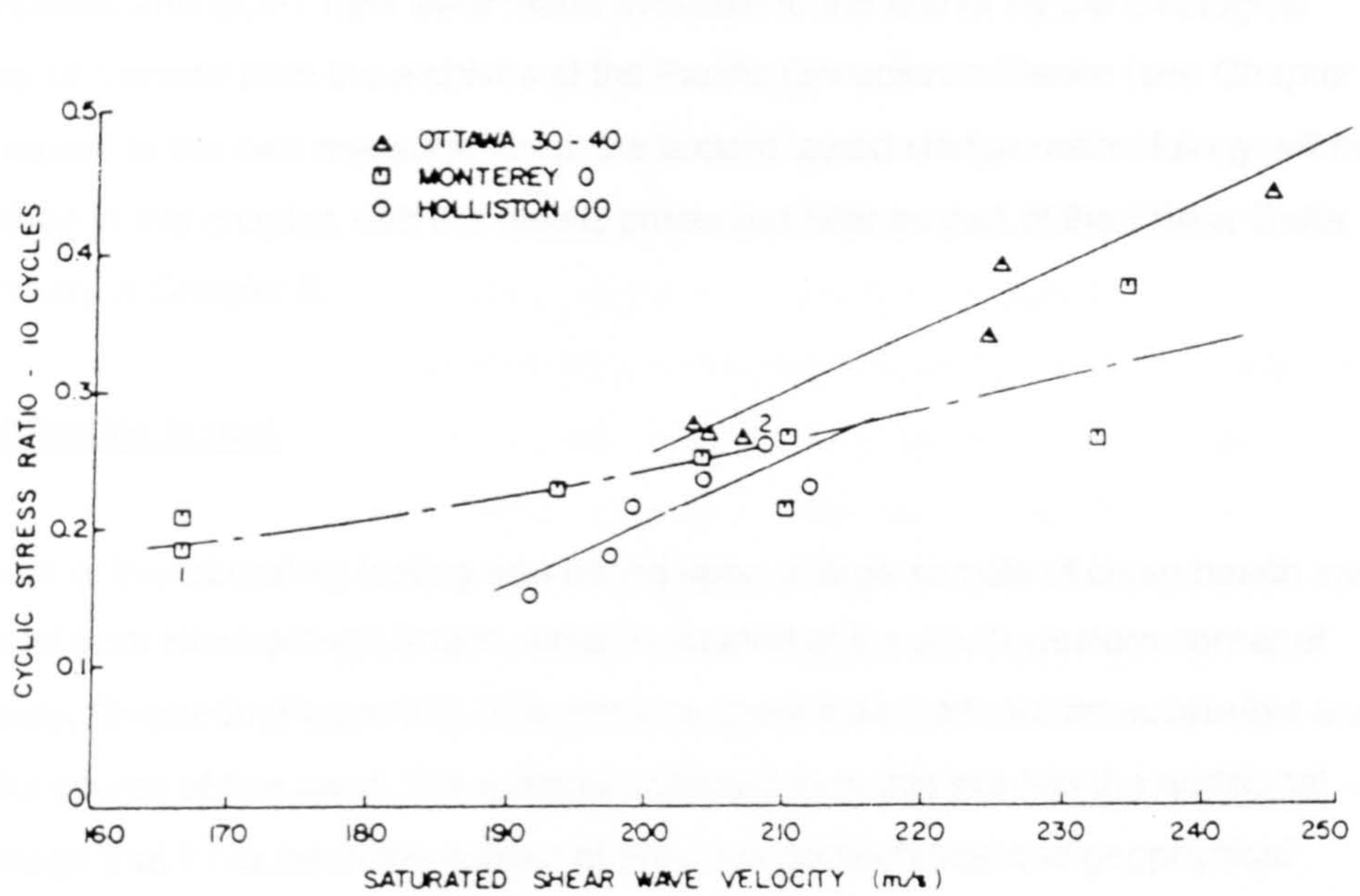

Figure 4.13. Relationship between shear wave velocity and liquefaction resistance in ten loading cycles: Ottawa, Monterey & Holliston sands (*after De Alba et al., 1984*).

CHAPTER 5.

MATERIALS AND METHODS.

5.1. Background.

The methods used in this research may be simply divided into two sections, laboratory testing and *in-situ* approaches. The laboratory work was based primarily around the testing of four different samples of sand using a triaxial cell equipped with piezoceramic shear wave bender transducers. A further sub-division of the laboratory work can be made into what may be generally termed, a 'geophysical technique', involving the generation and measurement of seismic shear waves, and a 'geotechnical technique', involving consolidated, undrained, monotonic triaxial testing. The associated *in-situ* component of the project involved interpretation of data acquired by Dr A. Davis & Dr D. Huws on behalf of the author using the UWB bottom towed sledge (Davis *et al.,* 1989) during two multidisciplinary research cruises on the Canadian Research Vessel, the *John P. Tully*. Complimentary field data, in the form of selected sub-bottom profiles, core descriptions and SCPT data were made available to the author by the Geological Survey of Canada from the archives at the Pacific Geoscience Centre (see Chapter 8). With regard to the field measurements, the bottom towed sledge methodology will be described in this chapter, with the results presented later as part of the Fraser Delta case study in Chapter 8.

5.2. Materials tested.

The bulk of the laboratory testing was based upon a large sample of clean beach sand collected from Newborough Beach, which is located at the south-western corner of Anglesey, Gwynedd (Figure 5.1). The site was chosen as it offered an accessible and plentiful source of fine sand. The material collected from this site has the additional advantage that it has been the subject of previous geotechnical and geophysical investigations by various researchers at UWB. During the laboratory test programme, in order to investigate the effects of increasing fines content on both the shear wave (S-wave) velocity behaviour and liquefaction potential of the sand, differing amounts of the non-plastic clay mineral, kaolinite, were added to the clean beach sand. This created two artificial sands, termed Newborough 5% and Newborough 10%, containing approximately 5% and 10% kaolinite respectively. In addition to these, a natural

sediment obtained from three closely spaced vibro-cores (PAR91A-01, PAR91A-02 & PAR91A-03) sited on the Fraser Delta, was also tested. This material was kindly provided by the Geological Survey of Canada. The index properties of the four test sands are summarised below in Table 5.1.

	Newborough 0%	*Newborough 5%*	*Newborough 10%*	*Fraser*
Mineralogy of sand fraction (%)				
...Quartz	90	90	90	50
...Rock fragments	8	8	8	50
...Other	2	2	2	0
% fines[1]	0	5	9	8
Mean grain size (μm)[1]	232	213	200	145
Variance[1]	0.218	0.458	0.626	0.440
Sorting[1]	0.467	0.676	0.791	0.663
B.S Classification[1]	Fine sand.	Fine sand.	Fine sand.	Fine sand.
Specific Gravity[1]	2.65	2.66	2.66	2.73
e_{min}[2]	0.666	0.619	0.589	0.759
e_{max}[2]	0.93	0.93	0.93	1.12

Table 5.1. Index properties of the sands used during laboratory testing.
[1] Determined in accordance with British Standard 1377: Part 2 (1990).
[2] Determined using a non-British Standards technique (see below).

Mineralogically, the Newborough 0% sand was composed predominantly (~90%) of sub-rounded to rounded clear, frosted or haematite stained quartz grains, with smaller amounts (~8%) of rock fragments, probably derived from North Walian volcanic and metamorphic sources. A small amount of calcite, in the form of very small shell fragments, was also present. In contrast, the Fraser Delta sand consisted of around 50% sub-angular to angular frosted quartz grains, and a further ~40% of angular fine grained, metamorphic rock fragments, primarily phyllites and schists; biotite and muscovite mica fragments made up the remainder. The high rock fragment content of the Fraser Delta sand, in particular the high percentage of often large (2-3mm across) biotite fragments, is indicative of the relative immaturity of this sediment compared to the beach sands. The grain size distribution curves for each sand are illustrated in Figure 5.2.

5.3. Laboratory Methods.

The laboratory methods used in this thesis may be broadly divided into three main groups: index properties, geotechnical methods and geophysical methods.

5.3.1. Index properties.

The index properties most commonly used to describe the physical characteristics of sands in liquefaction studies include the grain size distribution, grain shape, percentage of fine particles, specific gravity and range of possible densities. In this project these properties were defined according to B.S. 1377: Part 2 (1990), unless otherwise stated.

5.3.1.1. Grain size characteristics.

The grain size characteristics of a soil are possibly the most fundamental and, for sands at least, the most easily measured of all index properties. For this reason a number of engineering properties are either directly or indirectly related to particle-size characteristics, *e.g.* permeability and compressibility. Each sample tested was classified using the British standard range of particle sizes (see below).

Fine				Coarse						Very Coarse	
Clay	Silt			Sand			Gravel			Stone	
	Fine	Med.	Co.	Fine	Med.	Co.	Fine	Med.	Co.	Cobbles	Boulders
	6	20		200	600		6	20		200	
2			60	2			60				
μm				mm							

Table 5.2. British Standard range of particle sizes.
Med. - Medium, Co. - Coarse.

The grain size characteristics of the test sands in this study were determined using the dry sieve analysis procedure. Prior to this each sand was first washed and then dried at 105° for 24 hours before cooling in a desicator. The Newborough 0% sand was initially sieved through a 4mm sieve to remove any large rock and shell fragments.

5.3.1.2. Particle specific gravity (G_s).

Particle specific gravity of a material is the ratio of the weight or mass of a volume of the material to the weight or mass of an equal volume of water. It is simply defined as:-

$$G_s = \frac{W_s}{V_s \gamma_w} \qquad (5.1).$$

where, W_s = weight of solids,
V_s = volume of solids,
γ_w = unit weight of water.

In this study, G_s was determined by the density bottle method.

5.3.1.3. Minimum and maximum void ratios, e_{min} & e_{max}.

In the three phase soil model (i.e. solids, water, air) the ratio of void volume (i.e. water & air) to solid volume is known as the void ratio (e). A specific soil, and in particular sands and gravels, may exist over a wide range of densities or void ratios, with the actual void ratio of a soil usually lying somewhere between the two extremes, e_{min} & e_{max}. An often used measure of the relative state of compaction is provided by the relative density (D_r), which may be defined using:

$$D_r = \frac{e_{\max} - e}{e_{\max} - e_{\min}} \qquad (5.2).$$

In this study the values for e_{min} and e_{max} were calculated using a non British Standard technique. To obtain e_{min}, a known dry weight of moist sand was compacted into a sample mould of known dimensions. Compaction of the sample continued until no further volume reduction occurred; this ensured a state of densest packing was obtained. In contrast, e_{max} was calculated by allowing a known dry weight of saturated sand to gently settle down the length of a water filled measuring cylinder, allowing a very loose packing structure to form. In both cases, sample void ratio was calculated from a knowledge of the sample dry weight, volume and specific gravity, using:-

$$e = \left(\frac{V_T \times G_s \times \rho_w}{M_s} \right) - 1 \qquad (5.3).$$

5.3.1.4. Mineralogy of the sand fraction.

After wet sieving through a 63μm sieve, the sand fraction of the samples was further analysed for mineralogical composition and grain shape in a semi-quantitative manner using a binocular microscope.

5.3.2. Triaxial apparatus.

The basic items of standard laboratory triaxial equipment used in this research are listed below:

1. Wykeham Farrance 5000 Kgf Compression Test Machine, model WF10052/53.
2. Engineering Laboratory Equipment (ELE) 3500 KN/m^2 constant pressure apparatus, series EL27-432.
3. Wykeham Farrance oil dash pot system, model 13520.
4. Wykeham Farrance proving rings, serial numbers 3098 (max. load 2000lb), 9165 (max load 500kg) & 1912 (max load 400lb).
5. Soil-tech Ltd pore-pressure transducer, type WS-2000, linked to a Sandhurst Scientific Instrument Co., 8 channel digital display unit, model LH1600.

These items are illustrated in Plate 5.1. and briefly described below.

5.3.2.1. Wykeham Farrance Compression Test Machine.

The Wykeham Farrance 5000 Kgf compression test machine is a standard bench mounted, electronically controlled triaxial testing machine. Its electrical system utilises an A.C. current supply through a rectifier to a drive a 220 volt D.C drip proof motor. The platen speed, selected by digit switches on the front control panel, is variable between 0.0006mm and 6mm per minute, in steps of 0.0001mm. The selected speed will vary no more than 1% if the supply voltage is maintained to within ± 10% of its nominal value, and when any load is applied, by no more than 100%. The Jack Unit is composed of an accurately machined steel screw with bronze worm wheel, and steel worm mounted on angular ball races. The load itself is carried on high quality thrust bearings. A gearing selector lever, mounted on the main body of the machine, allows a more rapid platen adjustment prior to and subsequent to performing a test.

Key:-

1. Instrumented triaxial pressure cell.
2. Triaxial compression test machine.
3. Compression machine control box.
4. Amplifier.
5. Filter.
6. Pore-pressure digital display unit.
7. Oyo Sonic Viewer.
8. Pressure distribution board.
9. Constant pressure apparatus.
10. Proving ring.

Plate 5.1. Laboratory apparatus during testing.

3.

1.

4.

5.

7.

6.

2.

10.

8.

3.

1.

4.

9.

5.

2.

7.

6.

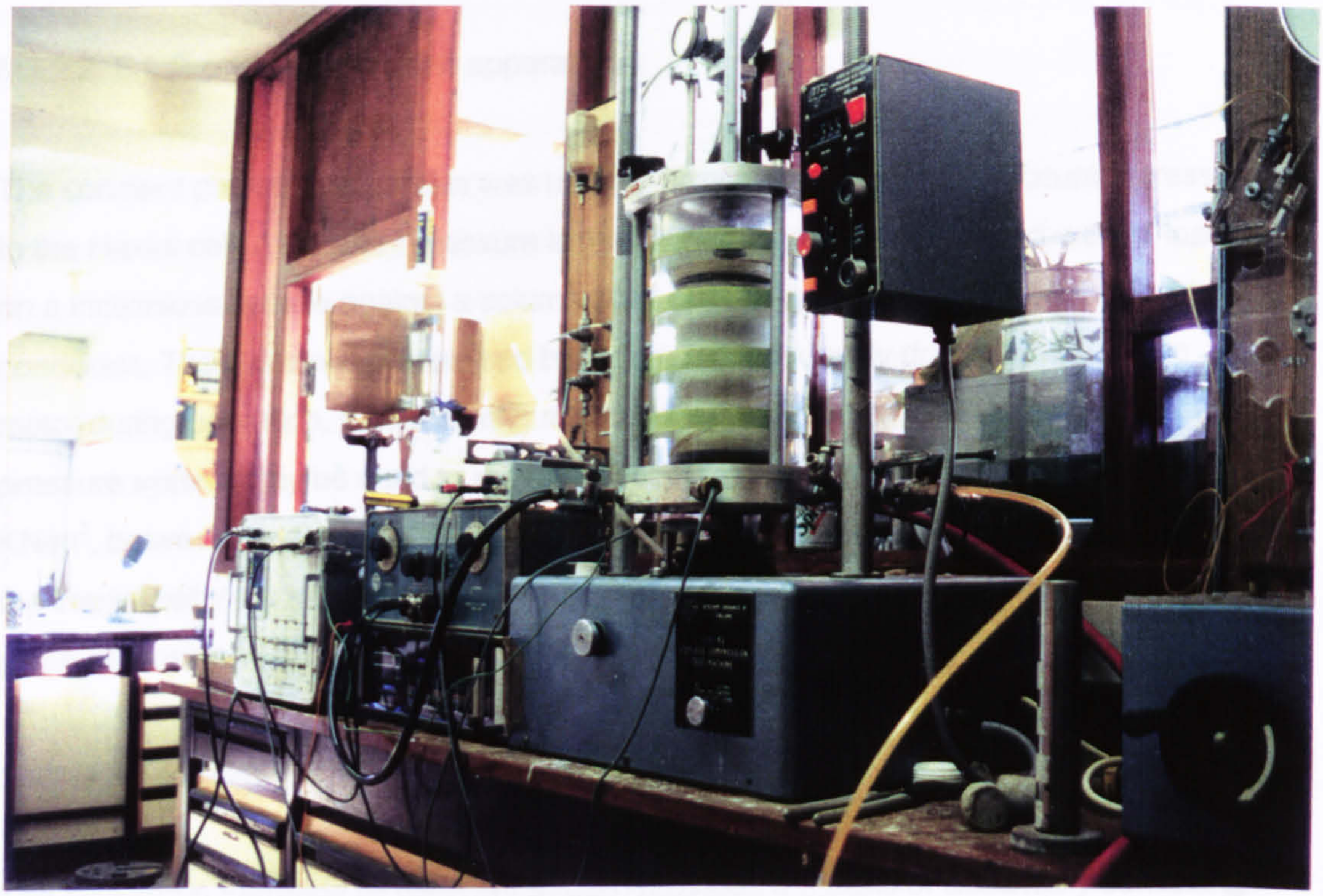

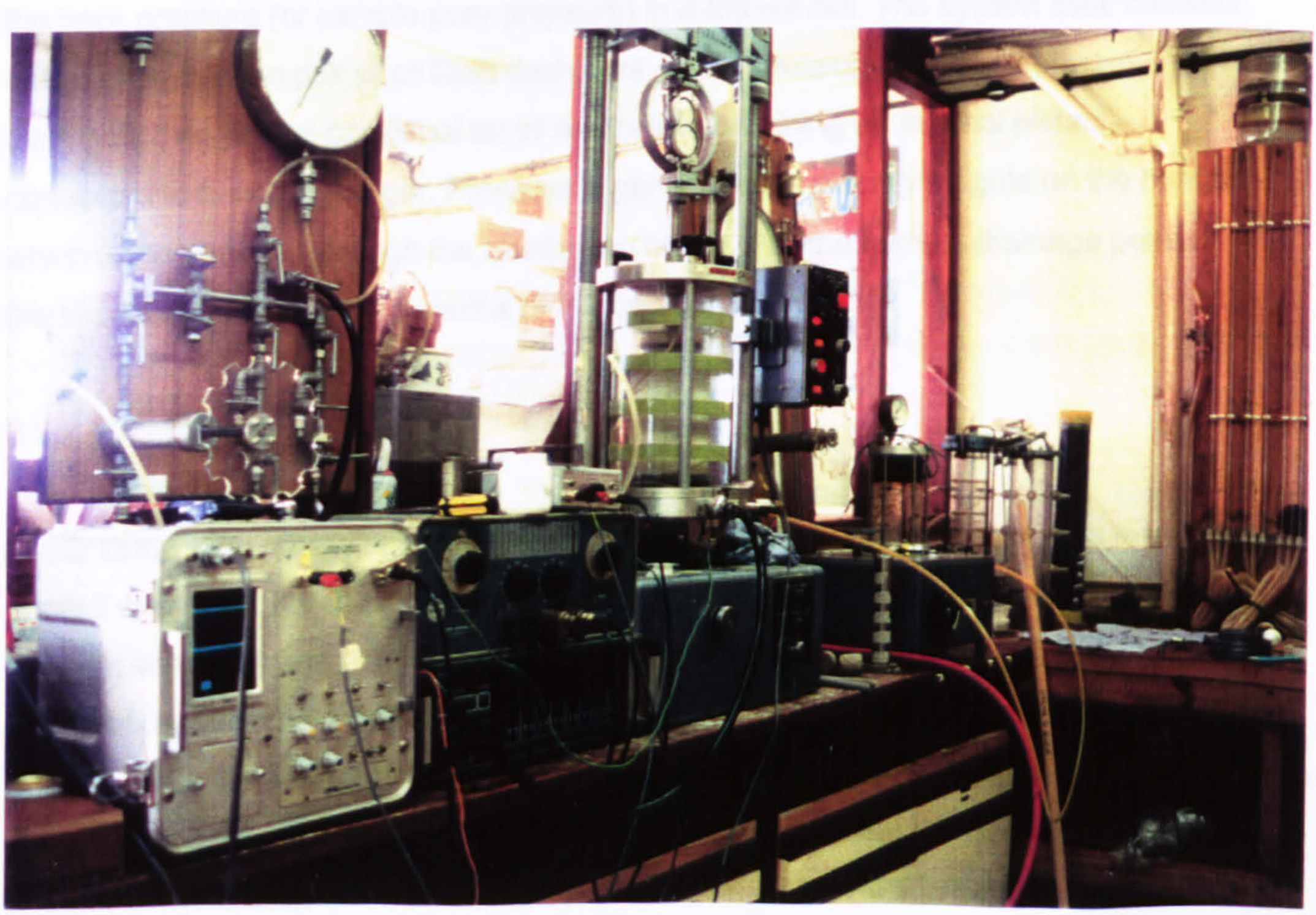

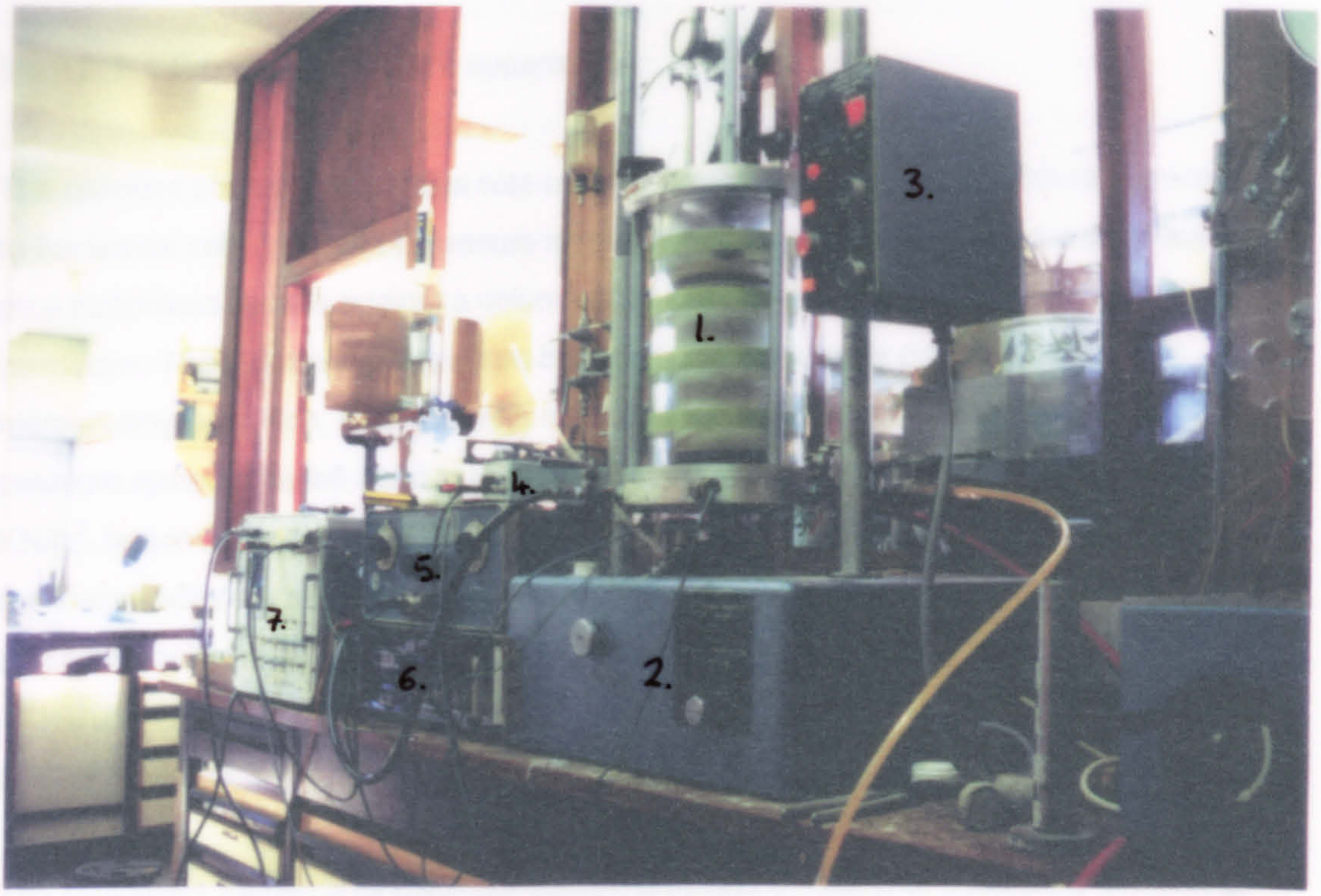
1.
2.
3.
4.
5.
6.
7.

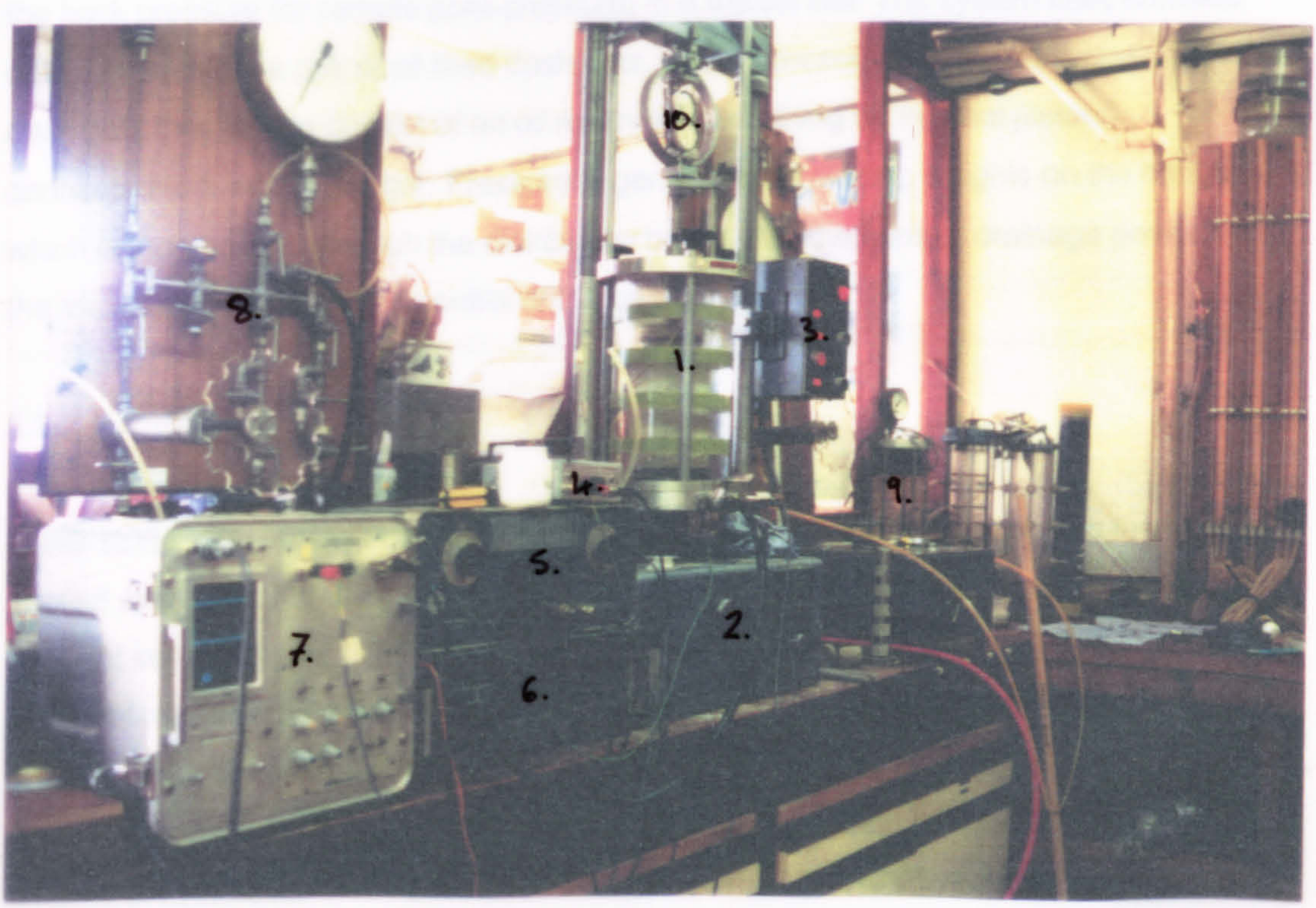
1.
2.
3.
4.
5.
6.
7.
8.
9.
10.

5.3.2.2. E.L.E constant pressure apparatus.

The constant pressure apparatus was used to provide a constant and accurate pressure to the triaxial cell. A constant pressure is maintained by balancing a 'dead-weight' load on a frictionless spindle against a column of oil operating under continuous feedback conditions. The system is pressurised by a pump, continuously driven by an electric motor during operation, thus ensuring maintenance of the required pressure. The pressure system may be used to provide a constant pressure in increments of 10 KN/m^2, between the limits of 200 KN/m^2 and 3500 KN/m^2. The pressure is transmitted to the triaxial cell via a transparent oil / water interchange vessel and a length of flexible pressure hosing.

5.3.2.3. Wykeham Farrance oil dash pot system.

The Wykeham Farrance oil dash pot system provides a means of accurately controlling the back pressure (or sample pore-pressure) in a triaxial cell. The system itself consists of two main parts: a pair of oil filled dash pots, and a pressure distribution board. The dash pots themselves consist of an oil reservoir, containing an internal piston, connected to a weight hanger. Pressure is generated by placing weights on the hanger, which is then passed through the distribution board, into the sample drainage ports of the triaxial cell, thus allowing control of the back pressure.

5.3.2.4. Calibrated Proving Rings.

In this study, high-tensile steel calibrated proving rings were used to measure the applied axial load. Three different proving rings were used for this purpose, each with different sensitivity and different maximum safe load characteristics. Upon loading, ring deformation was measured with a dial gauge, which was then used to the indicate applied stress via a suitable proving ring calibration. The stress - strain relationships resulting from a typical calibration are generally linear in nature, but display a certain amount of hysteresis.

In this study, calibration of the individual proving rings was achieved by first filling an empty pressure cell with distilled water. The proving ring was then fitted to the top beam

and carefully located on the loading ram. A series of cell pressures were then applied (in the range 200 -1000 kPa) and the displacement of the proving ring measured. Combined with a knowledge of the loading ram diameter, these data were then used to calculate the proving ring constant, which allows proving ring deformation to be directly related to applied stress (Figure 5.3).

In all the triaxial tests performed in this study, the axial load applied to the specimen was transmitted via a ram passing through a bush in the top of the cell. Any friction in this bush will cause errors when the axial load in the specimen is calculated. In the case of these experiments both the bush and ram were smooth and were well lubricated with high quality lithium based bearing grease. Any friction arising between the ram and the bushing could only arise as a result of lateral forces pushing the ram against the bushing. These lateral forces may arise from a non-uniform deformation of the test specimen itself, or from any slight mis-alignments in the loading system. Friction of this type may cause an error of between 1% & 3% of the axial load for most loading ranges. However, Bishop & Henkel (1964) conclude that

> '....for most commercial and research work, the simplicity of the apparatus is more important than the elimination of the errors of the magnitudes mentioned above.....'.

More modern triaxial apparatus tends to utilise a load cell mounted inside the triaxial cell, between the sample and the loading piston, which measures the actual load applied to the sample, thereby eliminating frictional problems.

5.3.2.5. Pore-pressure transducer.

Pore-pressure was measured using a Soil-tech pore-pressure transducer linked to an 8 channel digital display unit. The transducer itself consisted of a small flexible diaphragm, mounted in a small open ended chamber. Mounted on the back face of the diaphragm is a strain gauge. Upon the application of pressure the diaphragm deforms, causing the strain gauge to produce an electrical output directly proportional to the amount of deformation. This electrical output is then displayed on a suitable display unit, which can then be calibrated to display values of absolute pressure.

Before each test, the transducer was calibrated to ensure the recorded pore-pressures were accurate. This was achieved by applying a known pressure from the constant pressure apparatus to the transducer, and adjusting the digital display until the two values agreed. The pressure was then changed and the process repeated. Finally a 200 - 1000 - 200 kPa pressure loop was performed to check the calibration. A spreadsheet based regression analysis of the data was subsequently performed to further statistically check the calibration (see Figure 5.4). Pore-pressures calibrated in this way may be regarded as accurate to around ±2 kPa.

5.3.3. Geophysical apparatus.

For the measurement of seismic S-wavevelocity, the following apparatus and electronic instruments were utilised:

1. two geophysically instrumented Wykeham Farrance low pressure triaxial cells; initial sample diameters 50mm & 100mm;
2. Oyo Corporation New Sonic Viewer, model 5217A;
3. Kemo Ltd, variable gain amplifier and filter, model GB2;
4. Krohn-Hite filter, model 3100.

The above items / instruments are described in more detail below.

5.3.3.1. Geophysically instrumented triaxial pressure cells.

Two specially adapted triaxial cells were used in this study for simultaneous geotechnical-geophysical measurements. Both were equipped with shear wave 'bender' transducers as described below.

5.3.3.1.1. Small triaxial cell.

The small triaxial cell was the first of two triaxial cells to be used in this study; its developmental history is described by Schultheiss (1983). This cell is based upon a standard Wykeham Farrance low pressure triaxial cell, with a 38.1mm base and modified to take a sample of initial dimensions 50.8mm diameter by 101.6mm length. Compressional (P-wave) and shear (S-wave) transducers were mounted in the top and

bottom end platens of the cell, these being machined from perspex. The bottom platen acted as an adapter, fitting over the 38.1mm base of the cell. Each cap contained a centrally-mounted P wave transducer (not used in this study), and an off centre mounted, series connected, shear wave bender transducer, protruding around 10mm from the platen.

While the use of this cell allowed valuable experience to be gained in sample preparation, saturation and subsequent testing, the biggest disadvantage of the cell proved to be due to its small size. Because S-wave velocities are calculated between the tips of the bender transducers, the effective path length of the sample is unavoidable reduced in length to approximately 80mm. This short travel path has the effect of reducing the accuracy of measurement, simply because of the reduced travel time (i.e. a small error in travel time determination could lead to a potentially larger error in the calculated velocity). In practice, the data collected using this particular cell tended to be extremely 'noisy ', due to two main reasons:

1. P-waves also generated by the bender transducer masking the onset of the S-wave;
2. the 'near-field' component of the signal, also generated by the bender transducer.

Both theoretical and parametric studies (Viggrani & Atkinson, 1995) have shown that this near field component of the waveform, may mask the first arrival when the distance between the source and receiver are in the range 0.25 - 4 wavelengths, where wavelength (λ) can be estimated from:

$$\lambda = {}^{V_s}/_{f} \qquad (5.4).$$

where, f = mean frequency of the received signal.

Assuming a V_s = 200 m/s and a frequency of 7000 Hz (fairly typical values for a bender transducer generated S-wave in sand), λ = 28.6 mm. Therefore a minimum required path length to avoid these complex effects, should be at least 114mm.

Possibly the simplest method to reduce both these effects is to increase the effective path length, by employing a larger sample.

5.3.3.1.2. Large Triaxial cell.

This particular cell was originally developed during 1979 / 80 as a joint venture between P. J. Schultheiss, from UWB, P. Jackson and R. Baria, from the Engineering Geology unit at Institute of Geological Sciences and P. Strachan from the University of Newcastle. The developmental history and associated results are described in more detail by Schultheiss (1983) and Bates (1989). This cell is based on a Wykeham Farrance low pressure triaxial cell designed for testing samples of 100mm initial sample diameter (Figure 5.5). Within this study the sample height was initially 200mm to obtain the 2:1 length to diameter ratio needed to avoid any end restraint effects. The bottom platen contained a centrally mounted P-wave transducer and an off-centre, series connected shear wave bender transducer, protruding approximately 10mm into the sediment. The platen was bolted firmly to the metal base of the cell and sealed with a rubber 'O' ring. The top cap was of a similar construction, also containing a series mounted bender transducer, although in later experiments the P wave transducer was removed and replaced with an epoxy 'blank'. Specially drilled and sealed holes in the base plate allowed the signal wires from the transducers to be connected with the external shear wave measurement system.

In the event, the longer path length provided by the larger sample dimensions led to a superior signal quality and an improved resolution of the first arrival time of the shear wave. This was essentially due to:

1. increased time separation of the P & S-wave, by virtue of their different velocities;
2. a reduction in the onset masking effects of the 'near-field' components of the waveform.

5.3.3.2. Shear wave bender elements.

The bender transducers used in this study were constructed of the ceramic PZT-5B and were supplied by Morgan Matroc Limited, Transducer Products Division, Southampton. The transducers themselves were supplied in sheets of parallel or series poled ceramic, measuring approximately 45mm x 70mm x 1.5mm, and were prepared in the following way:

1. A small diamond tipped dentists circular saw, mounted on a milling machine, was used to cut the transducer from the larger sheet supplied by the manufacturers. Initial size of the transducer was approximately 10.5mm x 15mm x 0.5mm.
2. The signal wires were then carefully soldered to each face of the transducer.
3. The transducer and attached wires were then placed into a well greased perspex sample mould (Figure 5.6) and held in place using a pair of plastic pins, ensuring the transducer was held squarely and centrally.
4. An epoxy resin, composed of araldite (MY753) and hardener (HY951), was then poured into the sample mould. This particular combination of araldite and hardener was chosen because of its very low viscosity. Both products were supplied by Robnor Robnorganic Systems Limited, authorised distributors for Ciba-Geigy Plastics. The resin was carefully warmed using a small heat gun, to decrease viscosity and further assisting the removal of any small air bubbles.
5. After 24 hours, the transducers were carefully broken out of the mould and any excess epoxy removed. The circular holes in the epoxy coating, left by the plastic holding pins, and any air bubbles in the epoxy 'skin', were then filled using the same araldite / hardener combination. After both sides of the transducer had been treated, it was further shaped using a fine grade emery cloth. Once the transducer reached its required dimensions, the element was dipped into a small amount of resin, which further helped prevent water penetration. Final transducer dimensions were approximately 3mm x 12.5mm x 18.5mm.

The potted transducer was then cantilever mounted in the triaxial platen, again using epoxy resin. The signal wires were connected to the external signal cable, and the finished platen was assembled and sealed using bathroom silicone sealant and epoxy resin. Finally, before testing began, the porous stone was fixed in place. The slot through which the bender transducer penetrates through the stone was filled with Blu-Tak™ to prevent any sand grains inhibiting transducer movement.

Both parallel and series poled transducers were prepared using the above method. However, simple experiments on a small sample of potters clay suggested that a series - series arrangement proved equally satisfactory as the generally recommended series - parallel arrangement. The series - series arrangement also proved easier to fabricate due to a simpler wiring arrangement.

5.3.3.3. Oyo Sonic Viewer.

The Oyo Sonic Viewer is an oscilloscope designed specifically for measuring seismic velocities in rocks and sediments. Its main features include: a built in cathode ray tube, a small thermal printer, two channel memory, variable input & output gain, variable sampling time, and signal stacking and filtering facilities. The Sonic Viewer was used to both generate the signal pulse and receive the shear wave signal. The signal pulse consists of a 200 volt spike which induces resonance in the bender transducer, ensuring maximum signal strength. The resonant frequency of the bender depends upon the transducer dimensions and sediment stiffness. All travel time determinations using this system were based upon a visual velocity pick from the shear wave trace displayed on the cathode ray tube. Selected sample records were also recorded using the thermal printer. No data were recorded digitally.

5.3.3.4. Filters and amplifiers.

Although the Sonic Viewer has both variable input and output gains, signal stacking features and a simple high-cut filter, it was found that, especially with the larger triaxial cell, some form of external amplification was required to boost the received signal. Signal amplification was performed using a Kemo model GB2, variable gain amplifier. The signal was typically amplified by around 30 dB. The amplifier also contained a simple high and low cut filter. These were used to 'prefilter' the signal at 1Hz low-cut and 100 kHz high-cut. The amplified and pre-filtered signal was then passed to the Krohn-Hite filter for further removal of high frequencies (usually in the form of P-wave 'noise'). The signal typically was filtered at high-cut frequency of between 16 & 19 kHz.

5.4. Description of laboratory procedures.

The laboratory procedure used in this study may, for an individual sand sample be divided into three separate procedures: sample preparation, shear wave measurement and triaxial testing, each occurring consecutively.

5.4.1. Sample preparation.

Three commonly used procedures may be used for the preparation of sand samples for laboratory testing: moist tamping (moist placement or wet tamping), dry deposition, and water deposition (Ishihara, 1993). The basic requirements for all these techniques are to:

1. obtain homogeneous samples with a uniform structure,
2. create samples with a very high void ratio (ideally e_{max} or greater), to ensure a contractive response upon shear,
3. allow preparation of samples over a wide density range.

Each different sample preparation method may result in different initial sediment fabrics which can dramatically affect the cyclic strength of a material. In contrast, the ultimate, or steady state appears to be little affected by initial sediment fabric because of the generally large deformations involved (Robertson *et al.*, 1995). Using the dry deposition and water deposition sample preparation methods it is not generally possible to produce samples loose enough to give a strongly contractive response under shear. The moist tamping technique can however, provide samples of both dilative and contractive characteristics, depending on the initial void ratio at the time of sample preparation. Using this technique it is even possible to prepare samples with an extremely loose structure which may even exceed the calculated value of e_{max}, resulting in an extremely contractive response. This situation (i.e. extremely loose sediment structure, with local void ratios exceeding e_{max}) may also occur in certain sedimentary environments, in particular deltaic environments, although direct evidence for this is extremely hard to gather because of the near impossibility of sampling such loose sediments. However, it is for the reasons of ease of preparation and relative homogeneity that that the moist tamping sample preparation technique is possibly the most commonly used preparation method for the laboratory study of liquefaction phenomena. It was for the same reasons that this method was selected for the preparation of samples used in this study.

Essentially the method involved the following steps:-

1. Five or six equal, pre-weighed, oven-dried portions of sand were mixed with distilled water to a moisture content of about 5%, producing a characteristic 'cohesive' type of sand behaviour.
2. A rubber membrane was then stretched over the triaxial base platen, and secured with two rubber 'O' rings. The three sections of a split part sample former were then carefully placed over the lower platen, making sure not to trap any of the membrane between the mould sections.
3. The membrane was then stretched taut inside the split mould former and attached to the top of the mould. To ensure that the membrane remained tightly against the inside surface of the sample former, a small vacuum was maintained between the inside face of the former and the outside surface of the membrane. The vacuum was provided by a small vacuum pump, and the air was evacuated from the top of the sample former via a purpose drilled hole in each section of the former. The butt-joints of the sample mould were sealed with vaseline preventing excess air migration.
4. The orientation of the bender transducer on the bottom platen was then noted prior to assembling the triaxial cell.
5. One of the pre-weighed portions of moist sand was then carefully added to the mould and tamped to a pre-determined height using a small, flat bottomed tamper. This procedure was then repeated for the remaining sub-samples. The amount of tamping energy applied to each sub-sample determined the initial void ratio after preparation. Loose samples were prepared by using only a small amount of gentle tamping, while denser samples required more effort, usually in the form of an increased number of individual tamps.
6. The top platen was then carefully placed on top of the sample, and the rubber membrane sealed with two more 'O' rings, remembering to carefully align the top bender with the bottom platen orientation.
7. A small vacuum (of around 30-40 kPa) was then applied to the sample, allowing the split-former to be dismantled.
8. The pressure cell was then placed over the sample and secured to the base plate (ensuring no sand grains were attached to the main 'O' ring) and filled with water. This was then pressurised to the minimum confining pressure of 200 kPa.
9. To displace the air in the sample, carbon dioxide gas was then percolated through the sample from bottom to top, at a pressure of around 20-30 kPa for approximately 20 minutes. Waste CO_2 was bubbled through a large drum of water.

10. Distilled water was then flushed through the sample at a similar back pressure of around 20 kPa, until no further CO_2 bubbles were observed exiting the sample.
11. The top drainage tap was then closed and the sample confined to a pressure of 300 kPa. The back pressure was then raised to a pressure of 100 kPa and allowed to settle. This process was then repeated in steps of 100 kPa, until the cell pressure reached around 1000 kPa. The high back pressures, typically on the order of 800 kPa, ensured a high degree of saturation (see below).
11. Once a high level of saturation had been confirmed, the sample was ready for subsequent testing.

Been & Jefferies (1985) note that samples prepared using the method described above tend to contain thin looser bands between each tamped layer. In addition, denser samples tended to be more uniform than their looser counterparts. For a carefully prepared sample using the method described above they found the sample uniformity to be typically around ± 0.01 in terms of void ratio. In addition, they noted that as the thin looser layers are horizontal, their effect on triaxial shearing behaviour was of a small magnitude.

5.4.1.1. Sample saturation.

In triaxial testing it is vital to ensure that a sample is fully saturated. In undrained tests complete saturation is important to maintain the 'constant volume' assumption (a partially saturated sample may change volume, and hence void ratio, under a compressional load). Conventionally, high degrees of saturation are achieved by using large back pressures to force any gas into solution. In the case of this study, any air in the sample was displaced with more soluble CO_2. Once the cell pressure and back pressure reached the desired level, the bottom drainage valve was closed and Skempton's 'B' value calculated. This parameter is a very useful tool in indicating the degree of saturation of specimens in a triaxial cell, and was measured by simply raising the cell pressure by a known pressure, typically 40 kPa (Δ cell pressure), and recording the associated change in pore-pressure (Δ pore-pressure). The sample 'B value' was then calculated using:

$$B = \frac{\Delta \, Cell \, Pressure}{\Delta \, Pore \, Pressure} \qquad (5.5).$$

For a perfectly saturated sample, B = 1. For the purposes of this study the sample was regarded as being adequately saturated once the B value was greater than, or equal to 0.95 (see Figure 5.7).

5.4.2. Shear wave measurements - 'Geophysical technique'.

The measurement of S-wave velocity took place once the sample had been fully saturated and consolidated. V_s was then measured over a range of effective stresses. This is in contrast to the method proposed by (Robertson *et al.*, 1995), who simply measured the S-wave velocity during consolidation, prior to triaxial testing. The method proposed in this study consists of two parts, system calibration and shear wave measurement and is described in more detail below (system layout is illustrated in Figure 5.8).

5.4.2.1. System calibration.

Before the system described in Section 5.3.3. above was used to routinely measure the S-wave velocity behaviour of the sample, the system had to be calibrated. This was in order to quantify any time delays which may exist in the system. In the case of P-waves, this is a simple task, and involves measuring the P-wave velocity through water at various different path lengths in the cell. A regression analysis of the resulting data allows definition of the system delay (a negative y-axis constant indicates the delay). Calibration of bender transducers is a little more difficult due to the lack a suitable reference medium. Because of this, the system delay was in fact quantified using the low amplitude P-wave which is also generated by the bender transducers. Calibration was achieved by measuring the travel time of the P-wave generated by the bender transducers at different path lengths. A regression analysis of the data was then used to quantify the system delay (Figure 5.9).

This calibration showed that the system delay using the bender transducers was 0.011 micro-seconds. For the purposes of this study this delay can be regarded as insignificant because it is several orders of magnitude below the system resolution (Sonic Viewer sampling rate when measuring shear waves is 4.0 microseconds).

5.4.2.2. Shear wave measurement technique.

Once sample preparation had been completed, the S-wave velocity was measured over a range of effective stresses, typically between 30 - 400 kPa. This range in effective stress may be achieved in two ways:

1. holding the cell pressure constant and changing the back pressure, or
2. holding the back pressure constant and changing the cell pressure.

The advantage of the first method is that it allows close monitoring of changing pore-pressures via the pore-pressure transducer and hence accurate calculation of the effective confining stresses. The disadvantage of the second method is that due to the type of apparatus used there are only a certain number of possible steps cell pressure. In addition, this method involves the use of very high cell pressures (up to 1500 kPa), close to the upper limit of the triaxial cell and increasing the risk of water migration into the bender transducers.

A disadvantage common to both techniques is that, as the sample is essentially drained during changes in back pressure, small changes in void ratio may occur, resulting in a slight hysteresis effect in terms of void ratio during loading & unloading. However, this variation will probably be relatively insignificant in magnitude since the sample has already undergone its most significant change in volume during the previous consolidation stage of the procedure. On the basis of the various advantages and disadvantages described above it was decided to use the former method for the majority of testing.

The shear wave travel time at a specific effective stress was measured using the following procedure:

1. The bender transducer at the bottom of the sample was exited with a 200 volt spike pulse from the Sonic Viewer, generating a shear wave pulse travelling upwards through the sample.
2. The shear wave signal was received by the bender transducer at the top of the sample. This signal was then amplified, initially filtered at 100 kHz using the Kemo amplifier, and then filtered again at approximately 16 kHz using the Krohn-Hite filter

before being displayed on one of the two available channels on the cathode ray display screen of the Sonic Viewer.

3. Another shear wave was generated by the same procedure. However the received signal was this time filtered at approximately 19 kHz using the Krohn-Hite filter and displayed on the other available display channel.

4. The travel time was then determined based upon a visual analysis of the signal onsets of both signals. This 'dual filter' procedure was intended to some extent to quantify any changes caused by the high-cut filtering on the received waveform.

5. Once the travel time had been determined, the back pressure and hence the effective stress was changed, by either removing or adding weights onto the dash pot weight hangers. Once the back pressure settled (usually after ~ 1 minute), the whole process was repeated at the new value of effective stress.

Generally, around two to three unload - load loops were performed over a range of effective stresses of the order of 40 kPa to 400 kPa. Once this sequence had been completed, the cell pressure and pore-pressure were lowered in steps of 100 kPa in the reverse of the method described above. Once the cell pressure reached 200 kPa, a small negative pore-pressure of around - 40 kPa was applied to the sample. The remaining cell pressure was then carefully released and the pressure cell drained of water. The negative back pressure ensured maintenance of sample shape during this stage. The pressure cell was then removed and the sample dimensions (specifically sample height & circumference) measured to an accuracy of ± 0.25mm. This allowed both the subsequent calculation of both the S-wave velocity (derived from the sample length) and void ratio (derived from the sample volume).

The recorded pore-pressures, cell pressure, travel times and path length were entered into a worksheet designed by the author and running in 'Quattro™', which calculated void ratio, effective stress, and S-wave velocity , and presented in tabular form in Table 5.3. Void ratio was calculated using Equation 5.4 above, while S-wave velocity was calculated using:

$$Vs = \frac{Sample\ length\ -\ transducer\ penetration}{Travel\ time} \qquad (5.6).$$

where, distance units are in metres and time is measured in seconds and,
transducer penetration (in the large triaxial cell) = 18.00 mm.

S & P wave testing on a sample of Newborough beach sand, with 5% Kaolinite.
Date:- 8.2.95. (morning)
Filename:- smple2vs.wb1 ...test No. 8.

Weight of sample (g):-	2520.00
Initial height of sample (mm):-	199.50
Final height of sample (mm):-	199.50
Radius of sample (mm):-	49.82
Area of sample:-	76.87
Volume of sample:-	1533.52
Specific Gravity:-	2.66
Void ratio:-	0.619
Cell pressure (KPa):-	1000
P-wave delay time (nS):-	
Bender offset (mm):-	18.00

Regression Output:

Constant			1.64
Std Err of Y Est			0.01
R Squared			0.99
No. of Observations			26
Degrees of Freedom			24
		b	*a*
X Coefficient(s)		0.30	43
Std Err of Coef.		0.0057	
e min:-	0.619		
e max:-	0.930		
Dr (%):-	100		

Transducer reading	Back pressure (KPa)	Effective stress (KPa)	Travel time (uS)	Velocity. (m/s).	Log effective stress	Log Vs.	Regression curve
965	965	35	1424	127	1.54	2.11	127
955	955	45	1312	138	1.65	2.14	138
948	948	52	1232	147	1.72	2.17	144
939	939	61	1192	152	1.79	2.18	151
921	921	79	1108	164	1.90	2.21	163
891	891	109	992	183	2.04	2.26	180
880	880	120	972	187	2.08	2.27	185
863	863	137	956	190	2.14	2.28	193
850	850	150	944	192	2.18	2.28	198
832	832	168	888	204	2.23	2.31	205
824	824	176	912	199	2.25	2.30	208
801	801	199	840	216	2.30	2.33	216
796	796	204	868	209	2.31	2.32	217
765	765	235	808	225	2.37	2.35	227
765	765	235	812	224	2.37	2.35	227
733	733	267	776	234	2.43	2.37	236
729	729	271	784	232	2.43	2.36	237
718	718	282	772	235	2.45	2.37	240
709	709	291	740	245	2.46	2.39	242
699	699	301	732	248	2.48	2.39	244
678	678	322	724	251	2.51	2.40	249
669	669	331	720	252	2.52	2.40	252
650	650	350	704	258	2.54	2.41	256
632	632	368	680	267	2.57	2.43	260
624	624	376	676	268	2.58	2.43	261
608	608	392	664	273	2.59	2.44	265

Table 5.3. Example shear wave interpretation spreadsheet.

Once the effective stress - S-wave velocity behaviour of the sample had been determined, further spreadsheet analysis allowed the fitting of a curve through the data (see Section 6.2.2.3.).

5.4.3. Triaxial measurements - 'Geotechnical technique'.

The geotechnical section of the laboratory technique essentially involved a series of consolidated, undrained, monotonic triaxial tests. As described above, the consolidated undrained triaxial test involves the consolidation of a sample under drained conditions, followed by simple, undrained compression, during which the induced strain, stress, and pore-pressures are recorded. The data collected can then be used to calculate the peak shear strength and, in the cases of loose sands, the steady state shear strength. Traditionally, stress controlled triaxial tests are used to define the steady state strength, however more recent research has shown that both stress controlled and strain controlled tests may be satisfactorily used (Been & Jefferies, 1985). All tests in this study were strain controlled, and the sample was strained at 1% / minute.

An initial aim of this study was to directly measure V_s at steady state, but a number of practical factors prevented this. These included:

1. The definition of steady state, as described by Poulos (1981), requires that the sample be deforming 'at constant volume, constant shear stress and constant velocity'; the measurement of V_s between two moving platens would be very difficult to achieve with the apparatus used in these experiments.
2. Noise created by the individual grains moving past each other in the 'flow structure', associated with flow liquefaction, would also create large amounts of ambient noise, effectively masking any shear wave signal.
3. The triaxial drive motor creates a large amount of electrical noise, interfering with the Sonic Viewer and in turn strongly affecting signal quality.
4. Measuring V_s at 'steady state' once the test had been halted also proved impossible because a significant element of elasticity in the whole triaxial apparatus generally ensured a significant change in the stress conditions (in terms of the effective stress and deviator stress) once shearing halted.

For these reasons, it was chosen to define V_s at steady state based upon an analysis of the shear wave data collected prior to the triaxial test, and the mean confining pressure reached at steady state. This involves the assumption that changes in the various stress components (i.e. σ_1', σ_2' & σ_3') during shear have little or no effect on V_s (V_s was measured under isotropic conditions, while the effective confining stress at steady state is anisotropic in nature). Although there appears to be some conflicting evidence in the literature on the effects of stress ratio on V_s or G, (see discussion in Section 4.2.1) this assumption may be regarded as valid for the relatively small range of effective stresses encountered in these experiments.

5.4.3.1. Triaxial testing technique.

Once the sample dimensions had been measured, the pressure cell was placed over the sample and the cell once again filled with water. The proving ring was mounted on the triaxial crossbeam and aligned to fit the loading ram. The strain dial pedestal was also fitted to the top of the cell and roughly aligned with the strain dial. Two hardened steel safety rods were fitted to the top of the cell and located in two eyes mounted on the crossbeam. These rods prevent the cell jumping from the triaxial machine during strain. A confining pressure of 200 kPa was then applied to the sample, which was then re-consolidated in the manner described above. The pore-pressure transducer was calibrated. Once the cell pressure reached 1000 kPa and the back pressure was of the desired magnitude, the drainage tap was shut and the B value determined. If the sample was shown to be saturated, the height of the base platen was then adjusted so that the loading ram just rested upon the top sample platen. The proving ring dial, the strain dial readings, and the pore-pressure was then noted. Finally the strain rate was adjusted to allow straining at 1% / min.

The test was then allowed to run, with observations of stress and pore-pressure being made every 0.5mm. Once the test was completed, the back pressure and cell pressure were released, the pressure cell drained of water, and the sheared sample removed. The data were then entered into a spreadsheet which allowed calculation of the following parameters:- pore-pressure change, change in length, strain, axial load (deviator stress), major principle stress, minor effective stress, major effective stress and the effective confining stress. An example spreadsheet is shown in Table 5.4. The basis

TRIAXIAL COMPRESSION TESTING.

Date:- 8.2.95. (morning).

Sample Location:-	Newborough	Mass of sample (g):-	2520.00
Sample Depth:-		Initial volume (cm^3):-	1533.52
		Specific gravity:-	2.66
Proving Ring Number:-	3098	Void ratio:-	0.619
Rate of strain (mm/min):-	1.995	Porosity (%):-	38.2
Cell Pressure (K):-	1000		
Back Pressure (KPa):-	802	Skempton 'B' value:-	0.9
Effective Stress (KPa):-	198		
Initial length (mm)	199.50	Strain Dial Calibration:-	0.01 mm/Increment.
Radius of sample (mm).	49.82	Stress Dial Calibration:-	4.56 N/Increment.
Initial area of sample (cm^2):-	76.87		

Strain Dial Reading	Stress Dial Reading	Transducer reading.	Pore-Pressure KN/m^2	Pore-pressure change	Length of sample (mm).	Change in lgth. (mm).	Strain (%).	X-sectional area (m^2)	Axial load KN/m^2	Major principal stress	Minor effective stress	Major effective stress	Effective confining stress
0	0	802	802	0	199 50	0.00	0.00	0.007687	0.00	1000.0	198.0	198 0	198.00
50	60	805	805	3	199.00	0.50	0.25	0.007706	35.50	1035.5	195.0	230 5	206.83
100	360	842	853	51	198.50	1.00	0.50	0.007726	212.49	1212.5	147.0	359.5	217.83
150	600	842	842	40	198.00	1.50	0.75	0.007745	353.26	1353.3	158.0	511.3	275.75
200	750	828	828	26	197.50	2.00	1.00	0.007765	440.46	1440.5	172.0	612.5	318.82
250	880	812	812	10	197.00	2.50	1.25	0.007784	515.50	1515.5	188.0	703.5	359.83
300	1000	796	796	-6	196.50	3.00	1.50	0.007804	584.30	1584.3	204.0	788.3	398.77
350	1100	780	780	-22	196.00	3.50	1.75	0.007824	641.10	1641.1	220.0	861.1	433.70
400	1180	766	766	-36	195 50	4.00	2.01	0.007844	685.97	1686.0	234.0	920.0	462.66
450	1260	752	752	-50	195.00	4.50	2.26	0.007864	730.60	1730.6	248.0	978.6	491.53
500	1340	739	739	-63	194.50	5.00	2.51	0.007884	775.00	1775.0	261.0	1036.0	519.33
550	1420	725	725	-77	194 00	5.50	2.76	0.007905	819.16	1819.2	275.0	1094.2	548.05
600	1490	712	712	-90	193.50	6.00	3.01	0.007925	857.32	1857.3	288.0	1145.3	573.77
650	1570	698	698	-104	193.00	6.50	3.26	0.007946	901.02	1901.0	302.0	1203.0	602.34
700	1640	685	685	-117	192.50	7.00	3.51	0.007966	938.75	1938.8	315.0	1253.8	627.92
750	1710	671	671	-131	192.00	7.50	3.76	0.007987	976.28	1976.3	329.0	1305.3	654.43
800	1790	657	657	-145	191.50	8.00	4.01	0.008008	1019.29	2019.3	343.0	1362.3	682.76
850	1860	646	646	-156	191.00	8.50	4.26	0.008029	1056.39	2056.4	354.0	1410.4	706.13
900	1940	632	632	-170	190.50	9.00	4.51	0.008050	1098.94	2098.9	368.0	1466.9	734.31
950	2010	620	620	-182	190.00	9.50	4.76	0.008071	1135.60	2135.6	380.0	1515.6	758.53
1000	2090	606	606	-196	189.50	10.00	5.01	0.008092	1177.69	2177.7	394.0	1571.7	786.56
1050	2160	594	594	-208	189 00	10.50	5.26	0.008114	1213.92	2213.9	406.0	1619.9	810.64

Table 5.4. Example triaxial test interpretation spreadsheet.

of these calculations may be found in any standard geotechnical text book (*e.g.* Smith, 1990), and will not be repeated here.

5.4.3.2. Membrane penetration.

In any triaxial test, where a sample is enclosed within a membrane and is subjected to a confining pressure, there is some element of membrane penetration. During a typical consolidated, undrained triaxial test on a loose contractive sand, the membrane will tend to push outwards as the effective confining pressure is decreased in response to the build-up in pore-pressure. Consequently, some volume changes and drainage occur, with a corresponding decrease in void ratio. The void ratio changes associated with this type of membrane penetration can be regarded as a function of mean grain size and effective confining pressure. In an analysis based upon a sand with a grain size of 0.21 mm, Konrad (1990b) found that over a pressure range of 2,000 kPa, the change in void ratio would be on the order of 0.1%; for a sand with a mean grain size of 0.175mm the effect was even less marked. Because of the very small magnitude of these volume changes, membrane penetration effects were not corrected for in this study.

5.5. Analysis of system error.

The discussion of system error can, once again, be divided into two sub-sections: geophysical testing and geotechnical testing. The system error associated with each of these sections is discussed below.

5.5.1. Errors associated with the measurement of shear wave velocity.

Possibly the biggest single source of error when attempting to determine the S-wave velocity of a material in the laboratory is related to the difficulty in defining the precise signal onset time. This source of error is common within geophysical techniques which require the determination of a travel time from a signal that usually contains some element of random noise. Apart from the possibility that the 'wrong' onset may be selected, a variety of other factors, such as high noise levels, filtering effects, and poor signal quality, may contribute to making the absolute error associated with a particular measurement very difficult to quantify. Because of these reasons, for the purposes of this study, only the identifiable and measurable sources of error have been quantified.

From a simple analysis of the velocity travel time equation (Equation 5.7), two possible sources of systematic errors in the shear wave measurement system may be identified:

1. travel time determination errors,
2. errors associated with the measurement of the path length.

5.5.1.1. Travel time errors.

The systematic error associated with the determination of the precise travel time in this study is controlled to a large extent by the resolution of the Sonic Viewer. For the purpose of these measurements, the sampling rate of the Sonic Viewer was set at 4 microseconds. Assuming a high quality signal, the error associated with picking an accurate onset time were ± 4 micro-seconds. In terms of velocity, assuming a 180mm travel path and a velocity of 200 m/s, this represents an error of ± 1 m/s. Maximum measured velocities in this study were in the order of 350 m/s, giving associated error of ± 3 m/s. In this worst possible case, this represents an error of ± 0.9%.

5.5.1.2. Travel path measurement errors.

The travel path was measured with a steel ruler to an accuracy of ± 0.25 mm. Although more precise measurements could have been made, the author considered that this represented the limit to which path length could be resolved using this particular method. In terms of velocity, assuming a 180 mm travel path, and a velocity of 200 m/s, an error in distance of ±0.25 mm represents an error of ± 0.3 m/s. A velocity of 350 m/s would have an associated error in velocity of ± 0.5 m/s. Expressed as a percentage, this represents a maximum error of ± 0.14%.

In the worst case it appears that the physical, instrumental limitations of the system therefore account for a maximum possible error of ±1.04% over the range of velocities measured during laboratory testing. This represents an error of ± 2.08 m/s at a nominal velocity of 200 m/s.

5.5.2. System error; geotechnical measurements.

The main measurement parameters associated with the triaxial test in this study are void ratio, strain, deviator stress and the effective confining stress. The errors associated with each of these parameters are discussed below.

5.5.2.1. Void ratio.

The void ratio of the sample was determined based upon a knowledge of the dry weight, the specific gravity and the volume of the sample (see Equation 5.4). Dry sample weights usually of the order of 2200g were measured using a digital balance to an accuracy of ±0.1g; any weighing error is insignificant in subsequent void ratio calculations. Specific gravity was determined to four decimal places, as according to B.S 1377: Part 2 (1990) but these are conventionally only quoted to two decimal places. The errors associated with calculating void ratios using relative densities which have been determined to four decimal places are insignificant when compared to other potential errors and may therefore be ignored. However, the biggest potential source of error when calculating the void ratio proved to be errors associated with the sample volume measurements. Sample volume was derived from measurements of sample length and circumference which were made to an accuracy of ±0.25mm. Assuming an error of ± 0.25mm in determining both the sample length and circumference, the potential systematic error associated in the calculation of void ratio is approximately ± 0.005.

5.5.2.2. Strain.

Strain was calculated using a factory calibrated strain gauge, with a resolution of 0.01 mm. For a sample of a nominal 200 mm initial length, this leads to a maximum possible theoretical error in terms of strain of 0.005%.

5.5.2.3. Deviator stress.

Once again, the determination of the absolute error associated with deviator measurements is difficult due to the slight hysteresis associated with the proving ring calibration and ram friction effects. Quantifiable systematic error associated with the system was controlled dominantly by the accuracy with which a single reading could be

made from the stress dial. In reality, during the course of a triaxial test, especially during an early part of the test, when the deviator stress changes rapidly, the accuracy with which the stress dial could be measured was ± 5 dial increments. Using Proving Ring 3098 (used in the majority of tests), this corresponds to an error of ± 22.75N. This in turn corresponds to a systematic error in the prediction of deviator stress of around ± 3 kPa.

5.5.2.4. Effective confining stress measurements.

As mentioned above, the pore-pressure transducer was calibrated before each test using the constant pressure apparatus. This calibration ensured that the transducer was probably accurate to within ± 2 kPa. As mentioned above, the effective confining stress was calculated using Equation 5.8. below:

$$p' = (\sigma_1' + 2\sigma_3')/3 \qquad (5.7).$$

Working through this equation, with the errors described above and below (i.e. effective stress, deviator stress, etc.) indicates that in terms of effective confining stress, the system has a maximum theoretical resolution on the order of ± 2.3 kPa.

5.6. Summary of laboratory methods.

The laboratory apparatus described above allowed the routine measurement of both the geophysical and geotechnical properties of four different test sands, with a relatively small amount of quantifiable systematic error. This provided the basis for the combination of shear wave measurement and the conceptual framework of steady / critical state soil mechanics, and ultimately allowed laboratory results to be applied to the field.

5.7. Field Methods - the 'Seismic Sledge'.

The major field method used in this research was based on the 'Seismic Sledge', or 'Magic Carpet', seafloor shear wave refraction system, developed at the University of Wales, Bangor over the past 7-8 years (see Davis *et al.*, 1989; Huws, 1993). This instrument, deployed from the back deck of a research vessel, was designed specifically to measure the *in-situ* geophysical parameters of surficial marine sediments, and in

particular S-wave velocities and sediment electrical properties. Additional data presented in this project was collected using other techniques, in particular SCPTU's and sub-bottom profiles, however it should be noted that none of these field data were collected by the author.

5.7.1. System description.

The Seismic Sledge essentially represents a marine version of a conventional land based shear wave refraction array, relying on techniques which have long been used for reconnaissance engineering site investigations. The complete system has the capability to measure surface sediment electrical properties, compressional wave and shear wave velocities of the upper few metres of the sediment column (see Figure 5.10 & Plate 5.2). The system as used in this study is described in more detail in a series of publications by Davis *et al.* (1989), Huws (1990) and Huws (1993) and for this reason, only a brief description of the system will be given here. The sledge, initially designed to be deployed from the University of Wales' research ship, the *R.V. Prince Madog*, is composed of three principal components:

1. a seafloor towed sledge,
2. a geophone string,
3. ship-board system.

5.7.1.1. Towed seafloor sledge.

The towed seafloor sledge represents the 'heart' of the system and consists of a hydrodynamically stable towed instrument platform constructed mainly from galvanised steel tube and plate. The system is modular in nature and allows the relatively simple mounting of the different system components. Mounted within the steel 'roll cage' of the sledge are a pair of electro-magnetic slug sources and a small electronics package. The shear wave sources are mounted in opposing directions, perpendicular to the length of the sledge, and each consist of an 8000 turn copper coil and a free-moving metal slug, the latter contained within a metal tube running through the centre of the coil. Energising the coil causes the slug mass to accelerate down the metal tube, hitting an end-stop mounted rigidly against the sledge frame. This produces a sudden sideways movement of the sledge, creating in turn a horizontally polarised shear wave, with a dominant

Plate 5.2. a. The seismic sledge being deployed from the back deck of the *R.V John P. Tully*, showing the geophone string streaming out astern.

Plate 5.2. b. The 'Seismic sledge' prior to deployment from the *R.V John P. Tully.*

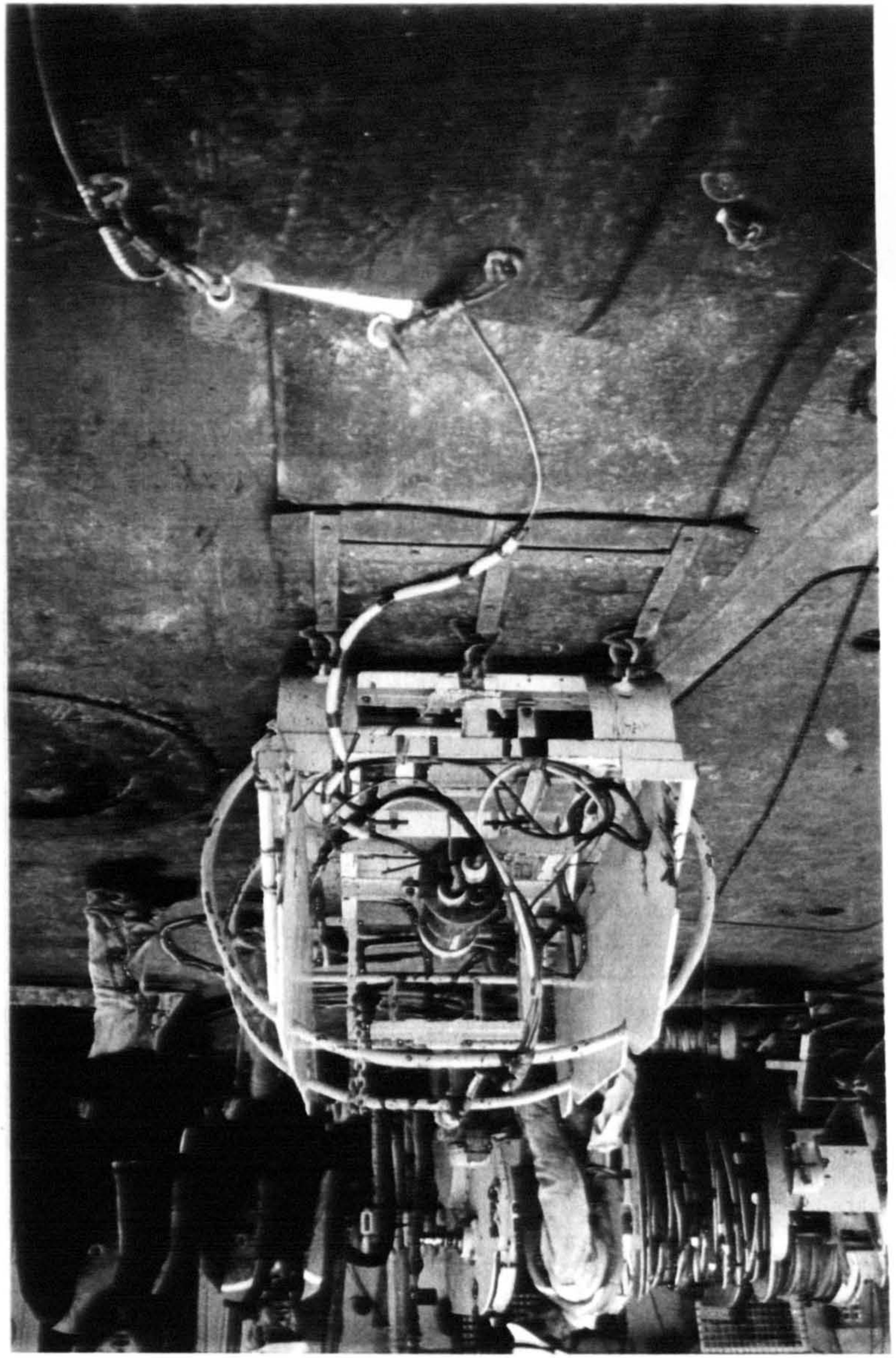

frequency of 20-30Hz. The slug is returned to its 'home' position by means of an elastic shock cord.

The electronics package is enclosed in a pressure sealed metal cylinder and mounted in the centre of the sledge. Contained within the cylinder are a series of pre-amplifiers, and a small geophone. The pre-amplifiers amplify the received signal before relaying it back to the ship and are mounted close to the receivers to limit amplification of any cable noise / pickup which may occur between the sledge and the ship.

5.7.1.2. Towed geophone string.

The geophone strings, consisting of a series of gimballed geophones, are located to the rear of the sledge and may be deployed in two different configurations: pseudo-underway and long offset.

The pseudo-underway version of the system consists of 6 stainless steel pans, each containing a 3-component, gimbal mounted geophone. These geophone pans are each mounted within an approximately 15m long by 1m wide semi-stiff rubber mat which both ensures adequate coupling between the pans and the seafloor and helps to maintain geophone alignment and spacing. The geophones are 1.96 metres apart, and attain a maximum offset of around 12m. The signal cables from each geophone are connected to the sledge mounted electronics package using a Valeport™ 24 pin underwater connector.

The long-offset system utilises 2 stainless steel geophone pans, once again each containing a 3-component, gimbal mounted geophone. These geophones are each deployed some distance from the sledge (up to a maximum of about 300m) and linked to the ship by a Kevlar tow cable and a signal cable.

5.7.1.3. Ship-board system.

Located on board the ship is the main deck control unit, a standard ABEM Mk 3 Terraloc engineering seismograph, and a Power Supply Unit (PSU), in this case a Geoacoustics, model 5420A. The seismograph digitally records and displays the data received from the geophones and also provides some element of limited post-processing capability.

The seismic data collected are stored on standard 3.5 inch diskettes which allow data (after suitable format conversion) transfer to other processing software. The sledge is linked to the ship by a steel tow-cable and a signal cable.

5.7.2. Mode of operation.

As may be noted from the system description above, the sledge may be operated in two different modes: the pseudo-underway and the long-offset system, the latter being the preferred mode for larger scale refraction measurements.

The pseudo-underway system, with the maximum geophone offset of around 12m, allows measurement of the shear wave properties of the surface sediments down to a depth of around 3m. Possibly the biggest advantage of the system when operated in this mode is that it allows the routine production of shear wave refraction 'profiles'. This is achieved as the ship steams slowly forward, by alternatively taking up and then paying out tow cable. The action of rapidly paying out the tow cable causes the sledge to become stationary on the seabed, allowing a low-noise shear wave measurement to be made. The slack cable is then taken in, ready to recommence towing on the seafloor and the whole process repeated.

The long-offset, or larger scale refraction system allows the investigation of sediment S-wave velocity - depth profiles to the order of a few tens of metres. This configuration utilises the sledge mounted shear wave sources and fixed reference geophone deployed from an anchored ship. The two 3-component geophone pans are then deployed remotely from the sledge, ready for the first shear wave measurement. Once a measurement has been completed, the geophones are then winched a short distance towards the ship and the test repeated. The distance from the shear wave sources to the geophones is calculated from an analysis of the direct compressional wave and a knowledge of the compressional wave velocity in seawater. Using this measurement method, a large scale, multi-channel refraction record may be constructed.

5.7.3. Interpretation procedure.

Conventionally, seismic refraction interpretations rely on a knowledge of both a forward and a reversed refraction shot. However, refraction data collected using the seismic

sledge, for logistical reasons can only be of a single ended nature. For this reason, pseudo-underway sledge data are best interpreted using a simple horizontal layer velocity model. The most commonly used model of this type in this project was the two layer model, as it provided the best representation of the sledge data collected on the Fraser Delta. Modelling of this type allows the calculation of an 'apparent' 1st layer velocity (V_{1app}), a 2nd layer velocity (V_2) and a depth to the first interface (D_1). For data collected and interpreted using the short offset system use, of this simple model may be regarded as sufficiently valid, as even a dipping refractor approximate to the horizontal over such a short offset.

The typical data interpretation sequence, which for both the pseudo-underway and long-offset systems were broadly similar, is described below:

1. Data retrieval onto the Terraloc, from floppy disk. Selected short offset and all long offset records were transferred into a basic PC based seismic interpretation package, Q'Seis™, allowing more complex filtering, and in the case of the long-offset data, compilation of a refraction profile.
2. Initial visual appraisal of data quality; poor quality records were discarded at this stage.
3. Signal enhancement, usually consisting of amplitude normalisation and digital filtering, the latter removing high frequency noise and pickup (typical filter setting, 40 Hz high cut).
4. Manual determination of individual travel times using the Terraloc or the processing package. If signal onsets were obscured by noise, later events were used.
5. Manual plotting of travel time data and best fit lines on graph paper.
6. Input of data into a spreadsheet, enabling calculation of layer velocities V_{1app}, V_2 and D_1.

This interpretative method allows the production of a S-wave velocity - depth profile of the surface layers of sediment, the depth of penetration depending primarily upon the geophone offset distance from the sledge and the *in-situ* velocity gradient. These data, especially when plotted against distance to produce S-wave velocity refraction 'profiles' are particularly useful as an initial reconnaissance tool, and may be used to identify areas of anomalously low velocities, which can then be the subject of further investigation.

5.7.4. Analysis of error when interpreting velocity - depth information.

Once again, the errors associated with this type of measurement may be divided into two basic groups, unquantifiable errors arising from poor quality data or invalid assumptions during data processing, and quantifiable errors. In common with the errors associated with the calculation of laboratory generated shear wave velocities, the two main components of error associated with *in-situ* shear wave velocities are:

1. travel time determination errors,
2. errors associated with the measurement of the path length.

5.7.4.1. Travel time errors.

In the case of *in-situ* shear wave measurements made using the seismic sledge, the fundamental sampling rate of the Terraloc is the biggest single source of quantifiable uncertainty. The ABEM Terraloc records 1000 samples per trace, regardless of record length. The minimum possible record length is 24ms, making the minimum sample time of 0.024ms. For a shear wave travelling at a typical 150m/s, recorded on a 200ms record, given a nominal receiver separation of 1.7m, an error of ± 0.024ms would yield an error of ± 3m/s. Therefore, provided that the signal onset may be accurately defined, and that the error in travel path is small in magnitude, the instrumental error of the seismograph is acceptable (Huws, 1993).

5.7.4.2. Travel path errors.

The biggest assumption made when calculating velocities from data collected using the seismic sledge is that each geophone unit is lined out to its full extent directly behind the sledge (Huws, 1993). Any mis-alignment of the geophone pans could however cause:

1. the distance between the two units to be shorter than expected, and
2. the horizontal component geophones to be not be exactly transverse and radial relative to the seismic source, thus resulting in an error of signal phase (and hence travel time).

5.7.5. Summary of field techniques.

The 'Seismic Sledge' provides an extremely useful method for the routine measurement of the *in-situ* shear wave properties of the top few metres of marine sediments. Depending on geophone configuration, the data collected may be used to produce either composite refraction 'profiles' or more detailed S-wave velocity - depth profiles (Huws, 1993). Possibly the sledge's most important current role is as a reconnaissance tool, allowing the identification of 'low velocity' zones, which represent low stiffness materials i.e. muds or loose sands. Potentially loose, and hence liquefiable materials, worthy of further, more detailed examination can be then identified by subsequent sampling procedures..

5.8. Conclusions.

The laboratory and *in-situ* techniques described provide the basis for a powerful tool for the investigation of both the geophysical and geotechnical properties of marine sediments, especially uncemented sands. The *in-situ* capability provided by the Seismic Sledge in particular further allowed the extrapolation of the stability analysis into the potentially liquefiable field situation of the offshore Fraser Delta.

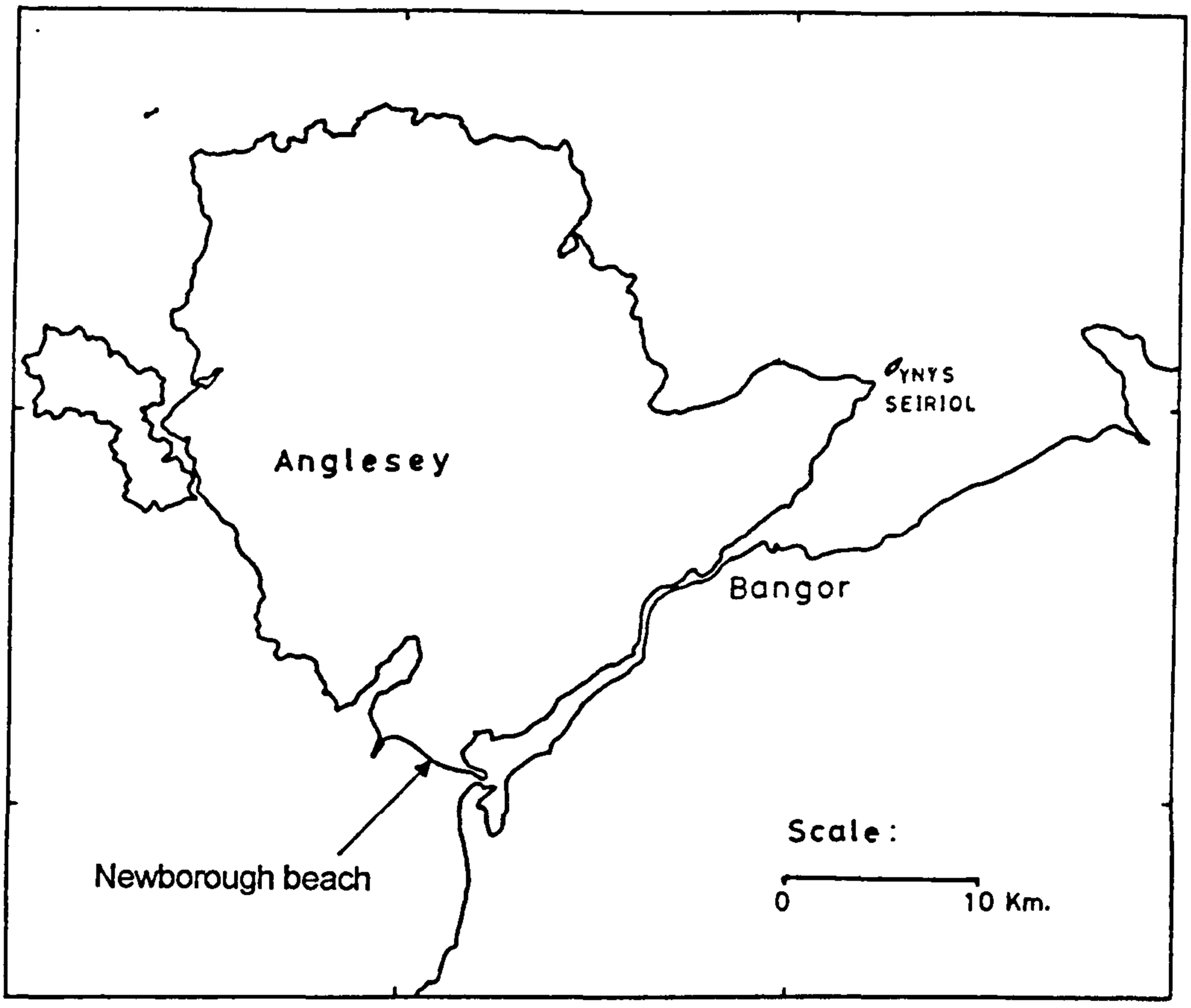

Figure 5.1. Newborough beach - location map.

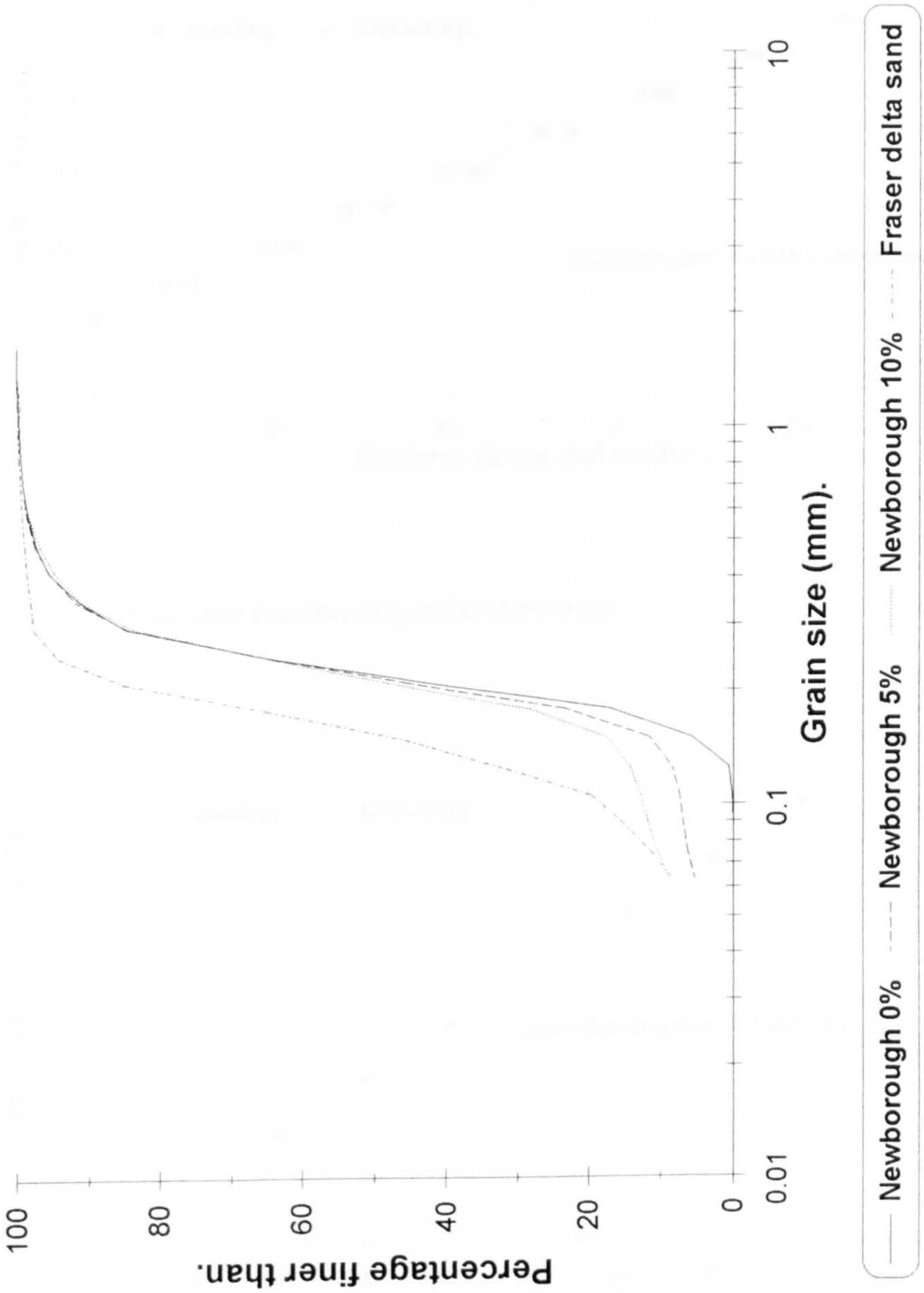

Figure 5.2. Grain size distributions for all laboratory sands tested.

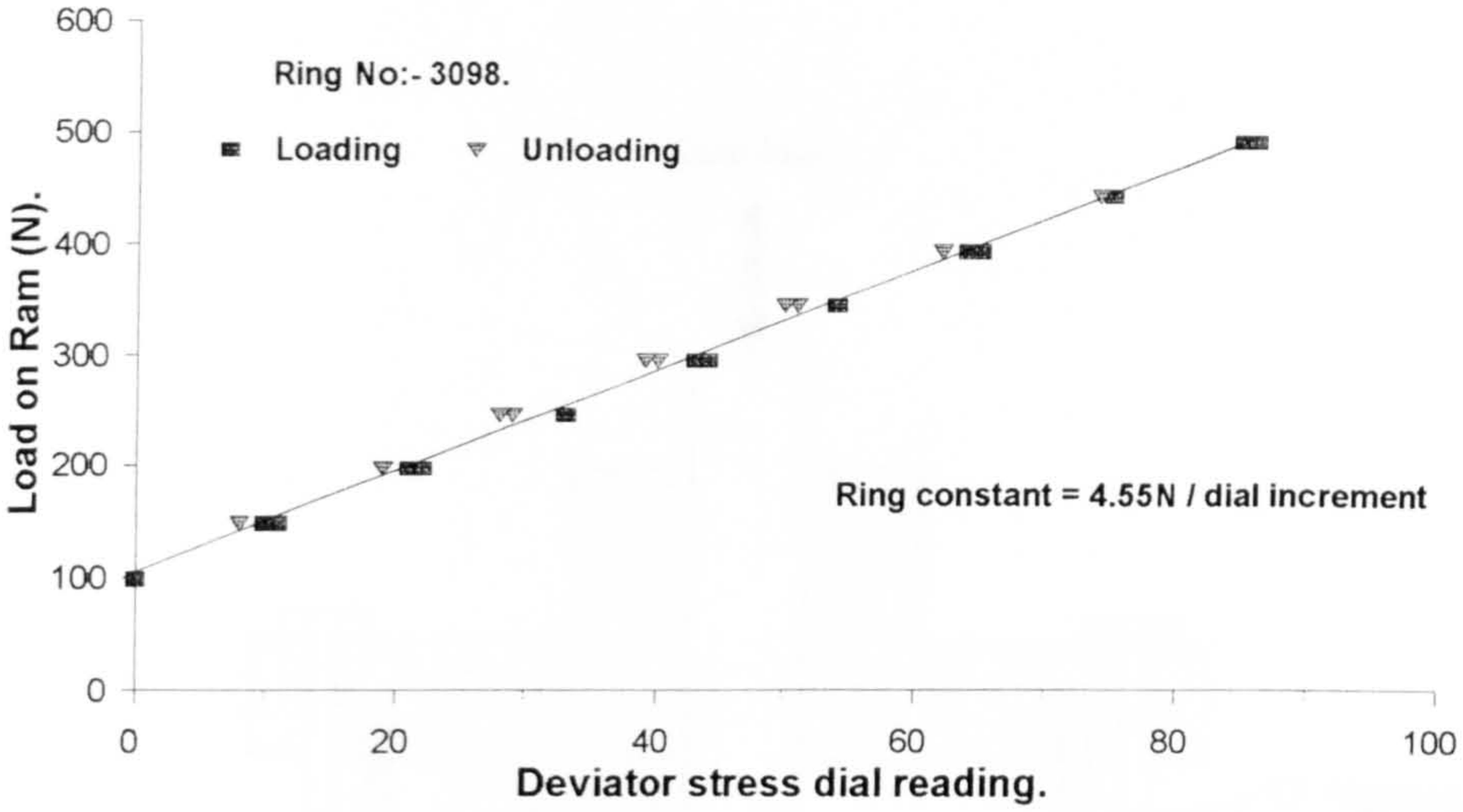

Figure 5.3. Example proving ring calibration data.

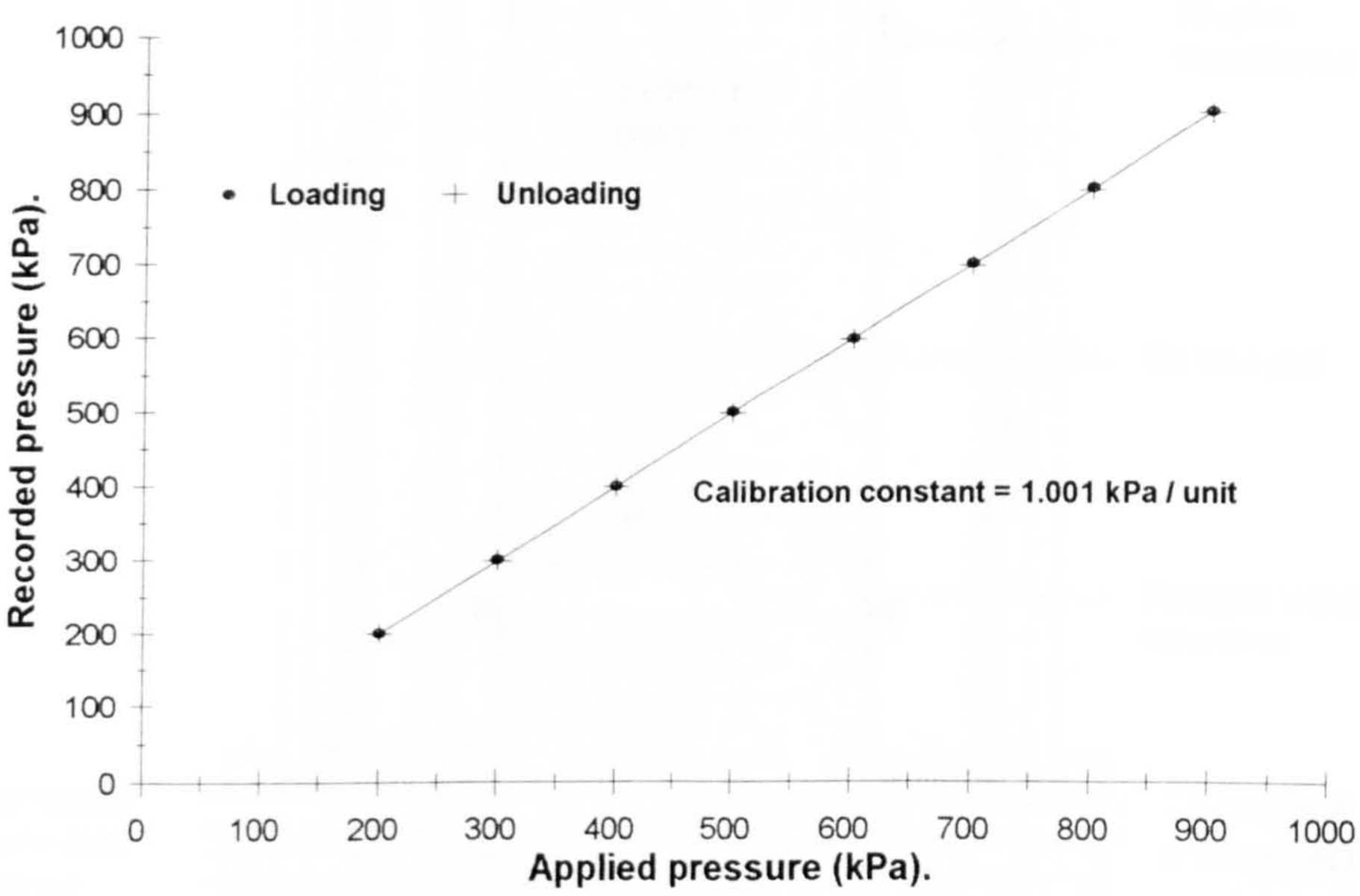

Figure 5.4. Example pore-pressure transducer calibration data.

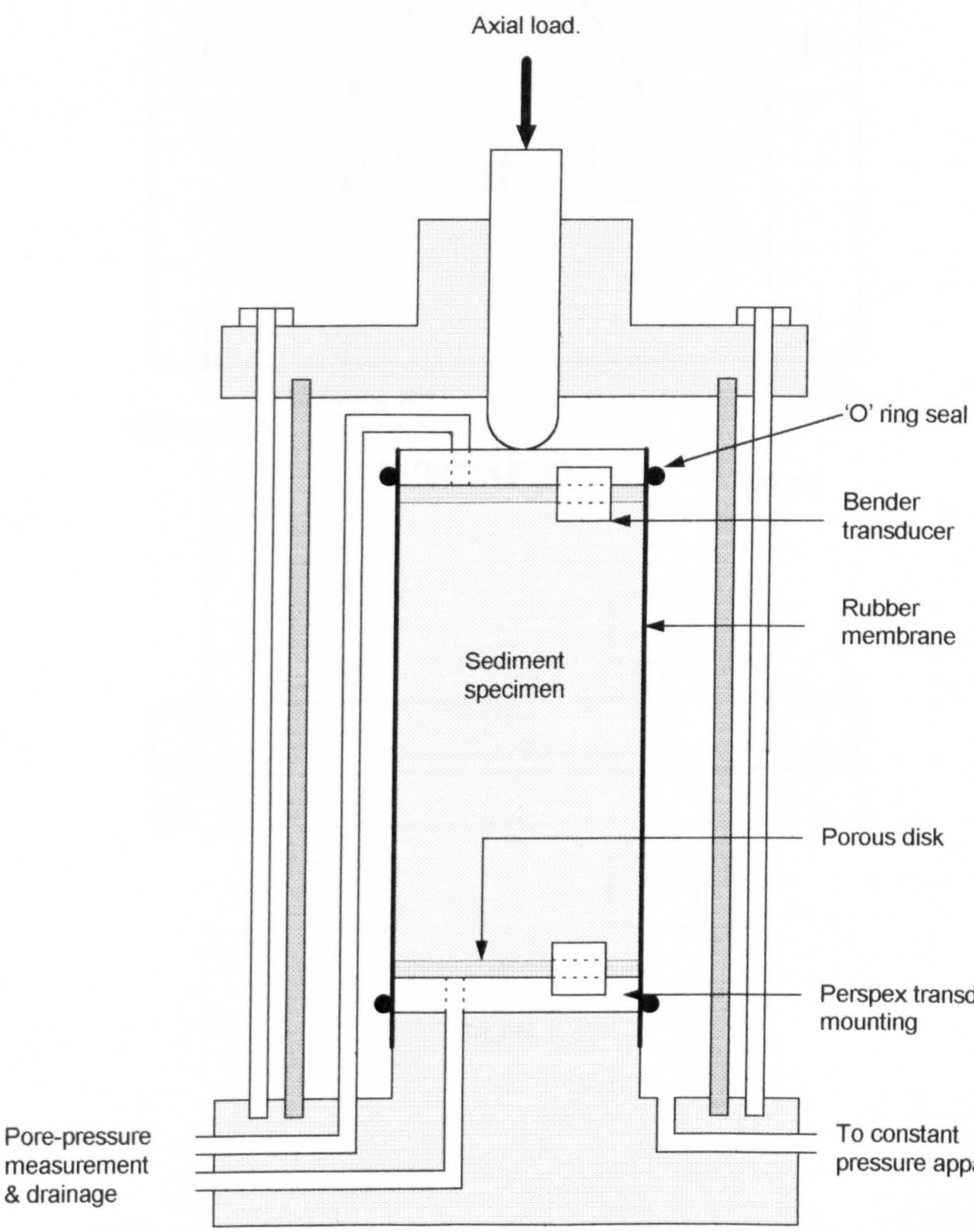

Figure 5.5. Schematic diagram of the large triaxial cell.

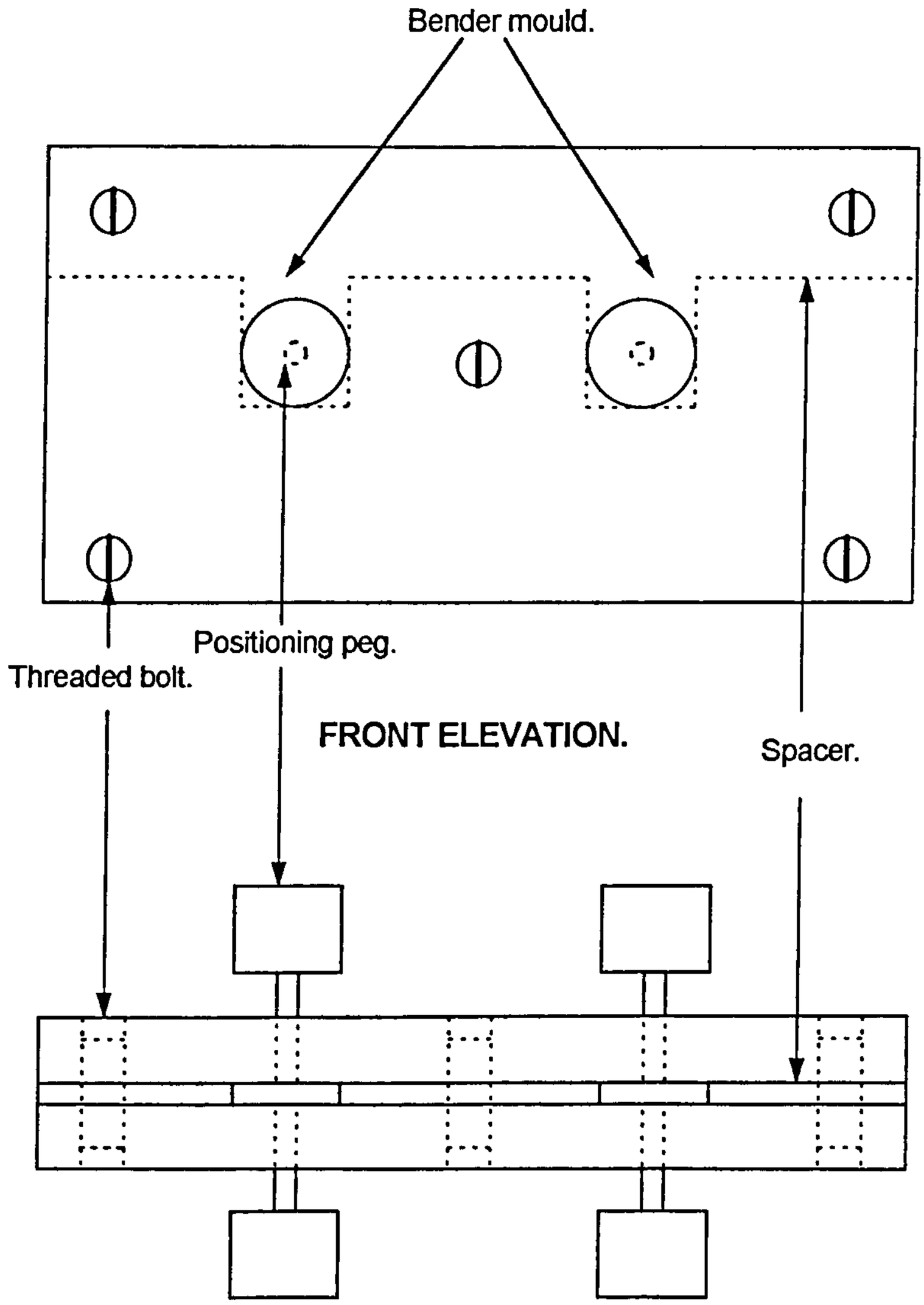

Figure 5.6. Detail of sample mould used in the manufacture of bender transducers.

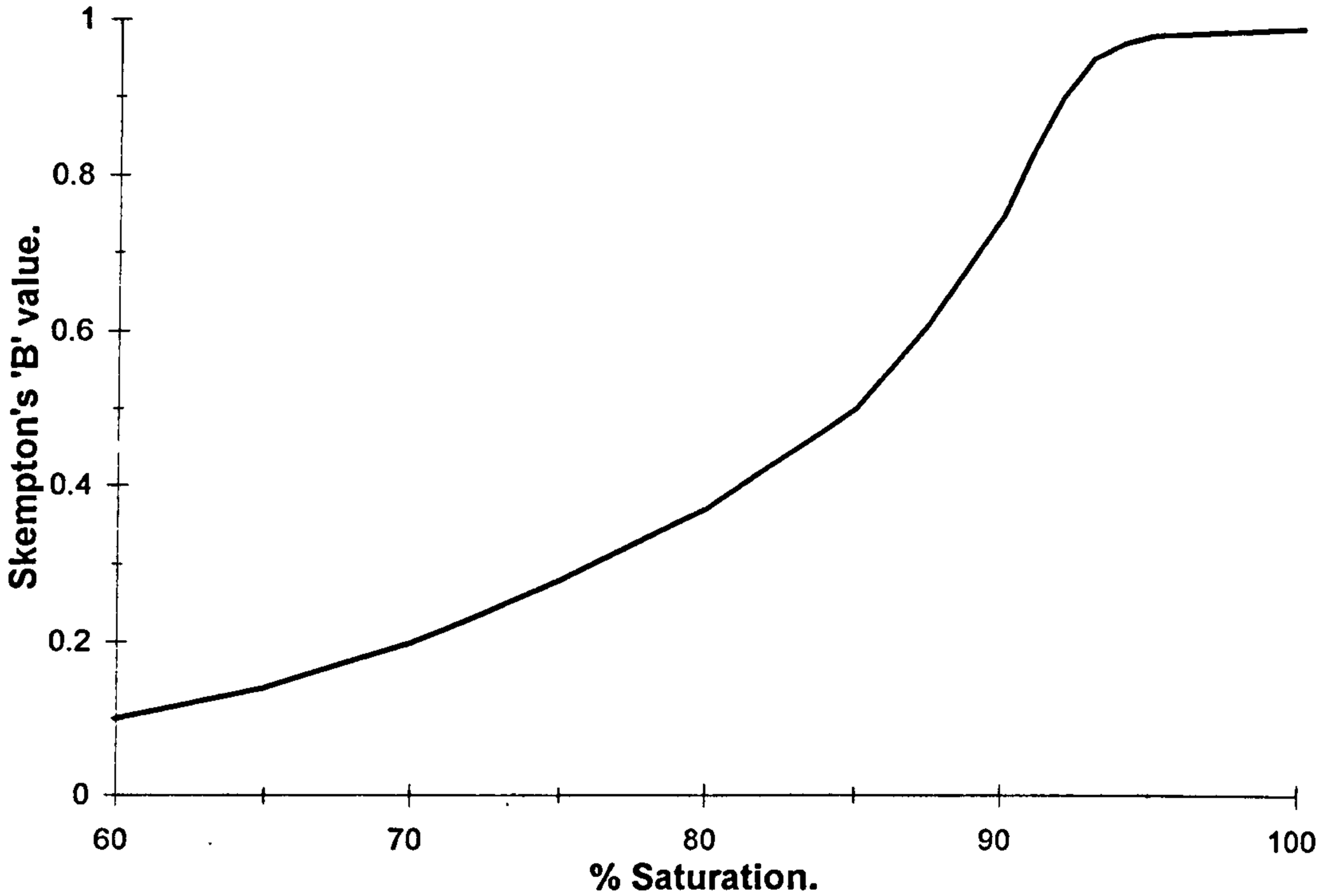

Figure 5.7. Approximate relationship between Skempton's 'B' value and sample saturation.

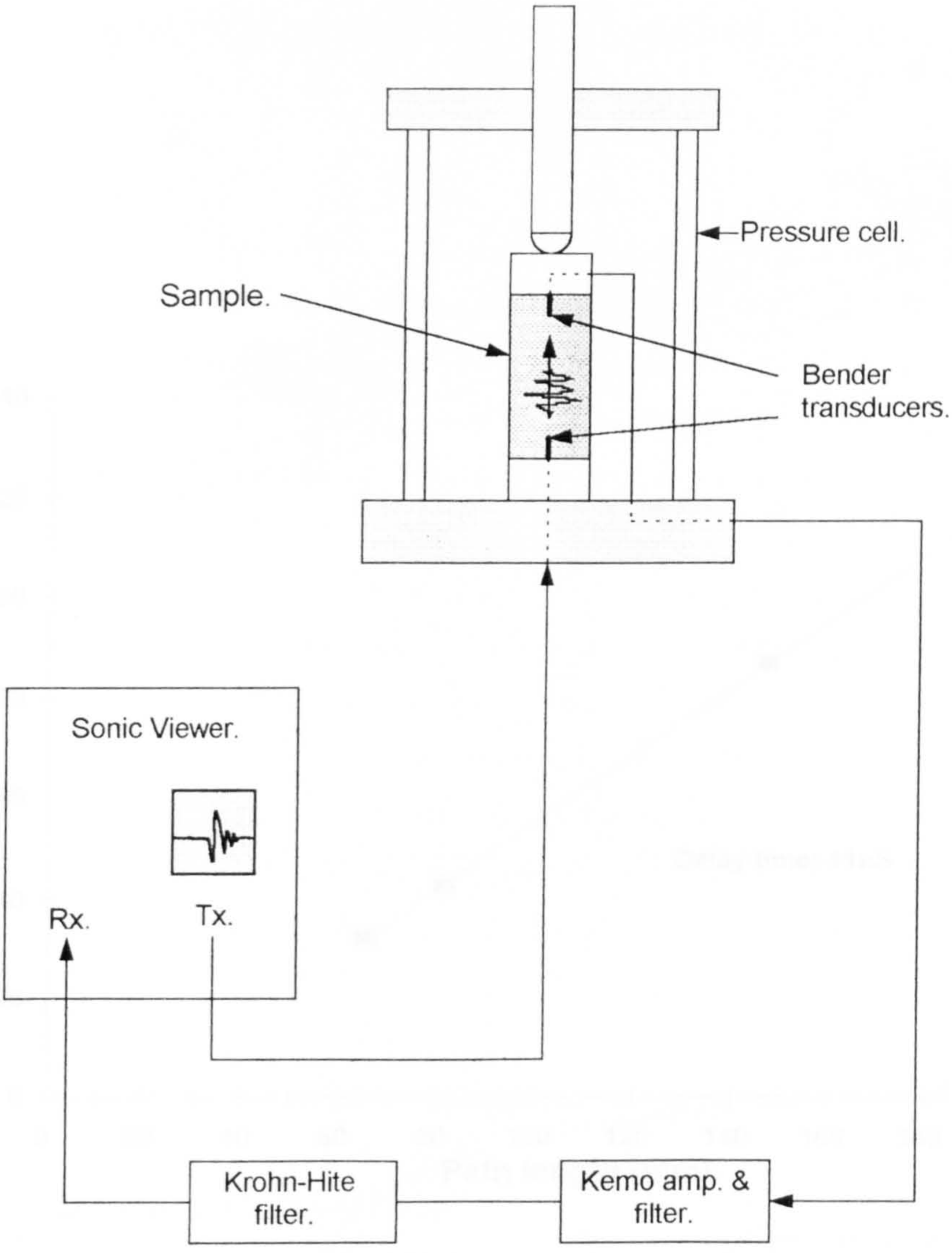

Figure 5.8. Diagrammatic representation of the shear wave measurement system.

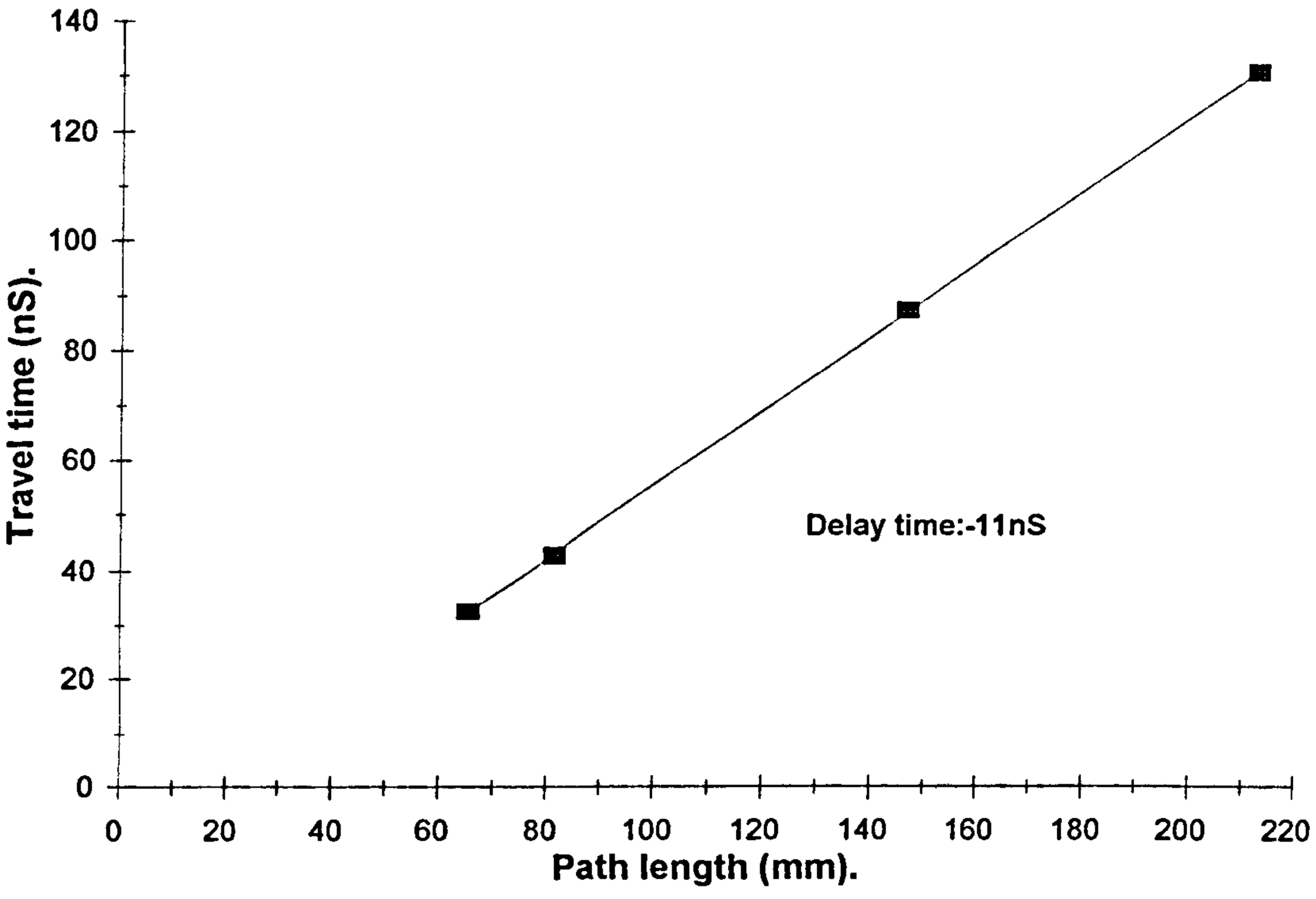

Figure 5.9. Example delay time determination for the instrumented triaxial apparatus.

a.

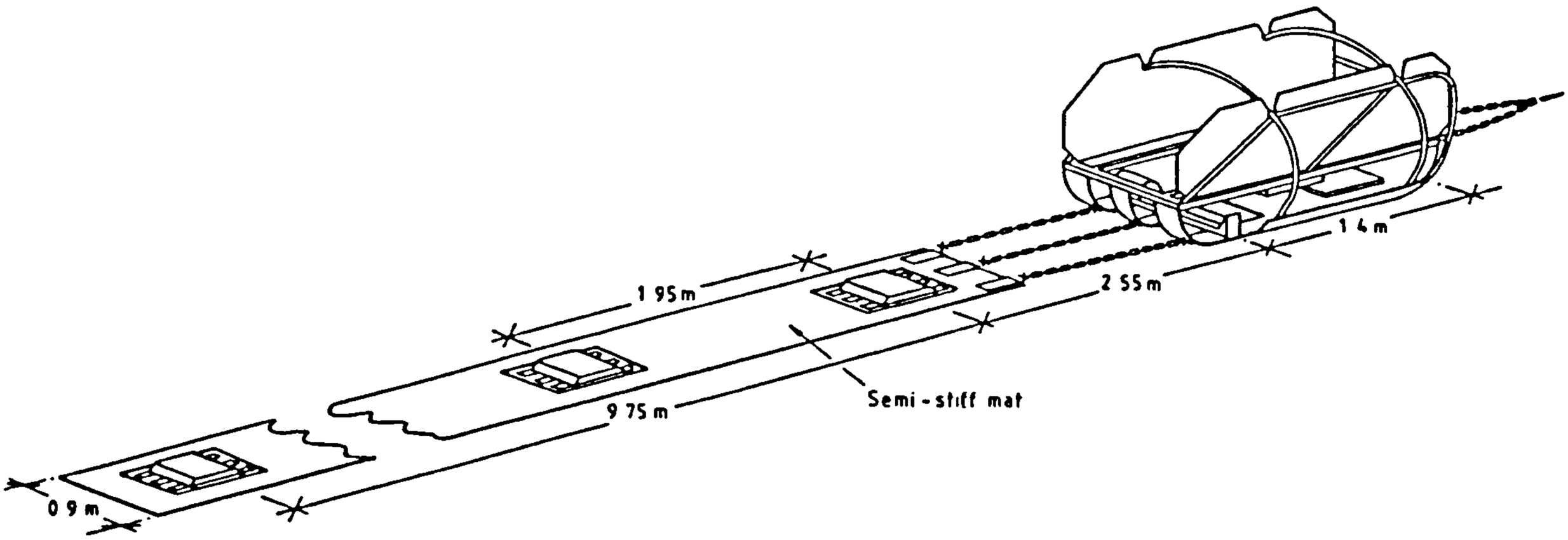

b.

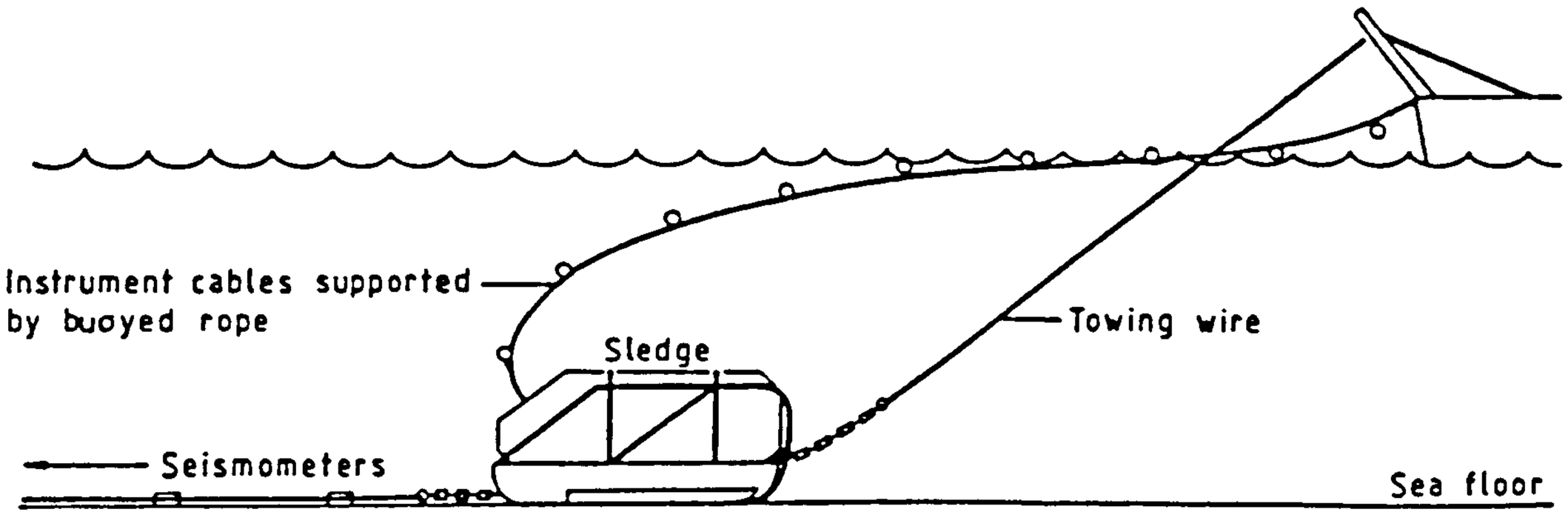

Figure 5.10. a. Seismic sledge pseudo-underway configuration; receiver layout.

Figure 5.10. b. Seismic sledge pseudo-underway configuration; deployment layout.

(*after Davis et al., 1989*)

CHAPTER 6.

LABORATORY RESULTS - SECTION 1.

CONVENTIONAL SHEAR WAVE VELOCITY AND TRIAXIAL DATA.

6.1. Introduction.

The laboratory testing component of this study involved a total of 60 combined shear wave velocity - triaxial tests using the 100mm sample diameter instrumented cell. A further 10 shear wave velocity only tests were performed using the same cell and a smaller number (~20) of preliminary tests were performed using the 50mm sample diameter triaxial cell. Of the 60 full tests completed, 35 were performed on the Newborough 0% sand, 8 on the Newborough 5% sand, 9 on the Newborough 10% sand, and finally 8 on the Fraser sand. The large number of tests carried out on the first sample was as a result of the experimental nature of the technique. The lesser number of tests performed on the latter samples represents possibly a more realistic number for the routine determination of shear wave and steady state parameters, the technique having been standardised by this stage. The laboratory data in this chapter will be described in two ways, firstly in purely observational terms during a 'typical' test, and secondly using a more in depth approach detailing the individual results for each sample.

6.2. Laboratory testing - general overview.

This section illustrates some of the general observations and trends noted during laboratory testing of all the sand samples. For simplicity these observations are discussed in the order in which they were noted.

6.2.1. Sample preparation and saturation.

The moist tamping method of sample preparation used in this study allowed the preparation of laboratory samples with a wide range of initial void ratios. Very dense, homogeneous samples (with densities close to e_{min}) and medium dense samples were prepared relatively easily. Loose samples were harder to prepare, with the upper limit of available sample densities prepared using this technique falling below the measured

value of e_{max}. The preparation and testing of very loose samples was found to be limited by two main factors:-

1. Excessive sample inhomogeneities, resulting from the method of preparation and subsequent consolidation.
2. The 200 kPa minimum confining pressure supplied by the constant pressure apparatus. A lower initial confining pressure could potentially allow the preparation of looser samples.

Once consolidation had been completed it was clear from a simple visual examination that the samples consisted of thin loose zones, sandwiched between thicker, denser zones, a feature noted by Been & Jefferies (1985). In the denser samples, these zones were less pronounced, however they became progressively more marked in looser samples. The presence of these thin, slightly looser zones did not appear to affect the large strain sample behaviour unduly, and for the purpose of this study, the samples were regarded as being essentially homogenous.

As previously mentioned, complete saturation of the sample is of great importance during triaxial testing. The use of CO_2 and high back pressures during sample preparation helped to ensure near total saturation of all samples tested. Measuring the increase in B value associated with increasing back pressures showed that pressures of the order of 700 - 800 kPa were required to ensure satisfactory sample saturation (see Figure 6.1 & 6.2).

6.2.2. Shear wave data.

The shear wave velocity behaviour of a specific sample was determined on the basis of 25 to 35 individual velocity determinations over a range of effective stresses, usually between 30 kPa and 400 kPa. Based upon the measurements made using the large 100mm diameter triaxial cell alone, the number of individual shear wave determinations made in this study was of the order of 2100. During testing, it was found that the two main controls on signal quality were sample saturation and filtering of the received signal. The two main controls on the actual velocity of the shear wave were found to be the effective confining stress and the void ratio. Each of these factors are briefly discussed below.

6.2.2.1. Sample saturation.

The saturation of the sample proved to have a major affect on received signal quality, especially when using the small 50mm diameter triaxial cell. Essentially it was found that in a sample which was not fully saturated, very high quality shear wave signals were obtained (Figure 6.3). However, once the sample was fully saturated this 'filtering' effect was less marked, and a corresponding reduction in signal quality was noted. The most likely cause of this effect is attenuation of the near field P-wave component of the signal by small gas bubbles in the pore-spaces. Other reasons for this attenuation effect could be due to changes in coupling characteristics, or liquefaction around the transducer once the specimen is fully saturated. In some extreme cases, at very low effective stresses using the small triaxial cell, these effects caused a degradation of shear wave quality to such an extent that no significant arrival could be identified (Figure 6.4).

6.2.2.2. Filtering effects.

Some type of filtering proved necessary throughout all tests in order to remove higher frequency (P-wave) components of the waveform which often masked the onset of the shear wave, especially at lower effective stresses. The disadvantage of filtering however, is that it may cause subtle changes in the signal, which may in turn alter the observed travel time. This effect increases directly with the bandwidth of filtering applied. For this reason, the signal was filtered as little as practicably possible. The effects of filtering upon a raw signal are illustrated qualitatively in Figures 6.5 & 6.6. As can be seen, the main effects of filtering frequencies above 19 kHz were:-

1. to remove the higher frequencies, in the first part of the signal,
2. to create in its place a lower frequency residual 'noise', rapidly attenuating with time,
3. to subtly alter the entire S-wave waveform.

6.2.2.3. Effective stress effects.

Effective stress was found to be the single most important factor controlling the shear wave velocity of a specific sample. Figure 6.7 illustrates a typical shear wave velocity - effective stress relationship obtained using the methods described above. Over the

stress range encountered in this study, this relationship was found to be geometrical in nature, and could be described using the formula:-

$$V_s = a \times p'^{b} \qquad (6.1).$$

where, a & b are sample constants.
p' = effective confining stress (in kPa).

To obtain a best fit curve, the coefficients a & b were calculated on the basis of a simple linear regression of the logarithm of p' versus the logarithm of V_s (see below). In this study a varied between 23.0 & 58.0 and b between 0.25 & 0.42.

The effects of changing effective stress also had an affect on the received shear wave signal itself. As mentioned above, to achieve an optimum signal, the bender transducers were operated at resonance, the frequency of which is dependent on both the transducer dimensions and sediment stiffness. For a specific sample, an increase in the confining stress results in an increase in stiffness, which in turn leads to an increase in the dominant frequency of the shear wave. This effect is illustrated qualitatively in Figures 6.8 & 6.9.

Below an effective stress of around 35 kPa, the precise onset of the shear wave was very difficult to determine, due mainly to the detrimental effects of long wavelength, low amplitude and long travel time on signal quality.

6.2.2.4. Void ratio effects.

The effects of varying void ratio on the velocity of the shear wave proved to be less significant than the effects of varying effective stress. However, the difference in recorded velocities for two samples of Newborough 0% sand with different void ratios are illustrated in Figure 6.10. Over the typical range of void ratios found in these sands, the relationship between void ratio and shear wave velocity at a specific effective stress was found to be generally linear in nature. This relationship will be discussed in more detail below.

6.2.3 Triaxial testing.

As mentioned above, some 60 consolidated, undrained triaxial tests were performed using the large 100mm diameter triaxial cell. For each sand type, these tests were completed over a range of initial void ratios and effective stresses. In agreement with the literature (*e.g.* Been & Jefferies, 1985; Konrad, 1990a; Konrad, 1990b), three distinct types of sample response were observed, consisting of the following:-

1. For loose sands, strong contraction, leading to steady state conditions,
2. For dense sands, strong dilation, leading to failure along a well defined shear plane,
3. For medium - dense sands, initial contraction, followed by limited dilation, leading to steady state conditions.

However, an additional fourth type of response was identified, occurring only in very loose samples and consisting of strong contraction, leading to complete liquefaction once the back pressure reached the cell pressure (Figure 6.11). In the case of the Newborough 0% test sand, this type of response made it extremely difficult to determine the steady state line based upon sands which displayed a strongly contractive response. For this reason, the steady state line of the Newborough 0% sand was, in part, defined upon the basis of dilative sample responses.

Both the shear wave velocity and triaxial data will be discussed more quantitatively below, treated separately for each test sand.

6.3. Results: Newborough 0% sand.

Newborough 0% sand provided the test bed for the proposed laboratory technique, and was used for testing in both the small and large triaxial cells. The results of the tests performed using the large triaxial cell are described below.

6.3.1. Shear wave data.

The results of all shear wave tests performed using the large triaxial cell are listed in Table 6.1 below. As can be seen, 45 individual shear wave tests were performed on Newborough 0%, over a wide range of void ratios, from a minimum of 0.719 to a maximum of 0.854. Test number 46, with a calculated void ratio of 0.666 represents the

determination of e_{mn}, and was not subject to any geophysical or geotechnical measurements. The preparation and testing of samples with a void ratio significantly looser than 0.854 proved impossible, due to the reasons described in Section 6.2.1 above. The minimum and maximum recorded shear wave velocity - effective stress curves, are illustrated in Figure 6.12 (a) and are quoted below:-

$$V_{s\min} = 35 \times \sigma'^{0.32} \qquad (6.2).$$

$$V_{s\max} = 43 \times \sigma'^{0.33} \qquad (6.3).$$

As mentioned in Chapter 4, these V_s - effective stress best fit curves were calculated using data collected during the geophysical section of the laboratory technique. More specifically, the sample constants a & b were derived on the basis of a simple linear regression of the shear wave - effective stress data which had been first transformed into a linear relationship by logging both axes. From the linear regression equation of these data, the a value was calculated from the inverse log of the intercept, while the stress exponent b was equal to the gradient of the regression line (Figure 6.12 b). The significance of this regression, and all other regression analyses in this project, were then tested using analysis of variance (ANOVA) (Zar, 1984), at a 95% confidence level. The results of this analysis are listed in Table 6.2 below.

Title	*Equation*	*Source*	*Df*	*M*	*F*	R^2	*p*
Eqn. 6.2.	y = 0.32x +1.55	Regression Residual	1 31	3.096 0.0006	4920	0.99	1.01×10^{-35}
Eqn. 6.3.	y = 0.33x + 1.63	Regression Residual	1 34	1.95 0.001	1594	0.98	3.77×10^{-30}

Table 6.2. Linear regression and ANOVA data for recorded V_{smin} & V_{smax} for Newborough 0% sand.

where, *Df* = degrees of freedom, *M* = Mean square value, *F* = F value, & a *p* value of less than 0.05 indicates a highly significant result.

As can be seen, the data analysed in this way display both very high R^2 values (~0.99) and extremely low significance values ($p \sim 4.0^{-30}$ - 1.0^{-35}). Although these values are partly a product of the way the data were derived, they do suggest that the data are statistically highly significant.

To illustrate the effects of void ratio on shear wave velocity, velocities may be calculated at a specific effective confining stress, using the individual sample constants derived for each sample. Figure 6.13 illustrates the variation of shear wave velocity with void ratio at a standard effective confining stress of 300 kPa. A simple linear regression of these data reveals that the shear wave velocity at 300 kPa may be related to void ratio, using:-

$$V_{s300} = 559 - 391e \qquad (6.4).$$

The regression data for this relationship are listed below in Table 6.3. Use of this relationship suggests that V_{s300} at e_{min} is of the order of 300 m/s, while V_{s300} at e_{max} is of the order of 195 m/s; this represents a maximum possible range of shear wave velocities at 300 kPa of 105m/s. These variations of S-wave velocity with void ratio are well within the calculated resolution of the measurement system.

Many investigators, e.g. Robertson *et al.* (1995), suggest that velocities can be normalised to a standard effective stress of 100 kPa. Simple linear regression analysis of the relationship between shear wave velocity normalised to 100 kPa and void ratio shows that:-

$$V_{s100} = 415 - 307e \qquad (6.5).$$

The upper and lower boundaries of these data are defined by:-

$$V_{s100\ upper} = 429 - 307e \quad ; \quad V_{s100\ lower} = 402 - 307e \qquad (6.6, 6.7).$$

These relationships are illustrated in Figure 6.14 and the regression data are listed below in Table 6.3. Use of Equations 6.5 - 6.7 ,and assuming that the V_s - e relationship remains linear in nature between e_{min} and e_{max}, suggests that V_{s100} at e_{min} is approximately 210 m/s ± 15 m/s. V_{s100} at e_{max} is of the order of 129 m/s ± 15 m/s; this represents a likely range of shear wave velocities at 100 kPa between e_{min} & e_{max} of the order of 81m/s.

Title	*Equation*	*Source*	*Df*	*M*	*F*	R^2	*p*
Eqn. 6.4.	$V_{s300} = 559\text{-}391e$	Regression Residual	1 43	0.03 0.0001	262	0.86	6.71×10^{-20}
Eqn. 6.5.	$V_{s100} = 415\text{-}307e$	Regression Residual	1 43	0.021 0.0003	63	0.58	5.94×10^{-10}

Table 6.3. Linear regression and ANOVA analysis of variance for Equations 6.4 & 6.5.

The regression data listed above clearly show that the relationship between normalised shear wave velocity and void ratio at both 300 & 100 kPa for Newborough 0% sand is highly significant.

These data may be presented in a slightly different format by rearranging Equations 6.1, 6.4 & 6.5, allowing a comparison between measured void ratio and predicted void ratio, based upon a knowledge of the effective confining stress and the sample constants of each individual sample. Based upon an effective confining stress of 300 kPa, void ratio may be predicted from shear wave velocity using:-

$$e_{pred} = \frac{\left(a \times p'^{b}\right) - 559}{-391} \qquad (6.8).$$

Assuming an effective stress of 100 kPa the relationship has the form:-

$$e_{pred} = \frac{\left(a \times p'^{b}\right) - 415}{-307} \qquad (6.9).$$

These relationships are illustrated in Figure 6.15 and the regression data are displayed below.

Title	*Equation*	*Source*	*Df*	*M*	*F*	R^2	*p*
Eqn. 6.8	y = 1.0x + 0.0003	Regression Residual	1 43	0.03 0.0001	262	0.86	6.71×10^{-20}
Eqn. 6.9.	y = 1.0x - 0.0007	Regression Residual	1 43	0.021 0.0003	63	0.58	5.94×10^{-10}

Table 6.4. Analysis of variance for comparison between measured and predicted void ratio.

On the basis of the *p* values both these relationships are highly significant. In the case of Equation 6.8. it appears that shear wave velocity may be used to predict the actual void ratio to within ± 0.025 (Figure 6.15 (a)). In the case of Equation 6.9, the slightly lower R^2 value once again reflects the slightly more scattered nature of these data. In this case, the shear wave velocity may be used to predict the actual void ratio to within ± 0.05. Both these values are significantly above the calculated system resolution, which in terms of void ratio is ± 0.003. These values are therefore probably either reflecting some other, unquantifiable source of error or influencing factor in the system . In both cases the regression line of the data lies very close to the '1 to 1' line.

The shear wave data described above may also be presented in the more general form of expression suggested by Hardin & Richart (1963), relating shear wave velocities to both void ratio and effective confining stress. Using the average value of the stress exponent from Table 6.1 above, the shear wave velocity of Newborough 0% may be predicted using the relationship:-

$$V_s = (84 - 60e)p'^{0.34} \qquad (6.10).$$

6.3.2. Triaxial data.

The triaxial data collected during testing on Newborough 0% sand are listed in Table 6.5. The test data were based upon the results of 35 consolidated, undrained triaxial tests. The range of void ratios tested displayed examples of all the types of sample response described in Section 6.2.3. above. As already mentioned, during testing considerable difficulties were encountered in defining the steady state point for highly contractive samples. Typically, the response of a very loose sample of Newborough 0% was strong contraction, leading to complete failure of the sample when the pore-pressure reached 100% of the cell pressure (Figure 6.11). This response was noted in test numbers 16, 17, 20, 22, 27, 29, & 43. No reference to this type of response is made in the literature. One possible explanation of this response could be that the extremely low effective confining stresses at steady state, common to very loose sand samples such as these, is below the resolution of the laboratory apparatus used in this study. Because of this problem, a number of steady state strengths were defined using slightly dilative sands, in which a poorly defined shear plane was observed to develop. This

may result in a small, but probably insignificant underestimation of the true steady state strength.

Figure 6.16 illustrates the state boundary surface, defined by three undrained tests on contractive and dilative sands. Figures 6.17 (a) & (b) illustrate the ultimate steady states for all tests, defined in the form of void ratio (e) versus the logarithm of effective confining stress at steady state (p'_{ss}), and deviator stress at steady state (q'_{ss}) versus p'_{ss}.

Typically steady state lines defined in e log-p' space and in the pressure range 10 - 1000 kPa are linear in nature and can be defined using an equation of the general form (Sladen *et al.* 1985):-

$$e_{ss} = e_1 - C_{ss} \log p'_{ss} \qquad (6.11).$$

In q - p' space the steady state line is also linear and may be defined using:-

$$q_{ss} = Mp'_{ss} \qquad (6.12).$$

where, e_{ss} = void ratio at steady state,
e_1 = intercept at 1 kPa,
C_{ss} = slope of the steady state line in e - log p' plane,
q_{ss} = shear stress at steady state,
M = slope of the steady state line in q - p' plane,
p'_{ss} = effective confining stress at steady state.

M can be related to the effective friction angle at steady state ϕ'_{ss}, using:-

$$M = \frac{6\sin\phi'}{3-\sin\phi'} \qquad (6.13).$$

The results of a simple linear regression analysis on the Newborough 0% data plotted in the e - log p' and q - p' planes are illustrated in Table 6.6 below.

Title	*Equation*	*Source*	*Df*	*M*	*F*	R^2	*p*
e - log p'	y = -0.043 logx + 0.887	Regression Residual	1 24	0.004 3.11	136	0.84	2.26×10^{-11}
q - p'	y = 1.28x	Regression Residual	1 24	1223667 235	521 4	0.995	1.38×10^{-29}

Table 6.6. Simple linear regression for the Newborough 0% sand steady state data.

From the results of these simple linear regressions, the following parameters may be used to define the steady state line of Newborough 0% sand:-

$e_1 = 0.877$, $C_{ss} = 0.043$, $M = 1.28$, $\phi_{ss} = 29°$.

These parameters are valid over the effective stress range 30 - 900 kPa.

Both these regressions display high R^2 values and extremely low p values and may therefore be regarded as being statistically significant.

From a knowledge of the material constants given above, the state parameter may be calculated using:-

$$\psi = e - e_{ss} \qquad (6.14).$$

This parameter, originally defined by Been & Jefferies (1985), represents the conventional method of defining sand state. Positive states indicate a possible contractive response, while negative states indicate a possible dilative response. However, because of the scatter of data around the mean steady state line (see Figure 6.17), the state parameter as measured in these tests does not necessarily represent best index of sediment state; this may be more readily measured by examining the change in effective confining stress ($\Delta p'$) during the triaxial test. However, by virtue of the methodology, this is only possible in a laboratory situation.

In order to compare data from a number of different tests, a number of authors have found it convenient to 'normalise' the recorded effective stress paths by dividing the stresses by the effective confining stress at steady state (Sladen *et al.* 1985). In this

manner the collapse surface, discussed in Section 3.3.1, may be established from tests with varying void ratios. Normalisation in this manner has the effect of reducing the steady state line to a single point, as the ratio q divided by p'_{ss} is always close to 1.2 at steady state. Figure 6.18 (a) illustrates the normalised stress paths for tests 13, 15 & 19. This figure clearly shows that loose samples, with the ratio $p/p'_{ss} > 1.0$, (Test No's 13 & 19) display a strongly strain softening response. In contrast, dense samples, with the ratio p/p'_{ss} < than 1.0 display a strain hardening response under undrained shear. Figure 6.18 (a) also shows that, in agreement with the literature, the ratio p/p'_{ss} at steady state for the Newborough 0% sand is approximately 1.2. Figure 6.18 (b), illustrates the collapse surface, defined by plotting the peak points of the normalised stress paths. For clarity only test number 15 is plotted. This diagram clearly illustrates that the collapse surface is distinct from the state boundary surface, representing the limit of stability under undrained loading conditions. As can be seen, only a limited number of tests resulted in a strongly contractive sample response, affecting the precision to which the slope of the collapse surface (M_L) may be determined. However, the results of a simple linear regression and an ANOVA analysis are given below:-

Title	*Equation*	*Source*	*Df*	*M*	*F*	R^2	*p*
Collapse surface	y = 1.25x - 0.05	Regression Residual	1 25	22 0.0023	9274	0.997	1.17×10^{-33}

Table 6.7. Regression analysis for the Newborough 0% sand collapse surface.

The regression analysis indicates that the slope of the collapse surface (M_L) is 1.25 for the Newborough 0% sand.

6.4. Results: Newborough 5% sand.

6.4.1. Shear wave data.

The results of shear wave testing on the Newborough 5% test sand are listed in Table 6.8 below. As can be seen, 8 complete tests were performed on this sample over a range of void ratios from a minimum of 0.619 to a maximum of 0.765.

Test Number	*Void ratio*	*a*	*b*
1	0.765	32	0.33
2	0.751	40	0.30
2	0.736	38	0.31
4	0.728	38	0.31
5	0.707	40	0.30
6	0.704	35	0.32
7	0.699	38	0.32
8	0.619	43	0.30
Mean.	**0.714**	**38**	**0.31**
Minimum value.	**0.619**	**32**	**0.30**
Maximum value	**0.765**	**43**	**0.33**
Standard deviation.	**-**	**3.3**	**0.01**

Table 6.8. Summary of shear wave test results on Newborough 5% sand.

Following an analysis of the above data, the minimum and maximum recorded shear wave velocity - effective confining stress curves, were identified. These $V_{s\min}$ and $V_{s\max}$ curves corresponded to the maximum and minimum recorded void ratios respectively and are quoted below:-

$$V_{s\min} = 32 \times \sigma'^{0.33} \qquad (6.15).$$

$$V_{s\max} = 43 \times \sigma'^{0.30} \qquad (6.16).$$

These relationships are illustrated in Figure 6.19, and the associated regression data are listed below.

Title	*Equation*	*Source*	*Df*	*M*	*F*	R^2	*p*
Eqn. 6.15	y = 0.33x + 1.51	Regression Residual	1 24	2.39 0.0007	3420	0.99	6.56×10^{-35}
Eqn. 6.16	y = 0.30x + 1.64	Regression Residual	1 24	2.34 0.0008	2815	0.99	2.15×10^{-26}

Table 6.9. Linear regression analysis for Equations 6.15 & 6.16.

Both these relationships have very high R^2 values and very low *p* values, indicating that in common with the shear wave data for the Newborough 0% test sand, these data are of a highly significant nature.

Figure 6.20 illustrates the variation of shear wave velocity with void ratio at an effective stress of 300 kPa. The results of a simple linear regression analysis on this data (results listed in Table 6.10 below) show that void ratio may be related to V_s at 300 kPa, using:-

$$V_{s300} = 376 - 212e \qquad (6.17).$$

Use of this equation suggests that V_{s300} at e_{min} is of the order of 245 m/s, while V_{s300} at e_{max} is of the order of 179 m/s; this represents a maximum possible range of shear wave velocities at 300 kPa of the order of 66 m/s. With regard to the errors associated with the measurement system, this variation in velocity with void ratio is well within the limits of system resolution.

A regression analysis of the same data, with the effective stress equal to 100 kPa, shows that void ratio may be related to V_{s100} using:-

$$V_{s100} = 278 - 165e \qquad (6.18).$$

The regression data for this relationship are listed in Table 6.10 below. As can be seen from this table, for both V_{s300} & V_{s100} the *p* value are several orders of magnitude lower than those associated with the Newborough 0% sand. This effect is mainly due to the significantly fewer individual tests (reflected by the degrees of freedom) that were performed on the Newborough 5% sand. However, despite this, the *p* values remain well below the critical 0.05 value, indicating that both these relationships are of a significant nature. The upper and lower boundaries of the V_{s100} data may be defined using:-

$$V_{s100\ upper} = 282 - 165e \quad ; \quad V_{s100\ lower} = 274 - 165e \qquad (6.19;\ 6.20).$$

Use of Equations 6.18 - 6.20 suggests that V_{s100} at e_{min} is approximately 180 m/s $\pm$ 4 m/s. V_{s100} at e_{max} is of the order of 125 m/s $\pm$ 4 m/s; this represents a likely range of shear wave velocities at 100 kPa between e_{min} & e_{max} of the order of 55 m/s. This experimental scatter of $\pm$ 4 m/s compares to an scatter of $\pm$ 15 m/s for the Newborough 0% test sand described above. The regression line and data boundaries for these data are illustrated in Figure 6.21.

Title	*Equation*	*Source*	*Df*	*M*	*F*	R^2	*p*
Eqn. 6.17.	$V_{s300} = 376\text{-}212e$	Regression Residual	1 6	0.012 0.0003	38	0.84	0.0008
Eqn. 6.18.	$V_{s100} = 278\text{-}165e$	Regression Residual	1 6	0.012 0.0003	45	0.86	0.0005

Table 6.10. Linear regression data for Equations 6.17 & 6.18.

Interestingly, in contrast to Newborough 0% sand, data normalised to 300 and 100 kPa both have very similar R^2 values, indicating that the degree of scatter for each relationship is approximately of the same order of magnitude, despite the potentially smaller range of velocities at 100 kPa (due to the dispersive nature of the V_s - p' curves).

As described above, normalised shear wave velocity may be used to predict the void ratio of laboratory samples. For shear wave velocity normalised to an effective confining stress of 300 kPa, the void ratio of laboratory specimens of Newborough 5% sand may be predicted using:-

$$e_{pred} = \frac{\left(a \times p'^{b}\right) - 376}{-212} \qquad (6.21).$$

For a shear wave velocity normalised to an effective confining stress of 100 kPa, the void ratio of laboratory specimens of Newborough 5% may be predicted using:-

$$e_{pred} = \frac{\left(a \times p'^{b}\right) - 278}{-165} \qquad (6.22).$$

These relationships are illustrated in Figure 6.22 and the regression data for these relationships are presented below.

Title	*Equation*	*Source*	*Df*	*M*	*F*	R^2	*p*
Eqn. 6.21.	y = 1.0x + 0.001	Regression Residual	1 6	0.012 0.0003	38	0.84	0.0008
Eqn. 6.22.	y = 1.0x - 0.002	Regression Residual	1 6	0.012 0.0003	45	0.86	0.0005

Table 6.11. Linear regression and ANOVA data for the comparison between measured and predicted void ratio.

From these data we can see that on the basis of the low *p* values, the relationship between measured and predicted void ratios, calculated from S-wave velocities normalised to two different effective confining stresses, is significant. Examination of Figure 6.22 (a) reveals that the predicted void ratio appears to predict the measured void ratio to better than ± 0.03. Figure 6.22 (b) indicates that based upon a normalised void ratio of 100 kPa the predicted void ratio appears to predict the measured void ratio by ± 0.025. Once again, despite the relatively high quality of these data, these calculated values appear to be significantly larger than the resolution of the system. However, in both cases the regression line lies very close to the '1 to 1' perfect correlation line.

Finally, expressed in its general form and based upon the data described above, the shear wave velocity behaviour of Newborough 5% sand may be summarised using:-

$$V_s = (65 - 38e)p'^{0.31} \qquad (6.23).$$

6.4.2. Triaxial data.

The triaxial data collected during testing on Newborough 5% sand are summarised in Table 6.12, below.

Test No.	e	p'_c (kPa).	p'_{ss} (kPa).	$\Delta p'_{ss}$ (kPa).	q'_{ss} (kPa).	q_{max} (kPa).	p' at q_{max} (kPa).	ψ
1	0.765	200	20	+180	22	240	205	0.044
2	0.751	197	66	+131	84	318	245	0.030
3	0.736	198	153	+45	192	329	249	0.015
4	0.728	200	181	+19	237	336	257	0.007
5	0.707	198	375	-177	506	530	375	-0.014
6	0.704	198	250	-52	320	351	266	-0.017
7	0.699	200	535	-335	710	713	535	-0.022
8	0.619	-	-	-	-	-	-	-

Table 6.12. Summary of triaxial test data on Newborough 5% sand.

In contrast to the Newborough 0% sand, this sand provided some excellent examples of contractive responses leading to a well defined steady state of deformation. Also immediately apparent from the triaxial testing was that this sand was 'more liquefiable' than the previously tested Newborough 0% sand, in that a sample of lower initial void ratio (i.e. denser state) could lead to the generation of raised pore-pressures upon shear. Example sample responses illustrated in normalised stress space are shown in Figure 6.23 (a). Figure 6.23 (b) illustrates the collapse surface, defined by plotting the peak points of the normalised stress paths. The results of a regression analysis on the collapse surface data are listed below:-

Title	Equation	Source	Df	M	F	R^2	p
Collapse surface	y = 1.15x + 0.26	Regression Residual	1 5	92 0.020	4548	0.999	1.36×10^{-08}

Table 6.13. Regression and analysis of variance for the Newborough 5% sand collapse surface.

This analysis shows that the slope of the collapse surface (M_L) is equal to 1.15 and is of an extremely significant nature.

Figure 6.24 (a) & (b) illustrate the steady state line defined in e - log p' and q - p' space respectively. The results of the simple linear regression analyses on these data are listed below.

Title	*Equation*	*Source*	*Df*	*M*	*F*	R^2	*p*
e -log p'	y = -0.05 logx + 0.836	Regression Residual	1 5	1.29 0.024	53	0.90	0.0008
q - p'	y = 1.32x	Regression Residual	1 5	193527 24	8010	0.999	3.3×10^{-9}

Table 6.14. Simple linear regression analysis for Newborough 5% steady state line.

The data listed in Table 6.14 illustrate that the steady state line defined in both the e -log p' and p' - q plane is statistically significant. The analysis also shows that the following parameters may be used to define the steady state line of Newborough 5% sand:-

$e_1 = 0.836$, $C_{ss} = 0.05$, $M = 1.32$, $\phi_{ss} = 30°$.

These parameters are valid over the effective stress range 20 - 600 kPa.

6.5. Results: Newborough 10% sand.

6.5.1. Shear wave data.

The results of shear wave testing on the Newborough 10% sand are listed below in Table 6.15. As can be seen, 9 complete tests were performed on this sand, over a range of void ratios from a minimum of 0.589 to a maximum of 0.730.

Test Number	*Void ratio*	*a*	*b*
1	0.690	29	0.35
2	0.681	33	0.34
2	0.671	35	0.32
4	0.675	35	0.32
5	0.634	36	0.32
6	0.640	33	0.34
7	0.643	30	0.35
8	0.589	26	0.38
9	0.730	24	0.36
Mean.	**0.661**	**31**	**0.34**
Minimum.	**0.589**	**24**	**0.32**
Maximum.	**0.730**	**36**	**0.38**
Standard deviation.	**-**	**4.0**	**0.02**

Table 6.15. Summary of shear wave testing data on Newborough 10% sand.

Once again, the minimum and maximum shear wave velocity - effective stress curves correspond to the minimum and maximum measured void ratios (test numbers 8 & 9). These data are illustrated in Figure 6.25 and quoted below:-

$$V_{s\min} = 24 \times \sigma'^{0.36} \qquad (6.24).$$

$$V_{s\max} = 26 \times \sigma'^{0.38} \qquad (6.25).$$

The regression data used to derive these values data are listed below.

Title	*Equation*	*Source*	*Df*	*M*	*F*	R^2	*p*
Eqn. 6.24	y = 0.36x + 1.39	Regression Residual	1 26	2.57 0.0006	4638	0.99	7.8×10^{-31}
Eqn. 6.25	y = 0.38x + 1.42	Regression Residual	1 26	2.01 0.0004	5281	0.99	1.45×10^{-31}

Table 6.16. Linear regression data for Equations 6.24 & 6.25.

As can be seen from the regression data listed above, both these relationships have very high R^2 values and very low *p* values, indicating that these data are extremely significant and have a very small variation around the best fit curve.

Figure 6.26 illustrates the variation of shear wave velocity with void ratio at an effective stress of 300 kPa. From a brief visual inspection of this illustration, it can be seen that once again void ratio appears to be approximately related to shear wave velocity. This relationship was quantified using a simple linear regression and ANOVA analysis. The results of the analysis (listed in Table 6.17 below) on these data illustrate that void ratio may be related to V_s at 300 kPa, using:-

$$V_{s300} = 380 - 248e \qquad (6.26).$$

Use of this equation suggests that V_{s300} at e_{min} is of the order of 234 m/s, while V_{s300} at e_{max} is the order of 149 m/s; this represents a maximum possible range of shear wave velocities at 300 kPa of the order of 85 m/s. Once again this change in S-wave velocity

with varying void ratio is theoretically resolvable by the laboratory measurement apparatus.

The relationship between shear wave velocity and void ratio at an effective stress of 100 kPa is illustrated in Figure 6.27. Simple linear regression of these data revealed that void ratio may be related to V_s at 100 kPa using:-

$$V_{s100} = 246 - 146e \qquad (6.27).$$

The upper and lower boundaries of these data are defined by:-

$$V_{s100\ upper} = 255 - 146e \quad ; \quad V_{s100\ lower} = 234 - 146e \qquad (6.28;\ 6.29).$$

Use of Equations 6.27 - 6.29 suggests that V_{s100} at e_{min} is approximately 160 m/s ± 12 m/s. V_{s100} at e_{max} is of the order of 110 m/s ± 12 m/s; this represents a likely range of shear wave velocities at 100 kPa between e_{min} & e_{max} of the order of 50 m/s. This experimental scatter resembles that determined for the Newborough 0% test sand of ± 15 m/s. The regression data for these relationships is listed below.

Title	*Equation*	*Source*	*Df*	*M*	*F*	R^2	*p*
Eqn. 6.26.	$V_{s300} = 380\text{-}248e$	Regression Residual	1 7	0.009 0.0006	15	0.64	0.006
Eqn. 6.27.	$V_{s100} = 246\text{-}146e$	Regression Residual	1 7	0.006 0.001	5	0..36	0.05

Table 6.17. Linear regression analysis for Equations 6.26 & 6.27.

In contrast to the previous two sands, these data display both significantly lower R^2 and *p* values. Although the linear relationship between void ratio and V_{s300} (Equation 6.26) remains significant in nature, the relationship between void ratio and V_{s100} displays a very low R^2 value (indicating a large data scatter) and a *p* value of 0.05, indicating that at a level of 95% confidence, this regression is only just significant. Possibly the simplest method of improving the statistical significance of these results would be to perform further tests over a wider range of void ratios.

When used to predict the void ratio of the laboratory samples, the relationships between void ratio and shear wave velocity have the form:-

$$e_{pred} = \frac{\left(a \times p'^{b}\right) - 380}{-248} \qquad (6.30).$$

where, p' = 300 kPa.

$$e_{pred} = \frac{\left(a \times p'^{b}\right) - 255}{-146} \qquad (6.31).$$

where, p' = 100 kPa.

The regression analyses for these data are listed in the table below.

Title	*Equation*	*Source*	*Df*	*M*	*F*	R^2	*p*
Eqn. 6.30.	y = 1.0x - 0.001	Regression Residual	1 7	0.009 0.0006	15	0.64	0.006
Eqn. 6.31.	y = 1.0x + 0.003	Regression Residual	1 7	0.0058 0.0011	5	0.36	0.05

Table 6.18. Linear regression analysis for the comparison between measured and predicted void ratio.

These relationships are illustrated in Figure 6.28. Once again these data are more significant for the shear wave velocity normalised to 300 kPa. The conclusion that can drawn from this observation is that when attempting to relate shear wave velocity to void ratio, normalising the S-wave to a higher effective confining stress generally increases the statistical confidence of the results. However, despite the apparent greater degree of scatter in the data, in both instances the mean lines through the data lie very close to the '1 to 1' perfect fit line.

The general formulae relating all three parameters (i.e. V_s, e & p') for the Newborough 10% sand is:-

$$V_s = (53 - 33e)p'^{0.34} \qquad (6.32).$$

6.5.2. Triaxial data.

The triaxial data collected during testing on Newborough 10% sand are summarised in Table 6.19, below. In common with the Newborough 5% sand, this sand provided some excellent examples of a contractive response leading to a well defined steady state of deformation.

Test No.	*e*	p'_c *(kPa).*	p'_{ss} *(kPa).*	$\Delta p'_{ss}$ *(kPa).*	q'_{ss} *(kPa).*	q_{max} *(kPa).*	p' *at* q_{max} *(kPa).*	ψ
1	0.690	196	27	+169	34	227	190	0.038
2	0.681	199	70	+129	88	318	246	0.029
3	0.671	199	96	+103	125	308	243	0.019
4	0.675	197	79	+118	104	313	240	0.023
5	0.634	198	435	-237	556	556	435	-0.018
6	0.640	197	345	-148	460	460	345	-0.012
7	0.643	198	190	+8	235	259	211	-0.009
8	0.589	200	-	-	-	-	-	-0.063
9	0.730	196	-	196	0	107	156	0.078

Table 6.19. Summary of triaxial testing data on Newborough 10% sand.

Example sample responses, defined in normalised stress space, are illustrated in Figure 6.29 (a). Figure 6.29 (b) illustrates the collapse surface, with a single stress path. Note again that the post-peak stress path crosses the collapse surface, confirming that the collapse surface only represents the limit of stability of a sand under undrained conditions and is distinct from the state boundary surface. The results of the simple linear regression analysis on the collapse surface are listed below:-

Title	*Equation*	*Source*	*Df*	*M*	*F*	R^2	*p*
Collapse surface	y = 1.19x + 0.173	Regression Residual	1 5	40 0.023	1715	0.997	1.55×10^{-07}

Table 6.20. Regression data for the Newborough 10% sand collapse surface.

The results of this analysis show that the slope of the collapse surface (M_L) is extremely significant and equal to 1.19.

Figures 6.30 (a) & (b) illustrate the steady state line defined in e - log p' and q - p' space respectively. The significance of these data were tested using linear regression, and the ANOVA analysis and the results are listed below.

Title	*Equation*	*Source*	*Df*	*M*	*F*	R^2	*p*
e -log p'	y = -0.05 logx + 0.769	Regression Residual	1 5	1.01 0.013	77	0.93	0.0003
q - p'	y = 1.29x	Regression Residual	1 5	144799 54	2672	0.998	5.12×10^{-8}

Table 6.21. Simple linear regression and analysis of variance for the steady state line for Newborough 10% sand.

These data clearly show that the steady state line defined in both the e - log p' and q - p' planes are both linear and of a highly significant in nature. From the results of these data, the following parameters may be used to define the steady state line of Newborough 10% sand:-

$e_1 = 0.769$, $C_{ss} = 0.05$, $M = 1.29$, $\phi_{ss} = 29°$.

These parameters are valid over the effective stress range 20 - 500 kPa.

6.6. Results: Fraser sand.

6.6.1. Shear wave data.

The results of shear wave testing on the Fraser Delta sand are listed below in Table 6.22 As can be seen, 8 complete tests were performed on this particular sample, over a range of void ratios from a minimum of 0.759 to a maximum of 0.882.

Test Number	*Void ratio*	*a*	*b*
1	0.861	49	0.27
2	0.871	44	0.28
2	0.882	42	0.29
4	0.878	44	0.28
5	0.878	37	0.30
6	0.814	41	0.29
7	0.830	50	0.26
8	0.759	58	0.25
Mean.	**0.847**	**45**	**0.28**
Minimum.	**0.759**	**37**	**0.25**
Maximum.	**0.882**	**58**	**0.30**
Standard Deviation.	-	**6.6**	**0.02**

Table 6.22. Summary of shear wave test results for the Fraser sand.

The minimum and maximum recorded shear wave velocity - effective stress curves were calculated as described previously and the regression data for this analysis are listed in Table 6.22 below. The curves themselves are illustrated in Figure 6.31, and the equations are quoted below:-

$$V_{s\min} = 37 \times \sigma'^{0.30} \qquad (6.33).$$

$$V_{s\max} = 58 \times \sigma'^{0.25} \qquad (6.34).$$

Title	*Equation*	*Source*	*Df*	*M*	*F*	R^2	*p*
Eqn. 6.33	y = 0.30x + 1.56	Regression Residual	1 28	3.34 0.001	2683	0.99	2.36×10^{-29}
Eqn. 6.34	y = 0.25x + 1.76	Regression Residual	1 12	0.87 0.0004	1987	0.99	1.06×10^{-14}

Table 6.23. Linear regression analysis for Equations 6.33 & 6.34.

Both these relationships have very high R^2 values and very low *p* values, indicating once again that the transformed data from which the relationships were calculated are of a highly significant nature.

Figure 6.32 illustrates the relationship between shear wave velocity and void ratio at an effective stress of 300 kPa. From a simple visual inspection, these data appear significantly more scattered than the previous three sand samples tested. The results of a simple linear regression analysis on these data show that void ratio may be related to shear wave velocity at 300 kPa, using:-

$$V_{s300} = 362 - 169e \qquad (6.35).$$

However, as can be noted from the regression data listed below in Table 6.24, these data are only significant at a level of 90% confidence. Part of the reason for this relatively poor correlation, especially when compared to the other test sand data described, could be due to the relatively small range of void ratios over which these measurements were performed. More specifically, most of these shear wave - void ratio measurements were made over a range, in terms of void ratio, of less than 0.1. The

reason for this small spread of void ratios is most likely due to the increased compressibility of the Fraser Delta sand, making the preparation of samples with a wide range of initial void ratios more difficult. Further shear wave velocity measurements, closer to the extreme values of e_{min} & e_{max}, could be used to further improve the statistical validity of this relationship.

Plotting the Fraser delta sand shear wave velocity and void ratio data, with the effective stress equal to 100 kPa, once again shows that the relationship between normalised shear wave velocity and void ratio is well scattered in nature. Simple linear regression of these data revealed that void ratio may be related to V_s at 100 kPa using:-

$$V_{s100} = 310 - 175e \qquad (6.36).$$

The upper and lower boundaries of this data is defined by:-

$$V_{s100\ upper} = 321 - 175e \quad ; \quad V_{s100\ lower} = 297 - 175e \qquad (6.37;6.38).$$

Once again these data are only significant at a 90% level of confidence.

Title	*Equation*	*Source*	*Df*	*M*	*F*	R^2	*p*
Eqn. 6.35.	$V_{s300} = 362 - 169e$	Regression Residual	1 7	0.005 0.001	4	0.30	0.09
Eqn. 6.36.	$V_{s100} = 310 - 175e$	Regression Residual	1 6	0.006 0.001	5	0..37	0.07

Table 6.24. Linear regression analysis for Equations 6.35 & 6.36.

In common with the discussion above, and recognising the increased statistical uncertainty surrounding these data, the following relationships may be used to predict the void ratio of laboratory prepared samples of Fraser Delta sand:-

$$e_{pred} = \frac{\left(a \times p'^{b}\right) - 362}{-169} \qquad (6.39).$$

where, p'=300 kPa

$$e_{pred} = \frac{\left(a \times p'^{b}\right) - 310}{-175} \qquad (6.40).$$

where, p'=100

The regression data associated with these relationships are listed below.

Title	*Equation*	*Source*	*Df*	*M*	*F*	R^2	*p*
Eqn. 6.39.	y = 1.0x - 0.003	Regression Residual	1 7	0.005 0.001	4	0.30	0.09
Eqn. 6.40.	y = 1.0x - 0.0001	Regression Residual	1 7	0.006 0.001	5	0.37	0.07

Table 6.25. Linear regression analysis for the comparison between measured and predicted void ratio.

Figure 6.34 (a & b) once again reflects the greater scatter of these data, with the scatter in both instances being of the order of ± 0.075 in terms of void ratio. However, despite this large degree of scatter, in both cases the respective regression lines lie very close to the '1 to 1' or perfect fit line.

Expressed in its most general form, the shear wave velocity behaviour of the Fraser delta sand may be described in terms of void ratio and effective confining stress using:-

$$V_s = (74 - 41e)p'^{0.28} \qquad (6.41).$$

6.6.2. Triaxial data.

The triaxial data collected during testing on the Fraser sand are summarised in Table 6.26 below.

Test No.	e	p'_c (kPa).	p'_{ss} (kPa).	$\Delta p'_{ss}$ (kPa).	q'_{ss} (kPa).	q_{max} (kPa).	p' at q_{max} (kPa).	ψ
1	0.861	202	238	-36	320	320	238	0.015
2	0.871	194	192	+2	260	260	192	0.022
3	0.882	201	114	+87	150	173	150	0.036
4	0.878	199	149	+50	195	195	149	0.031
5	0.878	199	134	+65	174	174	134	0.031
6	0.814	199	277	-78	377	377	277	-0.033
7	0.830	200	186	+14	253	253	186	-0.017
8	0.759	200	503	-303	720	720	503	-0.088

Table 6.26. Summary of triaxial test data on the Fraser delta sand.

In contrast to the two previous sand samples, this particular sand did not display any examples of a typical contractive response, rather it tended to fail after an initial pore-pressure rise, followed by a subsequent fall in pore-pressures, leading to what was interpreted as steady state conditions. Two examples of this type of response, defined in normalised stress space, are illustrated in Figure 6.35. Because of this lack of strongly contractive sample responses it was not possible to define the collapse surface for this particular sand.

Figures 6.36 (a) & (b) illustrate the steady state line defined in e - log p' and q - p' space respectively. Both these data sets were the subject of full linear regression analyses; the data from which they are derived are listed below.

Title	Equation	Source	Df	M	F	R^2	p
e -log p'	y = -0.19 logx + 1.29	Regression Residual	1 6	0.25 0.008	31	0.81	0.001
q - p'	y = 1.38x	Regression Residual	1 6	109070 11	9530	0.996	7.79×10^{-11}

Table 6.27. Linear regression data for the steady state line; Fraser Delta sand.

Both these regressions display high R^2 and p values and are statistically highly significant, displaying extremely low p values.

From the results of these analyses, the following parameters may be used to define the steady state line of the Fraser Delta sand:-

$e_1 = 1.29$, $C_{ss} = 0.19$, $M = 1.38$, $\phi_{ss} = 31°$.

These parameters are valid over the effective stress range 100 - 500 kPa.

6.7. Summary.

The data presented above describe in detail the geophysical and geotechnical properties of all four laboratory test sands. These data is of relatively standard form, and both types of data have been previously described for other materials by different authors. However, possibly the most unique part of this project is the integration of these two types of data, allowing correlations to be made between conventional geotechnical measures of liquefaction potential and geophysical parameters, in this case, shear wave velocity. The integrated data will therefore be presented in Chapter 7.

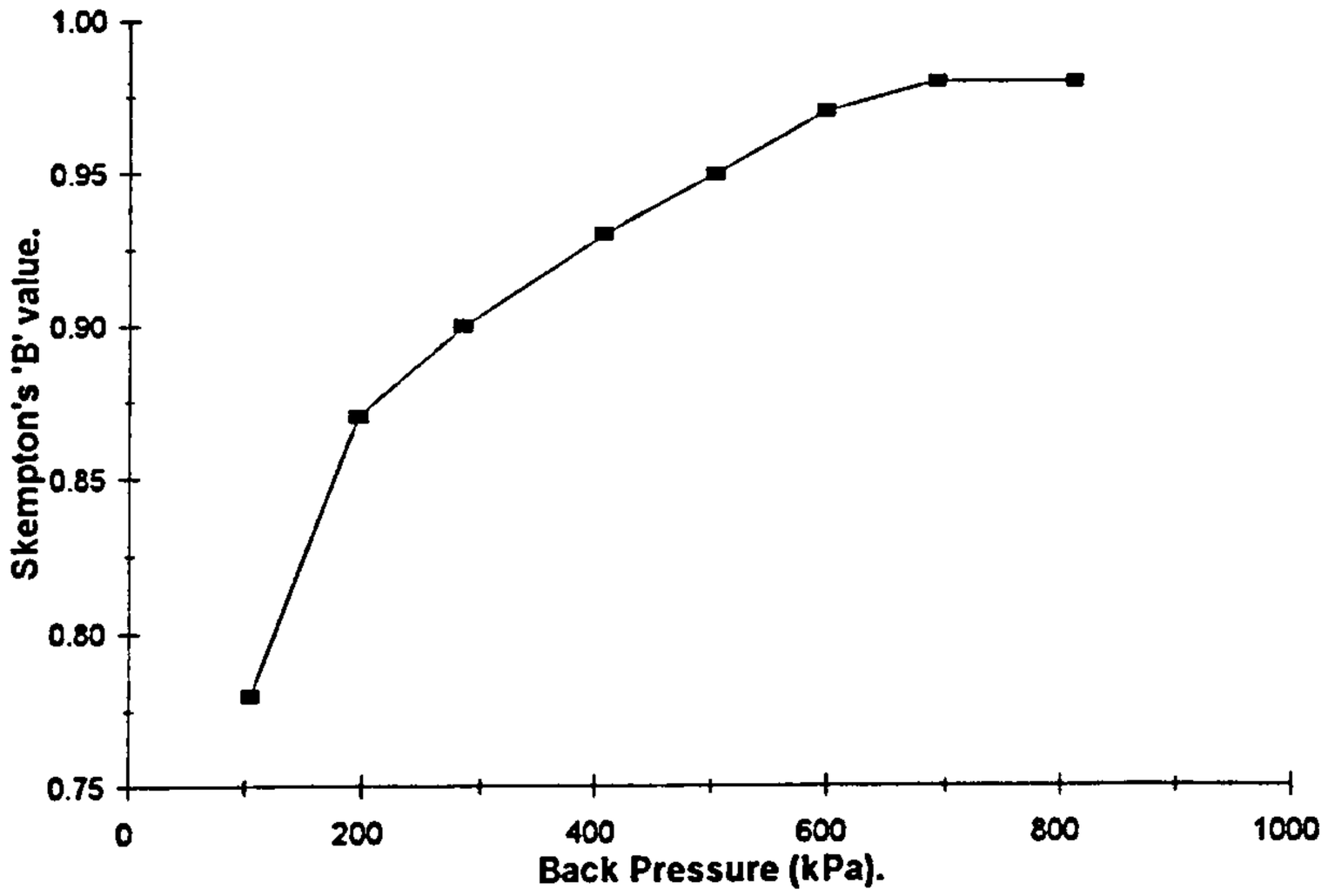

Figure 6.1. Example data set illustrating the increasing 'B' values with increasing back pressure.

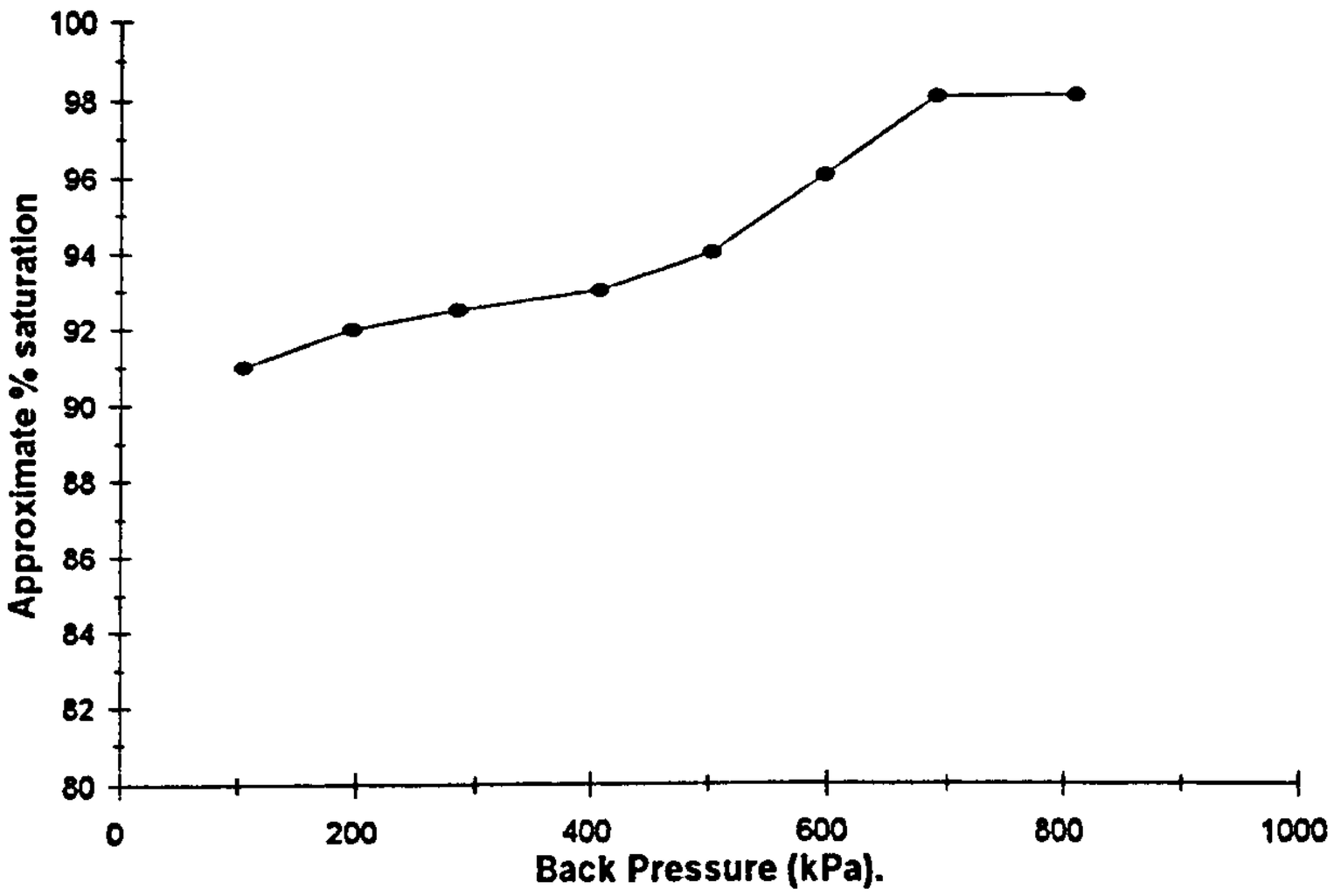

Figure 6.2. Example data illustrating the approximate percentage saturation of a sand sample during consolidation, inferred from Figure 6.1. above.

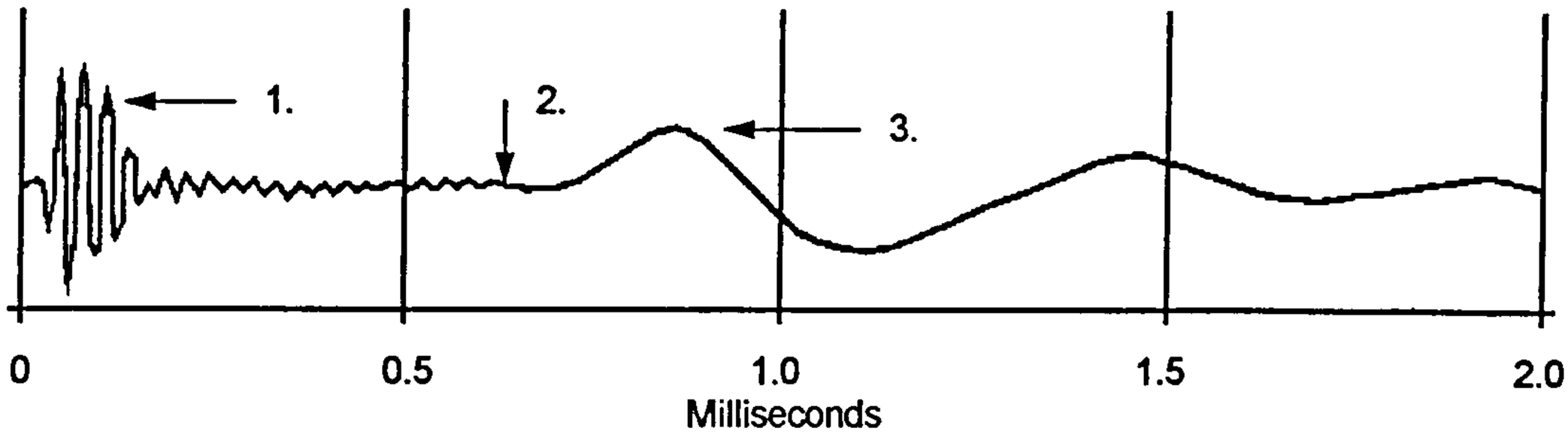

Figure 6.3. Typical unfiltered shear wave signal in an unsaturated medium, collected using the small 50mm triaxial cell.

1. Rapidly attenuated, high frequency P-wave component.
2. Shear wave onset.
3. Well defined, lower frequency shear wave.

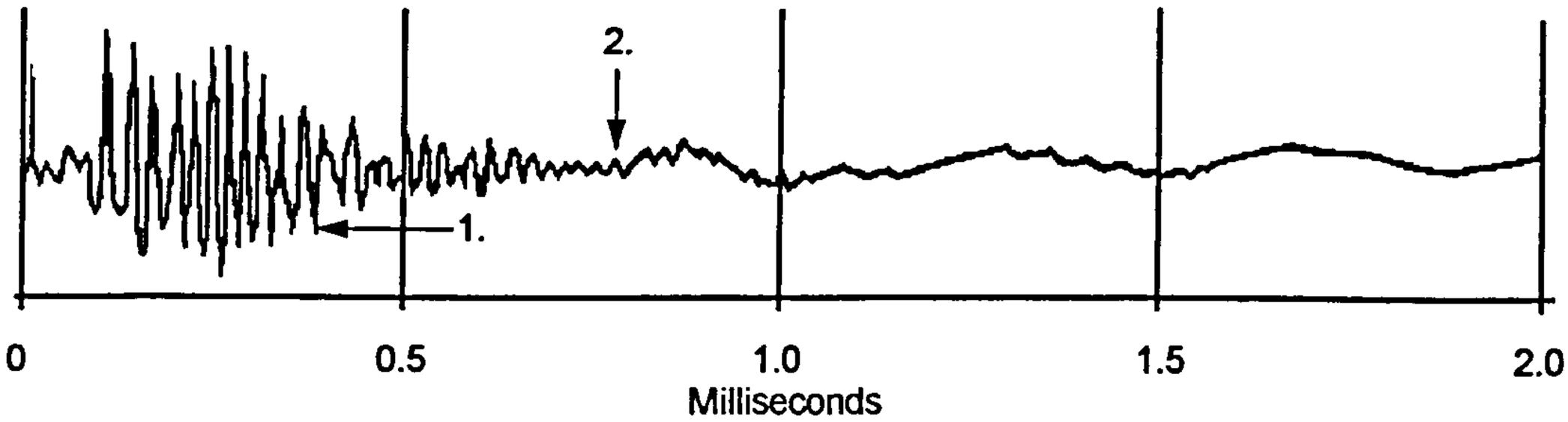

Figure 6.4. Typical unfiltered shear wave signal in a fully saturated medium, collected using the small 50mm triaxial cell.

1. High frequency P-wave component.
2. Poorly defined shear wave, with no obvious onset.

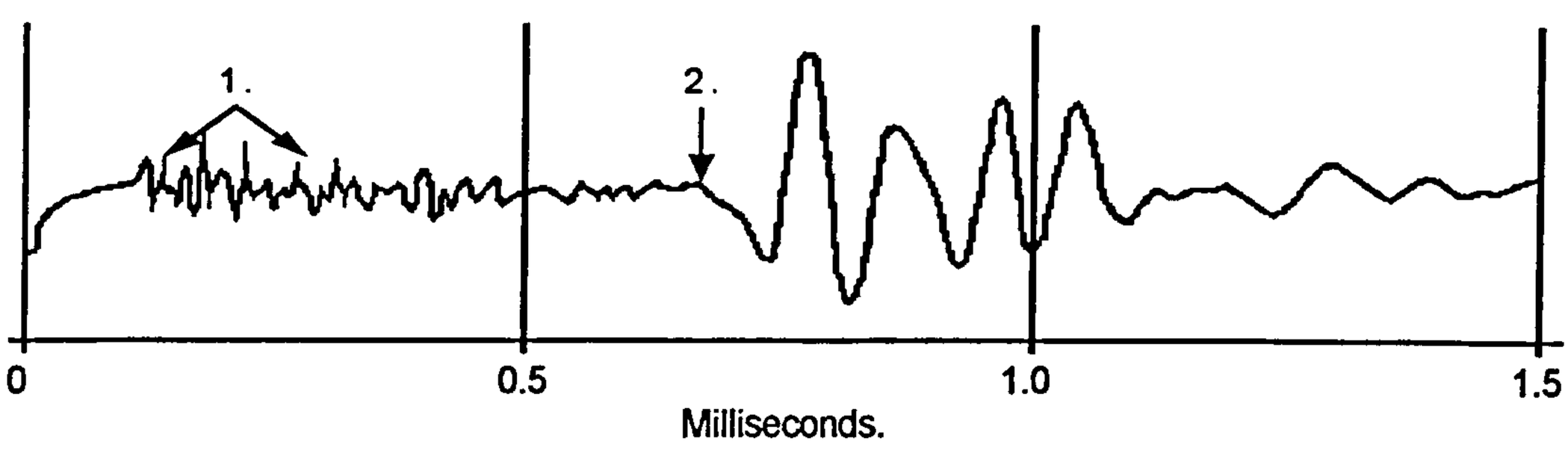

Figure 6.5. Unfiltered signal, collected using the large 100mm triaxial cell.

1. Unfiltered P wave or near field noise.
2. Shear wave onset.

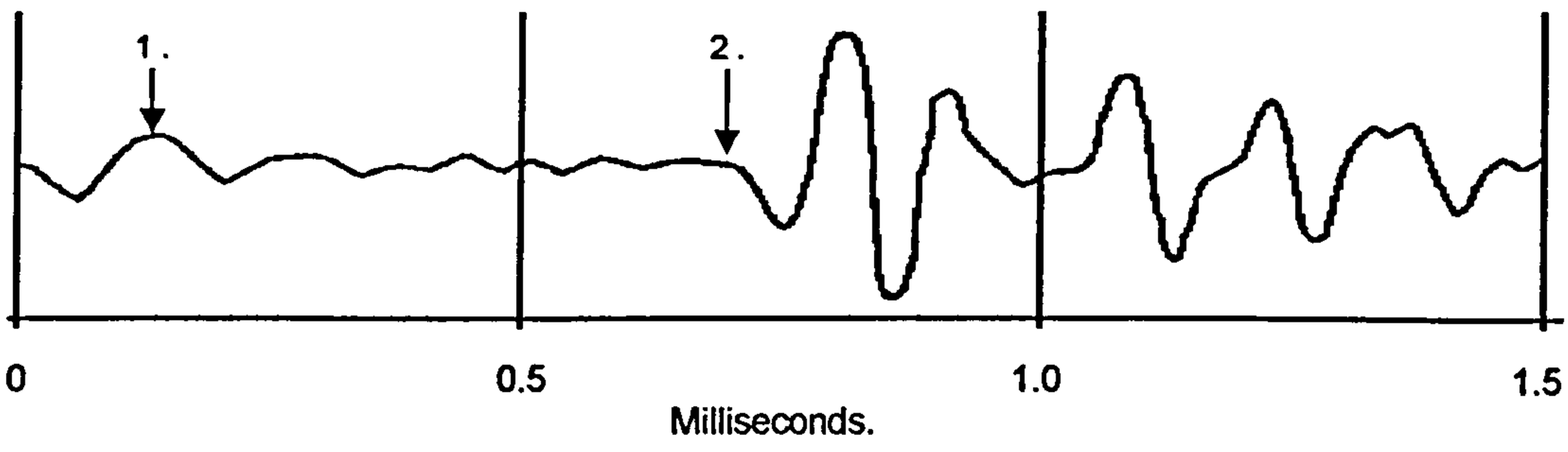

Figure 6.6. Filtered version of the signal illustrated in Figure 6.5 (19 kHz high cut).

1. Low frequency residual noise remaining after filtering.
2. Shear wave onset.

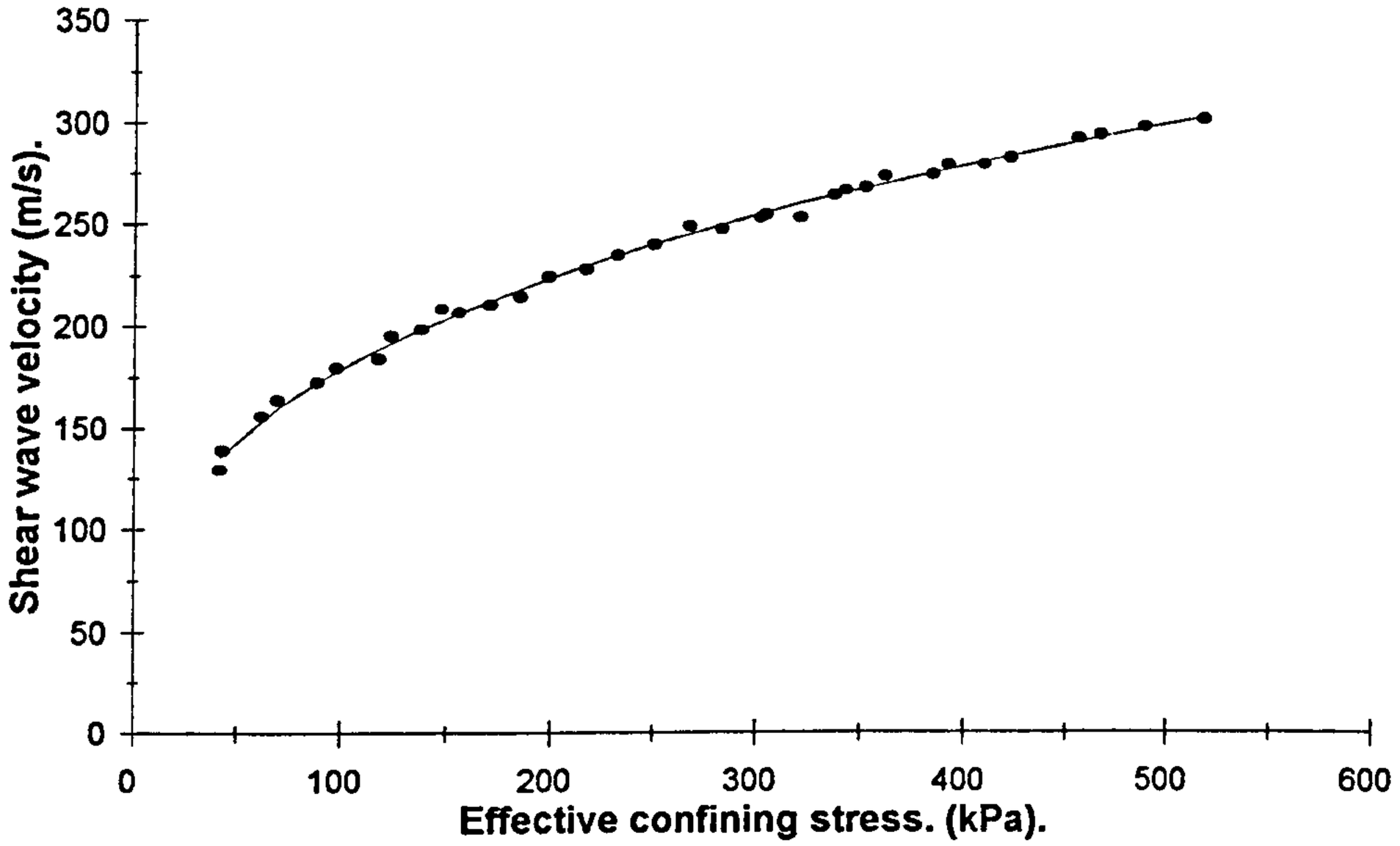

Figure 6.7. Example relationship between shear wave velocity and effective confining stress.

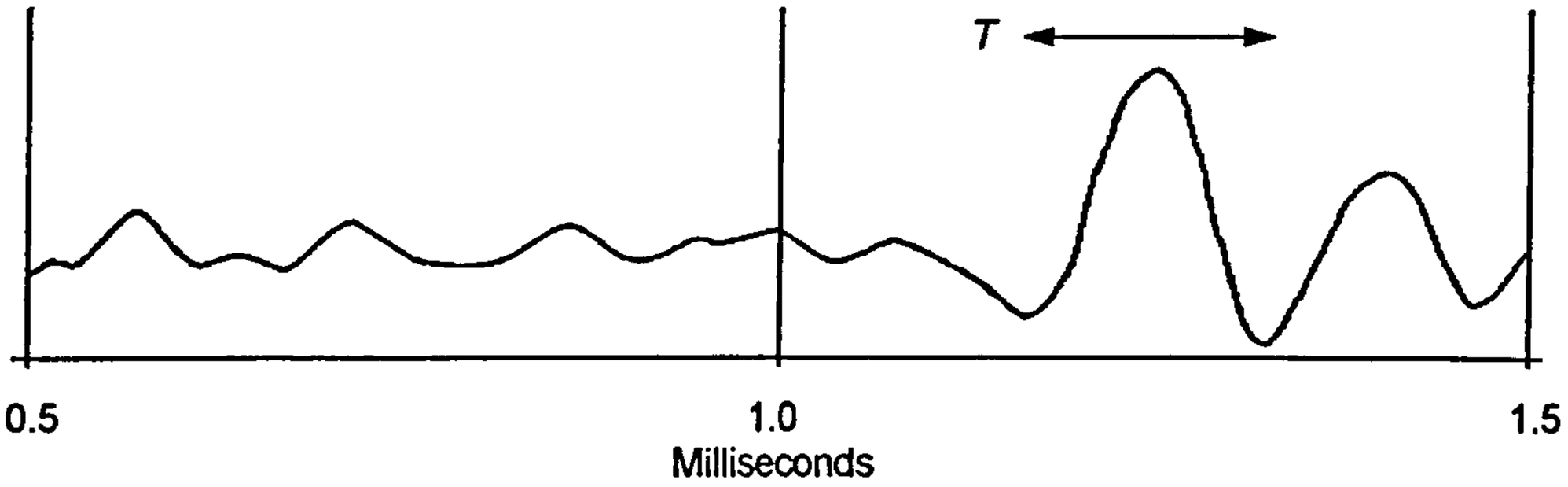

Figure 6.8. Example shear wave signal at effective stress of 68 kPa (test material Newborough 0% sand).

Period (*T*) :- 152μS.
Frequency :- 6579 Hz.

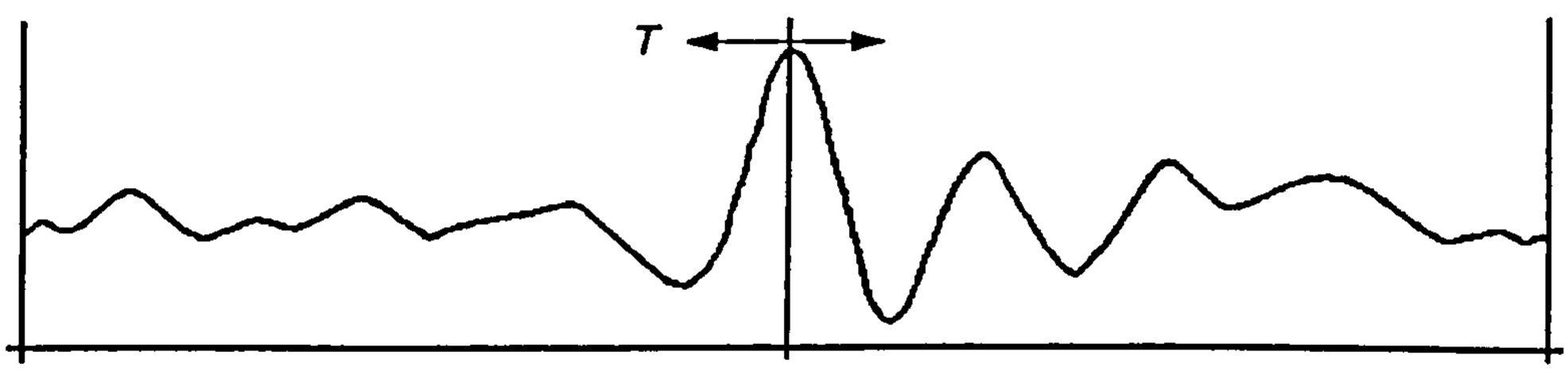

Figure 6.9. Example shear wave signal at an effective stress of 107 kPa (test material Newborough 0% sand)..

Period :- 122μS
Frequency :- 8197 Hz.

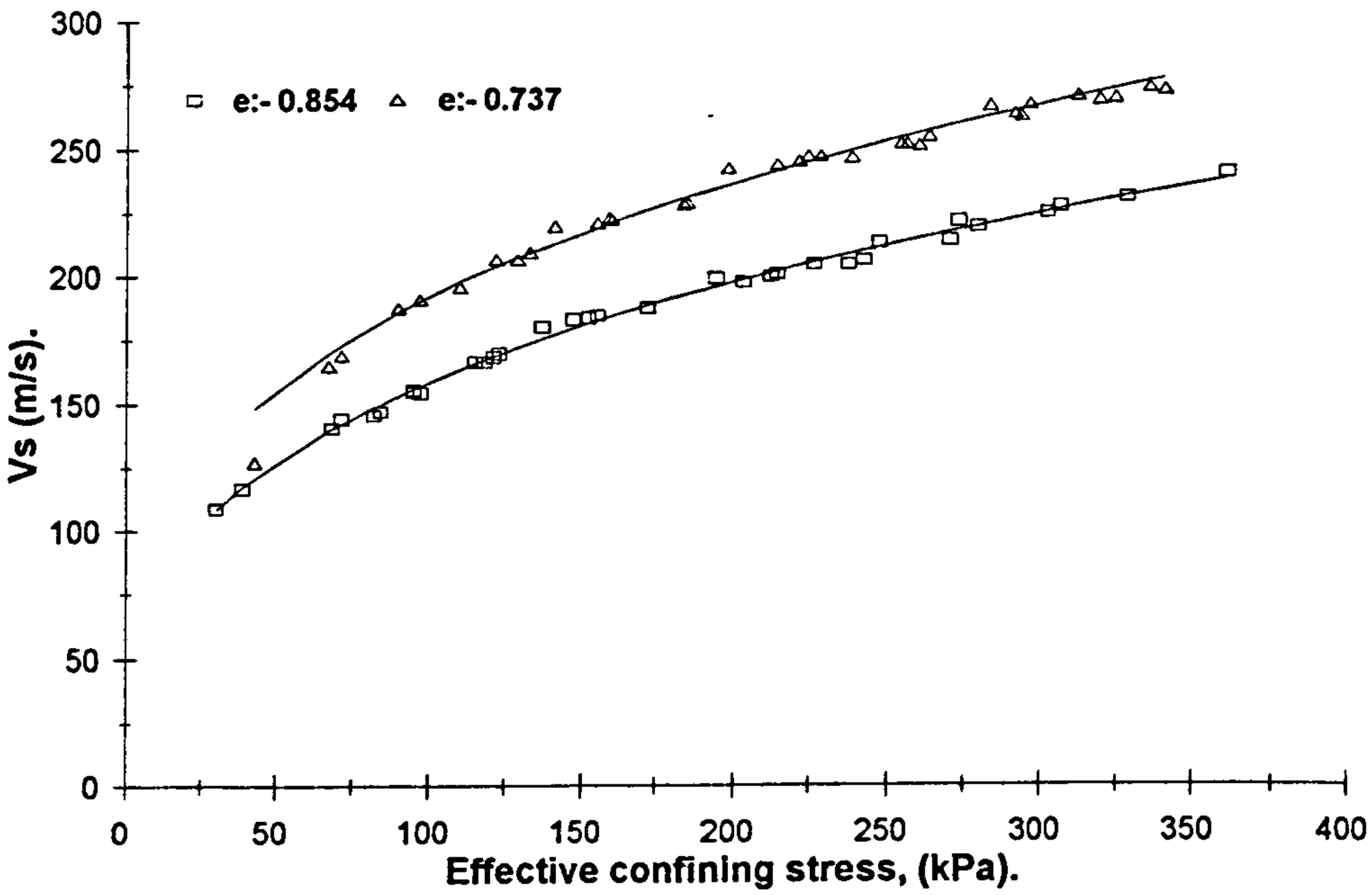

Figure 6.10. Effect of differing void ratio upon the shear wave velocity for different samples of Newborough 0% sand.

a.

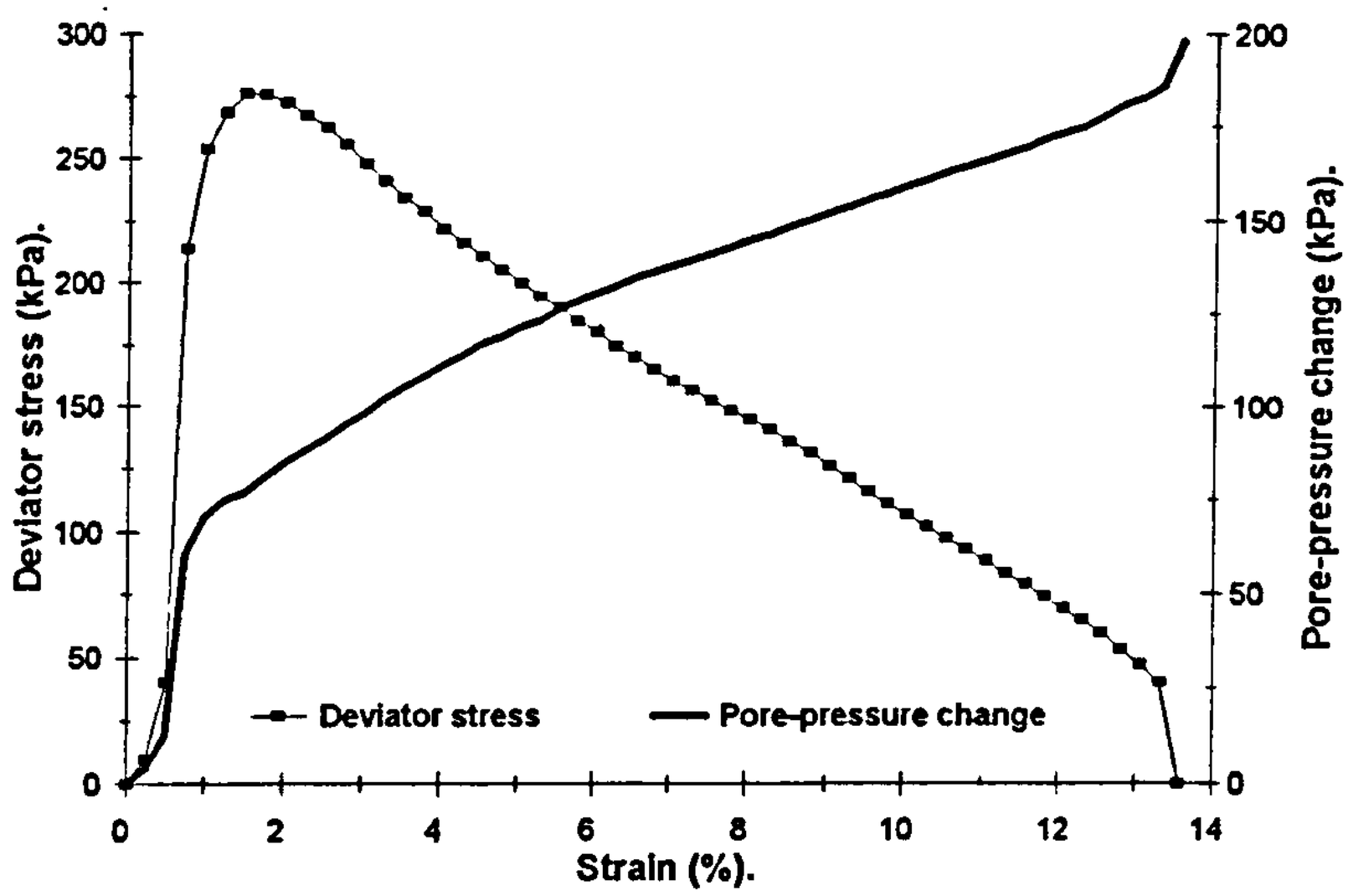

b.

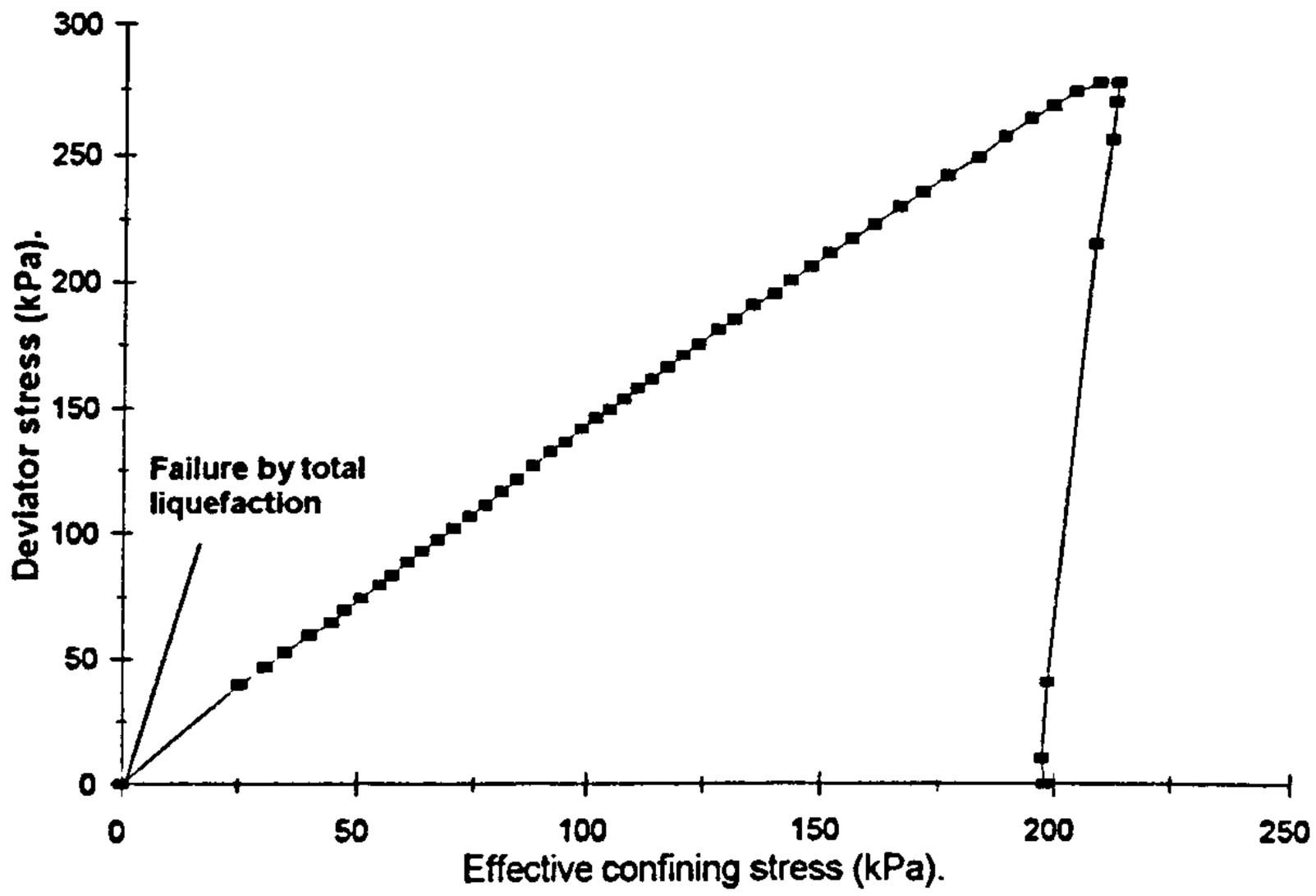

Figure 6.11. a & b. Undrained, contractive response of a loose sand, leading to failure by total liquefaction.

a.

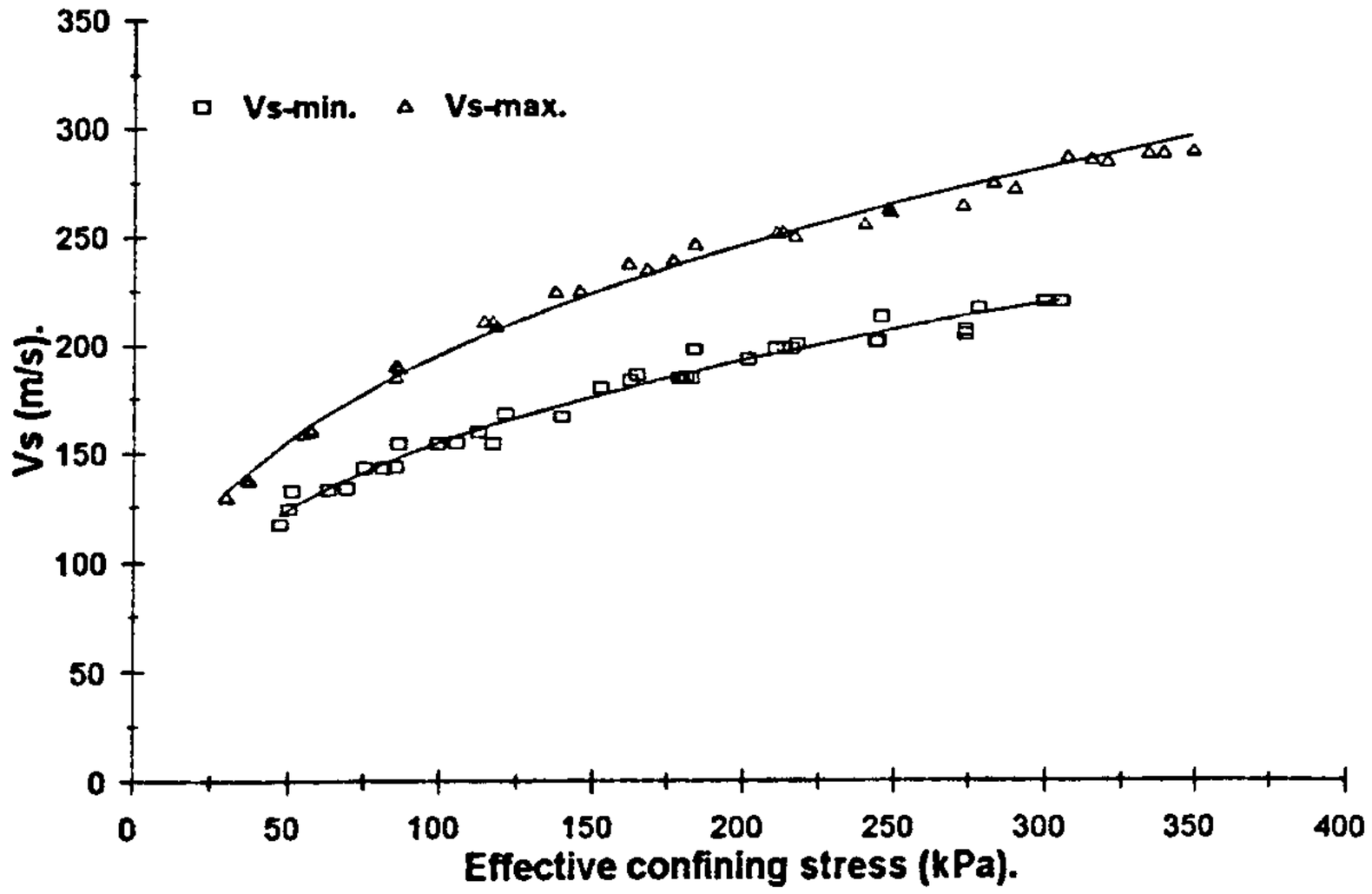

b.

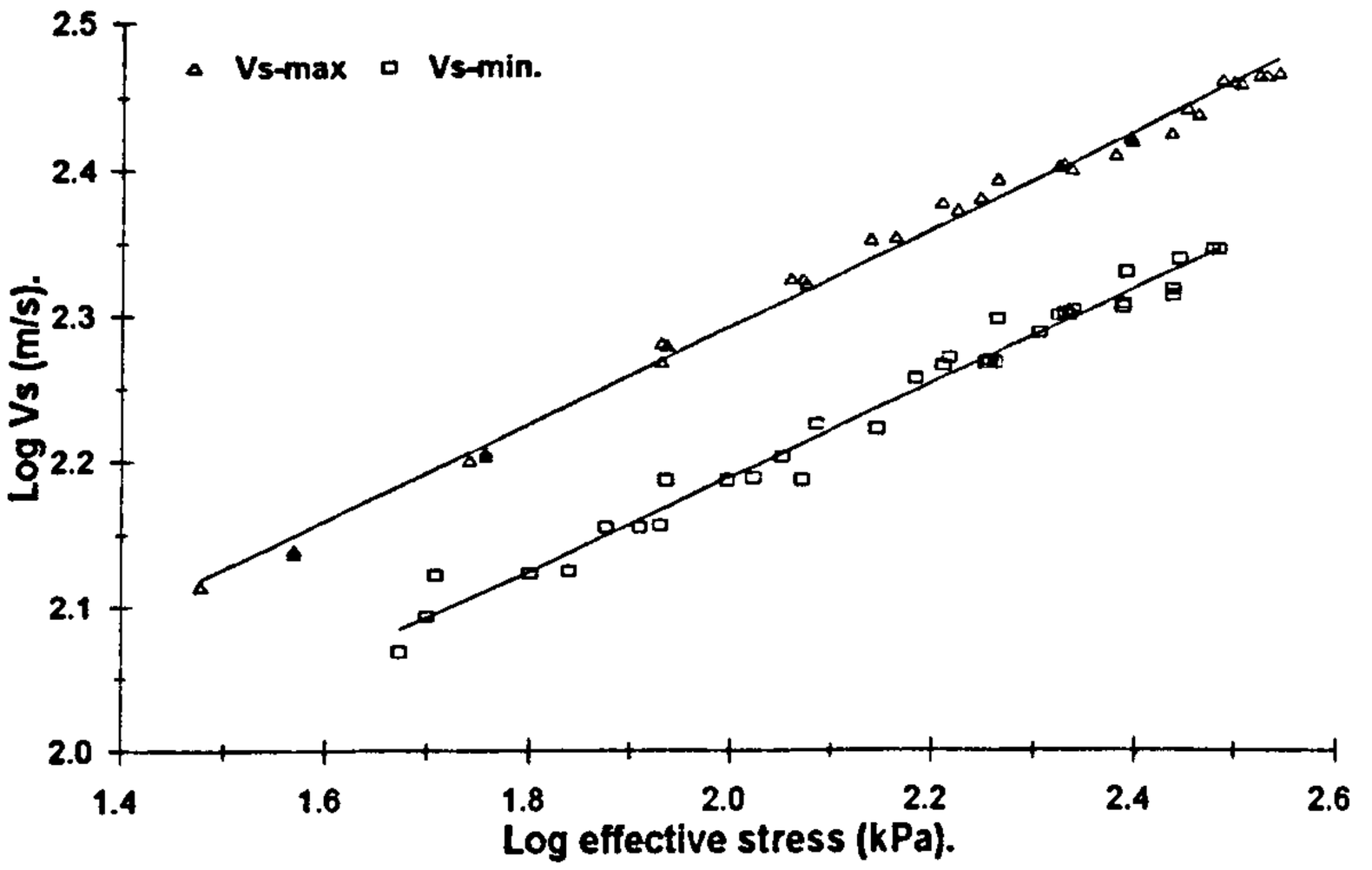

Figure 6.12. a. Minimum and maximum measured shear wave velocities, Newborough 0% sand.

Figure 6.12. b. Minimum and maximum velocities, Newborough 0% sand. Note logarithmic scale.

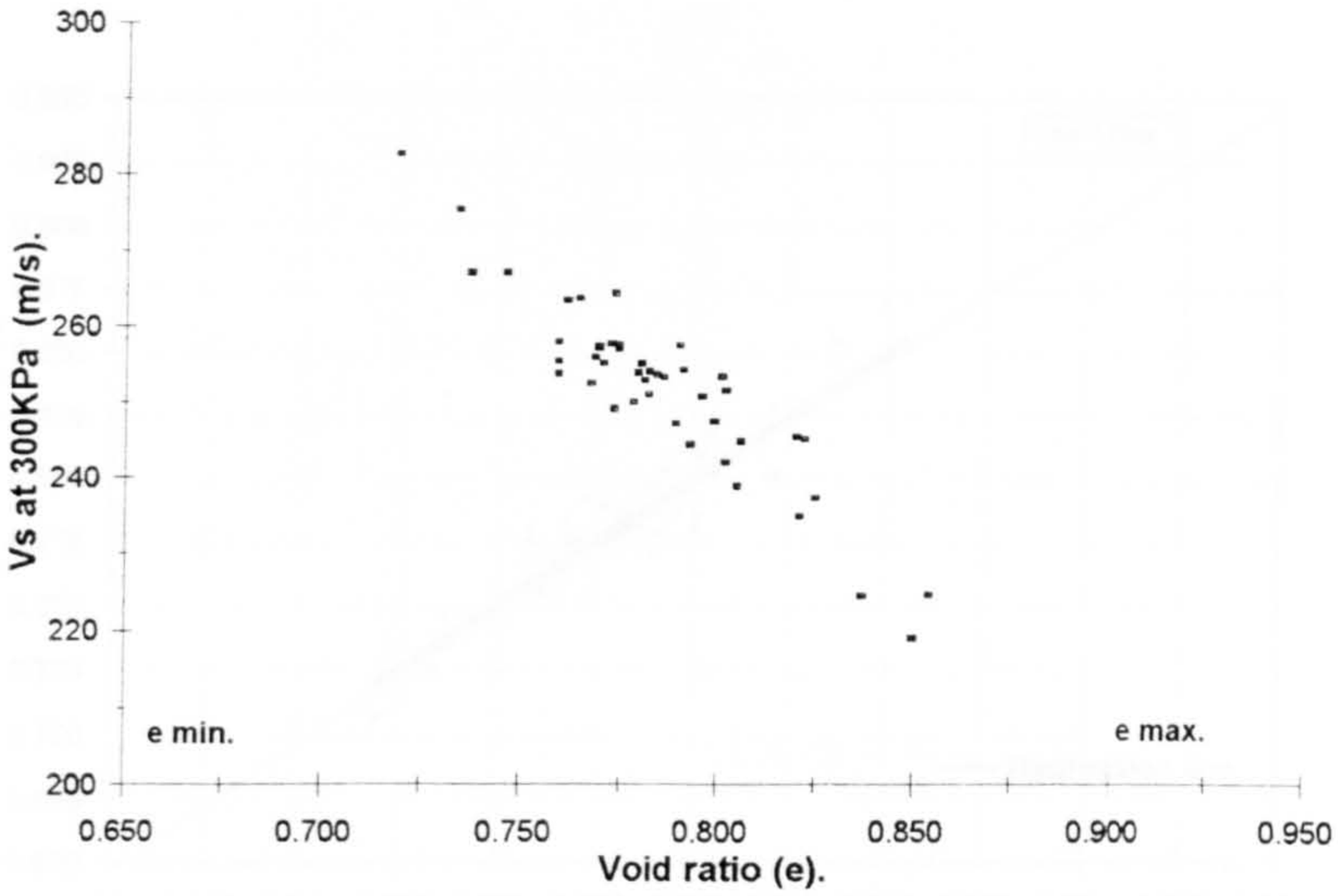

Figure 6.13. Relationship between void ratio and shear wave velocity, at an effective stress of 300 kPa.

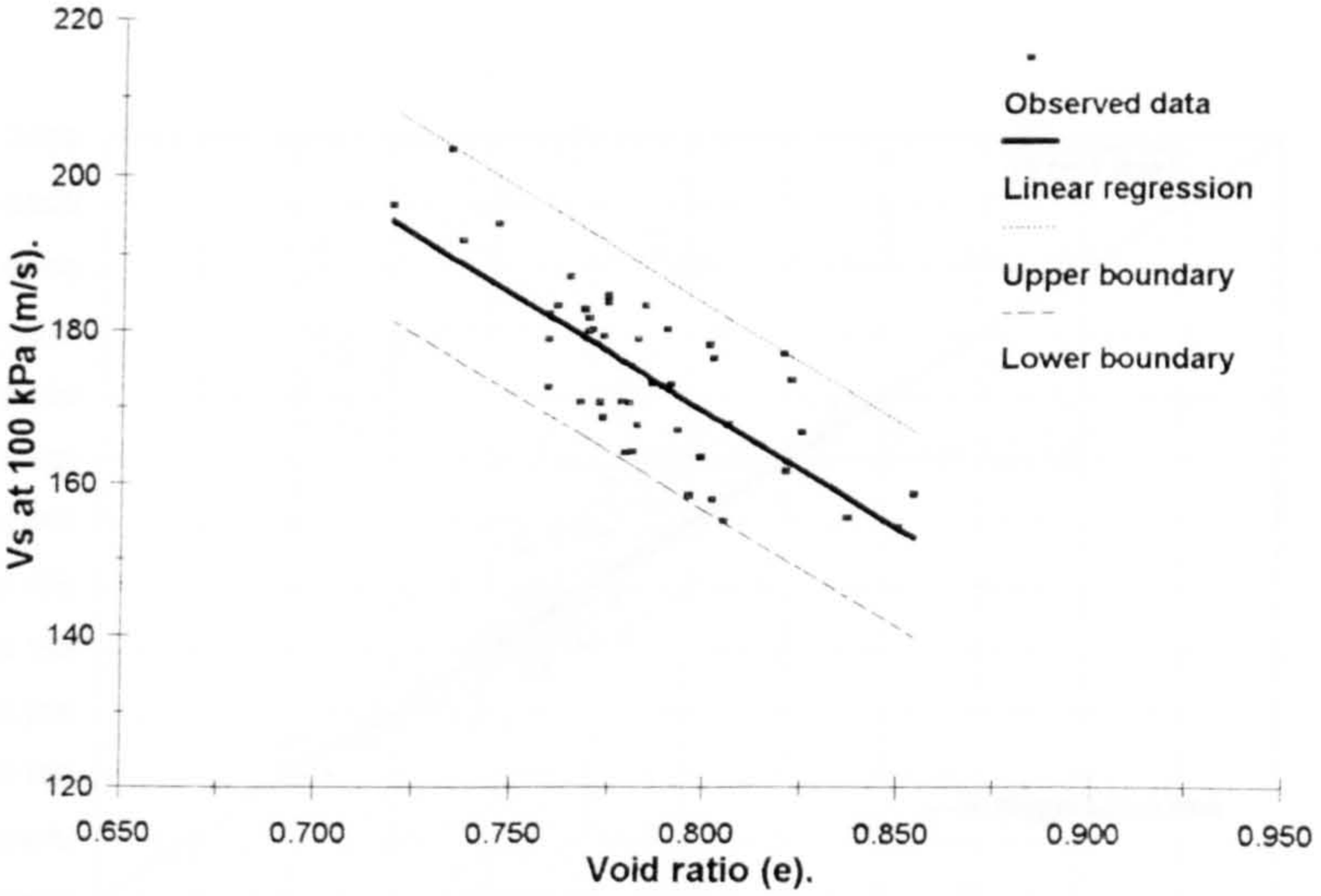

Figure 6.14. Relationship between void ratio and shear wave velocity, at an effective stress of 100kPa, illustrating regression line and data boundaries.

a.

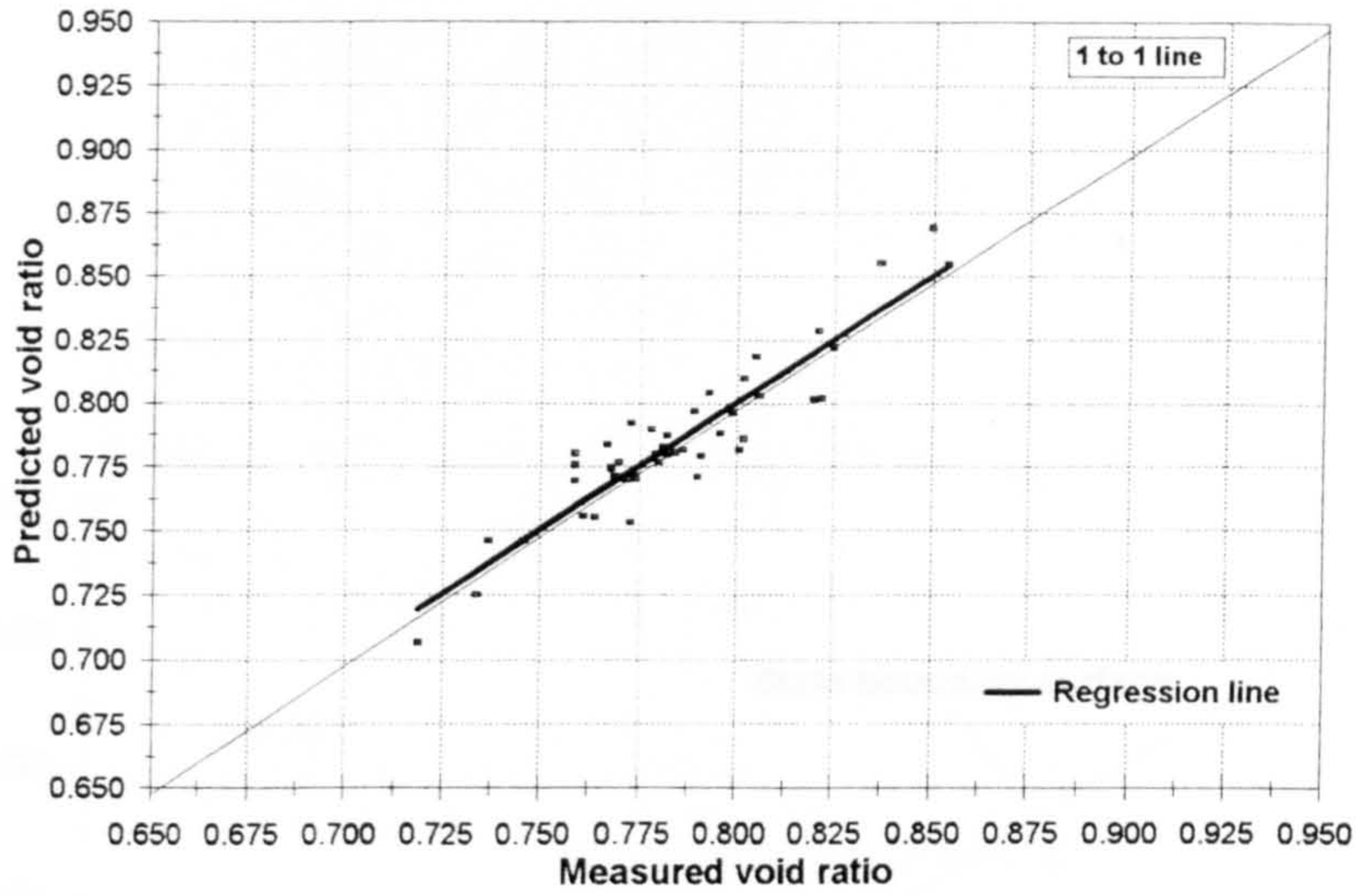

b.

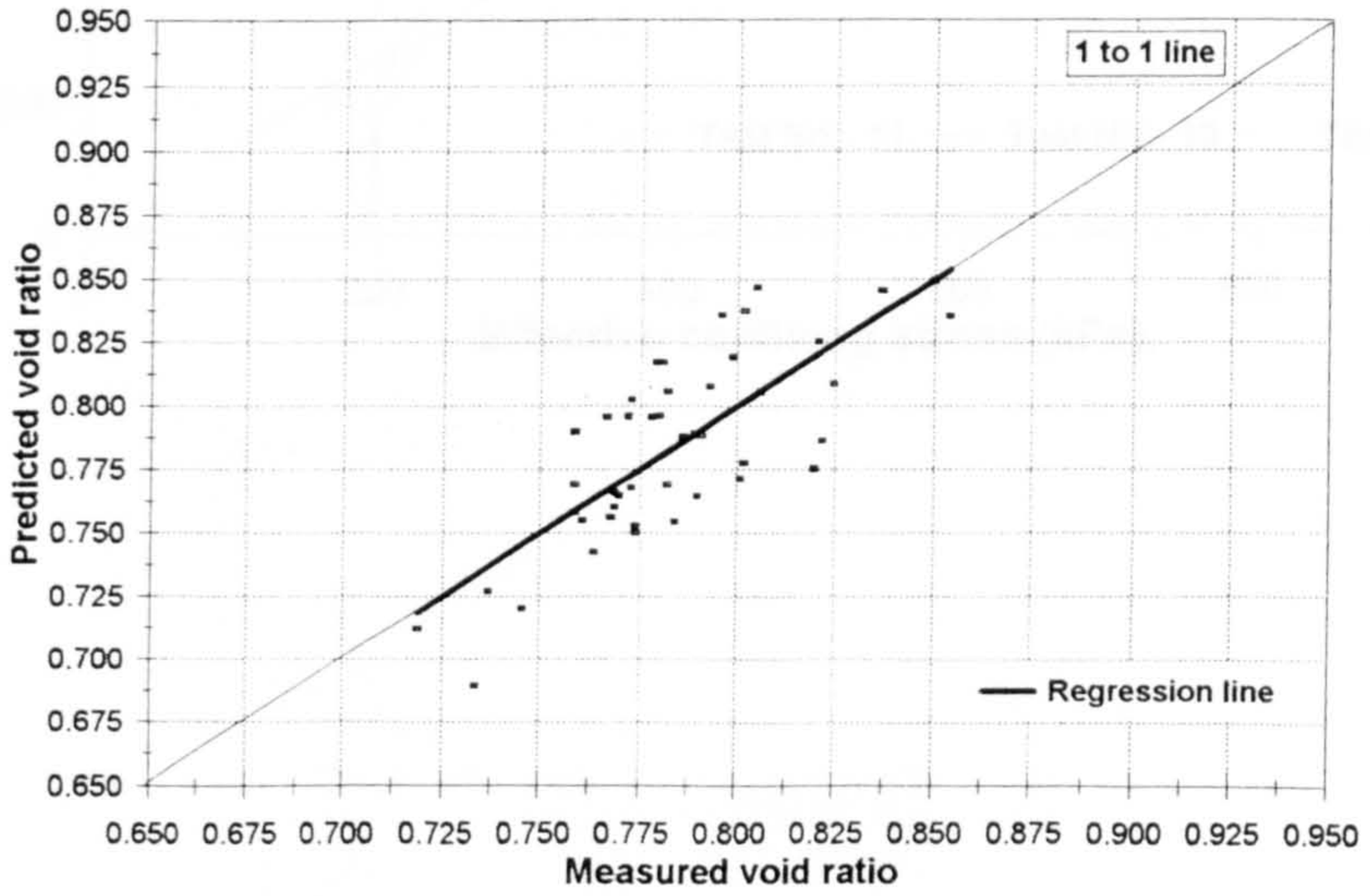

Figure 6.15. a. Comparison between measured and predicted void ratio, based upon shear wave velocities normailsed to 300 kPa.

Figure 6.15. b. Comparison between measured and predicted void ratio, based upon shear wave velocities normailsed to 100 kPa.

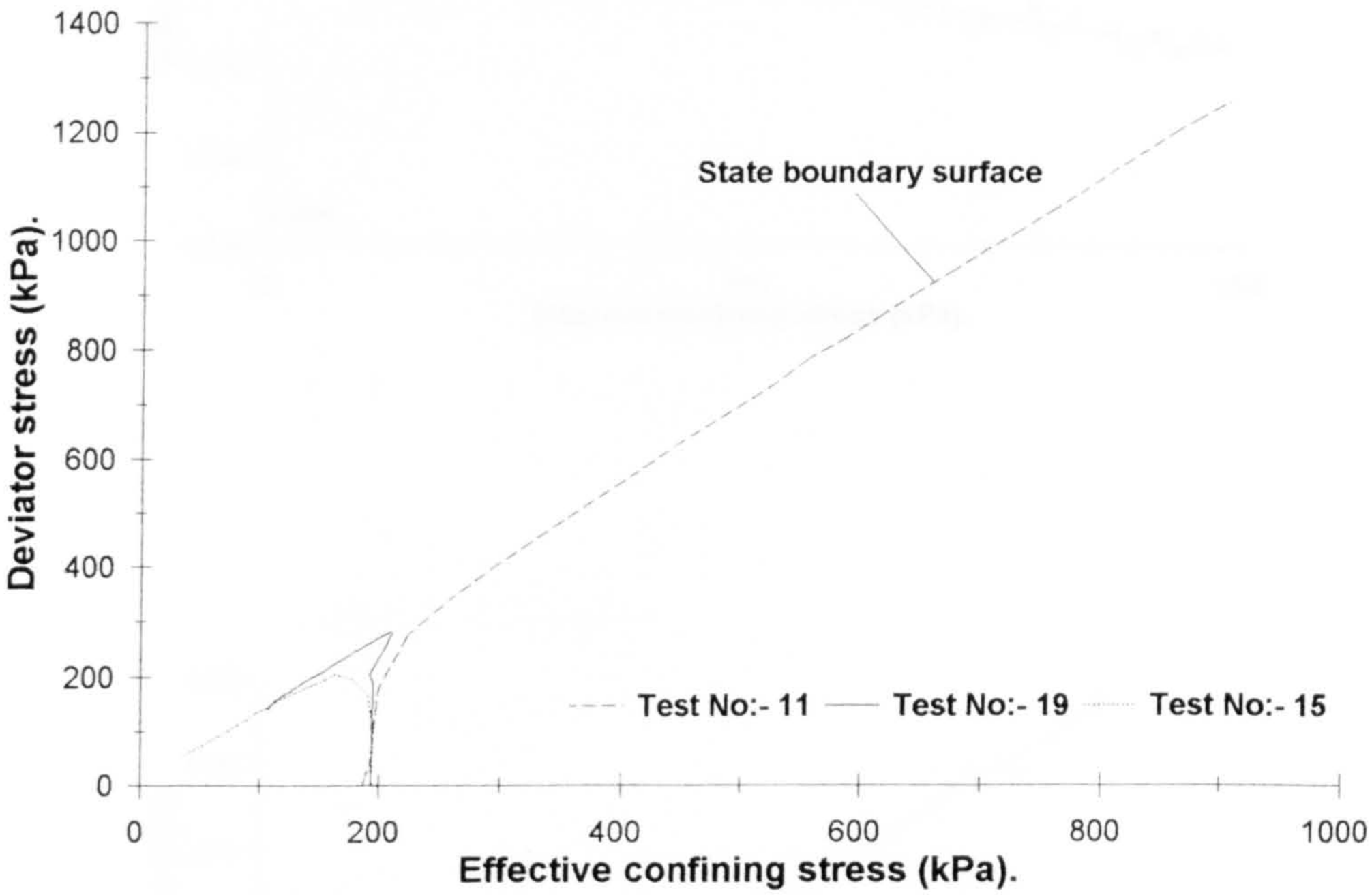

Figure 6.16. State boundary surface defined for Newborough 0% sand.

a.

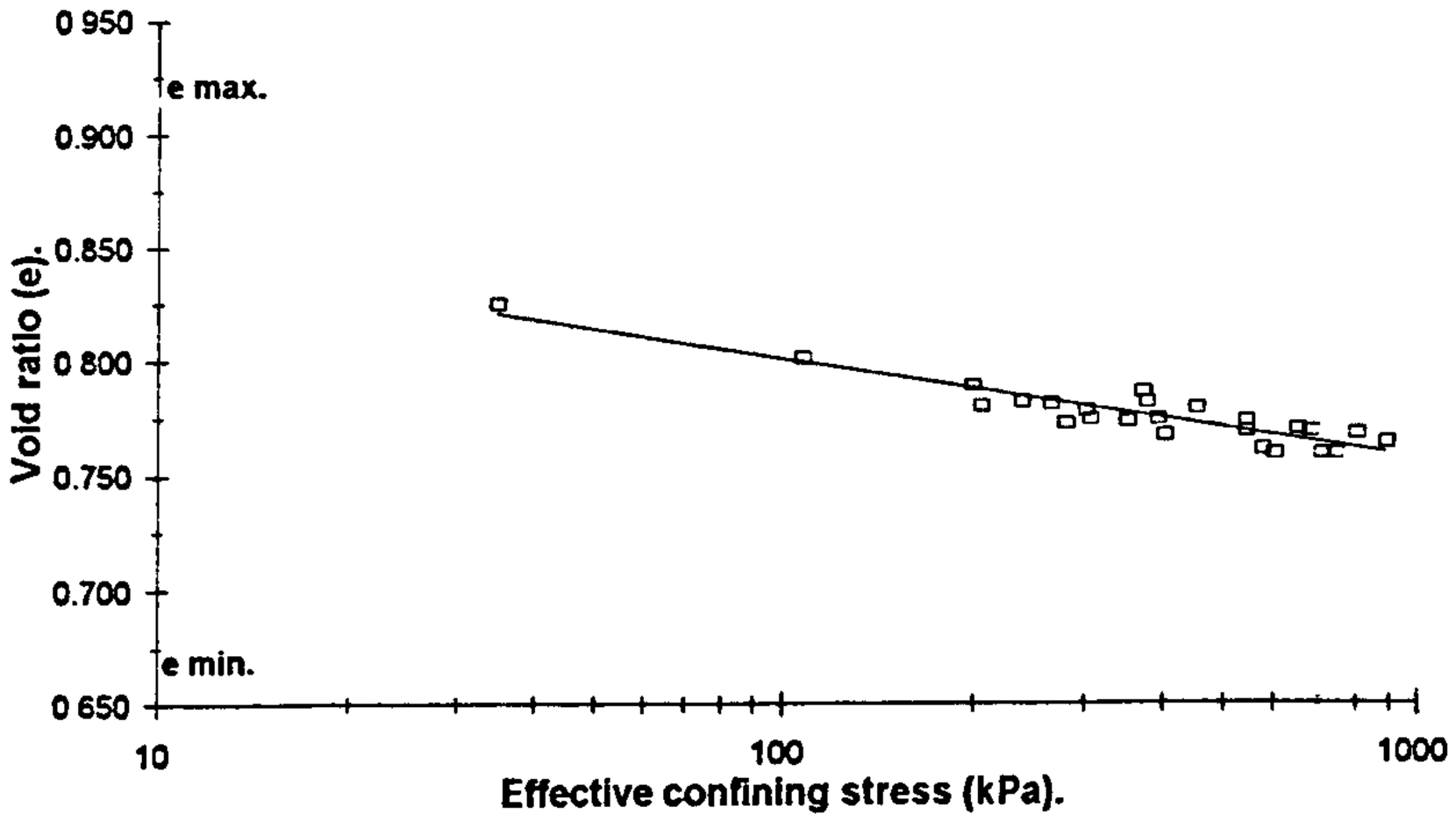

b.

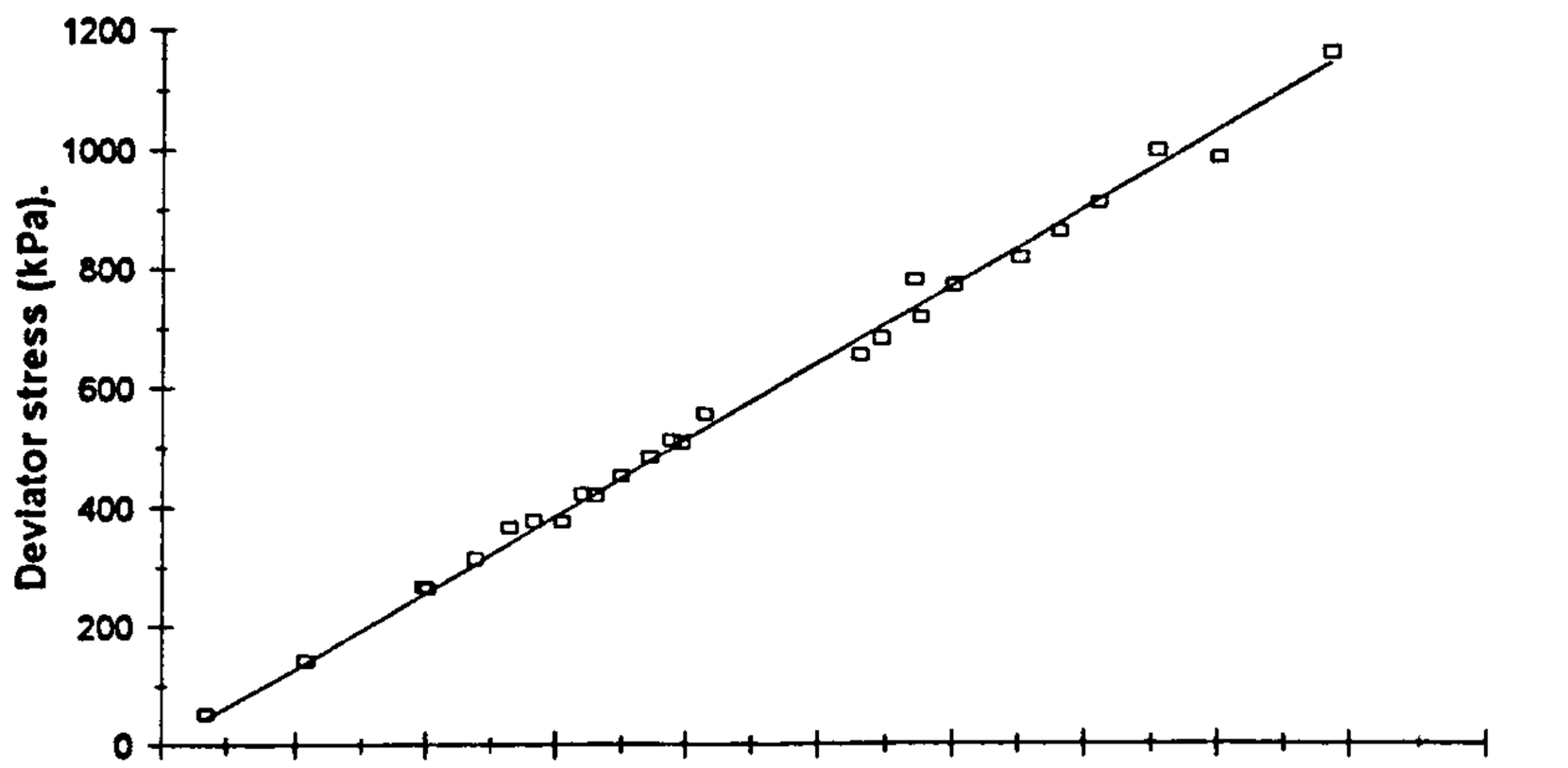

Figure 6.17. a & b. Newborough 0% sand steady state line.

a.

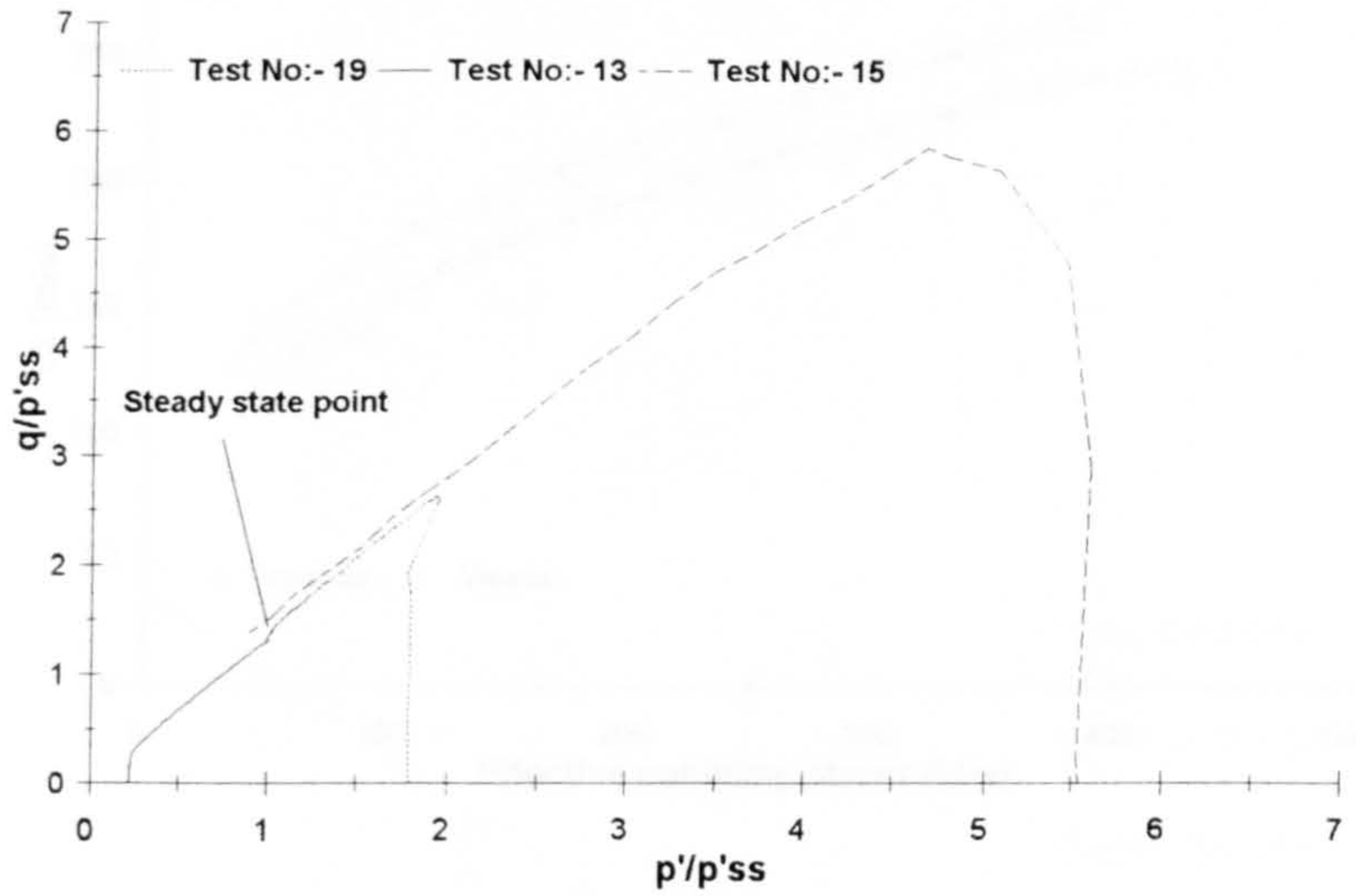

b.

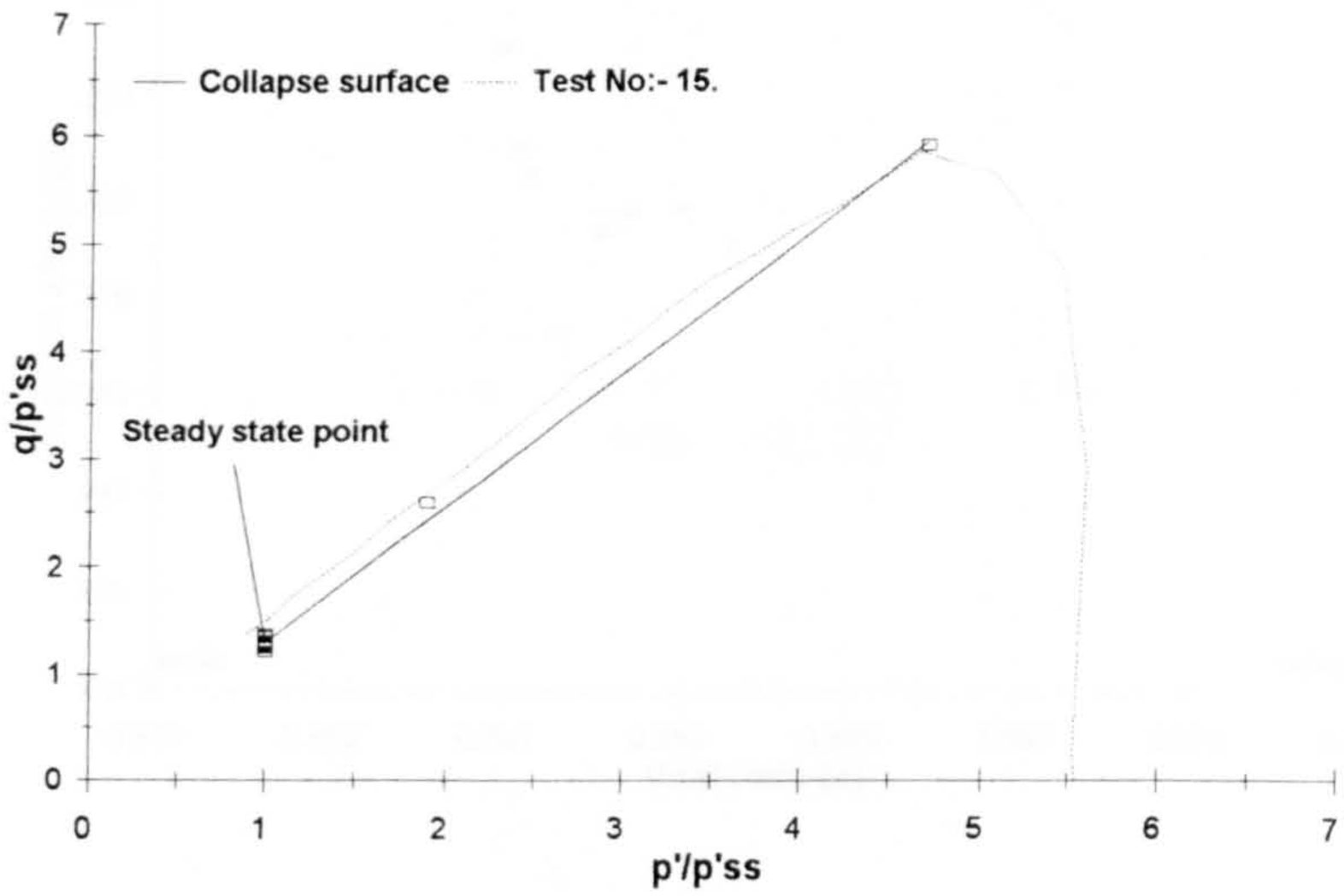

Figure 6.18. a. Selected normalised stress paths; Newborough 0% sand.

Figure 6.18. b. Collapse surface and peak points from normalised stress paths; Newborough 0% sand.
Note:- for calrity only one stress path is shown.

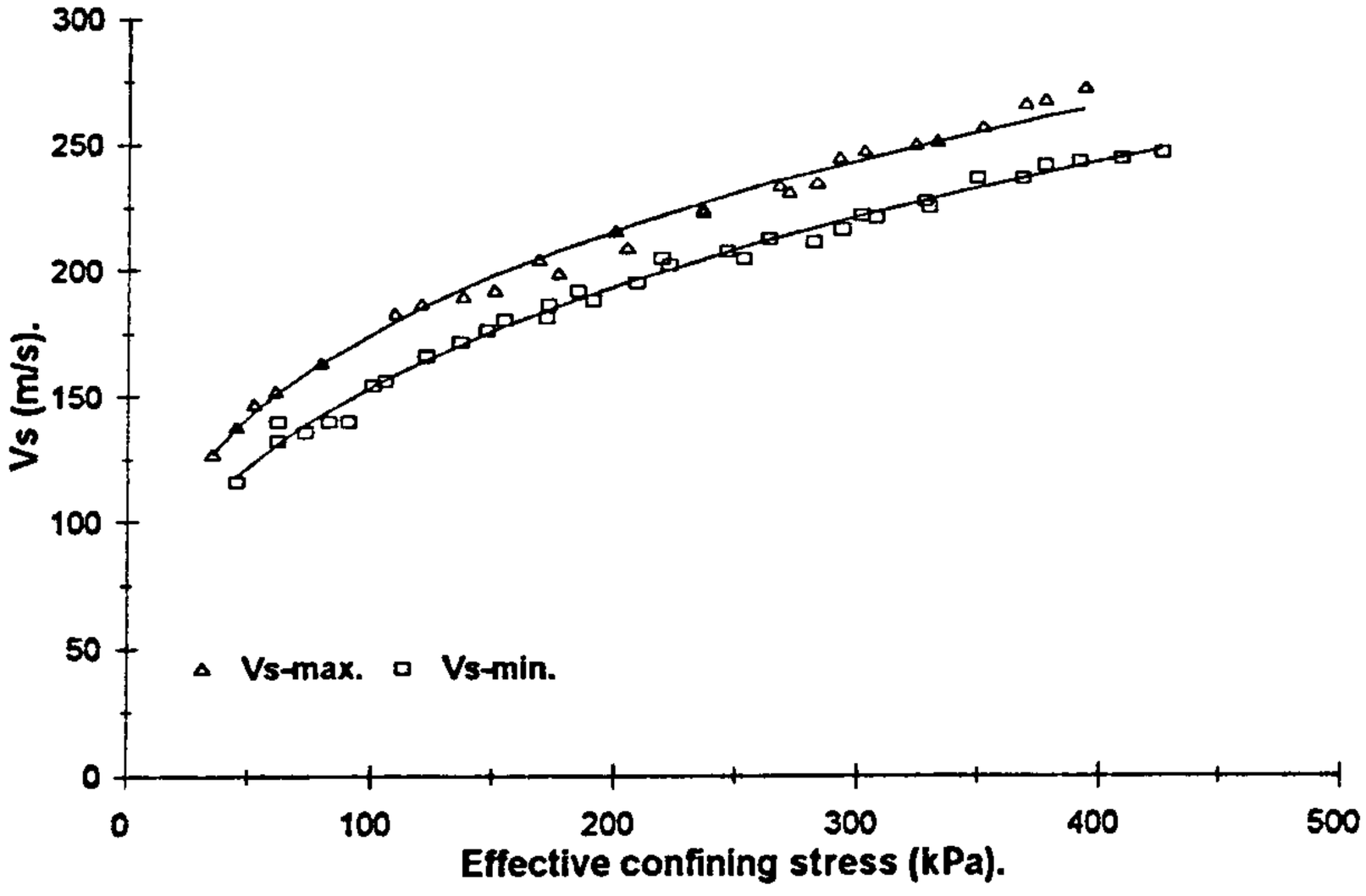

Figure 6.19. Minimum and maximum measured velocities; Newborough 5% sand.

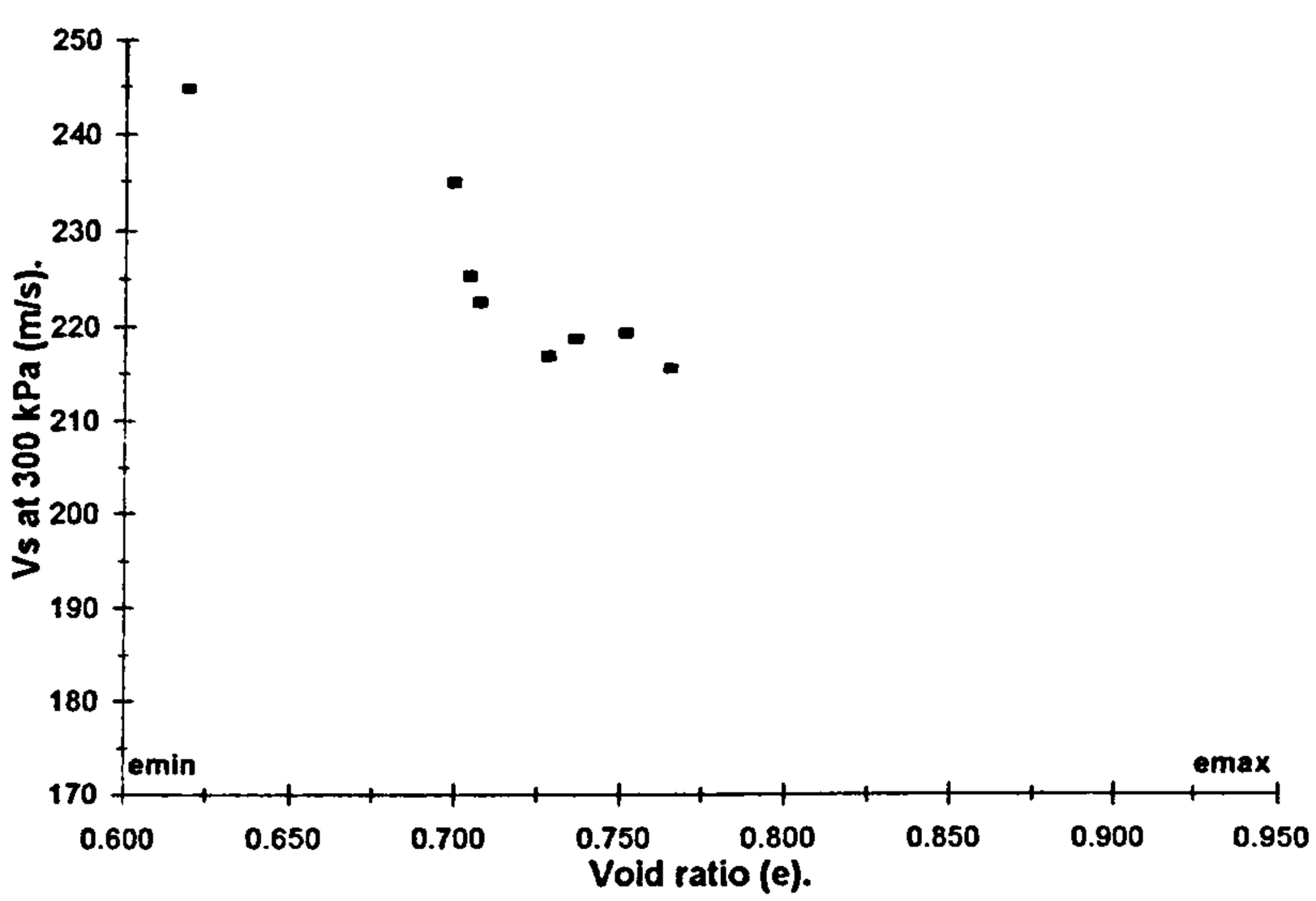

Figure 6.20. Relationship between void ratio and shear wave velocity, at an effective confining stress of 300 kPa.

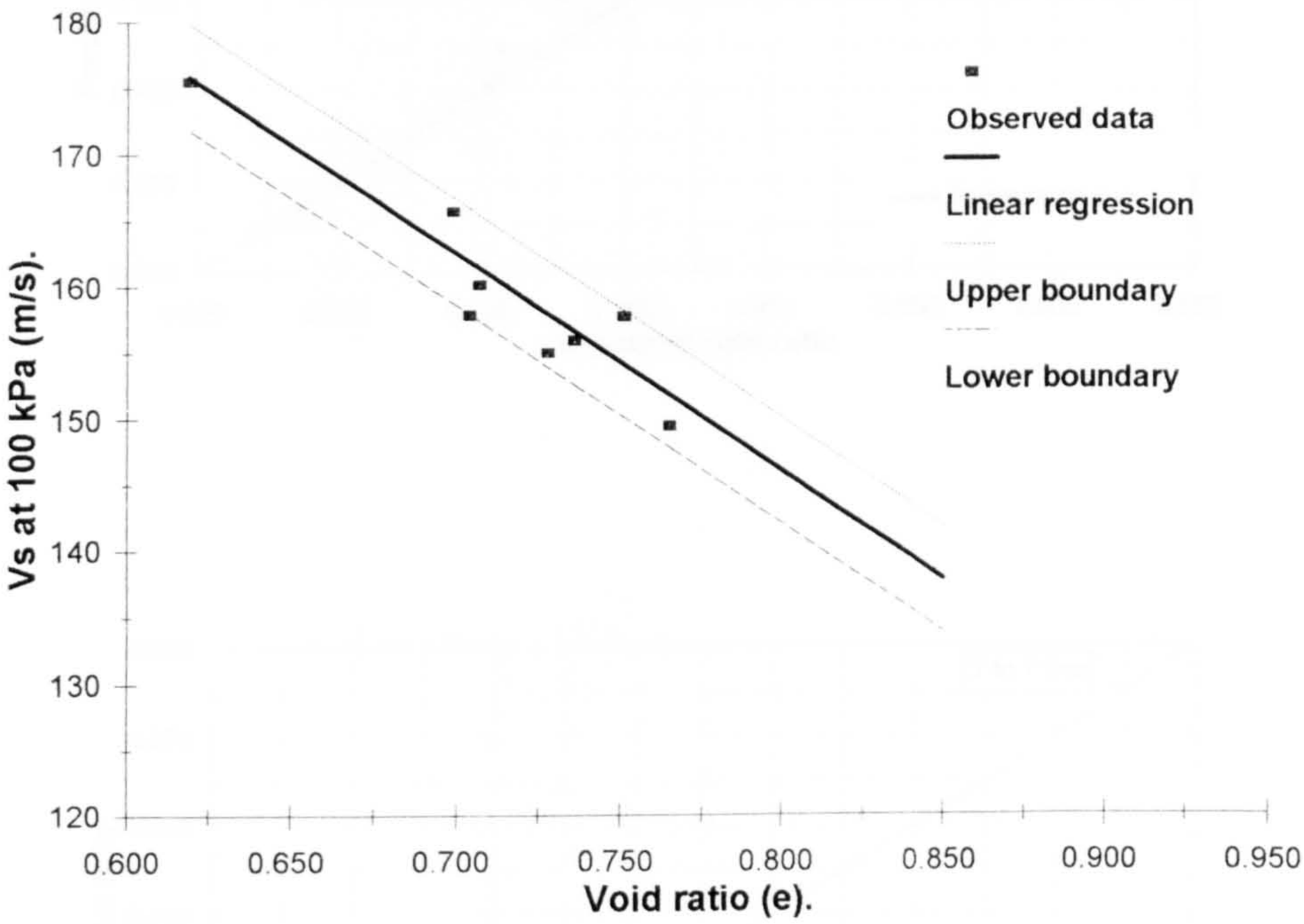

Figure 6.21. Relationship between void ratio and shear wave velocity, at an effective stress of 100kPa, illustrating regression line and data boundaries; Newborough 5% sand.

a.

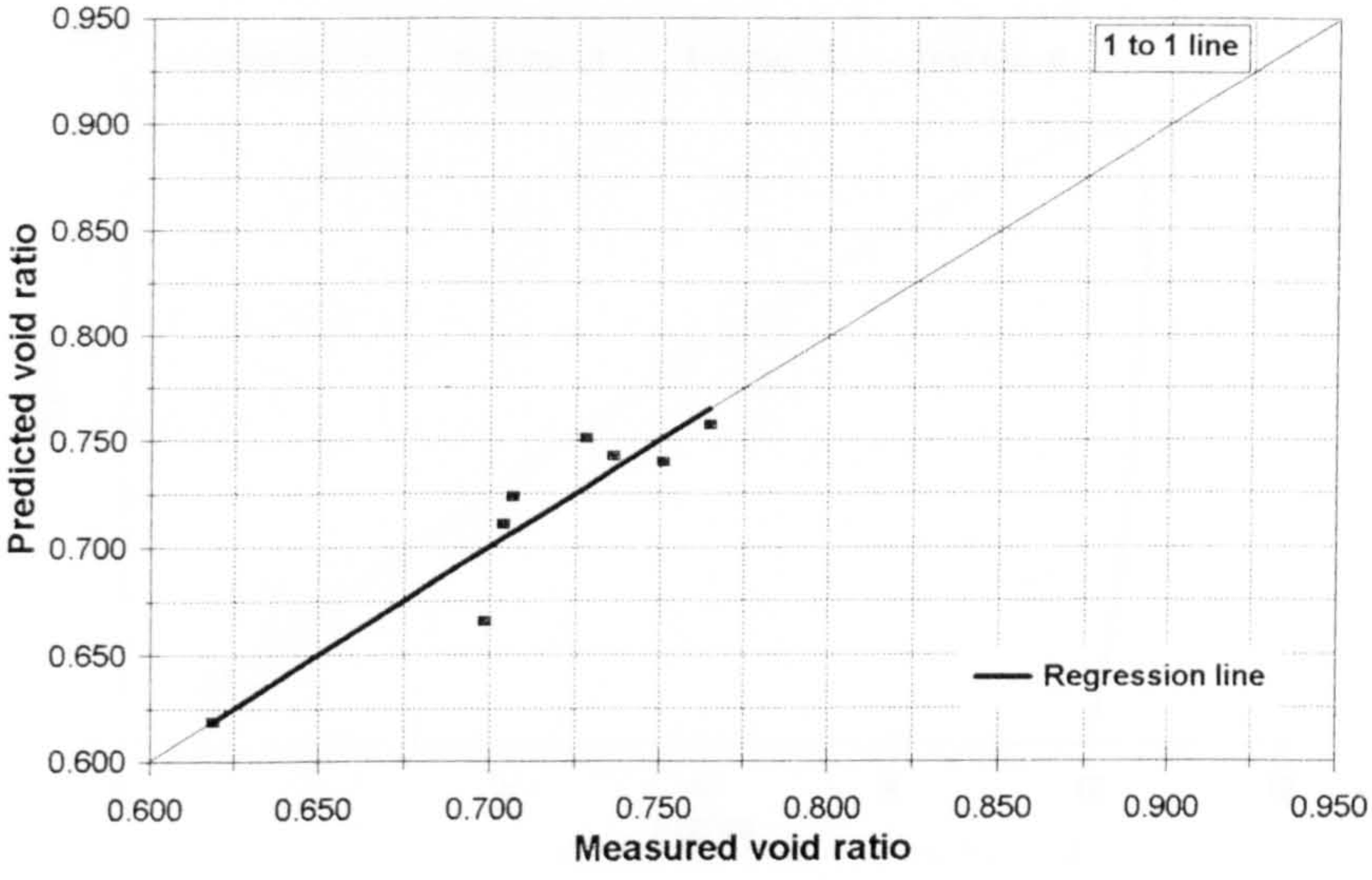

b.

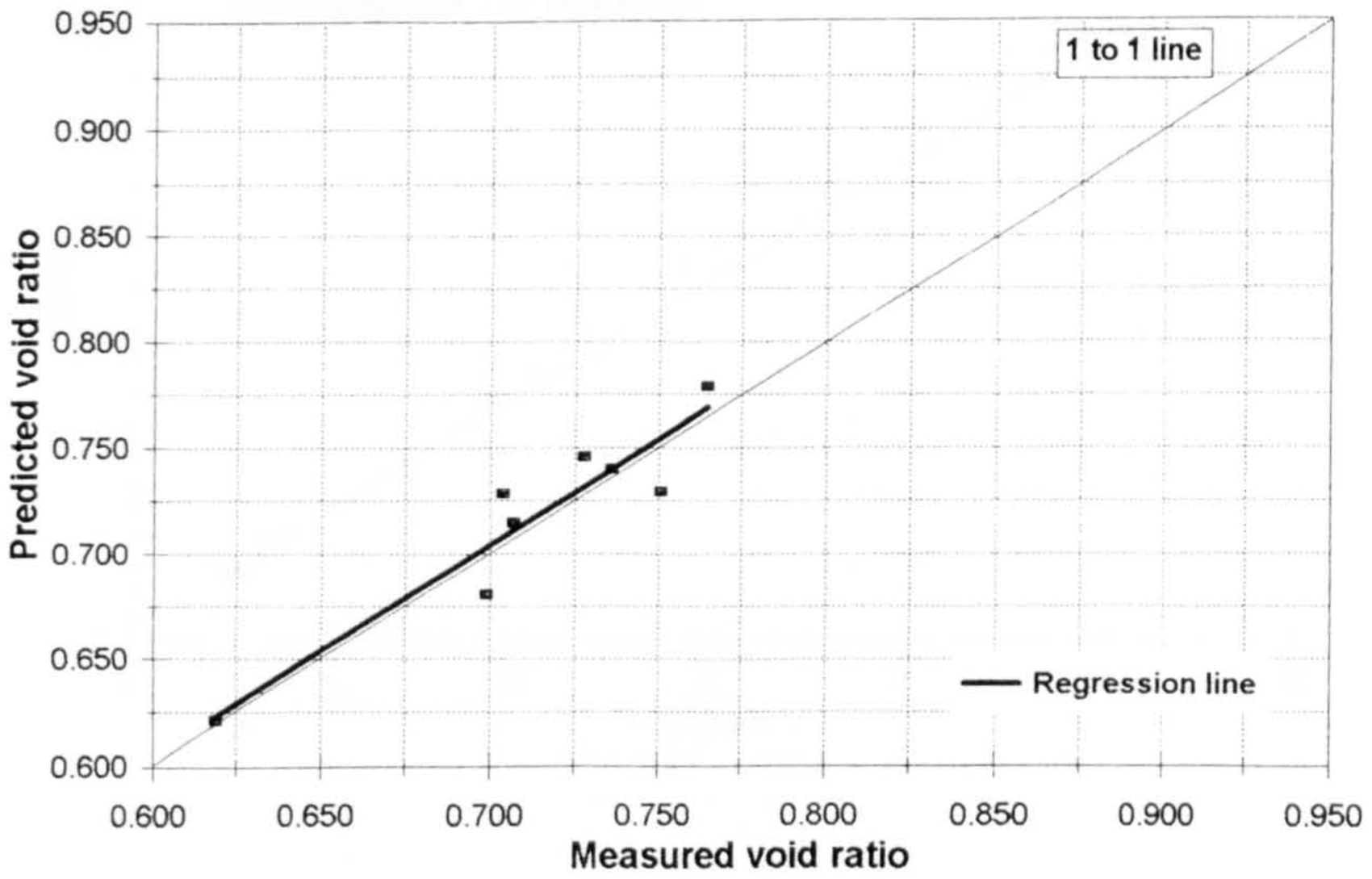

Figure 6.22. a. Comparison between measured and predicted void ratio, based upon shear wave velocities normalised to 300 kPa; Newborough 5% sand.

Figure 6.22. b. Comparison between measured and predicted void ratio, based upon shear wave velocities normalised 100 kPa; Newborough 5% sand.

a.

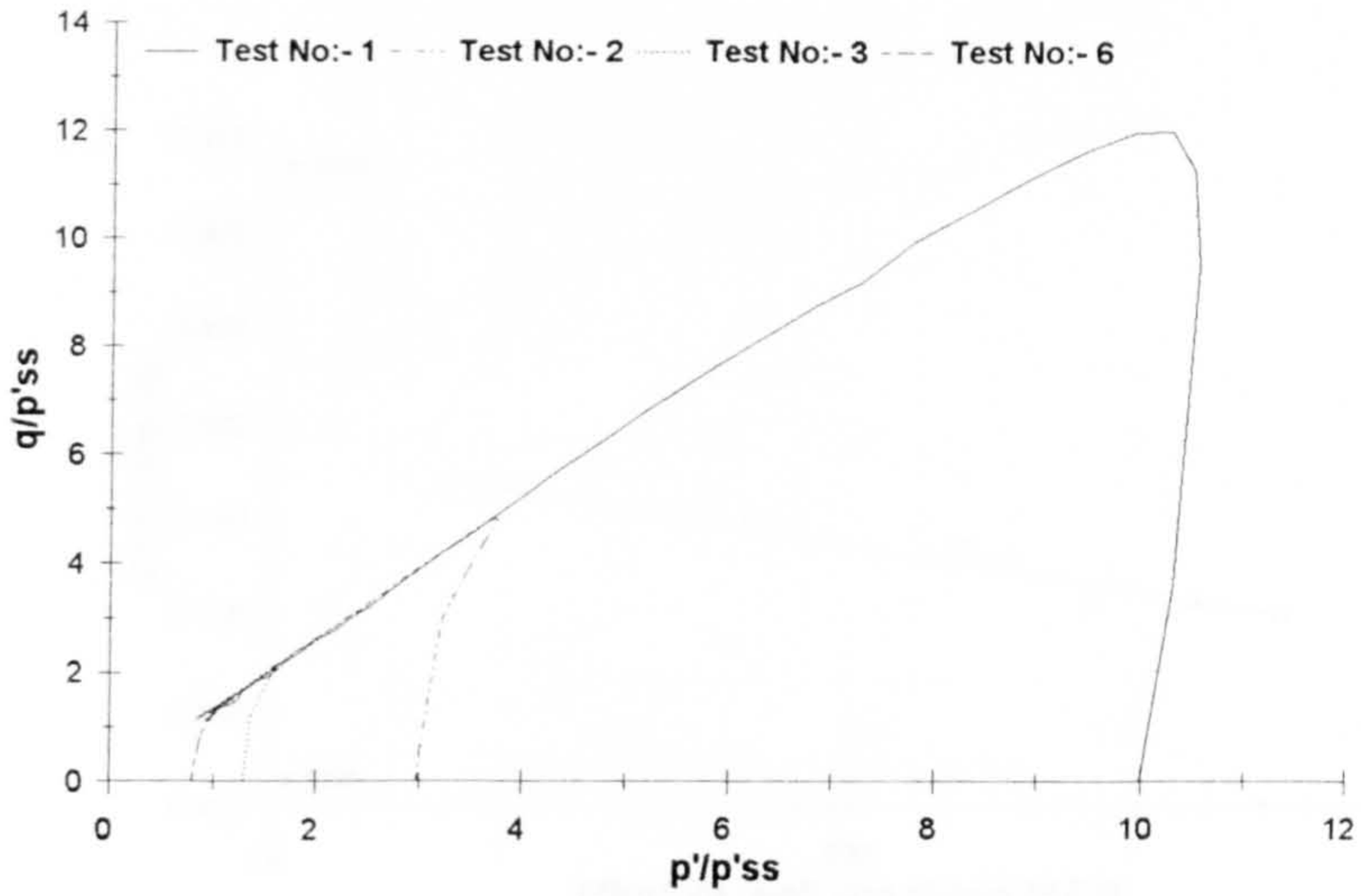

b.

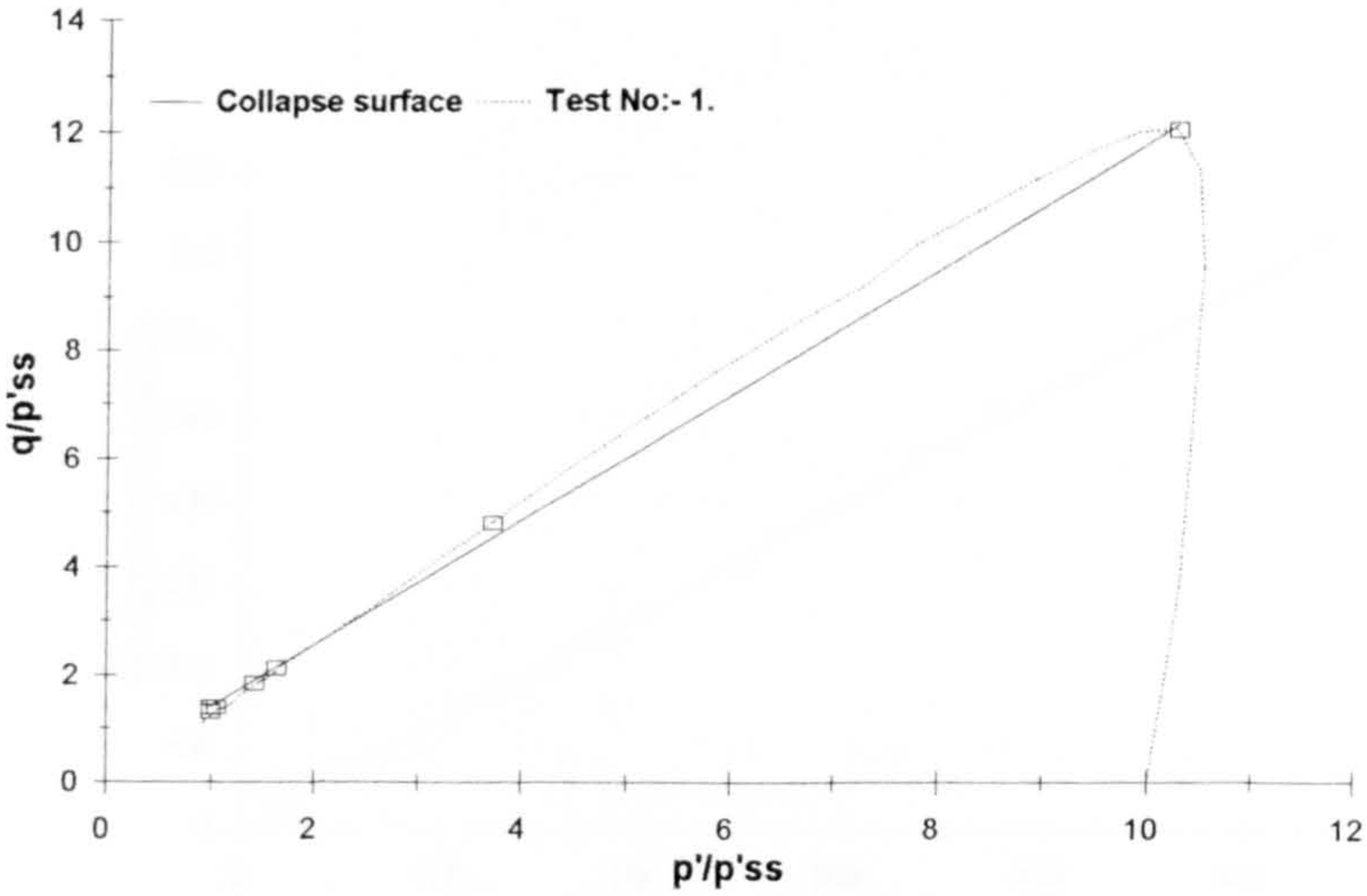

Figure 6.23. a. Selected normalised stress paths for Newborough 5% sand.

Figure 6.23. b. Newborough 5% sand; collapse surface.

a.

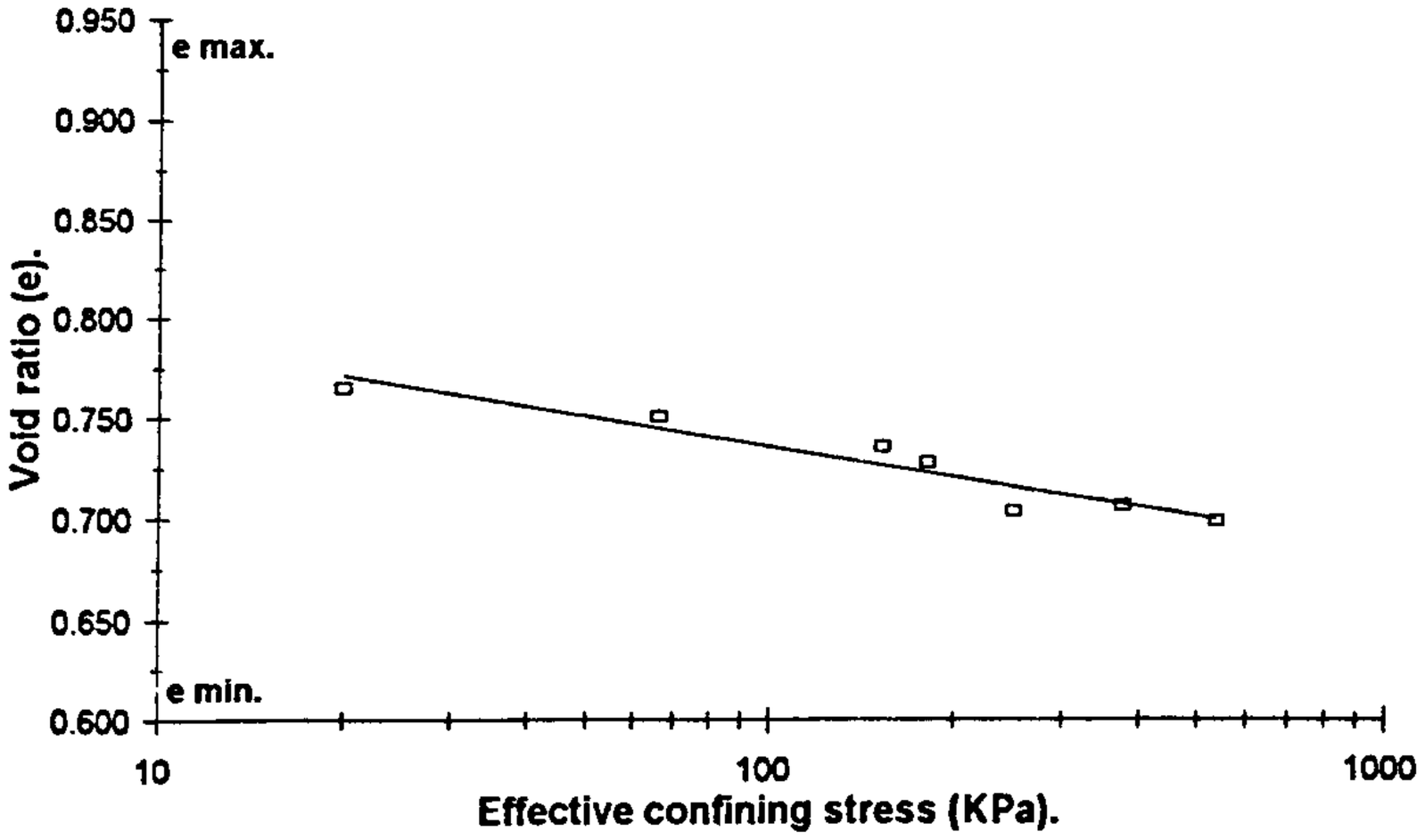

b.

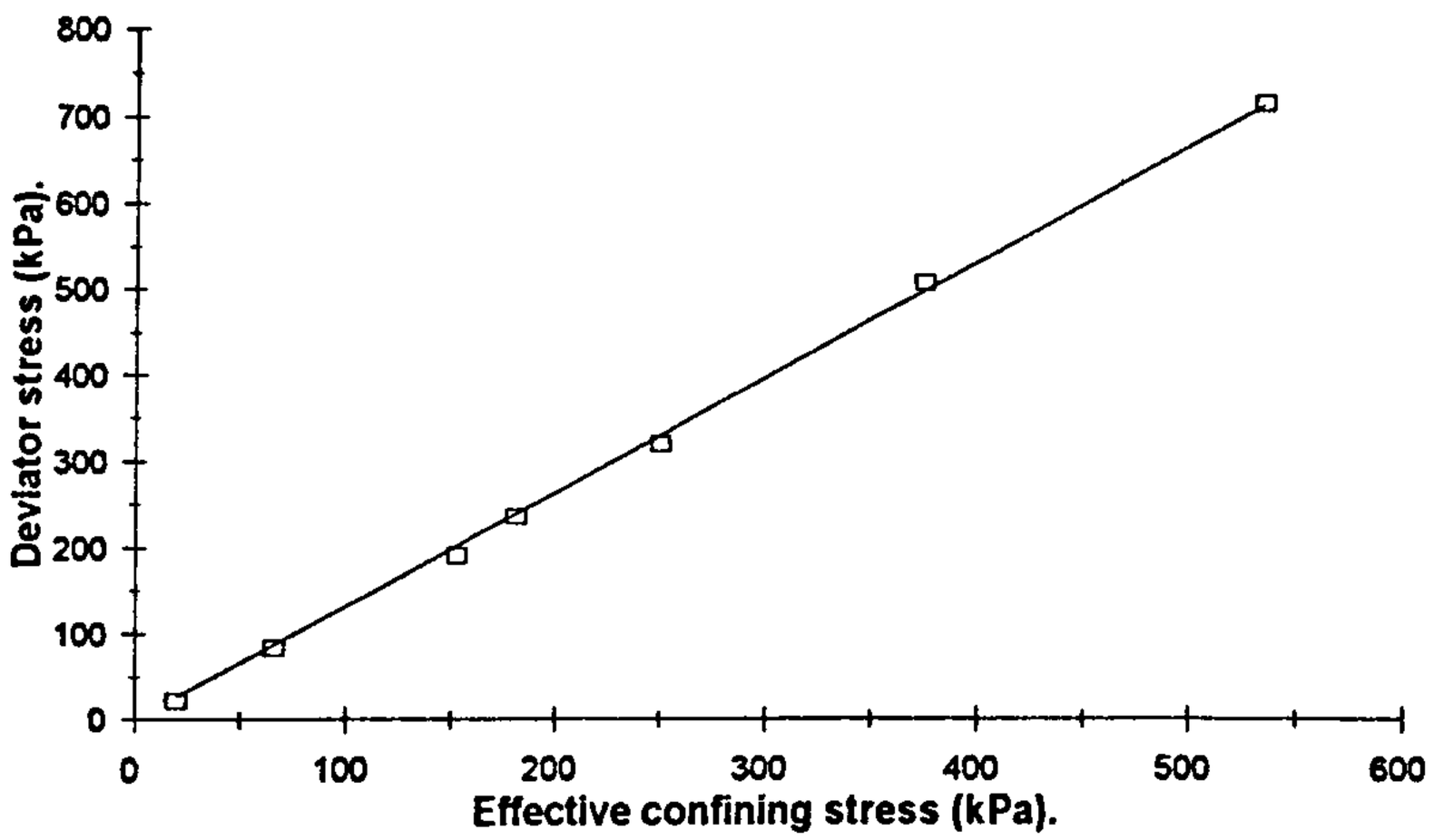

Figure 6.24. a & b. Newborough 5% sand; steady state line.

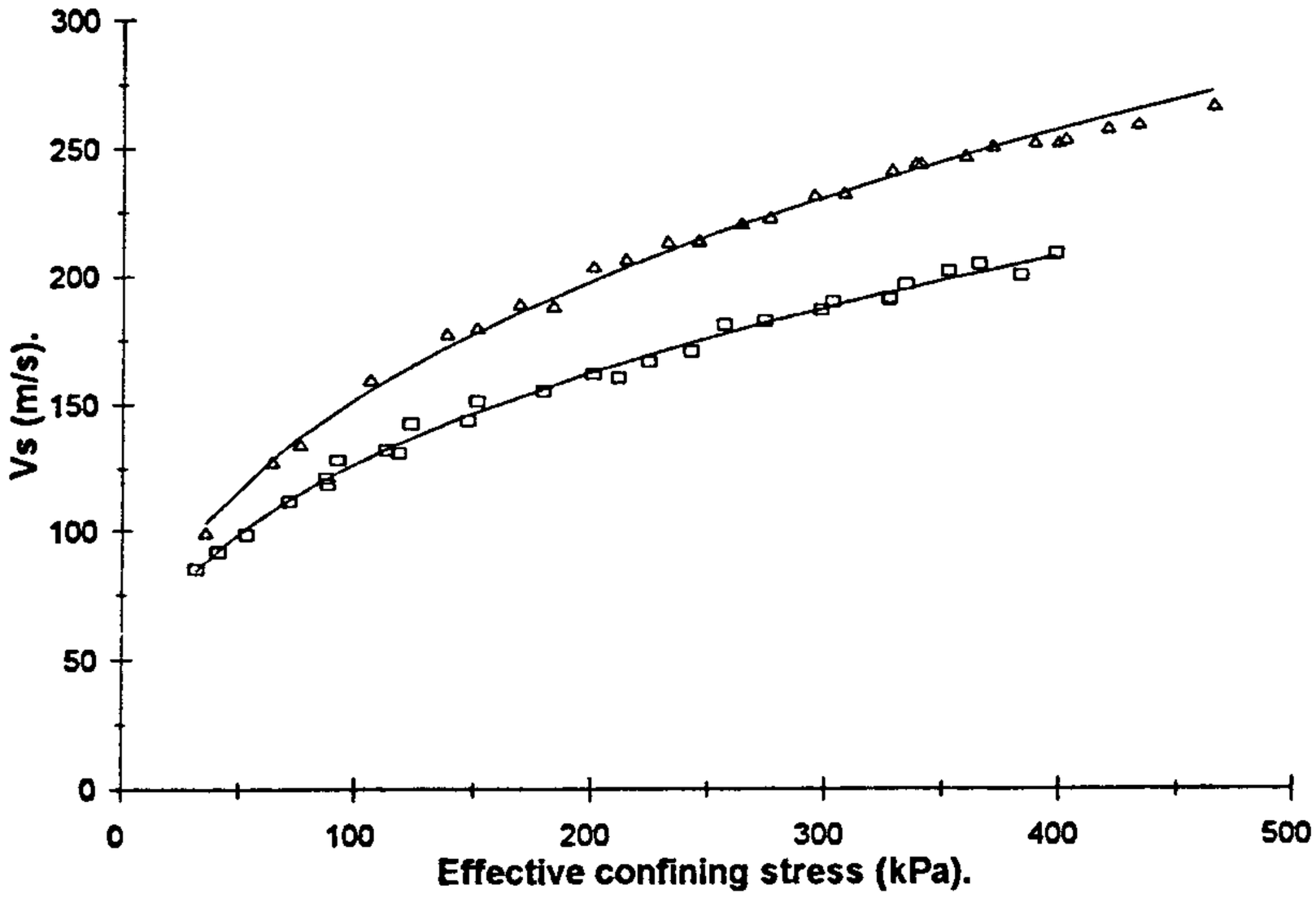

Figure 6.25. Mimimum and maximum recorded velocities; Newborough 10% sand.

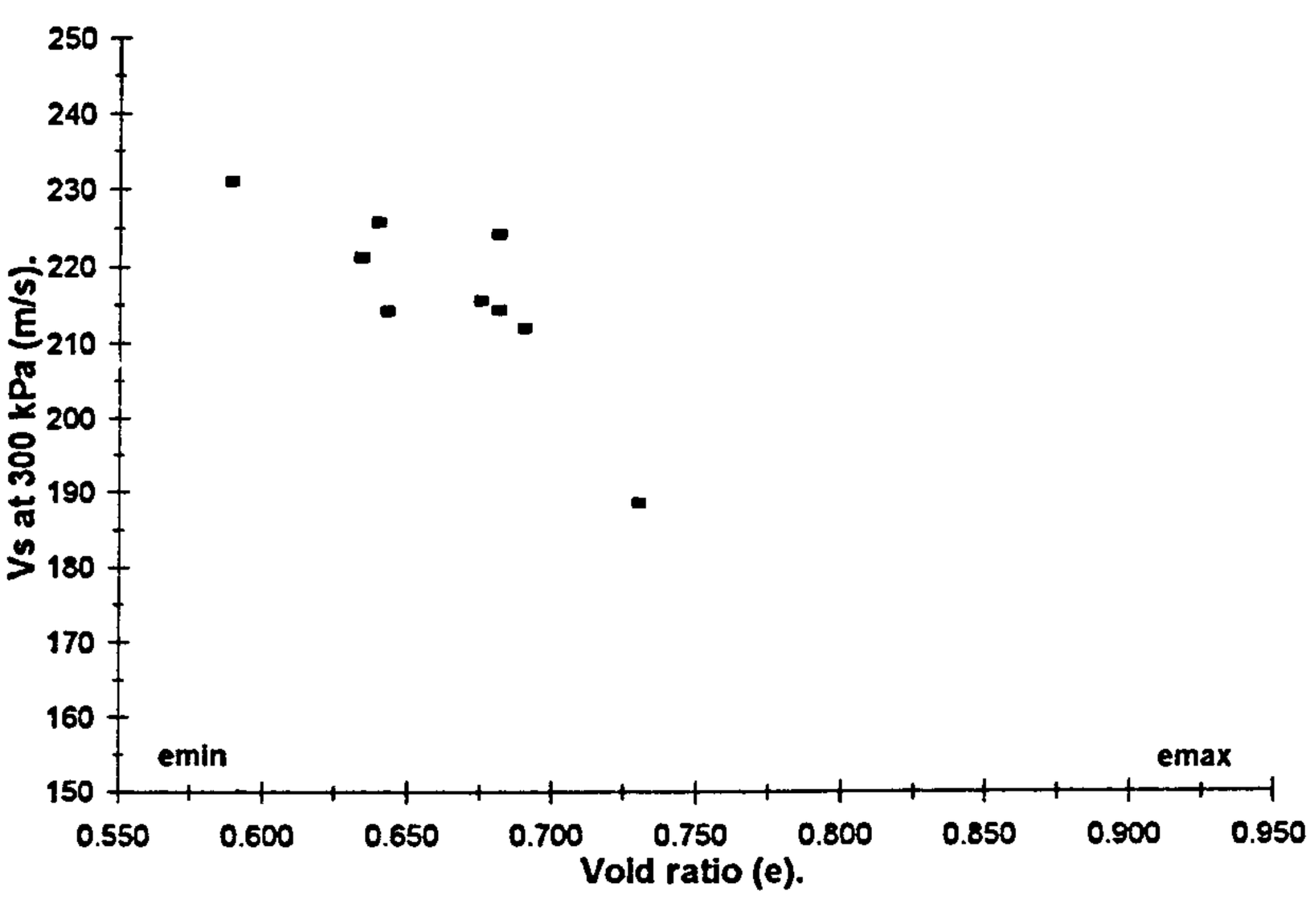

Figure 6.26. Relationship between void ratio and shear wave velocity, at an effective confining stress of 300 kPa.

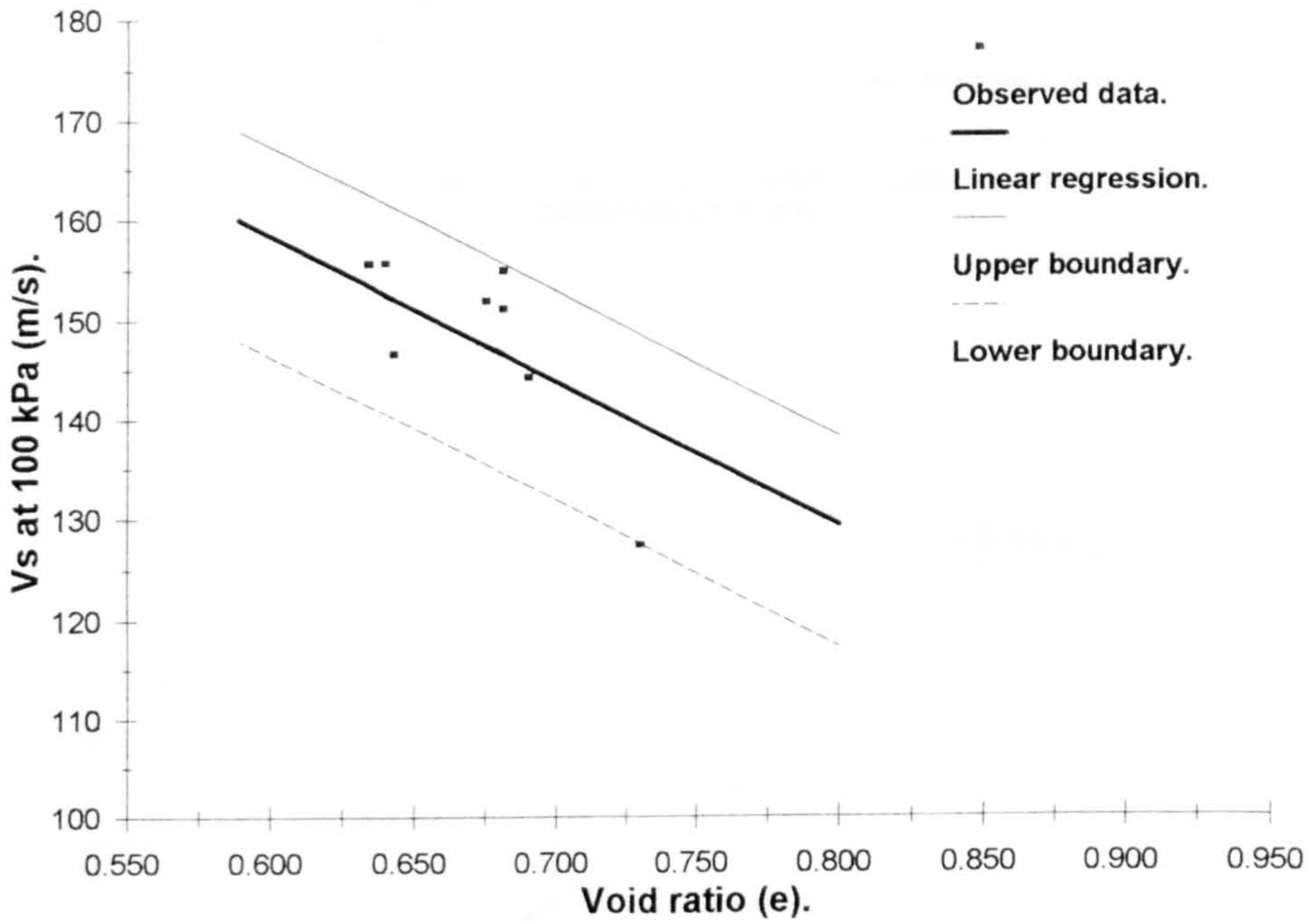

Figure 6.27. Relationship between void ratio and shear wave velocity, at an effective stress of 100kPa, illustrating regression line and data boundaries; Newborough 10% sand.

a.

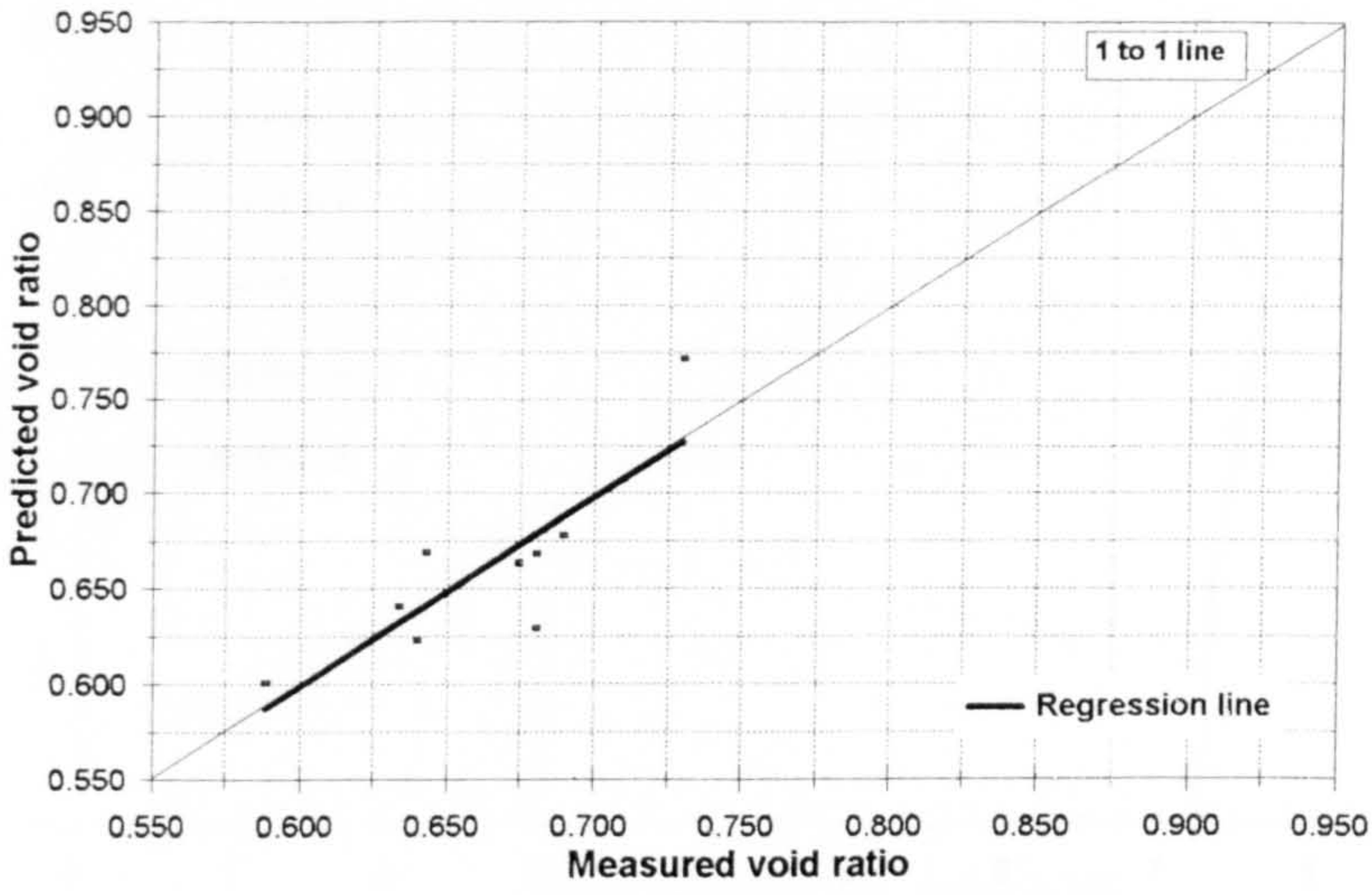

b.

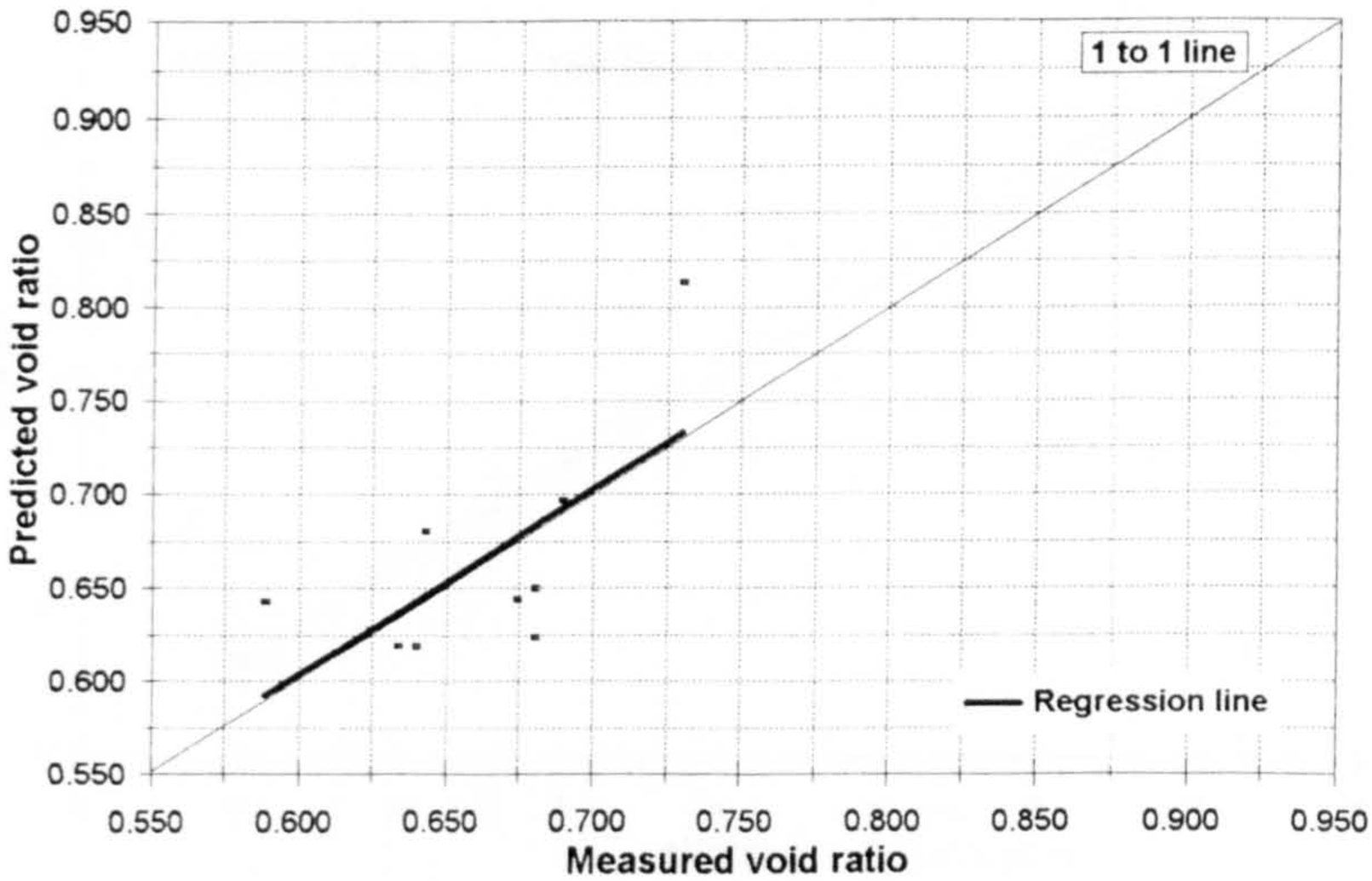

Figure 6.28. a. Comparison between measured and predicted void ratio, based upon shear wave velocities normalised to 300 kPa; Newborough 10% sand.

Figure 6.28. b. Comparison between measured and predicted void ratio, based upon shear wave velocities normalised to 100 kPa; Newborough 10% sand.

a.

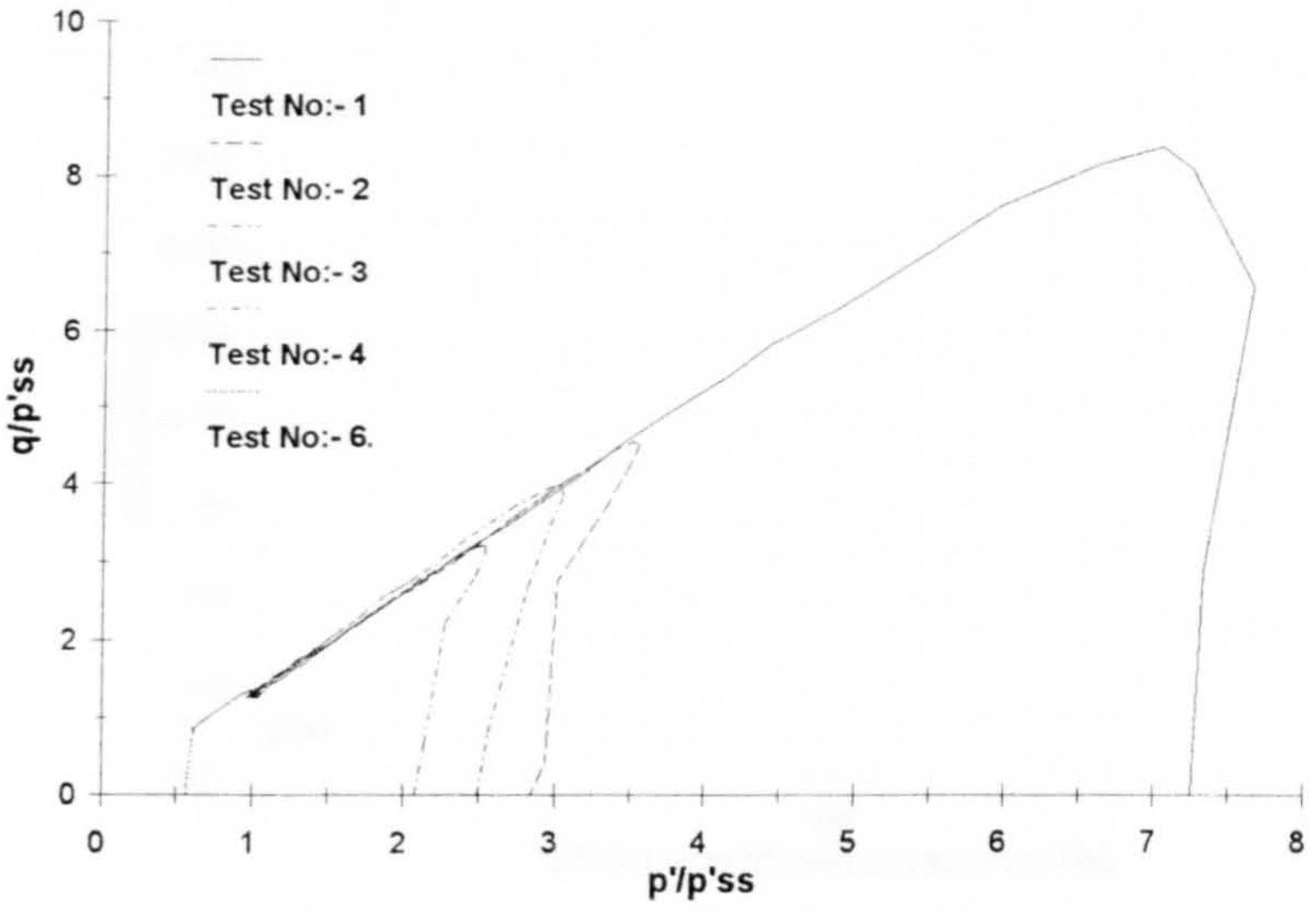

b.

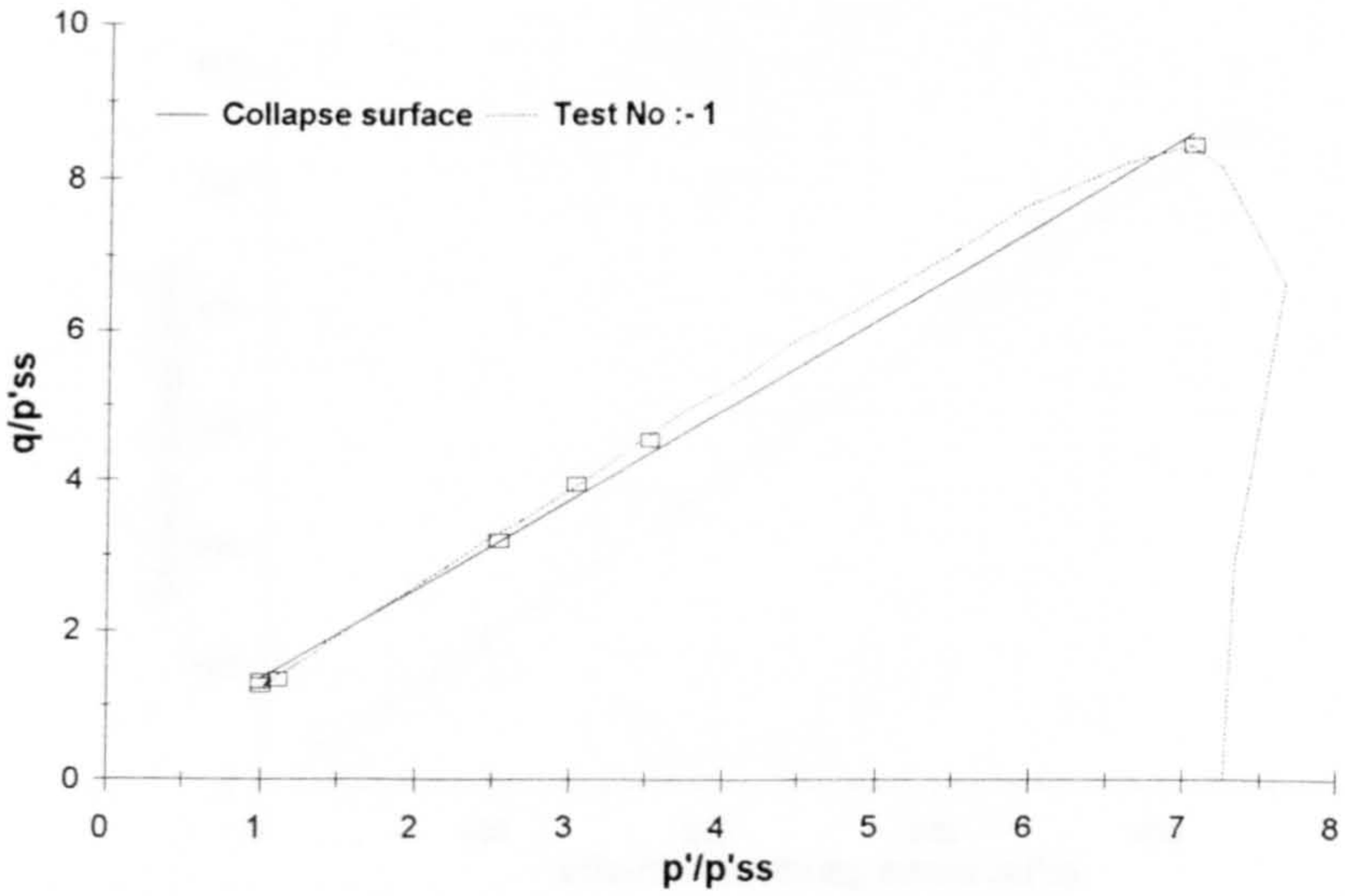

Figure 6.29. a. Newborough 10% sand; selected normalised stress paths.

Figure 6.29. b. Newborough 10% sand; collapse surface.

a.

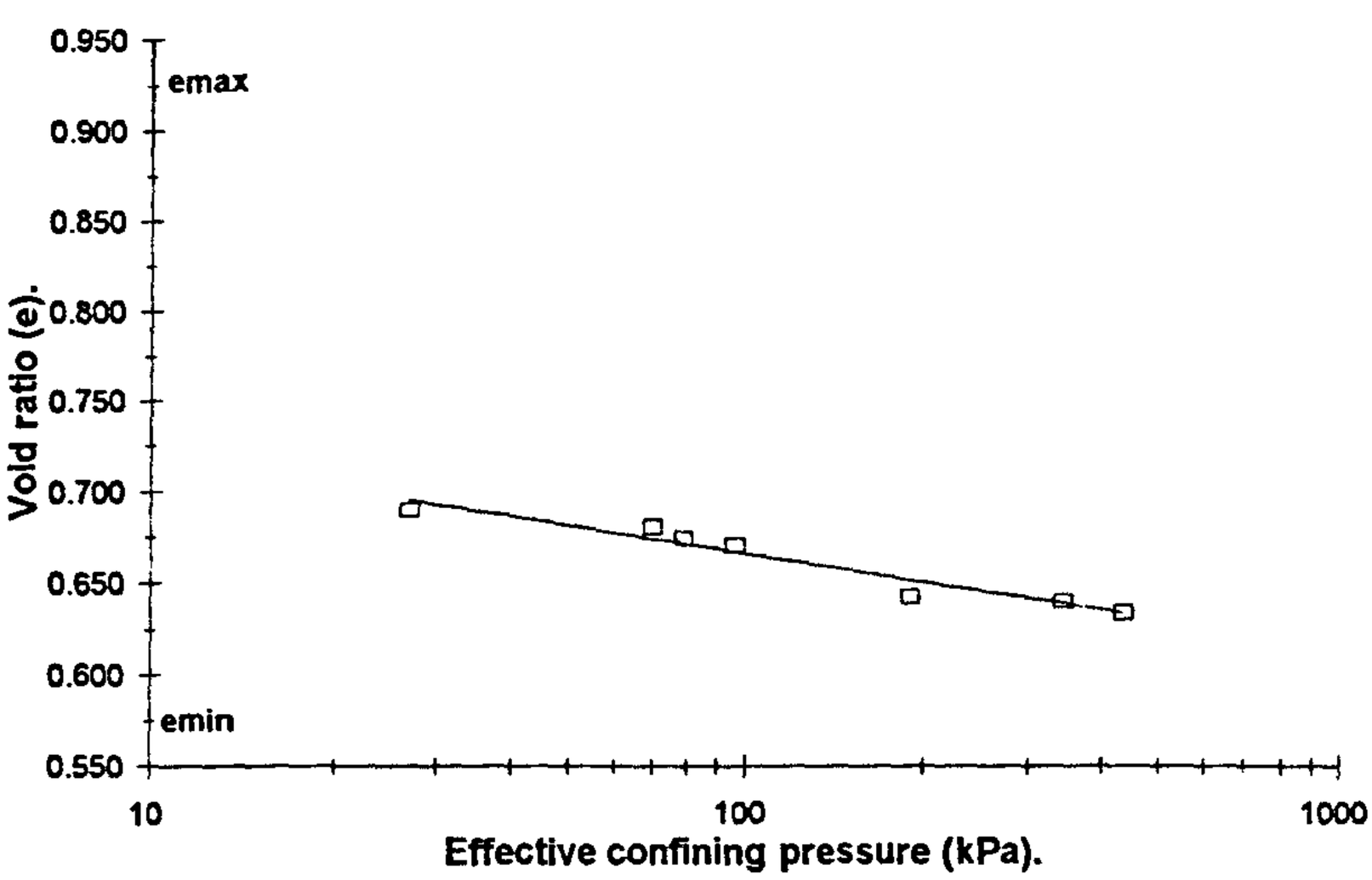

b.

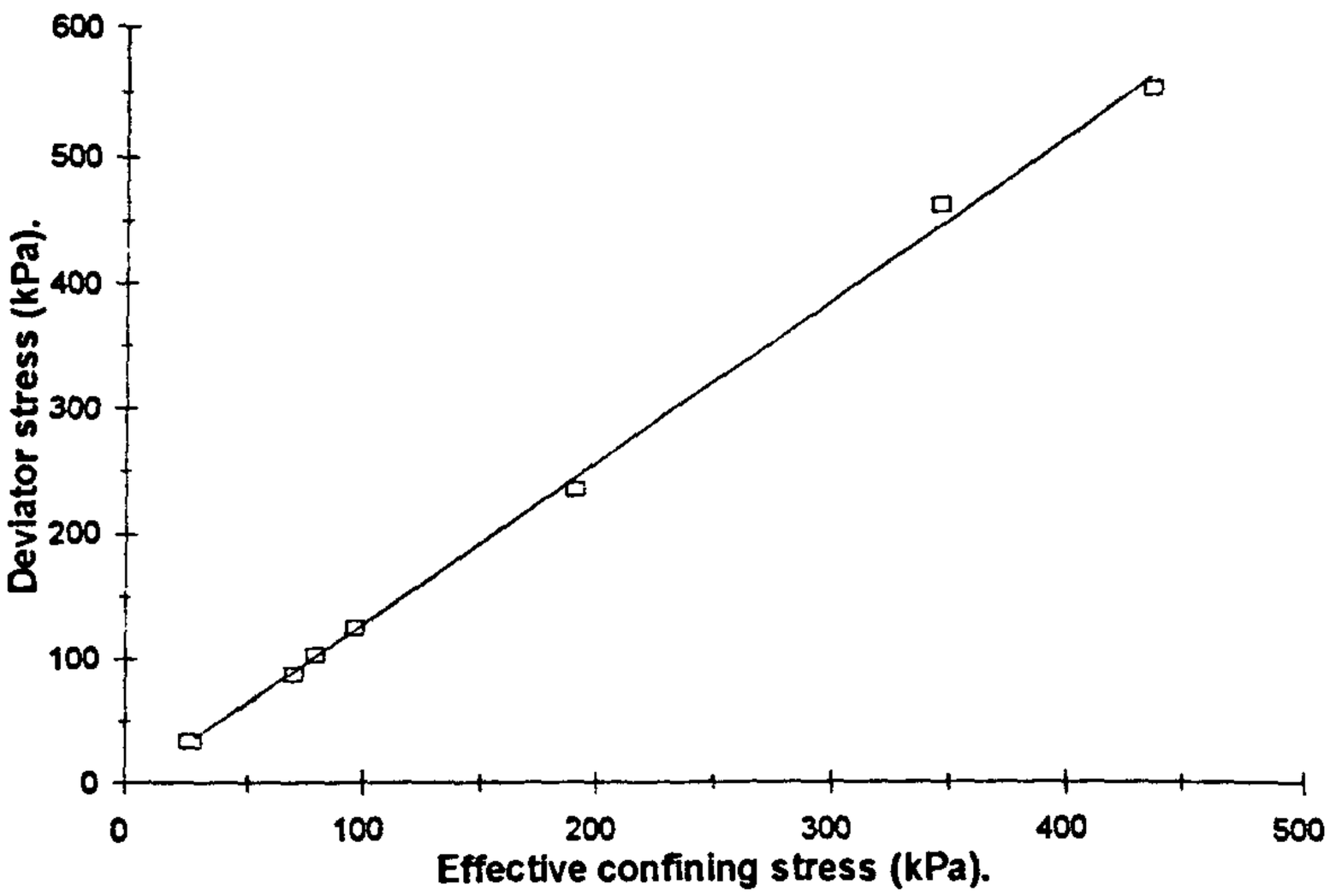

Figure 6.30. a & b. Newborough 10% sand; steady state line.

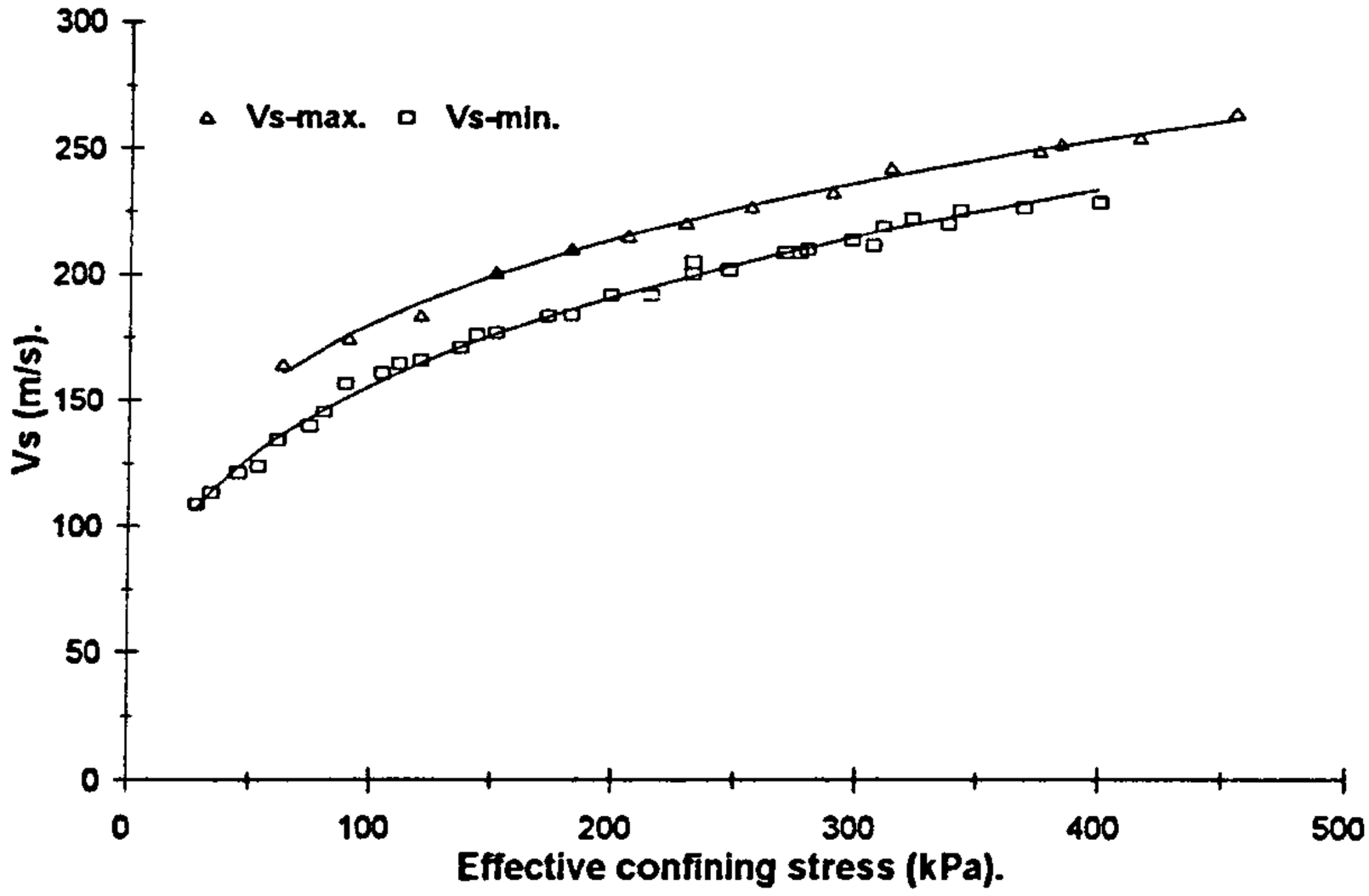

Figure 6.31. Minimum and maximum shear wave velocity curves; Fraser delta sand.

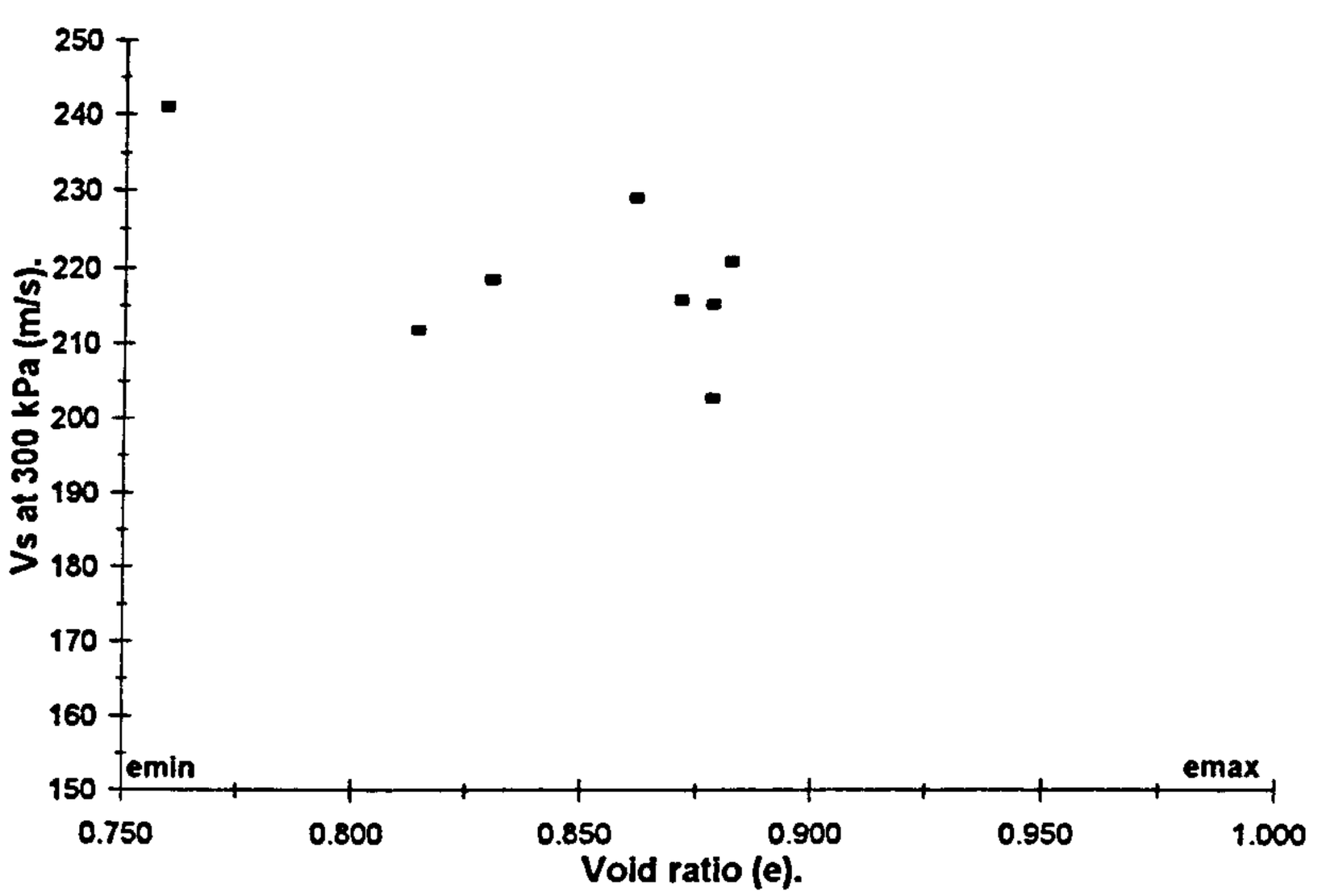

Figure 6.32. Relationship between void ratio and shear wave velocity, at an effective confining stress of 300 kPa.

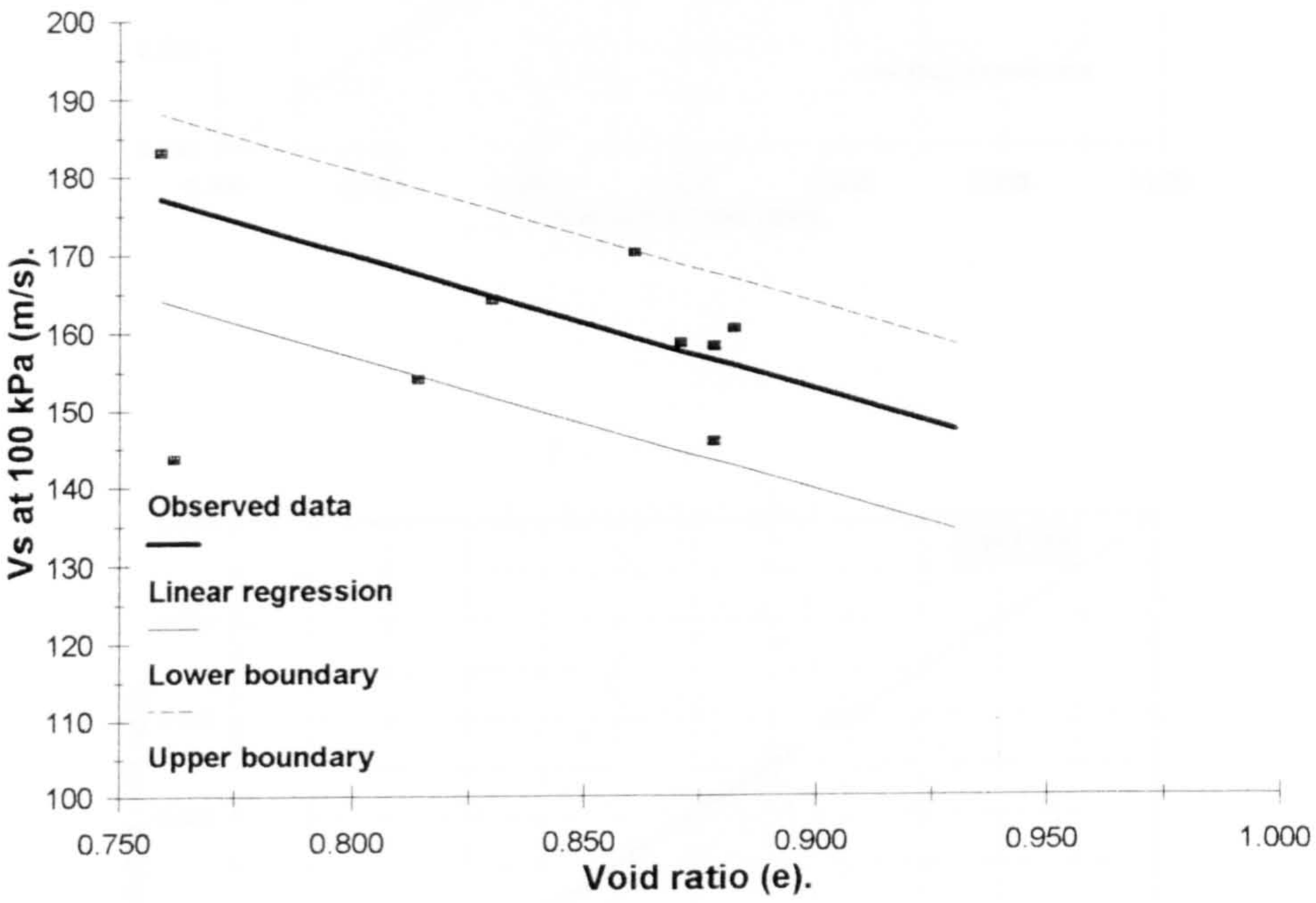

Figure 6.33. Relationship between void ratio and shear wave velocity, at an effective stress of 100kPa, illustrating regression line and data boundaries; Fraser Delta sand.

a.

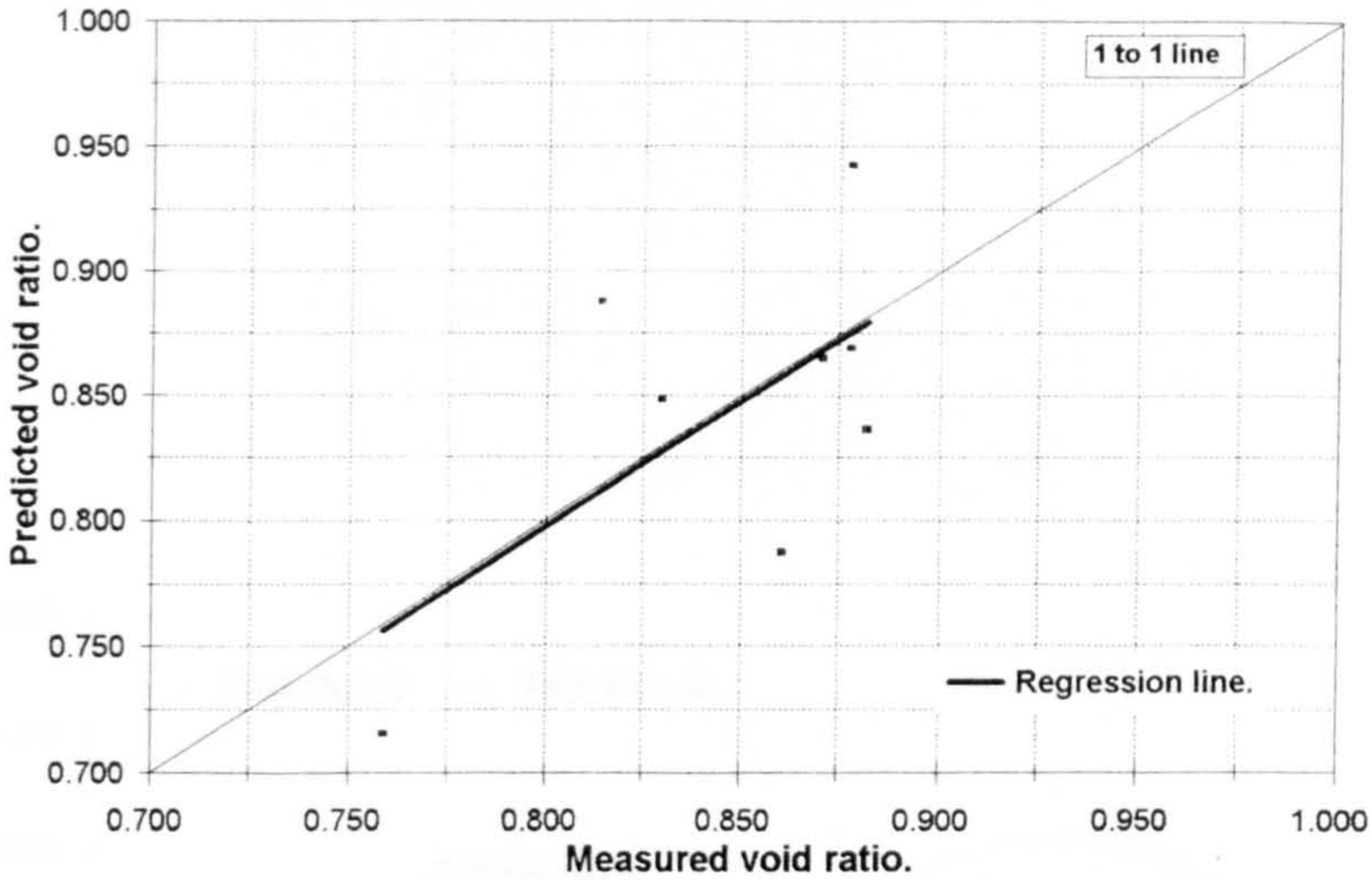

b.

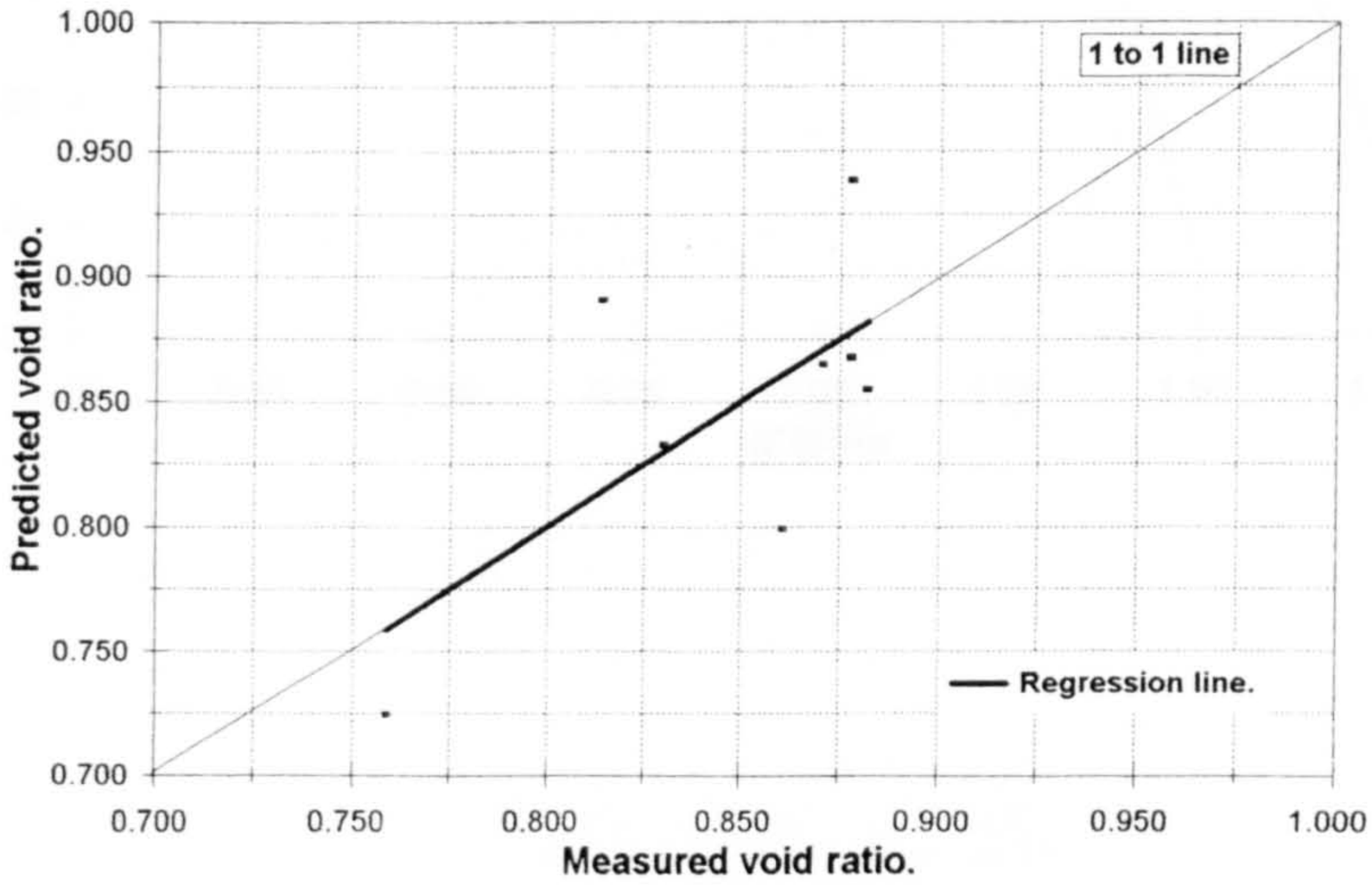

Figure 6.34. a. Comparison between measured and predicted void ratio, based upon shear wave velocities normalised to 300 kPa; Fraser Delta sand.

Figure 6.34. b. Comparison between measured and predicted void ratio, based upon shear wave velocities normalised to 100 kPa; Fraser Delta sand.

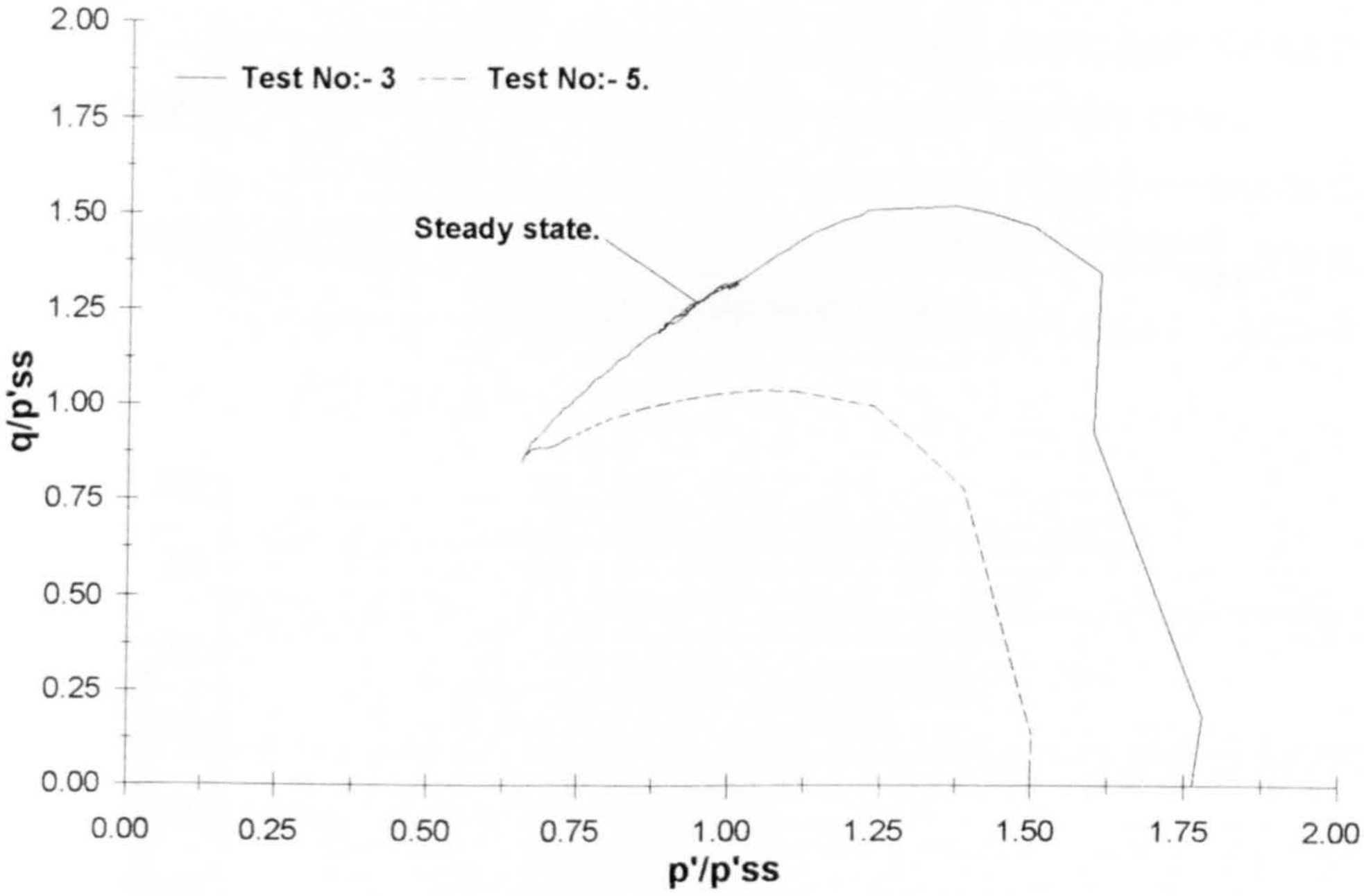

Figure 6.35. Fraser Delta sand; selected normalised stress paths.

a.

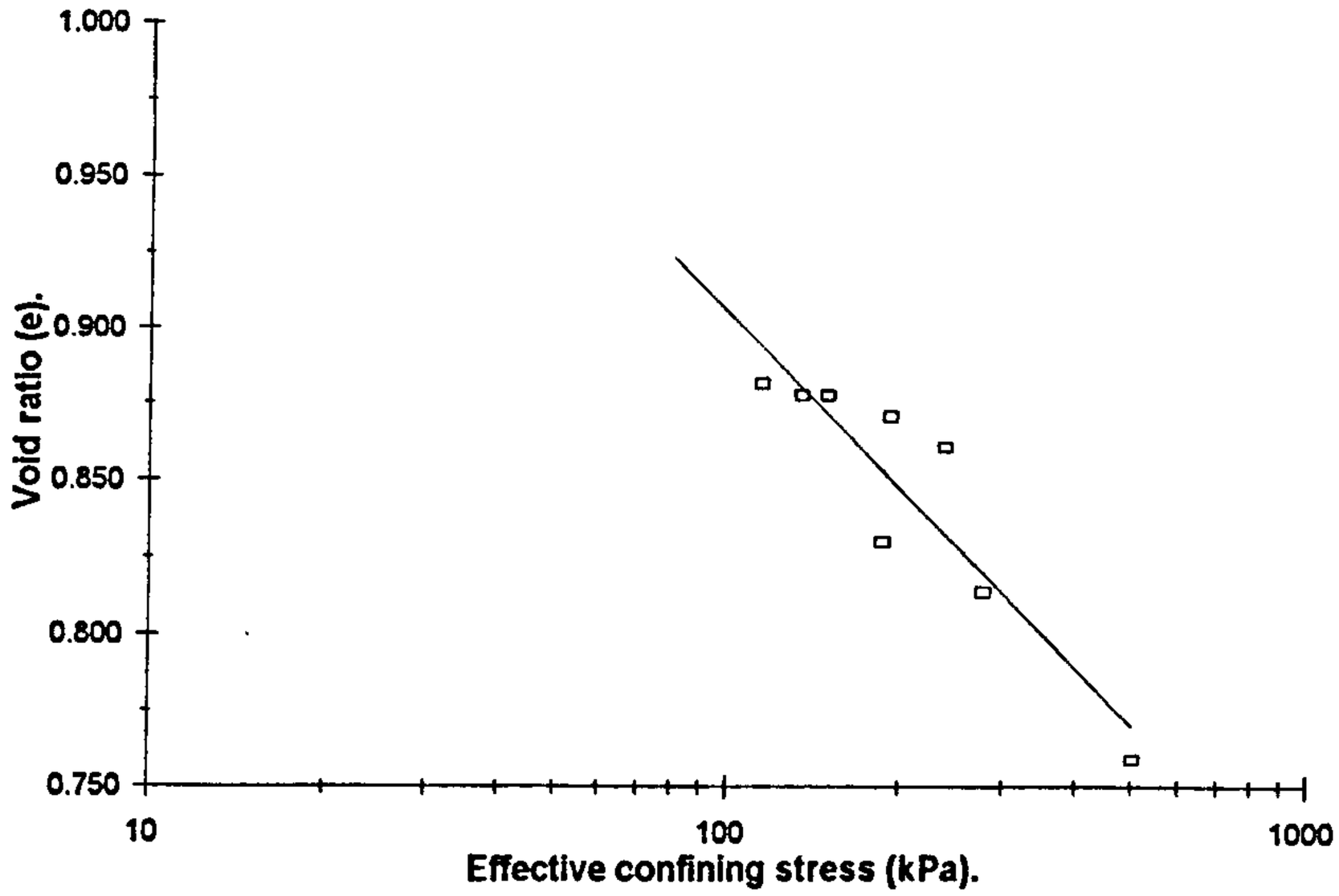

b.

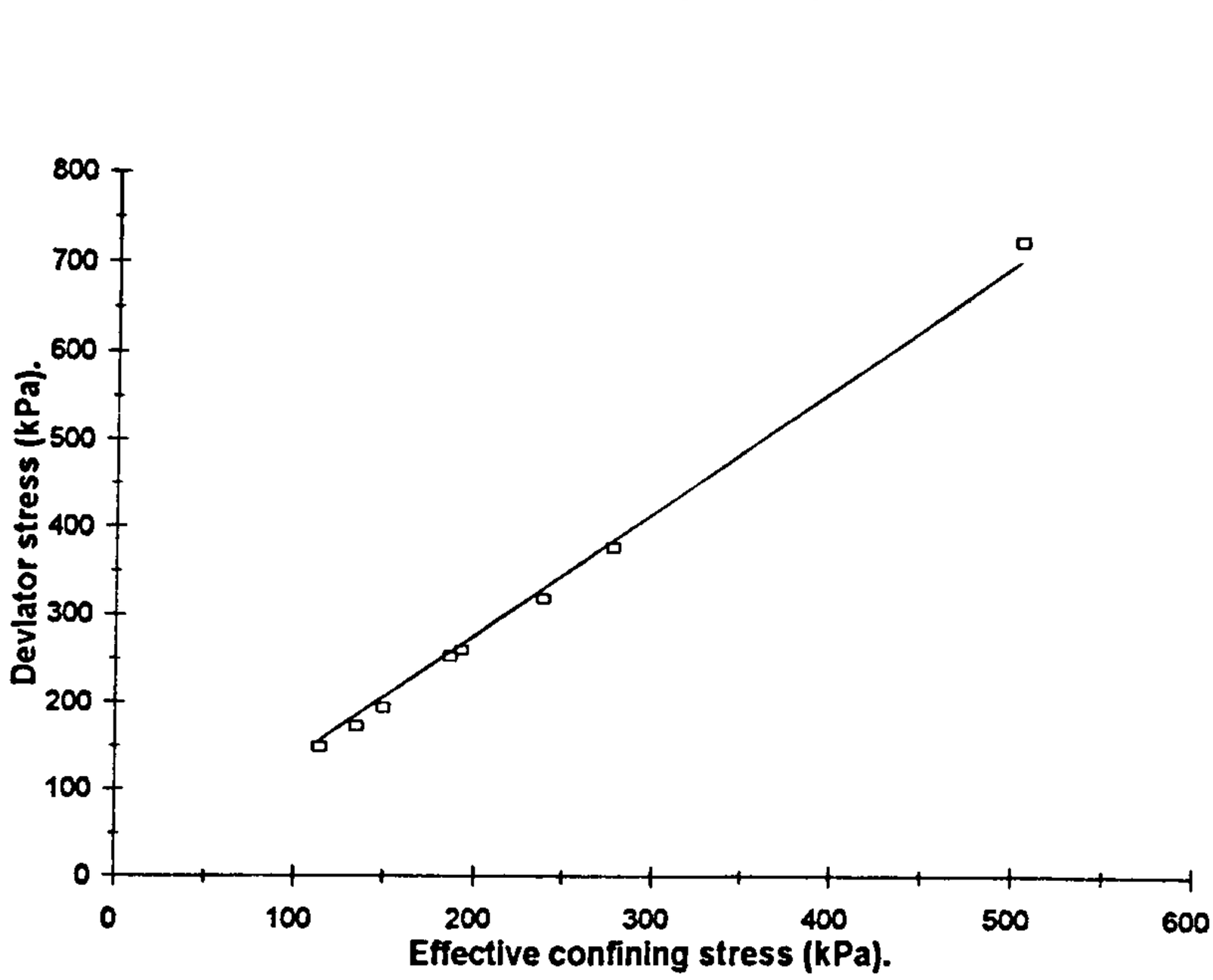

Figure 6.36. a & b. Fraser Delta sand; steady state line.

CHAPTER 7.

LABORATORY RESULTS - SECTION 2.

INTEGRATED GEOTECHNICAL & GEOPHYSICAL DATA.

7.1. Introduction.

In this chapter the separate geophysical and geotechnical results presented in the previous chapter will be integrated, allowing the detailed evaluation of the use of shear wave velocity in liquefaction prediction methods. The fundamental hypothesis of this procedure is that the shear wave velocity of a particular sand may be regarded primarily to be a function of both void ratio and effective confining stress, and may therefore be used as an index to either or both parameters. As no actual shear wave velocity measurements were taken during the course of the triaxial tests themselves due to the technical difficulties described in Section 5.4.3 above, the subsequent data are based upon the relationships between V_s, p' and e, presented in Chapter 6 above. The main assumptions of this method are therefore:

1. no significant change in void ratio takes place during the triaxial testing;
2. for a specific sample, V_s is solely a function of the effective confining stress, and is not significantly affected by any changes in stress ratio during triaxial testing;
3. any changes occurring to the soil fabric during shear will not have a significant effect on the shear wave velocity.

The first assumption can be considered to be valid, since it was shown above that high levels of saturation were achieved during sample preparation. The near-complete saturation means that the sample may be regarded as incompressible and therefore no volume (and associated void ratio) changes will occur during shear. In the case of assumption number two, there is conflicting evidence in the literature on stress ratio effects on the shear wave velocity, and this has been discussed in more detail in Section 4.2.1 above. From a consideration of this discussion, it may however be concluded that for the stress ratios encountered during testing, this assumption may be considered to be valid. Assumption number three is also important and is discussed in more detail by Tang & Clark (1993). These investigators did find small, but significant differences (~ 3m/s) between predicted and measured velocities during shear.

However, the author considers that these small differences are insignificant when compared to the potential errors incurred when attempting to directly measure velocities under shear, and in particular at steady state.

7.2. Inferred shear wave velocity behaviour during triaxial testing.

Based upon the assumptions listed above, the predicted shear wave velocity behaviour during undrained triaxial testing of a particular sand sample may be regarded as being dominantly a function of the changing effective confining stress. Any soil structure and stress ratio effects upon the velocity are small in magnitude when compared to the effective stress effects (see above) and were therefore ignored for the purposes of this study. Based upon this hypothesis, the predicted changes in shear wave velocity during testing on samples of loose, medium - dense and dense sand samples are illustrated below.

Figure 7.1 (a - c) illustrates the predicted shear wave velocity behaviour during triaxial testing of a loose sand. Figure 7.1 (a) illustrates the change in predicted V_s associated with increasing axial strain; Figure 7.1 (b) illustrates the change in predicted V_s with effective confining stress; Figure 7.1 (c) illustrates the change in predicted V_s associated with changing deviator stress. As can be seen from these diagrams, after an initial small increase at a strain of less than 1%, the shear wave velocity decreases to a constant 'steady state velocity' of around 90 m/s at a strain of greater than 10%.

Figure 7.2 (a -c) illustrates the shear wave velocity behaviour during triaxial testing of a dense sand. As previously, (a) illustrates the change in predicted V_s with increasing axial strain, (b) illustrates the change in predicted V_s with changing effective confining stress, and (c) illustrates the change in predicted V_s with increasing deviator stress. As can be seen, in contrast to the loose sand described above, the predicted shear wave velocity increases slowly, in response to the slowly increasing effective confining stress, until failure in shear occurred at around 20% strain, after which a small decrease in both velocity and confining stress occurred.

Figure 7.3 (a -c) illustrates the shear wave velocity behaviour during triaxial testing of a medium dense sand. a - c illustrate the data as previously described. As can be seen the shear wave velocity, after a small increase, decreases to a minimum of around 210

m/s at about 7.5% strain, at which point the pore-pressures ceased to rise and began to fall. The predicted shear wave velocity reaches a maximum value of 255 m/s at 25% strain, where the test was stopped.

Figure 7.4 (a -c) illustrates the shear wave velocity behaviour during triaxial testing of a loose sand, in which failure by complete liquefaction occurred. As can be seen, in a manner similar to the loose sand described above, after a small increase, the predicted shear wave velocity steadily decreased, corresponding to a steady decrease in effective confining stress, until at an axial strain of around 13.5%, at which time the pore-pressure reached the same magnitude as the confining pressure, the sample liquefied, lost all rigidity and the shear wave velocity dropped to zero.

As can be seen from Figures 7.1 (c), 7.2 (c), 7.3 (c) and 7.4 (c) ,the predicted shear wave velocity may be used as an alternative index of effective confining stress in a sand sample. It is therefore possible to define the state boundary surface (Figure 6.16) in terms of shear wave velocity and deviator stress; figure 7.5 (a) illustrates the state boundary surface for the Newborough 0% sand defined in terms of deviator stress versus predicted shear wave velocity. Figure 7.5 (b) illustrates the same data, but with logarithmic axes. As can be seen from both these illustrations, the surface defined in this manner appears to be of an approximately continuous nature.

7.3. Integrated data: Newborough 0% sand.

The individual relationships between shear wave velocity and void ratio, effective confining stress and deviator stress at steady state for the Newborough 0% test sand are described in detail below. The first, and possibly most important of these relationships represents the steady state line, defined in terms of shear wave velocity and effective confining stress. The definition of this line was an important initial aim of the project, as it potentially allows the definition of sediment consolidation state, purely on the grounds of a knowledge of shear wave velocities. However, during further analysis of the laboratory results it was found that other relationships exist between the predicted shear wave velocities, void ratio and deviator stress at steady state.

Figure 7.6 (a & b) illustrates the steady state line defined in terms of predicted shear wave velocity versus log effective confining stress (Figure 7.6 (a)), and shear wave

velocity versus effective confining stress (Figure 7.6 (b)). These data were produced by calculating the shear wave velocity at the effective confining stress at steady state using the appropriate sample constants, defined in the first part of the laboratory methodology. The use of log p' as the x-axis merely reflects the convention of plotting the steady state line using the same scale. As can be seen, Figure 7.6 (b) resembles a conventional V_s - p' curve, and may be described in the same manner, but it must be noted that these data were derived from tests on samples with a wide variety of initial void ratios and that each individual data point therefore represents a different void ratio, with a general increase in density at higher velocities. The best fit line through the data was calculated in the manner described for conventional $V_s - p'$ relationships (described above), and has the form:-

$$V_s = 35 \times p'^{0.35} \qquad (7.1).$$

The regression data for this relationship are presented below, and illustrate clearly that Equation 7.1 defined in this way has a high degree of statistical significance.

Title	*Equation*	*Source*	*Df*	*M*	*F*	R^2	*p*
Eqn. 7.1	y = 0.35x + 1.54	Regression Residual	1 24	2.26 0.0005	4517	0.99	7.67×10^{-29}

Table 7.1. Regression and ANOVA data associated with Equation 7.1.

This new form of state diagram essentially defines the 'critical shear wave velocity line' for Newborough 0% sand and can be regarded as being analogous to the steady state line. Any sample whose velocity, at a specific confining stress, falls significantly above the critical line will tend to dilate and strain harden under undrained shear; any sample whose velocity falls significantly below the critical line at a particular effective stress, will tend to contract, strain - soften, and potentially liquefy under undrained shear.

Figure 7.6 (c) illustrates the relationship between void ratio and predicted shear wave velocity at steady state. In this instance, predicted V_s replaces p' as the measure of stress, and there is an obvious similarity between this diagram and the conventional state diagram, illustrated in Figure 6.17 (a) above. The best fit line through these data has the general form:-

$$e'_{ss} = -c \times (\log V_s'_{ss}) + d \qquad (7.2).$$

where, e'_{ss} = void ratio at steady state,
$V_s'_{ss}$ = V_s at steady state,
c & d = sample constants = 0.124 & 1.078 respectively.

The regression data for this relationship is listed below.

Title	*Equation*	*Source*	*Df*	*M*	*F*	R^2	*p*
Eqn. 7.2	y = -0.124(log x) + 1.078	Regression Residual	1 23	0.235 0.002	134	0.85	4.63×10^{-11}

Table 7.2. Regression and ANOVA data associated with Equation 7.2

Figure 7.6 (d) illustrates the relationship between the deviator stress and shear wave velocity at steady state. On a logarithmic plot, there is clearly a linear relationship between the two parameters. The best fit line through these data has the general form:-

$$\log(q'_{ss}) = f \times (\log V_s'_{ss}) - g' \qquad (7.3).$$

where, q'_{ss} = deviator stress at steady state,
f & g' = sample constants = 2.74 & 3.99 respectively.

The regression data for this relationship are presented below.

Title	*Equation*	*Source*	*Df*	*M*	*F*	R^2	*p*
Eqn. 7.3	log (y) = 2.74 (log x) -3.99	Regression Residual	1 23	0.272 0.0001	1720	0.99	4.02×10^{-23}

Table 7.3. Regression and ANOVA data associated with Equation 7.3.

As can be seen from the results presented above, V_s is clearly a function of both void ratio, deviator stress and effective confining stress at steady state. Further, these relationships have high R^2 values, and p values well below the critical 0.05 value, indicating the high degree of significance that may be attached to these data.

7.3.1. Inference of sediment state from shear wave velocities.

As may be noted from the data presented above, the shear wave velocity of a particular sand is related to its void ratio, so it may be used as an index to sediment consolidation state, provided the effective stresses are accurately known. In contrast to expressing the state parameter as a function of void ratio (*e.g.* Been & Jefferies, 1985; Robertson *et al.* 1995) it seems logical to express the state parameter, when calculated from shear wave velocity, as a function of velocity. This new state index has been termed ψ_s and may be calculated using:-

$$\psi_s = -\left(V_s'_c - V_{s\,crit}\right) \qquad (m/s). \qquad (7.4).$$

where, $V_s'_c$ = measured (or calculated) shear wave velocity at a specific confining stress (m/s).
$V_{s\,crit}$ = critical shear wave velocity as defined in Figures 7.5 above, at the same effective confining stress (m/s).

In order to assess ψ_s as an index of sand consolidation state and hence liquefaction potential with particular reference to laboratory prepared sands, comparisons were made between ψ_s and both $\Delta p'$ and ψ (as defined by Been & Jefferies, 1985). These comparisons are illustrated in Figure 7.7 and described below.

Figure 7.7 (a) illustrates a direct comparison between ψ and $\Delta p'$. These data appear linear in nature and the scatter of data points around the regression line is a result data scatter around the steady state line illustrated in Figure 6.17 (a). The apparently anomalous data points at a $\Delta p'$ of approximately 200 kPa represent the samples of Newborough 0% sand that failed by complete liquefaction. Figure 7.7 (b) illustrates the relationship between ψ_s and $\Delta p'$. Once again the relationship appears to be approximately linear in nature, although the scatter of data around the mean line appears to be of a slightly greater magnitude. Figure 7.7 (c) illustrates a direct comparison between the two indices of sand state, ψ & ψ_s, and based upon simply a visual inspection, there appears to be a strong linear relationship between these two parameters. The regression and ANOVA analyses for these data are listed below.

Title	*Equation*	*Source*	*Df*	*M*	*F*	R^2	*p*
ψ - $\Delta p'$	$y = 5.56^{-5}x + 0.005$	Regression Residual	1 32	1545941 23539	66	0.66	2.96×10^{-9}
ψ_s - $\Delta p'$	$y = 0.016x + 0.831$	Regression Residual	1 32	1117344 35264	32	0.50	3.95×10^{-6}
ψ_s - ψ	$y = 414x - 1.27$	Regression Residual	1 43	0.04 0.0002	23 4	0.84	5.16×10^{-19}

Table 7.4. Regression & ANOVA data associated with Figure 7.7.

On the basis of the calculated *p* values, all these relationships appear to be significant in nature. However, on the simple basis of R^2 values for these data, ψ appears to be a better index of $\Delta p'$ than ψ_s. The fact that the two indices of state are linearly related to each other, suggests the viability of the proposed method.

A summary of the integrated geotechnical - geophysical data is presented in Table 7.5.

7.4. Integrated data: Newborough 5% sand.

The individual relationships between shear wave velocity and void ratio, effective confining stress and deviator stress for Newborough 5% sand are illustrated in Figures 7.8 (a - d); summarised data are listed in Table 7.6 below.

Test No.	*e*	p'_c *(kPa).*	$V_s'_c$ *(m/s).*	p'_{ss} *(kPa).*	$V_s'_{ss}$ *(m/s).*	$V_{s\ crit}$ *(m/s).*	ψ	ψ_s
1	0.765	200	188	20	86	196	0.044	8
2	0.751	197	193	66	141	195	0.030	2
3	0.736	198	192	153	181	195	0.015	3
4	0.728	200	192	181	190	196	0.007	4
5	0.707	198	196	375	237	195	-0.014	-1
6	0.704	198	197	250	205	195	-0.017	-2
7	0.699	200	207	535	284	196	-0.022	-11
8	0 619	198	217	-	-	195	-0.102	-22

Table 7.6. Summary of integrated laboratory data, Newborough 5% sand.

Figure 7.8 (a), illustrates the steady state line defined in terms of shear wave velocity versus log effective confining stress; Figure 7.8 (b) illustrates the same data, defined in

terms shear wave velocity versus effective confining stress. The best fit line through the data was calculated in the manner described above, and has the form:-

$$V_s = 32 \times p'^{0.35} \qquad (7.5).$$

The results of a regression analysis on this relationship are listed below.

Title	*Equation*	*Source*	*Df*	*M*	*F*	R^2	*p*
Eqn. 7.5	y = 0.35x + 1.50	Regression Residual	1 5	1.41 0.001	1326	0.995	2.94×10^{-7}

Table 7.7. Regression and ANOVA data associated with Equation 7.5.

These data clearly show that this relationship is once again significant in nature.

Figure 7.8 (c) illustrates a comparison between void ratio and shear wave velocity at steady state. Once again, from only a visual inspection of these data, there is obviously a clear linear relationship between these two parameters. The principle reason for this is due mainly to the strong inter-relationship between V_s and p'. The best fit line through these data has the form described in Equation 7.2 above and the calculated regression parameters:

$c = 0.140,\ d = 1.042$

The regression statistics for this relationship are displayed below.

Title	*Equation*	*Source*	*Df*	*M*	*F*	R^2	*p*
Vs - e	y = -0.14 (log x) + 1.042	Regression Residual	1 5	0.165 0.001	124	0.95	0.0001

Table 7.8. Regression and ANOVA data associated with the regression analysis between V_s & e, at steady state, for Newborough 5% sand.

Figure 7.8 (d) illustrates the relationship between the deviator stress and shear wave velocity at steady state. The best fit line through the data has the general form described in Equation 6.3, with the regression parameters:

f= 3.02, g' = 4.52.

Regression data are displayed in Table 7.9 below.

Title	*Equation*	*Source*	*Df*	*M*	*F*	R^2	*p*
Vs - q	log (y) = 3.02 (log x) - 4.52	Regression Residual	1 5	0.17 0.0002	878	0.99	8.2×10^{-7}

Table 7.9. Regression and ANOVA data for the relationship between shear wave velocity and deviator stress at steady state, Newborough 5% sand.

As can be seen from Tables 7.8 and 7.9, the relationships between the predicted shear wave velocity and both void ratio and deviator stress at steady state are of a statistically significant nature.

7.4.1. Inference of sediment state: Newborough 5% sand.

In order to compare the conventional and proposed indices of consolidation state for the Newborough 5% sand, ψ, ψ_s & $\Delta p'$ were calculated in the manner described above. Figure 7.9 illustrates the results of this comparison. Figure 7.9 (a), illustrates a direct comparison between ψ and $\Delta p'$. Despite the significantly fewer number of data points for this illustration, this relationship appears to be approximately linear in nature. Figure 7.9 (b) illustrates the relationship between ψ_s and $\Delta p'$. Here, the relationship also appears to be linear in nature, although in contrast to the Newborough 0% sand, the scatter of the shear wave data appears to be of a slightly lesser magnitude. Figure 7.9 (c), illustrates a direct comparison between the two indices of sand state, ψ & ψ_s. This relationship is again linear in nature, allowing the conclusion that ψ_s may be used as an index of sediment consolidation state for laboratory sands. However, it must be noted that the actual difference between a sample that showed a $\Delta p'$ of +200 and -200 kPa in terms of shear wave velocity is quite small, and is probably quite close to the real (unquantifiable) system resolution. This difference is also small in terms of void ratio, and illustrates that only a small change in density can dramatically alter the response of a particular sand to undrained shear. This remains a fundamental problem to the application of any sort of steady - state technique to the field, which can only be overcome to some extent by using a combination of field techniques.

The regression and ANOVA data for all Figures 7.9 (a, b & c) are given below.

Title	*Equation*	*Source*	*Df*	*M*	*F*	R^2	*p*
ψ - $\Delta p'$	y = 0.0001x + 0.01	Regression Residual	1 5	158001 7020	23	0.78	0.005
ψ_s - $\Delta p'$	y = 0.013x + 1.26	Regression Residual	1 5	163157 5989	27	0.81	0.003
ψ_s - ψ	y = 193.2x - 0.62	Regression Residual	1 6	0.0012 0.0003	46	0.87	0.0005

Table 7.10. Regression & ANOVA data associated with Figure 7.9.

These data indicate that in the case of Newborough 5% sand, ψ_s appears to be a more significant index of $\Delta p'$ than ψ. Once again, the relationship between the two independent indices of sediment consolidation state appears to be highly significant.

7.5. Integrated data: Newborough 10% sand.

The individual relationships between shear wave velocity and void ratio, effective confining stress and deviator stress for Newborough 10% sand are illustrated in Figure 7.10 (a - d); summarised data are listed in Table 7.11 below.

Test No.	*e*	p'_c *(kPa).*	$V_s'_c$ *(m/s).*	p'_{ss} *(kPa).*	$V_s'_{ss}$ *(m/s).*	$V_{s\,crit}$ *(m/s).*	ψ	ψ_s
1	0.690	196	183	27	92	183	0.038	8
2	0.681	199	195	70	140	195	0.029	-4
3	0.671	199	188	96	151	188	0.019	4
4	0.675	197	189	79	142	189	0.023	2
5	0.634	198	194	435	251	194	-0.018	-2
6	0.640	197	196	345	241	196	-0.012	-5
7	0.643	198	186	190	188	186	-0.009	6
8	0.589	200	198	-	-	198	-0.063	-6
9	0.730	196	163	-	-	163	0.078	29

Table 7.11. Summary of integrated laboratory data, Newborough 10% sand.

Figure 7.10 (a), illustrates the steady state line defined in terms of shear wave velocity versus log effective confining stress; Figure 7.10 (b) illustrates the steady state line, defined in terms shear wave velocity versus effective confining stress. For the Newborough 10% test sand, the best fit line through these data has the form:-

$$V_s = 29 \times p'^{0.36} \qquad (7.6).$$

Title	*Equation*	*Source*	*Df*	*M*	*F*	R^2	*p*
Eqn. 7.6	y = 0.36x + 1.47	Regression Residual	1 5	1.07 0.001	808	0.99	1.01×10^{-6}

Table 7.12. Regression and ANOVA data associated with Equation 7.6.

Figure 7.10 (c) illustrates a comparison between void ratio and shear wave velocity at steady state. The best fit line through these data has the form described in Equation 6.2 above and the regression parameters,

$c = 0.14$, $d = 0.97$.

The regression statistics for this relationship is displayed below.

Title	*Equation*	*Source*	*Df*	*M*	*F*	R^2	*p*
Vs - e	y = -0.14 (log x) + 0.97	Regression Residual	1 5	0.125 0.003	46	0.88	0.001

Table 7.13. Regression and ANOVA data associated with the regression analysis between V_s & e at steady state, for Newborough 10% sand.

Figure 7.10 (d) illustrates the relationship between the deviator stress and shear wave velocity at steady state. Once again, the best fit line through the data has the general form described in Equation 6.3, with the regression parameters:

$f = 2.81$, $g' = 4.02$

Regression data are displayed below.

Title	*Equation*	*Source*	*Df*	*M*	*F*	R^2	*p*
Vs - q	log (y) = 2.18 (log x) - 4.02	Regression Residual	1 5	0.138 0.0001	905	0.99	7.6×10^{-7}

Table 7.14. Regression and ANOVA data for the relationship between V_s & q at steady state, Newborough 10% sand.

The results of these analyses on these data show clearly that both these relationships are significant.

7.5.1. Inference of consolidation state: Newborough 10% sand.

Figure 7.11 (a - c) compares and contrasts the different indices of consolidation state for the Newborough 10% test sand, while the regression analyses for these relationships is presented below. Figure 7.11 (a), shows a direct comparison between ψ and $\Delta p'$. Once again, the data appear linear in nature although there appears a greater degree of scatter than recorded for the two previous sands. Figure 7.11 (b) illustrates the relationship between ψ_s and $\Delta p'$. This relationship reflects the greater scatter in the shear wave velocities for this sand (also noted above) and is not significant at a confidence level of 95%. Figure 7.11 (c), illustrates a direct comparison between the two indices of sand state, ψ & ψ_s. This diagram indicates that, despite the poor relationship between ψ_s & $\Delta p'$, ψ & ψ_s are statistically related to each other, suggesting that even in this case some estimate of consolidation state may be derived from laboratory shear wave velocity data. It also tends to confirm the hypothesis that in laboratory sands at least, ψ appears to the best index of sand state.

Title	*Equation*	*Source*	*Df*	*M*	*F*	R^2	*p*
Fig. 7.14 (a).	y = 0.0001x + 0.007	Regression Residual	1 5	124252 4148	30	0.83	0.003
Fig. 7.14 (b).	y = 0.018x + 0.93	Regression Residual	1 5	42829 20433	2	0.15	0.21
Fig. 7.14 (c).	y = 209x + 1.57	Regression Residual	1 6	0.008 0.0007	11	0.56	0.0012

Table 7.15. Regression & ANOVA data associated with Figure 7.11.

7.6. Integrated data: Fraser Delta sand.

The individual relationships between shear wave velocity and void ratio, effective confining stress and deviator stress for the Fraser Delta sand are illustrated in Figures 7.12 (a - d); summarised data are listed in Table 7.16 below.

Test No.	*e*	*p'c (kPa).*	*Vs'c (m/s).*	*p'ss (kPa).*	*Vs'ss (m/s).*	*Vs crit (m/s).*	*ψ*	*ψs*
1	0.861	202	206	238	215	191	0.015	-15
2	0.871	194	191	192	190	188	0.021	-3
3	0.882	201	196	114	167	191	0.035	-5
4	0.878	199	192	149	177	190	0.030	-2
5	0.878	199	179	134	159	190	0.030	-11
6	0.814	199	188	277	207	190	-0.034	-2
7	0.830	200	197	186	192	190	-0.017	-7
8	0.759	200	218	503	274	190	-0.088	-28

Table 7.16. Summary of integrated laboratory data, Fraser Delta sand.

Figure 7.12 (a) illustrates the steady state line defined in terms of shear wave velocity versus log effective confining stress; Figure 7.12 (b) illustrates the steady state line, defined in terms shear wave velocity versus effective confining stress. The best fit line through these data has the form:-

$$Vs = 31 \times p'^{0.34} \qquad (7.7).$$

Title	*Equation*	*Source*	*Df*	*M*	*F*	R^2	*p*
Eqn. 7.7.	y = 0.34x + 1.49	Regression Residual	1 5	0.29 0.001	292	0.98	1.25^{-5}

Table 7.17. Regression and ANOVA data associated with Equation 7.7.

Figure 7.12 (c) illustrates a comparison between void ratio and shear wave velocity at steady state. Once again there is a clear relationship between these two parameters. The best fit line through these data has the form described in Equation 6.2 above and the regression parameters:

$c = 0.51, d = 2.02$

The regression statistics for this relationship is displayed below.

Title	*Equation*	*Source*	*Df*	*M*	*F*	R^2	*p*
Vs - e	y = -0.51 (log x) + 2.02	Regression Residual	1 6	0.03 0.001	21	0.74	0.004

Table 7.18. Regression and ANOVA data associated with the regression analysis between V_s and e at steady state, for the Fraser Delta sand.

Figure 7.12 (d) illustrates the relationship between the deviator stress and shear wave velocity at steady state. Once again, the best fit line through the data has the general form described in Equation 6.3, with the regression parameters:

$f = 2.85, g' = 4.40$

The regression data for this relationship is displayed below.

Title	*Equation*	*Source*	*Df*	*M*	*F*	R^2	*p*
Vs - q	log (y) = 2.85 (log x) - 4.40	Regression Residual	1 6	0.037 0.0003	119	0.94	3.5×10^{-5}

Table 7.19. Regression and ANOVA data for the relationship between shear wave velocity and deviator stress at steady state, Fraser Delta sand.

In common with the other data of the same type described above, these relationships can all be regarded as statistically significant.

7.6.1. Inference of sediment state, Fraser Delta sand.

Figure 7.13 (a - c) compares and contrasts the different indices of consolidation state for the Fraser Delta sand, while the regression analyses for these relationships are presented below. Figure 7.13 (a) illustrates a direct comparison between ψ and $\Delta p'$. These data are significantly linear in nature, at a confidence level of 95%. Figure 7.13 (b) illustrates the relationship between ψ_s and $\Delta p'$. This particular relationship is also significantly linear in nature, although the data display a larger amount of scatter than Figure 7.13 (a). Figure 7.13 (c) illustrates a direct comparison between the two indices of

sand state, ψ & ψ_s. This diagram indicates that for the Fraser Delta sand, the relationship between ψ & ψ_s is only significant at a level of 90% significance.

Title	*Equation*	*Source*	*Df*	*M*	*F*	R^2	*p*
Fig. 7.17 (a).	y = 0.0003x + 0.008	Regression Residual	1 5	94564 2361	40	0.85	0.0007
Fig. 7.17 (b).	y = 0.072x - 4.1	Regression Residual	1 5	63975 7560	9	0.52	0.026
Fig. 7.17 (c).	y = 172x + 5.5	Regression Residual	1 6	0.005 0.001	4	0.32	0.08

Table 7.20. Regression & ANOVA data associated with Figure 7.13.

7.7. Summary.

The data described above clearly illustrate the various inter-relationships that exist between the predicted shear wave velocity and measured void ratio, effective confining stress and deviator stress at steady state. The relationships between these parameters are all generally of a significant nature, and it was shown that the shear wave derived index of sand state, ψ_s correlates well with the more conventional state parameter, ψ. The biggest additional advantage of shear wave methods, for the prediction of liquefaction potential by this technique is its relative ease and repeatability of measurement in the field. As an illustration of this, the application of shear wave based methods in liquefaction prediction in the field is described below, with reference to the potentially unstable site, of the Fraser River Delta, British Columbia.

(a).

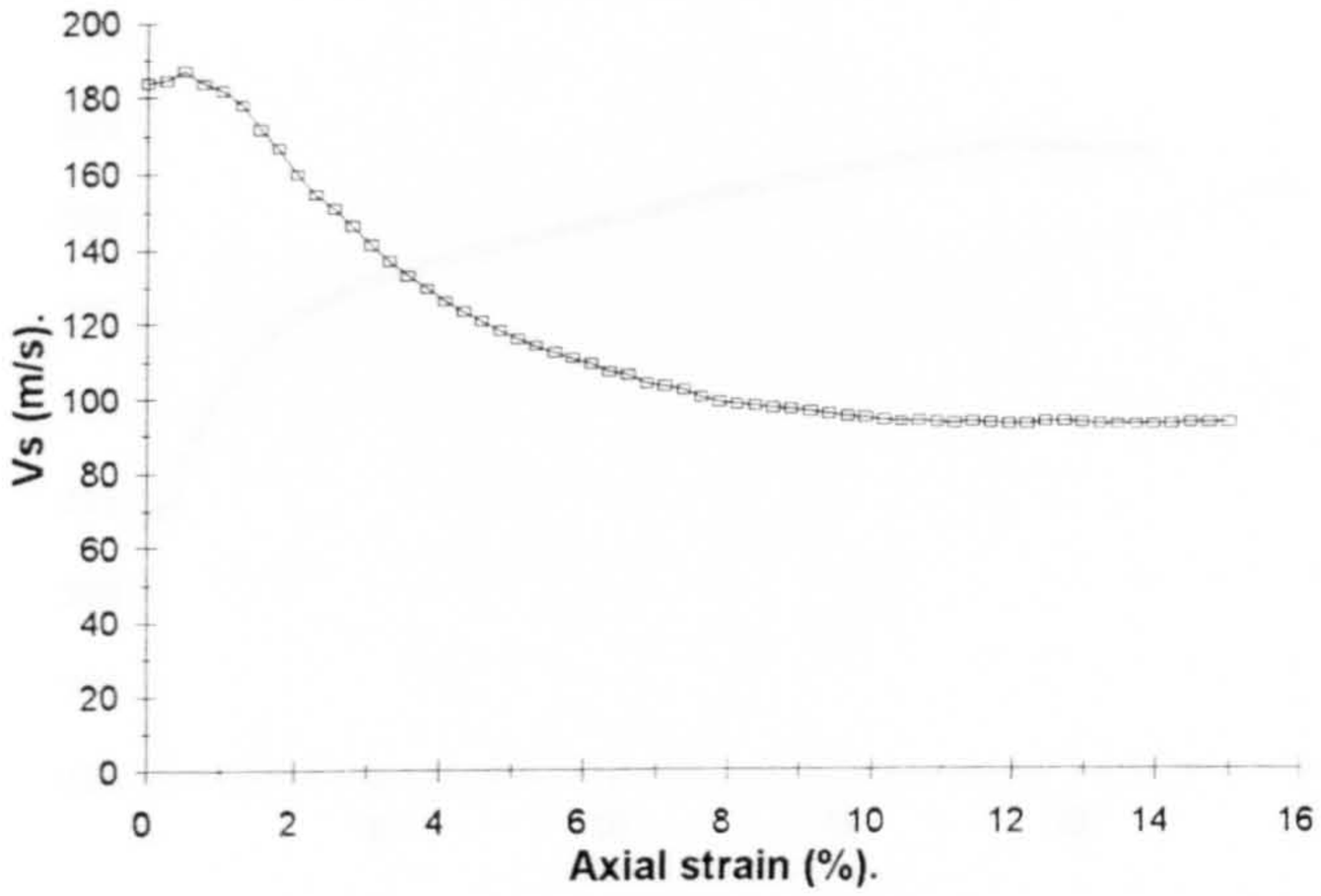

(b).

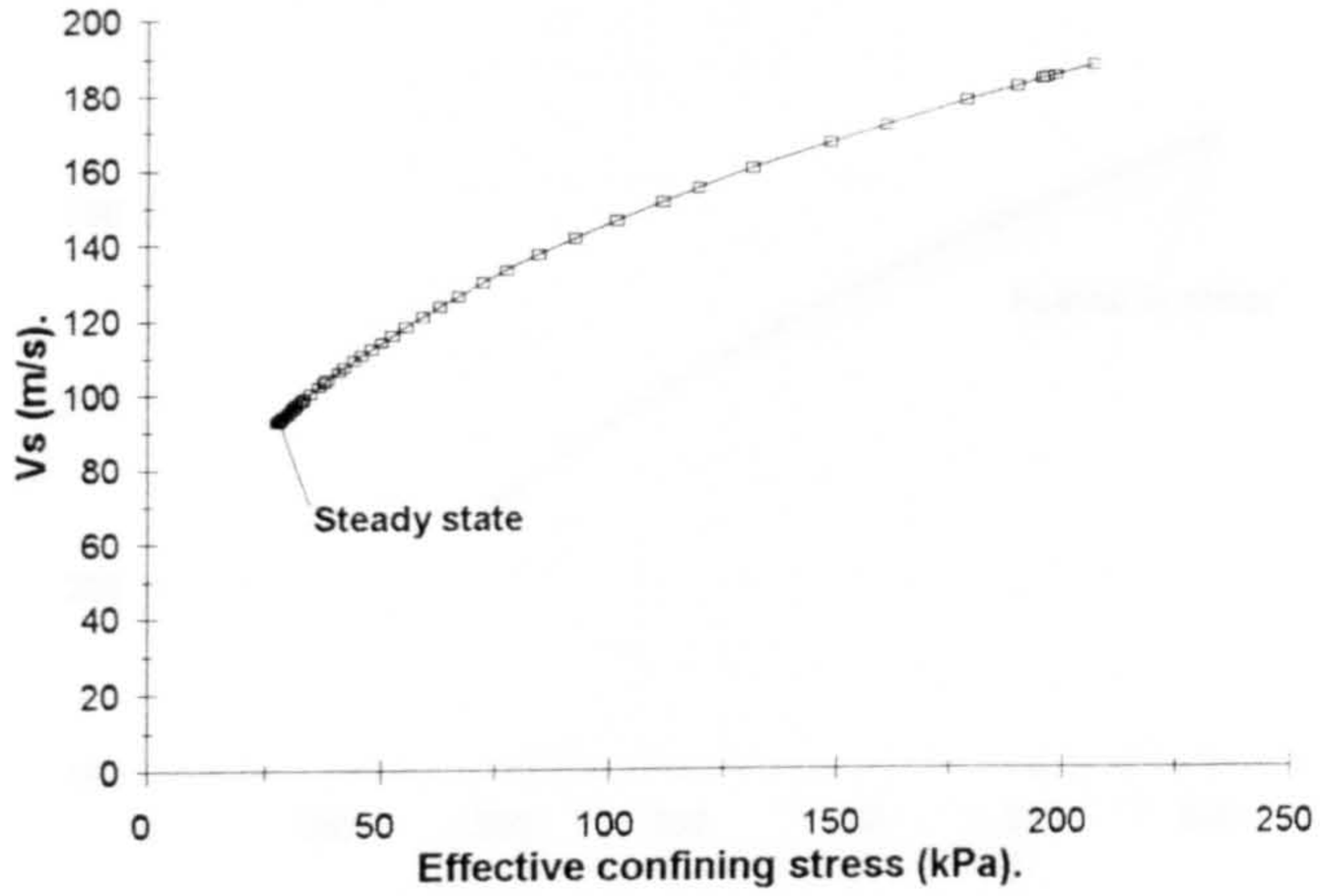

(c).

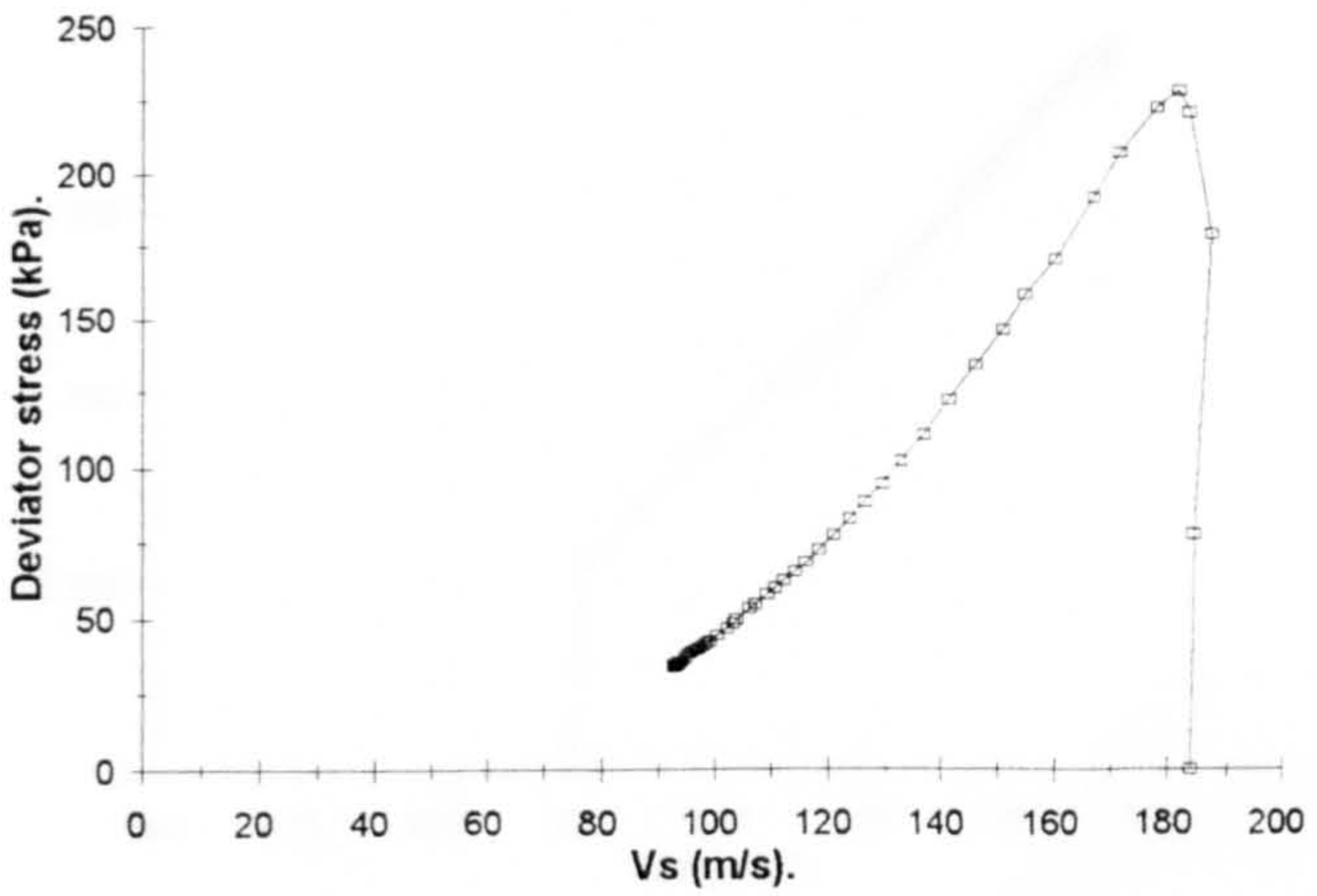

Figure 7.1. Predicted shear wave velocity response of a loose sand, under undrained shear.

(a).

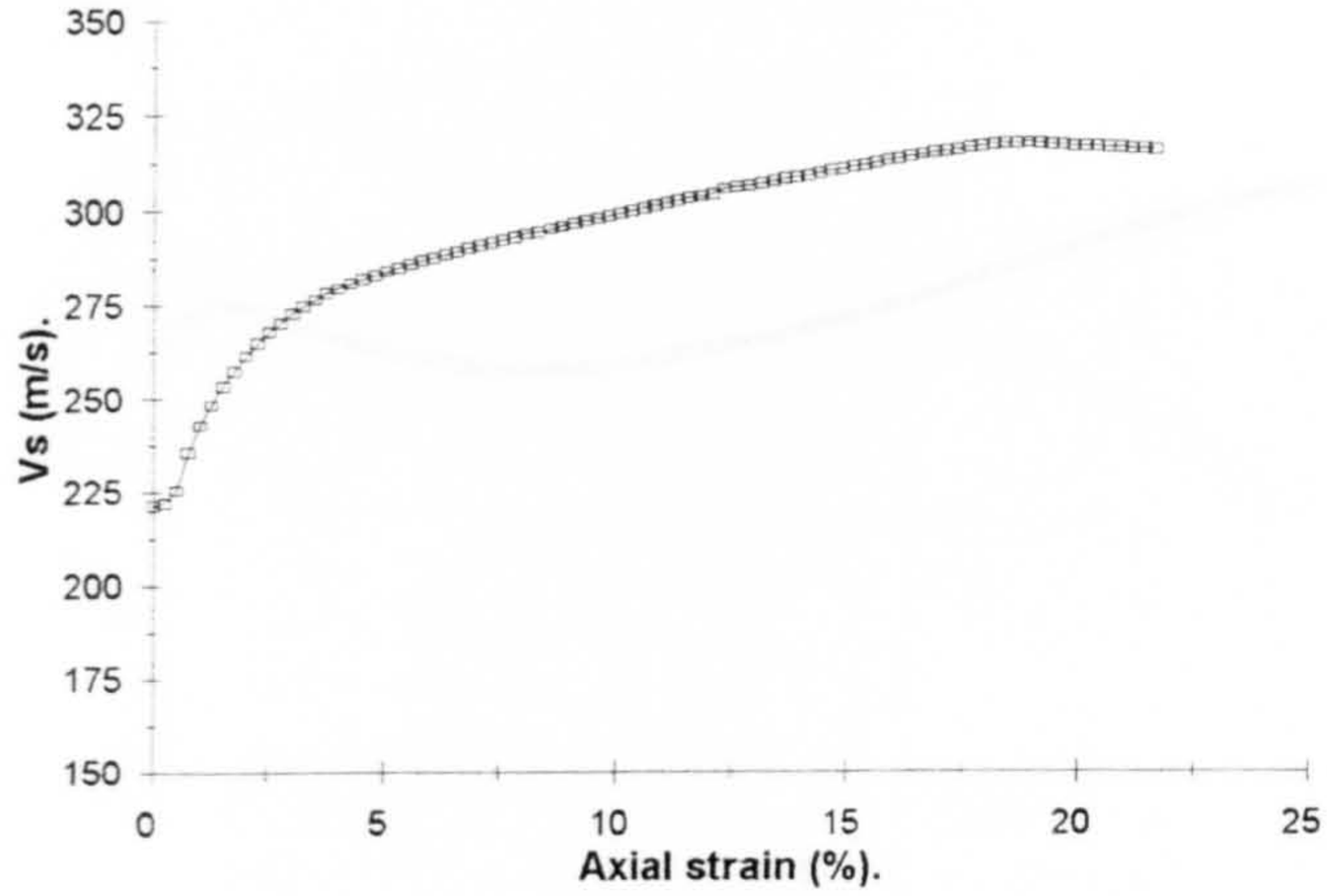

(b).

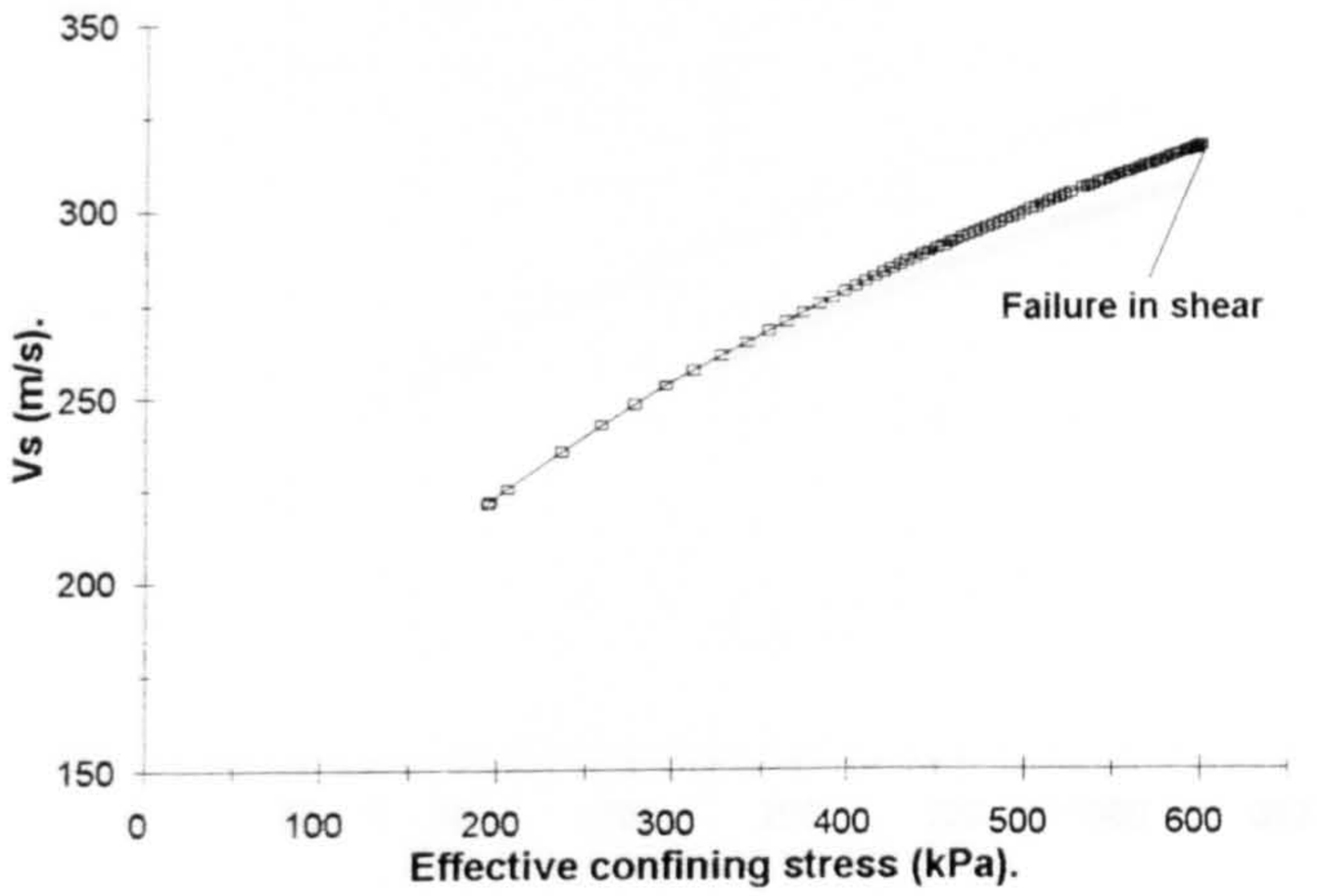

(c).

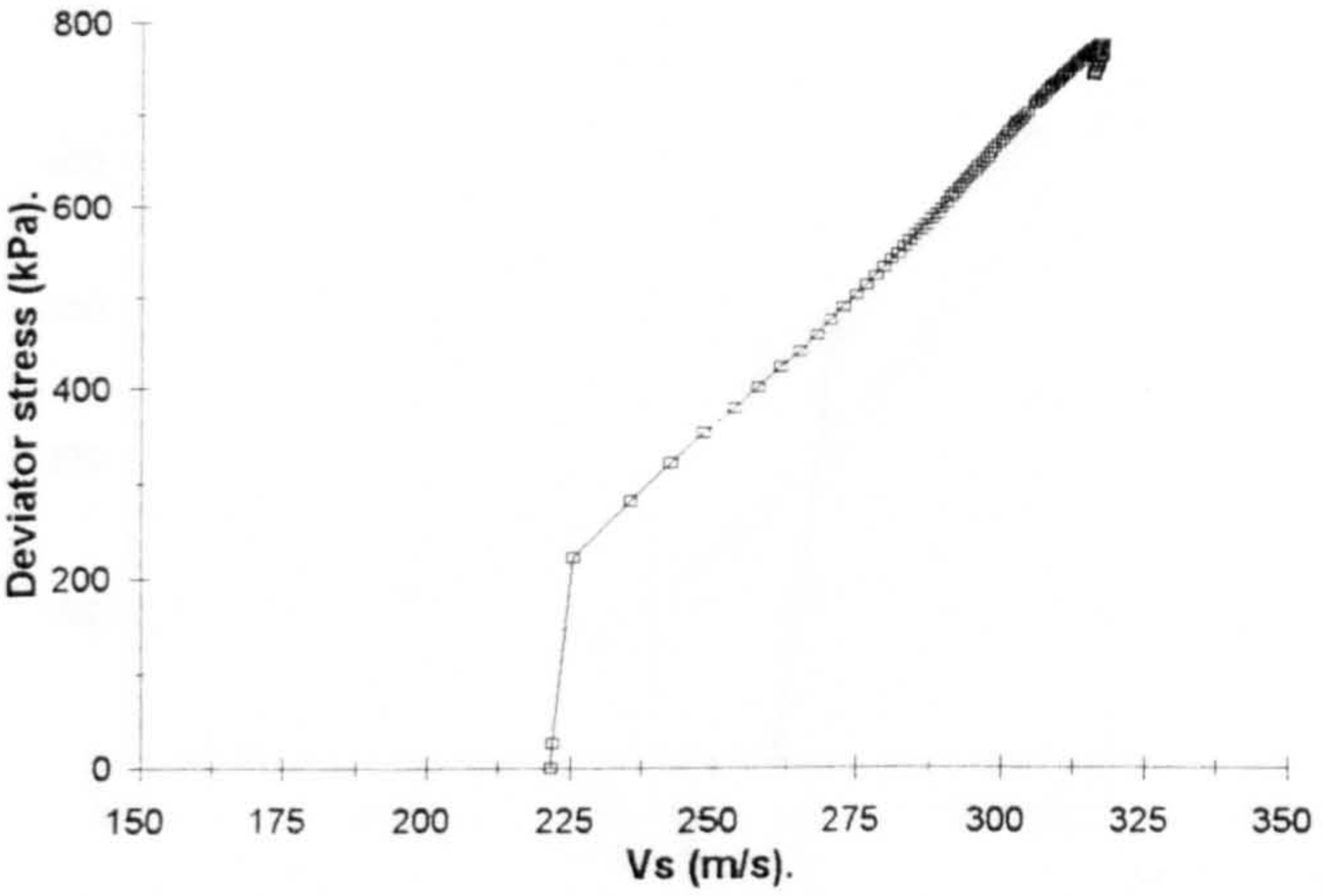

Figure 7.2. Predicted shear wave velocity response of a dense sand, under undrained shear.

(a).

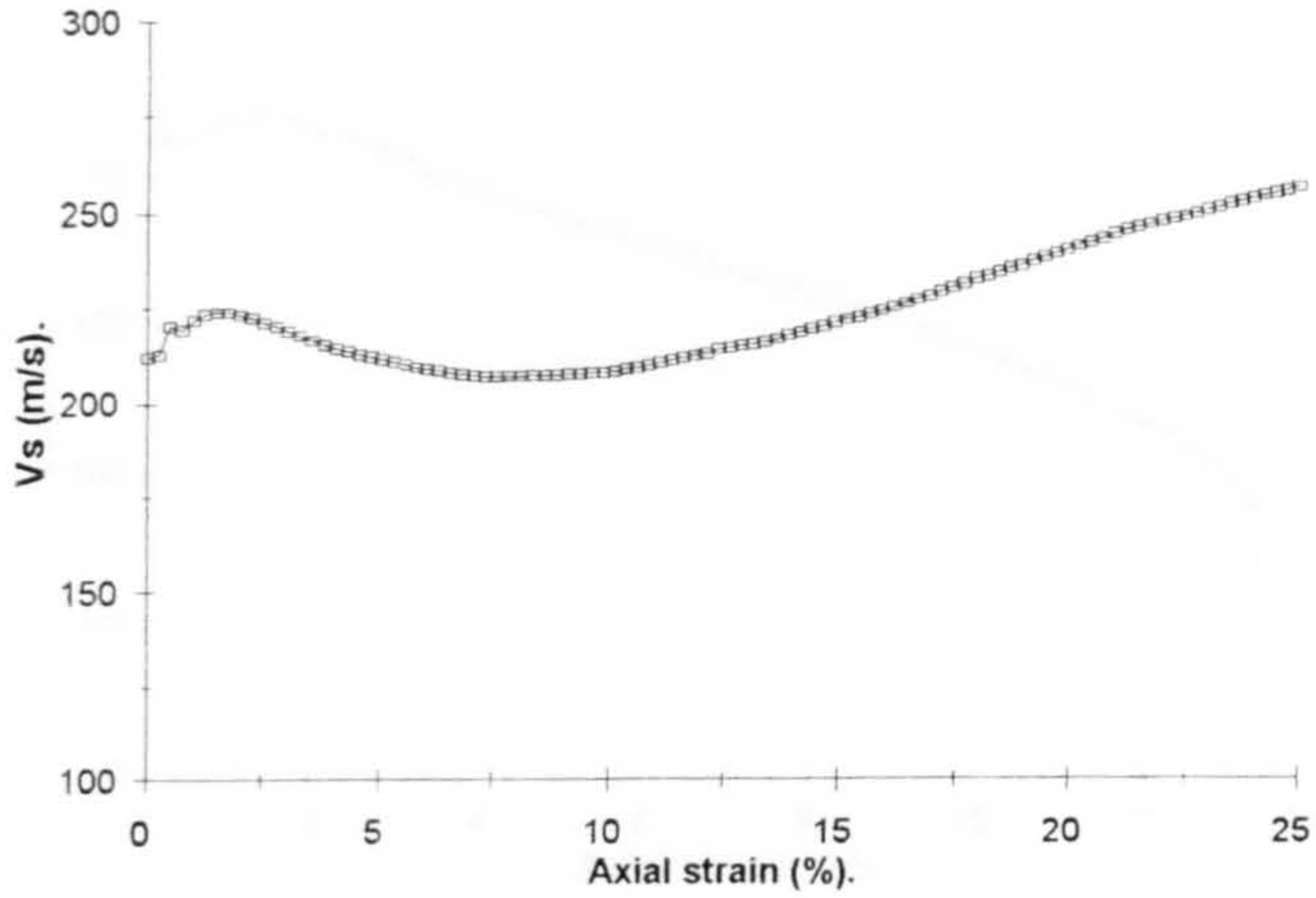

(b).

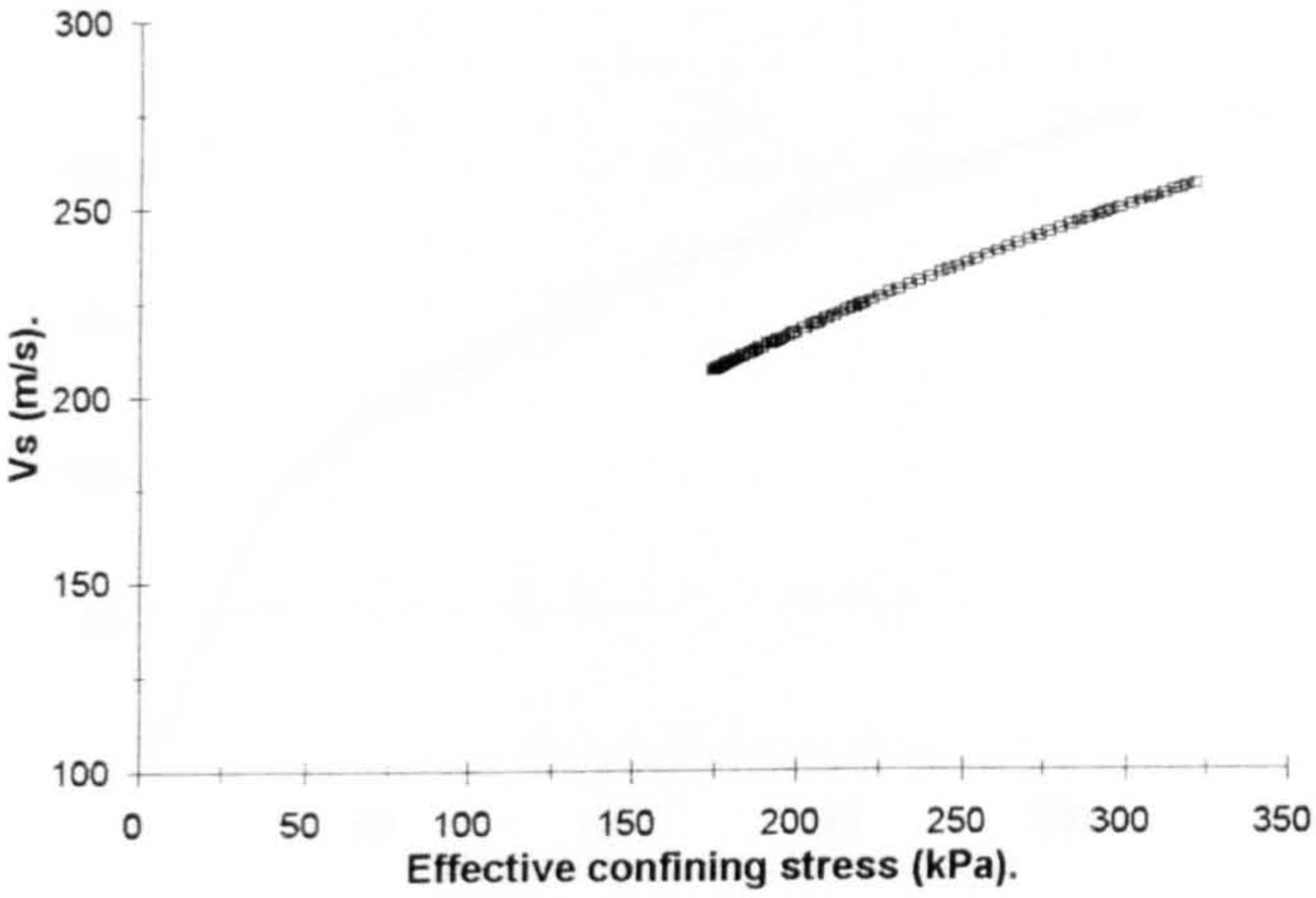

(c).

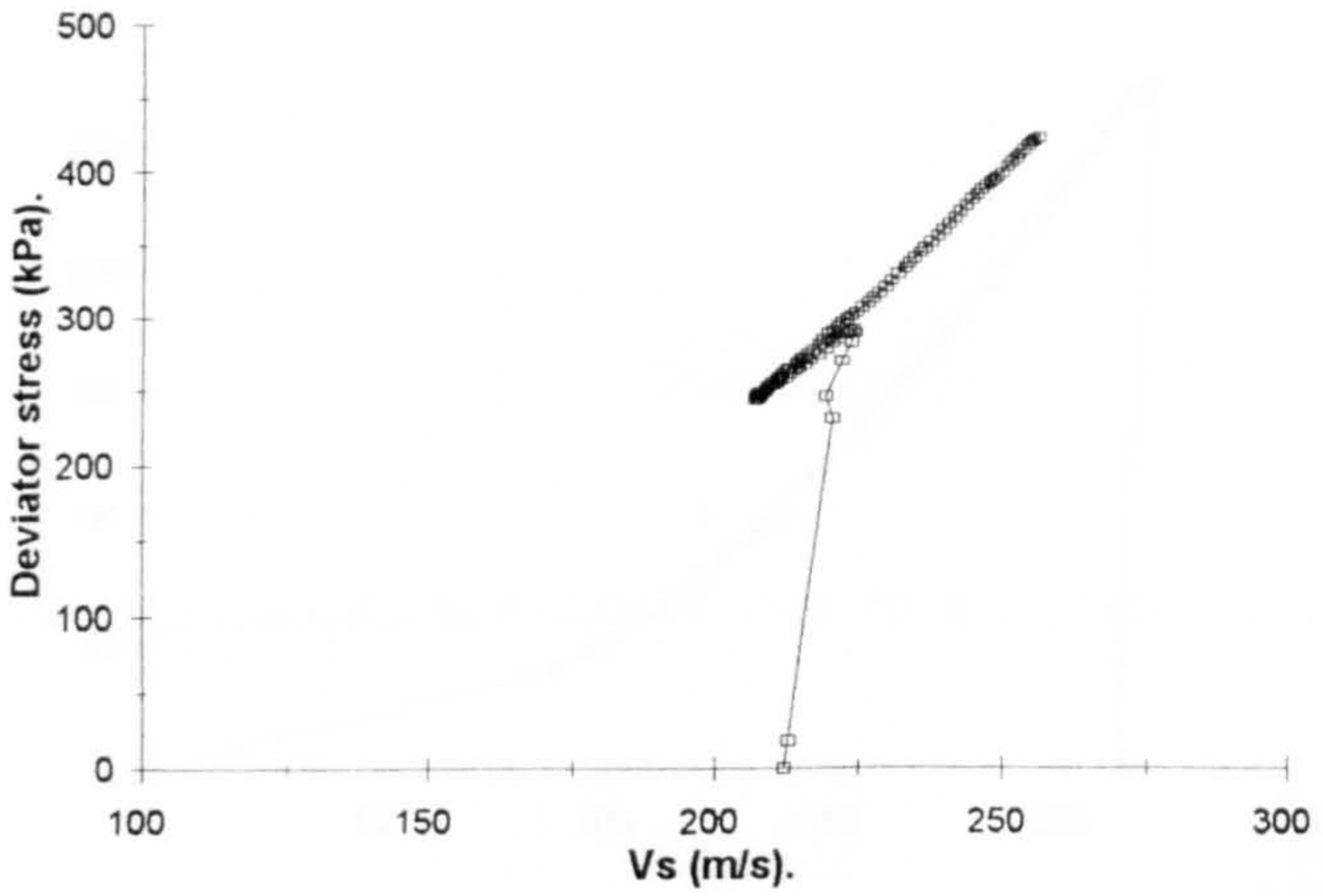

Figure 7.3. Predicted shear wave velocity response of a medium-dense sand, under undrained loading.

(a).

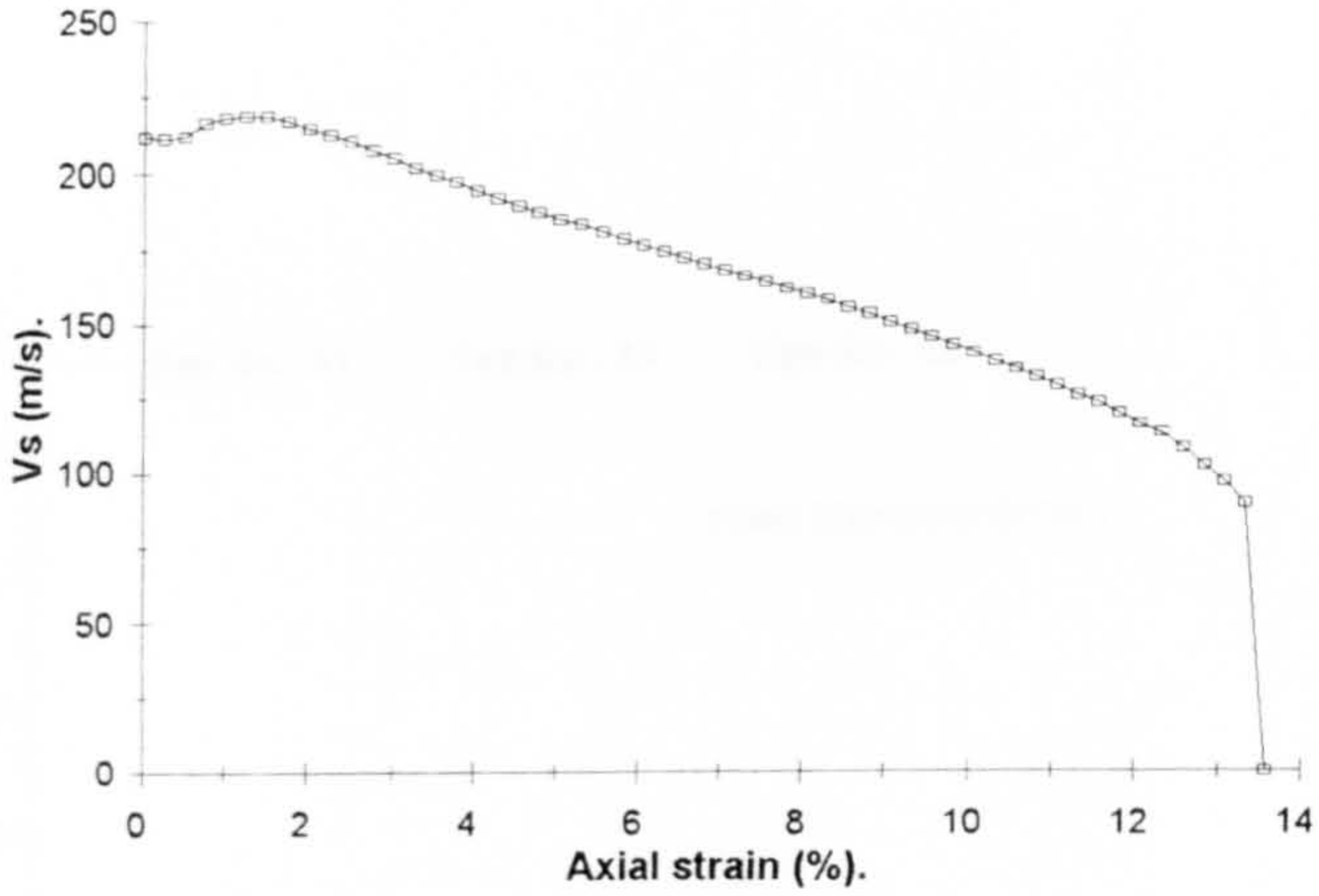

(b).

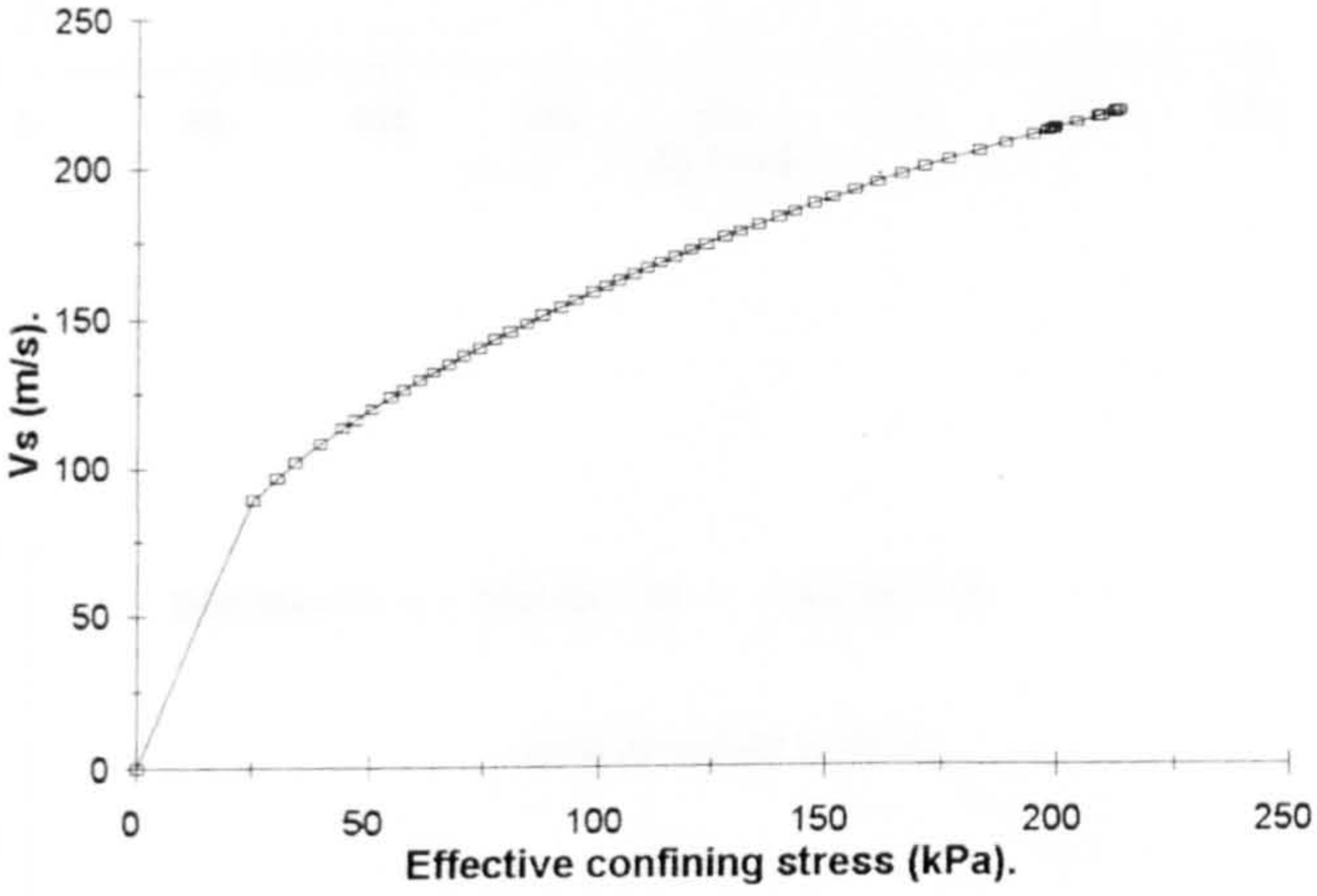

(c).

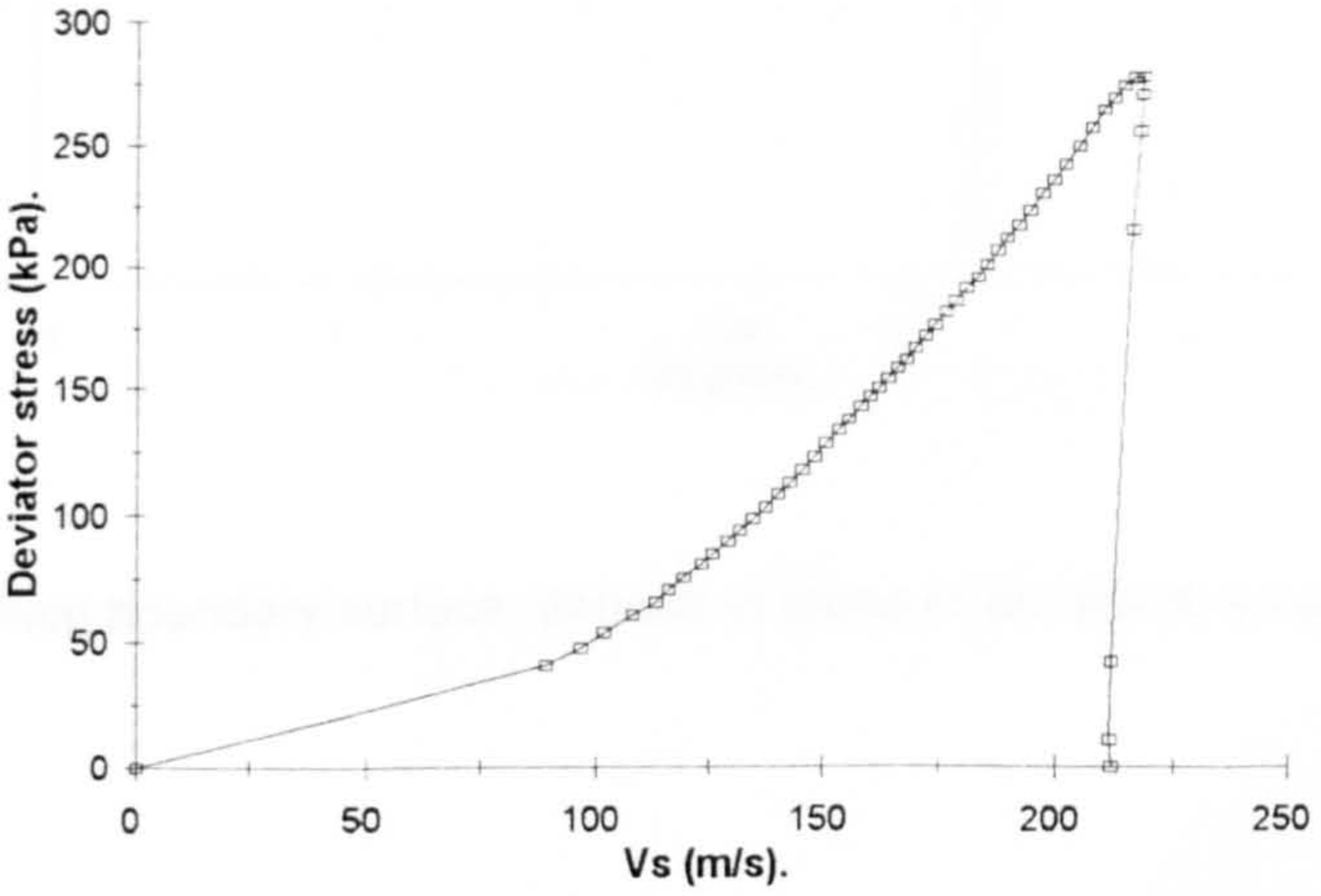

Figure 7.4. Predicted shear wave response of a very loose sand, under undrained loading, leading to complete failure by liquefaction.

(a).

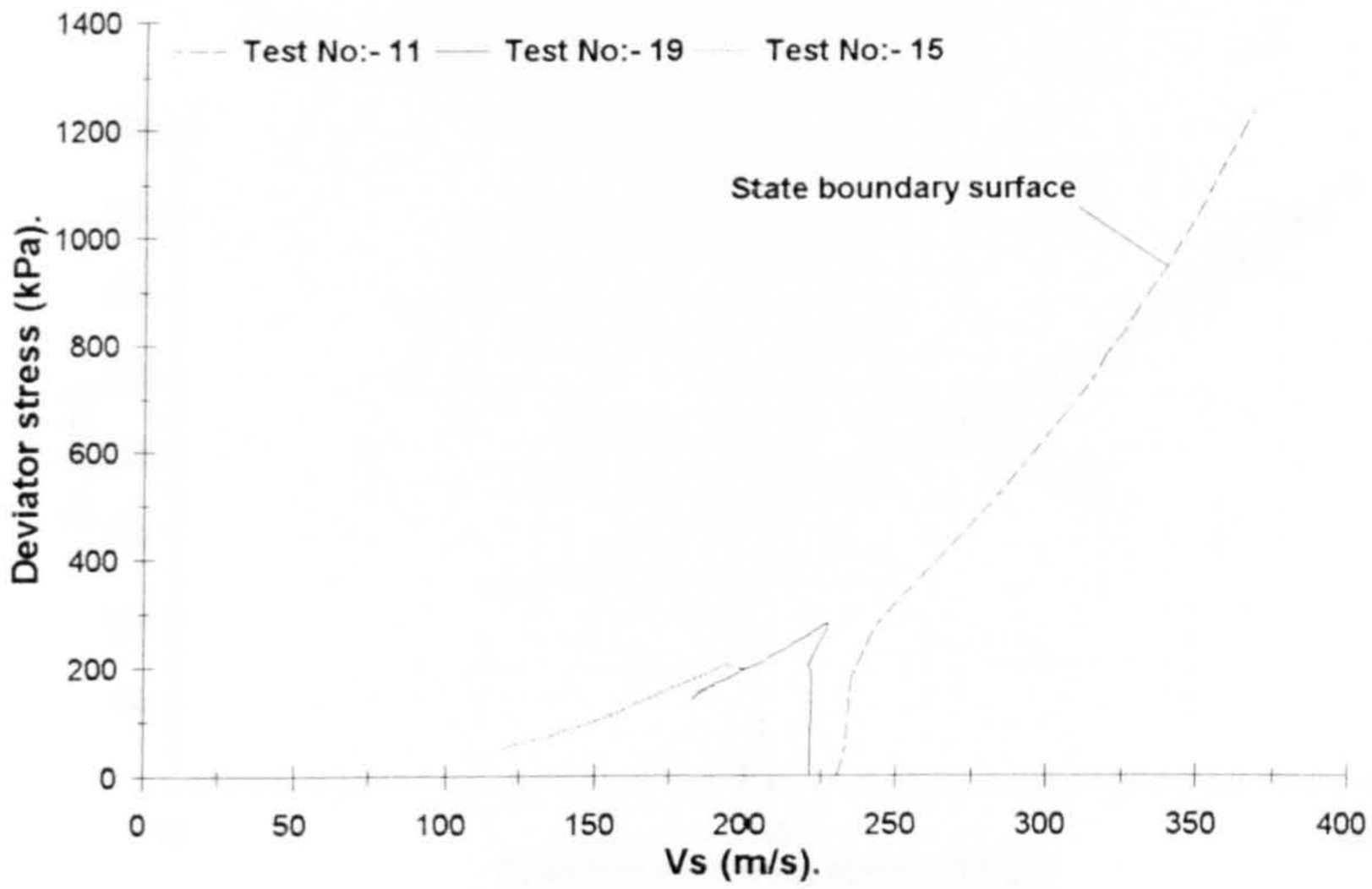

(b).

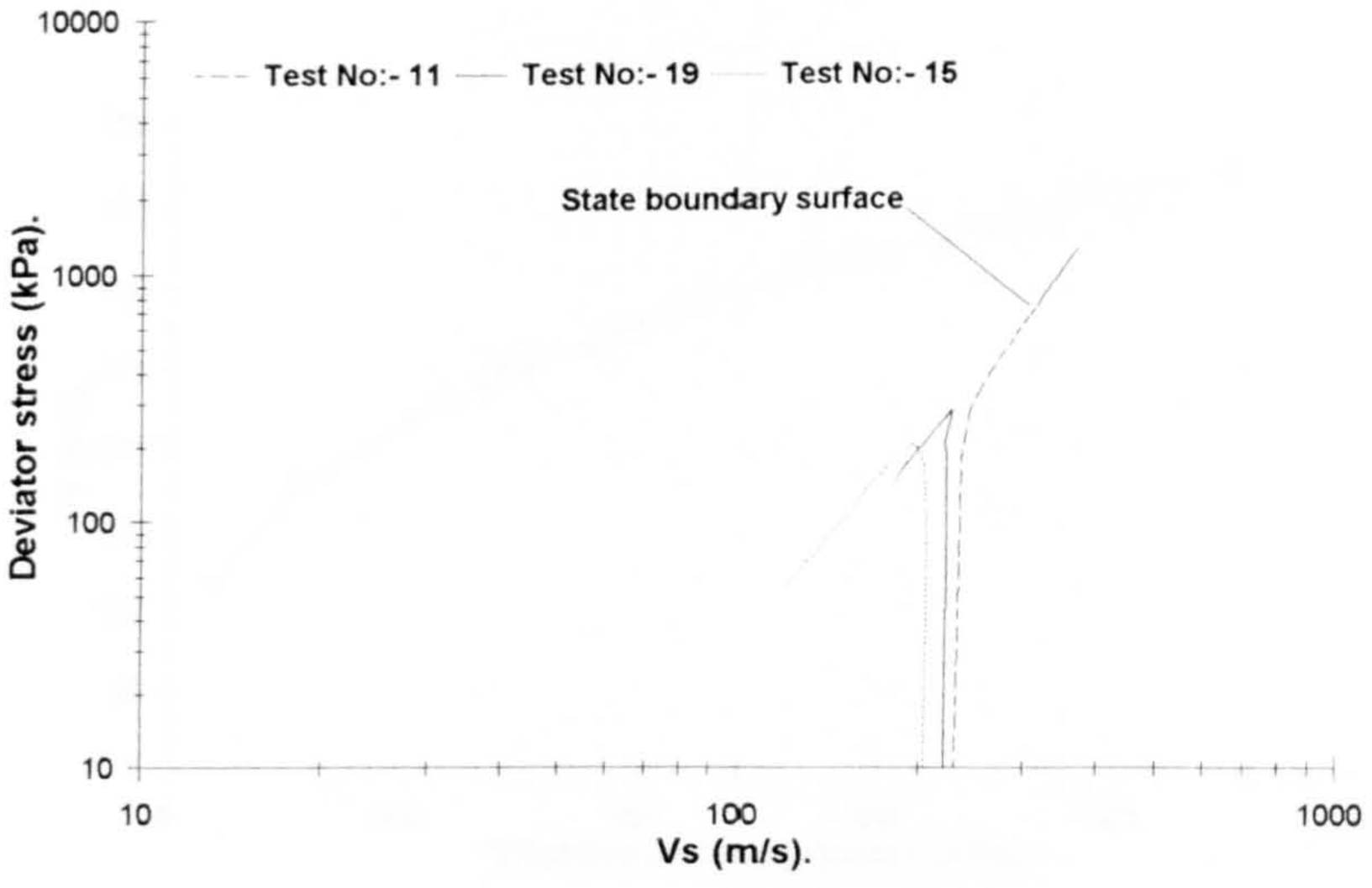

Figure 7.5. State boundary surface, defined in terms of predicted shear wave velocity.

(a).

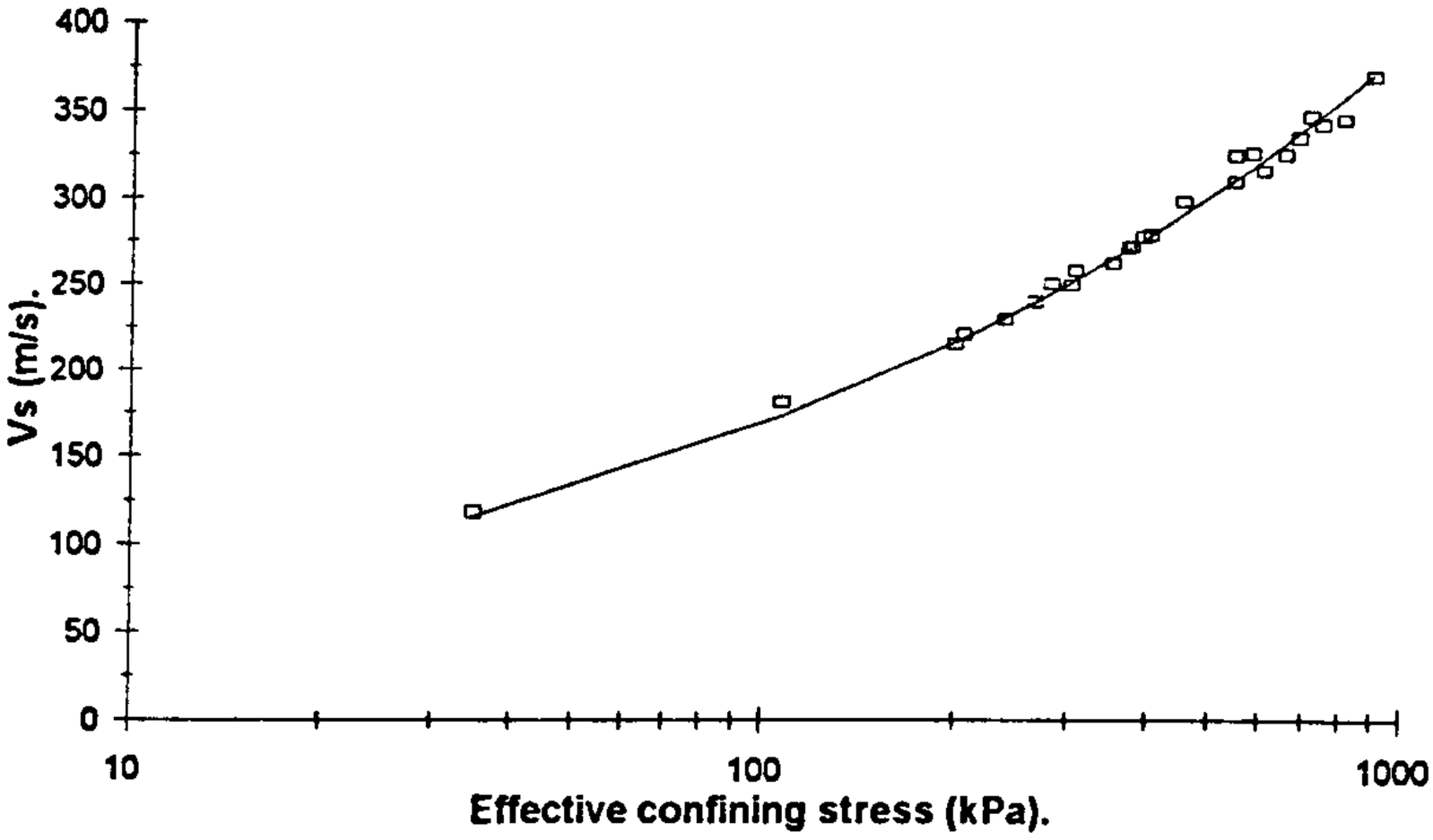

(b).

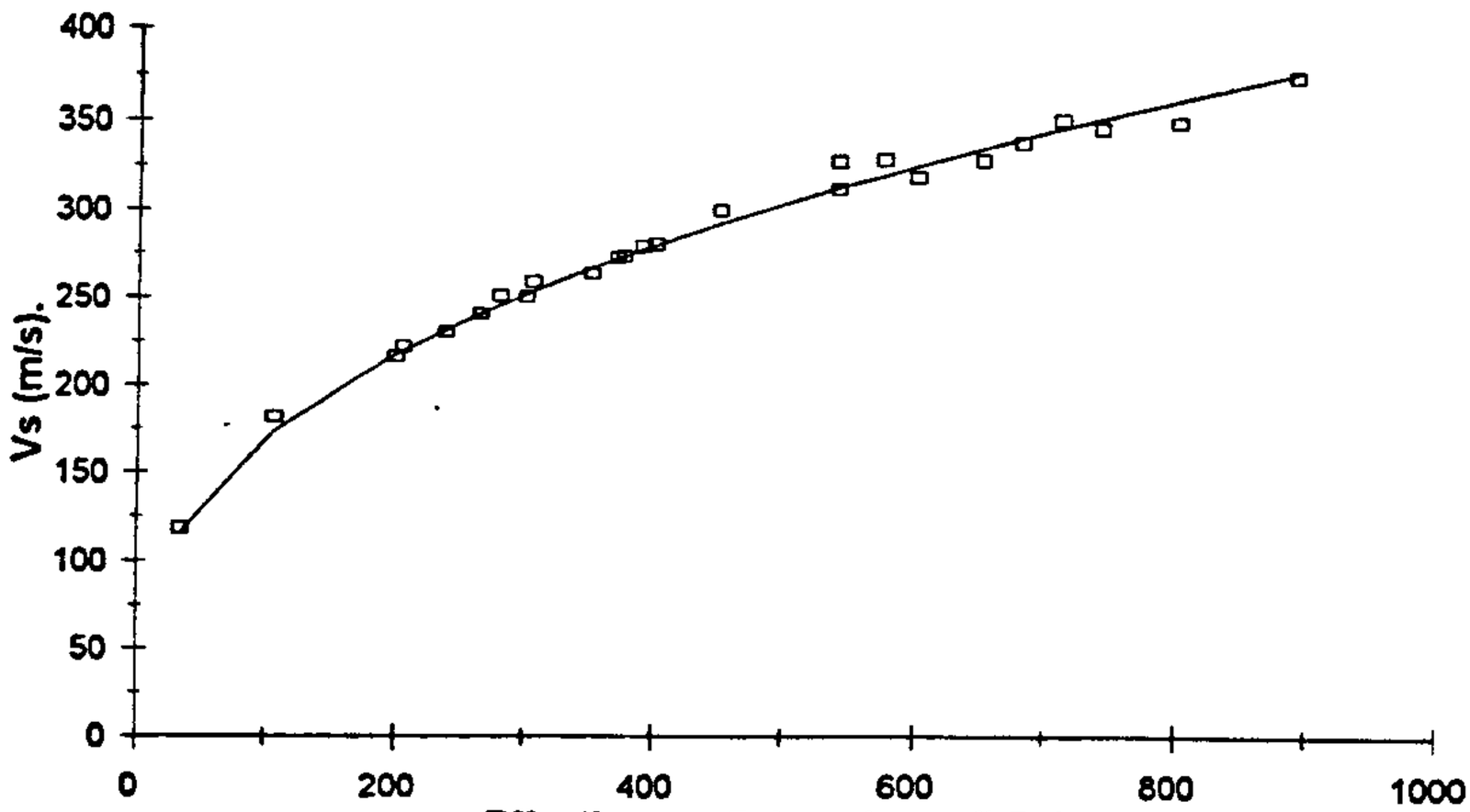

Figure 7.6. 'Critical shear wave velocity' line, defined for the Newborough 0% sand.

(c).

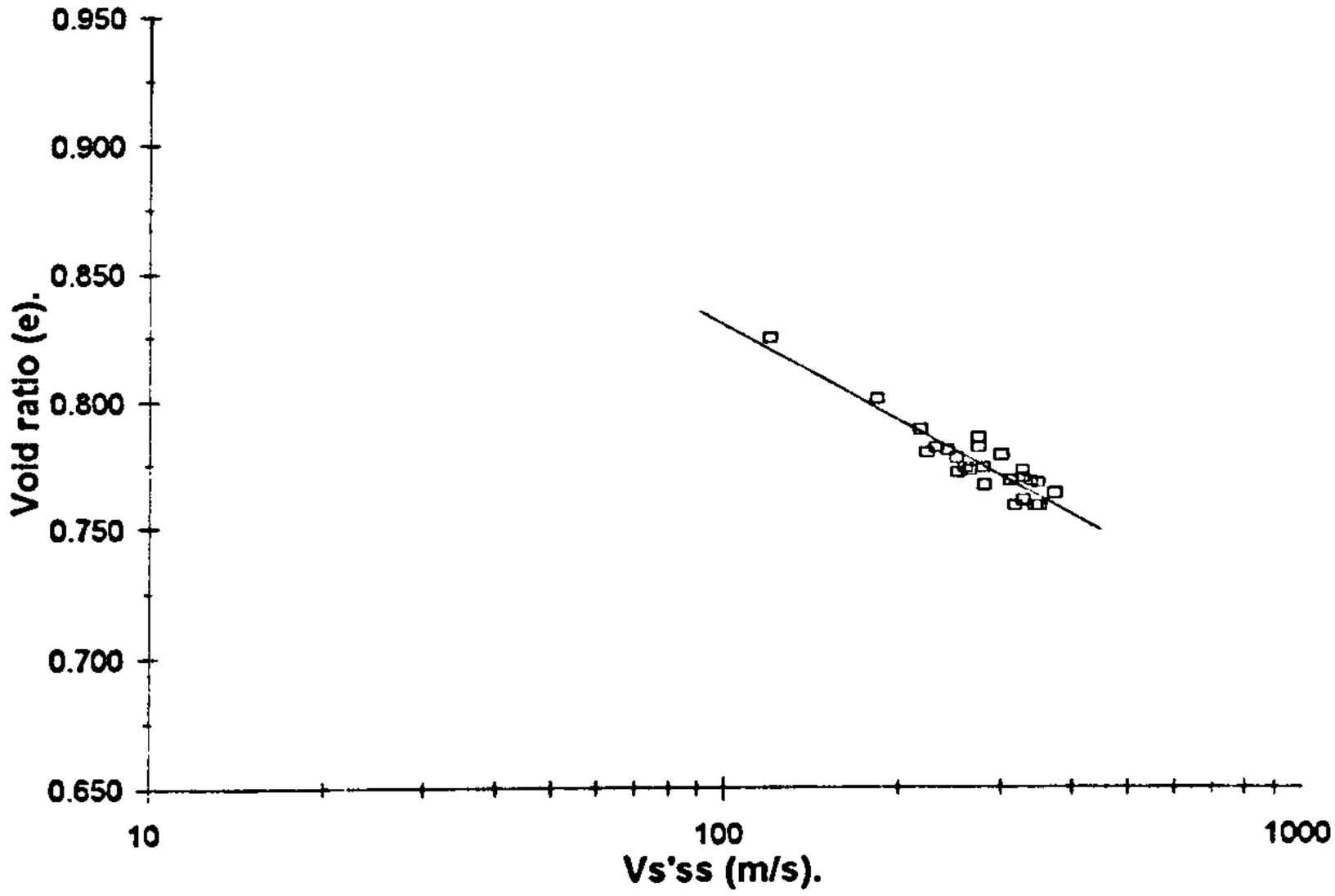

(d).

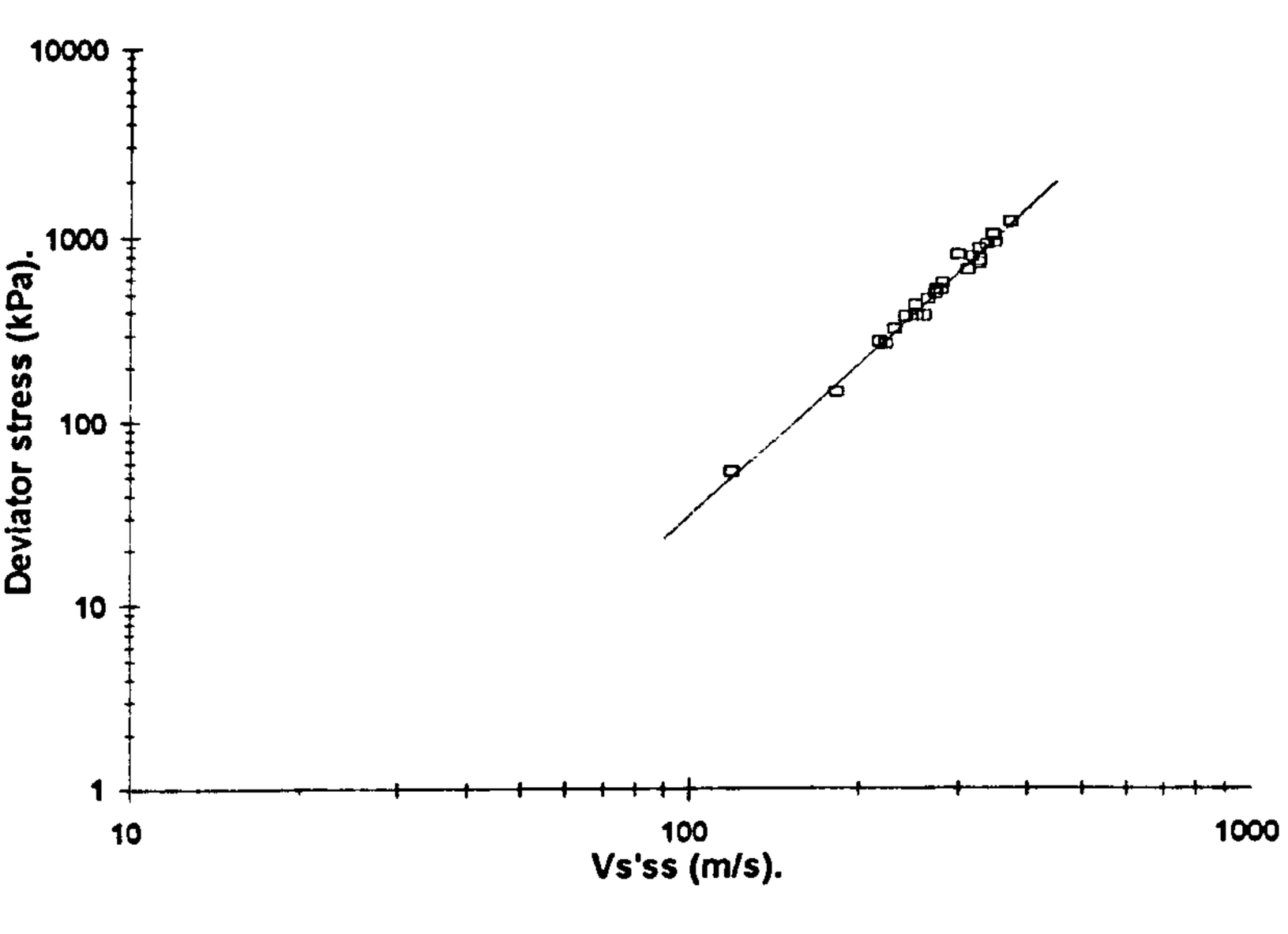

Figure 7.6 (cont). Relationship between void ratio, deviator stress and shear wave velocity, at steady state; Newborough 0% sand.

a.

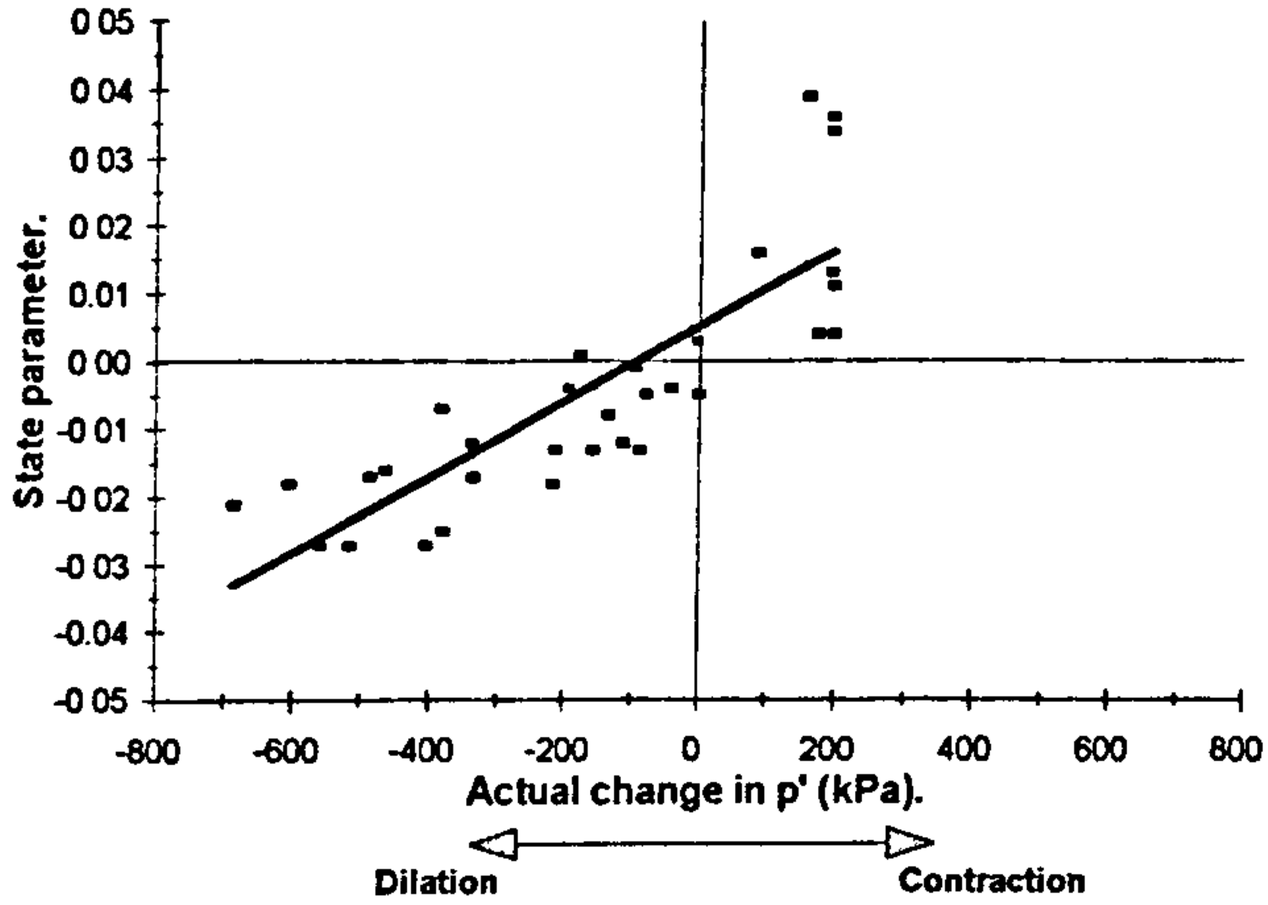

b.

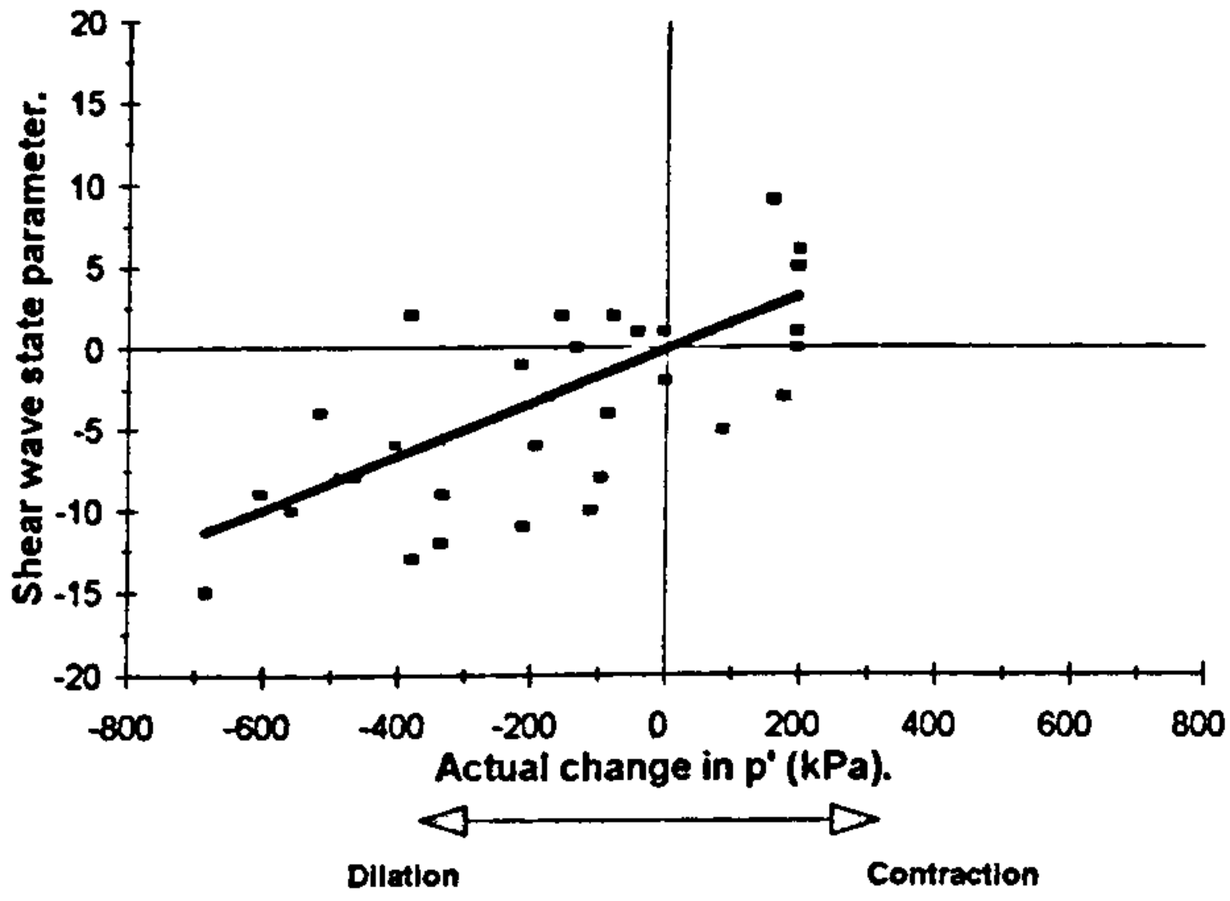

c.

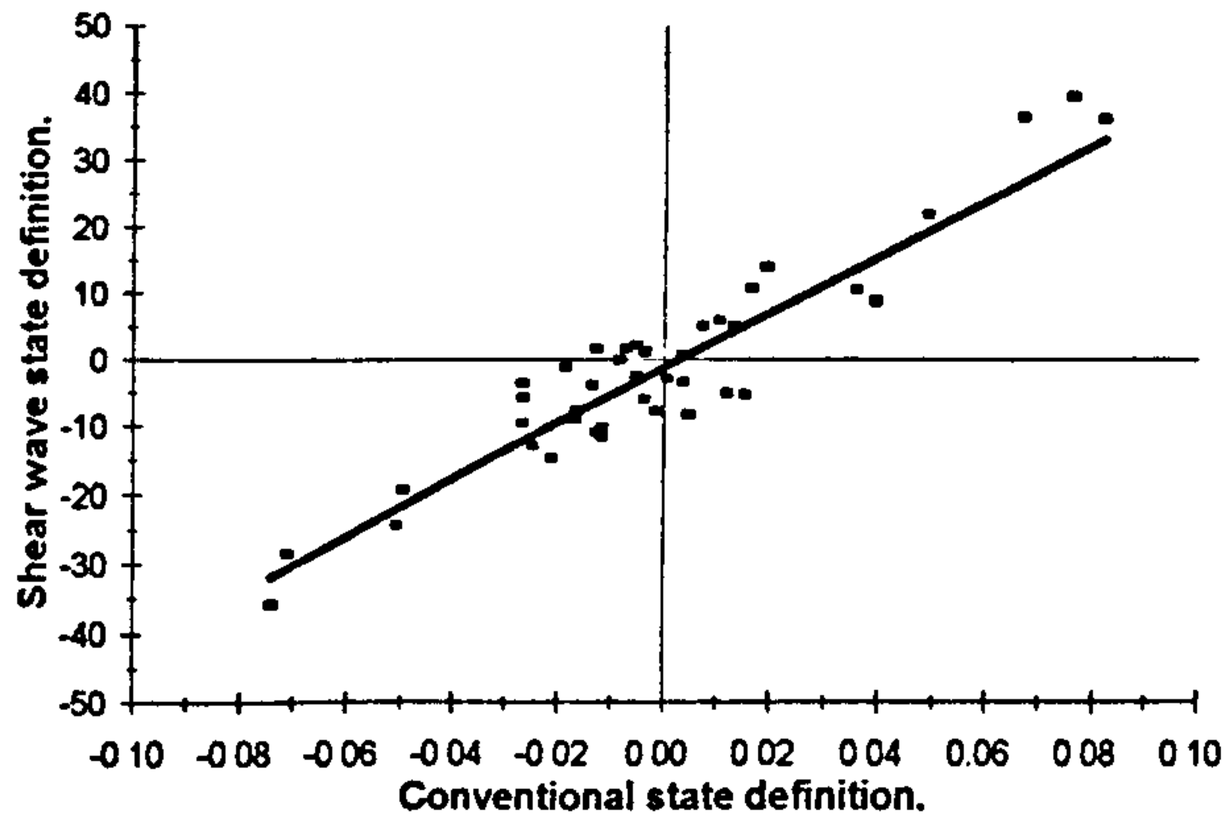

Figure 7.7. Comparison between different indices of sand consolidation state; Newborough 0% sand.

Note:- Figures 7.7 a & b illustrate data derived from triaxial testing only. Figure 7.7 c illustrates data from all tests on Newborough 0% sand.

a.

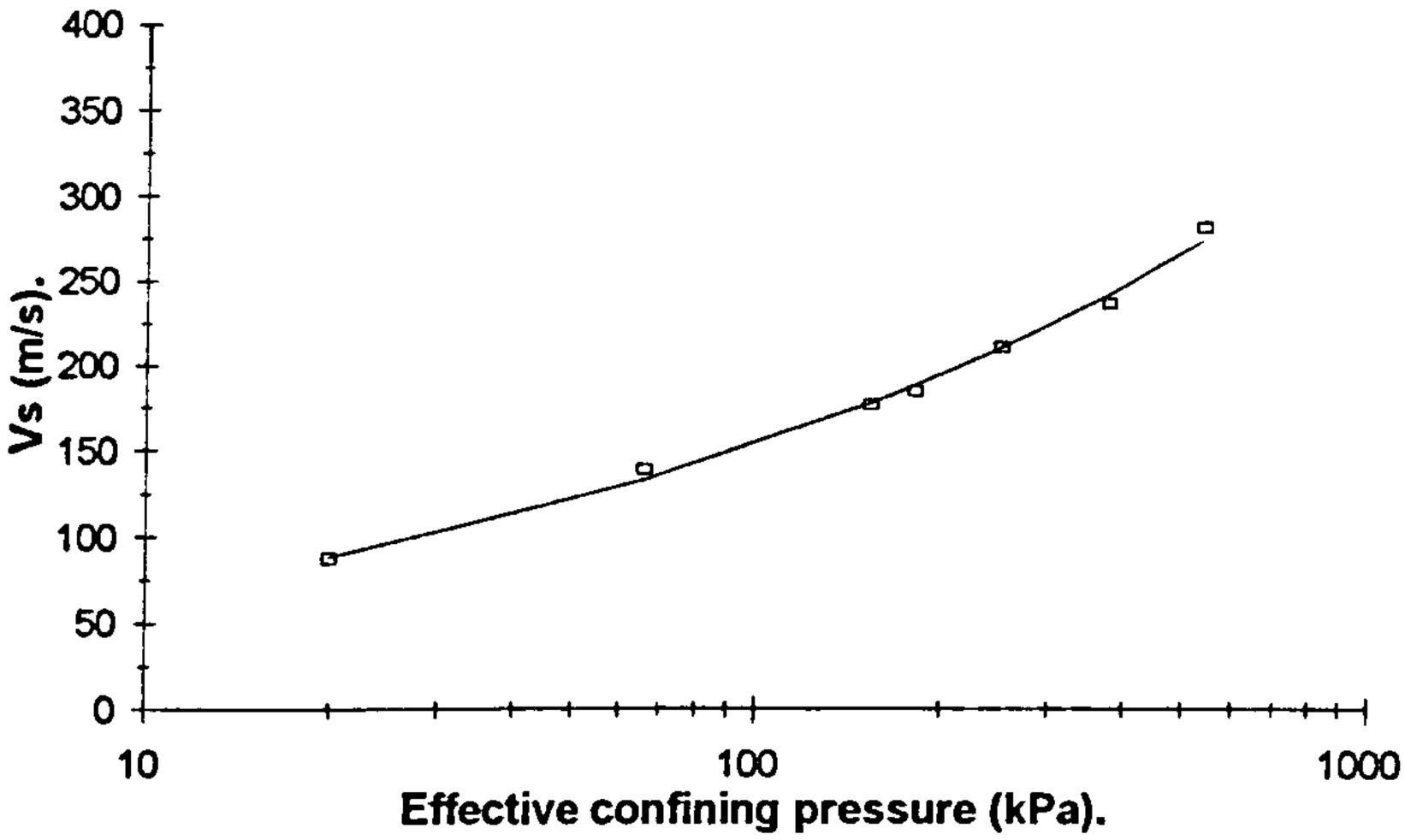

b.

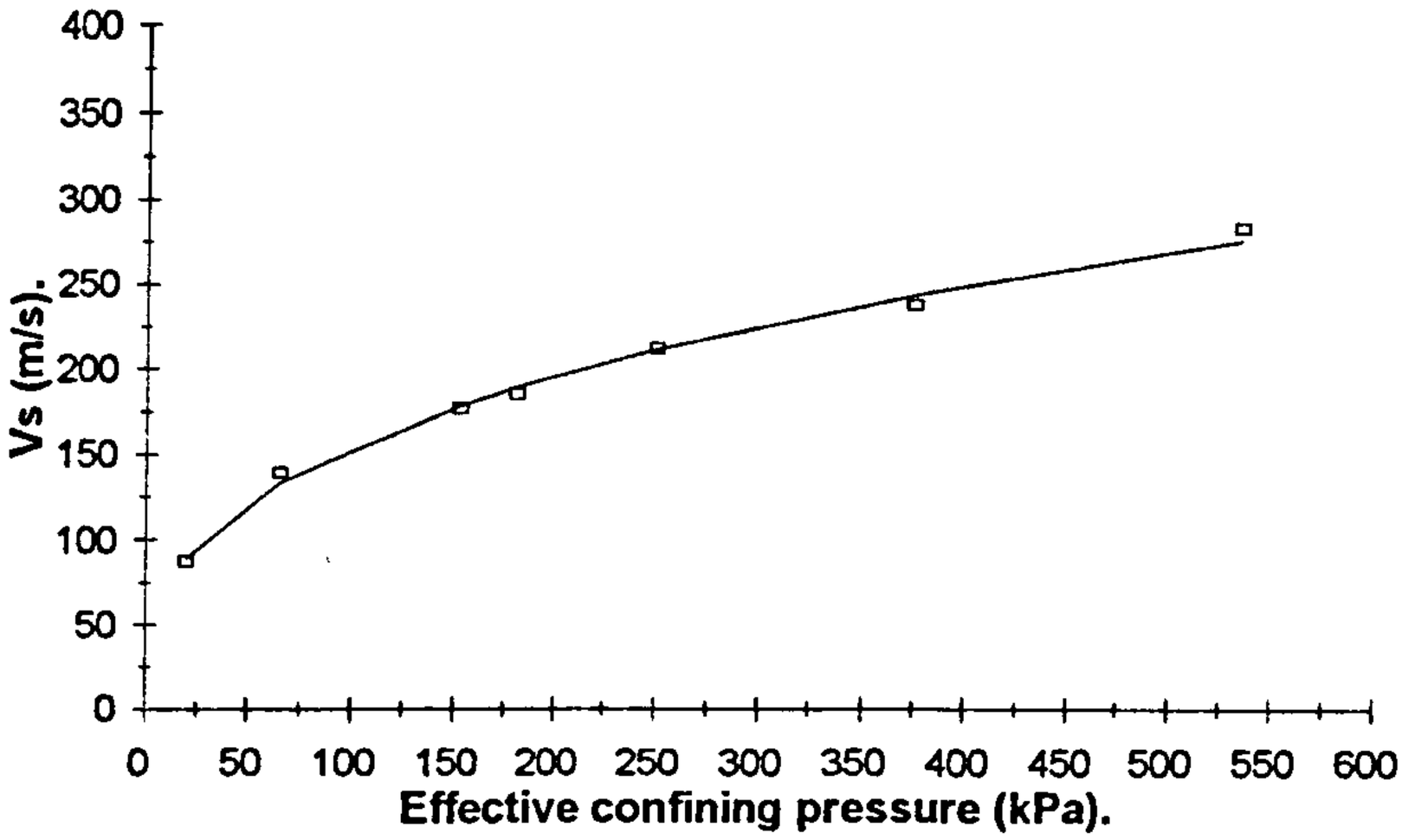

Figure 7.8. a & b. 'Critical shear wave velocity' line, defined for Newborough 5% sand.

c.

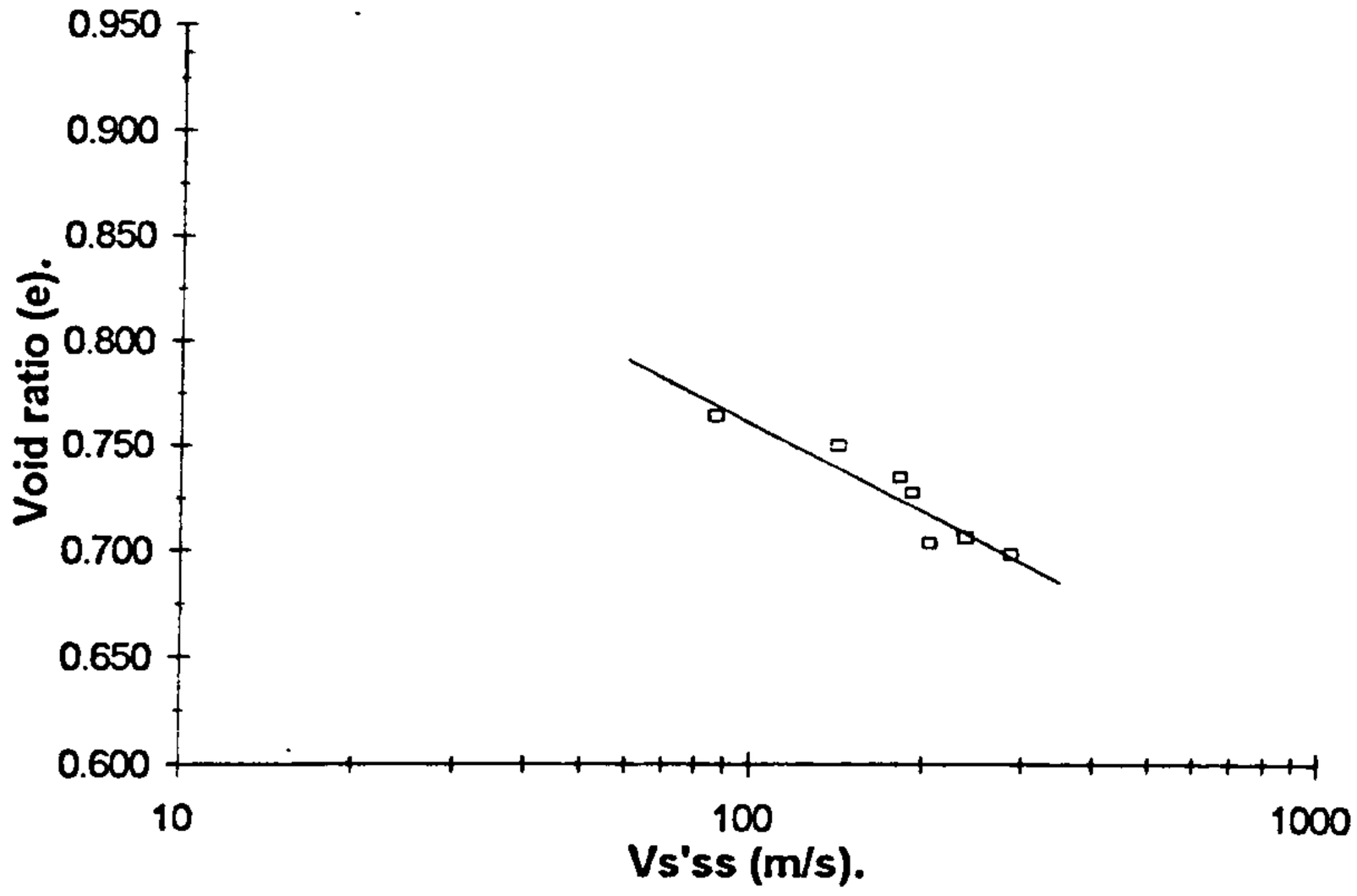

d.

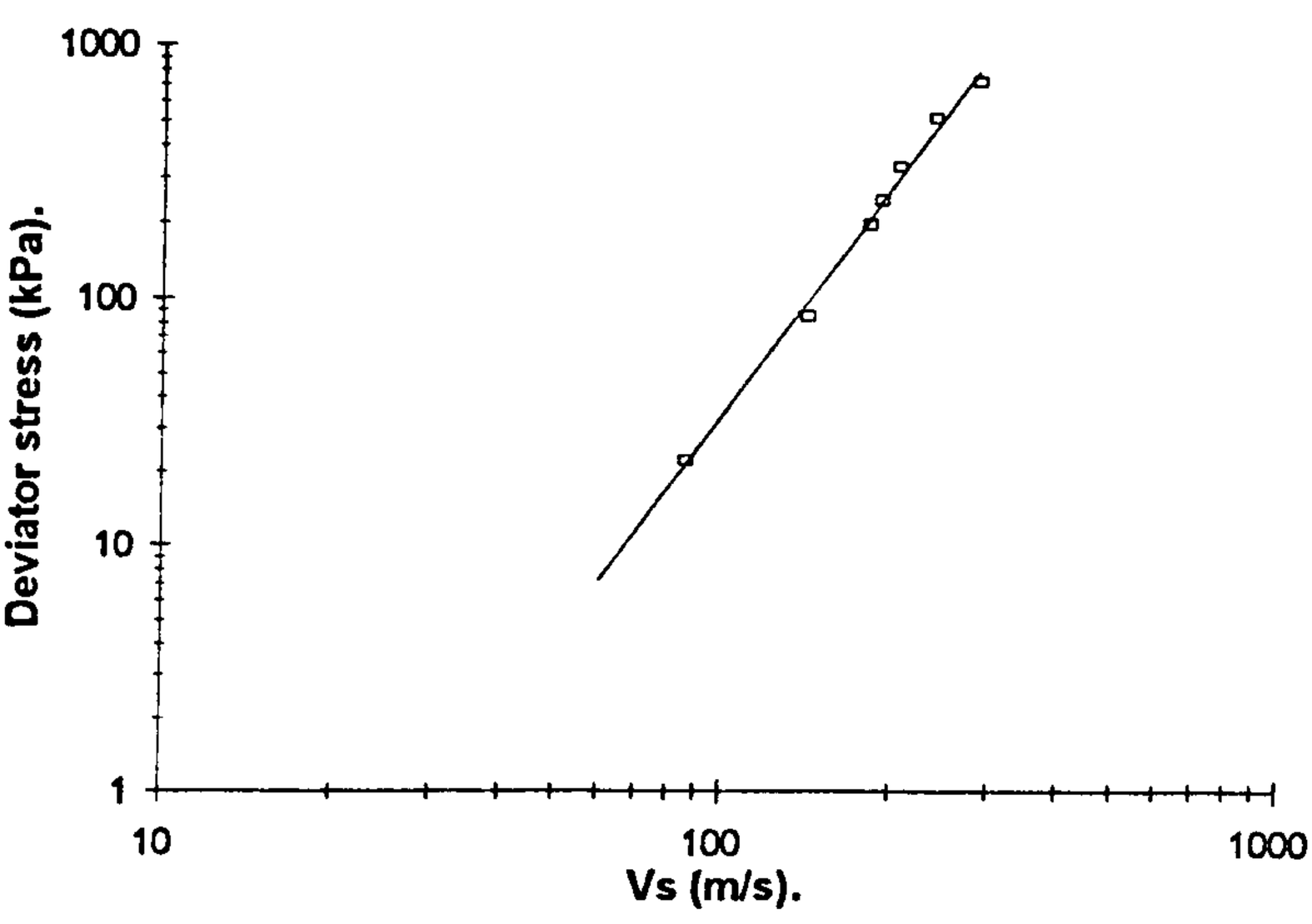

Figure 7.8. c & d. Relationship between void ratio, deviator stress and shear wave velocity, at steady state; Newborough 5% sand.

a.

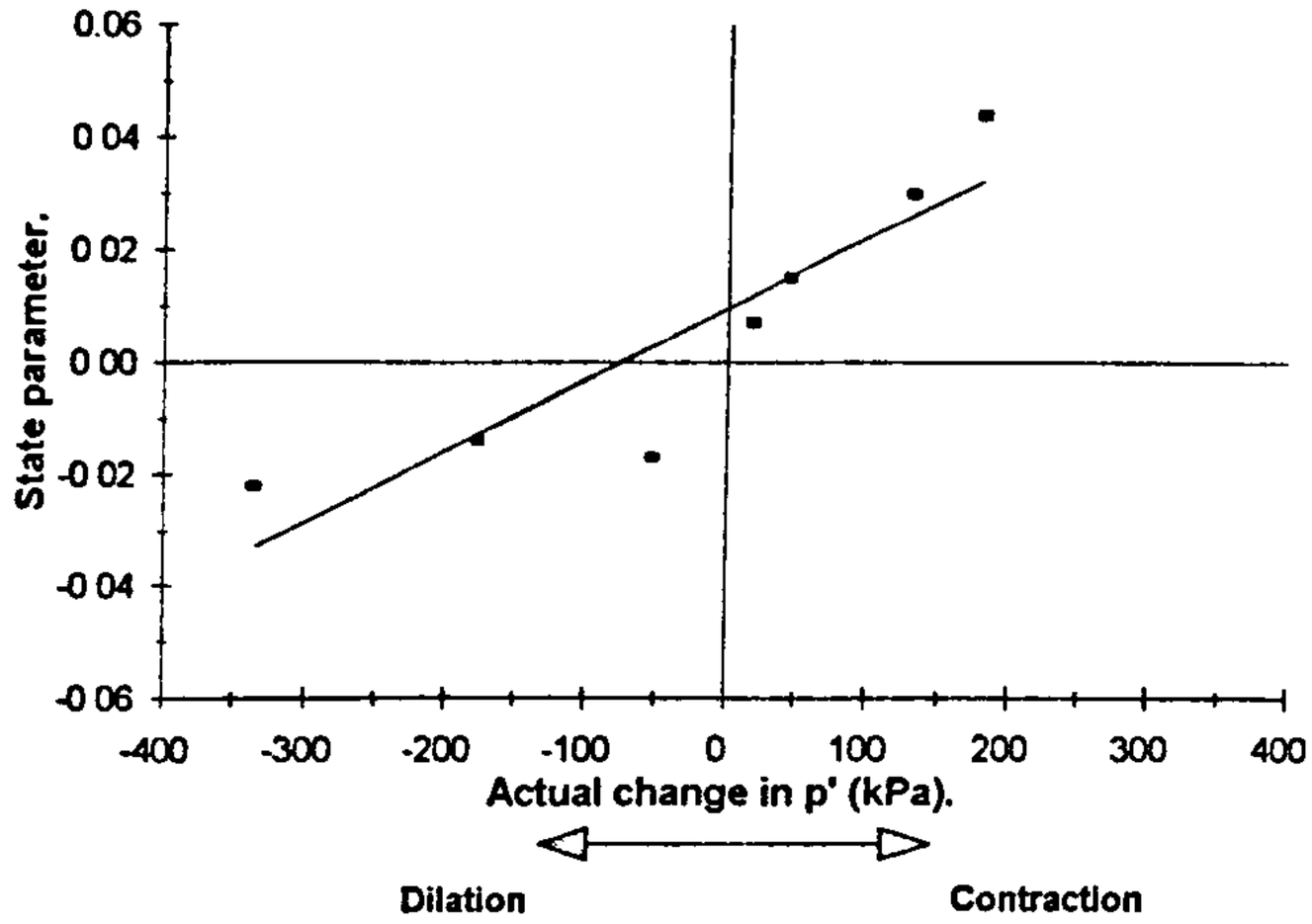

b.

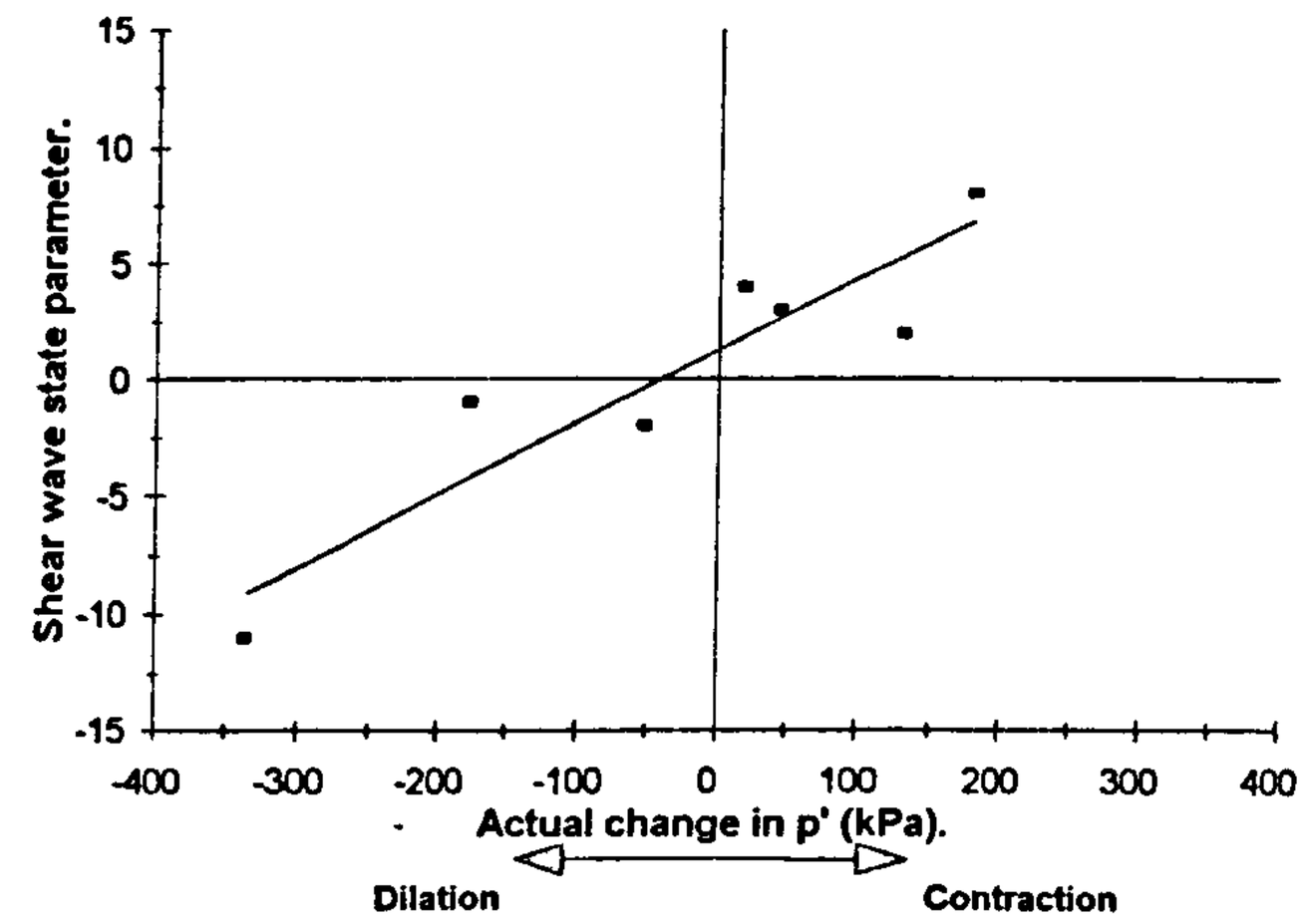

c.

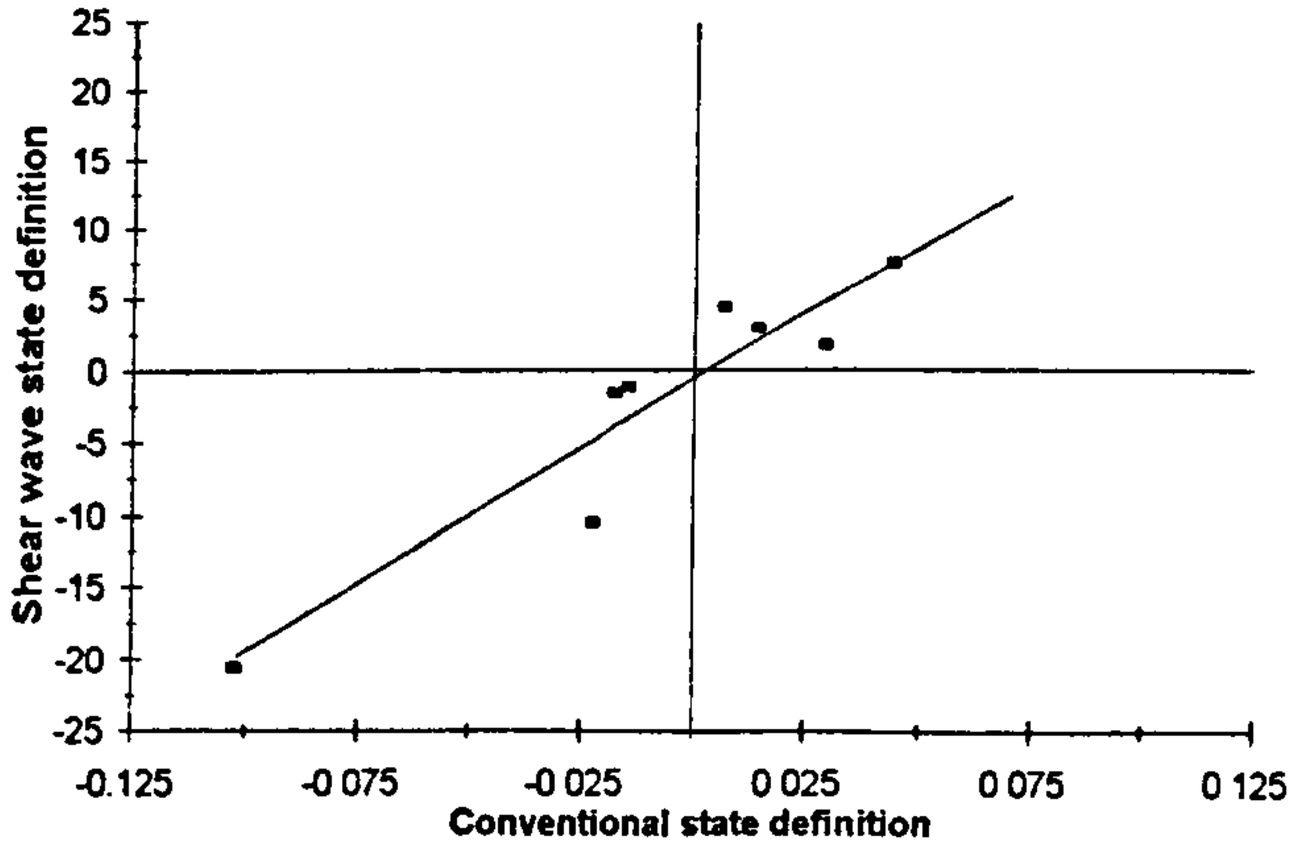

Figure 7.9. Comparison between different indeces of sand consolidation state; Newborough 5% sand.

a.

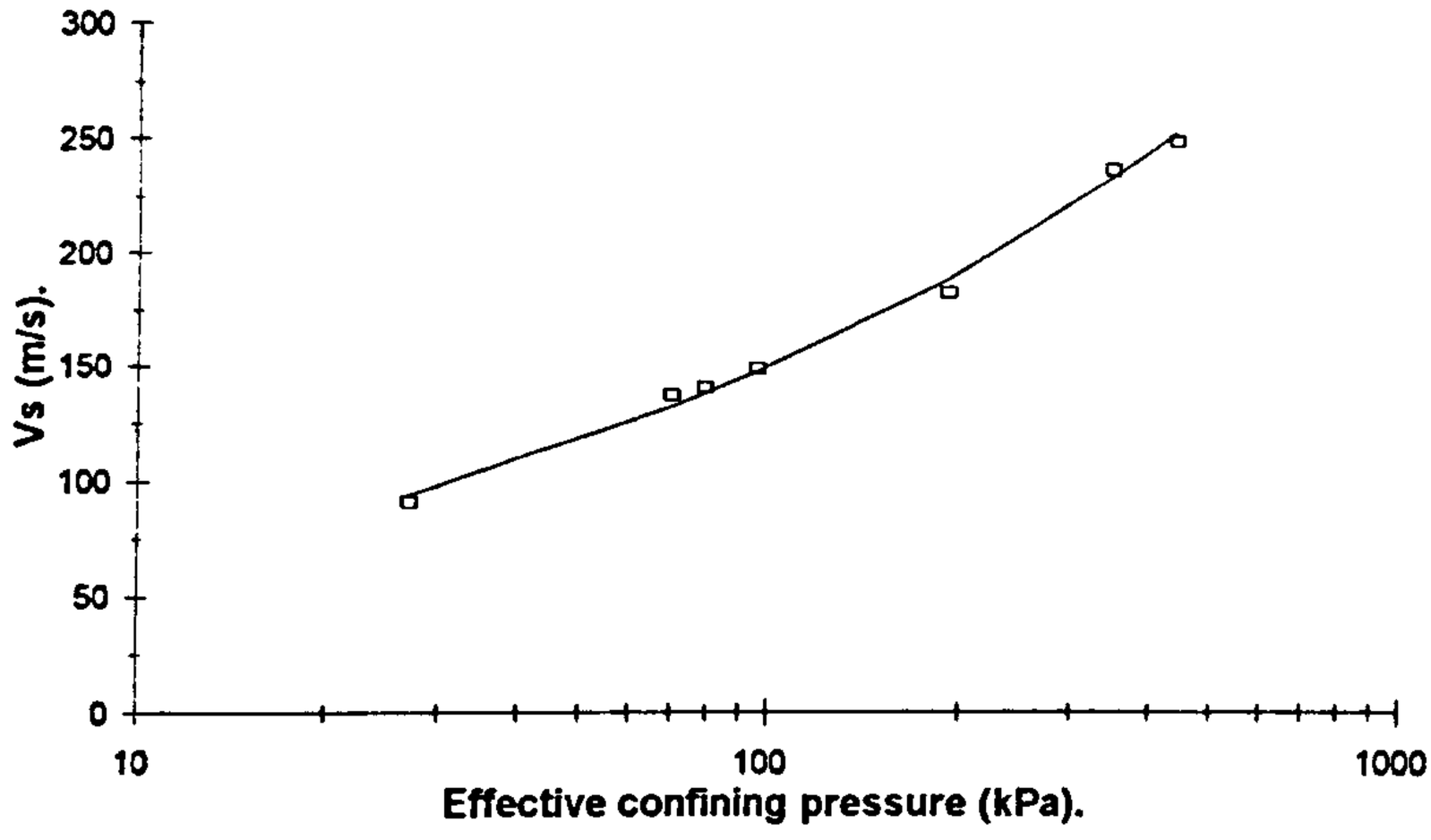

b.

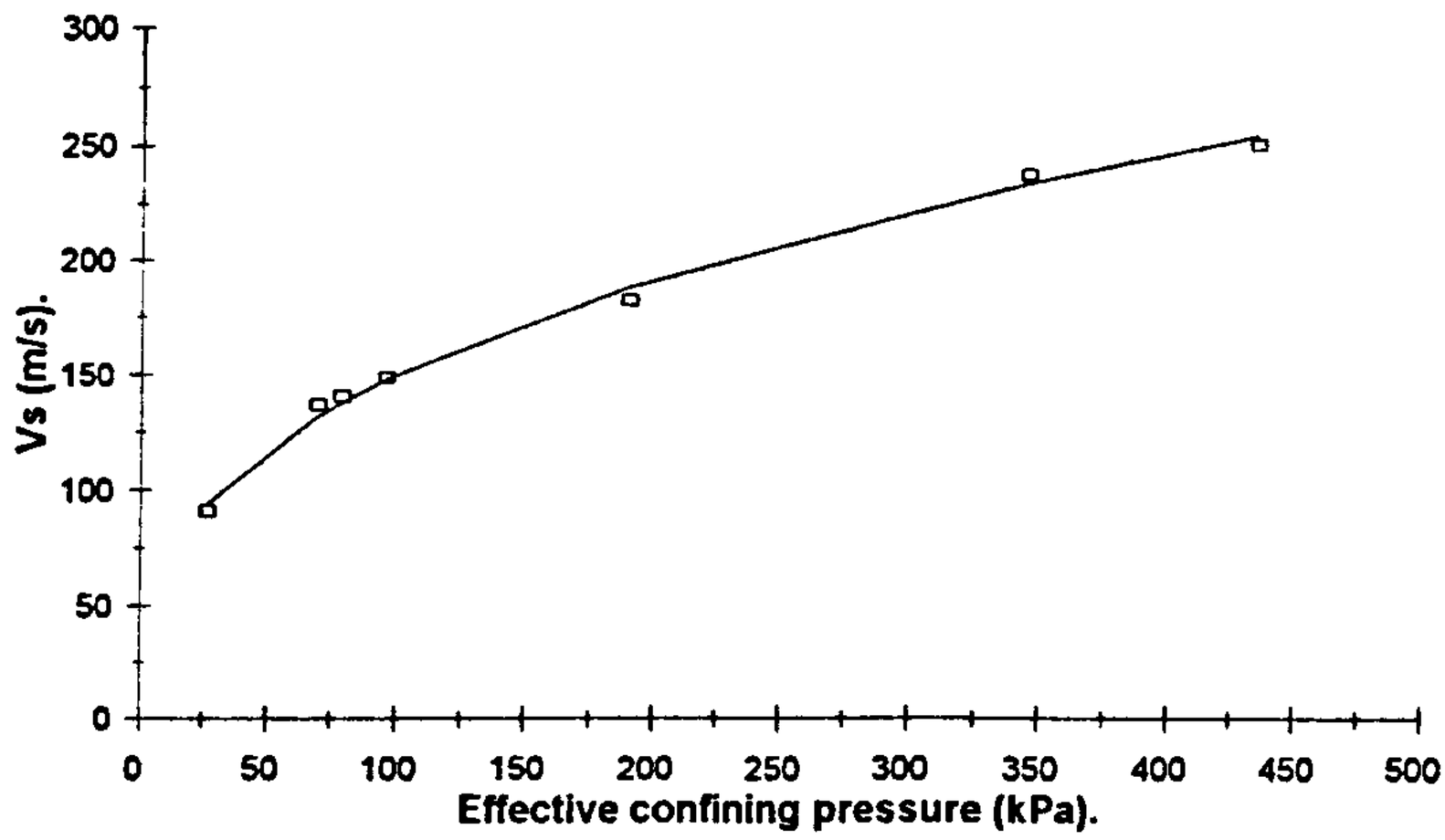

Figure 7.10. a & b. 'Critical shear wave velocity' line, defined for Newborough 10% sand.

c.

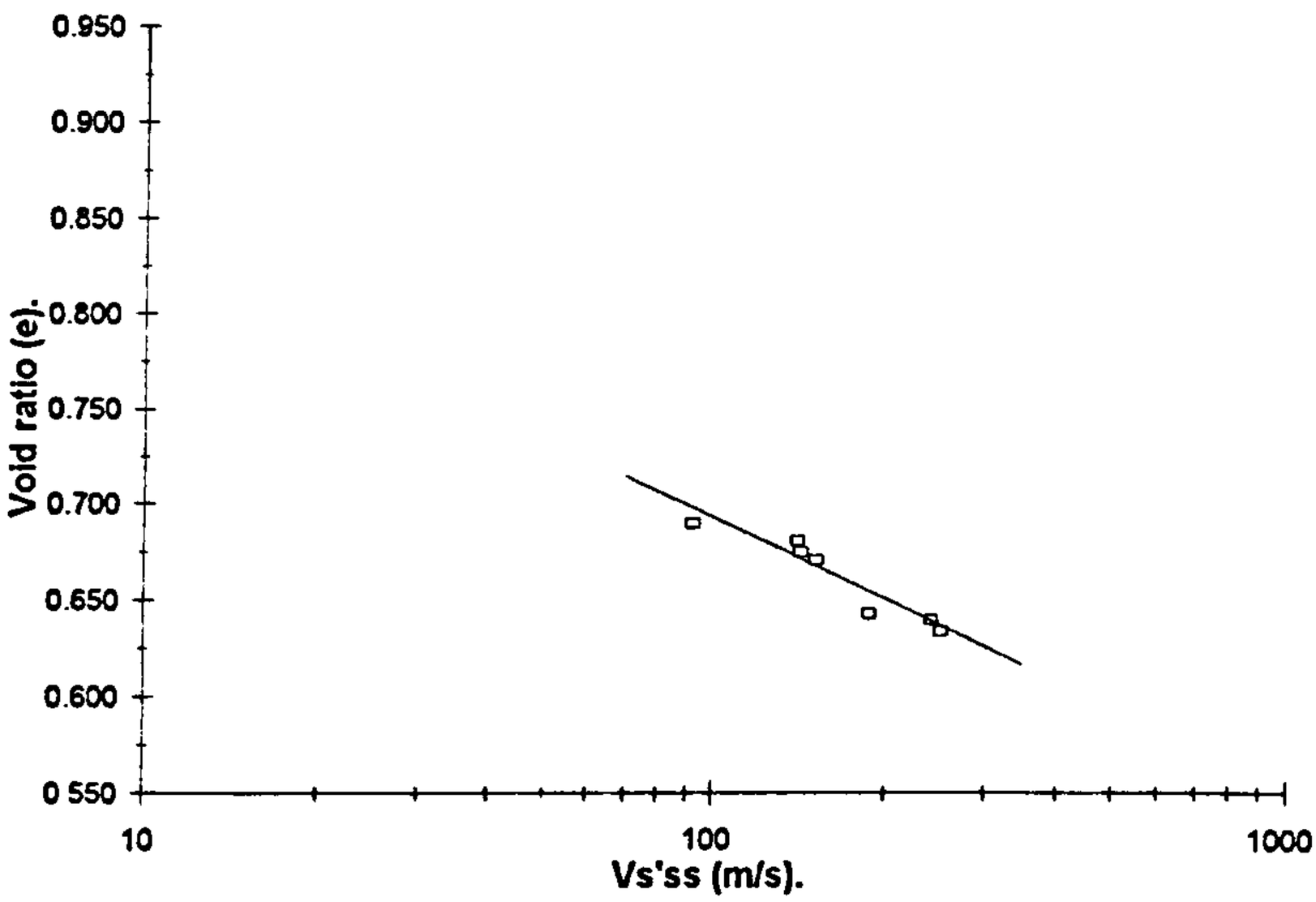

d.

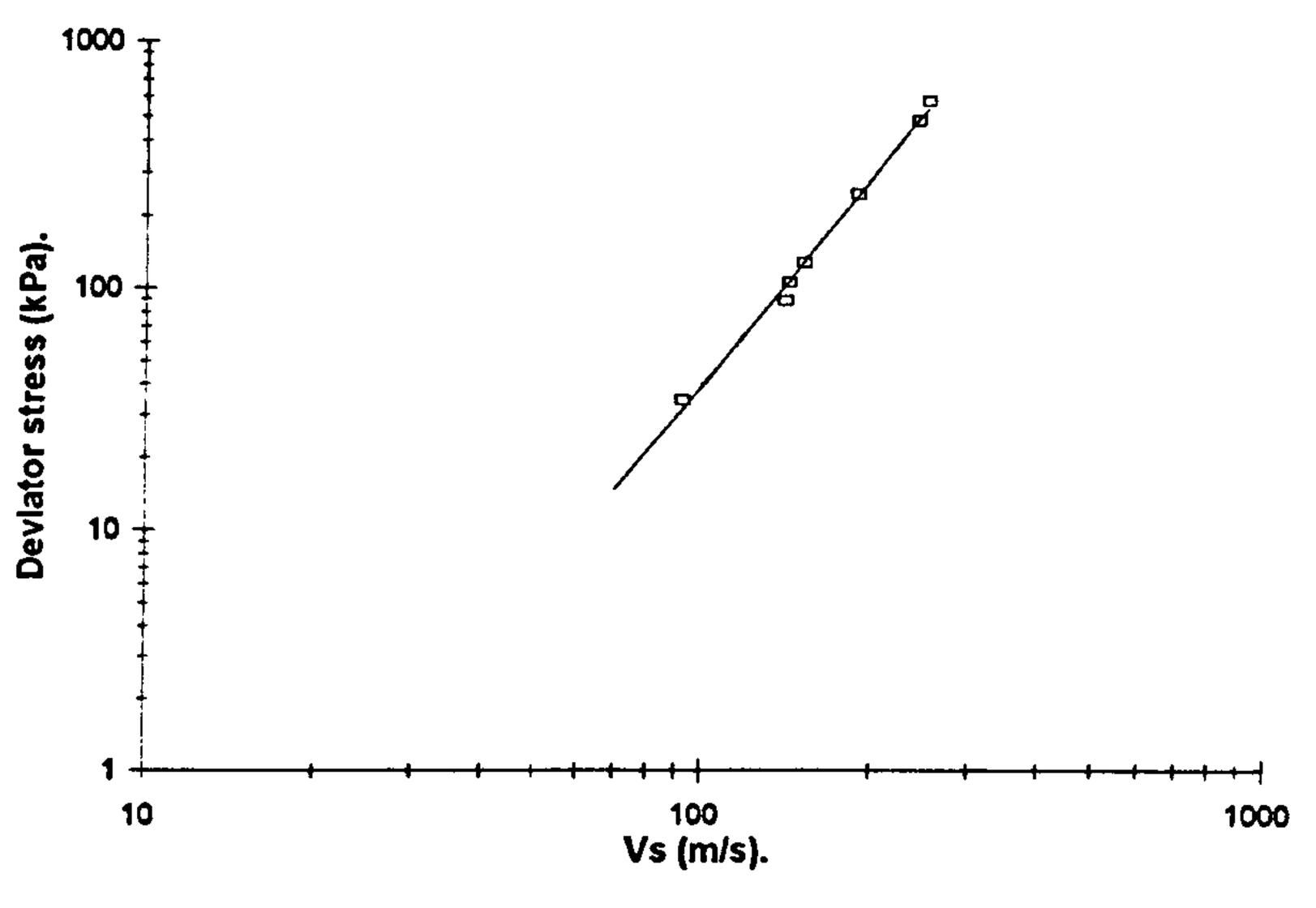

Figure 7.10. c & d. Relationship between void ratio, deviator stress and shear wave velocity, at steady state; Newborough 10% sand.

a.

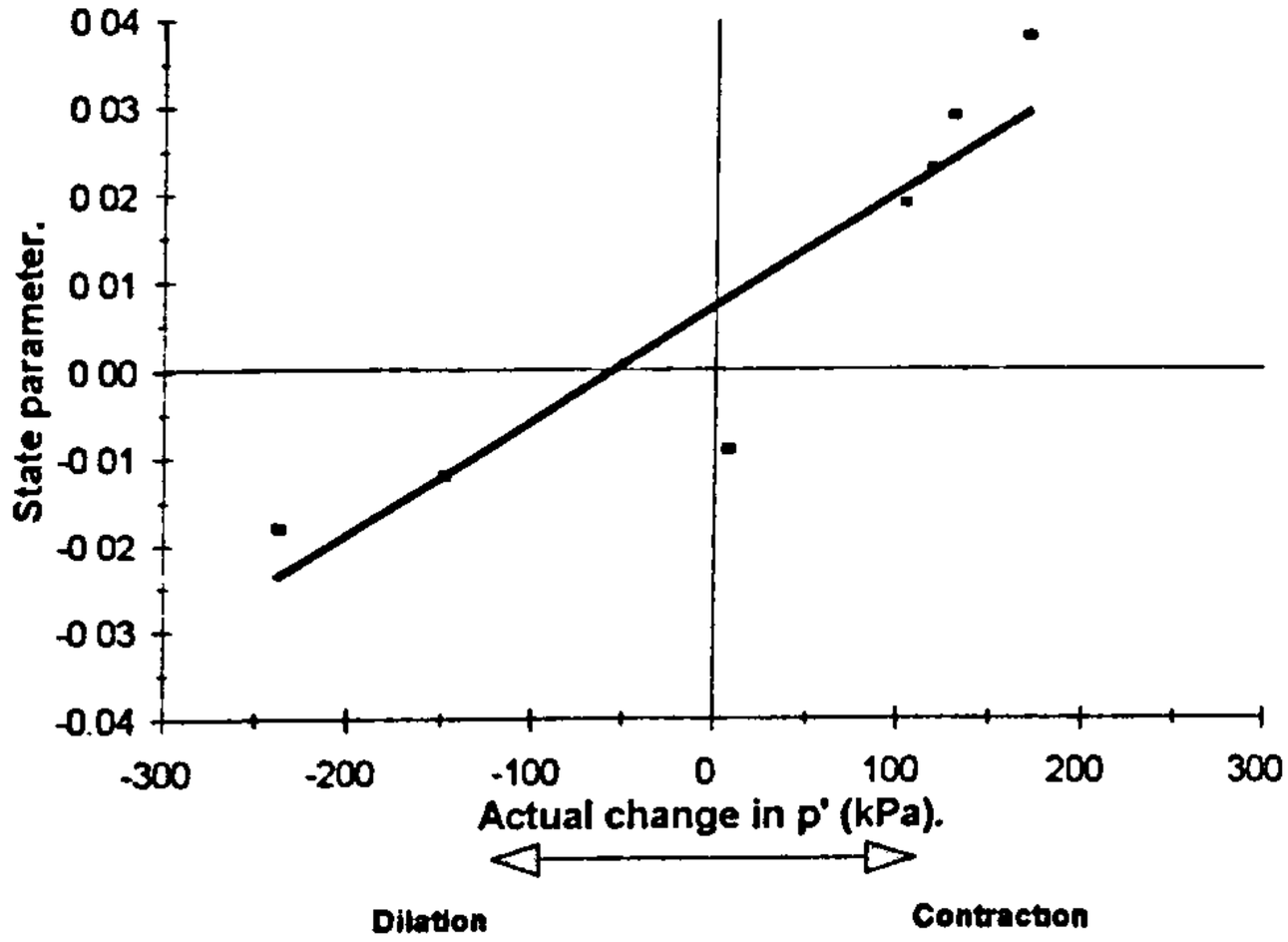

b.

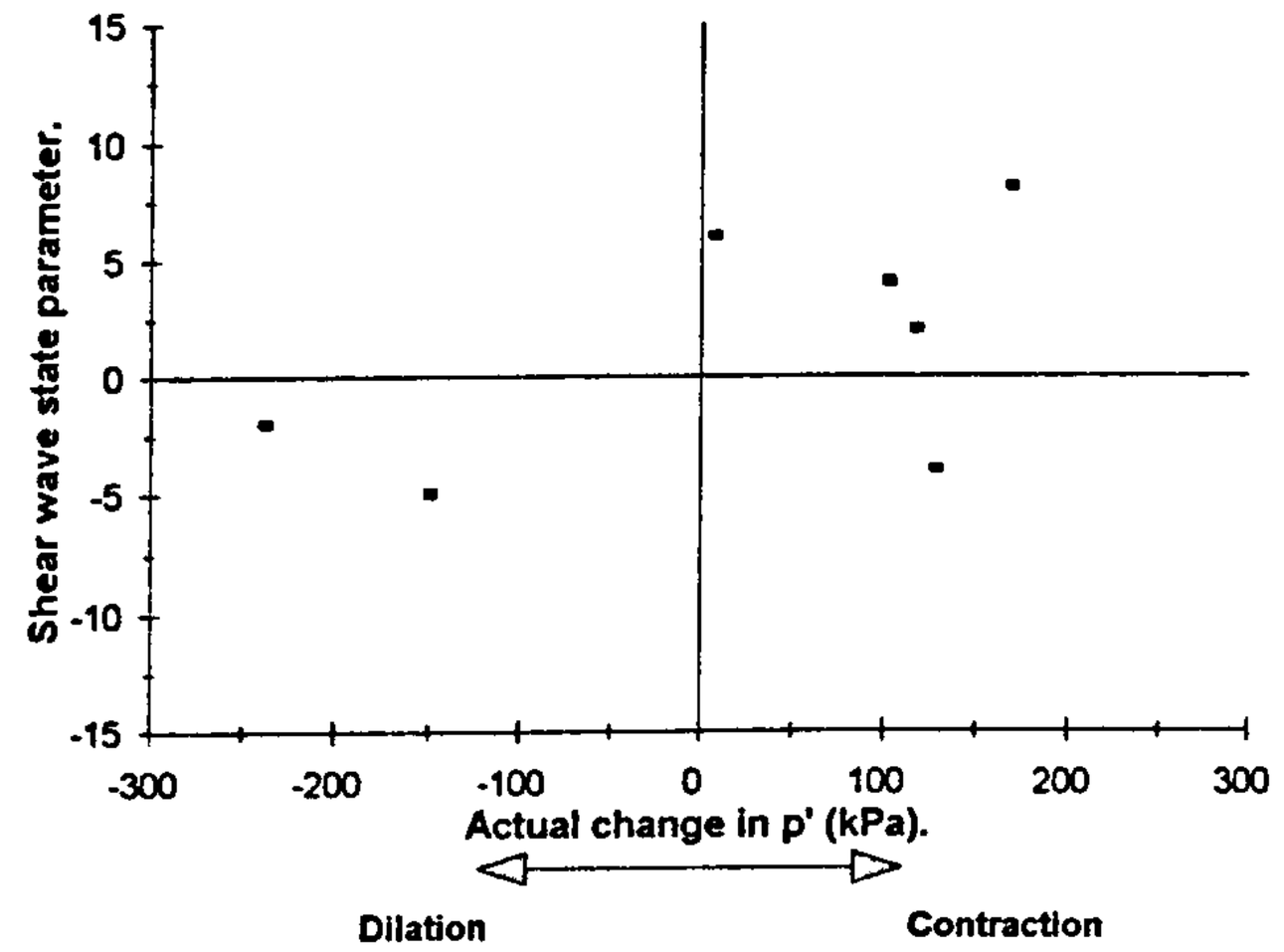

C.

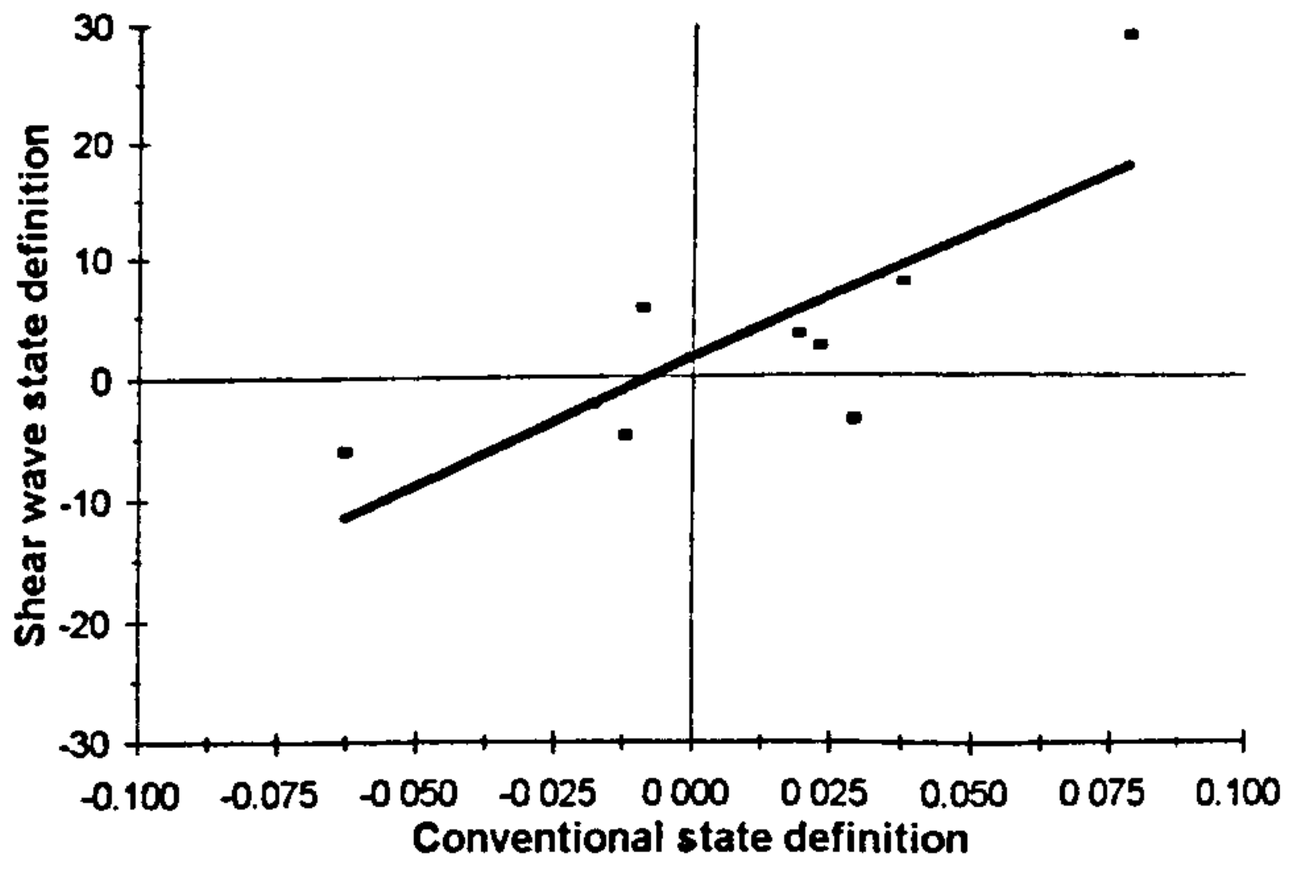

Figure 7.11. Comparison between different indices of sand consolidation state; Newborough 10% sand.

a.

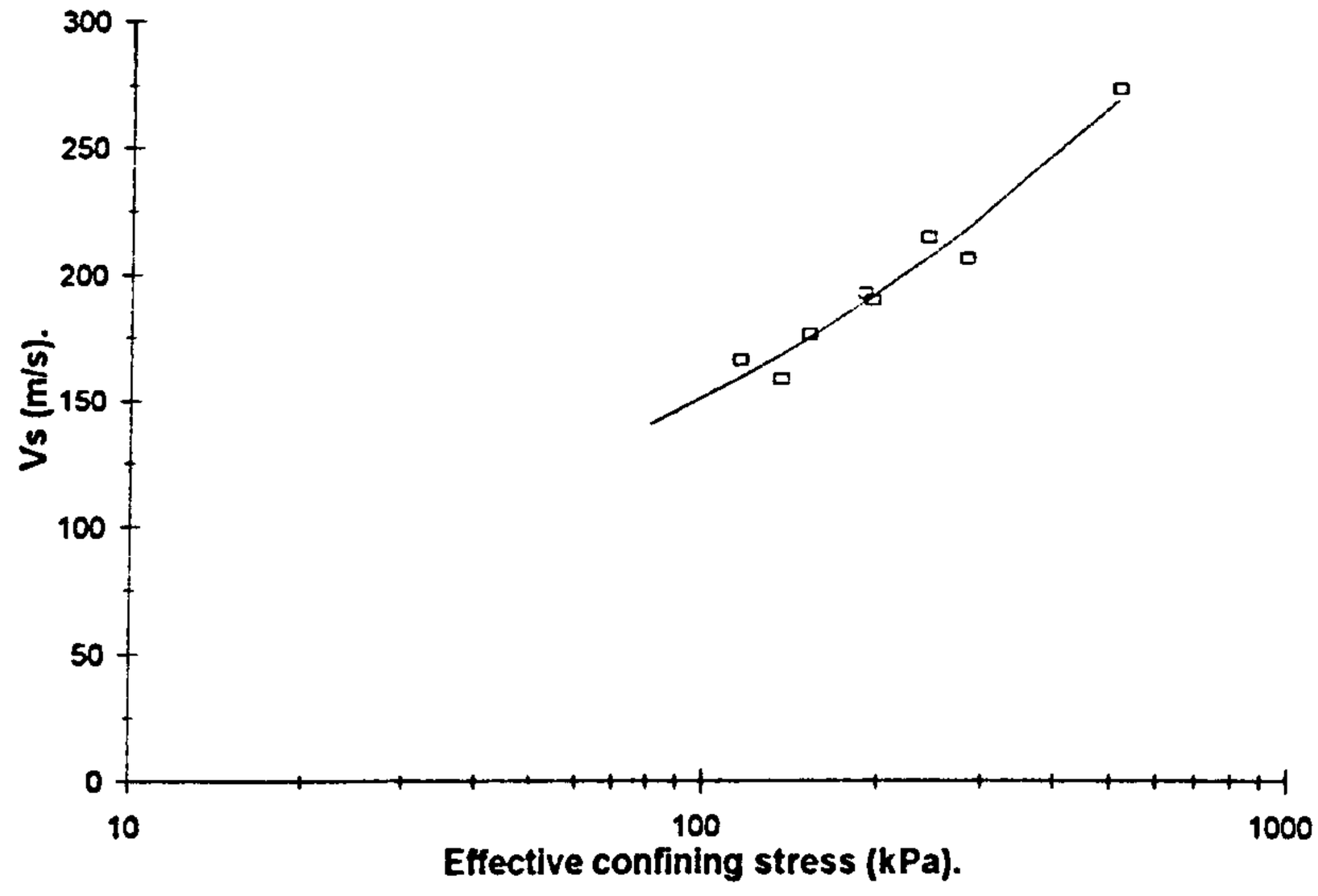

b.

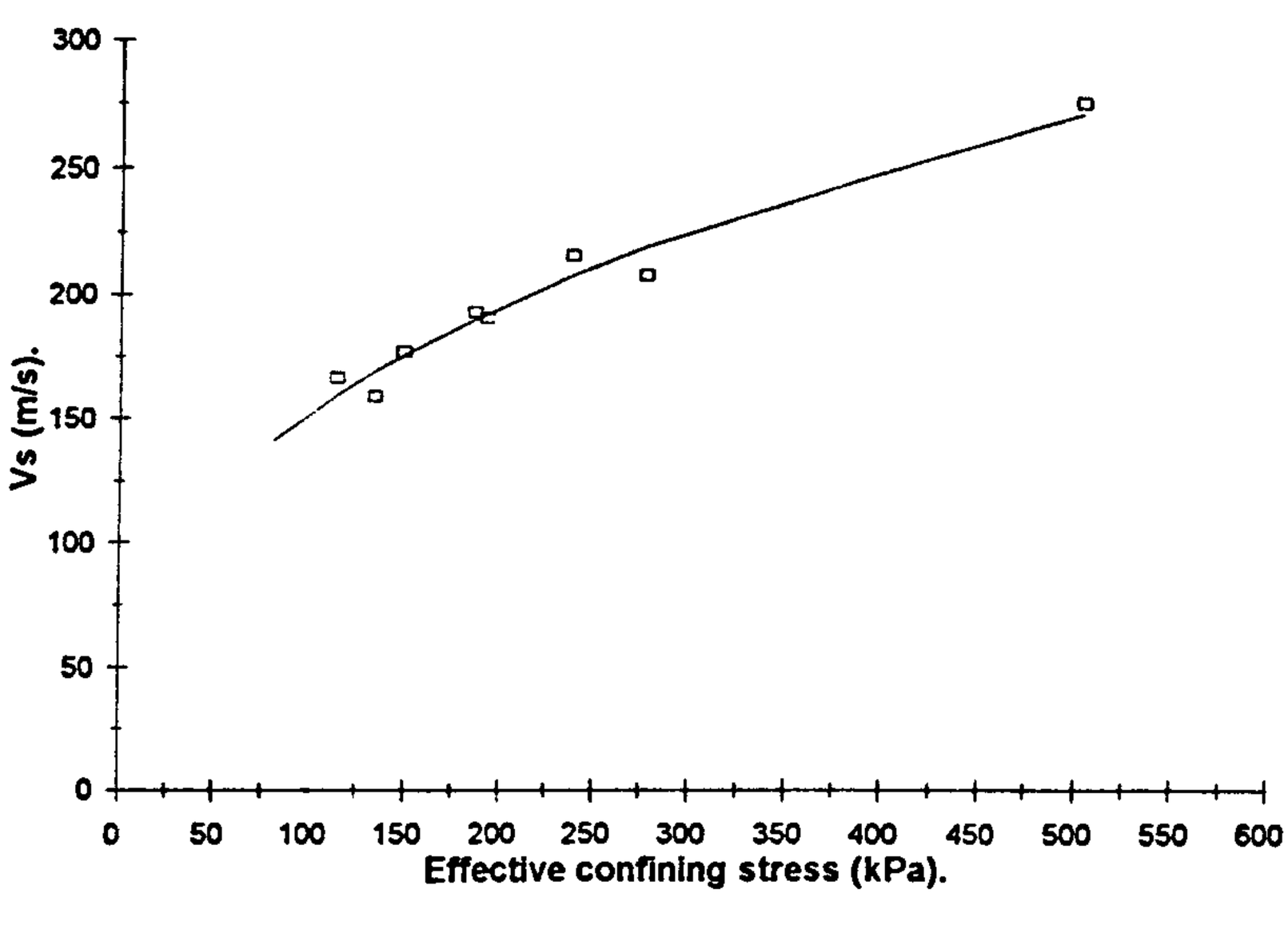

Figure 7.12. a & b. 'Critical shear wave velocity line', defined for the Fraser Delta sand.

c.

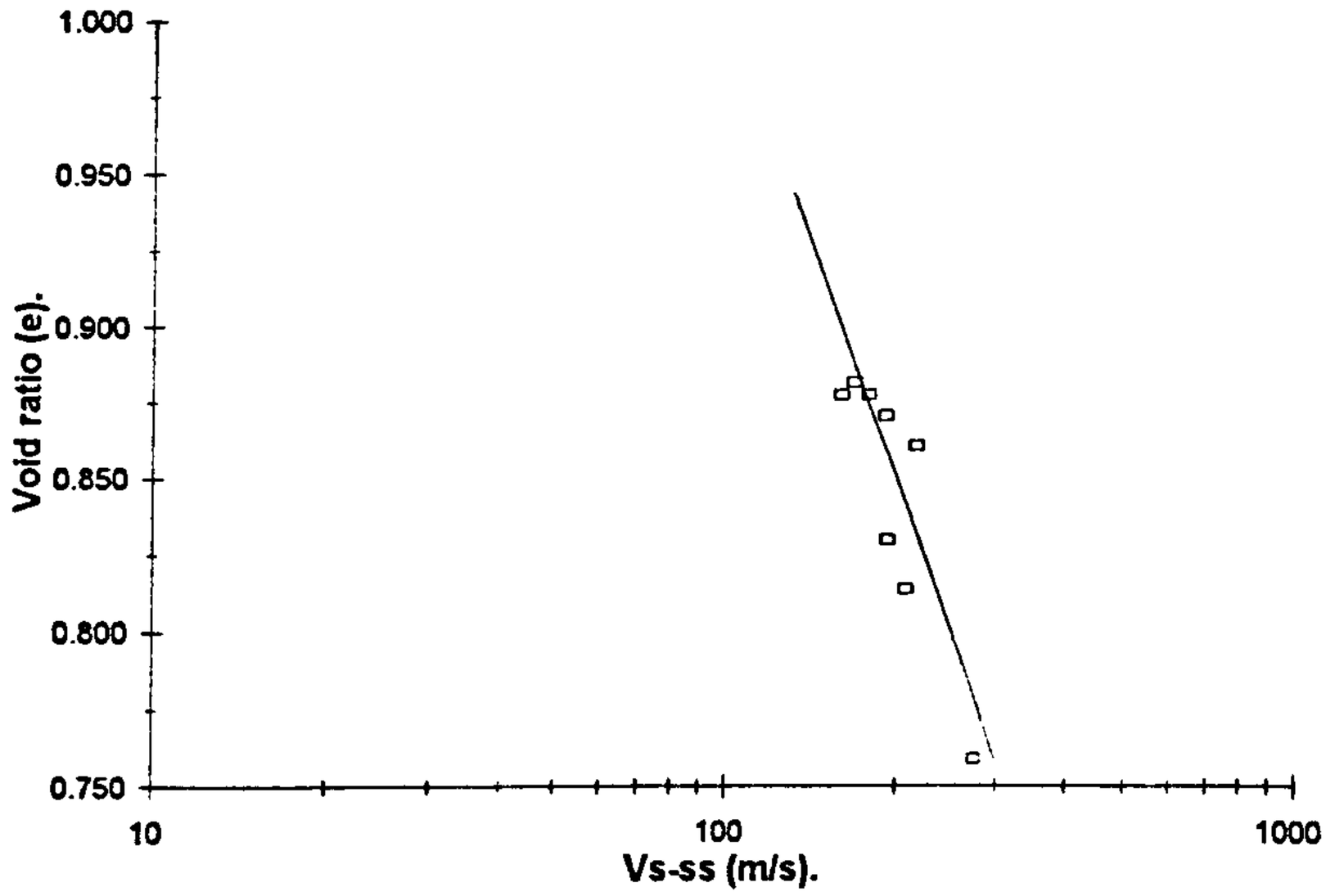

d.

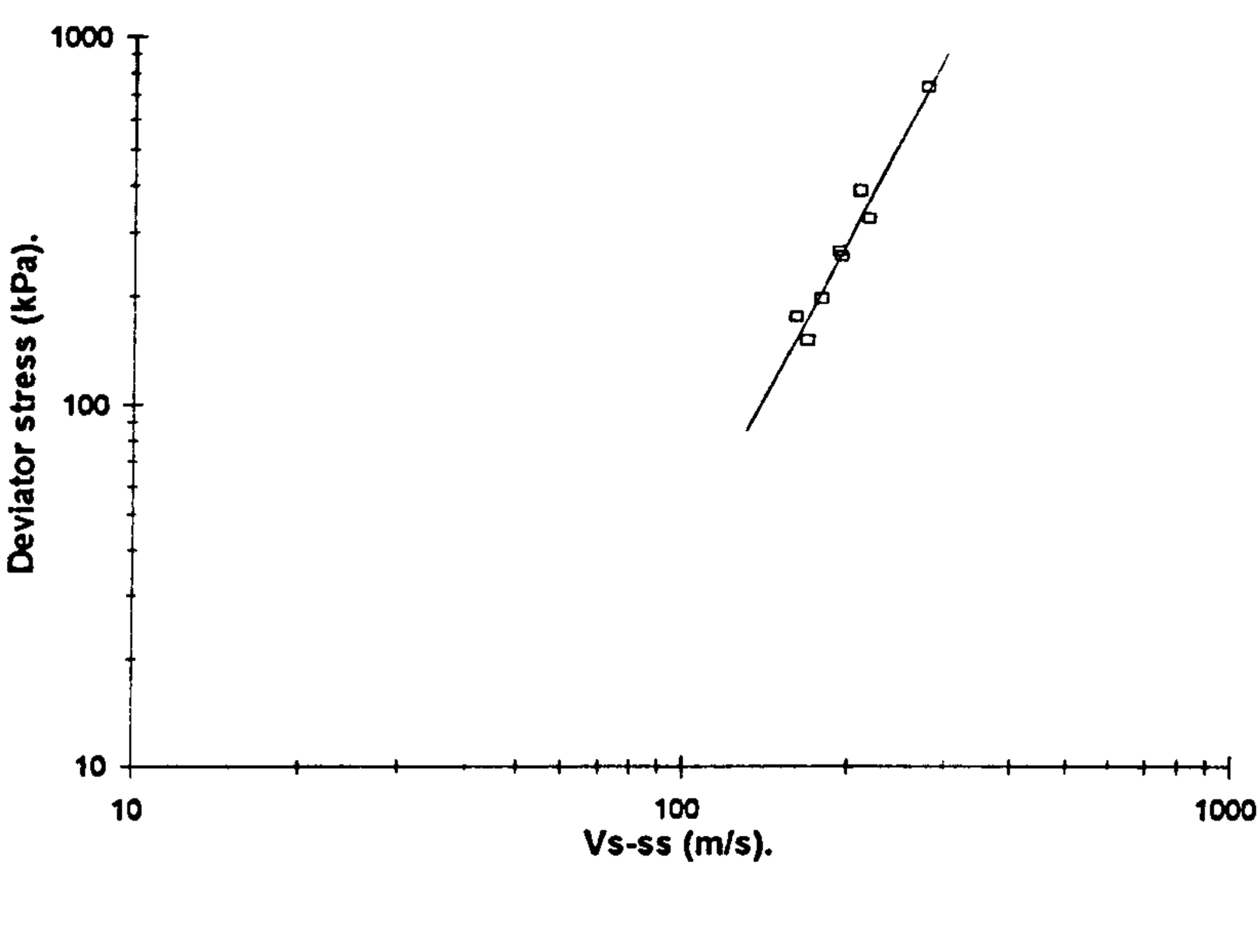

Figure 7.12. c & d. Relationship between void ratio, deviator stress and shear wave velocity, at steady state; Fraser Delta sand.

a.

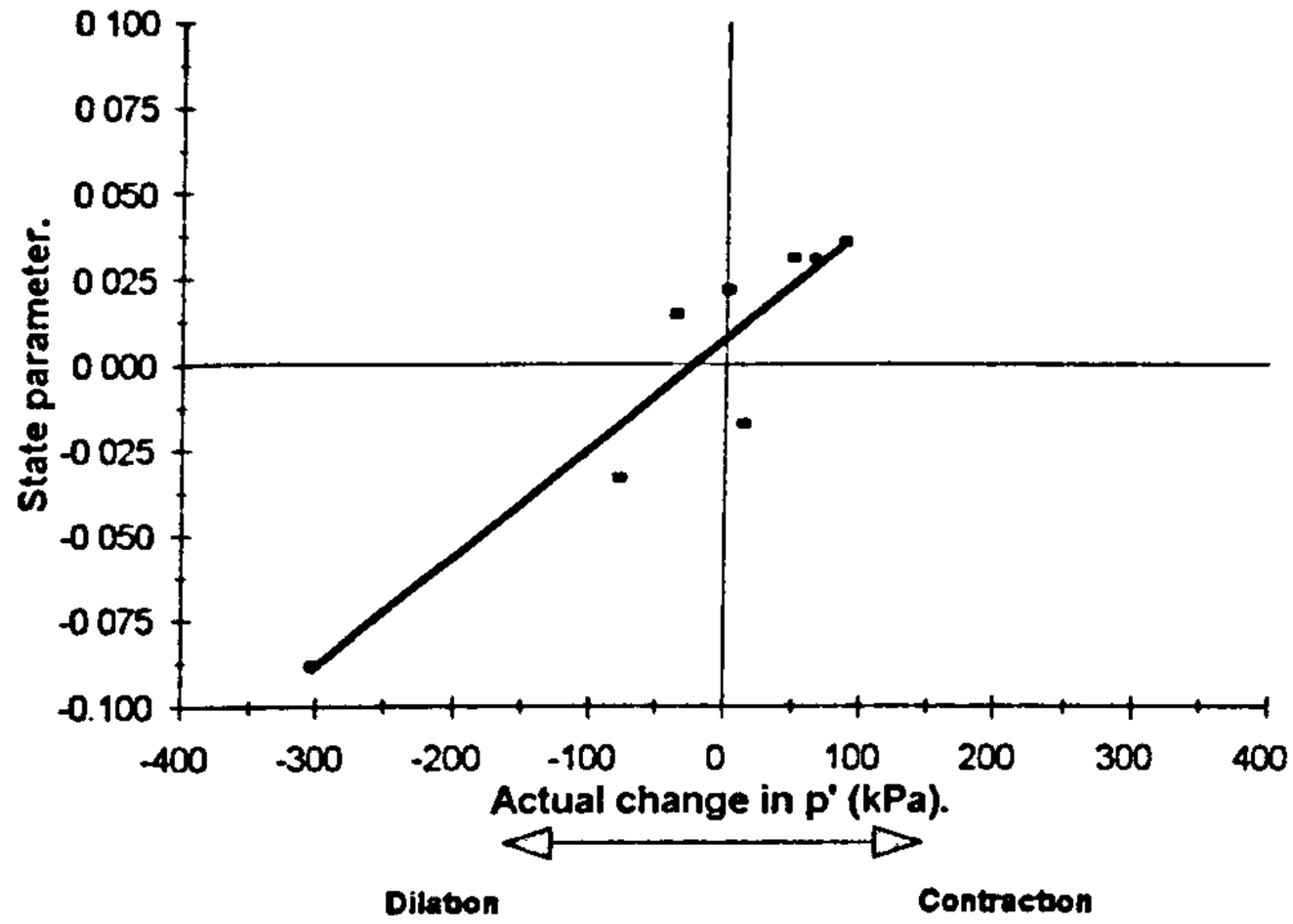

b.

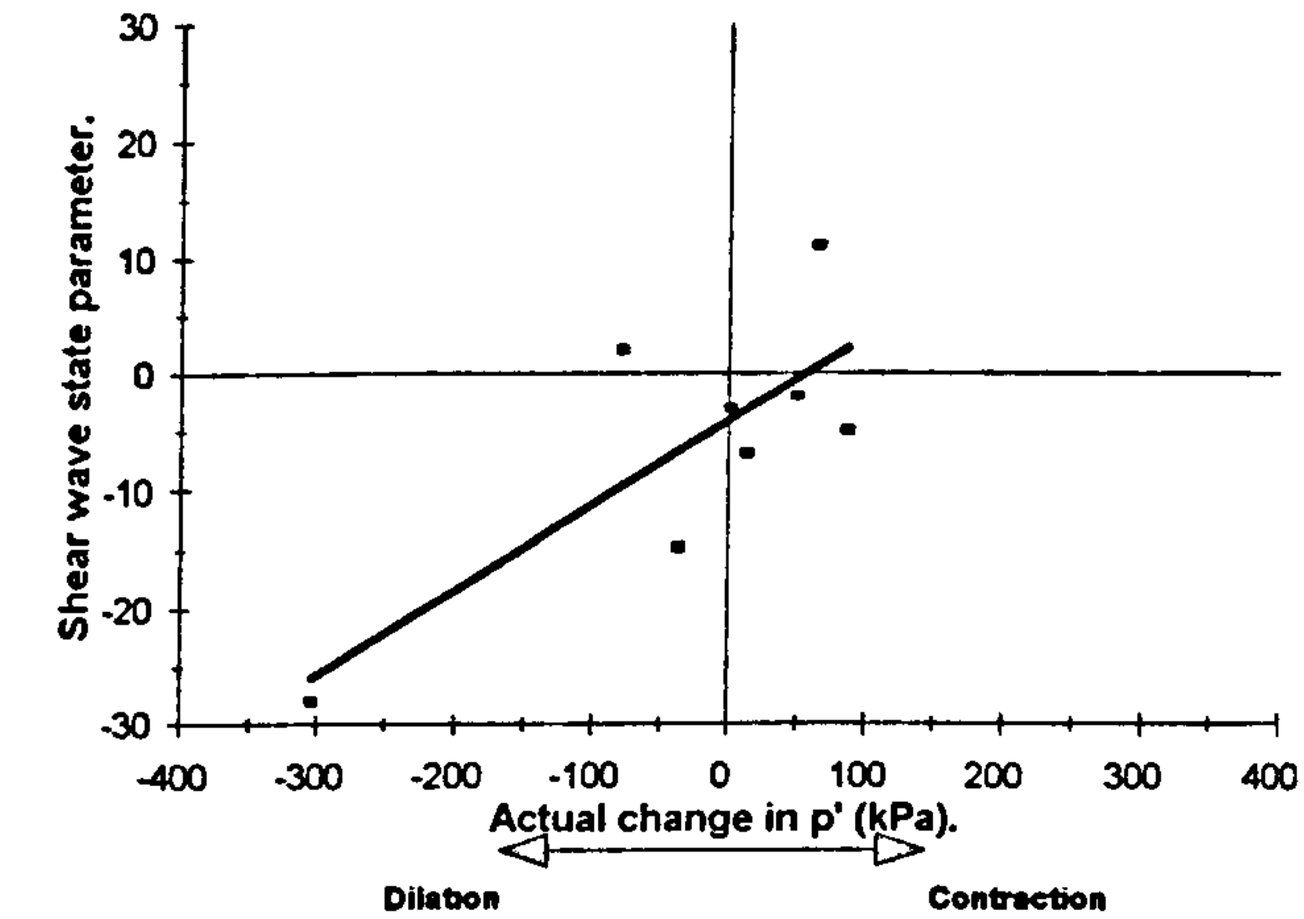

C.

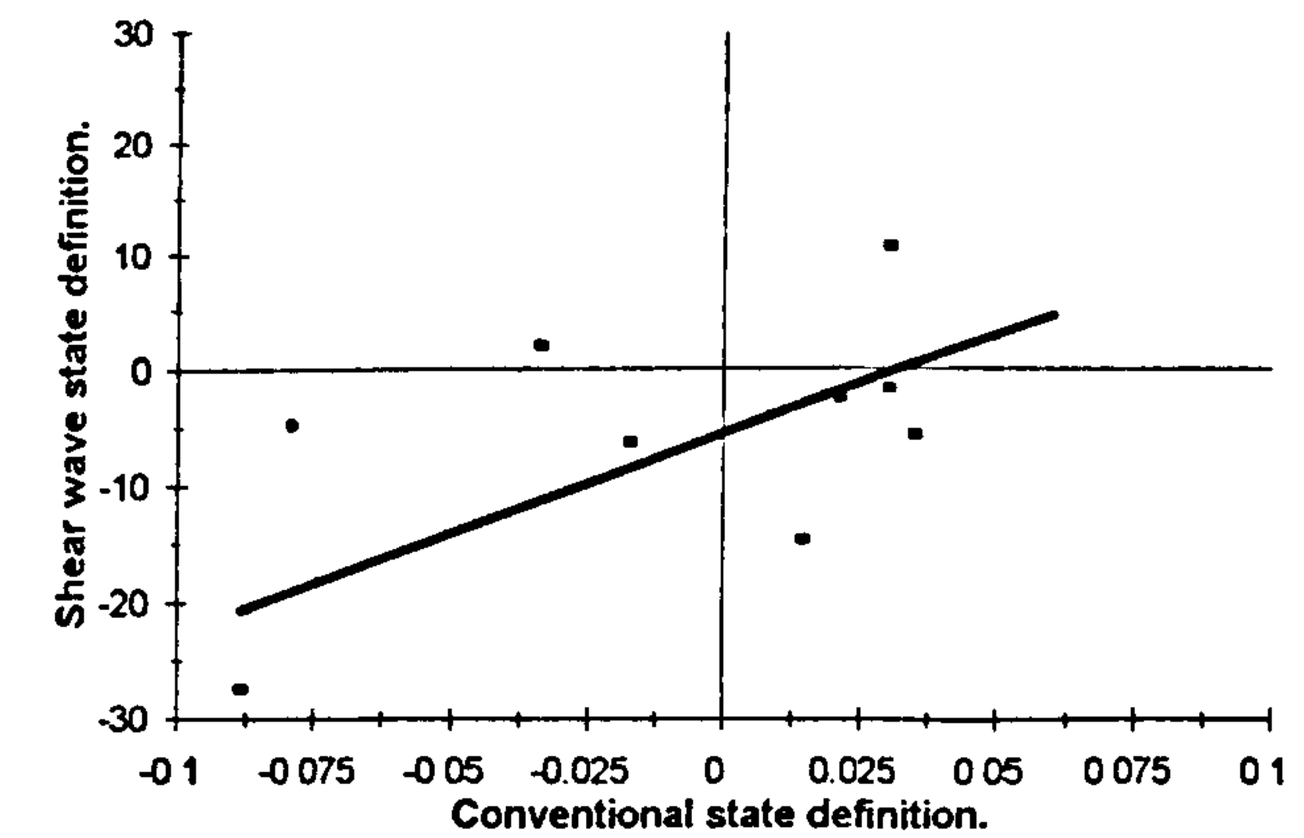

Figure 7.13. Comparison between different indices of sand consolidation state; Fraser Delta sand.

CHAPTER 8.

CASE STUDY: THE FRASER RIVER DELTA, BRITISH COLUMBIA. OVERVIEW AND FIELD RESULTS.

8.1. Introduction.

The Fraser Delta is the largest delta in western Canada, located in the extreme south-western corner of British Columbia, immediately south of the rapidly growing Vancouver Metropolitan area (Figure 8.1). The delta is an important agricultural area and much of its flat land is currently being urbanised by satellite communities, including Richmond, Tswawwassen and Ladner. Much of this land has either been reclaimed from the sea, or is very low lying, resulting in a heavy reliance on dykes to protect the area from inundation by the sea. The Fraser River itself has been confined, trained, and is continuously dredged to maintain deep navigable channels. The delta is of huge economic importance to the region. Built near the edge of the sub-aerial delta is Vancouver International Airport, currently undergoing a $350 million expansion involving large ground stabilisation works (Mosher and Barrie, 1995). Constructed out over the tidal flats of Robert's Bank, in the southern part of the delta, is the busiest passenger ferry terminal in the world, carrying approximately 51 million passengers a year (Mosher and Barrie, 1995). Adjacent to the ferry terminal lies Tswawwassen Coal Port, Canada's largest coal exporting terminal, which is currently undergoing a major expansion to enable handling of grain and container traffic, involving the biggest ground stabilisation effort ever undertaken in Canada (Mosher and Barrie, 1995). Crossing the Strait of Georgia, between the delta and Vancouver Island, are numerous power and communications cables; Vancouver Island has little or no power generating capacity of its own and is almost completely reliant on the power transferred through these submarine cables.

8.2. Setting.

The perimeter of the delta can be divided geographically into two parts, the southern and western portions, separated by Point Roberts Peninsula, a slightly elevated former island underlain by Pleistocene sediments. Gently sloping tidal flats extend up to 9km

from the dyked edge of the delta to the sub-tidal foreslope. The southern foreslope is quite poorly defined, sloping gently into about 30m of water. In contrast, the western slope of the delta dips at an average of 1.5° toward the semi-enclosed marine basin of the Strait of Georgia, terminating in some 300m of water approximately 5 to 10km seaward of the sub-aerial tidal flats.

8.2.1. Fluvial regime.

The Fraser River, which supplies sediment to the delta, drains an area of over 234,000km^2 and travels approximately 1400km from its headwaters in the Mount Robson Provincial Park, to its terminus in the Strait of Georgia; this represents the largest fluvial system on the Pacific coast of Canada. Runoff in the basin is dominated by the spring snowmelt, occurring between the beginning of May and the end of June; the mean annual flow measured at Hope, B.C., is 8,770 m^3/sec, ranging between a low of 5,130 m^3/sec and a peak of around 15,200 m^3/sec (Stewart and Tassone, 1989). Based upon 18 years of sediment data collected at Mission, 84km upstream of the river mouth, the mean annual sediment load is 17.3 million tonnes/year, of which approximately 35% is sand (particles > 0.063mm), 50% is silt (0.004-0.063mm) and 15% is clay (<0.004) (Environment Canada, 1988). During the period of high river discharge in the early summer, more than half the sediment discharged is sand, while throughout the rest of the year the river carries mainly silt and clay, with lower sediment concentrations corresponding to lower levels of river discharge.

8.2.2. Oceanographic regime.

Tides crossing the western delta-front are of mixed semi-diurnal type, with the range of spring tides averaging approximately 5m. This tidal range decreases both landward and, in the river channels, with increasing river discharge (Clague *et al.* 1983). Over the delta slope the north-westerly flood tide is somewhat stronger and of longer duration than the ebb tide; tidal currents run roughly parallel to the bathymetric contours, with a current turbulence maximum occurring at the break in slope. A well defined salt-water wedge intrudes into the distributary channels, which during winter can reach as far as 7 miles upstream, but during the summer freshet barely reaches as far as the inner edge of the tidal flats (Kostaschuk *et al.* 1989).

8.2.3. Tectonic regime.

Vancouver and the Fraser Lowlands are located within a belt of high seismicity that encompasses much of the western coast of British Columbia and the adjoining Washington State (Milne *et al.* 1978) (Figure 8.2). This high level of seismicity is associated with the relative motions of the America, Juan de Fuca, Explorer and Pacific Plates. In southern British Columbia the Juan de Fuca Plate is thought to be subducting beneath the Pacific Plate, while the Explorer Plate, a small crustal fragment to the north, may be underplating parts of Vancouver Island and the adjacent mainland (Clague *et al.* 1992). Reports of seismic activity in British Columbia date back to 1872 when an earthquake of estimated Richter magnitude 7 - 7.5 shook most of the settled Pacific North - West. The most damaging earthquake to hit south-western British Columbia in living memory occurred in 1946 on central Vancouver Island. This particular earthquake had a Richter magnitude of 7.2 and caused liquefaction in coastal areas up to 100km from its epicentre, with the runways at Vancouver Airport reportedly 'rolling like waves' (Rogers, 1980). Recent research suggests that there may be the possibility of a 'megathrust earthquake', with a magnitude of up to 9.2, with the epicentre located in the Cascadia subduction zone (Rogers, 1992), although this is still a matter of some debate (Campbell and Rotzein, 1992).

8.3. Modern sedimentary environments.

The Fraser Delta is dominantly composed of thick sequences of loose sands and silty sands underlain by non-lithified glacial/non-glacial material. These Quaternary deposits lie on a Tertiary bedrock characterised by high relief, with depths to bedrock ranging from 100m up to 1000m (Harris *et al.* 1995). Six sedimentary environments can be distinguished on the modern delta: the foreslope, the sub-aqueous platform, tidal flats, floodplain, peat bog and river channels (Figure 8.3).

8.3.1. Foreslope.

The western foreslope dips on average at 1.5° (ranging from 1 to 23°) to intersect the floor of the Georgia Strait at about 300m. Sedimentary environments close to the active distributary mouths are characterised by high sediment influx rates, sediments consisting of fine silty sands, and by lateral and down-slope movement of material by

gravity and strong bottom currents. Locally gullies cut the foreslope, formed by mass wasting or turbidity currents which are maintained by sliding of accumulated gully bottom sediments and the flushing action of tidal currents (Matthews and Shepard, 1962). Mass movements down these gullies redistribute deposits on the delta slope and locally deform the foreslope deposits (Luternauer and Finn, 1983; McKenna *et al.* 1992).

Sedimentation further away from the distributary channels reflects the lower energy levels of the deeper water, with lower sedimentation rates and generally finer grained sediments, in particular silts and silty clays. Deeper water foreslope sediments are bedded parallel to the submarine slope, and in places consist of laminated and bedded fine sand and sandy to clayey silt (Clague *et al.* 1983).

8.3.2. Sub-aqueous platform.

The sub-aqueous platform is inclined at approximately 0.5° and lies between the foreslope and the lowest low tide level. The break in slope marking the seaward edge of the sub-aqueous platform coincides with the maximum depth of vigorous wave and current turbulence (Luternauer and Murray, 1973). The sediments in this zone consist of well sorted fine and medium sands which are discharged through the river channels during periods of high flow and then subsequently distributed along the delta front by longshore currents (Luternauer and Murray, 1973).

8.3.3. Tidal flats.

The tidal flats, inclined at an angle of about 0.05°, form a zone around 6km wide which is bordered on the seaward side by the lowest low tide level and on the landward side by a discontinuous fringe of marsh and muddy sediments (Clague *et al.* 1983). Close to its seaward border the sediments are dominantly sandy, grading upslope into a 1 - 2 km wide zone of silt, sand and sandy silt, eventually leading to the edge of continuous marsh vegetation. Further landward still, increasing entrapment of fine sediments by marsh vegetation results in the substrate becoming predominantly silty. Within 1 - 1.5 km of the dykes, the upper tidal flat is covered by tidal marsh, which is dominated by salt tolerant rushes and sedges of the Cyperaceae family.

8.3.4. Floodplain.

Inland of the tidal flats is the dyked portion of the intra-delta. Parts of this area are as much as 1m below extreme high tide level and therefore would experience occasional flooding by the sea if not dyked. The sediments that underlie much of this area consist of very slightly inclined, sandy to clayey silts of overbank and uppermost intertidal origin (Clague *et al.* 1983). Much of this sediment accumulated in fresh and brackish marshes and swamps bordering both existing and former distributary channels of the Fraser River. Sediments deposited in this environment commonly contain, in addition to sedge and tree pollen, small amounts of pollen and spores from freshwater plants such as water plantain (*Alisima plantago-aquatica*), scouring rush (*Equisetum sp.*), skunk cabbage (*Lysichitum americanum*) and buckbean (*Menyanthes trifoliata*) (Clague *et al.* 1983).

8.3.5. Bogs.

Much of the Eastern part of Lulu Island is covered by organic deposits. These deposits, up to 8m thick in places, lie on a poorly drained substrate close to the low tide level, and began to accumulate once the surface of the delta was high enough to avoid regular inundation by the sea (Matthews and Shepard, 1962). The continued succession of marsh plants has eventually led to the growth of the moss *Sphagnum*, leading ultimately to the formation of domed peat bogs.

8.3.6. River Channels.

River channel deposits are typically coarser grained in nature, with modern channels being typically floored by coarse sand containing scattered pebbles. These modern channels may be naturally scoured to as much as 22m below mean sea level, although they are now almost constantly dredged to maintain a navigable depth. The average amount of material removed from the Fraser River's navigable channels between 1975 and 1985 has been estimated at 4.3 million m^3 / year. Of that 4.0 million m^3 / year is from the main channel between New Westminster and Sand Heads (Stewart and Tassone, 1989).

8.4. Stratigraphy and Holocene delta growth.

8.4.1. Delta plain.

The stratigraphy of the Fraser Delta plain (Figure 8.4) and tidal flats has been defined from a series of boreholes (Williams & Roberts, 1989; Clague *et al.* 1991), in addition to a large database of engineering test holes and cone penetration test results (Monahan *et al.* 1993b).

Sediments of the delta are on average 120m thick (Matthews & Shepard, 1962) and lie unconformably on Pleistocene sands and clays of glacial origin. The deepest borehole on the delta is reported to have penetrated 216m of sand and silt before reaching Pleistocene material (Clague *et al.* 1983).

Topset sediments thin and climb westward, being from up to 40m thick at the apex of the delta to 20m or less at the western margin of the sub-aerial delta plain. The lowest portion of these topset sediments form a sand unit 10 to 20m thick, with a sharp base and consisting of one or more fining upward sequences. This unit is nearly continuous under the eastern tidal flats and sub-aerial delta plain, but becomes less well defined in the western tidal flats, where foreslope silts are commonly overlain by thin silty sands. This probably represents a distributary channel complex (Monahan *et al.* 1993a), with the accumulation of channel sands occurring primarily where distributaries cross the tidal flats, and to a lesser extent where they cross the sub-aerial delta plain. These distributary sand units are capped on the tidal flats by intertidal sands and silts, while on the delta plain they tend to be overlain by bioturbated sands and silts, often containing shell debris; these have been interpreted as having been deposited in a tidal flat environment (Williams & Roberts, 1989; Monahan *et al.* 1993a). Above these tidal flat deposits lie rooted or organic rich sediments deposited in a floodplain environment.

8.4.2. Foreslope.

The south-western sector of the foreslope represents the most intensively studied part of this particular environment, with a large database of both cores and seismic profiles already in existence (Hart *et al.* 1992a). The foreslope sediments in this region typically consist of up to 120m of sands dipping at an average of 2°, grading seaward into

bioturbated muds deposited on the lower foreslope. Locally in the upper foreslope, units of interlaminated to interbedded sands occur, up to 30m thick in places and grading down-slope into underlying silts. These coarser grained units are thought to represent the distributary mouth sand lobes. Deeper in the section, interbedded with foreslope silts are units of fine to medium fine sand arranged in one or more fining upward sequences, which may represent gravity flow deposits which bypassed the upper foreslope in conditions similar to those existing on the modern delta slope seaward of the main distributary mouth (Hart *et al.* 1992b).

The foreset sequence described above lies conformably above the bottomset silt and clay sediments (Clague *et al.* 1991). These sediments are similar to those that are presently accumulating in the deep basins of the Strait of Georgia, west and north-west of the Fraser delta.

8.4.3. Evolution of the Fraser Delta.

A detailed account of the evolution of the Fraser Delta is provided by Clague *et al.* (1983) and Williams & Roberts (1989). A summarised account, based on these papers, is provided below.

1. *~12,000 years ago.* The piedmont glacier covering the Fraser Lowland began retreating northwest up the Strait of Georgia and eastwards up the Fraser Valley. These lowland areas recently freed from their ice cover were rapidly inundated by the sea. Large amounts of sediment were discharged into the sea during this time from the rapidly decaying glaciers, rapidly forming deltas and submarine outwash fans.

2. *~11,000 years ago.* Much of the Fraser Lowland had emerged from the sea, with sediments being deposited in a range of fluvial, deltaic, marine and lacustrine environments. The rapidly melting Cordilleran Ice Sheet supplied huge amounts of sediments and meltwater to the Fraser River until about 10,000 years ago, at which time ice had completely disappeared from lowland valleys and plateau's of the British Columbia interior.

3. *9000 - 8000 years ago.* With sea level some 13m lower than at present, the Fraser Delta began its growth into the Strait of Georgia from its apex near New Westminster.

During this period it extended some 6.5km into the Strait, resulting in some 0.3m of aggradation on the eastern part of the delta.

4. *8000 - 6000 years ago.* Rising sea level induced some 8m of vertical accretion, while the delta front extended another 3.7km westward.

5. *6200 - 5800 years ago.* Peat accumulations (dated at 6025 +/- 105 years BP) indicate a stillstand, during which progradation of the delta continued steadily, with the delta front moving around 1.5km further seaward.

6. *5800 - 4500 years ago.* Sea level began rising again, initially quite rapidly, and subsequently slowing, allowing the development of peat bogs on the eastern delta surface. Lateral progradation continued, extending the delta front a further 1.65km seaward and resulting in a further 2.2m of vertical accumulation of floodplain deposits.

7. *4500 - 2250 years ago.* The sea rose slowly to its present level, accompanied by a further 2m of vertical delta growth and a lateral progradation of around 4km.

8. *2250 - present day.* The sea level has remained stable, the delta has prograded another 5.4km to its present position and natural aggradation of the delta surface has caused around 0.27m of vertical accretion.

8.5. Evidence of onshore delta instability.

Fraser Delta sub-aerial sediments strongly resemble those which liquefied at Niigata, Japan during the Magnitude 7.2, 1964 earthquake which caused widespread damage, and marked the beginning of intensive research on liquefaction phenomena. Because of the Fraser Delta's similarity to Niigata, the first obvious question to ask is: has the delta liquefied in the past, in response to earthquake loading? No historical record makes any specific reference to liquefaction, but it must be remembered that south-western British Columbia has only been settled for a relatively short period (~150 years). However, physical evidence does indicate that liquefaction has occurred slightly further back in the geological record. The main physical evidence can be found from detailed descriptions of palaeo-liquefaction features in surface deposits (Clague *et al.* 1992). The commonest of these features are sand dykes, which represent the subsurface

expression of sand boils or sand volcanoes. These features occur when, as a result of earthquake shaking, a buried sand unit liquefies and the resulting excess pore-pressures escape upwards, fracturing, eroding, and possibly even deforming overlying sediments, producing sand dykes, sand sills and sand boils.

Clague *et al.* (1992) describe such palaeo-liquefaction features at various sites on the Fraser Delta. The most commonly described manifestation of these features are sand dykes and sills, which show certain spatial similarities in that they consist of sand similar in texture to that of the underlying foreset sediments from which they are generally derived. In addition, the dykes range in thickness from 1mm to 30cm, cutting steeply through overlying sediments, characteristically with a sharp contact. Radiocarbon dates indicate that all observed features on the delta are less than 3500 years old, and it is likely that the sand bodies were emplaced during one or more brief events separated by lengthy periods during which no such features formed.

8.6. Evidence of offshore delta instability.

The offshore Fraser Delta (illustrated in Figure 8.5) has now been intensively studied using a variety of geophysical instruments including: Huntec Deep Tow Seismic systems, the IKB Seistec, 5in^3 airgun, a dual channel sidescan sonar, and echo sounders. Data quality is of a generally high standard, but varies locally often due to the 'masking' effects of interstitial gas. On the basis of the geophysical data collected, the delta front may be subdivided into five distinct physical areas: the undisturbed delta front, area's of shallow rotational sliding, submarine channel and failure complex, the Foreslope Hills, and the Roberts Bank failure wedge.

8.6.1. Undisturbed delta slope.

The largest single area of undisturbed delta slope lies on the upper to middle slope, north of the main channel, and covers an area of about 19.6 x 10^6m^2. Another slightly smaller area of undisturbed slope sediments lies south of the main channel, around a water depth of between 150m and 240m, and is associated with moderate seafloor slopes (Hart *et al.* 1992c).

These areas are seismically characterised by a smooth seafloor (featureless on sidescan sonar imagery), underlain by continuous parallel reflectors draping deeper relief. In places these reflectors grade through 'wavy' reflectors into underlying 'chaotic reflectors' (Hart *et al.* 1992c). Cores collected in these areas of undisturbed sediments reveal that they gradually change in character downslope. Close to the top of the slope, sediments consist dominantly of medium sands interbedded with very fine silts, probably representing the seasonal fluctuations in river discharge. Further downslope, at around 120m, sediments tend to consist of bioturbated very fine sandy silts, which were likely deposited from fine sediment plumes originating from the river mouth. Dispersal of these fine grained sediments is mainly to the north-west, reflecting the orientation of the dominant flood tide currents along the delta slope.

8.6.2. Shallow rotational sliding.

Immediately south of the main channel, on the relatively steep upper to middle slope, there is an area of approximately 7.8 x $10^6 m^2$ where the seafloor consists of rounded, asymmetrical blocks, typically with a relief of around 2-3m (Hart *et al.* 1992c). These blocks are aligned parallel to the bathymetry and are typically 40-60m wide (upslope-downslope dimension), and may be as much as 100m long (alongslope dimension). Within each block reflectors are discontinuous, dip upslope, and are typically truncated downslope. Cores from this area indicate the sediments to be dominantly gassy muds, containing occasional sand laminations. These block features are interpreted as being formed as a result of shallow rotational sliding of delta slope sediments. Recent data indicate that, due to an absence of sediment draped over the deforming blocks, instability is both recent and ongoing (Hart *et al.* 1992c).

8.6.3. Submarine channel failure complex.

Submarine channels are a relatively common feature on the delta slope. The most intensively studied channel, named the Sand Heads Sea-valley, is approximately 5.25km long and crosses a major portion of the delta slope. Other channels to the north lack any signs of recent erosion, and probably represent relict features from the 1800s, when the main distributary channel was located some distance to the north of its present position. In addition, two small channels are present on the southern portion of the upper slope, one being traceable for 2.25km, while the other shorter channel extends only

600m. McKenna *et al.* (1992) identify five large scale mass-wasting events near Sand Heads between 1972 and 1985. The largest of these events took place on June 30, 1985 and involved over 1 x $10^6 m^3$ of sediments. Slope retrogression exceeded 350m, forming a large gully, extending to within 100m of the Sand Heads Lighthouse (Figure 8.6). Slopes before and after the event were steep, 10 - 17° and 6 - 20° respectively, with the steepest post-event slopes occurring at the head of the gully near the centre line of the main channel.

The Sand Heads Sea-valley system is composed of three related components (Kostaschuk *et al.* 1992):-

i) upslope tributary channels,
ii) a single sinuous channel,
iii) distributary channels at the base of the delta-front.

8.6.3.1. Tributary channels.

Seaward of the river mouth at Sand Heads the delta front is dissected by as many as eleven separate channels (Kostaschuk *et al.* 1989). A number of these terminate a little way offshore, some join to form the main sea-valley to the north, and two others join to the south, themselves joining the sea-valley at around 100m depth. In the upper reaches of the channel, gradients may be as much as 23°, decreasing gradually to approximately 2° at around 115m depth. Channel walls are typically steep (19°-22°) and covered in features indicating small scale mass movements, including linear gullies, arcuate slump scars and bowl shaped depressions. Channel walls are flat or slightly inclined in cross-section. Inter-channel surfaces range from smooth and featureless to severely deformed surfaces disrupted by ridges, mounds and pits, all indicative of small scale slump failure.

8.6.3.2. Sinuous Channel.

This middle section of the sea-valley contains five distinct corners and begins at a depth of around 110m, stretching downslope until about 205m at which point it bifurcates into two distributary channels. Channel gradients range from 2° over its upper reaches to around 0.7° towards its lower end; width varies according to position, but in general

declines from 470m to 280m, while depth decreases from 18m to 7m. The floor of the channel is hummocky with irregular ridges extending across the channel in areas between the valley corners. A sinuous sub-channel runs down the thalweg of the sea-valley, resulting in benches or terraces representing former positions of the sea-valley floor. The valley sidewalls are covered by gullies, slumps and chutes similar to those in the tributary zone.

8.6.3.3. Distributary channels.

As mentioned above, the sinuous channel splits into two sub-channels at a depth of around 205m. The northward of these channels bifurcates further downslope, while the southern channel, curves southward and continues downslope. Channel gradients range from 1.1° to 0.7°, widths from 125m to 55m and depths from 1m to 2m.

8.6.4. The Foreslope Hills.

The Foreslope Hills form a region of rounded 'hills' and troughs extending several kilometres in a north to north-northeast direction, at the base of the slope in the central strait. These features have over 10m of relief between hill and trough axes, and are separated by a few hundred metres. Seismic data for the area indicate that the hills comprise distinct blocks of sediment, some of which appear to be fault bounded. The blocks can be over 50m thick, and comprise the middle to upper portion of the postglacial sediment column (Hart *et al.* 1992c). Stratification within each block dips landward, generally in contrast to reflector geometry observed on undisturbed parts of the delta slope. Recent sedimentation patterns in the region are complex. Hill crests probably represent zones of non-deposition, or even active erosion, while the troughs represent zones of accumulation, dominantly by muds. Elsewhere, onlapping high-amplitude reflectors occur in troughs, while chaotic reflectors are locally present. These 'ponded' deposits cover an area of around $2.6 \times 10^6 m^2$ and probably represent sediments which would otherwise have built a turbidite fan, had they not been intercepted by the relief of the Foreslope Hills.

The origin of these hills has been the subject of some considerable debate over the past decade or so. Early interpretations suggested that the undulating topography was the result of a single large failure, followed by remoulding and deposition (Tiffin *et al.* 1971;

Hamilton, 1987). More recently, better quality seismic data have led to the interpretation that the features as having been formed by *in-situ* processes of rotational slipping of cohesive sediments, generated by downslope extension (Hart *et al.* 1992c).

8.6.5. Roberts Bank failure wedge.

The existence of the Roberts Bank failure wedge was first suggested in 1982, when interpretation of airgun data suggested that failure deposits off Roberts Bank may form part of a 'wedge', pinching out downslope and along slope to the southeast (Hart *et al.* 1992b). Despite physical problems associated with obtaining good quality seismic data for the wedge (due to interstitial gas and the sandy nature of the sediments), more recent surveys (circa.1992) have confirmed the existence of the feature and have shown it to consist of a wedge of sediment locally over 50 milliseconds thick and characterised by 'wavy' or discontinuous reflectors (Figure 8.7). The base of the wedge is clearly defined as a series of prominent landward dipping reflectors which may represent shear surfaces. The failure wedge represents possibly the biggest 'risk' for the region as a whole, as both the coal port and ferry terminal have been built directly upslope from this feature.

8.7. Seismic stability of the Fraser River Delta.

Much research work has been carried out on the Fraser Delta, in particular on the sub-aerial delta, where access is easy and conventional liquefaction assessment techniques (i.e. SPT, CPT and more recently SCPT) have been used. Based upon an analysis of these data, Bryne & Anderson (1987) predict that if Richmond should be subjected to the design earthquake of Magnitude 7.5 as used in the 1985 National Building Code of Canada, the damage would be as follows:-

'1. Most buildings will suffer some damage due to uneven ground movements as a result of the liquefaction of the underlying soils. Cracks in the ground surface will be common, and where these cracks run beneath buildings severe damage will occur. Taller buildings are supported on piles and may suffer damage if the soil surrounding the piles liquefies. In the event damage to high rise structures may result from high lateral forces induced by resonance if they are not adequately designed.

2. The highway system may be disrupted due to lateral spreading and fissuring, resulting in vertical faults of up to 0.5m. The major bridges are expected to withstand the earthquake with little damage, but the approaches may suffer some damage, and lateral spreading of the abutment fills may disrupt access to the bridges.

3. The dykes will be severely damaged by cracking. Serious flooding could occur unless these are not repaired rapidly.

4. The water, sewage, gas, electrical and telephone services in the area will suffer light to moderate damage.

5. Fires will be initiated by the earthquake. The disruption of water supplies will hamper fire-fighting, so that fires may get out of control, and a conflagration is a possibility.

6. The possibility of a damaging tsunami or earthquake generated tidal wave is remote'.

The effects on the offshore delta are more difficult to quantify, due mainly to the conditions of restricted access presented by submarine sites. Luternauer and Finn (1983) suggest in their analysis based upon standard penetration test data, that the delta front sediments may resist earthquake motions characterised by peak acceleration between 10-12% of gravity and 15 significant cycles of motion. However, the recent discovery of the failure wedge below Roberts Bank, and the documentation of mass wasting events at Sand Heads, does indicate that during a significant shaking event there is the potential for some sort of large failure on the delta front. Because of the difficulty in physically testing the offshore sediments of the Fraser Delta, more recently a greater emphasis has been placed on *in-situ* testing using geophysical methods. This need for improved *in-situ* techniques for the prediction of liquefaction provided the initial impetus for research for this particular Ph.D. The results of this research, applied specifically to the Fraser Delta 'situation' are described below.

8.8. Field results: background.

Most of the field data presented in this chapter were collected by other investigators during two multi-disciplinary research cruises in November 1992 and 1993, aboard the

Canadian research ship, *John P. Tully.* In total, some 650 individual shear wave measurements were made by Dr A. Davis and Dr D. Huws using the seismic sledge, between Roberts Bank Coal Port and Sand Heads. Where possible, these data have been interpreted by the author to give information on the shear wave velocity - depth structure of the surficial Fraser Delta sediments. In addition, the data from two SCPTU tests collected by ConeTec Investigations Ltd[1] from a floating platform off Roberts Bank Coal Port were also obtained, courtesy of the Geological Survey of Canada. These data provided infomation on both the geotechnical and geophysical sediment properties to a depth of approximately 27m. These data also provided the opportunity to directly compare a more conventional CPT based approach for predicting liquefaction potential with the shear wave method proposed in this project.

The sediment samples used for laboratory analysis in this study were retrieved from three closely spaced vibro-cores (PAR91A-01, PAR91A-02 & PAR91A-03) collected on the Fraser Delta in 1991 during a Geological Survey of Canada research cruise (See Figure 8.8). Triaxial testing conducted as part of this Ph.D project and described previously, determined the steady state parameters for this sediment, and these results will now be used to quantify the *in-situ* liquefaction potential of Fraser Delta sediments.

8.9. Shear wave sledge data.

The shear wave sledge was deployed in both short offset (pseudo-underway) and long offset modes during both research cruises. Of these, the most successful were three short offset deployments (described in more detail below). The longer offset data suffered from more logistically related deployment problems, and as a result, the data were significantly poorer in quality. As a result, a full analysis of the long offset data was not possible.

Position fixing on board the ship during the cruise was achieved using a Global Positioning System. Sledge shot positions were acquired from the ships navigation log and a knowledge of the time of shot. Positions listed below reflect the position of the ship and have not been corrected for the layback of the sledge (usually 30 - 50 m

[1] ConeTec Investigations Ltd,
9113 Shaughnessy St,
Vancouver,
British Columbia,
V6P 6R9.

behind the ship) because this figure is less than the resolution of the position fixing system (typically ±100m). Survey tracks of these deployments are illustrated in Figure 8.9.

8.9.1. Short offset data.

The data obtained from analysis of the short offset shear wave sledge measurements were used where possible to determine velocity - depth information for the top 2-3m of sediment. This approach provides useful initial information on the surficial sediment properties, and allows the production of shear wave velocity refraction 'profiles', which may further allow the identification of anomalous areas, worthy of further investigation.

In total, some 600 individual short offset shear wave refraction shots were performed using the sledge. Overall data quality proved to be variable; the highest quality records allowed travel times to be extracted from the onsets of the shear wave signals on each geophone, allowing a 'complete' analysis of the data in terms of surficial velocities, and depths to the main refractors (Figure 8.10). On other records, time information could be extracted using the first trough, peak, or occasionally a later feature, allowing solely velocities to be calculated. The worst quality records were dominated by low frequency background reverberation, high frequency P-wave noise, and pickup from the signal impulse. In this latter case, no feature could be reasonably picked, and such records were excluded from any further analysis.

Once data had been extracted from each individual record, the subsequent time - distance graphs usually had the form illustrated in Figure 8.11. As can be seen from this illustration, the general form of these data allows velocity - depth interpretation based upon a simple two layer velocity model. Clearly it is an oversimplification to attempt to describe the top 2-3m of sediment using a simple two - layer velocity model of this type, when in fact it is more probably characterised by a strong velocity gradient. The apparent surface layer velocity V_1 must therefore be regarded as an average figure for that particular layer. Because of the use of an apparent surface layer velocity, the depth to the first refractor must also be regarded as being approximate in nature. However, using this approach, a useful and useable measure of the bulk properties of the surficial sediment can be obtained.

As mentioned above, three complete deployments (Deployment 1, 3 and 4) were fully interpreted and the results of this analysis is presented below.

8.9.1.1. Sledge deployment No. 1.

The data comprising Deployment No. 1, were collected on 9.11.93 and ran NW - SE over Roberts Bank towards the Coal Port in a water depth of approximately 50m. A total of 139 individual records were collected of which 73 were interpreted to reveal the apparent velocities and depth to the first refractor; an additional 35 records revealed velocity information only. A Huntec deep-tow boomer profile (PGC 91-01, Line A10) was obtained from the archives at the Pacific Geoscience Centre, running SE - NW (Figure 8.8 & 8.12) along the sledge profile. Analysis of the sub-bottom data revealed that the area consisted dominantly of sand waves. The interpreted results of the shear wave data in terms of velocity are illustrated in Figure 8.13 (a), and approximate depth to the first refractor in Figure 8.13 (b). Although the data are vertically exaggerated, on a small scale (10-100m) there appears to be a fairly random variation of measured velocities. Further, over the length of the profile, there does not appear to be any great overall trend to the data. Summarised deployment statistics are given in Table 8.1 below. While realising that spatial measurements do not generally lend themselves to simple statistical treatment, assuming that there is no long term trend to the data, the following may be used to give some impression of the range of values obtained from this deployment.

	Mean	*Min*	*Max*
Apparent V_1 (m/s).	43	29	66
V_2 (m/s).	85	67	105
Approximate depth to refractor (m).	-1.2	-2.0	-0.7

Table 8.1. Summarised data for Deployment No. 1.

Based upon this assumption, an 'average' velocity - depth profile may be defined; this is illustrated in Figure 8.14. In the interests of simple comparison, the 'critical shear wave velocity' derived from the laboratory testing programme is also displayed. Clearly, there appears to be a close agreement between the field derived and laboratory derived shear wave data. Assuming that the sediment tested in the laboratory is representative of those measured in the field, this provides a clear justification that combined laboratory

/ field shear wave techniques may be used to derive similar velocities. These data also illustrate the sediments in this region at least are close to their 'critical velocities'.

8.9.1.2. Sledge Deployment No. 3.

The data comprising Deployment No. 3 were collected on 18.11.92 and again the profile ran approximately NW - SE over Roberts Bank towards the Coal Port. A total of 68 individual records were collected of which 57 were interpreted to reveal the apparent velocities and depth to the first refractor. No sub-bottom control data are available for this profile, but it is likely that the surface of the delta is dominated by sand waves. The interpreted results of the shear wave data are illustrated in Figures 8.15 (a & b). Once again on a small scale (10-100m) there appears to be significant variation in the data, but over the length of the profile there does not appear to be any overall trend to the data. Based upon the assumptions discussed previously (Section 8.9.1.1), the range and mean values of V_{1app}, V_2 and the approximate depth to the first refractor are summarised below.

	Mean	*Min*	*Max*
Apparent V_1 (m/s).	33	19	71
V_2 (m/s).	79	59	111
Apparent depth to refractor (m).	-1.45	-2.25	-0.76

Table 8.2. Summarised data for Deployment No.3.

From these data an 'average' velocity - depth profile may be defined; this is illustrated in Figure 8.16. Once again the sledge data compares well with the 'critical shear wave velocity' line, derived from the laboratory testing and provides further justification for 'combined techniques of the type proposed in this thesis.

8.9.1.3 Sledge Deployment No. 4.

The data comprising Deployment No. 4 were collected on 19.11.92 and again ran approximately SE - NW from Roberts Bank towards Sands Heads, in a water depth of approximately 50m. A total of 106 individual records were collected of which 86 were interpreted to reveal apparent velocities only. Fourty -five records were interpreted to reveal the apparent velocity structure of the surficial seabed sediments. The results of

this analysis are illustrated in Figures 8.17 (a & b). As can be seen, on a small scale there appears to be a significant variation in the data. As before, over the length of the profile there does not appear to be any overall trend to the data. Summarised deployment statistics are given below.

	Mean	*Min*	*Max*
Apparent V_1 (m/s).	41	24	74
V_2 (m/s).	84	65	117
Apparent depth to refractor (m).	-1.36	-2.34	-0.84

Table 8.3. Summarised data for Deployment No.4.

Based upon these data, the 'average' velocity - depth profile is illustrated in Figure 8.18.

8.9.2. Long offset shear wave data.

Long offset data were recorded on 5.11.93 and 6.11.93, in the dredged basin to the west of the Coal Terminal. For this, two 3-component geophones were deployed some distance from the sledge, with the ship at anchor. The geophones were then gradually winched towards the sledge in an attempt to produce a cumulative refraction profile. The ranges between the sledge and the geophones were calculated from a knowledge of the direct P wave travel time in water between the sledge and the first geophone (Figure 8.19). Note that the first obvious arrival represents the true direct wave, while the stronger, distinct arrival is in fact the sea-surface reflected arrival. Assuming a seawater P-wave velocity of 1500m/s, the calculated ranges to the first geophone were (error bars are based upon a P-wave velocity variation of ±20m/s):

Record Number.	*Shot Number*	*Travel Time (ms)*	*Distance to 1st geophone pan (m).*
55	13	92	138 ±2
53	12	88	132 ±2
50	11	93	140 ±2
47	10	102	153 ± 2.5
44	9	111	167 ±2.5
41	8	124	186 ±2.5
38	7	129	194 ±3
36	6	131	197 ±3
33	5	134	201 ±3
30	4	133	200 ±3
26	3	140	210 ±3
23	2	140	210 ±3
21	1	148	222 ±3

Table 8.4. Ranges to 1st geophone.

The range data displayed above in show a gradual reduction in shot - receiver distance. However, the last record (record number 55) actually appeared to be further away than the previous shot despite the geophone cable having been winched in a short distance. This effect may have been caused by cable drag as a result of ship motion, causing the sledge and hence source to move separately, relative to the geophone pans.

The filtered and unfiltered transverse components of the signal are illustrated in Figure 8.20 (a & b). As can be seen, there are no obvious shear wave arrivals amongst the background noise on either the filtered or unfiltered data. This poor signal to noise ratio could be due to high levels of low frequency background noise generated by the nearby coal-port, or could be due to poor coupling between the geophones and / or source and the surface sediment. This lack of any distinct signal unfortunately prevented further analysis of the long offset data.

8.10. SCPTU data.

The data used in this study have been taken from a cone penetration based study conducted between September 20, 1993 & September 26, 1993, and are described in more detail in an initial report by ConeTec Ltd. (1993). The SCPT data were collected using a 10 ton compression cone, with a standard tip area of 10 cm^2 and a friction sleeve area of 150 cm^2. The cone was designed with an equal end area friction sleeve and tip end area ratio of 0.85. The pore-pressure filter was located immediately behind the cone tip and was saturated in glycerine under vacuum immediately prior to penetration. This equipment was used to collect the following data at the standard interval of 5cm: cone bearing (q_c), sleeve friction (F_s), dynamic penetration pore-pressure (U_t) and cone inclination (I). Shear wave signals propagating downwards from the surface source were recorded at the mid points of the 1m test intervals, during pauses in penetration for the addition of additional push rods. The seismic energy sources themselves consisted of small 'seismic caps', located 6.5m away from the cone sounding hole, and detonated electronically at the mudline. All the tests were carried out from a floating platform statically positioned with spuds and anchors.

8.10.1. CPT interpretation.

The CPT data are described in more detail below. The inferred stratigraphic profiles at each CPT test location are based upon relationships between cone bearing, sleeve friction and dynamic pore-pressure. The friction ratio ($R_f = F_s/q_c$ x 100%) is a calculated parameter which is used to identify the soil type and is based upon empirical results relating soil type and soil behaviour. In general, soft cohesive soils have high friction ratios, low cone bearing pressures and generate large positive excess pore-pressures during penetration. In contrast, cohesionless soils have lower friction ratios, high cone bearing pressures and generate small excess pore-pressures during penetration. The soil behaviour type zone numbers used to infer sediment type, are detailed below.

Rf soil classification zone.	*Soil Type.*
1.	Sensitive fine grained.
2.	Organic material
3.	Clay
4.	Silty clay
5.	Clayey silt
6.	Sandy silt
7.	Silty sand
8.	Fine sand
9.	Sand
10.	Gravely sand.

Table 8.5. Soil behaviour type zone numbers (*derived from CPINT v 5.0*).

8.10.1.1. SCPT 6.

SCPT 6 was collected on 24.9.93 and penetrated 29.2m below the mudline. The data from this test are presented in Figure 8.21(a-d). The soil type zone numbers (defined above) are displayed in Figure 8.22 and indicate that below a depth of approximately 8m, the soil profile is dominantly composed of sandy silts, silty sands, and fine sands. Figure 8.23 illustrates the inferred relative density, calculated by P.A. Monahan at the University of Victoria, B.C, using the CPT interpretation software, CPTINT, version 5.0. These data indicate that two distinct zones appear to exist, the first lying between around 7.5m and 13.5m where the inferred relative density ranges between approximately 70 - 35%; the second, looser zone exists between around 17.5m and 27.5, where the inferred relative density ranges between approximately 5 - 30%. Figure 8.24 illustrates the CPT data plotted on the diagram of the type defined by Robertson and Campanella (1985). As can be seen, most of the data fall within the zone

determined by Robertson & Campanella (1985) as being at risk of liquefaction. Figure 8.25 illustrates the shear wave velocity profile measured during this test, and the average velocity - depth interpretation from the short offset sledge data for deployment number 1. As can be seen from the SCPT data, there is a rapid velocity increase between 5m and 8m, followed by a more gradual increase between 8m and 27m. Although the data are of a different vertical extent, there appears to be a general agreement between the velocities derived from the seismic sledge and the SCPT. This agreement illustrates the usefulness of the seismic sledge, especially for rapidly surveying surficial seabed sediments.

8.10.1.2. SCPT 7.

SCPT 7 was also collected on 24.9.93 and penetrated 29.25m below the mudline. The data are presented in Figure 8.26 (a - d). The soil type zone numbers are displayed in Figure 8.27 and indicate that below 3m the soil profile is dominantly composed of sandy silts, silty sands, and fine sands. No relative density data are available for this particular CPT. Figure 8.28 illustrates the CPT data again plotted on the diagram of the type defined by Robertson & Campanella (1985). As can be seen, most of the data fall within the zone determined by Robertson & Campanella (1985) as being at risk of liquefaction. Figure 8.29 illustrates the shear wave velocity profile measured during the test, and the average velocity - depth interpretation from the short offset sledge data for deployment number 1. The SCPT derived velocities once again clearly display a rapid increase between a depth of approximately 5m and 7m, followed by a more gradual increase between 8m and 27m.

8.11. Inference of sediment state.

Before any inference of sediment state can be made, certain assumptions have to be considered; these are listed below:-

1. Homogeneity. All laboratory tests were performed on samples of a known grain size and having an approximately homogeneous fabric. In the field, it is extremely rare to find any significant thickness of naturally deposited sediment which does not vary in terms of either grain size distribution or fabric. This in turn is due to the variability of the spatial and temporal controls on the sedimentary environments. From an analysis of boomer

records, the Roberts Bank area of the Fraser Delta is characterised sand waves which are probably fairly homgeneous in terms of sediment type, both laterally and with depth, a conclusion confirmed by Robertson (*pers. comm*, 1995). The layering noted in the interpretation of the short offset sledge data is probably a function more of density changes, rather than a drastic shange in sediment type. In the case of this study, any shear wave velocity variations away from the 'predicted', is assumed to be largley a function sediment density.

2. Representative samples. It is assumed that the sediment recovered in the three vibro-cores from the delta is representative of that tested by the SCPT's and seismic sledge on Roberts' Bank.

3. Shear wave velocities. As noted above (Section 4.2.8), the shear wave velocity of a particular sediment tends to increase with age, as cememtation between the individual sediment grains increases. It is however assumed that the shear wave velocities recorded in the freshly deposited, normally consolidated samples in the laboratory are similar to those recorded at Roberts Bank. For this reason, the whole method described above is limited to uncemented sands only.

If these assumptions can be regarded as valid, the consolidation state of sediments tested by the SCPTs at Roberts Bank may be inferred based upon laboratory and field shear wave velocity measurements.

8.11.1. SCPT 6.

Figure 8.30 (a) shows the observed shear wave velocity field data, with the 'critical shear wave velocity' line plotted through it. As can be seen, the critical velocity runs directly through the data, indicating that some of the assumptions described above may be valid. Figure 8.30 (b) illustrates the shear wave state for SCPT 6, calculated using:-

$$\psi_s = -\left(V_{s\,meas} - V_{s\ crit}\right) \qquad (8.1).$$

where, $V_{s\,meas}$ = V_s measured *in-situ*.

$V_{s\,crit}$ = Critical V_s, at the same estimated depth, derived from the laboratory curve.

As can be seen, between 4 & 6m there appears to be a zone of potentially highly liquefiable sediment. However from an analysis of the inferred sediment type, the sediment in this zone is known to be composed of sensitive fine grained material (*i.e.* sediment not tested in this study), and must therefore be ignored. This is due to the fact that the Cone Penetration Tests were located on the tidal flats, where the surface sediments are likely to be finer than their sub-tidal counterparts. Between around 6m and 17.5m, ψ_s is dominantly negative, indicating a possible dilative or strain stiffening response to earthquake loading. Between around 17.5m and 27.5m, ψ_s appears to be more dominantly positive, indicating on the basis of the measured shear wave velocities, that this zone may be at risk from liquefaction. Interestingly these two zones appear to correlate very well with the two zones of inferred relative density described above (see Section 8.3.1.1) from the CPT analysis. Both data sets are plotted in Figure 8.31 which clearly shows that there is an approximate correlation between the inferred relative density derived from CPT measurements, and ψ_s derived from shear wave velocity measurements. As such, this is probably the strongest single piece of evidence indicating that shear wave velocity may be used to indicate sediment consolidation state. In addition, Figure 8.32 illustrates a direct comparison between the inferred relative density and ψ_s based upon interpolated ψ_s values between the depth of 10m and 27m. The correlation coefficient of these data is -0.61, indicating that for this particular data set, a strong relationship between CPT based measures of liquefaction potential and ψ_s exists. The ultimate conclusion that may then be drawn from this analysis is there is some correlation between shear wave velocity and cone penetration resistance.

8.11.2. SCPT 7.

Figure 8.33 (a) illustrates the observed field shear wave velocity data and the 'critical shear wave velocity' line for the Fraser Delta sand. As can be seen, the critical velocity runs directly through the data, indicating once again in this particular instance the validity of the technique. Figure 8.33 (b) illustrates the shear wave state for SCPT 7, calculated using Equation 7.1 above. As can be seen, between 4 and 6m there appears to be a zone of highly liquefiable sediment, but as before the sediment in this zone is not composed of silty or fine sand, and must therefore be ignored from this analysis. Below 6m the sand state, based upon the shear wave velocity, appears to 'zig-zag' between

negative and positive consolidation states down the profile. This could be indicative of a series of alternating 'loose' and 'dense' layers. As mentioned above, no inferred relative density data are available for this particular CPT data set.

8.12. Summary.

The data described above illustrate clearly that there appears to be a strong correlation between conventional geotechnical liquefaction assessment methods and those shear wave methods proposed in this study. This relationship is especially clear for the comparison between inferred relative density and ψ_s, for SCPT 6. It is also clear from these data that the relative ease of measurement of shear wave velocities, using both the systems described above appears to outweigh the physical disadvantages of the method, in particular the sensitivity of shear wave velocity to changes in void ratio, outlined in more detail above. Finally, the high degree of agreement between the data sets produced with the two methodologies has the more important implication that significant amounts of liquefiable sediments do exist in the upper 20 - 30m of the Fraser Delta, around Roberts Bank.

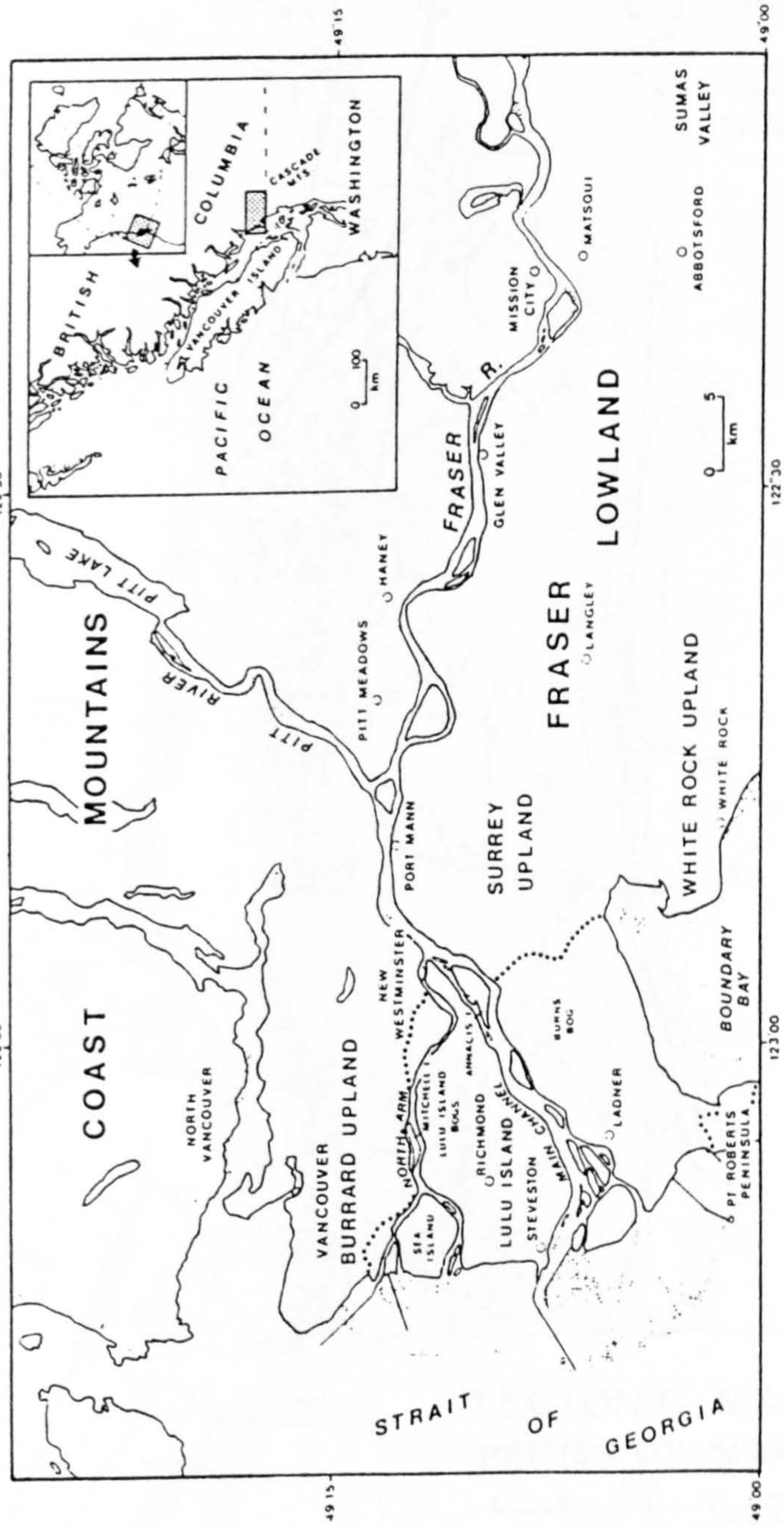

Figure 8.1. Fraser River Delta - location and general setting (*after Clague et al., 1983*).

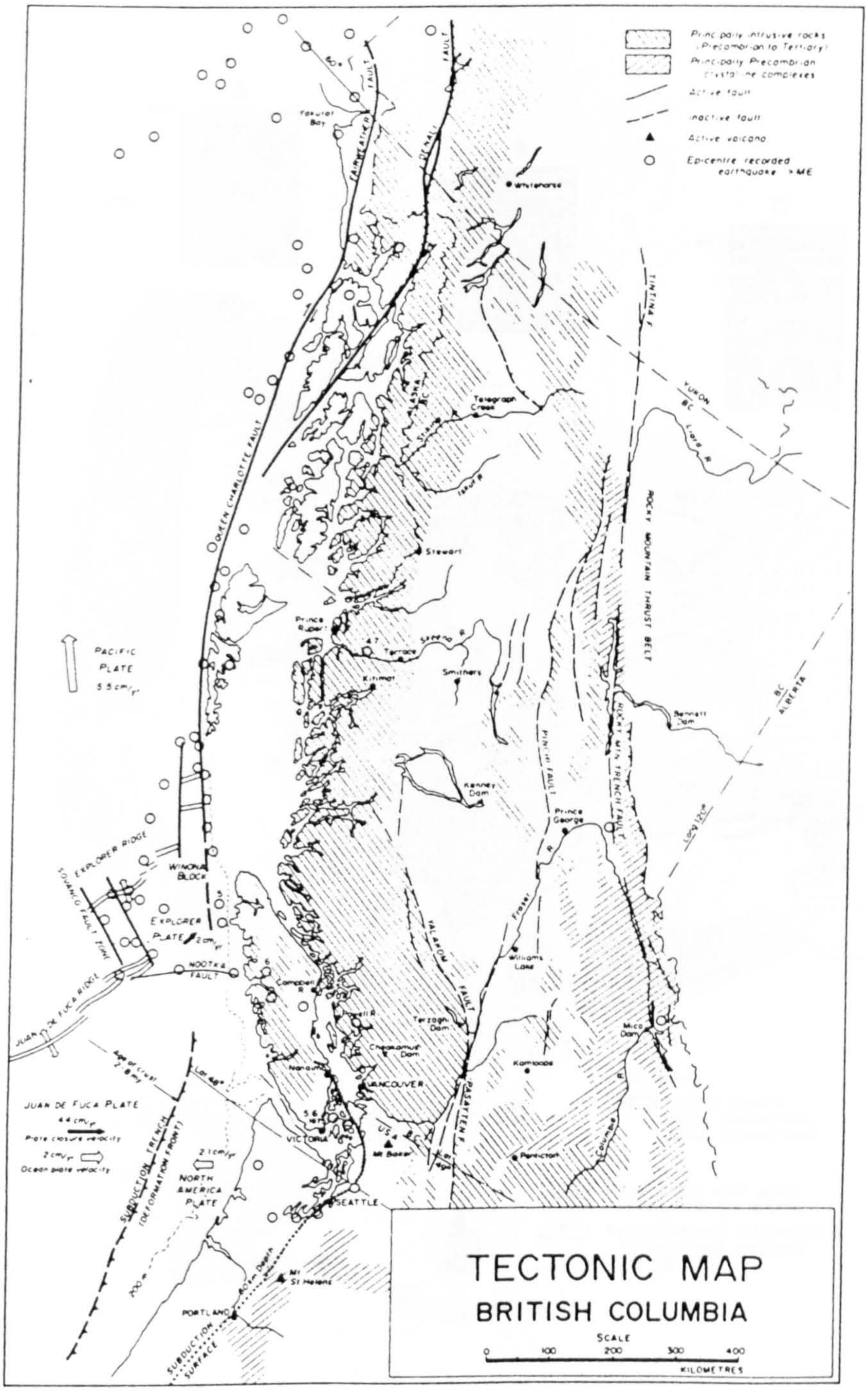

Figure 8.2. Tectonic map of British Columbia (*after Murty, 1992*).

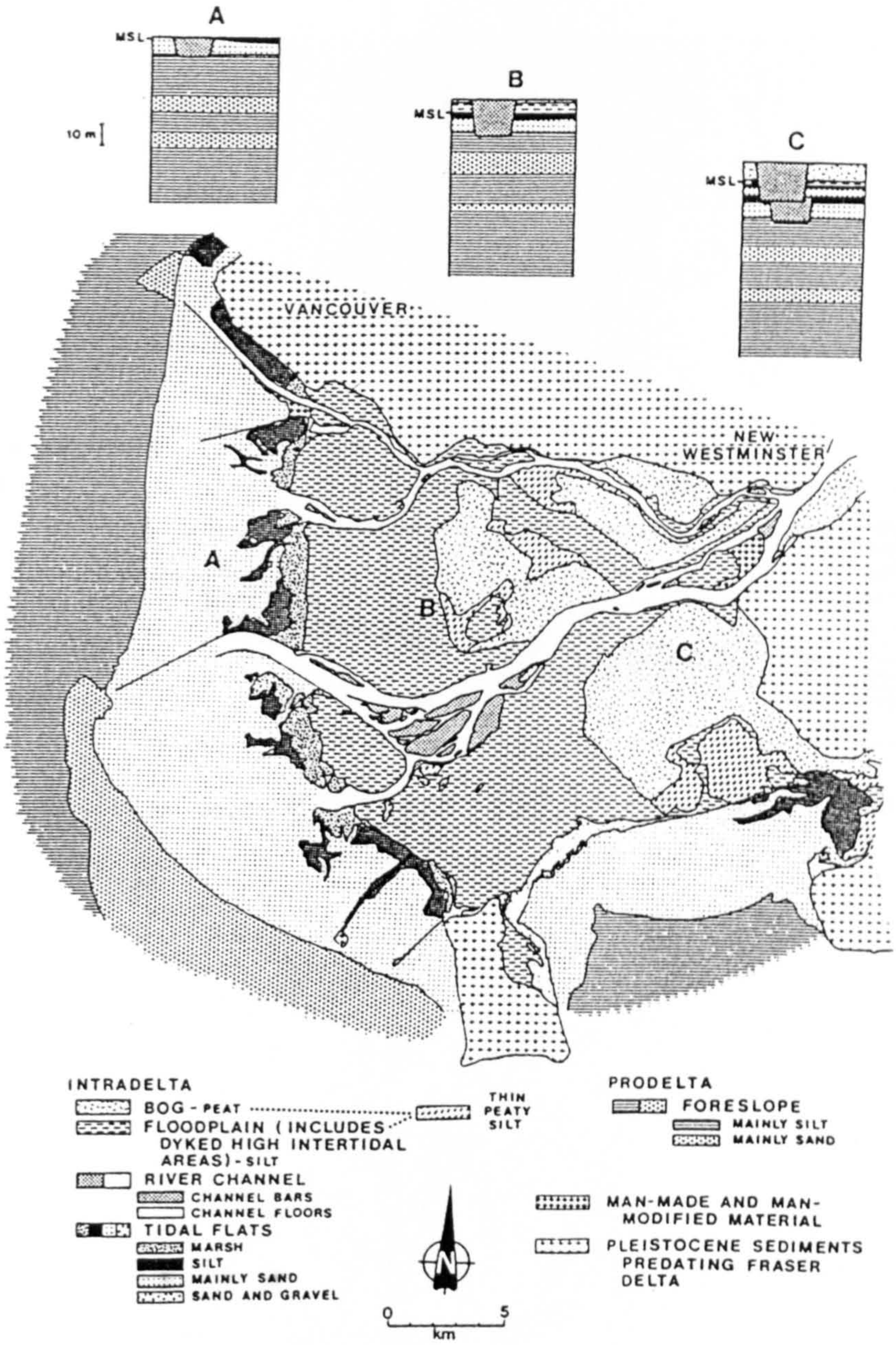

Figure 8.3. Sediments and sedimentary environments of the Fraser Delta (*after Clague et al., 1983*).

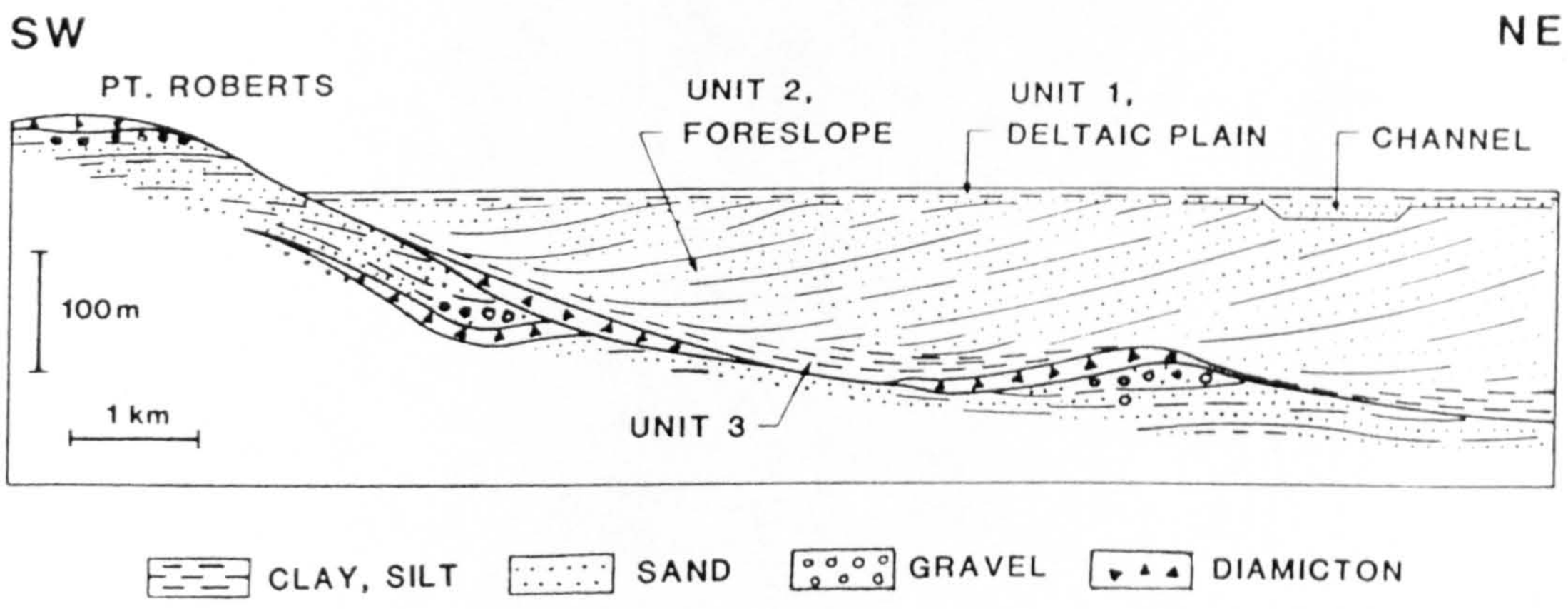

Figure 8.4. Schematic cross section of the Fraser Delta, from Burns Bog to Point Roberts, showing stratigraphic relationships of Quaternary deposits beneath the southern Fraser delta. Holocene deltaic sediments overlie an irregular surface developed on a complex Pleistocene fill (shaded area). Note vertical exaggeration. (*after Clague et al, 1991*).

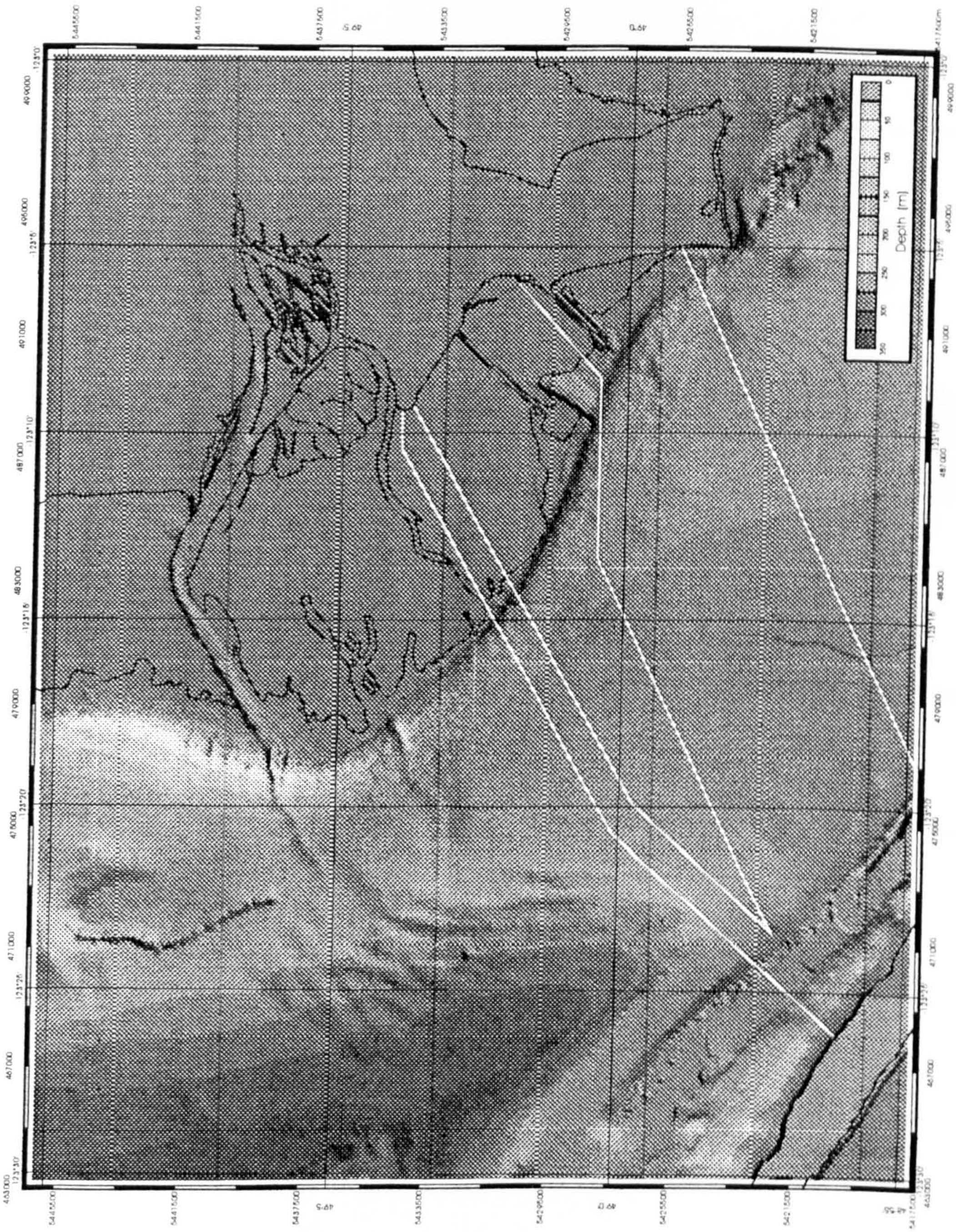

Figure 8.5. Offshore Fraser Delta bathymetry (white lines enclose the power cable corridor).
Courtesy of Geological Survey of Canada.

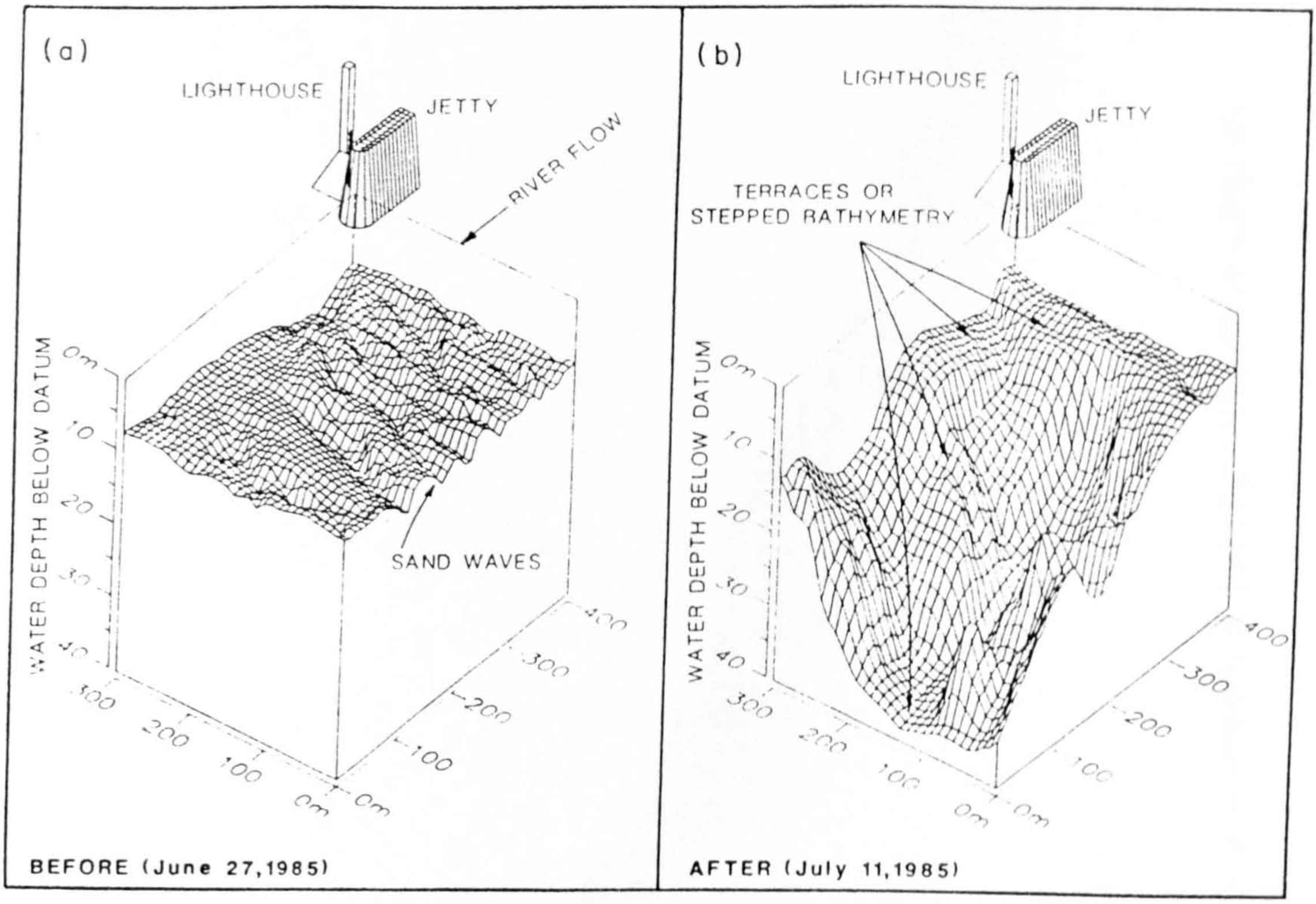

Figure 8.6. Computer generated isometric view of the 1985 mass wasting event at Sand Heads (*after McKenna, et al., 1992*).

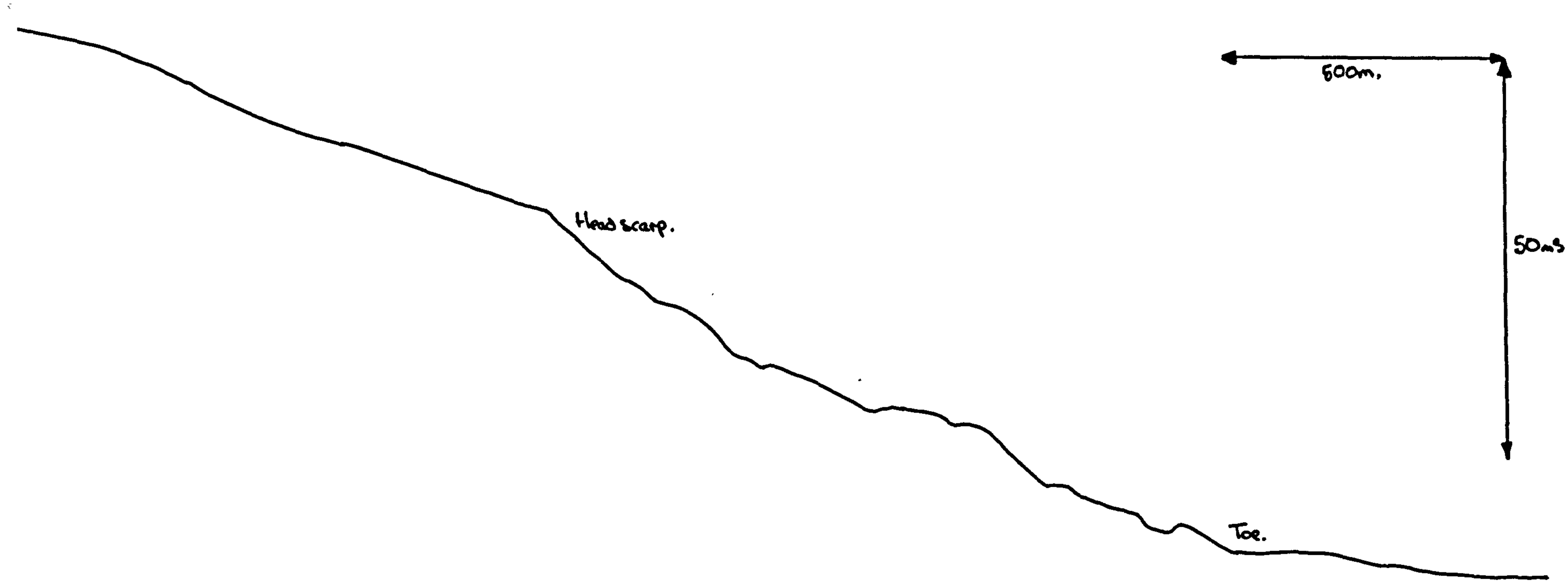
Head scarp.
500m.
50ms.
Toe.

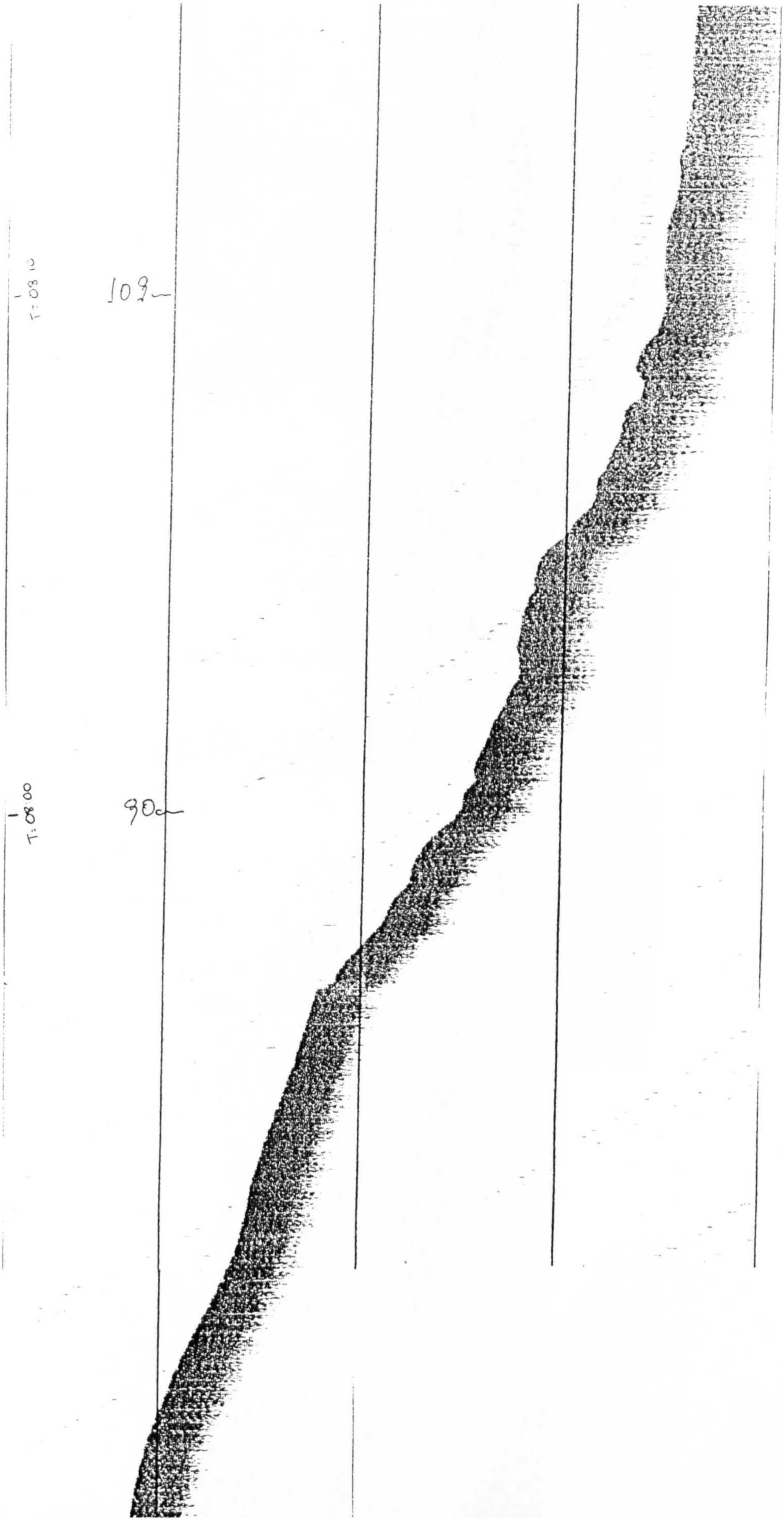

Figure 8.7 (a). 12KHz echo-sounder profile of the Roberts Bank failure wedge (line PGC93-29).

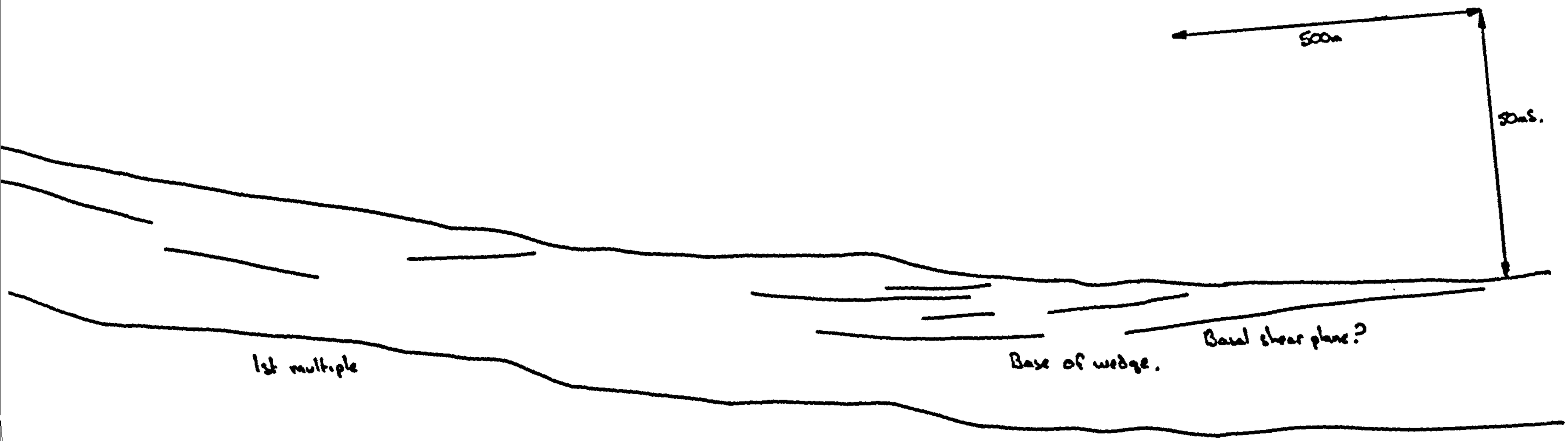
500m
50mS.
Basal shear plane?
Base of wedge.
1st multiple

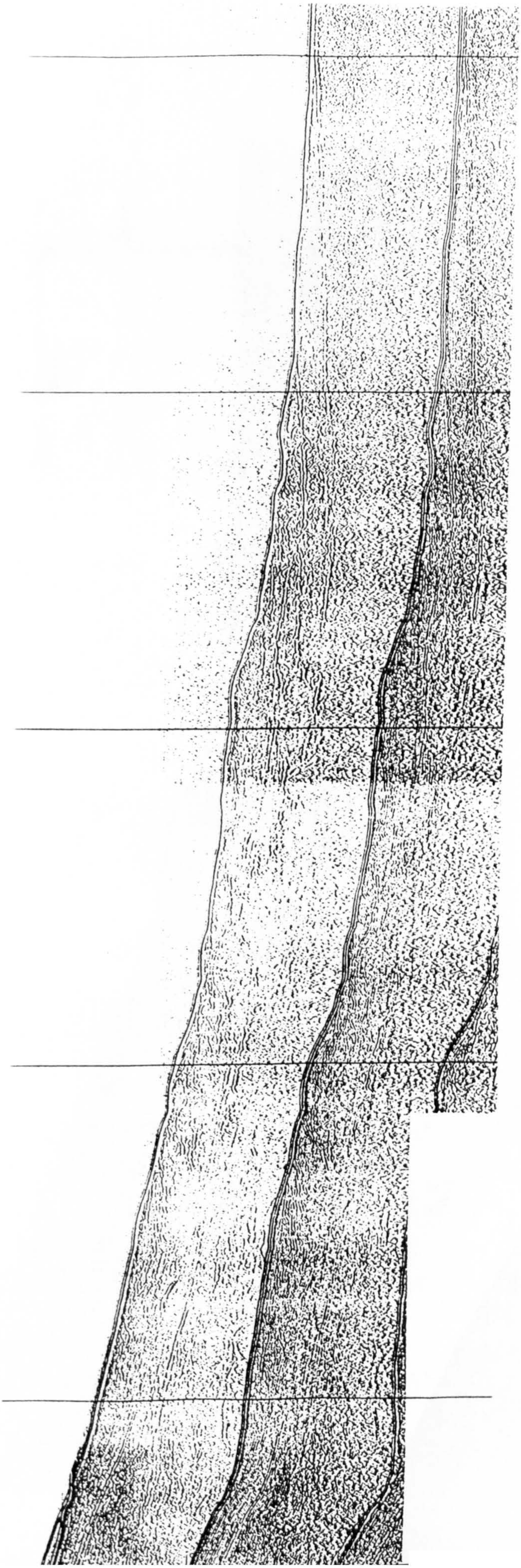

Figure 8.7 (b). Huntec deep-tow boomer profile of the Roberts Bank failure wedge (line PGC93-29)

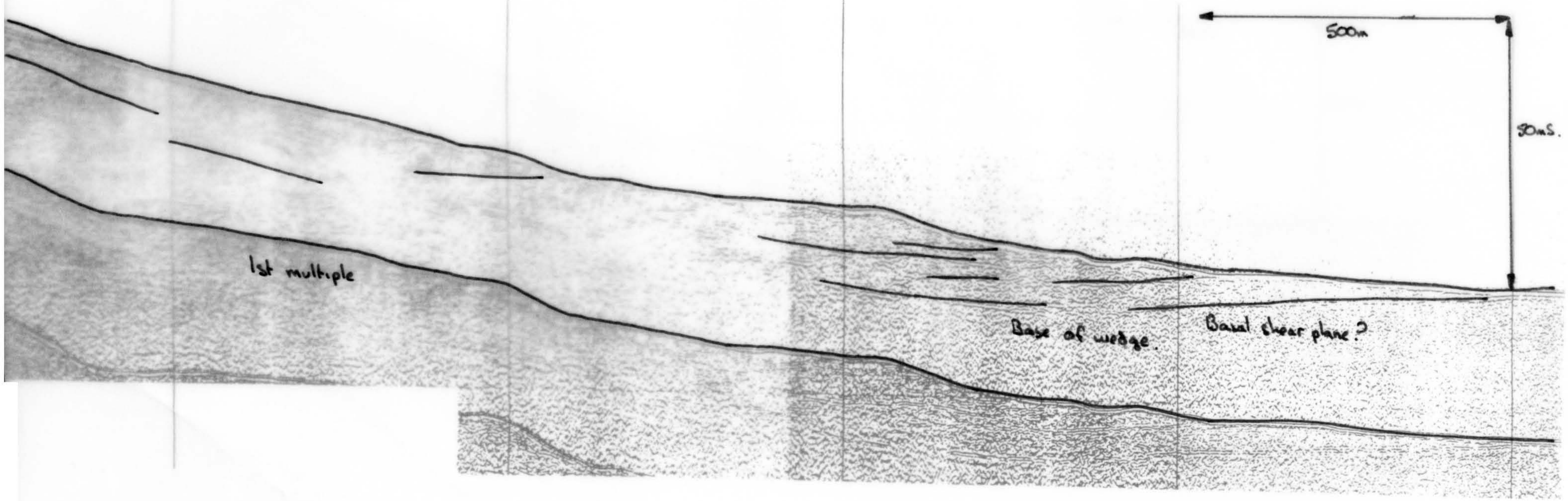

Figure 8.7 (b). Huntec deep-tow boomer profile of the Roberts Bank failure wedge (line PGC93-29)

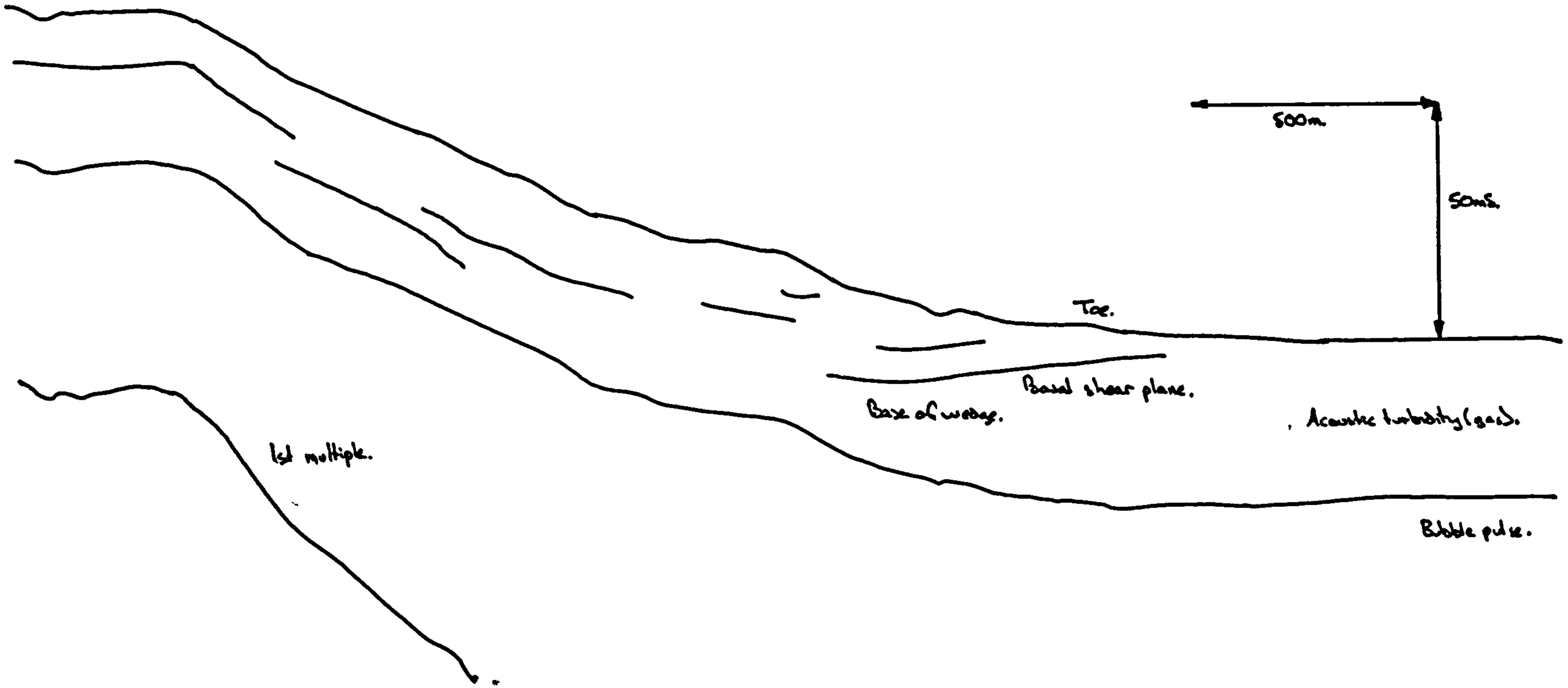
500m.
50ms.
Toe.
Basal shear plane.
Base of wedge.
Acoustic turbidity (gas).
1st multiple.
Bubble pulse.

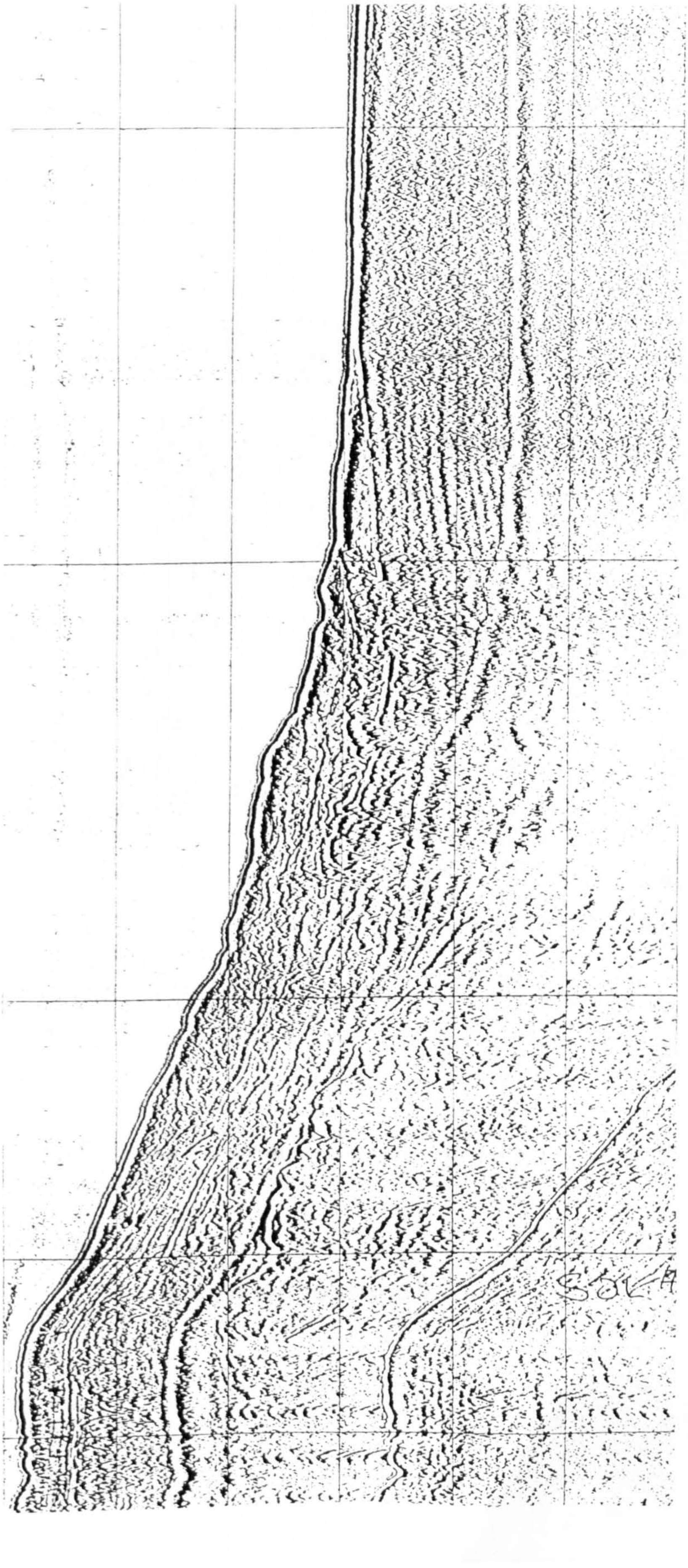

Figure 8.7 (c). 5in^2 air-gun profile of the Roberts Bank failure wedge (line PGC93-29).

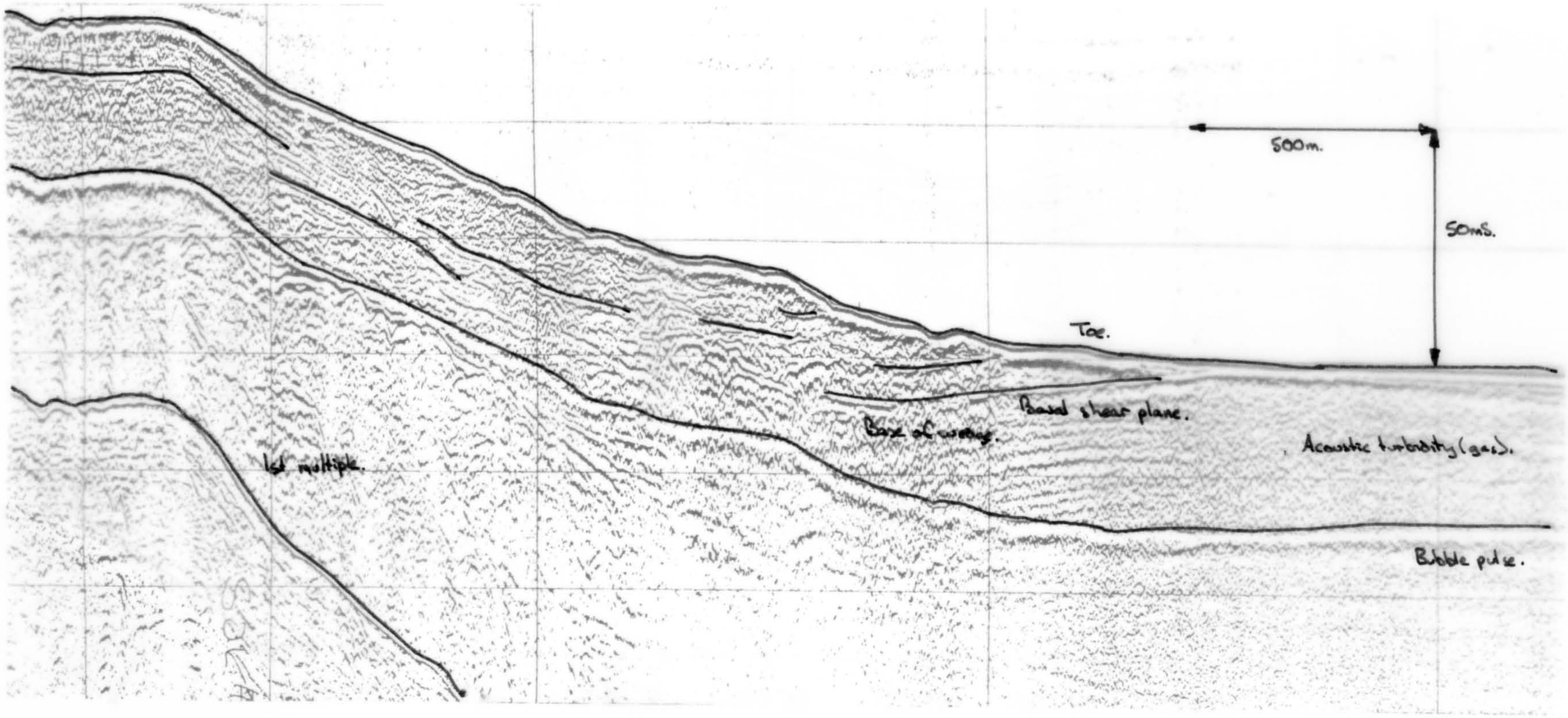

Figure 8.7 (c). 5in^2 air-gun profile of the Roberts Bank failure wedge (line PGC93-29).

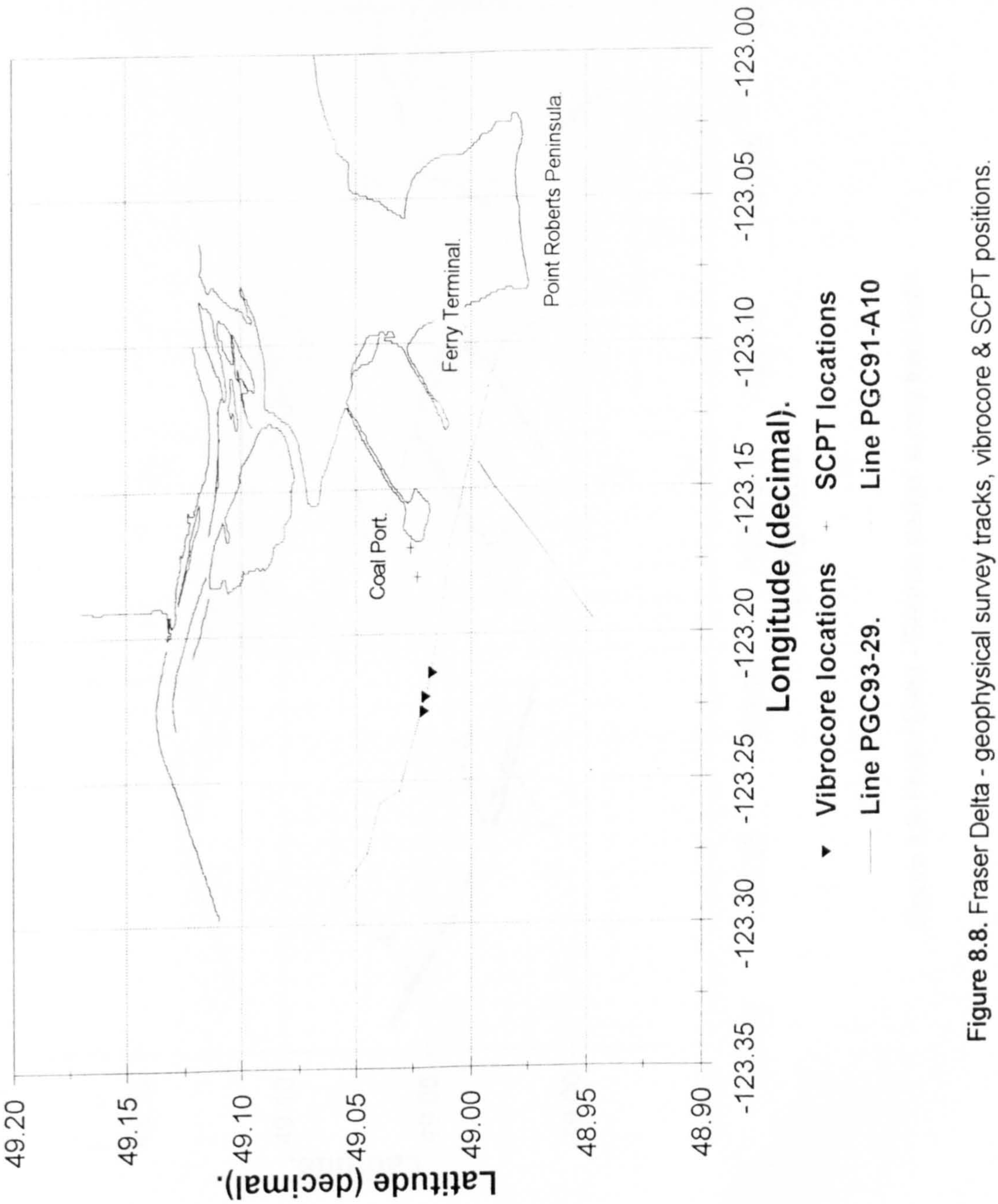

Figure 8.8. Fraser Delta - geophysical survey tracks, vibrocore & SCPT positions.

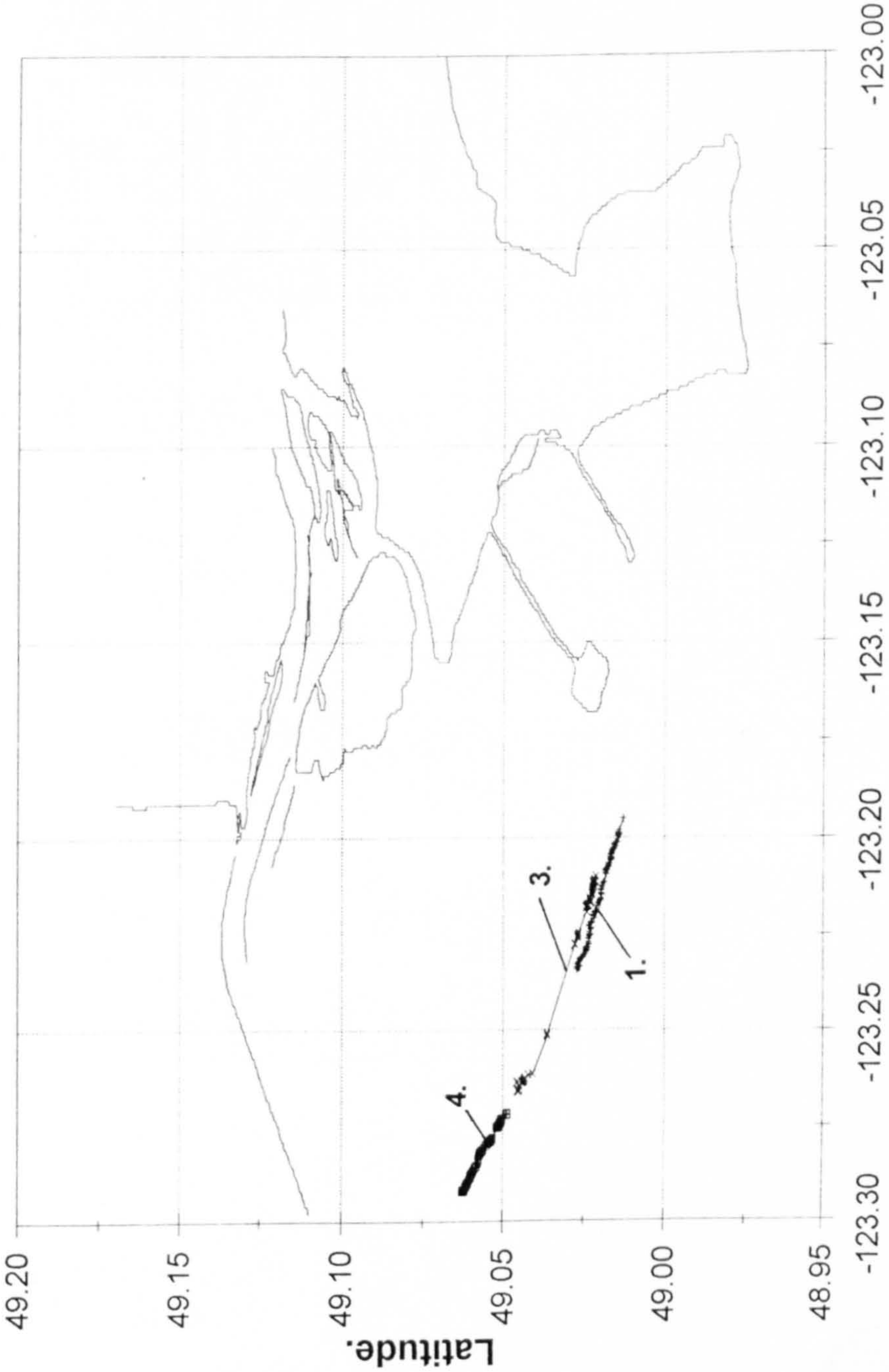

Figure 8.9. Fraser Delta - 'Seismic sledge' survey track lines.

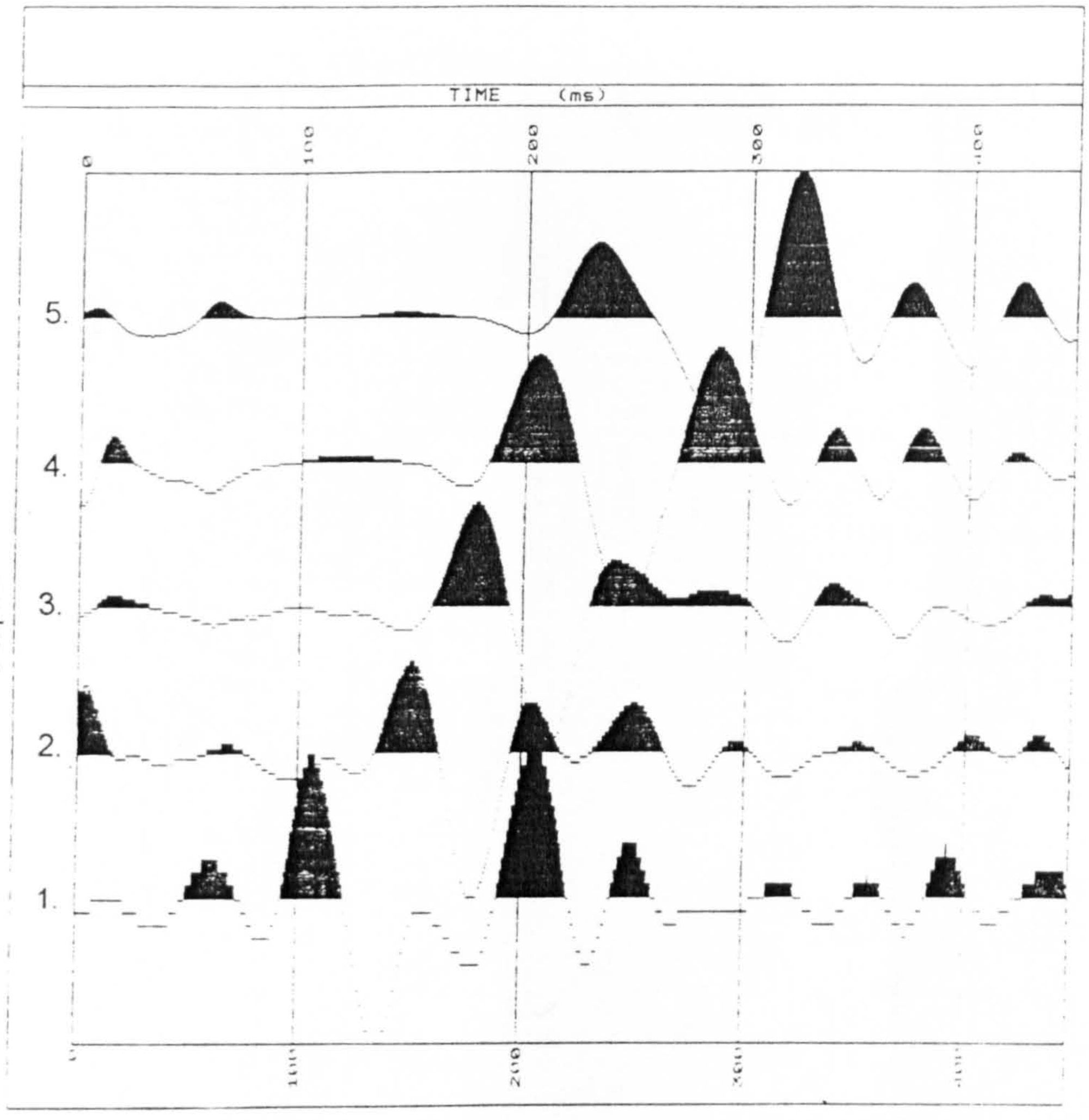

Figure 8.10. Example filtered, normalised, pseudo-underway sledge shear wave record.

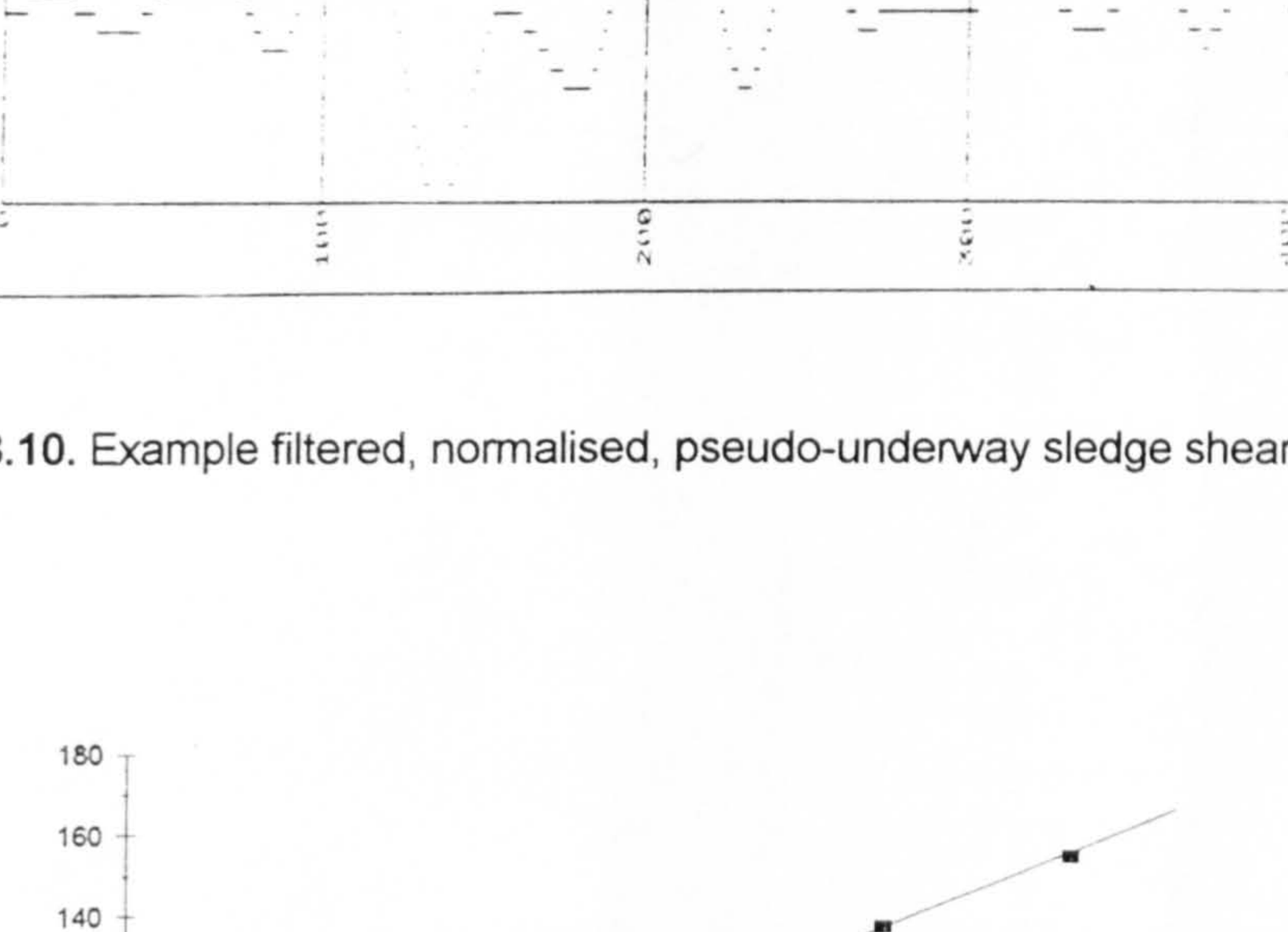

Figure 8.11. Typical time - distance graph derived from pseudo-underway sledge data.


30ms.
Sand waves.
1st multiple.

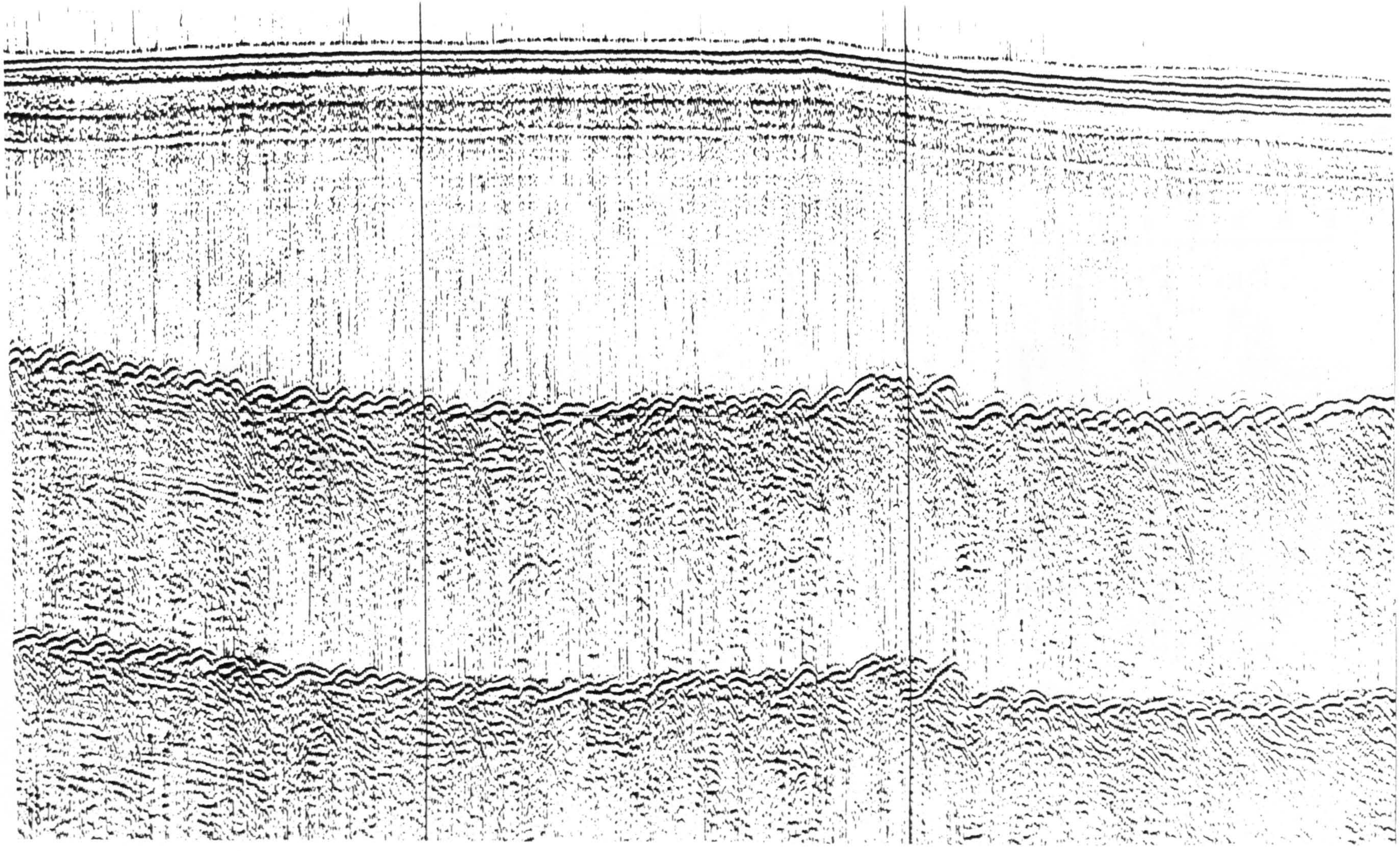

Figure 8.12. Typical section of Huntec DTS boomer record, along a section of sledge transect.

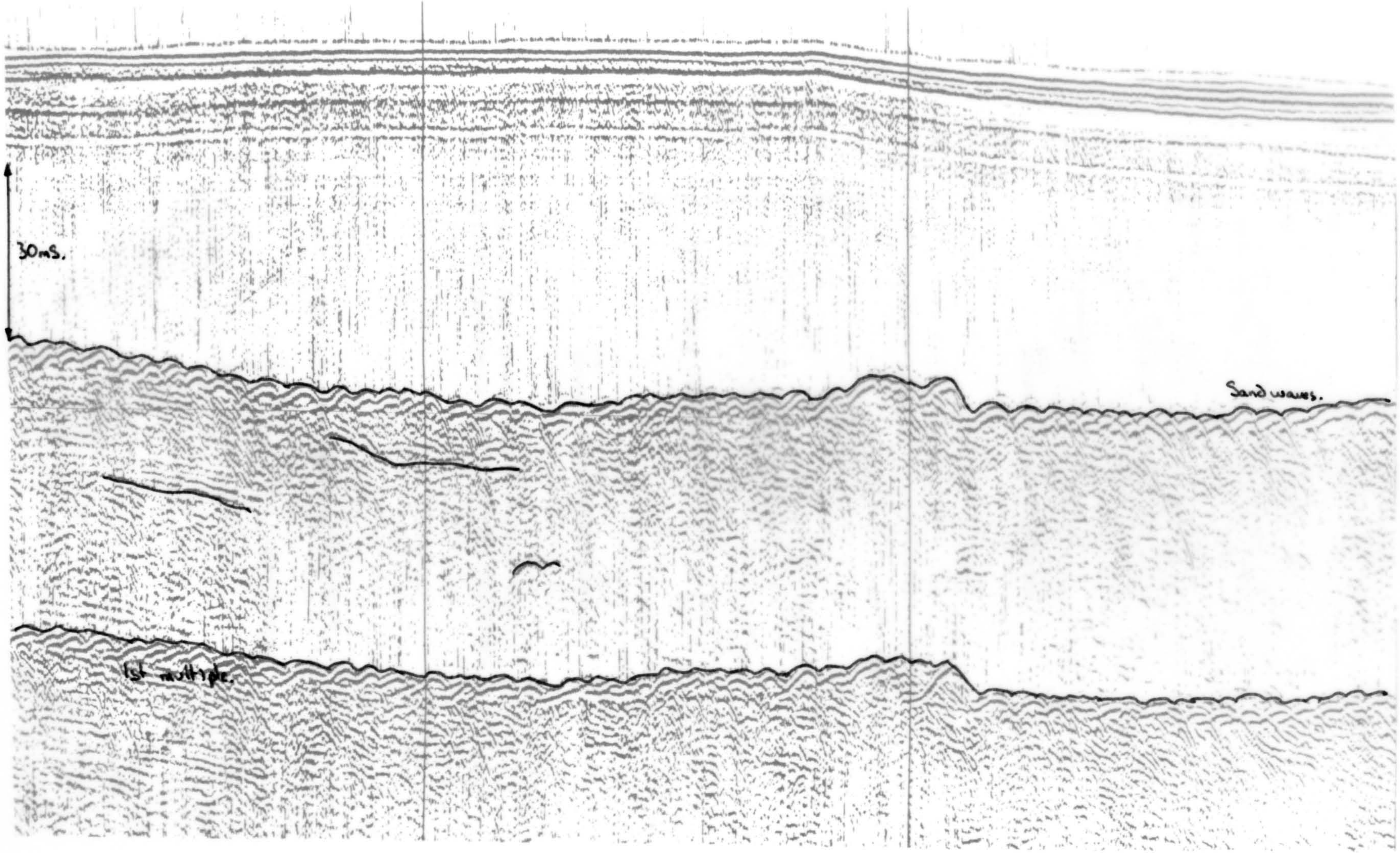

Figure 8.12. Typical section of Huntec DTS boomer record, along a section of sledge transect.

a.

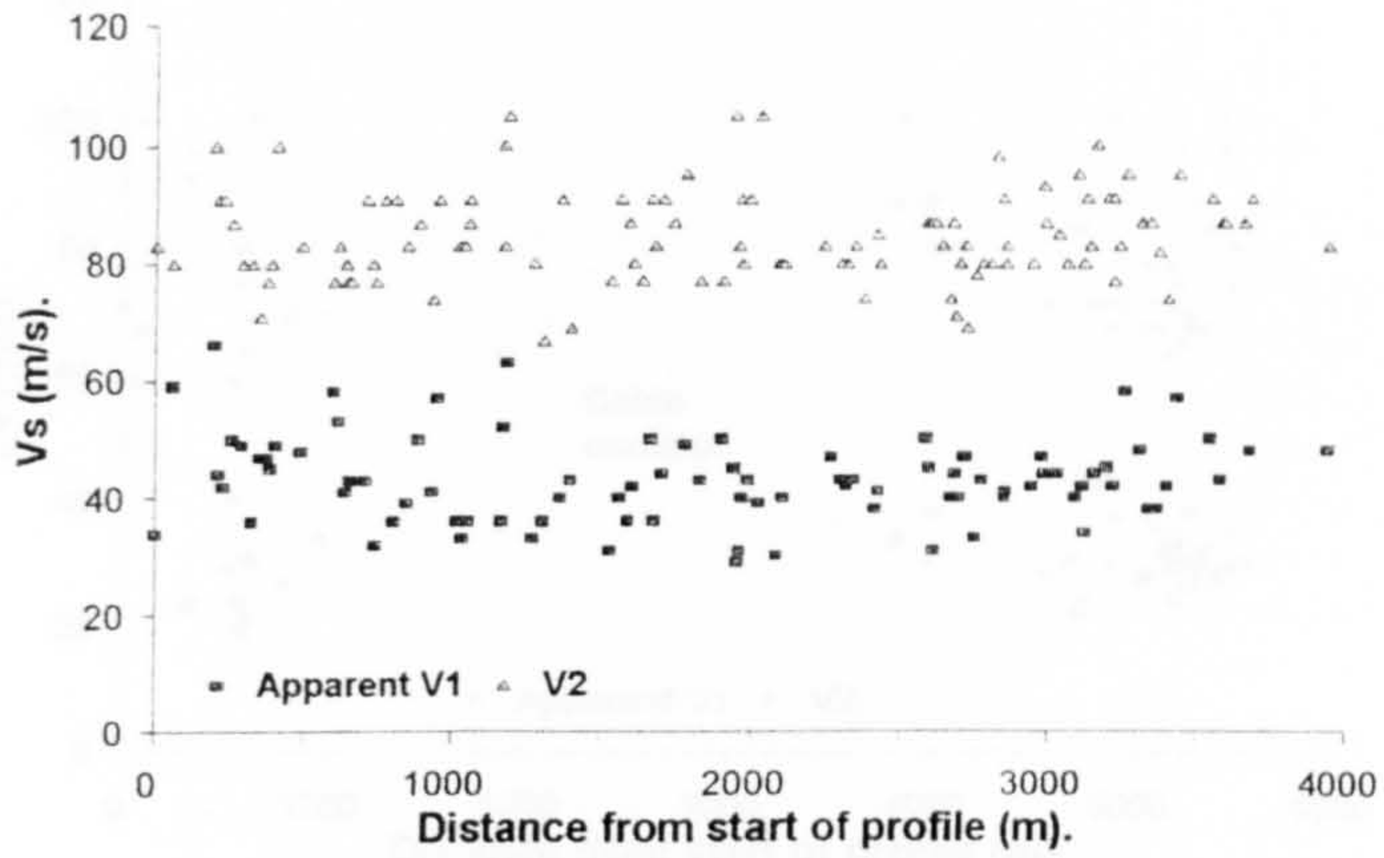

b.

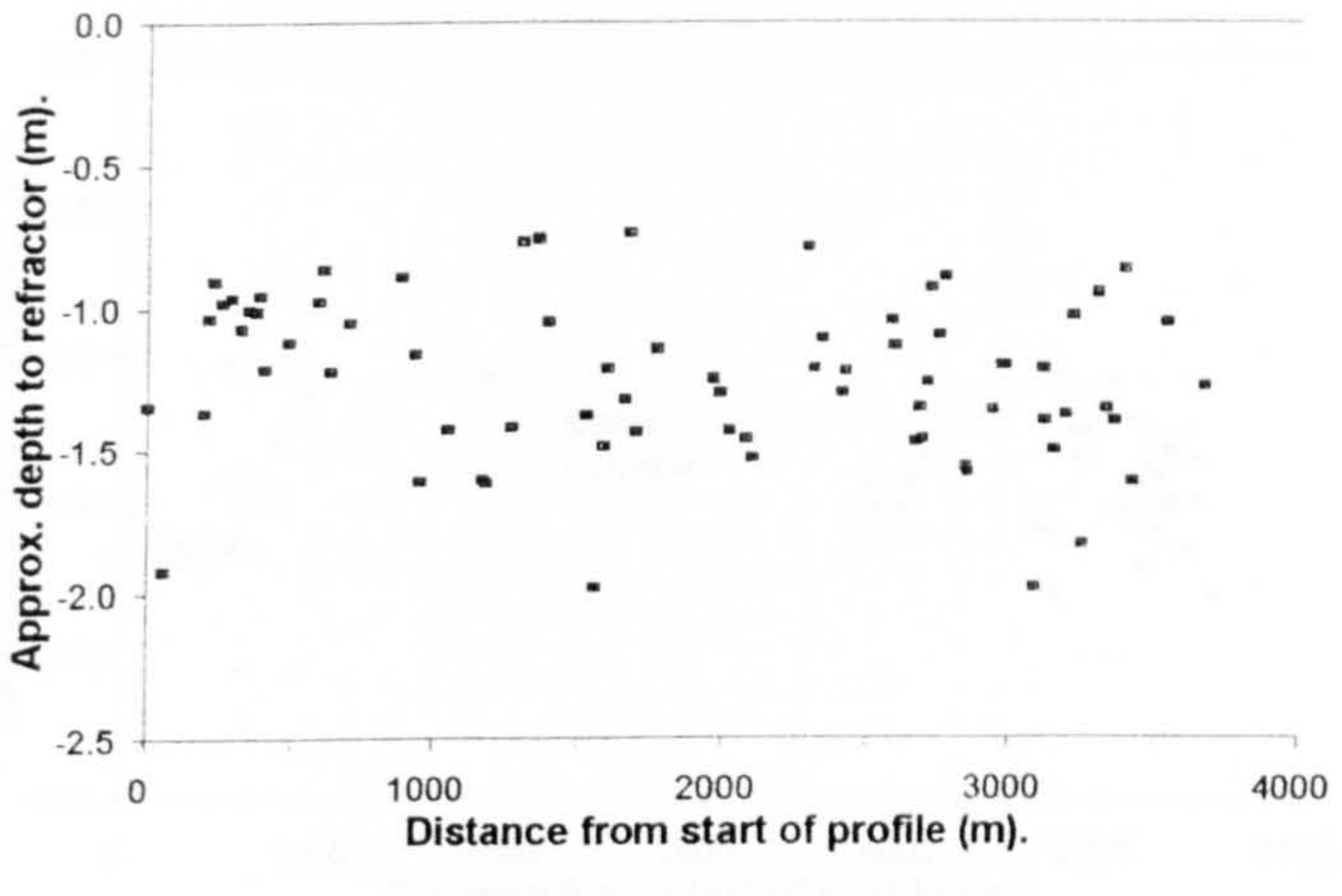

Figure 8.13. a. Shear wave velocity profile, deployment 1.
Figure 8.13. b. Approximate depth to refractor, deployment 1.

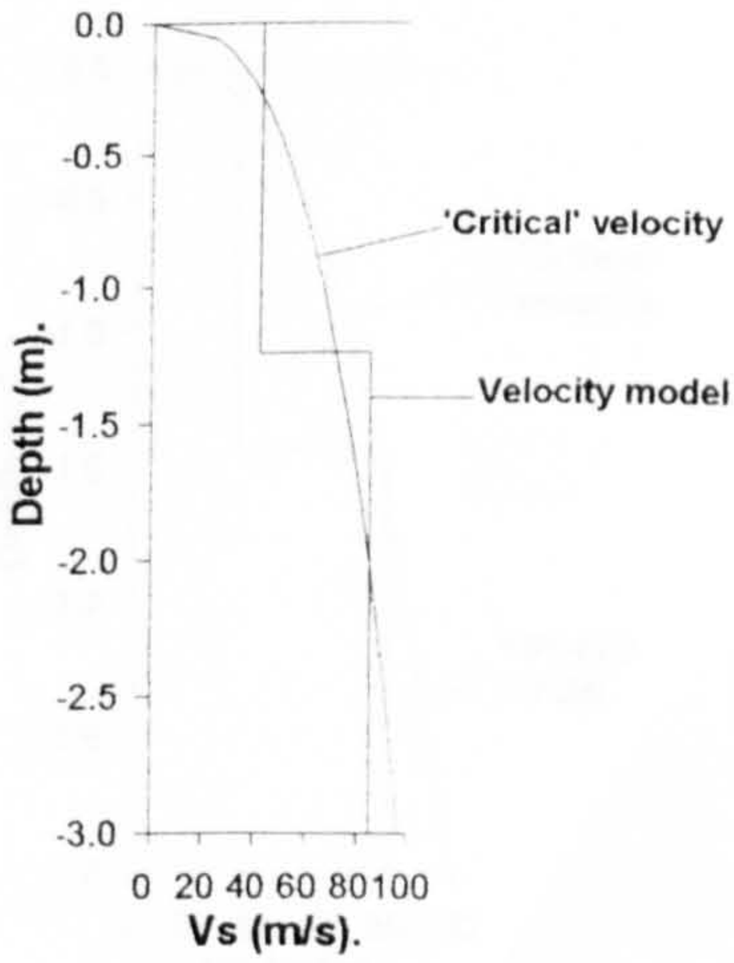

Figure 8.14. 'Average' velocity-depth model, deployment 1.

a.

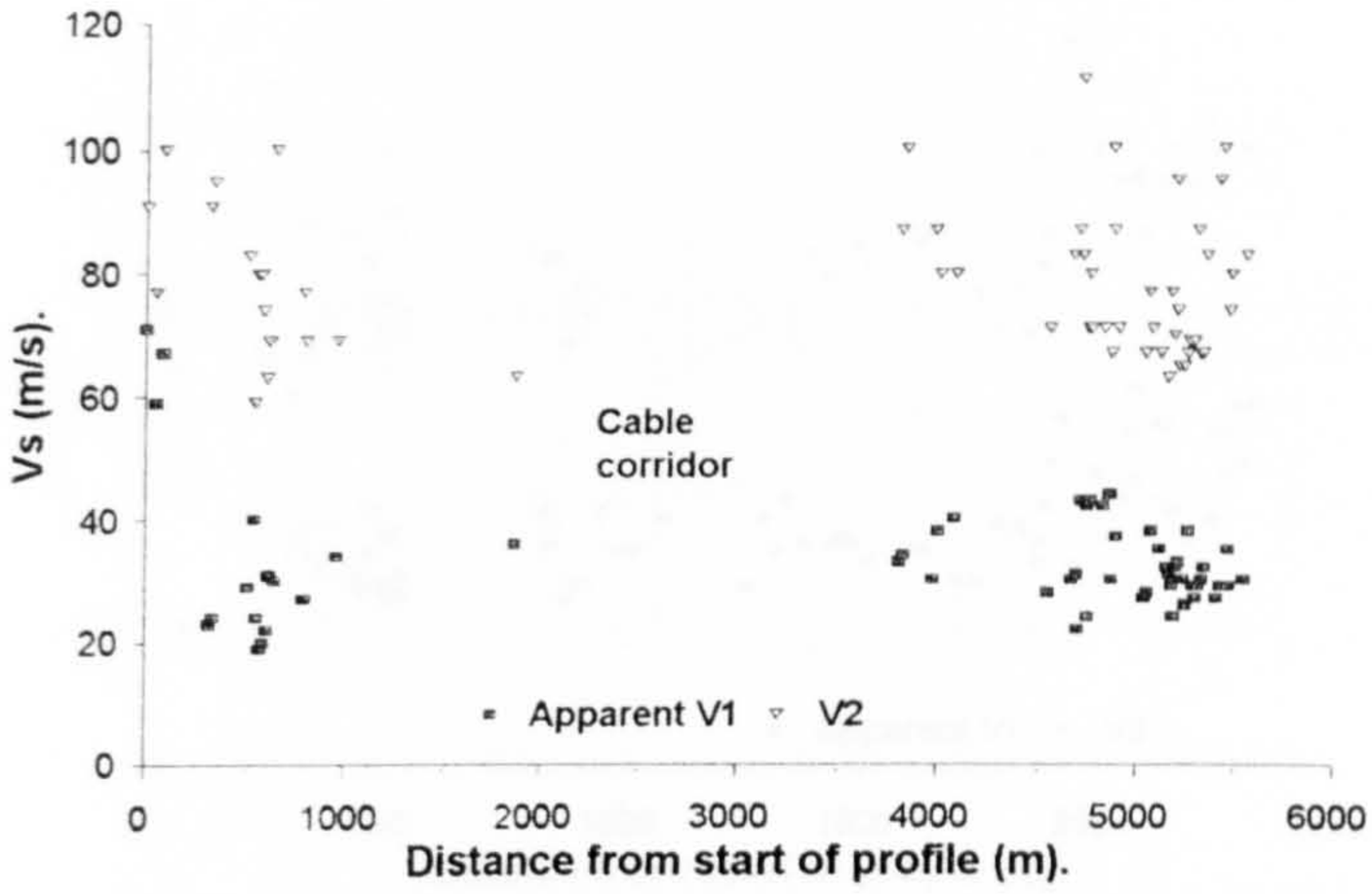

b.

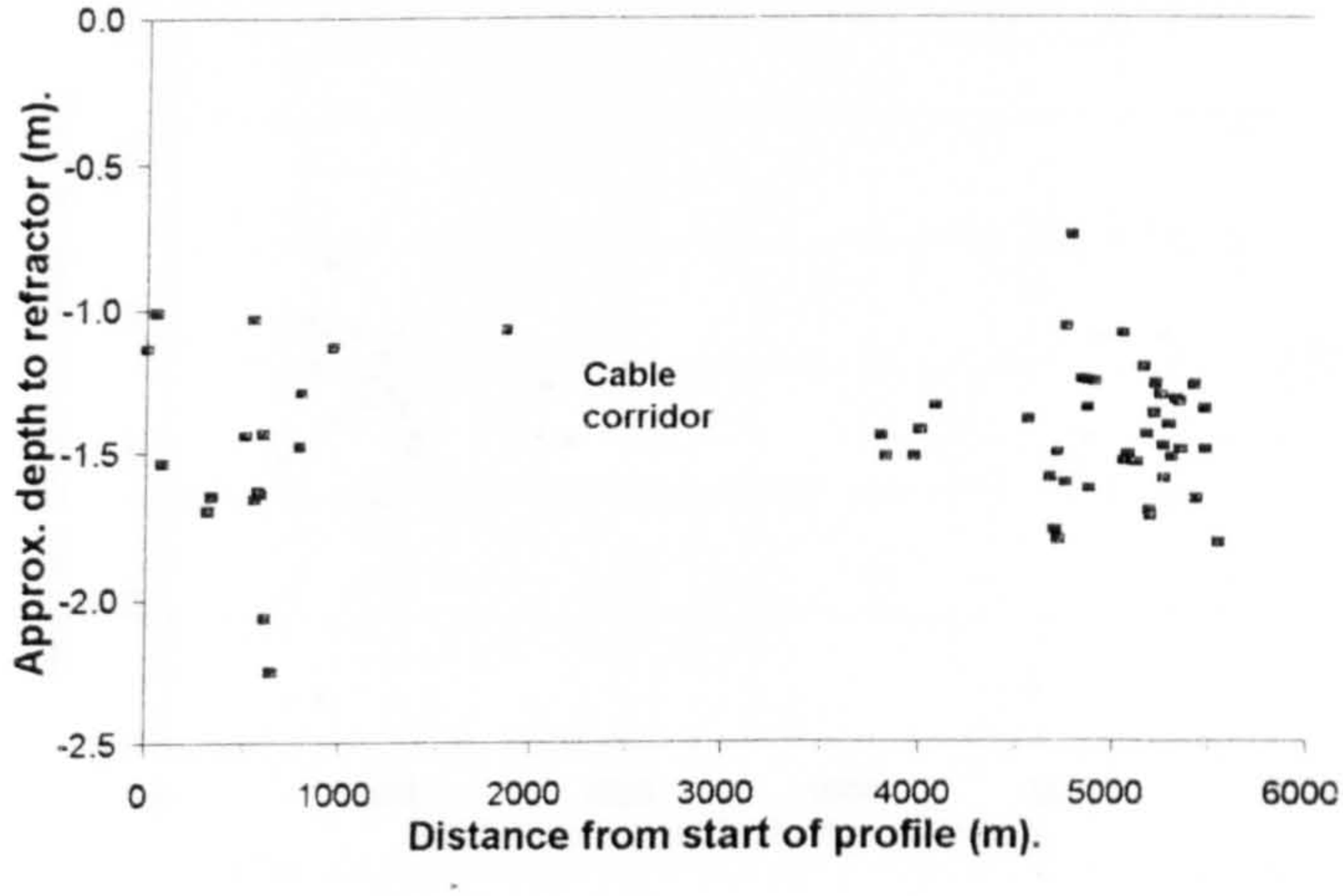

Figure 8.15. a. Shear wave velocity profile, deployment 3.
Figure 8.15. b. Approximate depth to refractor, deployment 3.

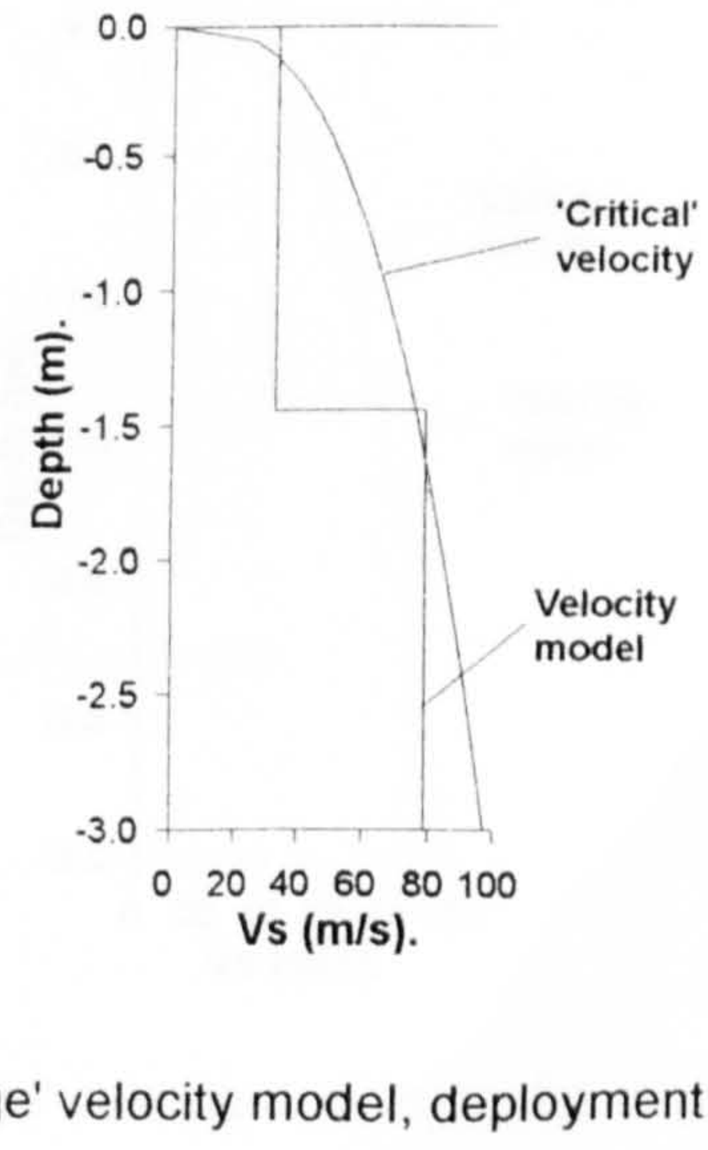

Figure 8.16. 'Average' velocity model, deployment 3.

a.

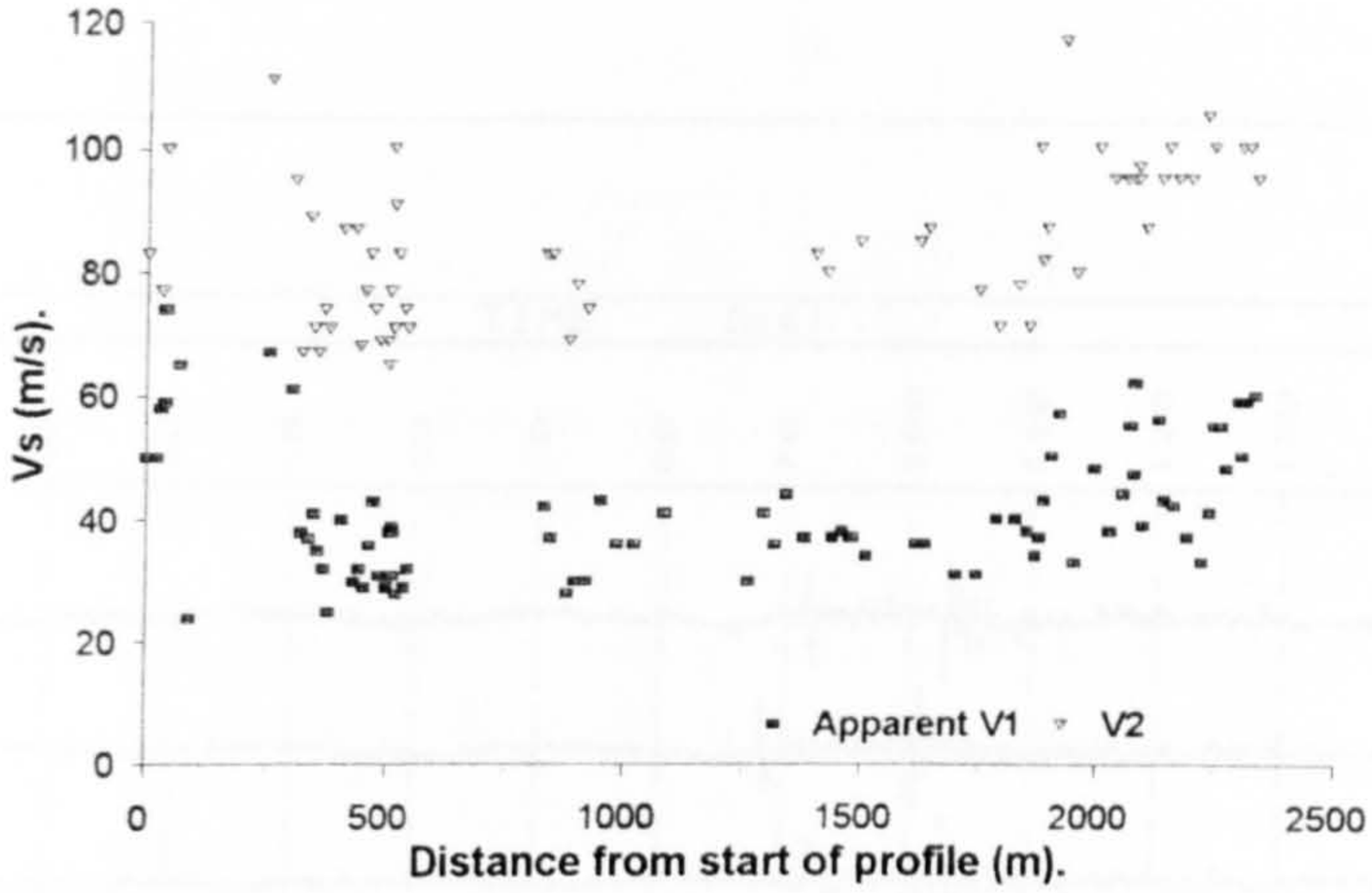

b.

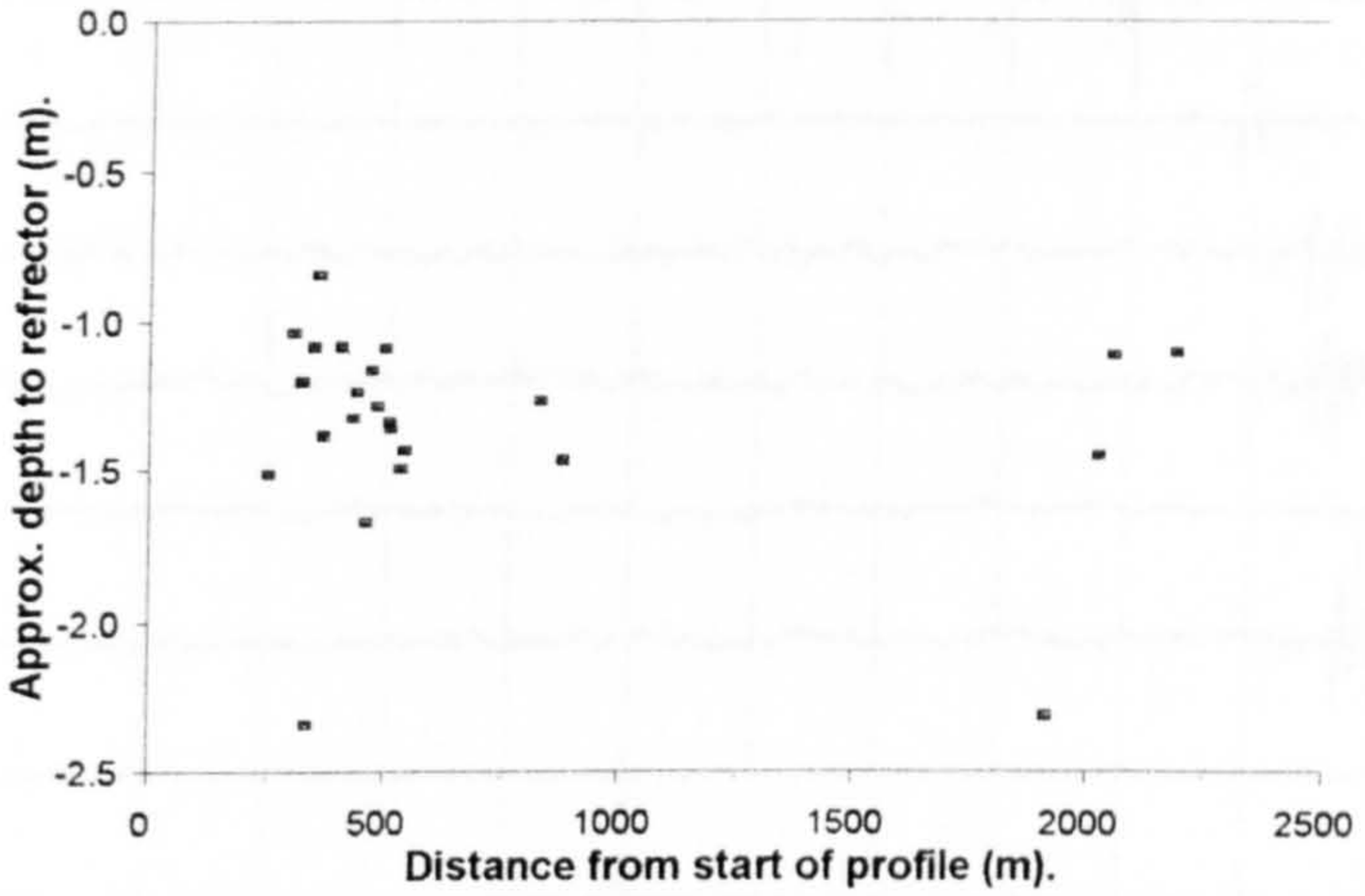

Figure 8.17. a. Shear wave velocity profile, deployment 4.
Figure 8.17. b. Approximate depth to refractor, deployment 4.

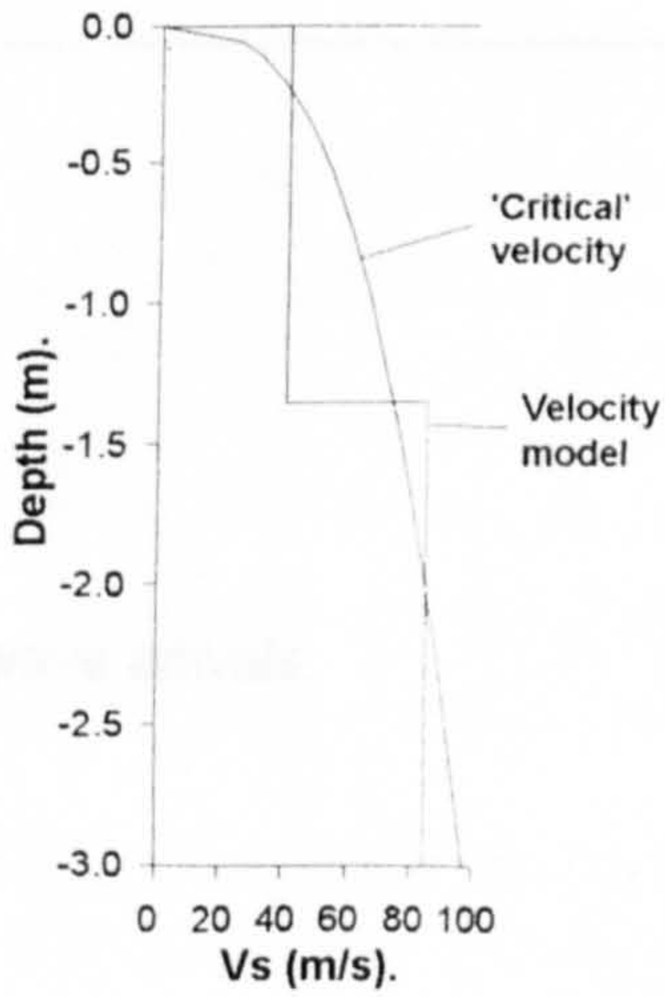

Figure 8.18. 'Average' velocity - depth model, deployment 4.

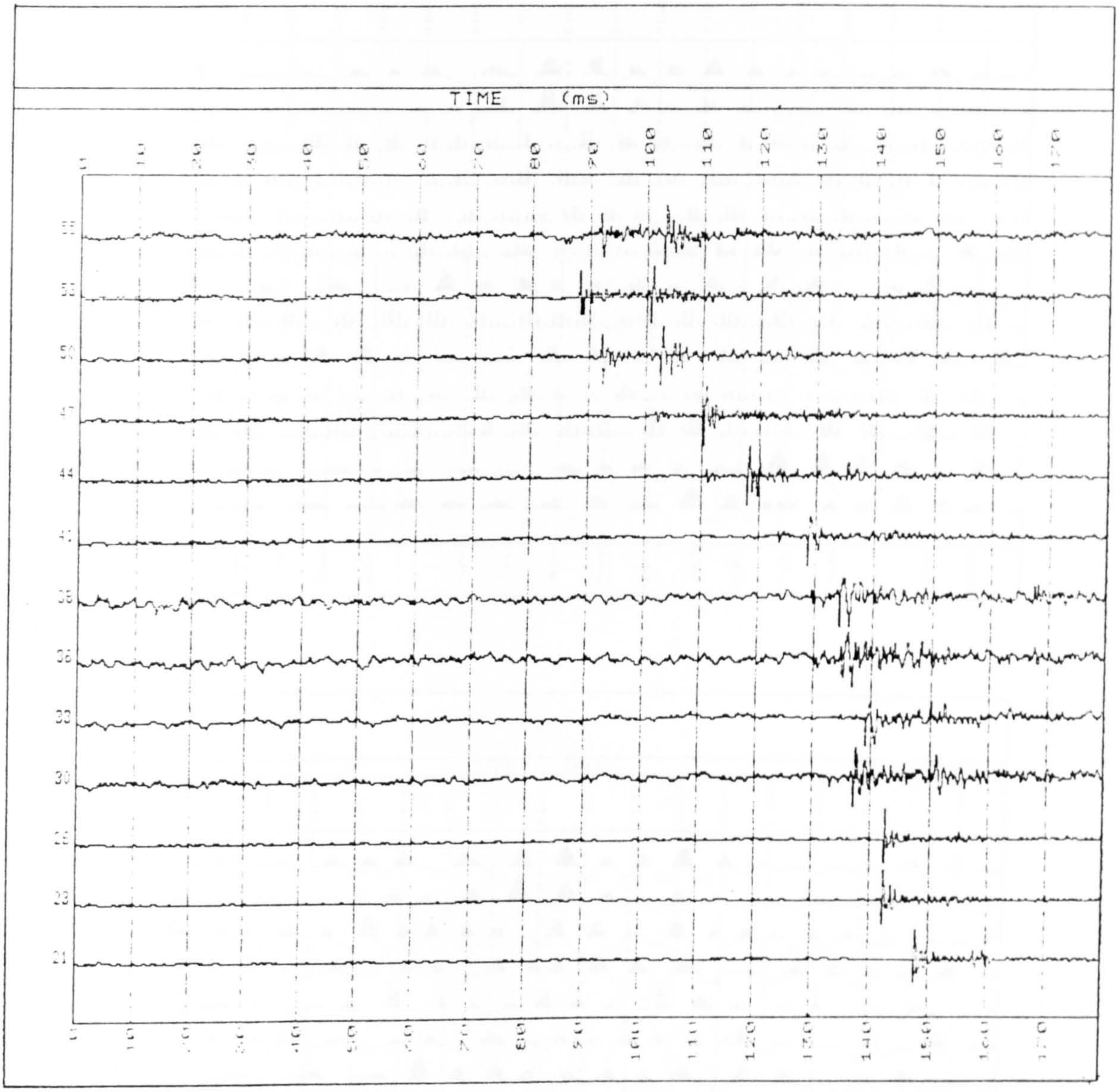

Figure 8.19. Long offset data - P-wave arrivals.

a.

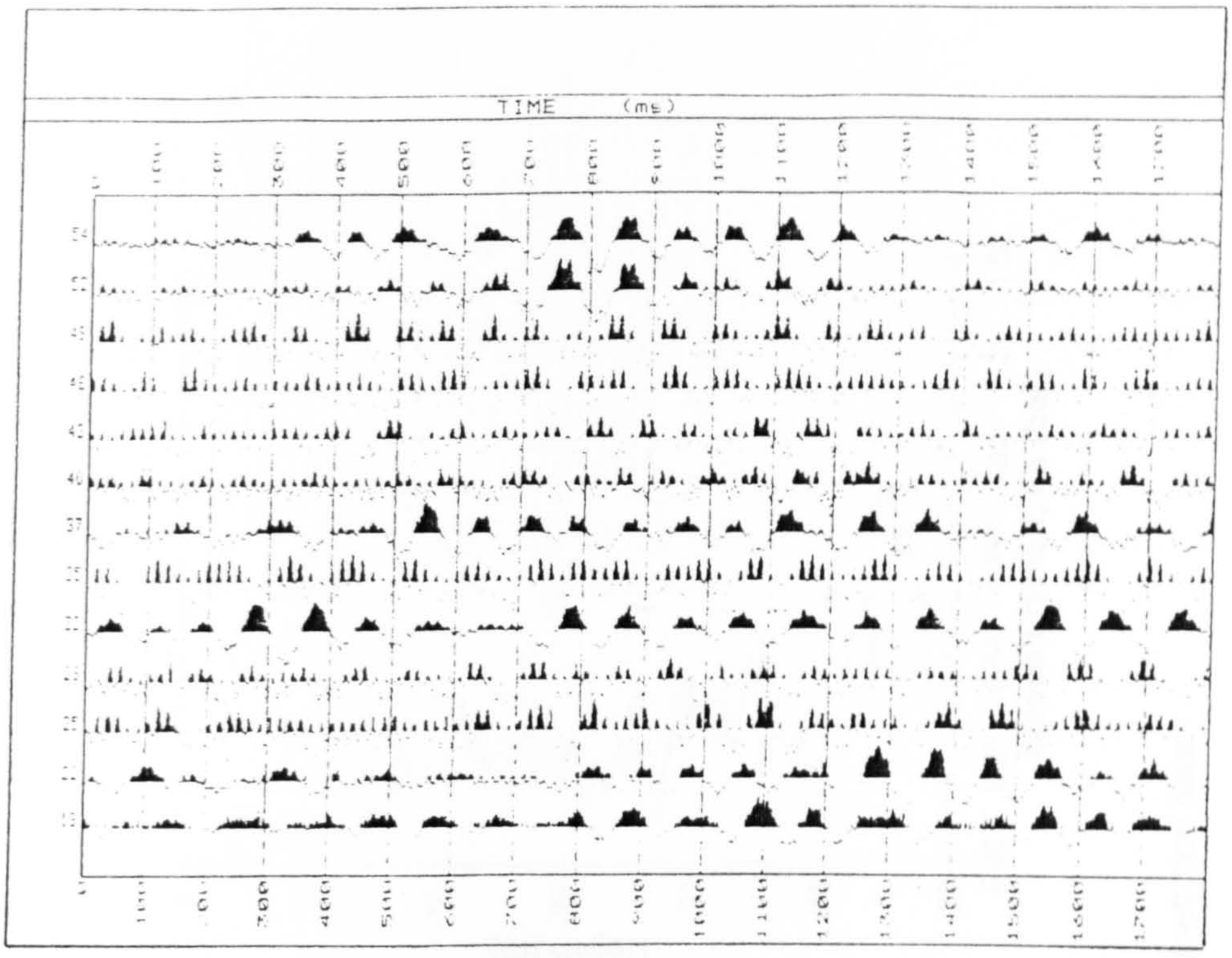

b.

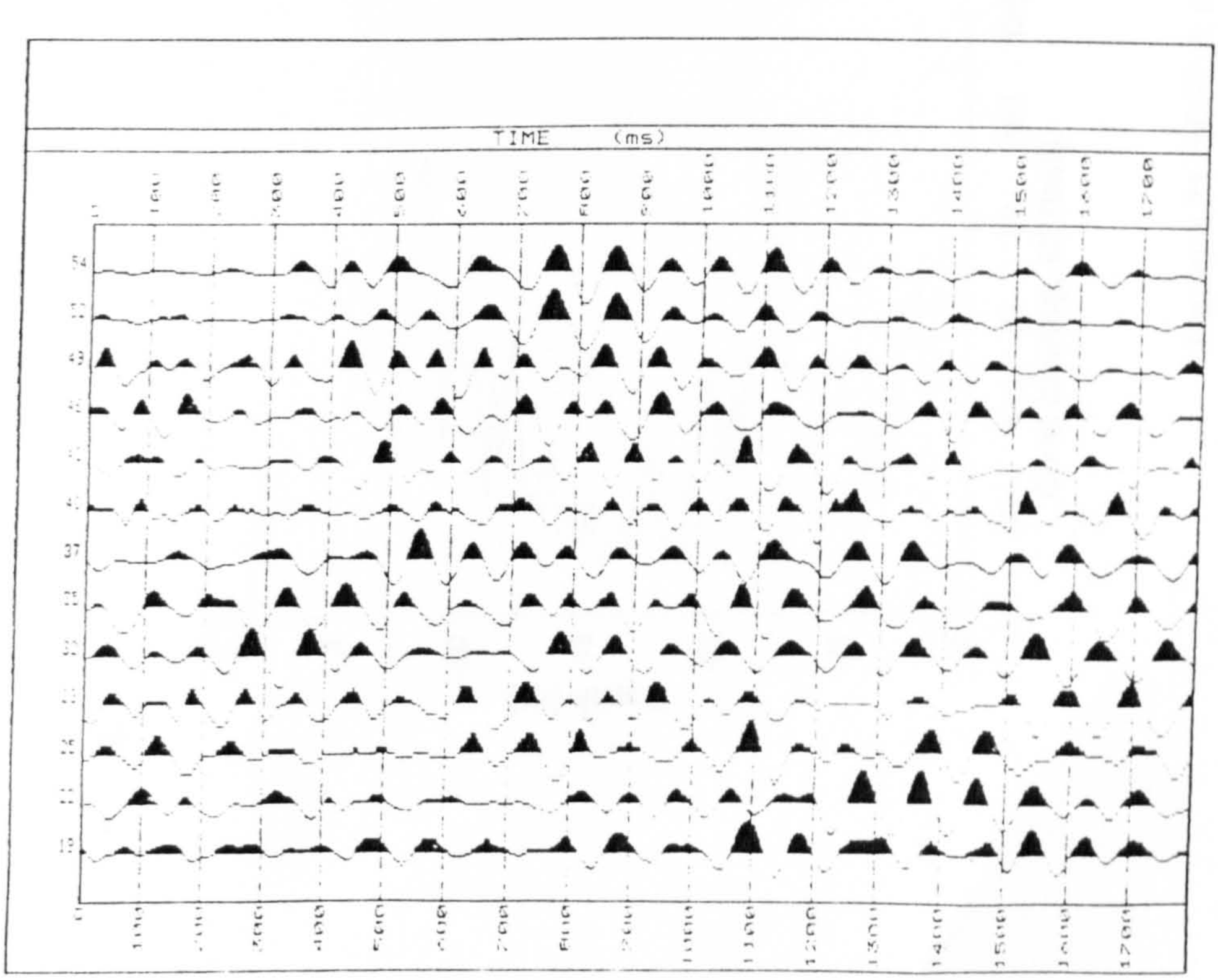

Figure 8.20. Unfiltered (a) and filtered (b) long offset shear wave data.

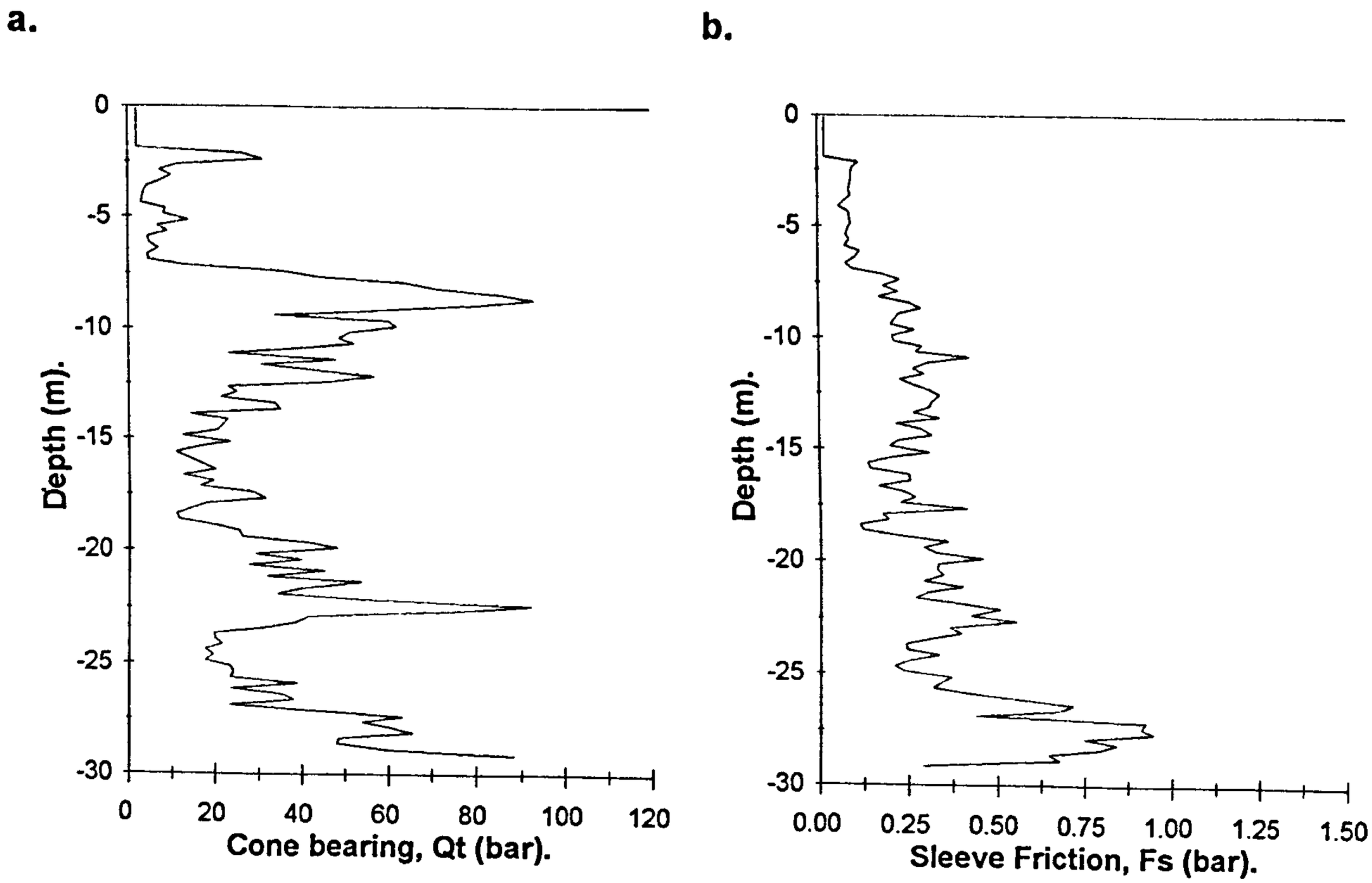

Figure 8.21. SCPT 6; raw penetration data.

c.

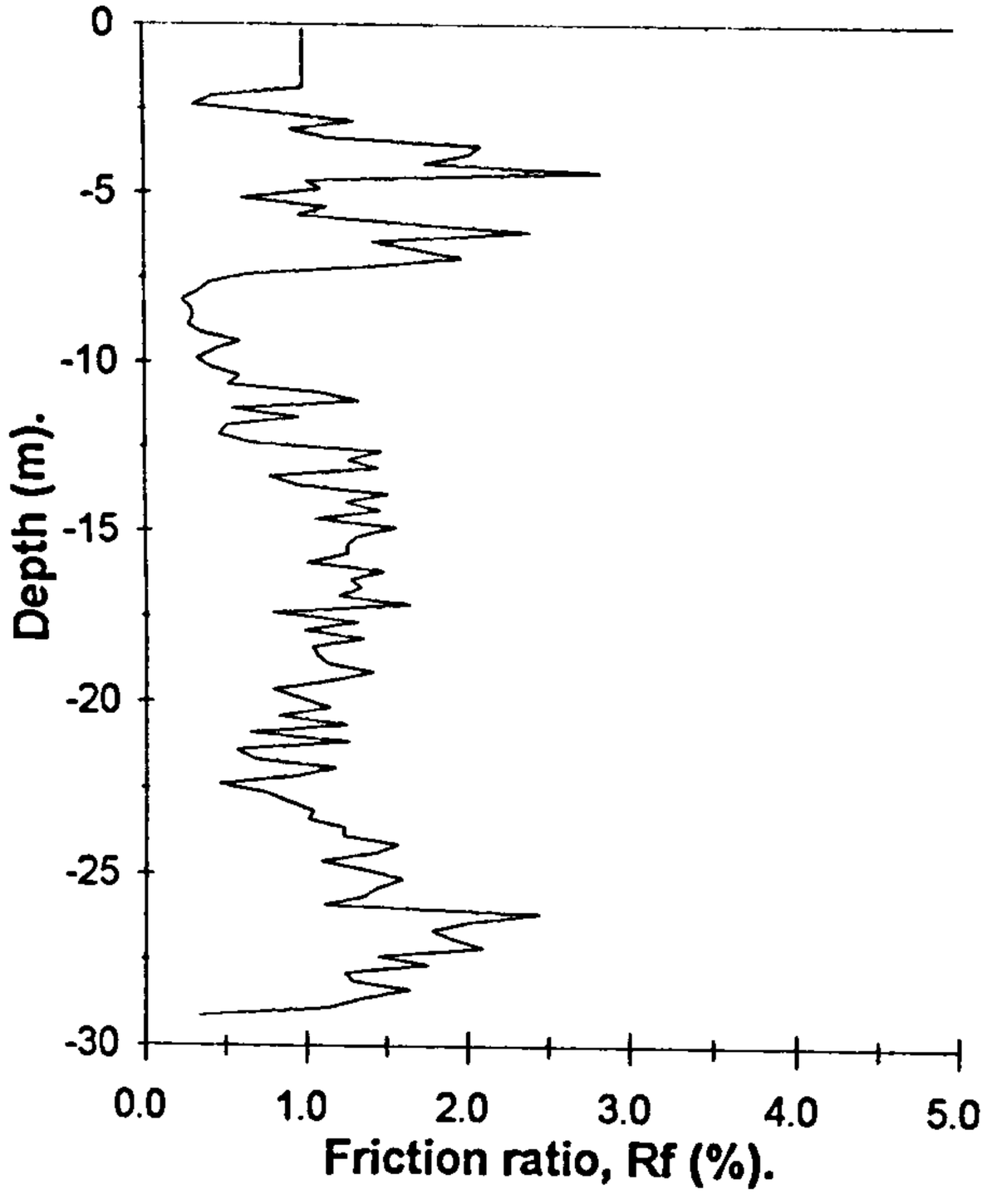

d.

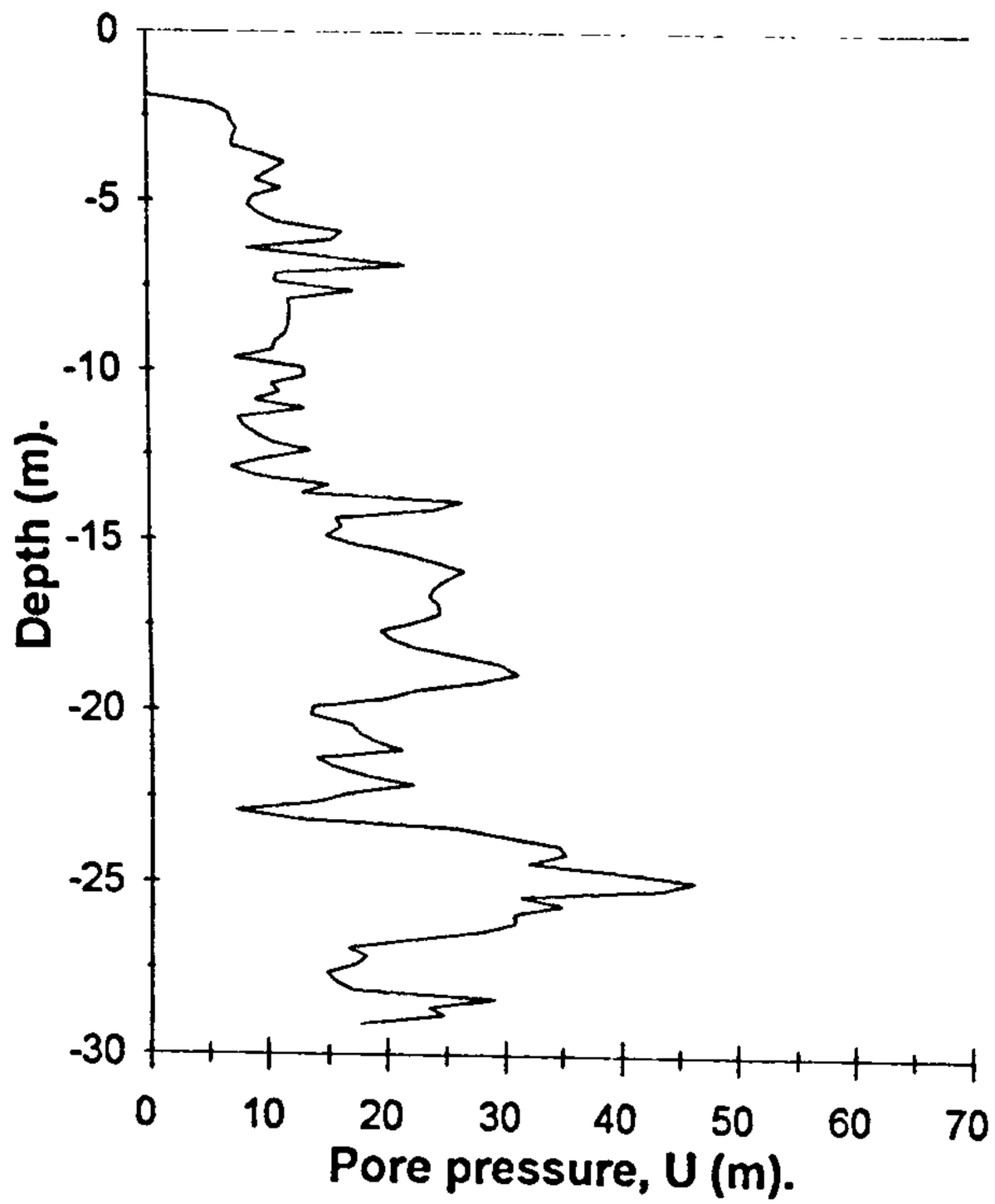

Figure 8.21 (cont). SCPT 6; raw penetration data.

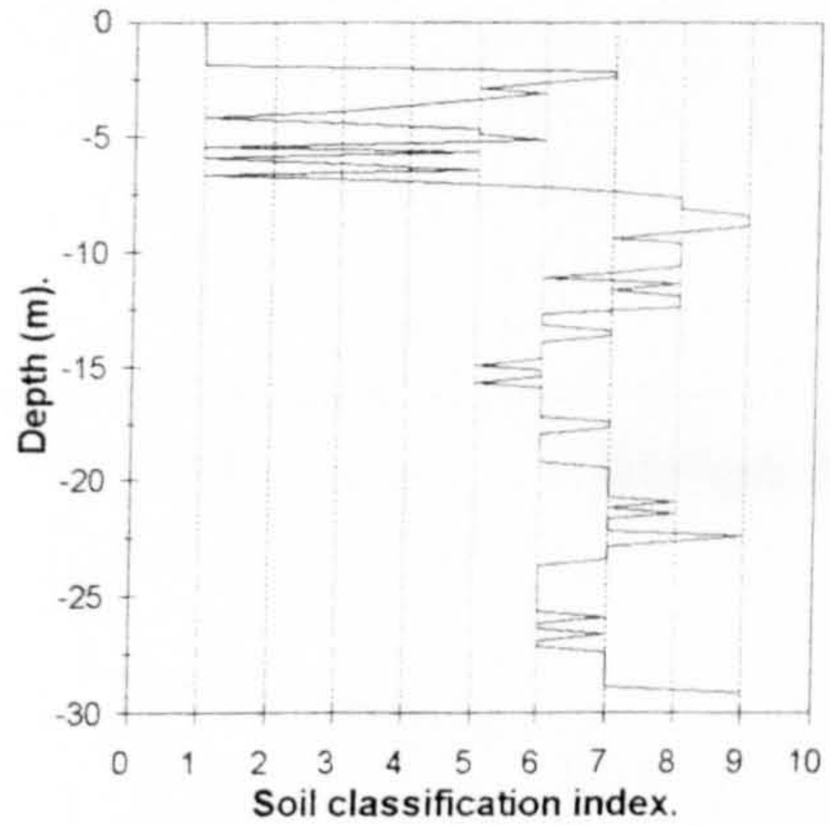

Figure 8.22. Soil zone classification, SCPT6.

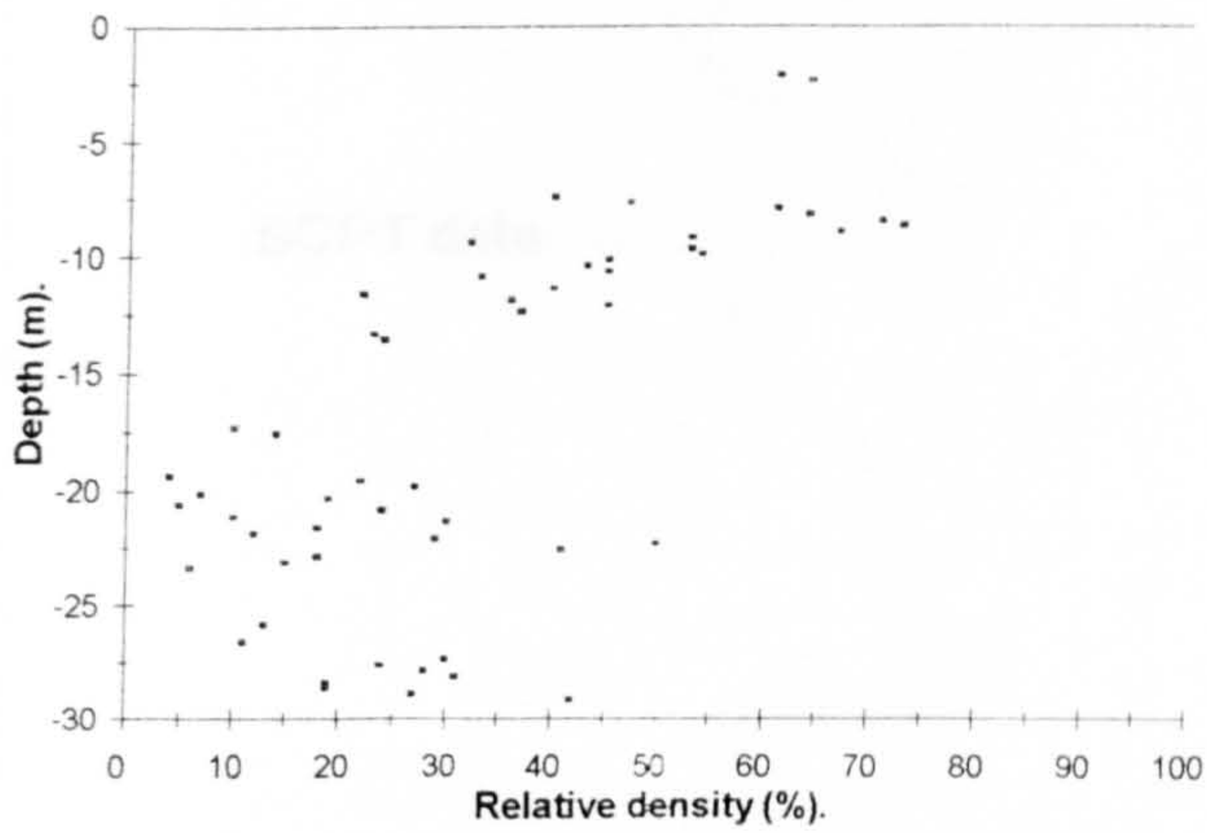

Figure 8.23. Inferred relative density, SCPT6.

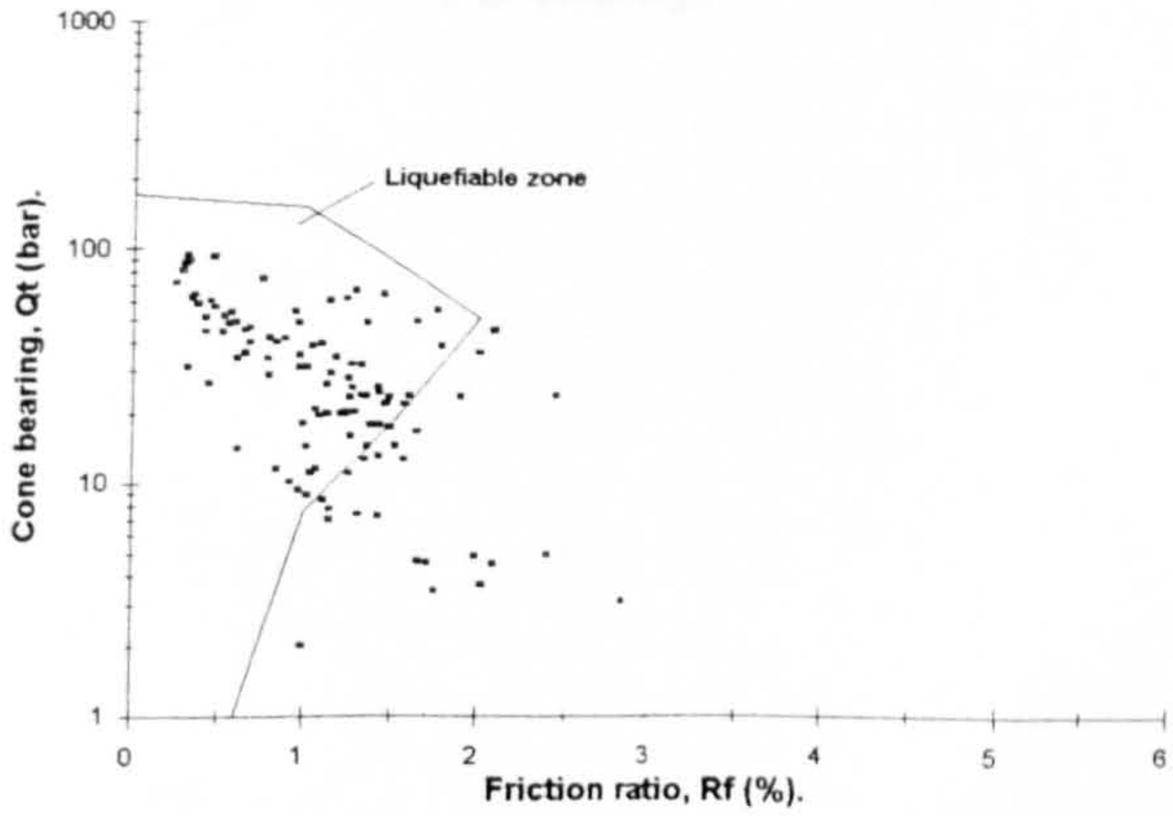

Figure 8.24. CPT soil classification chart, SCPT6.
(after Robertson & Campanella, 1985).

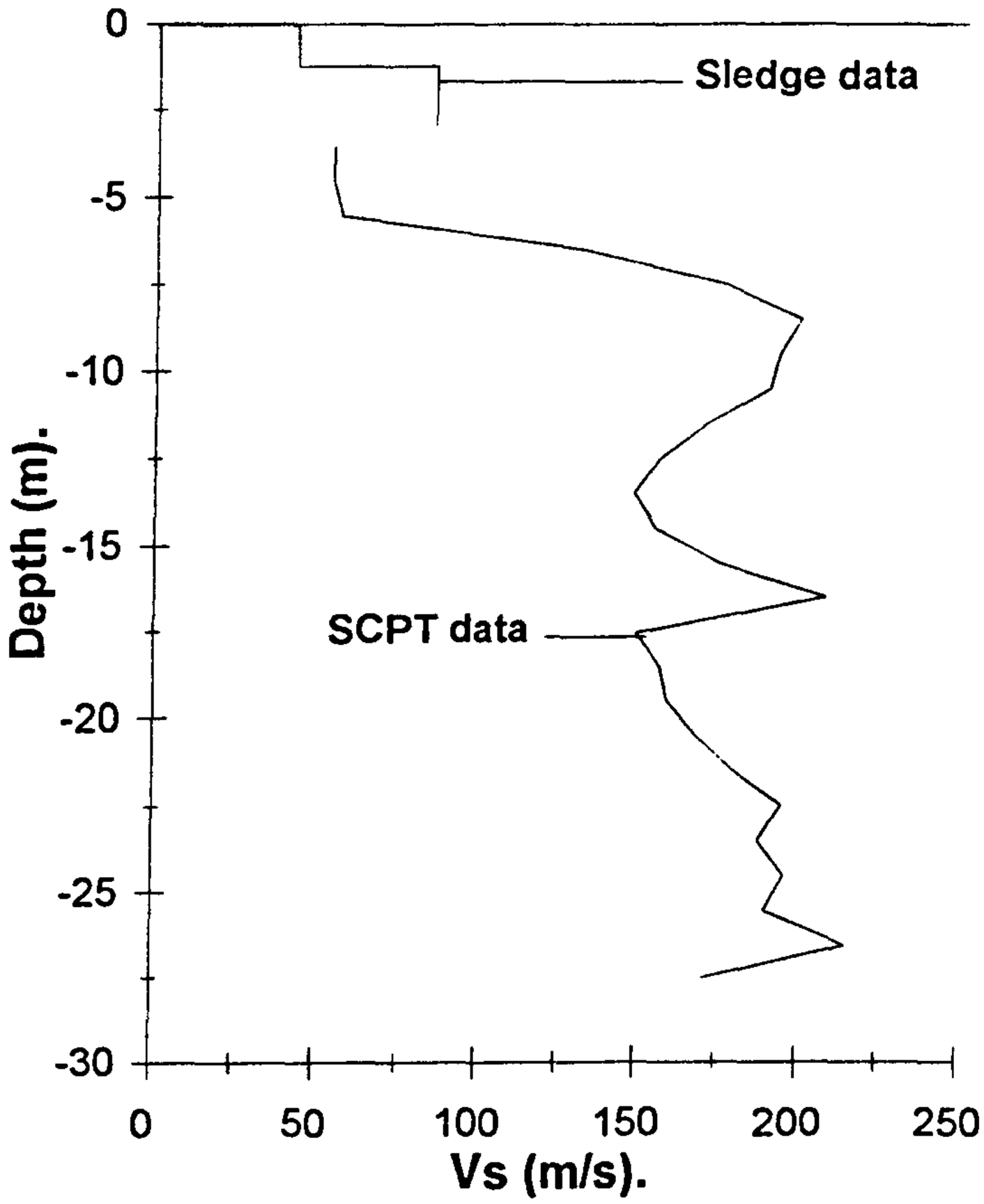

Figure 8.25. Shear wave velocity profile (SCPT 6) and surficial velocities from the 'Seismic Sledge'.

a.

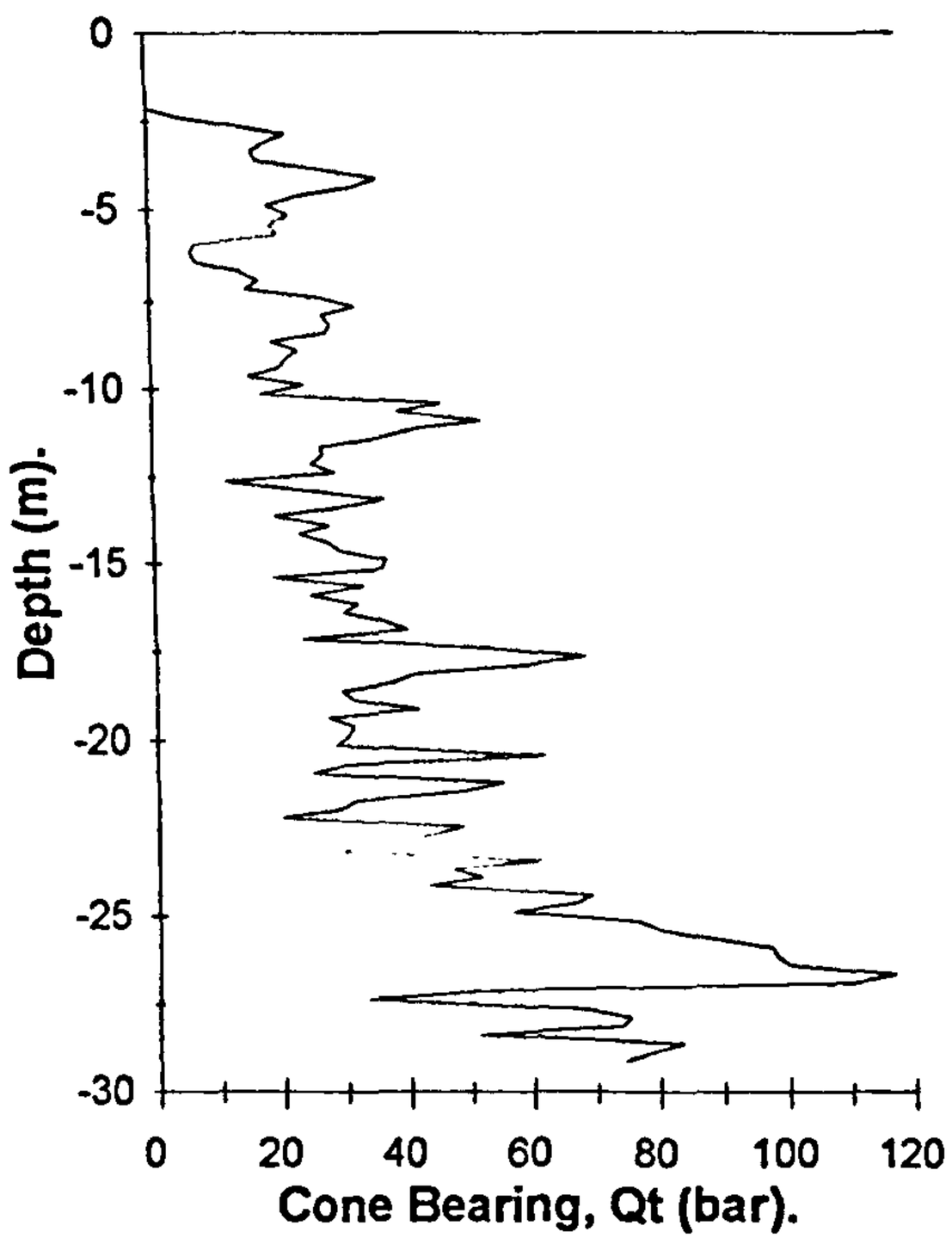

b.

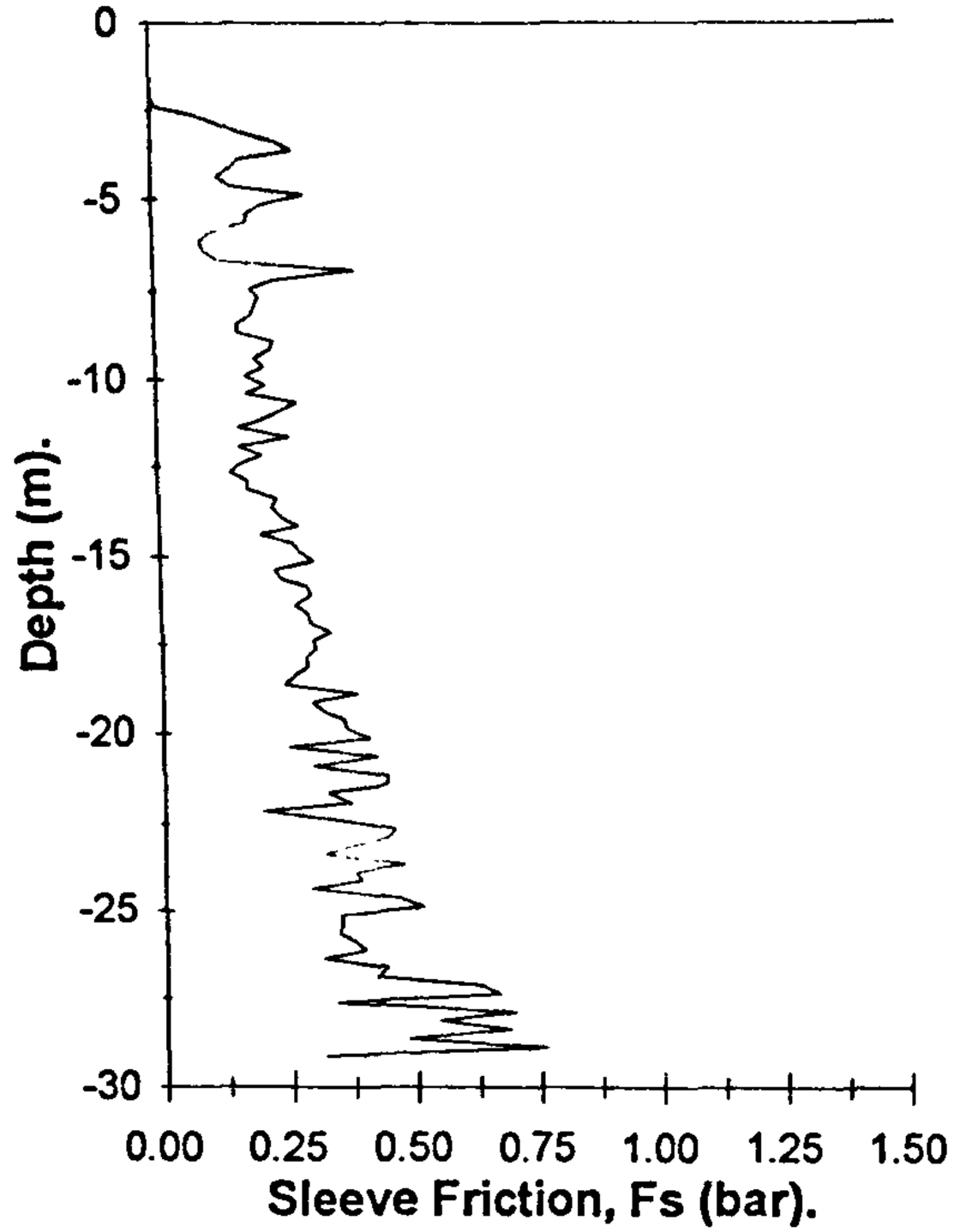

Figure 8.26. SCPT 7; raw penetration data.

c.

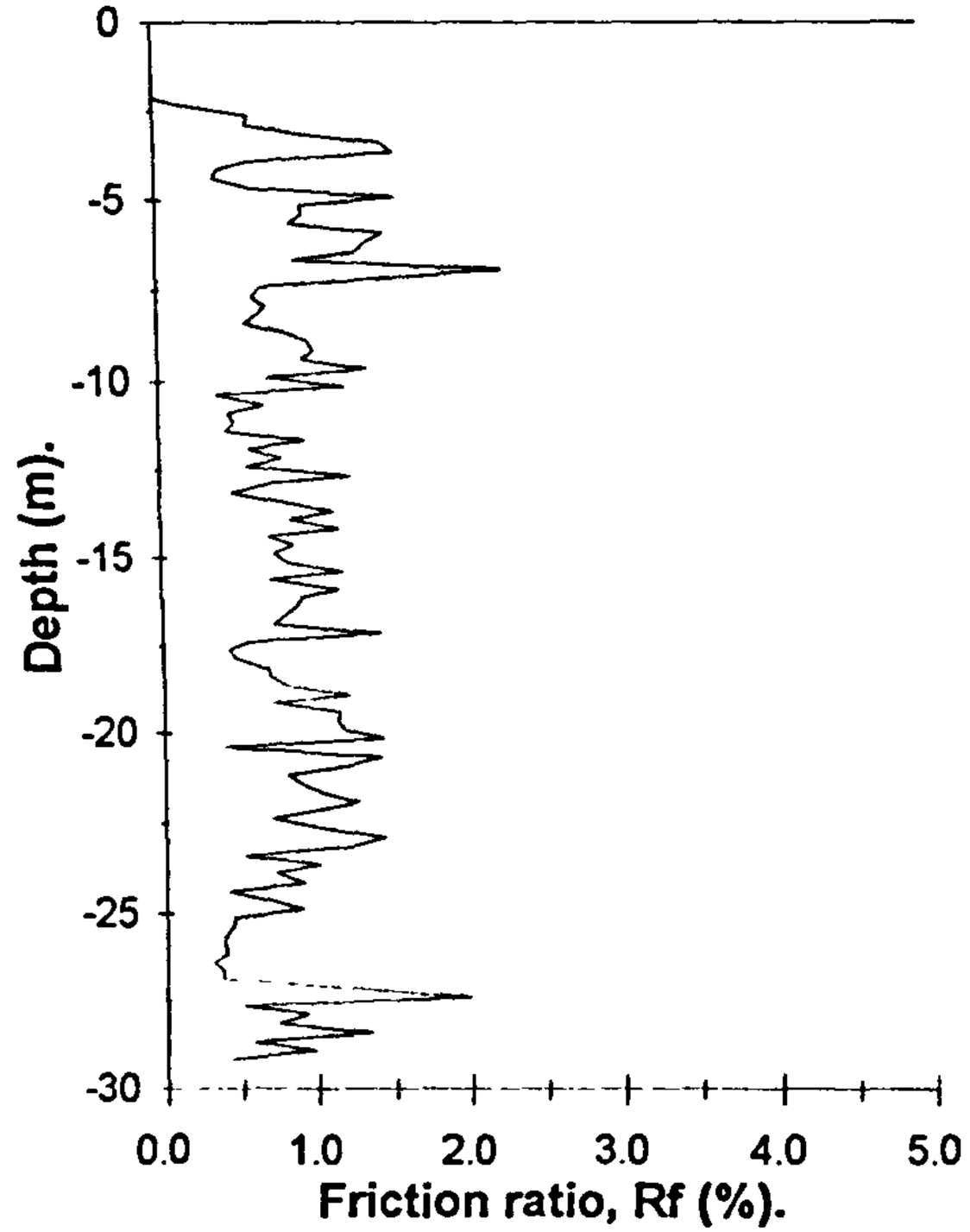

d.

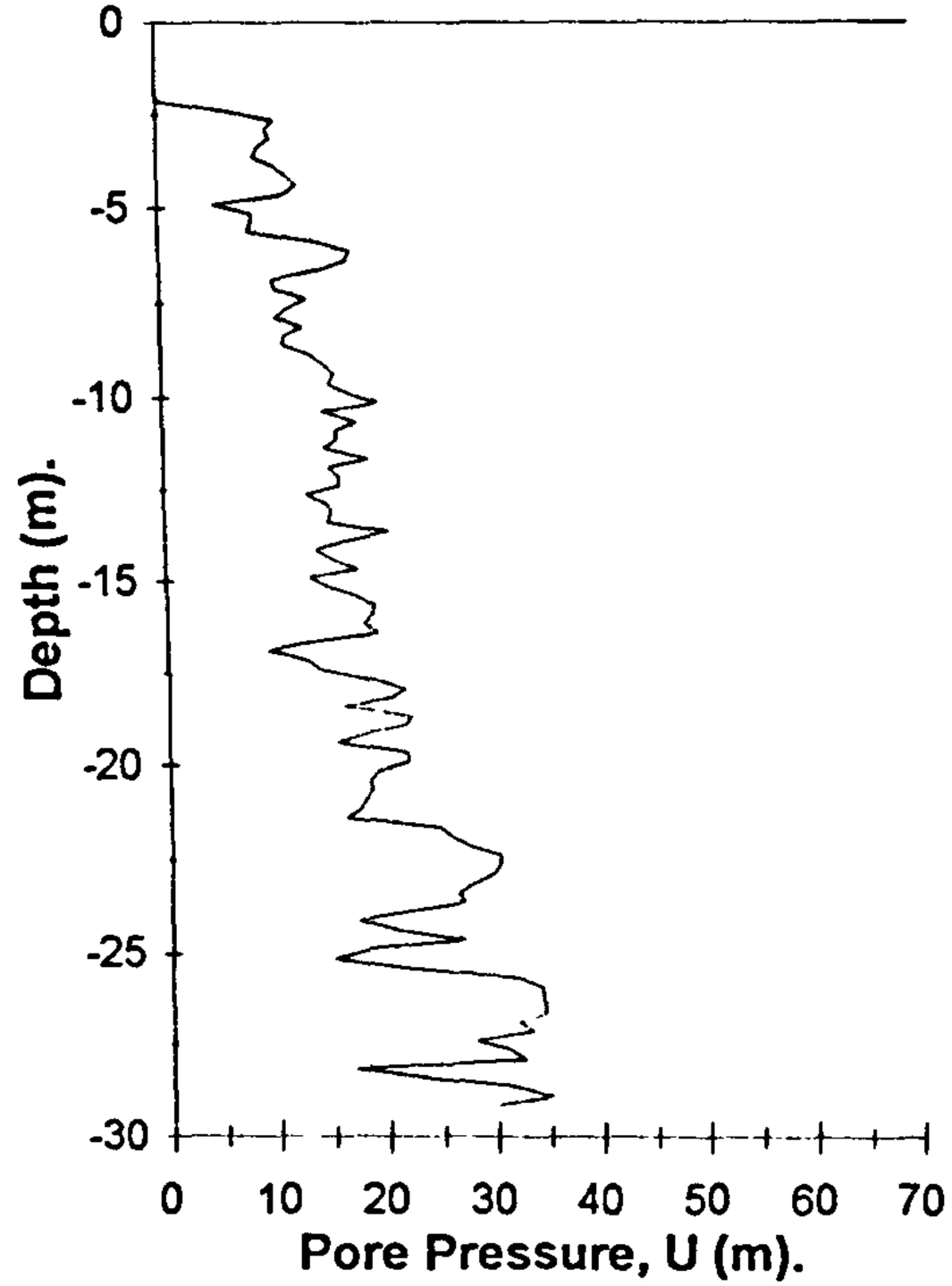

Figure 8.26 (cont). SCPT 7; raw penetration data.

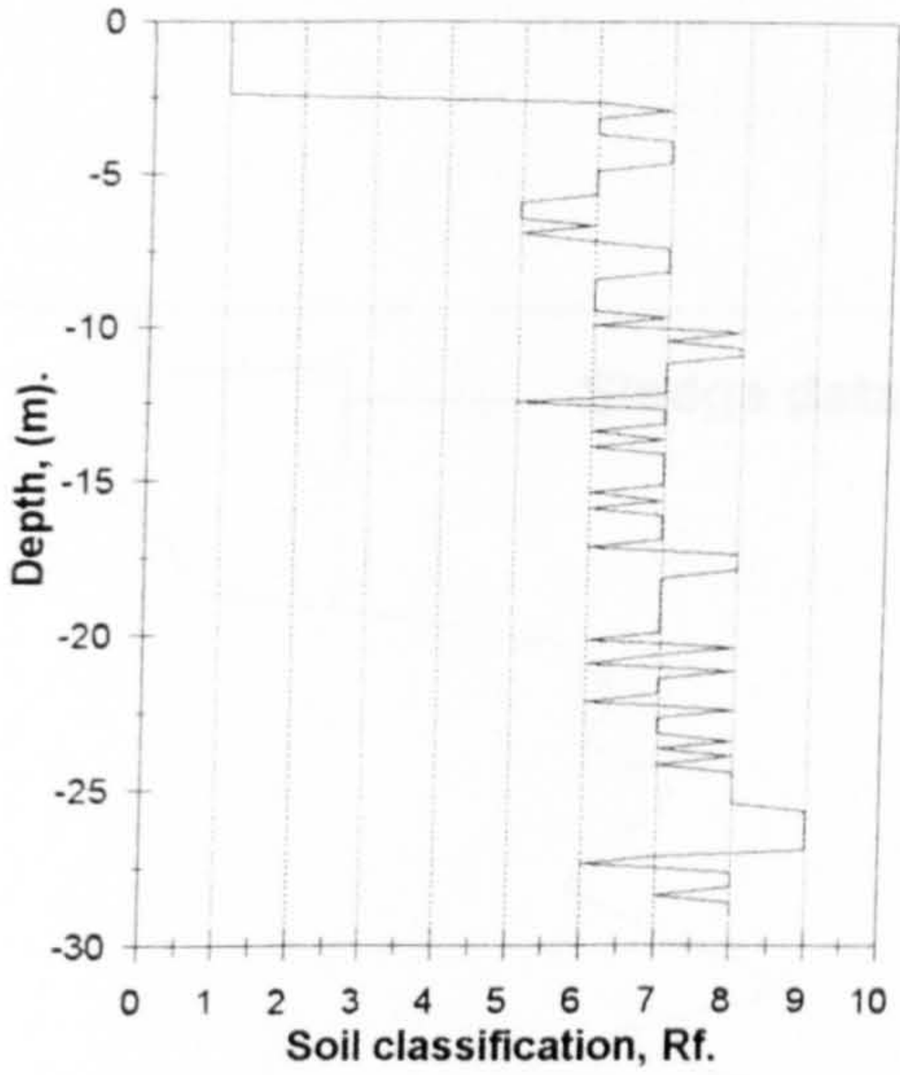

Figure 8.27. Soil zone classification, SCPT7.

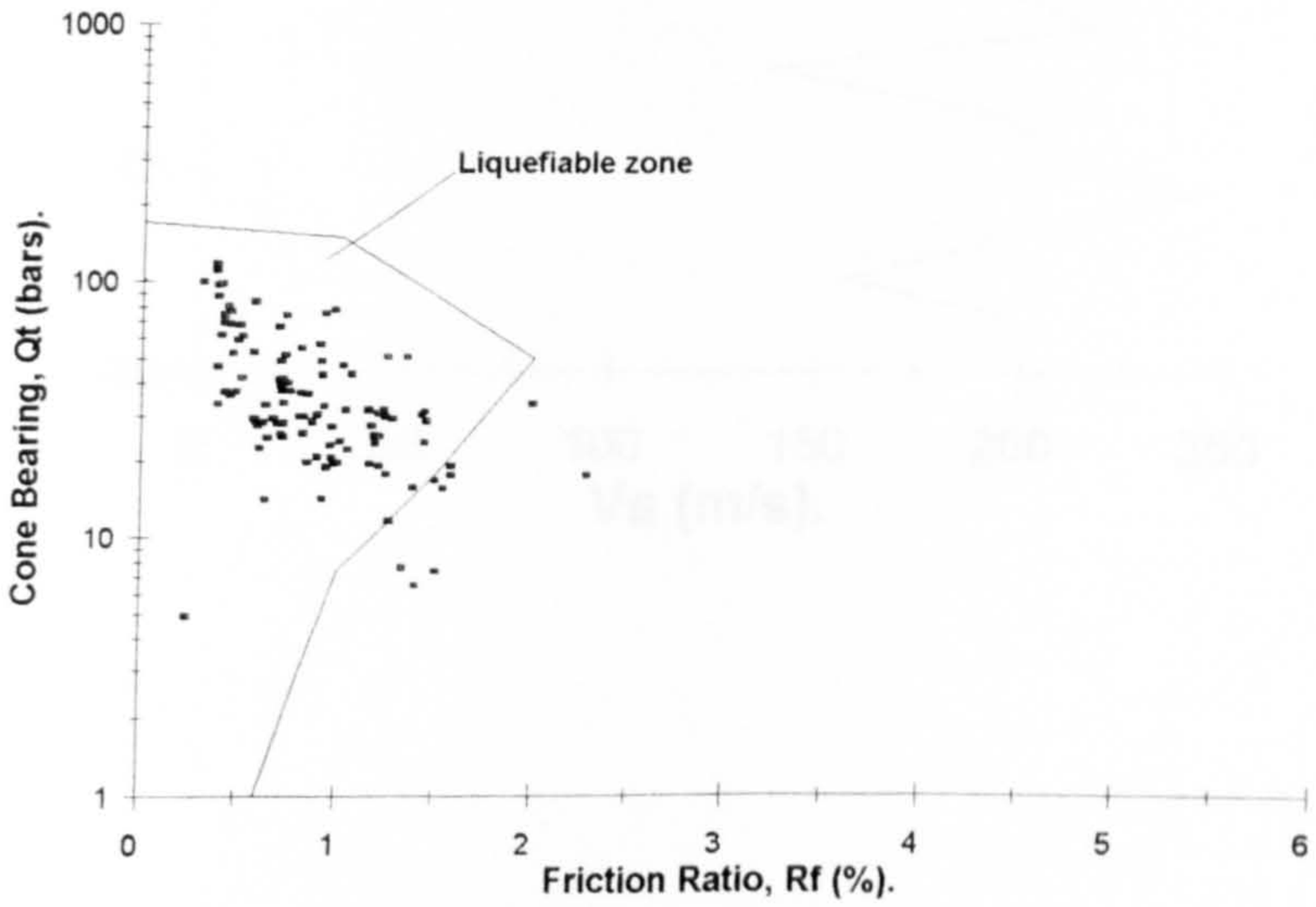

Figure 8.28. CPT soil classification chart, SCPT7.
(after Robertson & Campanella, 1985).

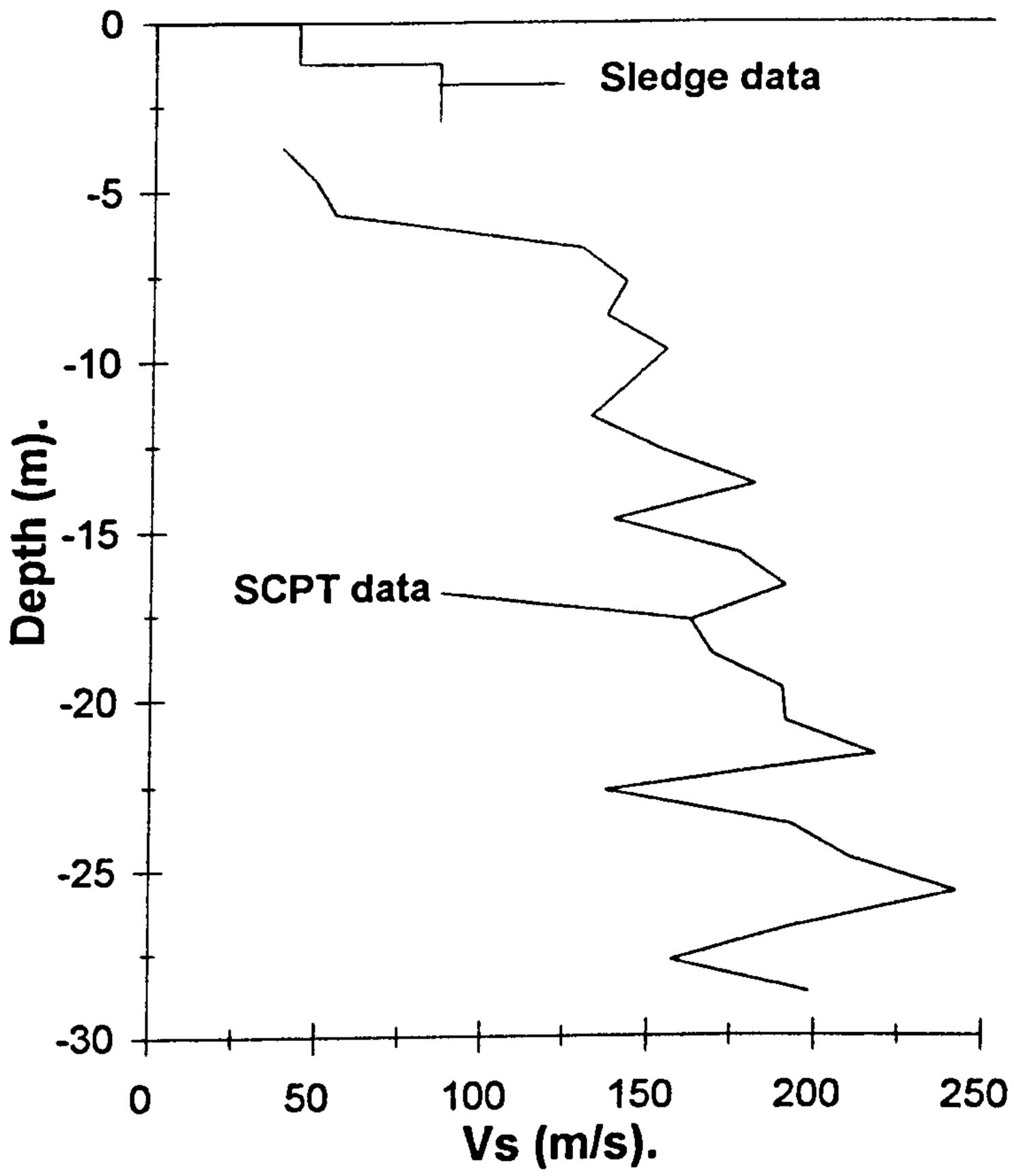

Figure 8.29. Shear wave velocity profile (SCPT 7) and surficial velocities from the 'Seismic Sledge'.

a.

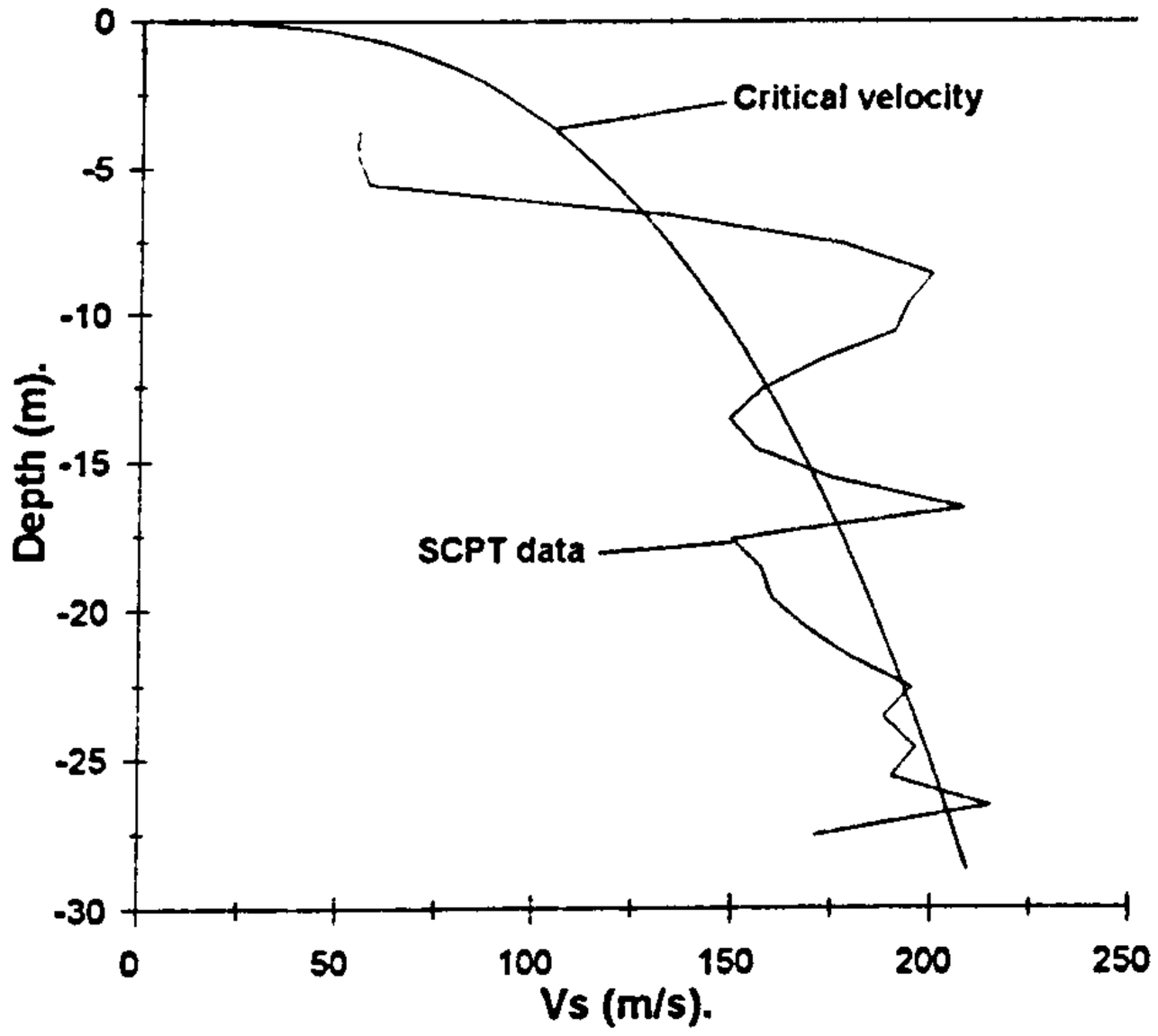

b.

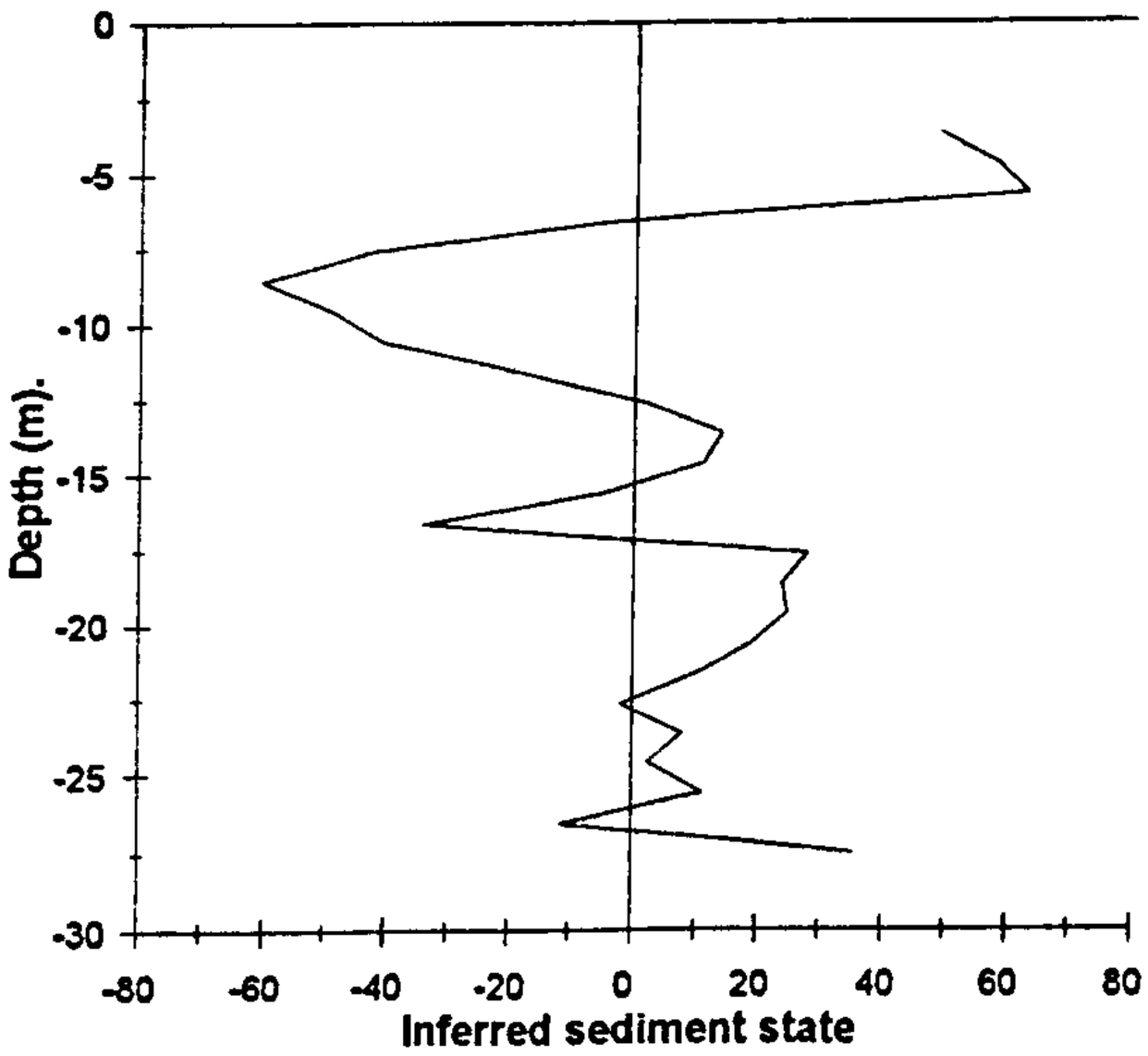

Figure 8 30. a. Shear wave velocity profile (SCPT 6) and laboratory derived critical velocity curve.

Figure 8.30. b. Sediment consolidation state inferred from shear wave velocity measurements, SCPT6.

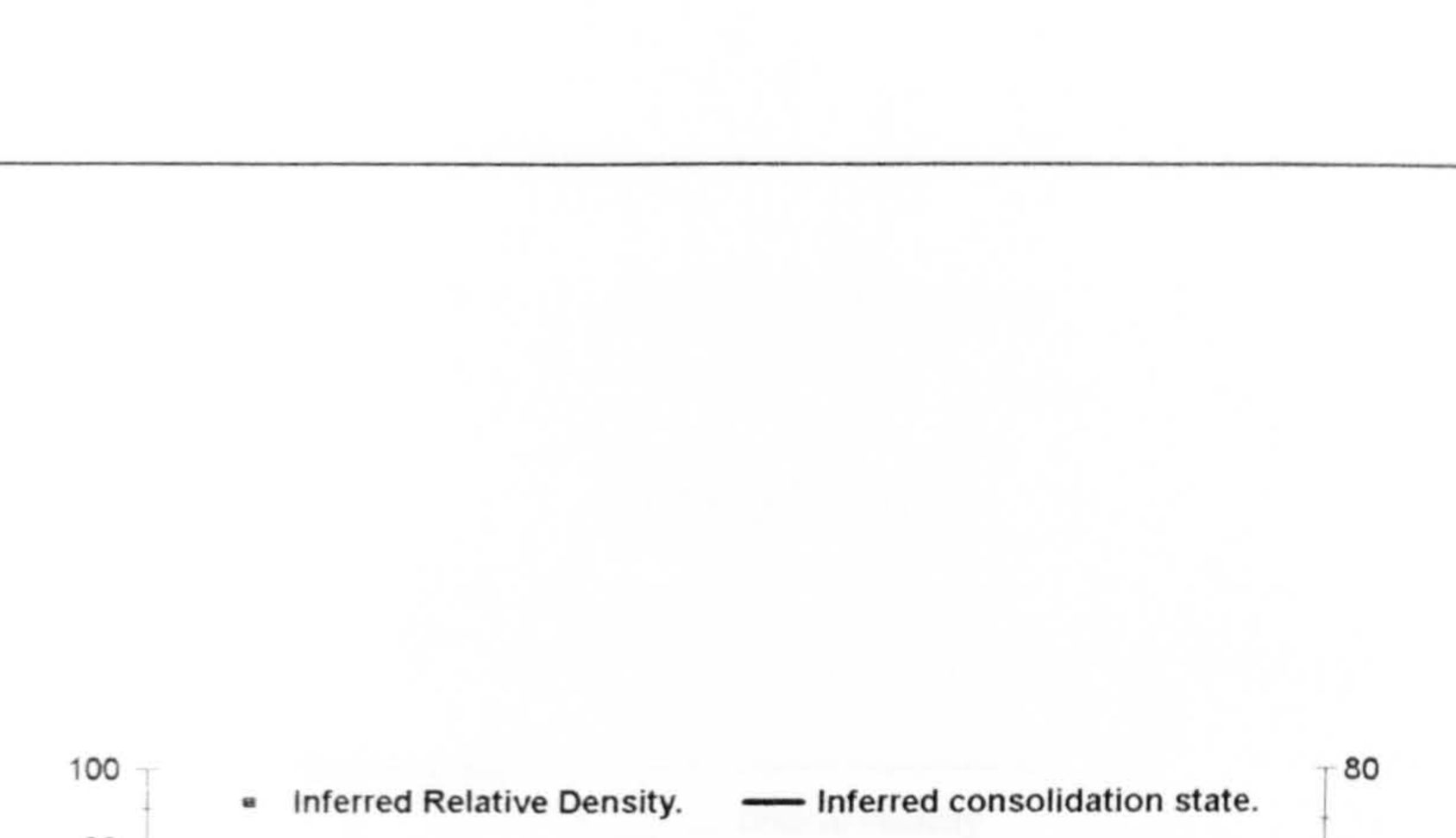

Figure 8.31. Inferred relative density and inferred consolidation state, SCPT 6.

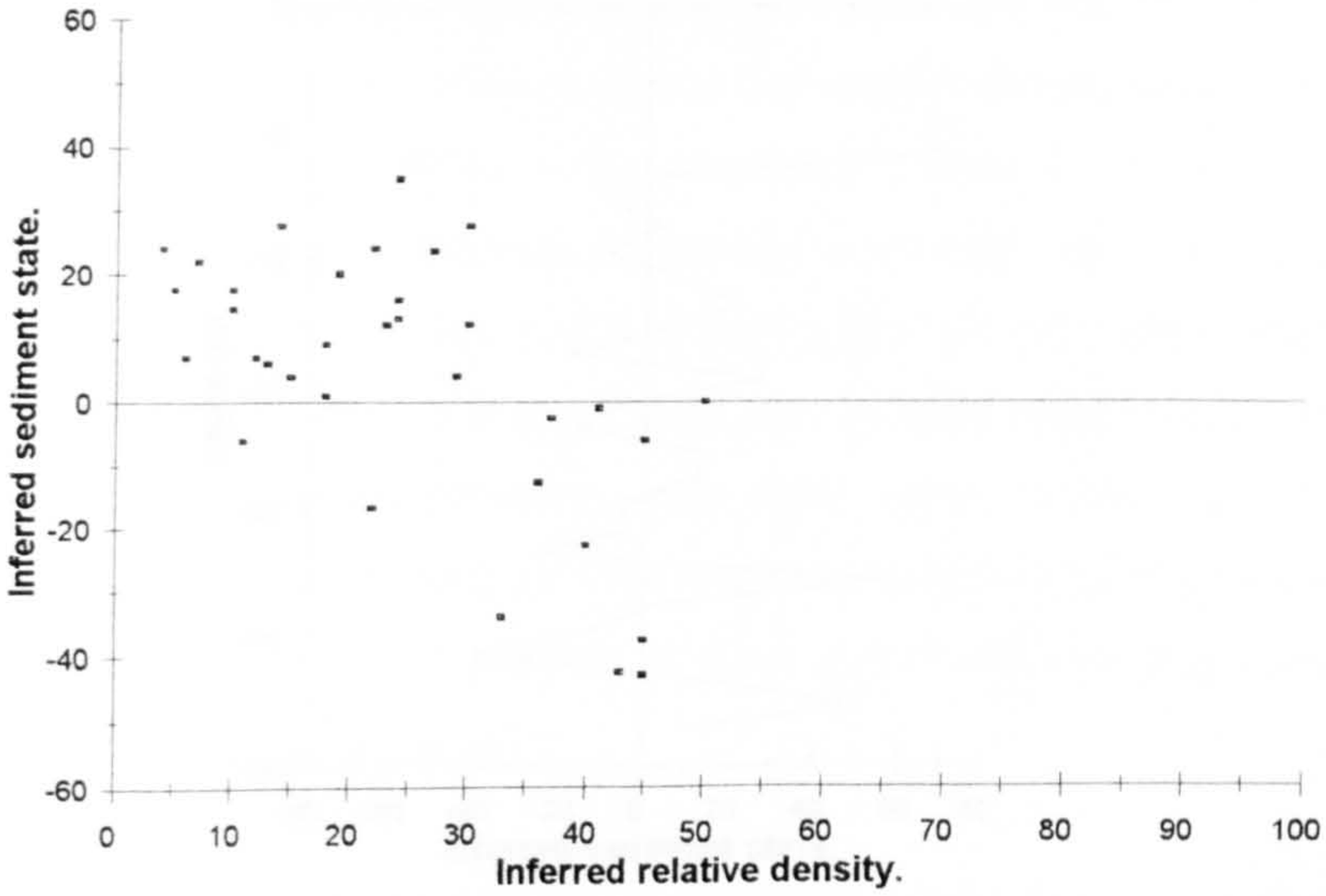

Figure 8.32. Relationship between inferred relative density and inferred consolidation state, SCPT6.

a.

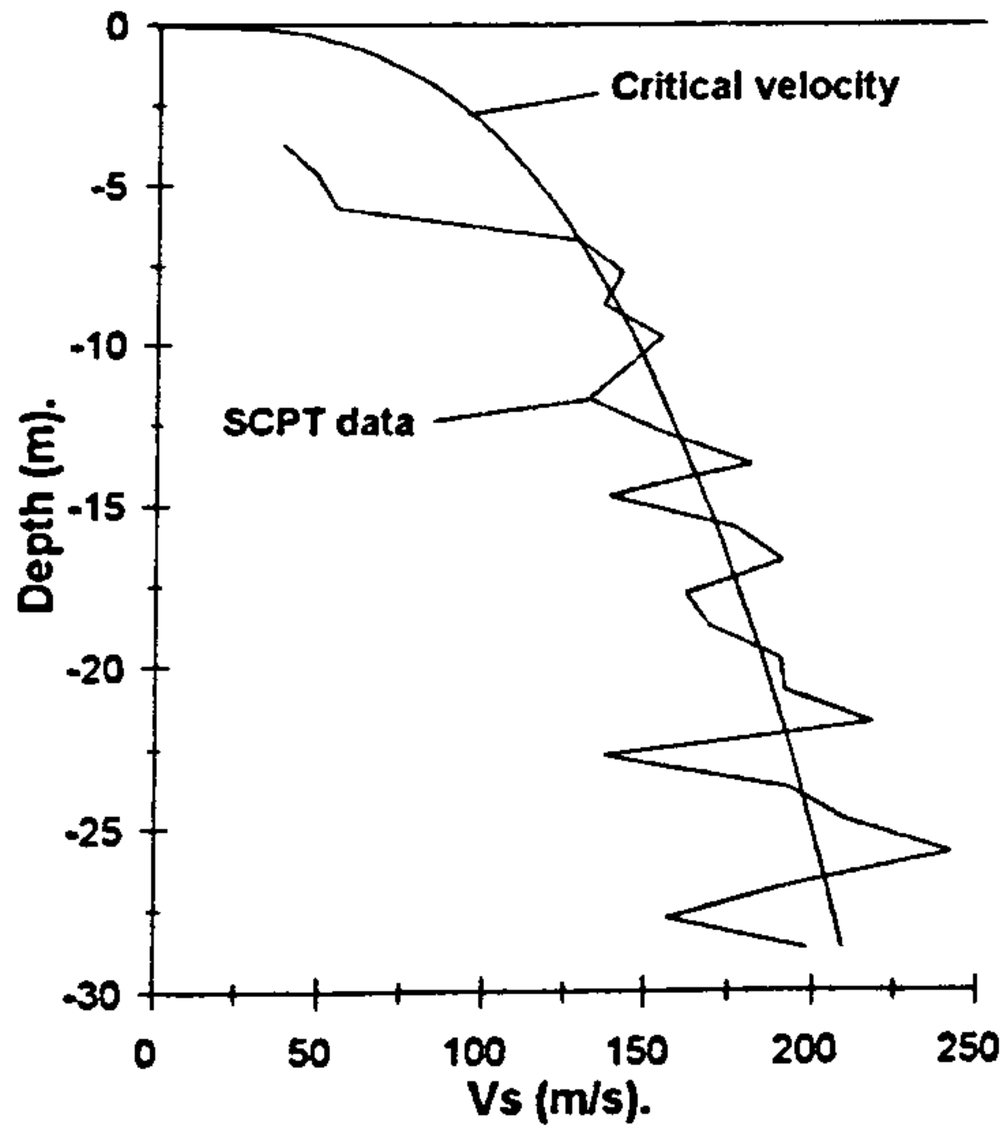

b.

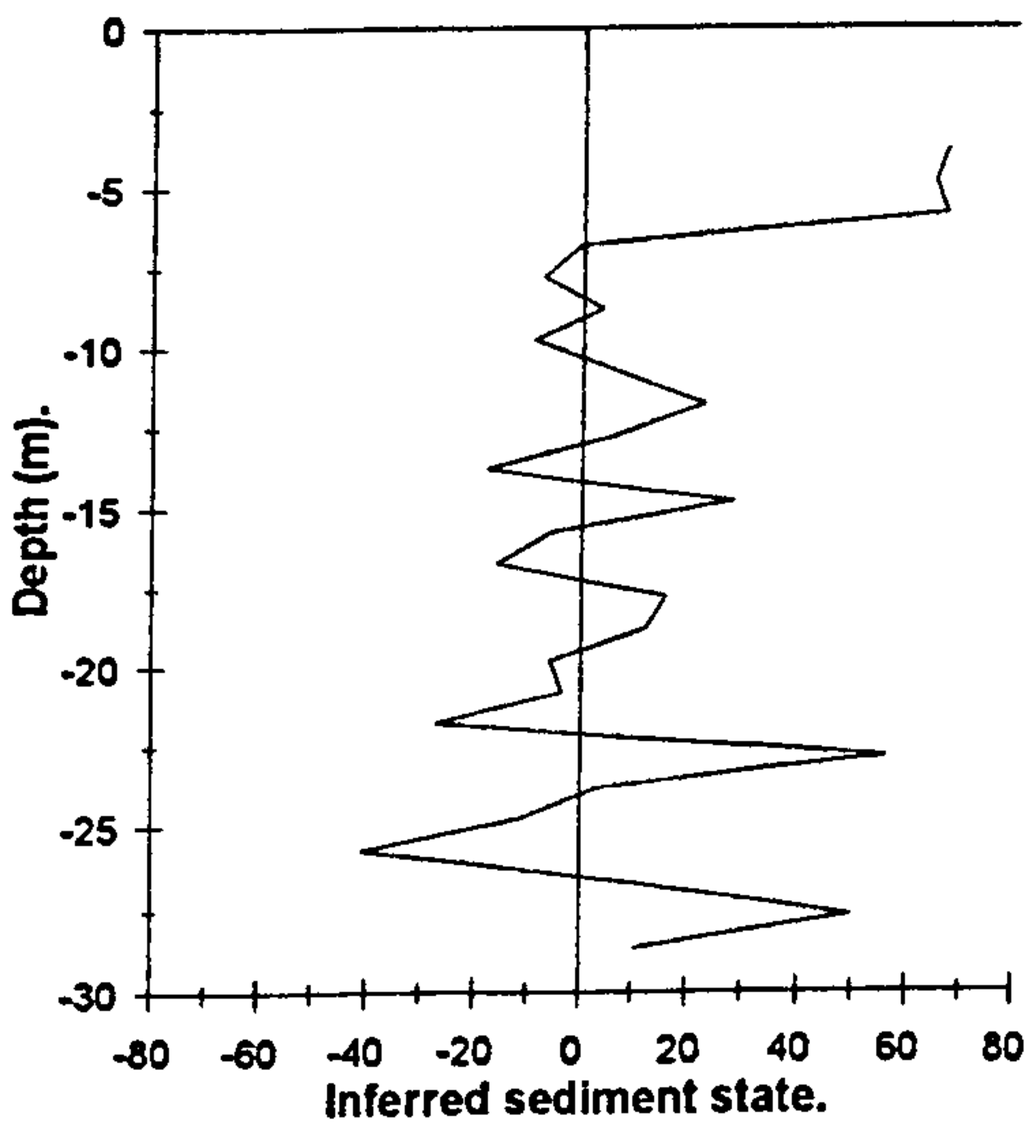

Figure 8.33. a. Shear wave velocity profile (SCPT 7) and laboratory derived critical velocity curve.

Figure 8.33. b. Sediment consolidation state inferred from shear wave velocity measurements, SCPT7.

CHAPTER 9.

DISCUSSION.

9.1. Introduction.

The results presented in Chapters 6, 7 and 8 provide strong laboratory evidence that consolidation state, and hence liquefaction potential, of laboratory sands may be estimated from a knowledge of the 'critical shear wave velocity line' and the *in-situ* shear wave velocity of a particular sediment body. The 'critical shear wave velocity line' itself may effectively be determined by measuring shear wave velocities over a range of effective stresses, prior to conventional steady-state testing procedures. Of the four different test sands investigated during the course of this study, the shear wave velocity based state index, ψ_s, proved to be significantly related to either the change in effective confining stress, $\Delta p'$, or the state parameter, ψ, at a confidence level of 95%.

In the field, previous attempts to measure ψ have primarily been based upon calibrated cone penetrometer testing, a technique which has well recognised deficiencies (Sladen, 1989). From an analysis of the laboratory and field results presented in Chapter 8, it appears that a combination of laboratory and field based velocity measurements can be used to give some estimate of the *in-situ* consolidation state, and hence liquefaction potential, of saturated sandy deposits. These estimates correlate well with other, more conventional cone penetration based indices of liquefaction potential. This suggests that, due primarily to the relative ease of measurement, repeatability and reliability, estimates of liquefaction potential based upon shear wave velocity measurements may be at least as good as other, more commonly used, predictive techniques. This relative ease of measurement becomes even more significant in offshore areas, and investigating 'difficult to sample' soils.

In order to overcome some of the inevitable limitations of the field shear wave procedure, it is strongly recommended that shear wave velocities should be used to predict liquefaction potential in the field only as part of a more fully integrated site investigation, involving both geophysical and geotechnical methodologies. Precise estimations of consolidation state based solely on velocities should be confined to the well defined boundary conditions of the laboratory. However, use of this procedure,

especially in an initial reconnaissance role, does offer the advantage of providing a first estimate of liquefaction potential in areas which may previously have been regarded as essentially unquantifiable.

Before any further discussion of the integrated data is made, the various geophysical and geotechnical aspects of the laboratory and field data will be discussed with relevance to existing published literature. In the interests of simplicity, the results will be subdivided into laboratory and field, and further subdivisions thereof.

9.2. Laboratory data.

9.2.1. Shear wave data.

The fundamental effects of varying effective confining stress, void ratio and fines content, on the shear wave velocity of uncemented sands were investigated during the testing of the three Newborough sands. In good agreement with the literature, the test programme showed that the shear wave velocity of a laboratory prepared sand is significantly affected by variations in all three variables. On a more practical approach, the Fraser Delta sand was tested to provide laboratory data which were used in conjunction field derived velocities measured *in-situ*.

9.2.1.1. Confining pressure effects.

The effects of effective stress upon the shear wave velocity of a laboratory prepared sand are well quantified and have been described in more detail in Section 4.2. The laboratory shear wave data in this study, derived from some 2000 individual velocity determinations, illustrate that for a specific sample of known void ratio the relationship between effective confining stress and shear wave velocity may be described using an equation of the form:-

$$V_s = a \times p'^{b} \qquad (m/s). \qquad (9.1).$$

where, a and b = sample constants,
p' = effective confining stress (kPa).

The summarised data for all the four sand samples tested during this study are presented below.

Sample constants	*Newborough 0%*	*Newborough 5%*	*Newborough 10%*	*Fraser Delta sand*
a: mean	**37 ± 2***	**38 ± 2**	**31 ± 2**	**45 ± 2**
a: max	57	43	36	58
a: min	23	32	24	37
b: mean	**0.34 ± 0.02**	**0.31± 0.02**	**0.34 ± 0.02**	**0.28 ± 0.02**
b: max	0.41	0.33	0.38	0.30
b: min	0.28	0.30	0.32	0.25
Pressure range (kPa)	20-400	20-400	20-400	20-400
Void ratio range	**0.719 - 0.854**	**0.699 - 0.763**	**0.589 - 0.730**	**0.759 - 0.878**

Table 9.1. Summarised sample constants and range of void ratio tested for all samples.
* Error values calculated from an analysis of the system error listed in Section 5.5.

As described above, for a specific sample, these constants were obtained from the statistical analysis of usually around 20 -30 individual shear wave velocity determinations over an effective stress range of approximately 25 - 400 kPa. Typically the transformed velocity - effective stress relationship had an R^2 value of the order of 0.99 and p values well below the critical value of 0.05. These statistics indicate that the data collected using the laboratory apparatus described in this study had relatively little data scatter around the mean, and were significant at a level of 95% confidence. Table 9.2 (below) provides a summary of other published data.

Material	*a: mean*	*b: mean*	*b:limits*	*Reference*
Ottawa sand (dry). p' > 96 kPa	-	0.238	0.23 - 0.25	(Hardin and Richart, 1963)
Ottawa sand (sat). p' > 96 kPa*	-	0.252	0.24 -0.26	"
Ottawa sand (dry). p' < 96 kPa	-	0.293	0.27- 0.31	"
Ottawa sand (sat). p' < 96 kPa	-	0.420	0.39 - 0.44	"
Ottawa sand (sat).		0.26	-	(Robertson *et al.* 1995)
Red Wharf Bay sand.	73	0.27	-	(Bates, 1989)
Alaska sand (sat).	-	0.26	-	(Cunning *et al.* 1995)
Syncrude sand (sat).	-	0.26	-	(Cunning *et al.* 1995)
In-situ sands (sat).		0.28	-	(Hamilton, 1976)
Marine Clay	26.49	0.22	-	(Baldwin *et al.* 1991)
	22.83	0.19	-	"

Table 9.2. Summarised sample constants compiled from the literature.
* *(sat)* indicates sample saturated with water.

The physical characteristics of the sediments described in Table 9.2 above are listed below.

Material	*Description.*	*% Fines.*	*D_{50} (mm)*	*Reference.*
Ottawa sand.	Uniform quartz sand.	0	No. 20 - 30*.	(Hardin and Richart, 1963)
Ottawa sand (C109).	Uniform quartz sand.	0	0.35	(Robertson *et al.* 1995)
Red Wharf Bay sand.	Beach sand.	-	0.15	(Bates, 1989)
Alaska sand.	Marine tailings sand.	31.7	0.12	(Cunning *et al.* 1995)
Syncrude sand.	Uniform tailings sand.	12.5	0.17	(Cunning *et al.* 1995)

Table 9.3. Summarised sand sample descriptions.
* U.S standard sieve sizes.

As can be seen, there is a reasonable agreement between the sample constants quoted in the literature and those derived from this study. The most noticeable feature of this comparison however, is the small difference (of the order of 0.04 - 0.06) between the published and quoted stress exponent, b, with particular reference to the Newborough sands. This difference may be partly a function of the error associated with these data (which is generally unquantified in the literature), but one possible reason for any small remaining discrepancy may be the small differences between the physical properties of the individual sands tested. The Fraser Delta sand has a more comparable stress exponent with the published data listed above, possibly due to its greater similarity in terms of mean grain size. This agreement with the published data further suggests that any small deviations from the published data are material-related rather than an artefact of the measuring system. The shear wave velocity - effective stress curves for all the samples tested (at an assumed void ratio of 0.700) are illustrated graphically in Figure 9.1. As can be seen, differences in the physical properties of the individual sands have resulted in a maximum difference in velocities at an effective confining stress of 300 kPa of around 85 m/s. Based upon the error values calculated in Section 5.5, at this confining stress these differences may be regarded as being significant in nature. In the case of the Newborough sands, the differences between the velocity behaviour of the different sands must simply be a function of the varying fines content.

Figure 9.2 illustrates a comparison between a typical velocity - effective stress curve collected during this study and other published data. The data recorded by Bates (1989), based upon Red Wharf Bay sand, were obtained using a similar apparatus to that used by the author, the only differences being method of sample preparation and the specific signal generation and acquisition equipment. The data presented by

Robertson *et al.* (1995), based upon Ottawa (C 109) sand were, also collected using a modified Wykeham Farrance triaxial cell fitted with bender elements. As can be seen, there is a good agreement between data collected by the author and that published in the literature, in particular between the Ottawa and Newborough 0% sands. This agreement probably reflects the physical similarities between the two sands in terms of mean grain size, void ratio, and sample preparation methodology for these particular tests. The slightly greater difference between the Newborough 0% and the Red Wharf Bay sand is most likely a result of differences in sediment physical properties and sample void ratio; Bates (1989) does not quantify this latter variable.

This brief discussion provides strong evidence that the shear wave velocity - effective stress curves obtained in this study compare well with other published data, both in general form and numerical similarity. Any small differences between these and published data are in all probability likely to be explained by small differences in the physical characteristics of the individual sands.

9.2.1.2. Void ratio effects.

The effect of void ratio upon shear wave velocities has also been quantified by various authors who report a general increase in velocity with decreasing void ratio (i.e. velocities increase with increasing sample density, due mainly to the increased number of particle contacts). This relationship, in the range of void ratios encountered in sands at least, may be generally regarded as being linear in nature, and has been discussed in more detail in Section 4.2.

The results from this study also demonstrate a significant linear relationship between void ratio and shear wave velocity at a specific effective confining stress. The linearity of the relationship also tends to become more significant at higher effective stresses. Using a knowledge of the best fit line through the data of this type and the individual sample constants a and b, the laboratory shear wave velocities may be used to predict laboratory sample void ratios (*e.g.* Figure 6.15). These relationships have a range of significances, but it is interesting to note that in all cases the best fit line is almost coincident with the '1 to 1' perfect fit line.

The general relationship between the shear wave velocity, void ratio, and effective confining stress can be expressed in the form proposed by Hardin and Richart (1963) as:-

$$V_s = (m_1 - m_2 e) p'^{b} \qquad (9.2).$$

where, m_1 and m_2 are sample constants.

The data collected in this study may be presented in this form; the summarised data collected are listed in Table 9.4 below.

Sand type.	m_1	m_2	b
Newborough 0%	84	60	0.34
Newborough 5%	65	38	0.31
Newborough 10%	53	33	0.34
Fraser Delta and	79	41	0.28

Table 9.4. Summarised sample constant data.

Based upon an experimental study of Ottawa sand, Robertson *et al.* (1995) and Cunning et al. (1995) provide a similar, alternative relationship, normalising the velocities to 100 kPa (P_a) using the general relationship:-

$$V_s = (n_1 - n_2 e)\left(\frac{p'}{P_a}\right)^{b} \qquad (9.3).$$

where n_1 and n_2 are sample constants.

The data collected in this study may also be expressed in the form suggested by Robertson *et al.* (1995) and Cunning *et al.* (1995). These data are summarised below.

Sand type.	n_1	n_2	b
Newborough 0%	415	307	0.34
Newborough 5%	278	165	0.31
Newborough 10%	246	146	0.34
Fraser	310	175	0.28

Table 9.5. Summarised sample constant data, (*after Robertson et al., 1995 and Cunning et al., 1995*).

Figure 9.3 illustrates a comparison between the normalised shear wave velocity - void ratio relationship of the sands tested in this study, based upon Equation 9.3 above. As

can be seen, all the sand samples appear to differ, either in terms of gradient or relative position. Once again, in the case of the Newborough sands, this difference must be to some extent due to the varying fines content. The difference between the Fraser Delta sand and the Newborough sand probably reflects broader differences between the individual test sands, in terms of fines content, mean grain size, grain shape and sand mineralogy.

Table 9.6. (below) illustrates typical sample constants based upon both Equation 9.2 and 9.3, quoted in the literature.

Sand type	m_1	m_2	n_1	n_2	b	*Reference*
Round grained sands $0.3 < e < 0.8$	111	51	-	-	0.25	(Hardin and Richart, 1963)
Angular grained sands $0.6 < e < 1.3$	104	34.9	-	-	0.25	"
Ottawa sand	-	-	381	259	0.26	(Robertson *et al.* 1995)
Alaska sand			307	167	0.26	(Cunning *et al.* 1995)
Syncrude sand			311	188	0.26	"

Table 9.6. Summarised published sample constant data.

As can be seen from the tabulated results above, the sample constants of the sands tested in this study and those listed in the literature appear to be broadly similar, with any differences attributable to physical differences between the individual sands.

Figure 9.4 provides an interesting comparison between actual data collected in this study for Newborough 0% sand and data collected by Robertson *et al.* (1995) using Ottawa sand. As can be seen, although the Ottawa sand data covers a greater range of void ratios (achieved by using a variety of different sample preparation techniques), there is a remarkable degree of agreement between the two data sets. This is probably a result of the similarities between the two sands and the data collection methodology.

Figure 9.5 (a) illustrates a comparison between the shear wave velocity - void ratio relationship from this study and the relationships for round grained and angular sands published by Hardin and Richart (1963) (listed above). Bearing in mind that the typical data scatter associated with these data is of the order of ±13m/s, the Fraser sand relationship agrees very well with the data presented by Hardin and Richart (1963), falling between the two extremes of angular and rounded sands. This suggests that the Fraser Delta sand, based upon an analysis of the void ratio and velocity data alone, is

sub-rounded to sub-angular in nature. The Newborough sands however, fall significantly below Hardin and Richart's (1963) data, although the Newborough 5% and 10% sands have a broadly similar gradient. Once again, this may be a function of differing mean grain size. Figure 9.5 (b) illustrates a comparison between the data collected from this study and that collected by Robertson *et al.* (1995) and Cunning *et al.* (1995) for Ottawa and Syncrude sands, (listed above). As can be seen, the Ottawa (C109), Syncrude and Alaska sand lie within very much the same range as the Newborough sands. Any residual differences which exist between the void ratio - shear wave velocity relationship for each sand type are therefore in all probability due to small differences in the physical characteristics of each sand.

9.2.1.3. Effects of increasing fines content.

The effect of physically increasing the fines content of a particular sand, as opposed to testing different sands with different fines content, is an area which seems to have attracted little published research effort. However, Han *et al.* (1986) and Nur *et al.* (1991) describe experiments investigating the effects of porosity and clay content on wave velocities in cemented sandstones, with particular relevance to deep well logging. Despite the fact that these measurements were made on sandstone samples at a confining pressure of 40MPa and a pore-pressure of 1.0MPa, both authors note a significant decrease in shear wave velocity with increasing clay content. Based upon a best least squares analysis of 75 different sandstone samples, Han *et al.* (1986) suggest the following relationship:-

$$Vs = 3.52 - 4.91\phi - 1.89C \quad \text{(km/s)}. \qquad (9.4).$$

where, ϕ = porosity,
C = fractional clay content.

This relationship is illustrated in Figure 9.6, and clearly shows a distinct decrease in shear wave velocities with increasing clay content over a range of porosities. Nur *et al.* (1991) suggest that this effect is due to the softening, or lubrication, of grain contacts by clay particles between the individual grains, partly by virtue of the large surface area of the clay particles. In addition, this velocity reduction effect could be due to the fact that the shear wave velocity of clays is generally lower than sands, and that the mixing of

sands and clays results in a reduction in observed velocities due to a simple 'mixing' or 'dilution' effect.

The effect of increasing fines content on a sand which otherwise remained unchanged, is illustrated by the tests on the Newborough (0%, 5%, 10%) sands, as seen in Figure 9.7. As can be seen, in general agreement with Han *et al.* (1986) and Nur *et al.* (1991), the effect of adding fines particles to the Newborough sand was to distinctly decrease the shear wave velocity (at a specific void ratio and effective stress).

Figure 9.8 illustrates the effects of increasing fines content for other sands in the literature. This shows that for different individual sands, the simple relationship between fines content and velocity at a specific effective stress is less well defined. Despite a very general decrease in velocities with increasing fines content, differences in mineralogy, grain size and shape, appear to overshadow this effect in natural, unconsolidated sands. One possible reason for the apparently anomalous Alaska sand may be that being a tailings sand, many of the fine particles are composed of crushed rock fragments which behave differently from clay minerals although being of a similar size.

9.2.2. Triaxial data.

Traditionally, the steady state of deformation for a particular sand is measured using consolidated, undrained triaxial testing techniques, and has been found to be solely a function of the initial void ratio, irrespective of initial stress conditions. The testing of a number of samples with differing initial void ratios allows the determination of the steady state line (SSL) for a particular sand. At effective confining pressures of less than around 1000 kPa, this generally straight line divides sand states that will contract and potentially liquefy from those that will dilate, and strain stiffen under undrained shear. Been and Jefferies (1985) defined the state parameter, ψ, for sands, quantifying sand consolidation state, with reference to the steady state line. Various different authors have recorded the steady state parameters for a variety of different sands. As might be expected, each individual sand displays its own unique steady state line, in terms of both gradient and relative position in e - log p' space, a result of the differing mechanical properties of each sand. Further, from published data it is generally accepted that the

addition of fine particles to a sand will have the effect of increasing the gradient of the SSL.

The steady state parameters of the four test sands were determined in the laboratory in this study using consolidated, undrained, strain controlled triaxial tests. The testing procedure adopted in this study allowed the steady state parameters of the four individual sands to be determined. In addition the effect on the steady state behaviour of adding fine particles to a particular sand could be quantified. The summarised steady state parameters of the four test sands are illustrated below.

Sand Type.	C_{ss}	e_1	M	ϕ'_{ss}	M_L	*Pressure range.*
Newborough 0%.	0.04	0.887	1.28	29°	1.25	30 - 900 kPa
Newborough 5%.	0.05	0.836	1.32	30°	1.15	20 - 600 kPa
Newborough 10%.	0.05	0.769	1.29	29°	1.19	20 - 500 kPa
Fraser Delta sand.	0.19	1.290	1.38	31°	-	100 - 500 kPa

Table 9.7. Steady state parameters for sands tested in this study.

The steady state lines of the four sands tested, defined in e - log p' space and q - p' space, are illustrated in Figure 9.9 (a and b) respectively. As can be seen from Figure 9.9 (a), the individual steady state lines of the test sands occupy both different relative positions in e - log p' space and have differing gradients, presumably dependant on the mechanical properties of each sand. Two interesting points can be noted from this diagram, with particular relevance to the Newborough sands. The first is that the addition of fine particles has caused a dramatic shift downwards of the SSL in e - log p' space, of the order of 0.05 in terms of void ratio. This has the obvious implication that sands containing significant amounts of fines are potentially more 'liquefiable' under undrained loading, i.e. a sand containing fines must be denser to ensure a dilative, strain - stiffening response. This type of response is also described by Been and Jefferies (1985) and Sladen *et al.* (1985). The second point to note is that there appears to be only a very small increase in gradient due to the addition of fine particles to the clean sand, and no apparent difference in gradient between the Newborough 5% and 10% sands. The well documented increase in gradient with increasing fines content must therefore be more strongly affected by a decrease in the actual grain size distribution as a whole, rather than the simple addition of fine particles *per se.* The mean grain size control on SSL gradient is illustrated in the comparison between the Newborough 10% and Fraser Delta sands, which have a broadly similar fines content

(9% - 8% respectively), but a different mean grain size (200μm - 145μm) and corresponding different SSL gradient (0.05 - 0.19). Figure 9.9 (b) illustrates the SSL in q - p' space. As can be seen from this figure, there is no obvious trend in the data; however examination of Table 9.7. reveals a general increase in the gradient of the SSL in q - p' space. This appears to agree well with Sladen *et al.* (1985) who also noted a very small increase in M with increasing fines content.

Table 9.8 lists the steady state and collapse parameters of a number of different sands described in the literature. Clearly there is a good agreement between the parameters obtained from this study and those quoted below.

Sand Type	C_{ss}	e_1	M	ϕ'_{ss}	M_L	*Pressure range.*
Nerlerk 0%[1]	-	-	1.19	30	0.62	-
Nerlerk 2%[1]	0.04	0.88	1.20	30	0.60	-
Nerlerk 12%[1]	0.07	0.80	1.24	31	0.59	-
Leighton Buzzard[1]	0.08	1.00	1.19	30	0.54	-
Ottawa (C109)[2]	0.075	0.926	1.20	-	-	-
Toyoura[2]	0.06	1.048	-	-	-	100 - 1000 kPa
Lornex[2]	0.34	1.762	-	-	-	> 200 kPa
Alaska[3]	0.117	1.485	1.48	-	-	-
Syncrude[3]	0.027	0.928	1.31	-	-	-

Table 9.8. Steady state and collapse parameters for various sands.
[1] Sladen *et al.* (1985), [2] Robertson *et al.* 1995), [3] Cunning *et al.* (1995)

The index properties of those sands not already mentioned are listed below.

Material	*Description.*	*% Fines.*	D_{50} *(mm)*	*Reference.*
Nerlerk 0%.	Fine uniform sand.	0	0.23	(Sladen *et al.* 1985)
Nerlerk 2%.	Fine uniform sand.	2	0.28	"
Nerlerk 12%.	Fine uniform sand.	12	0.28	"
Leighton Buzzard	Medium uniform sand.	0	0.86	"
Toyoura.	Fine uniform sand.	0	0.164	(Ishihara, 1993)
Lornex.	Angular quartz sand.	0	-	(Robertson *et al.* 1995)

Table 9.9. Index properties of sands mentioned above (Alaska and Syncrude sands are described in Table 9.3).

Figure 9.10 (a and b) illustrates a comparison between two of the test sands (Newborough 0%, and the Fraser Delta sand), and some of the sands listed above, defined in e - log p' space and q - p' space respectively. With reference to Figure 9.10 (a), there is considerable variation between the individual sand types in terms of both relative position and gradient. Once again, these variations are most probably a result of different mechanical properties of the sands, which themselves must ultimately be a

function of variations in grain size, shape, fines content and mineralogy. Figure 9.10 (b) also shows that in q - p' space there is a good agreement between the data collected in this study and data presented in the literature. There appear to be no obvious trends in these data, and the variation between the individual sand types is once again probably a result of the differing mechanical properties of the sands.

9.2.3. Integrated laboratory data.

Various authors over the past 20 or so years have attempted to use seismic velocities to reveal a wide range of sediment properties, (*e.g.* Baldwin *et al.* 1991; De Alba *et al.* 1984; Stumpel *et al.* 1984; Tang and Clark, 1993; Taylor Smith, 1993; Theilen and Percher, 1991), with a variety of success. While common correlations between seismic properties (*e.g.* P and S-wave velocities, attenuation) and mechanical sediment properties including shear strength, permeability, porosity, etc. have been published, a full description of these is beyond the scope of this discussion. However, common to all studies is the recognition that the use of seismic wave velocities (and attenuation) to predict sediment physical properties offers the potential for obtaining undisturbed *in-situ* data on the bulk sediment properties. This advantage becomes even more significant when attempting to study the physical properties of *in-situ* marine, lacustrine, estuarine or deltaic sediments with a minimum of disturbance.

Suggestions that shear wave velocity may be used as an index to liquefaction potential are based upon a relatively small number of field and laboratory evidence. The field based studies (*e.g.* Youd and Wieczorek, 1984), although useful, tend to be site specific, making any specific conclusions difficult to apply to other geographical areas. Much of the previous laboratory work investigating the inter-relationships between shear wave velocity and liquefaction potential has been performed using modified cyclic triaxial cells (e.g. De Alba *et al.* 1984), based upon the Berkeley approach to liquefaction prediction. In the authors view this does not represent the most intuitive approach to the problem.

Prior to the start of this project, and despite its obvious advantages not least in terms of testing simplicity, the combination of shear wave velocity measurement and steady / critical state concepts had not received any detailed research attention. However, data from this study and studies by Robertson *et al.* (1995) and Cunning *et al.* (1995)

performed independently and simultaneously seem to suggest that the shear wave velocity of an uncemented sand may be used to aid the prediction of liquefaction potential, especially when combined with other, more conventional, investigative techniques.

9.2.3.1. Modelled shear wave velocity behaviour during shear.

Results from the separate geotechnical and geophysical portions of the proposed technique have been integrated in Chapter 7. At the root of this integration of large and small strain measurements were three major assumptions (listed in Section 7.1). These assumptions were necessary due mainly to the difficulty in measuring shear wave velocities during steady state triaxial testing. Obviously some of these assumptions could be removed if velocities could be measured on an instantaneous basis during strain, however it was felt by the author that the development of such a laboratory apparatus was beyond the brief of this particular research project. The three main assumptions on which the integration of the data are based are likely to remain valid for most of the conditions encountered during undrained triaxial testing of the type used in this study. This conclusion is supported to some extent by Tang and Clark (1993) who compared modelled and measured velocities during triaxial testing and found any differences to be of only a very small magnitude (~3m/s). The use of these assumptions allows the modelling of shear wave velocity during triaxial testing on sands for the four typical responses observed during laboratory testing. The results of this modelling have been illustrated in Figures 7.1 - 7.4. Conceptually these models are very simple in nature, as they assume that under undrained loading the only parameter affecting the shear wave velocity is the changing effective confining stress, which for a first order approximation such as this, appears reasonable. Taking this model a step further allows the state boundary surface to be defined in terms of deviator stress and predicted shear wave velocity (*e.g.* Figure 7.5).

9.2.3.2. Integration of velocity behaviour with steady / critical state parameters.

The integration of predicted shear wave velocity at steady state with the conventional steady / critical state parameters of void ratio, effective confining stress and deviator stress has also been illustrated in Chapter 7. The individual relationships between these parameters are summarised in the general formulae below.

$$V_s'_{ss} = a \times p'_{ss}{}^{b} \qquad (9.5).$$

$$e_{ss} = -c \times \left(\log V_s'_{ss}\right) + d \qquad (9.6).$$

$$\log\left(q'_{ss}\right) = f \times \left(\log V_s'_{ss}\right) - g \qquad (9.7).$$

Table 9.10 (below) summarises the test data with reference to Equation 9.5, defining the 'critical velocity line'.

Sand type.	*a*	*b*
Newborough 0%	*35*	*0.35*
Newborough 5%	*32*	*0.35*
Newborough 10%	*29*	*0.36*
Fraser Delta sand.	*31*	*0.34*

Table 9.10. Summarised test data, with reference to Equation 9.5.

This relationship includes the effects of both varying void ratio and effective confining stress, and essentially divides dilative from contractive sand states in a manner similar to the state diagram defined in e - log p' space. Two interesting features can be noted from these data. The first is that for the Newborough sands, the sample constant a shows a steady decrease with increasing fines content, and that all the a constants are significantly below the corresponding average value for each test sand. The second interesting feature is that the stress exponent b, is consistently higher than the average value for each test sand, although in this case there appears no obvious trend in the data. A comparison between the 'critical shear wave velocity lines' for all the test sands is illustrated diagramatically in Figure 9.11 (a and b). As can be seen, for the Newborough sands at a specific effective stress, the addition of fines resulted in a gradual decrease in the critical velocity. Figure 9.12 illustrates the critical velocity line, defined in e - log p' space with some data recorded for loose and dense samples of Newborough 0% sand. Considering the loose sand first; all the recorded data points for this sand fall below the critical velocity line, indicating a contractive response under shear. However, at lower effective stresses, the difference between the measured velocities and the critical velocity decreases significantly. Projecting an imaginary line through these data points will show that at very low effective stresses (~ 10 kPa) the response of this sand will become dilative. In the case of the dense sand, the opposite is

true; all the measured data points lie above the critical velocity line, indicating a dilative response under shear. However, projecting these data towards higher effective stresses shows that the response may become contractive at stresses of greater than ~1500 kPa. This dependence on the state of stress (i.e. loose sands dilating at low effective stresses and vice versa) is a fundamental part of the steady state model. The fact that it is reflected in the velocity - state model is an extremely strong piece of evidence, confirming the validity of this research.

The Table below lists the summarised data for Equation 9.6.

Sand type	c	d
Newborough 0%	0.124	1.078
Newborough 5%	0.140	1.042
Newborough 10%	0.140	0.970
Fraser Delta sand.	0.510	2.020

Table 9.11. Summarised test data, with reference to Equation 9.6.

These data are illustrated diagramatically in Figure 9.13. In this case, predicted shear wave velocity at steady state replaces effective confining stress as the measure of stress. As can be seen, these data resemble the conventional state diagram (defined in e -log p' space) very closely. This is a result of the strong relationship between shear wave velocity and effective confining stress. In common with the triaxial results described previously, the most significant effect of the addition of fines was to decrease the shear wave velocity at any particular effective stress. Once again, the effect on the gradient of the line is less marked.

Sand type.	f	g
Newborough 0%	2.74	3.99
Newborough 5%	3.02	4.52
Newborough 10%	2.81	4.02
Fraser Delta sand.	2.85	4.40

Table 9.12. Summarised test data, with reference to Equation 9.7.

The data summarised in Table 9.12 above are illustrated diagramatically in Figure 9.14. In contrast to the examples listed above, there appears to be no obvious trend in the data.

These data show clearly that the predicted shear wave velocity at steady state is related to the conventional steady state parameters of void ratio, effective confining stress and deviator stress. Because of the inter-relationships which clearly exist between these parameters, there is obviously a strong case for integrating the geophysical and geotechnical data, allowing the estimation of essentially geotechnical behaviour on the basis of small strain geophysical test results.

9.2.3.3. Inference of consolidation state from shear wave velocities.

As mentioned in Section 3.3.1, in the field of steady / critical state soil mechanics, sediment consolidation state is expressed by the state parameter, ψ, which is essentially the difference between the *in-situ* void ratio and the void ratio at steady state. ψ was originally defined by Been and Jefferies (1985) and found to correlate well with other engineering design parameters, such as the angle of phase transformation, the peak shear stress and the pore-pressure at phase transformation. Undoubtedly, ψ does in fact represent by far the best index of sediment consolidation state available, especially under laboratory conditions. However, in the field, the direct measurement of *in-situ* void ratio, from which the state parameter may be calculated (with a knowledge of the steady state properties of the particular material), is extremely difficult.

In the case of this study it was chosen to express the consolidation state calculated from shear wave measurements, in terms of shear wave velocity and a new state index, ψ_s (Section 7.3.1). This is in contrast to the work of Cunning *et al.* (1995) and Robertson *et al.* (1995), who go a step further and calculate ψ directly from laboratory and *in-situ* field shear wave velocity measurements. This direct approach may represent somewhat of an over simplification, as it intrinsically suggests that void ratios may be defined accurately in the field from an analysis of the shear wave velocity alone, which in practice is an extremely difficult task. The advantage of ψ_s over ψ calculated from velocity measurements then, is that consolidation state is estimated only in terms of a simple velocity difference, which does not directly imply that *in-situ* void ratios may be predicted from shear wave velocities alone.

Figures 7.8, 7.11, 7.14 and 7.17 (above) illustrate the comparison between ψ, ψ_s and $\Delta p'$, and the summarised statistics are presented below.

Sand type	*Relationship*	*Df*	R^2	*p*	*significance**
Newborough 0%	$\psi - \Delta p'$	32	0.66	2.96×10^{-9}	S
"	$\psi_s - \Delta p'$	32	0.50	3.95×10^{-6}	S
"	$\psi_s - \psi$	43	0.84	5.16×10^{-19}	S
Newborough 5%	$\psi - \Delta p'$	5	0.78	0.005	S
"	$\psi_s - \Delta p'$	5	0.81	0.003	S
"	$\psi_s - \psi$	6	0.87	0.0005	S
Newborough 10%	$\psi - \Delta p'$	5	0.83	0.003	S
"	$\psi_s - \Delta p'$	5	0.15	0.21	NS
"	$\psi_s - \psi$	6	0.56	0.0012	S
Fraser sand.	$\psi - \Delta p'$	5	0.85	0.0007	S
"	$\psi_s - \Delta p'$	5	0.52	0.026	S
"	$\psi_s - \psi$	6	0.32	0 08	S^1

Table 9.13. Summarised statistics for the relationships between ψ, ψ_s and $\Delta p'$.
* Significant at a level of 95% confidence interval.
S^1 Significant at a level of 90% confidence.
S = significant relationship, $p < 0.05$
NS = non-significant relationship, $p > 0.05$

Several important points can be noted from Table 9.13:-

1. The number of individual measurements strongly influences the significance of the relationship; the data from the numerous Newborough 0% sand tests are therefore far more significant than the other test sands on which fewer individual tests were performed.
2. Based upon an analysis of the individual R^2 and p values, ψ is a more significant index to $\Delta p'$ and hence consolidation state than ψ_s.
3. In all but one case, the relationship between ψ_s and $\Delta p'$ is significant.
4. In all cases, the relationship between ψ and ψ_s is significant.

These observations show that in all but two cases, the relationships between ψ_s, ψ and $\Delta p'$, for all the test sands are significant at a 95% confidence level. This allows the conclusion that shear wave velocity may indeed be used as an index of consolidation state. With the benefit of hindsight, it becomes obvious that more individual tests on each sample could have improved the statistical significance of these relationships. However, with particular reference to Figures 7.8, 7.11, 7.14 and 7.17 (presented previously in Chapter 7), it can be seen that small changes in void ratio may produce relatively large differences in undrained behaviour. Corresponding ψ_s values are therefore correspondingly low, and it could be argued that in some cases they may fall below the theoretical system resolution, making precise conclusions about the sediment

consolidation state difficult to draw. In the field, which is by definition less homogeneous than laboratory conditions, these conclusions may be even more difficult to make. This remains the fundamental problem with the proposed method, and is due principally to the relative insensitivity of shear wave velocity to void ratio, especially when compared to effective confining stress effects. This is the main reason why the author suggests an integrated geophysical - geotechnical approach to site investigation, with a number of CPT's or SCPT's combined with shear wave velocity techniques or other geophysical techniques (*e.g.* electrical methods), allowing an increase in available data at little additional cost. The greatest advantage of shear wave velocity over other, currently used and theoretically more accurate methods, is the ability to test *in-situ*, in areas which would be otherwise difficult to sample. In relative terms, the author is in no doubt that the use of shear wave profiles to predict the liquefaction potential of a site represents a significant improvement on SPT based methods, not least in terms of repeatability and reliability.

An example of the way shear wave velocity information may be used as part of a more, integrated geophysical - geotechnical study was given in Chapter 8, and the implications of the results of that study are discussed below.

9.3. Field study.

The Fraser River Delta provides an interesting example of a potentially unstable delta situated in an area of high earthquake risk. Much work has already been completed by a number of authors on the sub-aerial part of the delta, using conventional land based techniques, and accordingly, the liquefaction risk of many of the sub-aerial sediments has been quantified. Work on assessing the risk of offshore liquefaction, leading to the potential failure of part of the delta front and in turn a tsunami of significant magnitude, has progressed more slowly. Even in the relatively shallow waters of Roberts Bank, the chances of recovering an 'undisturbed' sediment sample are so low as to be practically and economically impossible. In shallow water, CPT and SCPT based methods have been used, with the rig mounted upon a floating barge, but once again costs are likely to increase dramatically. In deeper water, standard geophysical site investigation equipment has been used to define the seabed and subsurface morphology, e.g. side-scan sonar, echo-sounder and sub-bottom profiling techniques. The data resulting from these various different studies have proved useful, although in some parts of the delta,

interpretation has been hampered by the presence of shallow gas and the sandy nature of the sediments (preventing sub-bottom penetration). These standard techniques have however, provided valuable details on the sub-surface structure of the delta and have allowed the identification of various potentially hazardous sub-surface features, e.g. the Roberts Bank failure wedge. With the possible exception of some *in-situ* pore-pressure measurements (Christian, 1993), very little information on the *in-situ* mechanical properties of the delta sediments has been published further than establishing that they are of a generally sandy and fairly loose nature.

It is in this type of essentially data starved scenario that the usefulness of shear wave velocity as some measure of liquefaction potential becomes obvious.

9.3.1. Seismic sledge data.

The short offset shear wave sledge data collected on and around Roberts Bank were presented in Chapter 8. As can be seen, these data have been interpreted to produce a series of refraction 'profiles' (Figures 8.13, 8.15, 8.15). These profiles are characterised by small scale spatial variability (of the order of 10-100m), probably due to localised sediment grain size / density variations, superimposed on a larger scale trend (on the order of 100-1000's m). In the case of these data, there appears to be no significant large scale shear wave velocity variation, suggesting that for the sediments tested, there are no significant large scale variations in the sediment type or structure. Assuming this to be true, a *qualitative* comparison may be attempted, allowing some idea of average sediment conditions in the upper 3 metres of the delta. These data are presented below.

Deployment No.	*Mean apparent V_1 (m/s)*	*Mean V_2*	*Mean approximate depth to 1st refractor (m).*
1	43	85	-1.2
3	33	79	-1.5
4	41	84	-1.4

Table 9.14. Summarised shear wave - depth relationships, Fraser River Delta.

This Table illustrates, qualitatively at least, that the shear wave velocity in the upper 1m of the surface sediments is generally of the order of 40 m/s, increasing to around 80m/s at a depth of about 1.3m.

These data can be considered extremely useful in the sense of an initial reconnaissance role, allowing the identification of both small and large scale surface sediment variability, and giving some useful 'surficial sediment velocities'. However, due principally to the lack of depth penetration, which is in turn a function of the maximum source - receiver range, other shear wave data had to be employed in the detailed analysis of *in-situ* sediment consolidation state.

9.3.2. SCPTU data.

Probably the most significant (in a depth and site specific sense) shear wave data were provided by the Geological Survey of Canada, in the form of two detailed SCPT sections. This data set had the advantage of concurrent CPT measurements, allowing a direct comparison between shear wave velocity and CPT based liquefaction interpretative methods. However, when attempting to infer the larger scale stability behaviour of the delta front, this particular data set has the obvious disadvantage of a limited spatial extent.

This data, in effect, ties all the data collected during this study together, in that it allows both a comparison between *in-situ* shear wave velocities derived using two different methods, and liquefaction potential estimates made from entirely separate geotechnical and geophysical procedures. This data is discussed in more detail in Chapter 8, and allows some interesting conclusions:

1. Shear wave velocities derived from the 'Seismic Sledge', appear to be in close agreement with velocities derived from SCPTU data.
2. Shear wave velocities derived from both field methods appear to be in close agreement with the 'critical velocity' derived from laboratory based measurements.
3. Both geophysical and geotechnical methods of liquefaction analysis appear to indicate the possibility of liquefaction occurring, under significant shaking.

These significant conclusions illustrate that the type of combined laboratory / field technique proposed in this study is valid for the initial and subsequent, investigation of potentially liquefiable offshore areas.

9.4. Summary.

Based upon the results of this relatively small study it can be concluded that certain zones of the top 20 - 30 m of sediments of the offshore Fraser River Delta around Roberts Bank are potentially liquefiable. If valid, this poses a significant risk of ground failure of the delta front under large scale earthquake loading conditions. The consequences of such an event potentially dwarves the effects of a similar land based liquefaction event. A worst case scenario of a significant earthquake event on the Fraser Delta front could include the re-activation of the Roberts Bank Failure Wedge, consequent large scale damage to the Coal and Ferry terminals, initiation of a significant tsunami in the Strait of Georgia, with resulting damage to coastal installations and the severing of power and communications links between the British Columbian mainland and Vancouver Island. Given that the general conclusions of this study are correct, and that they appear to agree well with other studies, the next urgent question to be asked is 'what can be regarded as a significant earthquake, in terms of triggering liquefaction and further, how can the potential risks of such an shaking event be minimised or mitigated against?'.

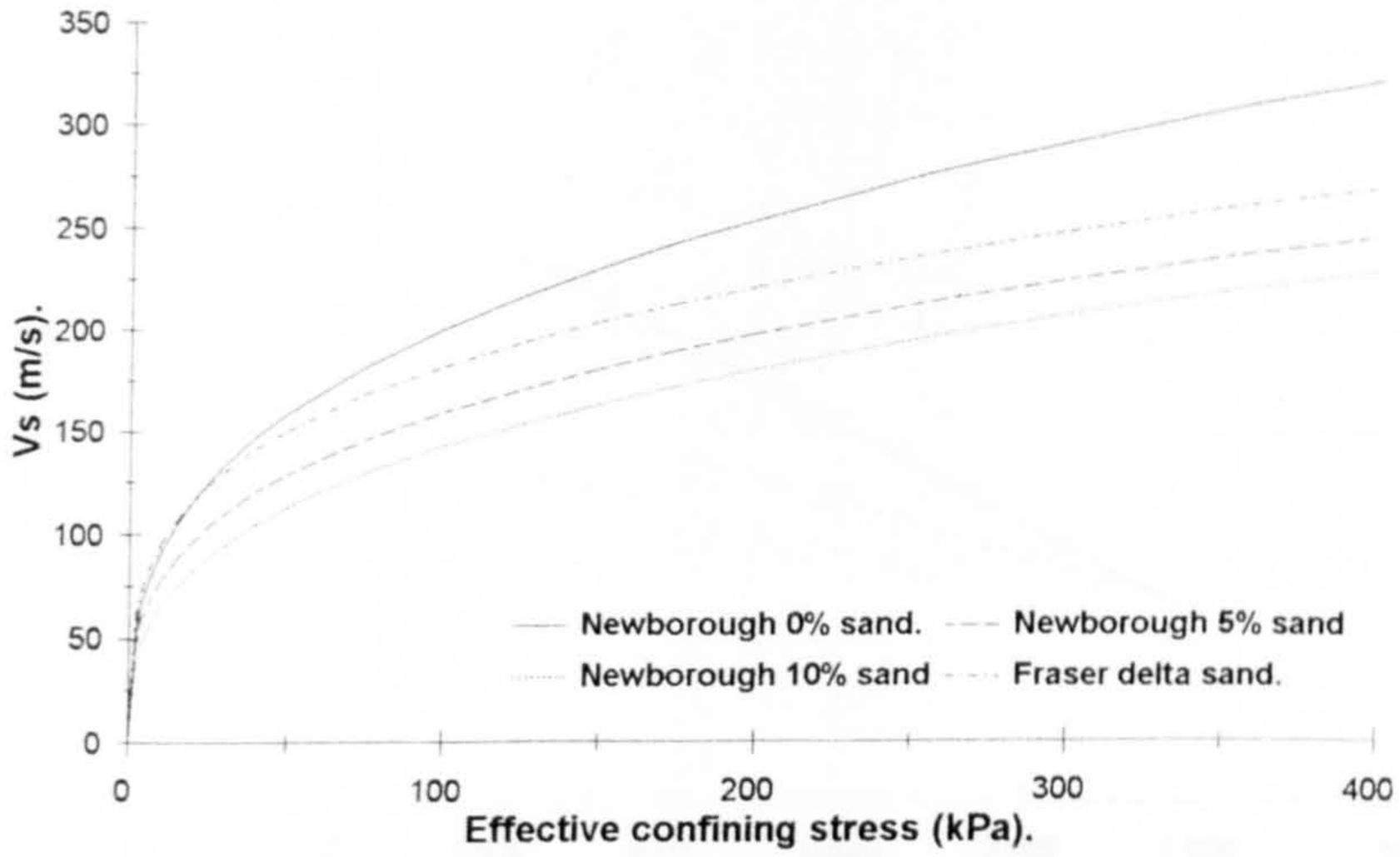

Figure 9.1. Summarised shear wave velocity - effective stress curves for all test sands Void ratio :- 0.700 for all samples.

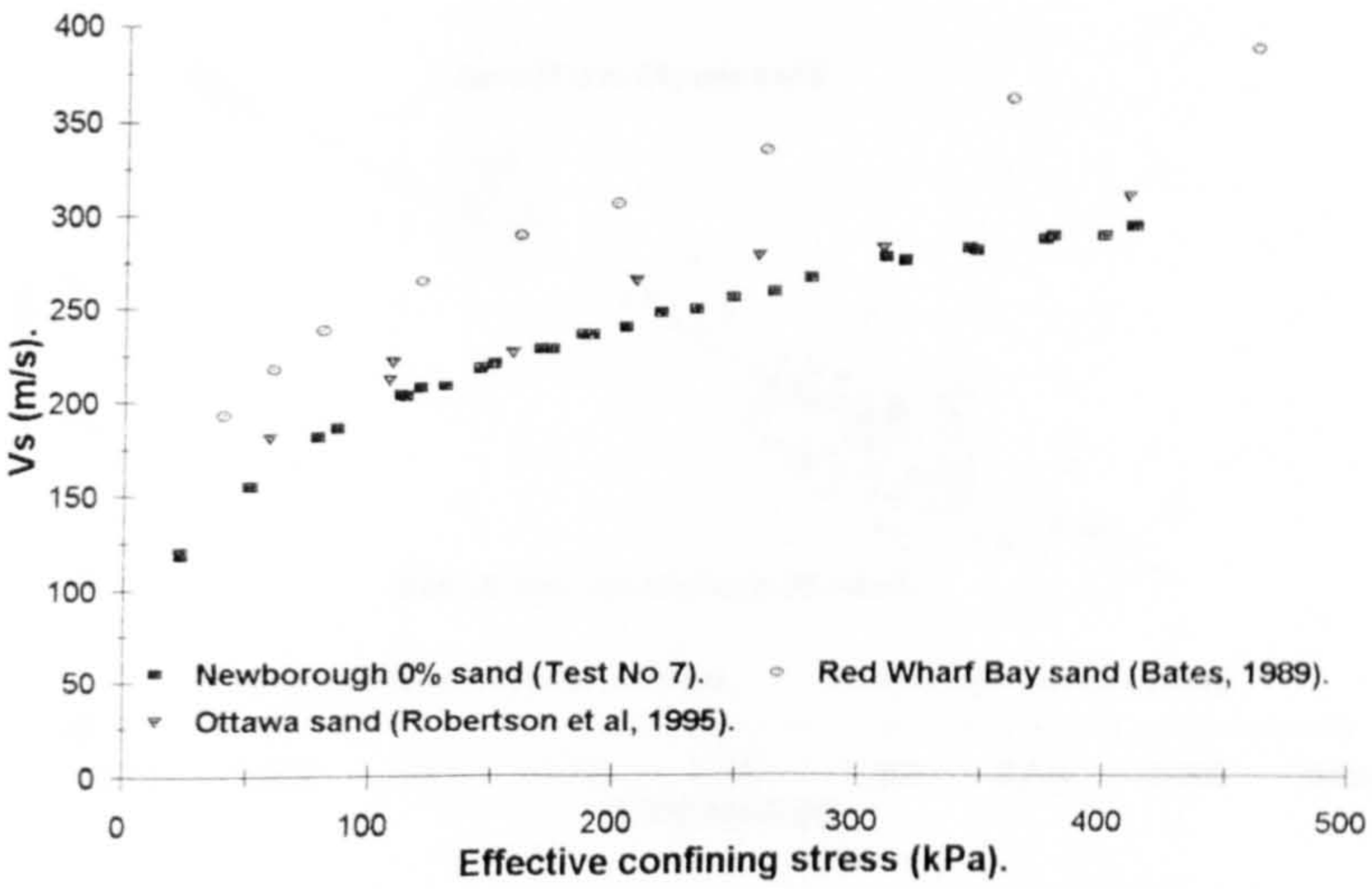

Figure 9.2. Qualitative comparison of typical Vs - p' data from this study and examples from the literature.

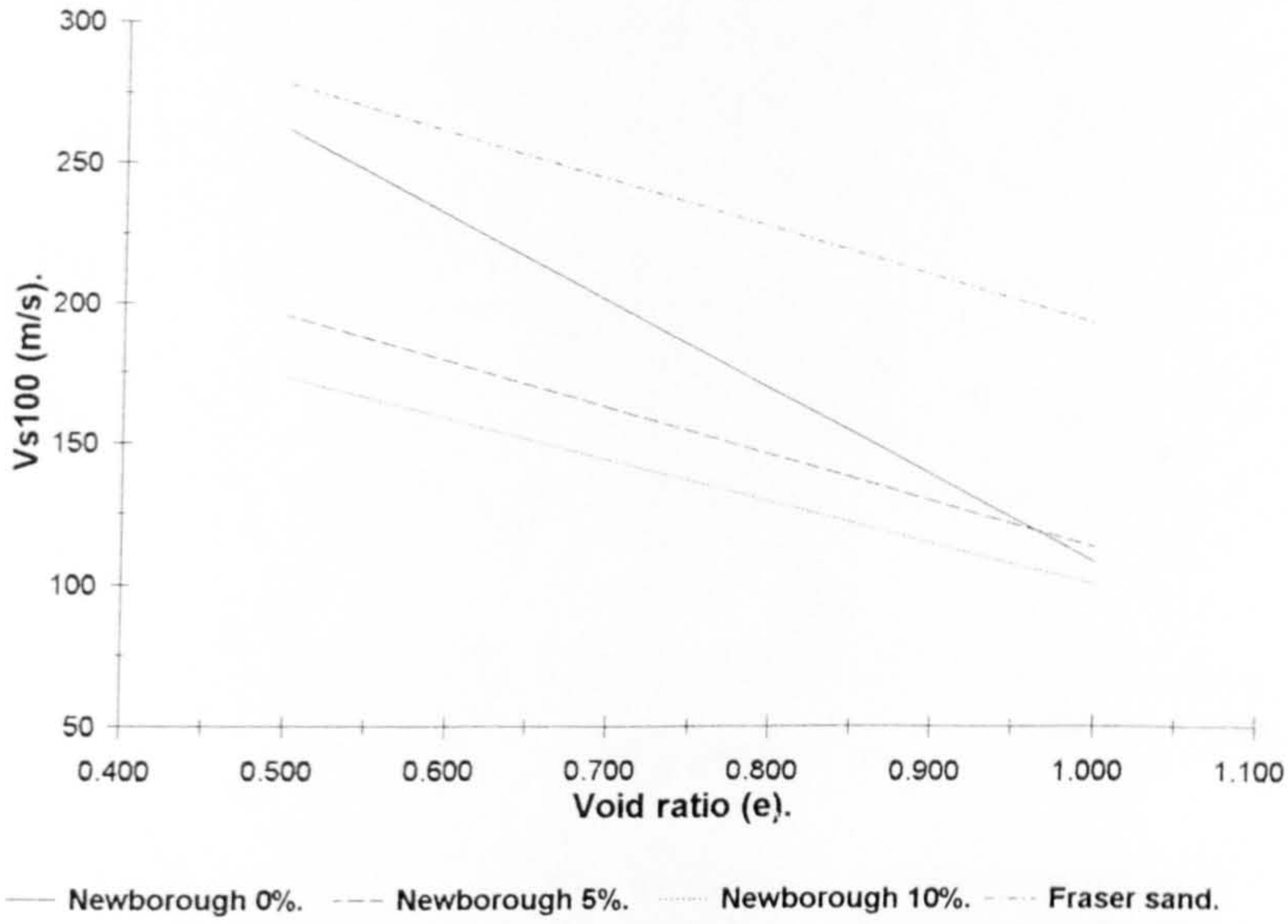

Figure 9.3. Comparison of Vs - e relationships, for all sands tested.

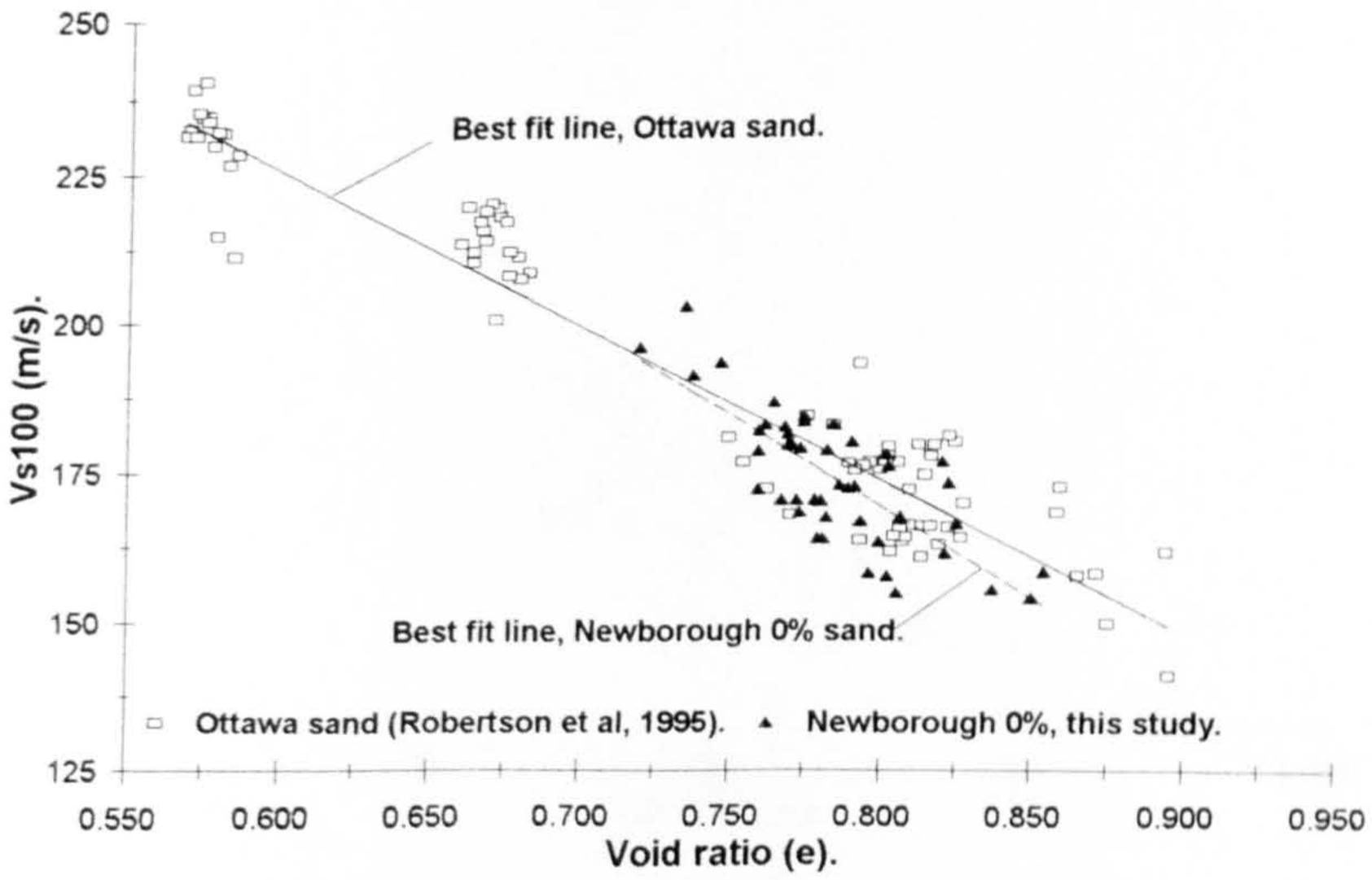

Figure 9.4. Detailed comparison between the Vs - e relationships of Ottawa and Newborough 0% sands.

a.

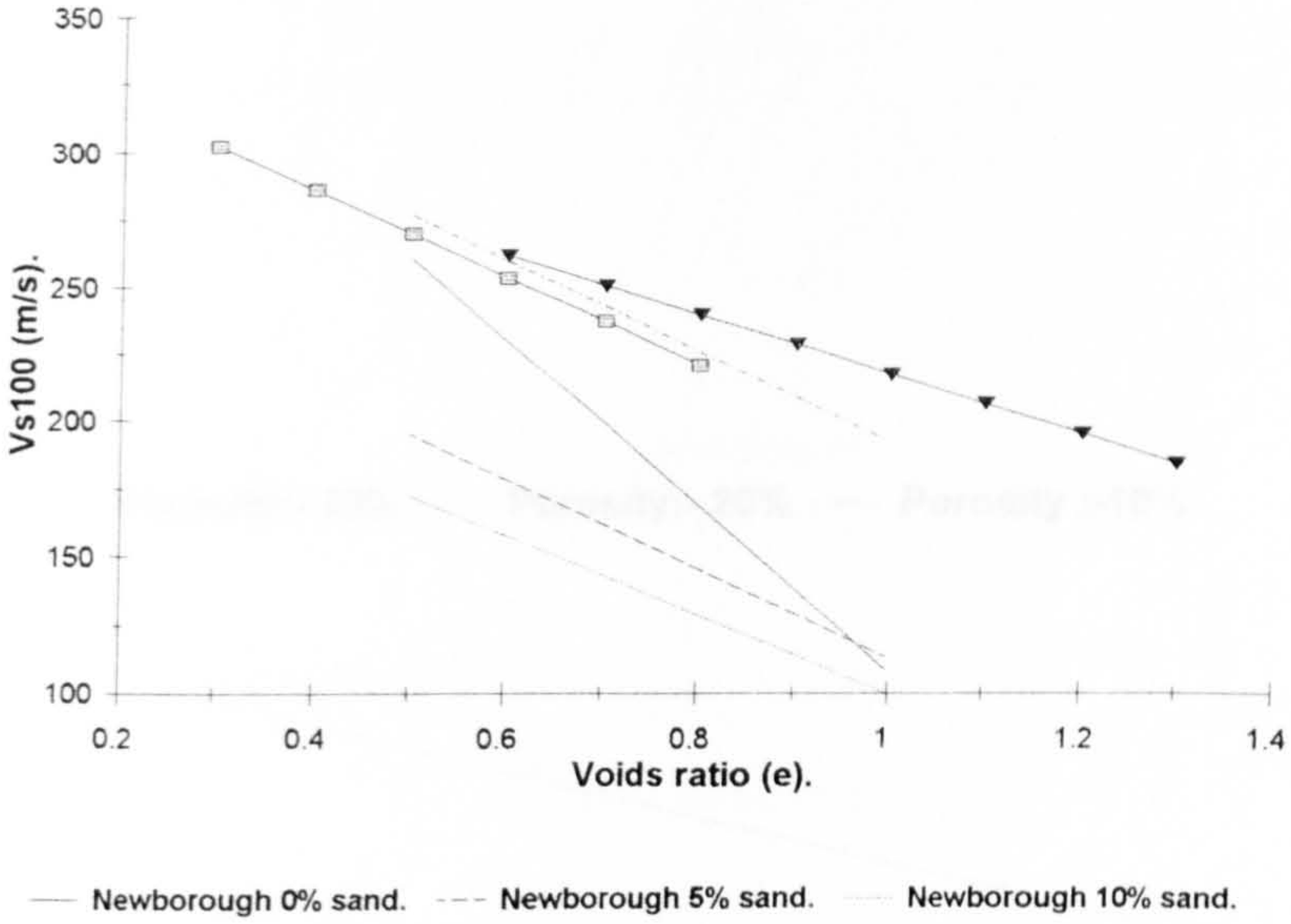

b.

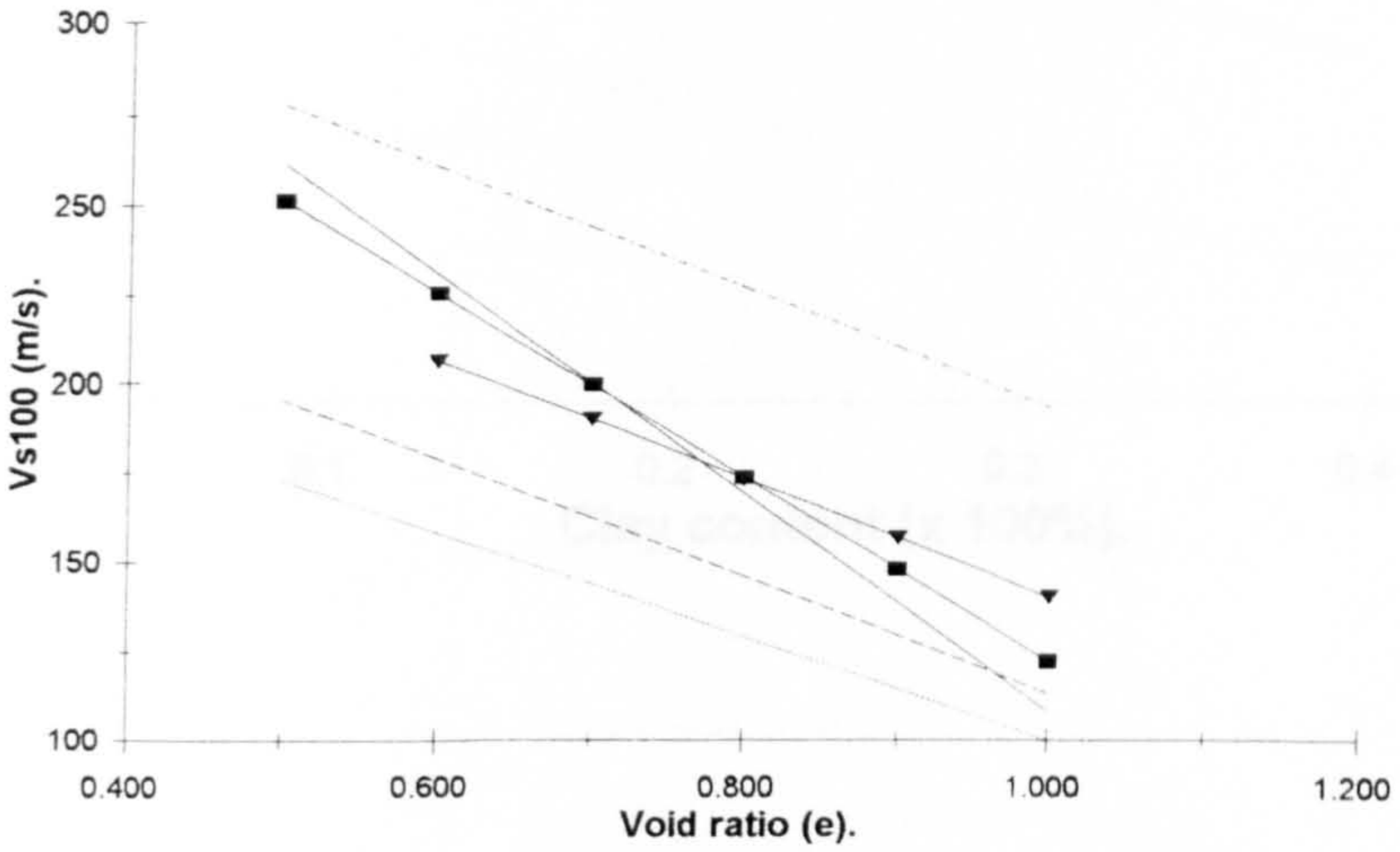

Figure 9.5. a. Comparison between Vs - e relationships from this study, and those obtained by Hardin & Black, 1963 (rounded and angular grained sands).

Figure 9.5. b. Comparison between Vs - e relationships from this study and those obtained by Robertson et al, 1995, and Cunning et al, 1995. (Ottawa and Syncrude sands).

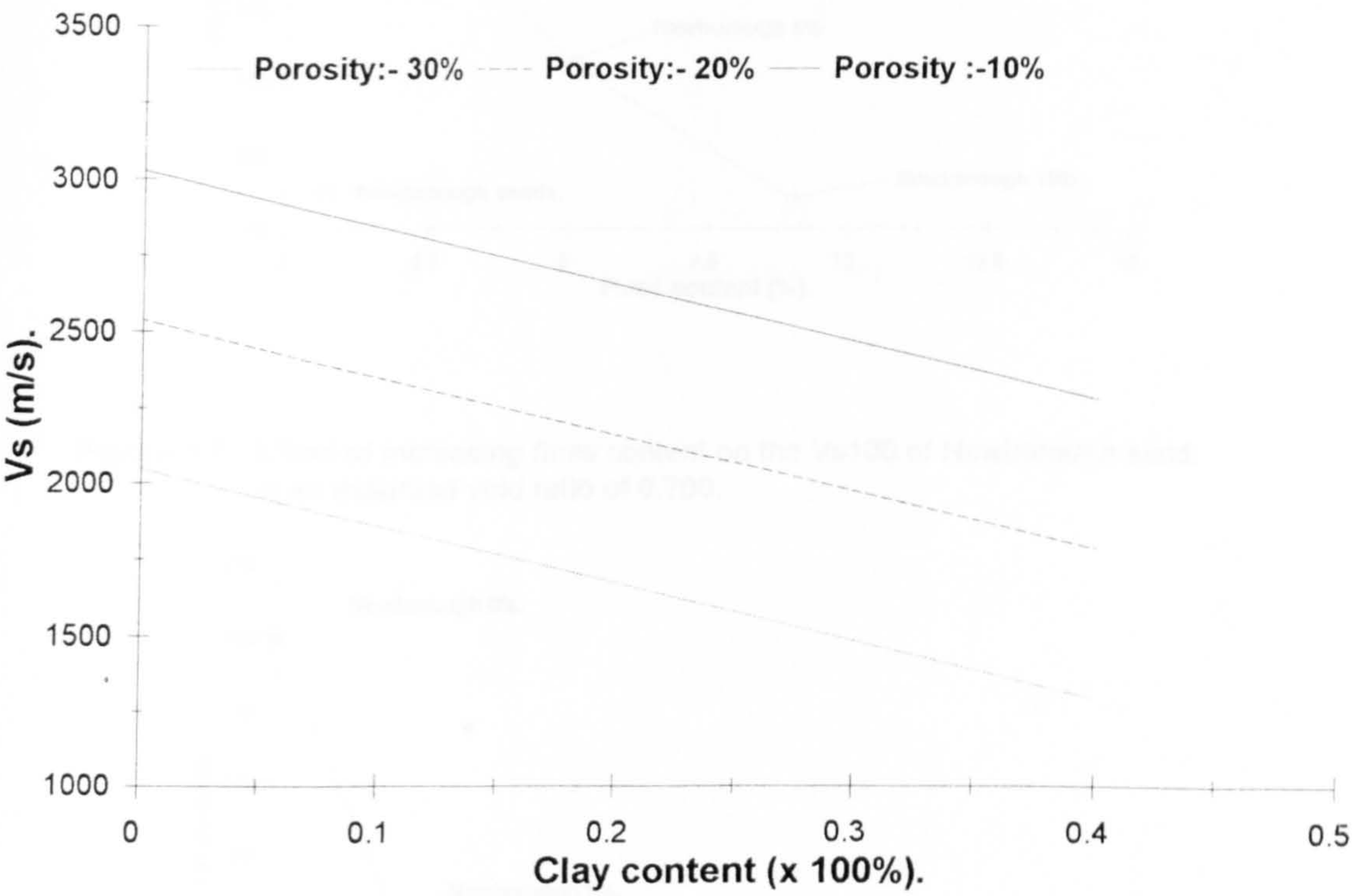

Figure 9.6. Illustration of the effect of increasing clay content on saturated sandstones over a range of porosities (*after Han et al., 1986*).

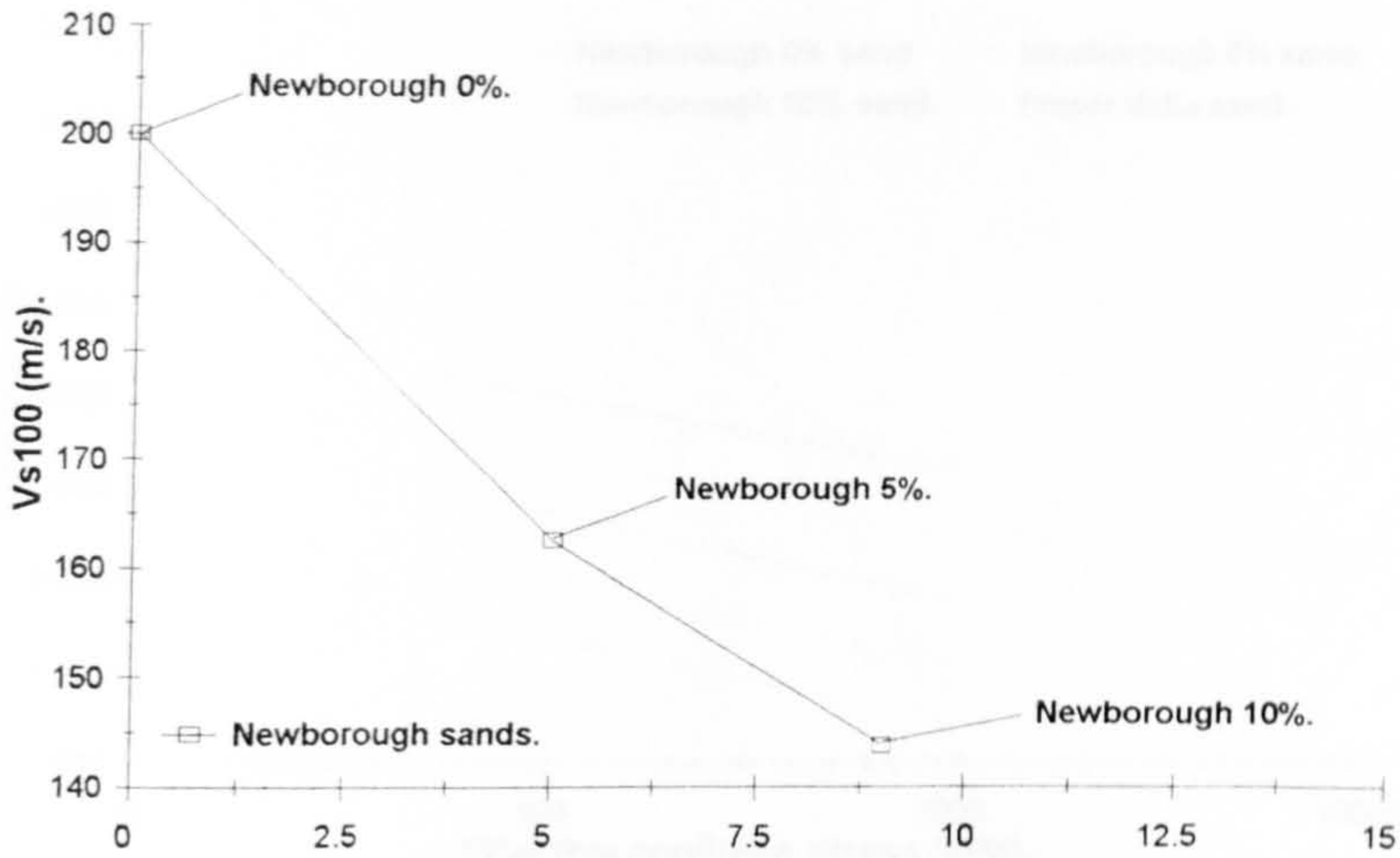

Figure 9.7. Effect of increasing fines content on the Vs100 of Newborough sand, at an assumed void ratio of 0.700.

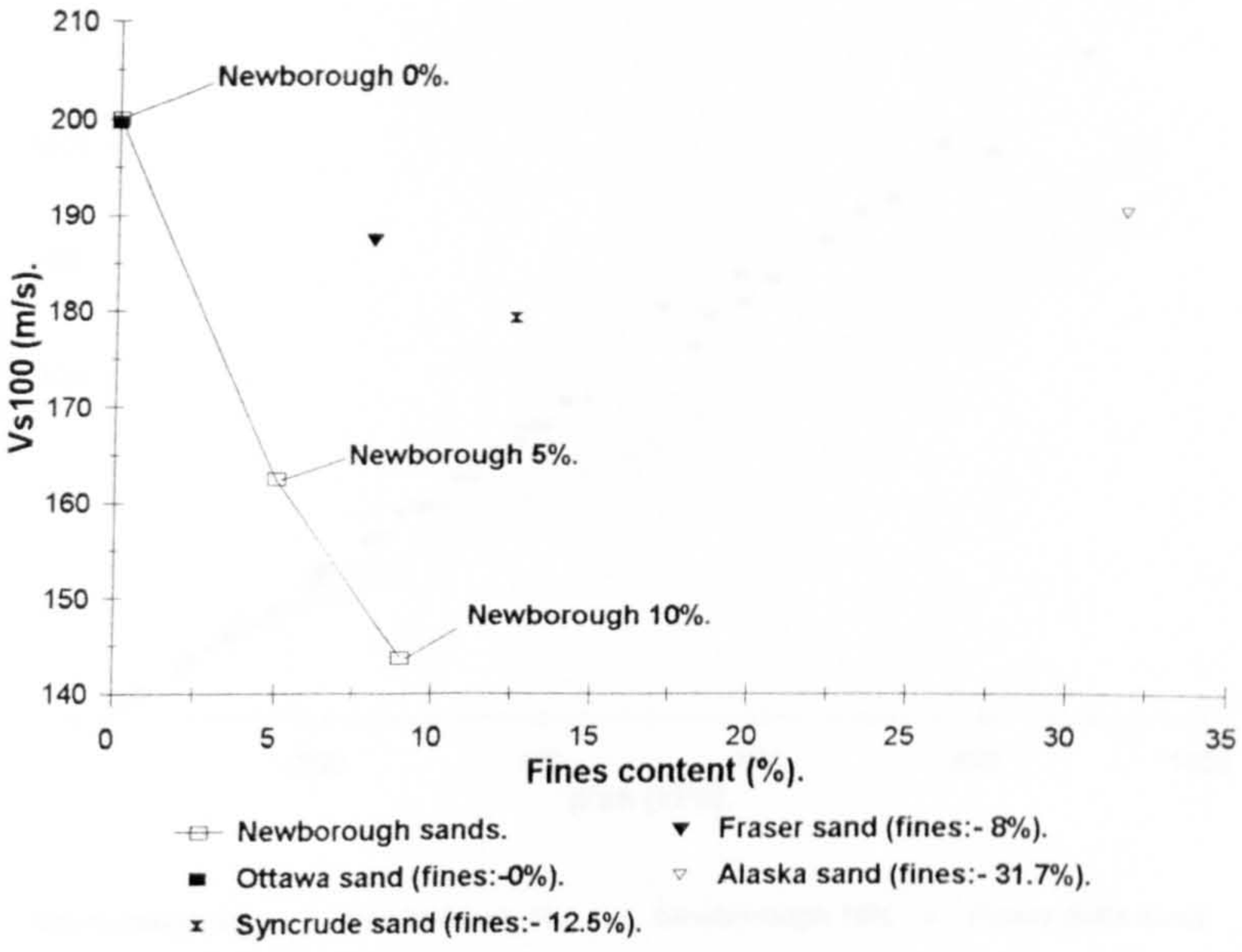

Figure 9.8. Relationship between Vs100 and fines content for different data published in the literature.

a.

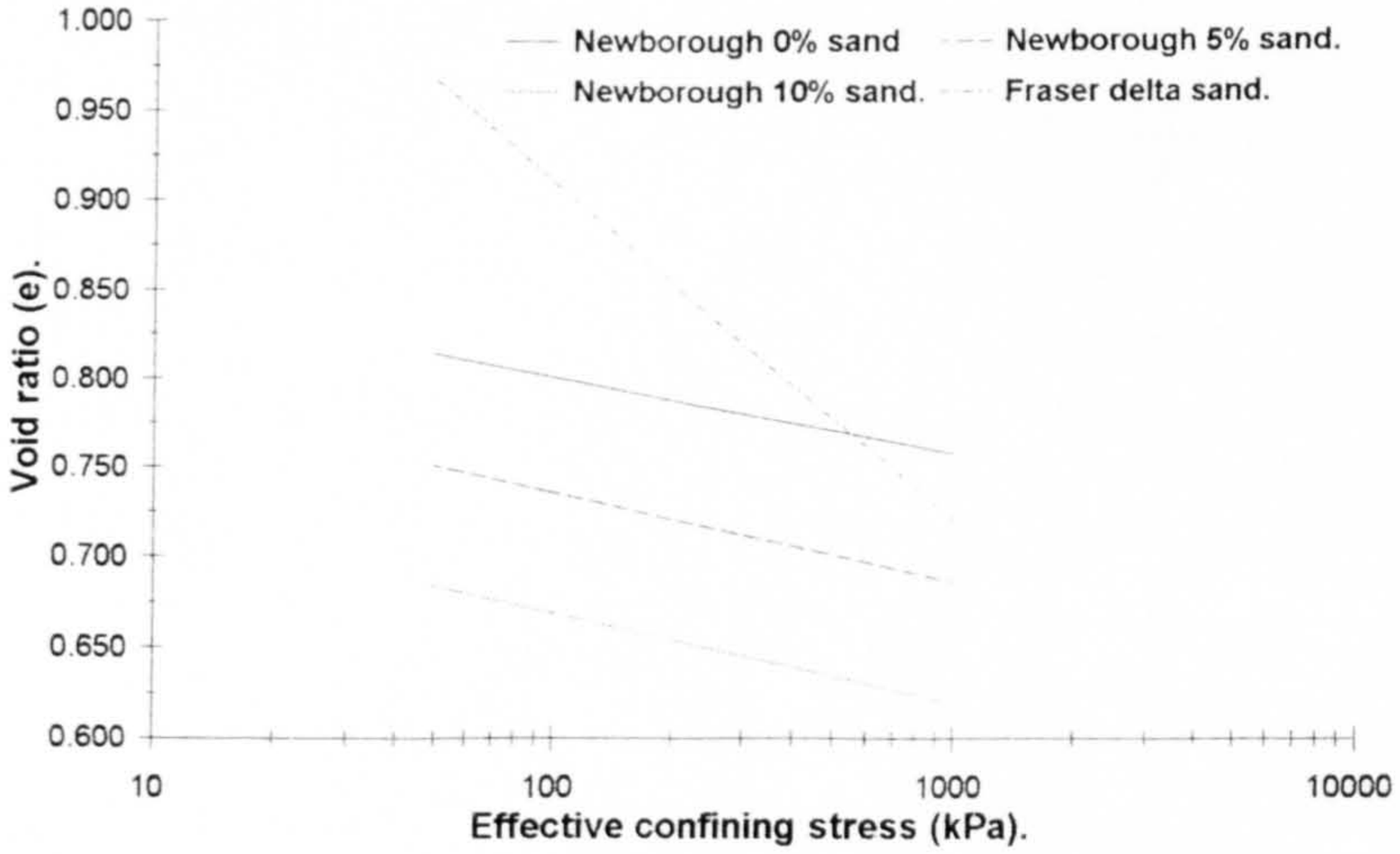

b.

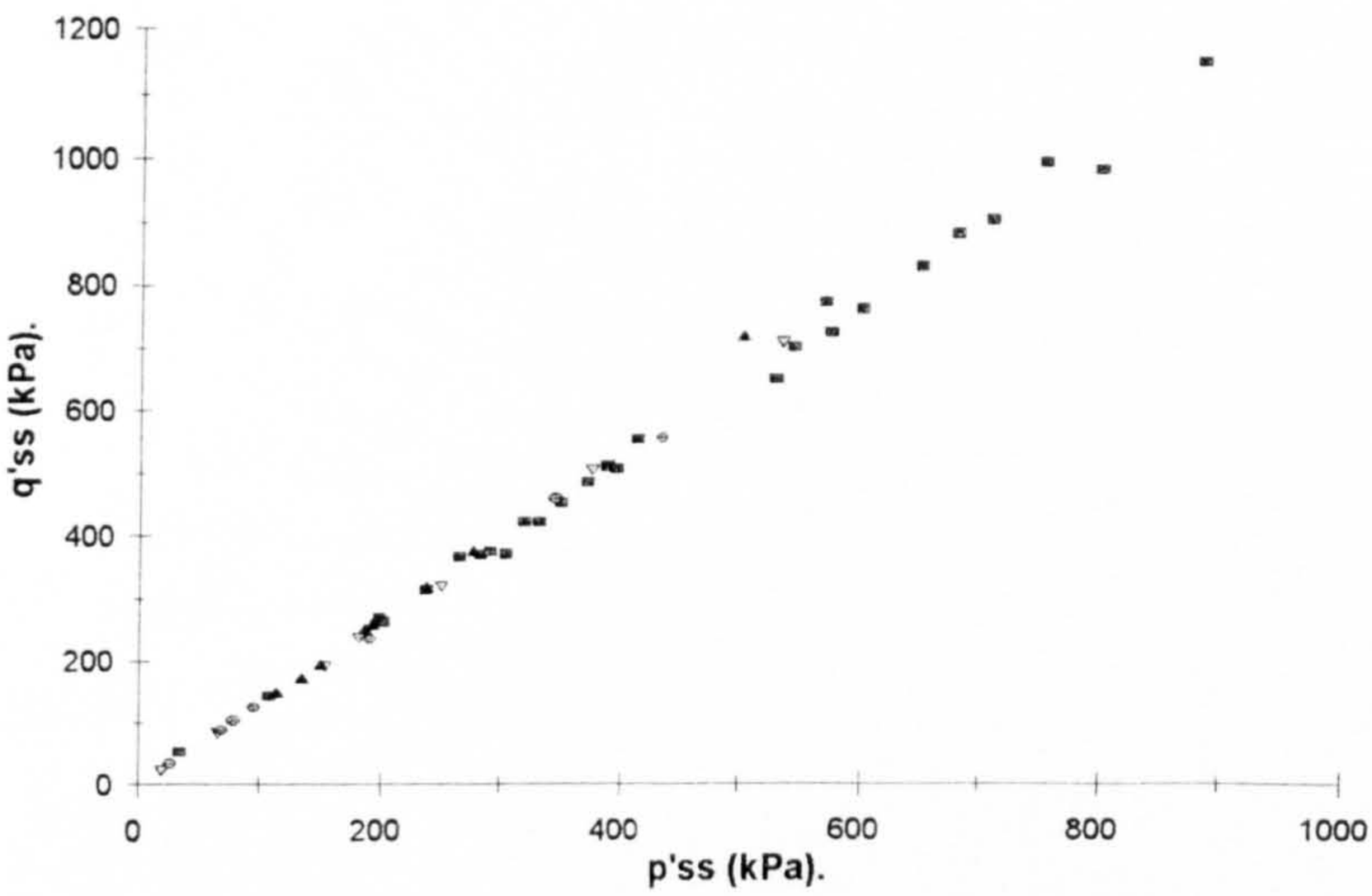

Figure 9.9. a. Steady state lines defined in e - log p' space, for the four test sands in this study.

Figure 9.9. b. Steady state data, defined in q - p space, for the four test sands.

a.

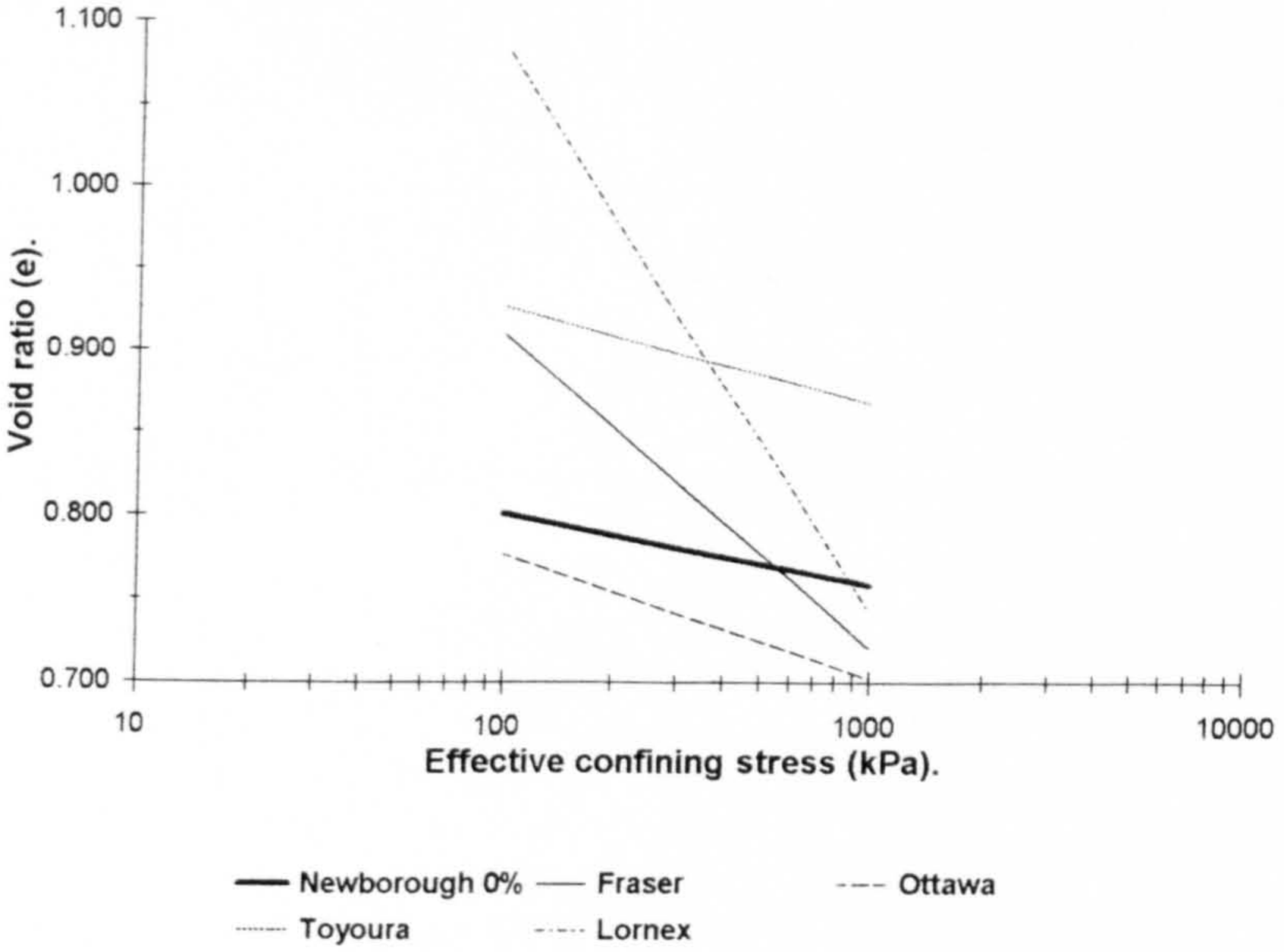

b.

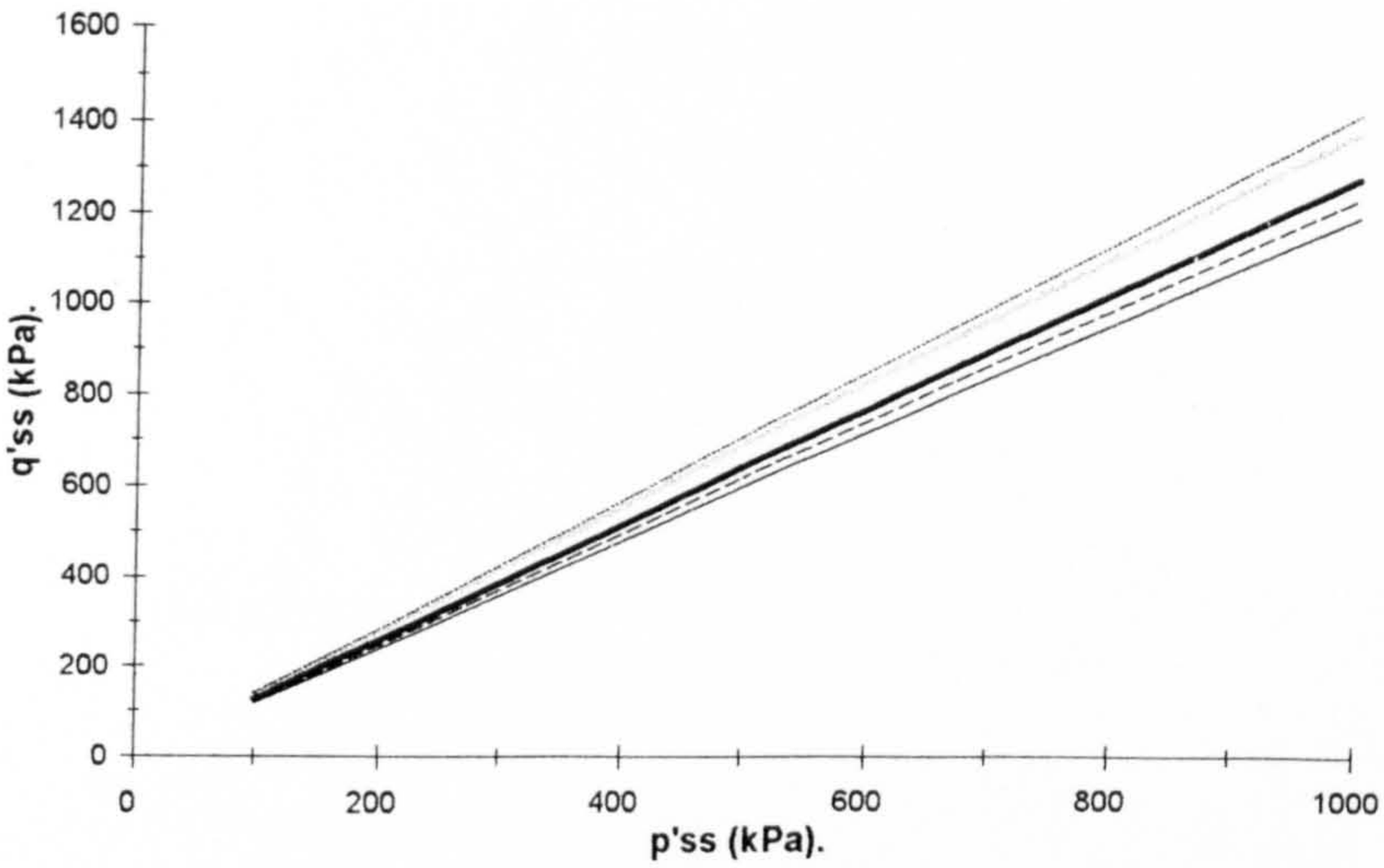

Figure 9.10. a. Comparison of selected steady state lines (this study) and those from the literature (Ottawa, Toyoura, Lornex).

Figure 9.10. b. Comparison of selected steady state lines (this study) and those from the literature (Ottawa, Toyoura, Lornex).

a.

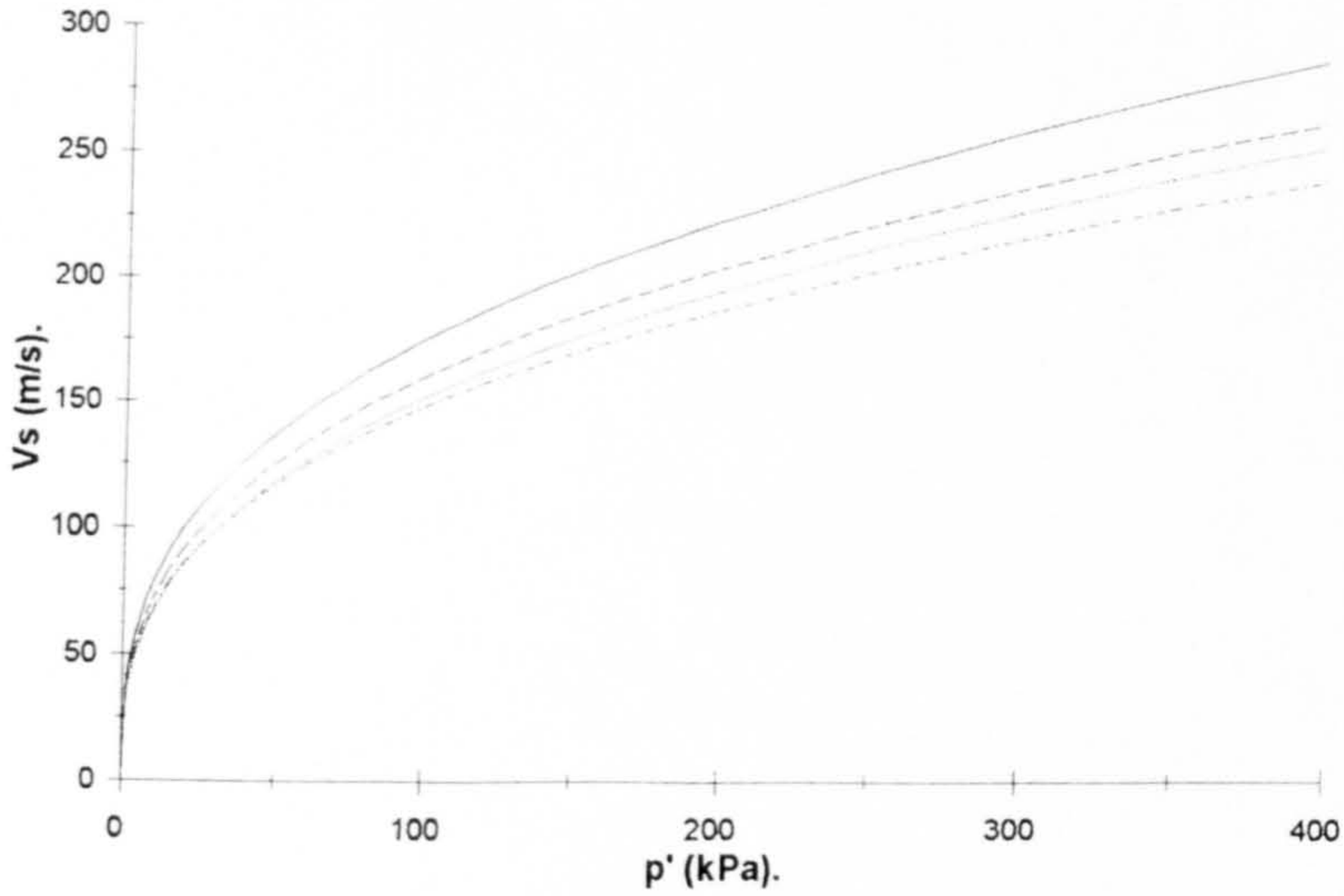

b.

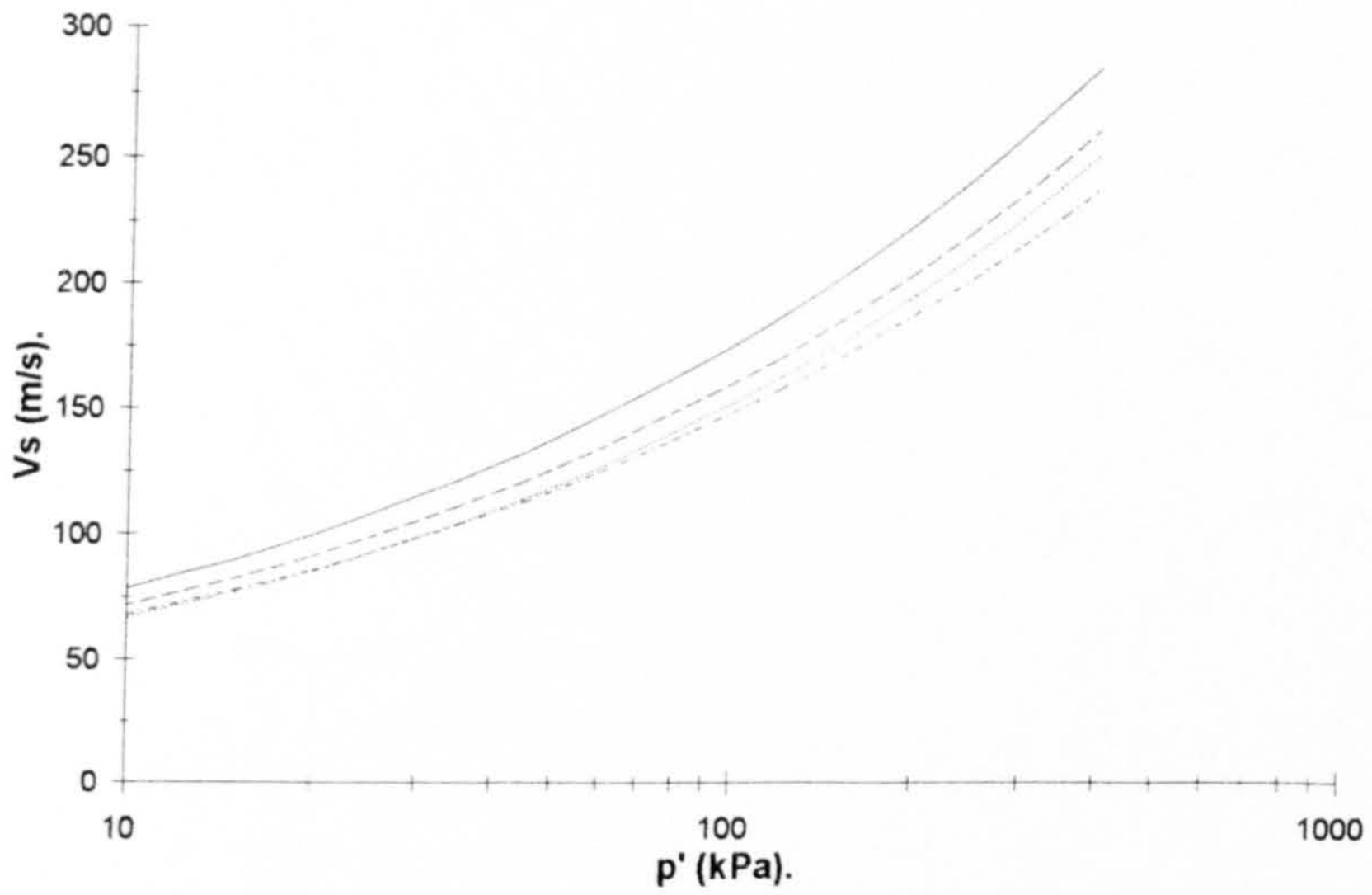

Figure 9.11. a. 'Critical shear wave velocity line' defined in Vs - p' space.

Figure 9.11. b. 'Critical shear wave velocity line' defined in Vs - log p' space.

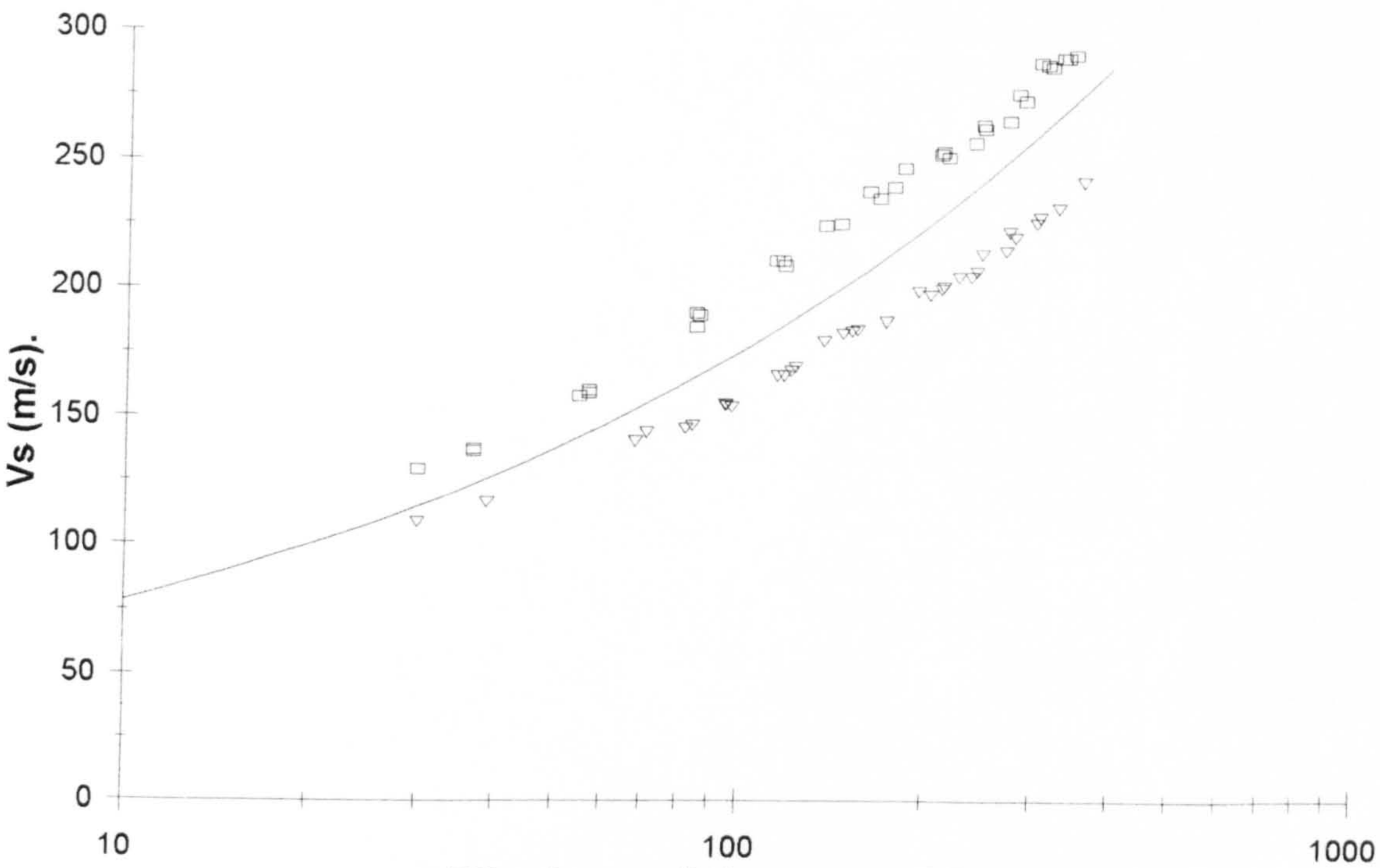

Figure 9.12. Newborough 0% 'critical velocity line', with additional laboratory measurements of shear wave velocity on loose and dense samples of the same sand.

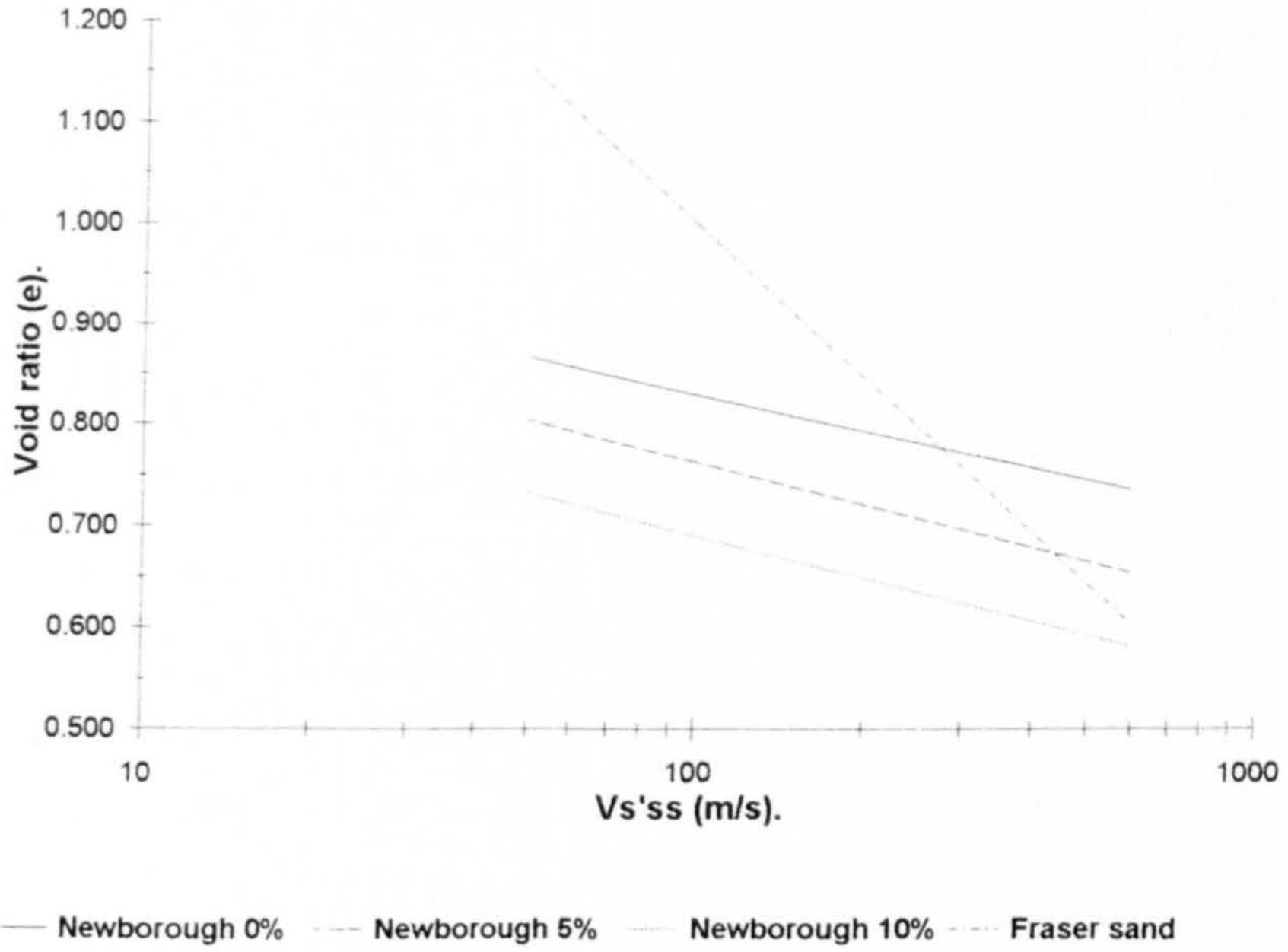

Figure 9.13. Steady state lines of all four test sands, defined in e - log Vs space.

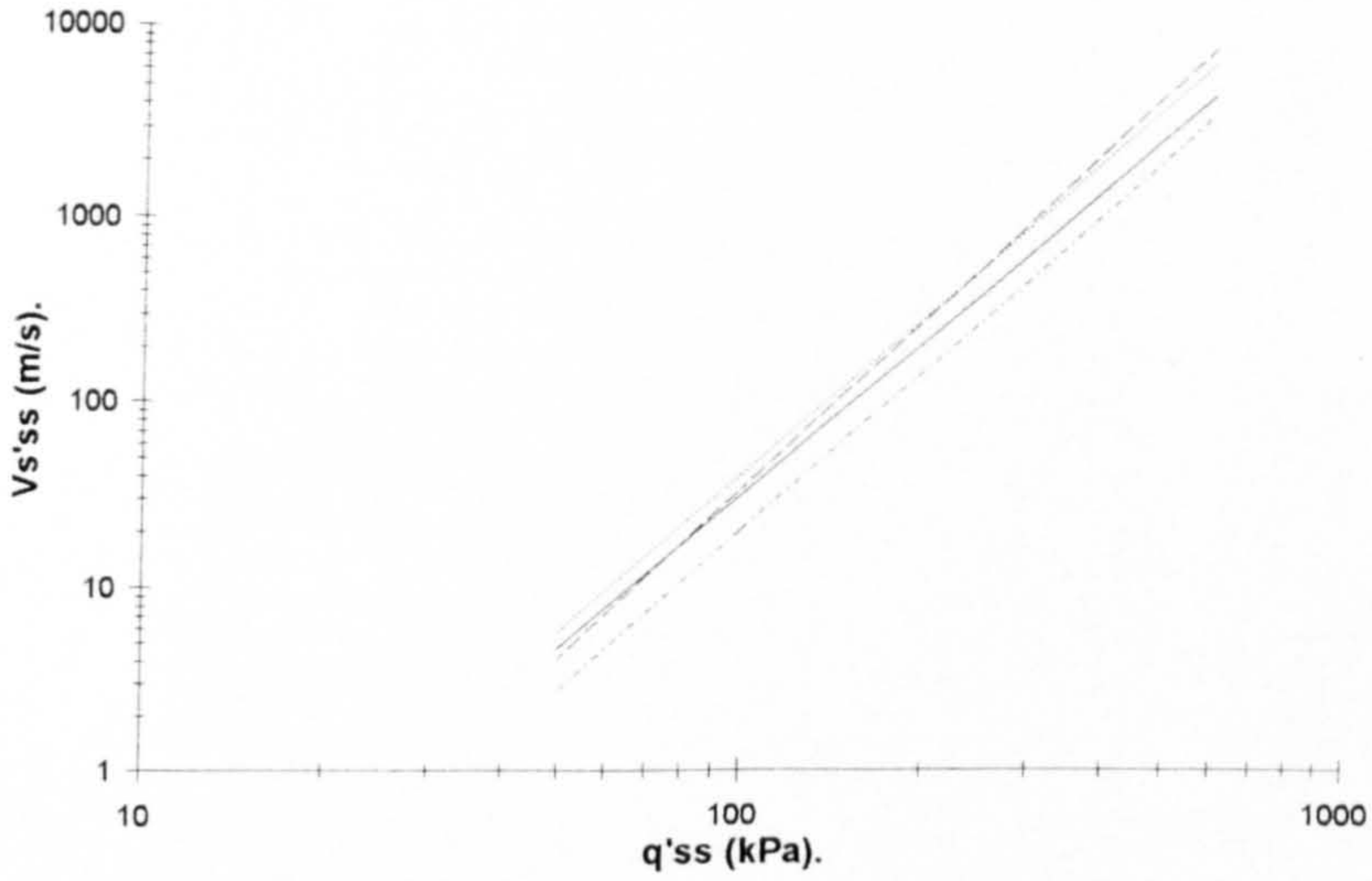

Figure 9.14. Steady state lines of the four test sands defined in log Vs - log q space.

CHAPTER 10.

CONCLUSIONS.

10.1. Introduction.

This research project represents an attempt to solve what may be regarded as an engineering problem, using a previously unattempted integration of generally accepted engineering methods and less conventional geophysical methods. As is obvious from the layout of the previous chapters, initial work was concentrated in the laboratory, and these findings were then applied to a field situation: the Fraser River Delta. Because the project and the thesis is so clearly divided into sections of laboratory and field research, it is inevitable that the conclusions will fall into similar sub-divisions.

10.2. Laboratory work.

The laboratory work may be further subdivided with conclusions concerning the measurement of shear wave velocities and steady state parameters initially treated separately, and then integrated.

10.2.1. Shear wave data.

The following conclusions may be drawn from the laboratory shear wave data:-

1. The shear wave velocity of uncemented sands may be routinely measured over a wide range of effective confining stresses using piezoelectric 'bender' elements potted in epoxy resin and mounted in the platens of a standard triaxial cell.
2. The disruptive 'near field' effects on the received waveform, described by Viggrani & Atkinson (1995), may be significantly reduced by increasing the travel path length. This was achieved using larger than 'normal' sample sizes; in the case of this study, sample size was nominally 200mm long, with a diameter of 100mm.
3. Adequate shear wave signals could be produced by using series poled transmitters and receivers, in contrast to the generally recommended series - parallel receiver - transmitter transducer arrangement. This has the significant advantage of simplifying transducer fabrication.

4. Shear wave velocities (V_s) for a specific sand sample are most strongly influenced by the effective confining stress (p'). For the four different test sands investigated during this study, shear wave velocity could be related to effective confining stress using the following general formulae:-

Newborough 0% sand, $V_s = 37 \times p'^{0.34}$ *(10.1)*

Newborough 5% sand, $V_s = 38 \times p'^{0.31}$ *(10.2).*

Newborough 10% sand, $V_s = 31 \times p'^{0.34}$ *(10.3).*

Fraser Delta sand, $V_s = 45 \times p'^{0.28}$ *(10.4).*

5. At a specific confining stress, the shear wave velocity of an uncemented, laboratory prepared sand is linearly related to the void ratio. Effective confining stress and void ratio may be related to shear wave velocity using the following general relationships:-

Newborough 0% sand, $V_s = (84 - 60e)p'^{0.34}$ *(10.5).*

Newborough 5% sand, $V_s = (65 - 38e)p'^{0.31}$ *(10.6).*

Newborough 10% sand, $V_s = (53 - 33e)p'^{0.34}$ *(10.7).*

Fraser Delta sand, $V_s = (79 - 41e)p'^{0.28}$ *(10.8).*

The effective stress range over which these relationships were obtained was in the range 20 - 400 kPa.

6. The addition of fine particles to a particular sand had the effect of (at a specific confining stress) decreasing the measured velocity. This decrease in velocity with increasing fines content is not as well defined in natural sands with varying fines content, suggesting that this effect is, in practice restricted to artificially prepared sands.

10.2.2. Triaxial data.

1. The steady state parameters of a sand may be defined using relatively simple consolidated, undrained triaxial tests on loose sands.
2. The steady state parameters of the four sands tested in this study are listed below.

Sand Type.	C_{ss}	e_1	M	ϕ'_{ss}	M_L	*Pressure range.*
Newborough 0%.	0.04	0.887	1.28	29°	1.25	30 - 900 kPa
Newborough 5%.	0.05	0.836	1.32	30°	1.15	20 - 600 kPa
Newborough 10%.	0.05	0.769	1.29	29°	1.19	20 - 500 kPa
Fraser Delta sand.	0.19	1.290	1.38	31°	-	100 - 500 kPa

Table 10.1. Steady state parameters defined for the four sands in this study.

3. The addition of fine particles of kaolinite to a sand dramatically lowered the position of the SSL in e log p' space, by as much as 0.05 in terms of void ratio. In contrast to much of the published literature, the addition of fine particles did not have any great influence on the gradient of the SSL.

10.2.3. Integrated geophysical - geotechnical data.

1. The shear wave velocity during undrained triaxial testing may be simply modelled by relating the velocity to the changing effective confining stress, using formulae such as Equations 10.1 - 10.4 above.
2. The calculation of a shear wave velocity at the steady state of deformation defines a 'steady state velocity' for a particular sand.
3. Plotting a number of steady state velocities in V_s - p' space allows the definition of a 'critical shear wave velocity line'. This boundary divides sand states with potentially contractive and dilative responses. In e - log p' space, the critical shear wave velocity line may be defined using:-

	Effective stress range.	
Newborough 0%, $V_s = 35 \times p'^{0.35}$	30 - 900 kPa.	*(10.9).*
Newborough 5%, $V_s = 32 \times p'^{0.35}$	20 - 600 kPa.	*(10.10).*
Newborough 10%, $V_s = 29 \times p'^{0.36}$	20 - 500 kPa.	*(10.11).*
Fraser Delta sand, $V_s = 31 \times p'^{0.34}$	100 - 500 kPa.	*(10.12).*

4. The void ratio at steady state may be estimated from a knowledge of the modelled shear wave velocity at steady state using,

Newborough 0%, $e_{ss} = -0.124(\log V_s'_{ss}) + 1.078$ *(10.13).*

Newborough 5%, $e_{ss} = -0.140(\log V_s'_{ss}) + 1.042$ *(10.14).*

Newborough 10%, $e_{ss} = -0.140(\log V_s'_{ss}) + 0.970$ *(10.15).*

Fraser Delta sand, $e_{ss} = -0.510(\log V_s'_{ss}) + 2.020$ *(10.16).*

5. The deviator stress at steady state may be related to the shear wave velocity at steady state using,

Newborough 0%, $\log(q'_{ss}) = 2.74(\log V_s'_{ss}) - 3.99$ *(10.17).*

Newborough 5%, $\log(q'_{ss}) = 3.02(\log V_s'_{ss}) - 4.52$ *(10.18).*

Newborough 10%, $\log(q'_{ss}) = 2.81(\log V_s'_{ss}) - 4.02$ *(10.19).*

Fraser Delta sand, $\log(q'_{ss}) = 2.85(\log V_s'_{ss}) - 4.40$ *(10.20).*

6. A new, shear wave velocity based index to sediment consolidation state, termed ψ_s, may be defined using:-

$$\psi_s = -(V_s'_c - V_{s\,crit}) \qquad (10.21).$$

where $V_{s\,crit}$ is the critical shear wave velocity at the same effective confining stress as the measured velocity, $V_s'_c$.

7. In the majority of cases, ψ_s was significantly related to both $\Delta p'$ and ψ at a confidence level of 95%. However in the laboratory at least, ψ proved to be a generally superior index to consolidation state than ψ_s.

10.3. Field data.

1. The seafloor shear wave refraction sledge may be used to produce shear wave refraction profiles. In the case of the Fraser Delta, the refraction data were interpreted to provide an 'apparent' V_1, V_2 and approximate depth to the first refractor. These measurements showed that in general the shear wave velocity of the upper 1m of sediment is of the order of 40 m/s, increasing to approximately 80m/s, at a depth of around 1.3m.

2. Shear wave velocities derived in the laboratory and from the seismic sledge in the field agree well with data derived from SCPT measurements for equivalent depths.
3. Analysis of liquefaction potential using shear wave and standard CPT based methods displayed a good qualitative agreement, illustrating that each method may be used to derive a similar conclusion.
4. Results from an analysis from both shear wave velocity and CPT based measurements illustrate that certain zones of the upper 20 - 30m of the sediment column of Roberts Bank will behave contractivley during shear, making liquefaction a distinct possibility.

10.4. Recommendations for further research and development.

Assuming an unlimited budget, the following recommendations may be made for further research:-

10.4.1. Laboratory based recommendations.

1. Use of a more modern triaxial apparatus, which will allow improvements to be made in terms of both improved monitoring of void ratio, shear wave velocities and data acquisition procedures.
2. Incorperation of electrodes into the triaxial cell, allowing the measurement of the electrical properties of the sample at steady state, in addtion to the shear wave properties.
3. Study of an increasing range of sand / clay mixtures and natural sediments to further quantify the effects of fines content on shear wave velocities.
4. Use of a cyclic triaxial apparatus allowing study of the commonly conflicting conclusions derived from cyclic and static test procedures.
5. Use of a six-degrees-of-freedom shake table to further study the relationships between purely triaxial derived conclusions and those derived from the *quasi* field conditions available from shake table testing.
6. Use of a calibration chamber and Cone Penetrometer rig, to further study the relationships between ψ, ψ_s and cone penetrometer based parameters.

10.4.2. Field based recommendations.

Many of the possible improvements to the shear wave sledge hardware are listed in Huws (1990), and will therefore be not listed in any further detail here. However, from the authors' own experience of the system the following improvements could offer further advantages, in terms of both data acquisition and interpretation:

1. Increasing the number of long - offset geophones could greatly increase long offset data acquisition.
2. Addition of a further source at the other end of the receiver string would allow both forward and reverse shot data to be collected, thus allowing improvements in the way the data collected can be interpreted.
3. Increasing the 'short offset' receiver string allowing an increased depth of investigation, thus extending the specific liquefaction investigations.
4. Increased number of geophones in the receiver string, allowing improved resolution of velocity - depth variability.
5. Sledge mounted cone penetrometer, allowing simultaneous detailed geotechnical analysis of surface sediments, and the production of depth profiles for a direct comparison.

10.5. Concluding comments.

The main aim of this Ph.D project was to thoroughly investigate the use of shear wave velocity as a tool for the prediction of liquefaction potential, initially with specific reference to laboratory prepared sands. Following on from this, any laboratory relationships elucidated were to be further applied in an attempt to quantify in some way the stability of the offshore Fraser River Delta. Additional use was to be made at this time of a large existing *in-situ* geophysical and geotechnical data set. The laboratory section of the study systematically revealed both the advantages and the limitations of the shear wave velocity approach to liquefaction prediction, particularly when combined with the theory of steady / critical state soil mechanics. The field study revealed the potential for using shear wave velocity methods in an attempt to quantify the liquefaction potential in otherwise difficult to sample sediments. The fact that the proposed shear wave method and conventional methods produced broadly similar conclusions can only add to the viability of the proposed technique. However, a balanced view of the use of

shear wave velocity in liquefaction prediction is extremely important and, as has already been stated, the methods described above are at their most useful as part of a fully integrated geotechnical - geophysical site investigation.

CHAPTER 11.

REFERENCES.

Alarcon-Guzman, A., Leonards, G. A., & Chameau, J. L. (1987). Undrained monotonic and cyclic strength of sands. Journal of Geotechnical Engineering, 114(10), 1089-1109.

Baldwin, K. C., De Alba, P. A., & Jones, A. N. (1991). Relationship between acoustic and mechanical properties of two marine clays. In J. M. Hovem, M. D. Richardson, & R. D. Stoll (Eds.), Shear Waves in Marine Sediments. (pp. 95-102). La Spezia, Italy: Kluwer Acacdemic Publishers.

Bates, C. R. (1989). Dynamic soil property measurements during triaxial testing. Geotechnique, 39(4), 721-726.

Been, K., Crooks, J. H. A., Becker, D. E., & Jefferies, M. G. (1986). The cone penetration test in sands: part I, state parameter interpretation. Geotechnique, 36(2), 239-249.

Been, K., & Jefferies, M. G. (1985). A state parameter for sands. Geotechnique, 35(2), 99-112.

Been, K., Jefferies, M. G., Crooks, J. H. A., & Rothenburg, L. (1987). The cone penetration test in sands: part II, general inference of state. Geotechnique, 37(3), 285-299.

Been, K., Jefferies, M. G., & Hachey, J. (1991). The critical state of sands. Geotechnique, 41(3), 365-381.

Bennell, J. D., & Taylor-Smith, D. (1991). A review of laboratory shear wave techniques and attenuation measurements with particular reference to the resonant column. In J. M. Hovem, M. D. Richardson, & R. D. Stoll (Eds.), Shear Waves in Marine Sediments. (pp. 83-93). La Spezia, Italy: Kluwer Academic Publishers.

Bishop, A. W., & Henkel, D. J. (1964). The measurement of soil properties in the Triaxial Test. (2 ed.). Edward Arnold Ltd.

Bjerrum, L., & Landra, A. (1966). Direct simple shear tests on a Norwegian quick clay. Geotechnique, 16, 1-20.

Bowles, J. E. (1992). Engineering properties of soils and their measurement (4th ed.). McGraw-Hill.

Bryan, G. M., & Stoll, R. D. (1988). The dynamic shear modulus of marine sediments. Journal of the Acoustical Society of America, 83(6), 2159-2164.

Bryne, P. M., & Anderson, L. D. (1987). Earthquake Design in Richmond, British Columbia, Version II. No. Soil Mechanics Series No. 109). University of British Columbia, Dept. of Civil Engineering.

Campbell, D. D., & Rotzein, J. L. (1992). Deterministic basis for seismic design in British Columbia. In Geohazards, '92. Geotechnique and natural hazards, (pp. 71-78). Vancouver: BiTec Publishers Ltd.

Canada, E. (1988). Sediment data, British Columbia, 1986 No. Enivironment Canada, Inland waters, Water Resources Branch.

Cao, Y. L., & Law, K. T. (1992). Energy dissipation and dynamic behaviour of clays under cyclic loading. Canadian Geotechnical Journal, 29, 103-111.

Casagrande, A. (1936). Characteristics of cohesionless soils affecting the stability of slopes and earth fills. Journal of the Boston Society of Civil Engineers., January.

Casagrande, A. (1975). Liquefaction and cyclic deformation of sands: a critical review. In Procedings of the 5th American Conference on Soil Mechanics and Erthquake Engineering, (pp. 80-133). Buenos Aires.

Castro, G. (1975). Liquefaction and cyclic mobility of saturated sands. Journal of the Geotechnical Engineering Division, ASCE, 101(GT6), 550-569.

Castro, G., & Christian, J. T. (1976). Shear strength of soils and cyclic loading. Journal of the Geotechnical Engineering Division, ASCE, 102(GT9), 887-894.

Castro, G., Seed, R. B., Keller, T. O., & Seed, H. B. (1992). Steady-state strength analysis of Lower San Fernando Dam slide. Journal of Geotechnical Engineering, 118(3), 406-427.

Chandler, R. J., Leroueil, S., & Trenter, N. A. (1990). Measurements of the permeability of London Clay using a self-boring pressuremeter. Geotechnique, 40(1), 113-124.

Charlie, W. A., Scott, C. E., Siller, T. J., Bulter, L. W., & Doehring, D. O. (1995). Estimating liquefaction potential of sand using the Piezovane. Geotechnique, 45(1), 55-67.

Christian, H. A. (1993). In-situ measurement of consolidation and permeability of soft marine sediments. In L. Boone, R. Mckenna, M. Paulin, & K. Witney (Ed.), Proceedings of the 4th Canadian Conference on Marine Geotechnical Engineering, 2 . St. Johns, Newfoundland.

Clague, J. J., Luternauer, J. L., & Hebda, R. J. (1983). Sedimentary environments and postglacial history of the Fraser Delta and lower Fraser valley, British Columbia. Canadian Journal of Earth Sciences, 20, 1314-1326.

Clague, J. J., Luternauer, J. L., Pullan, S. E., & Hunter, J. A. (1991). Postglacial deltaic sediments, southern Fraser River Delta, British Columbia. Canadian Journal of Earth Sciences, 28(9), 1386-1393.

Clague, J. J., Naesgaard, E., & Sy, A. (1992). Liquefaction features on the Fraser Delta: evidence for pre-historic earthquakes? Canadian Journal of Earth Sciences, 29, 1734-1745.

Clough, G. W., Lwabuchi, J., Rad, S. N., & Kuppusamy, T. (1989). Influence of cementation on liquefaction of sands. Journal of Geotechnical Engineering, 115(8), 1102-1117.

ConeTec Ltd. (1993). Results of CPT, RCPT, SCPT & SASW Testing at Roberts Bank and Sand Heads, Fraser River Delta, Vancouver, British Columbia No. Atlantic Geoscience Centre.

Cullingford, G., Lashine, A. K. F., & Parr, G. B. (1972). Servo-controlled equipment for dynamic triaxial testing of soils. Geotechnique, 22(3), 526-529.

Cunning, J. C., Robertson, P. K., & Sego, D. C. (1995). Shear wave velocity to evaluate the in-situ state of cohesionless soils. Canadian Geotechnical Journal: Preprint.

Davis, A. M., & Bennell, J. D. (1985). Dynamic properties of marine sediments. In T. Akal & J. M. Berkson (Ed.), Ocean seismo-acoustics. Low frequency underwater acoustics. NATO conference series IV, Marine sediments, 16 (pp. 501-510). La Spezia, Italy: Publihed in co-operation with NATO scientific affairs & the Plenum Press c. 1986.

Davis, A. M., Bennell, J. D., Huws, D. G., & Thomas, D. (1989). Development of a seafloor geophysical sledge. Marine Geotechnology, 8, 99-109.

De Alba, P., Baldwin, K., Janoo, V., Roe, G., & Celikkol, B. (1984). Elastic wave velocities and liquefaction potential. Geotechnical Testing Journal, 7(2), 77-87.

Dikmen, S. U., & Ghaboussi, J. (1984). Effective stress analysis of seismic response and liquefaction: theory. Journal of Geotechnical Engineering, 10(5), 628-658.

Dobry, R., Stokoe II, K. H., Ladd, R. S., & Youd, T. L. (1981). Liquefaction susceptability from shear wave velocity. In American Society of Civil Engineers National Convention, . St. Louis, Missouri.

Drnevich, V. P. (1972). Undrained cyclic shear of saturated sand. Journal of the Soil Mechanics & Foundations Division, ASCE, No SM8, 807-825.

Dyvik, R., & Madshus, C. (1985). Lab measurements of Gmax using bender elements. In V. Kholsa (Eds.), Advances in the art of testing soils under cyclic conditions (pp. 186-196). ASCE.

Fahey, M., & Randolph, M. F. (1984). Effect of disturbance on parameters derived from the self-boring pressuremeter tests in sands. Geotechnique, 34(1), 81-97.

Finn, W. D. L. (1972). Soil dynamics liquefaction..... In Microzonation for safer construction research & application, 1 (pp. 87-111). Seattle.

Finn, W. D. L., Bransby, P. L., & Pickering, D. J. (1970). Effect of strain history on liquefaction of sand. Journal of the Soil Mechanics and Foundation Division; Proceedings of the ASCE, 96(SM6), 1917-1934.

Finn, W. D. L., Lee, K. W., & Martin, G. R. (1977). An effective stress model for liquefaction. Journal of the Geotechnical Engineering Division, ASCE, 103(GT6), 517-533.

Ghaboussi, J., & Dikmen, S. U. (1984). Effective stress analysis of seismic response and liquefaction: case studies. Journal of Geotechnical Engineering, 110(5), 645-658.

Grainger, G. D., & Lister, N. W. (1962). A laboratory apparatus for studying the behaviour of soils under repeated loading. Geotechnique, 12, 3-14.

Green, G. E., & Reades, D. W. (1975). Boundary conditions, anisotropy and sample shape effects on the stress-strain behaviour of sand in triaxial compression and plane strain. Geotechnique, 25(2), 333-356.

Hamilton, E. L. (1976). Shear wave velocity versus depth in marine sediments: a review. Geophysics, 41(5), 985-996.

Hamilton, T. S. (1987). The Foreslope Hills of the Fraser Delta: implications for Tsunamis in the Georgia Strait. International Journal of the Tsunami Society, 5(1), 15-33.

Han, D., Nur, A., & Morgan, D. (1986). Effects of porosity and clay content on wave velocities in sandstones. Geophysics, 51(11), 2093-2107.

Hardin, B. O., & Black, W. L. (1968). Vibration Modulus of Normally Consolidated Clay. Journal of the Soil Mechanics and Foundation Division; Proceedings of the ASCE, 94(SM2), 353-369.

Hardin, B. O., & Drnevich, V. P. (1972). Shear modulus and dampling in soils: measurement and parameter effects. Journal of the Soil Mechanics and Foundation Division; Proceedings of the ASCE, 98(SM6), 603-624.

Hardin, B. O., & Richart, F. E. J. (1963). Elastic wave velocities in granular soils. Journal of the Soil Mechanics and Foundation Division; Proceedings of the ASCE, 89(SM1), 33-69.

Harris, J. B., Hunter, J. A., Luternauer, J. A., & Finn, W. D. L. (1995). Earthquake hazards of the Fraser Delta, British Columbia: sediment thickness, shear wave velocity and site response. In Victoria '95 GAC/MAC Annual Conference, (pp. 42). Victoria, British Columbia.

Hart, B. S., Hamilton, T. S., Barrie, J. V., Currie, R. G., & Prior, D. B. (1992a). Marine geophysical and geological surveys of the Fraser delta slope and adjacent Strait of Georgia: 1991 Geophysical survey track lines and 1983-1992 core locations. (Open file 2543). Geological Survey of Canada.

Hart, B. S., Horel, G., Olynyk, H. W., & Frydecky, I. (1992b). An airgun seismic survey of the Fraser Delta slope, offshore British Columbia. Current Research, Part E, Geological Survey of Canada, 33-39.

Hart, B. S., Prior, D. B., Hamilton, T. S., Barrie, T. S., Barrie, J. V., & Currie, R. G. (1992c). Patterns and styles of sedimentation, erosion and failure, Fraser Delta slope, British Columbia. In Geohazards'92. Geotechnique and Natural Hazards, (pp. 365-372). Vancouver: BiTec Publishers Ltd.

Hepton, P. (1989) Shear wave velocity measurements during penetration testing. PhD, University of Wales, Bangor.

Holzer, T. L., Youd, T. L., & Hanks, T. C. (1989). Dynamics of liquefaction during the 1987 Superstition Hills, Califomia, Earthquake. Science, 244(7 April), 57-59.

Huws, D. G. (1990). A system to measure the in-situ physical properties of marine sediments. Underwater Technology, 16(1), 30-32.

Huws, D. G. (1993) Measuring and modelling the in-situ physical properties of marine sediments. Ph.D, University of Wales, Bangor.

Ishihara, K. (1993). Liquefaction and flow failure during earthquakes. Geotechnique, 43(3), 351-415.

Jewell, R. J., Fahey, M., & Wroth, C. P. (1980). Laboratory studies of the pressuremeter test in sand. Geotechnique, 30(4), 507-531.

Jones, S. E. (1990) Geophysical properties of surficial intertidal sediments: textural and biological controls. Ph.D, University of Wales.

Jones, S. E., & Jago, C. F. (1991). Small scale in-situ measurements of SH velocity in surficial sedimentary deposits: localized testural and biological controls. In J. M. Hovem, M. D. Richardson, & R. D. Stoll (Eds.), Shear Waves in Marine Sediments, (pp. 313-320). La Spezia, Italy: Kluwer Academic Publications.

Kawakami, F., & Asada, A. (1966). Damage to the ground and earth structures by the Niigata earthquake of June 16, 1964. Soils and Foundations, 6(14-30).

Keary, P., & Brooks, M. (1991). An Introduction to Geophysical Exploration. Blackwell Scientific Publications.

Koizumi, K. (1966). Changes in density of sand subsoil caused by the Niigata earthquake. Soils and Foundations, 6(2), 38-44.

Konrad, J. M. (1990a). Minimum undrained strength of two sands. Journal of Geotechnical Engineering, 116(6), 932-947.

Konrad, J. M. (1990b). Minimum undrained strength versus steady-state strength of sands. Journal of Geotechnical Engineering, 116(6), 948-963.

Kostaschuk, R. A., Luternauer, J. L., McKenna, G. T., & Moslow, T. F. (1992). Sediment transport in a submarine channel system: Fraser River Delta, Canada. Journal of Sedimentary Petrology, 62(2), 273-282.

Kostaschuk, R. A., Stephan, B. A., & Luternauer, J. L. (1989). Sediment dynamics and implications for submarine landslides at the mouth of the Fraser River, British Columbia. Current Research, Part E, Geological Survey of Canada, 207-212.

Kramer, S. L. (1989). Uncertainty in steady state liquefaction evaluation procedures. Journal of Geotechnical Engineering, 115(10), 1402-1419.

Kuberis, R. H., & Vaid, Y. P. (1990). Corrections for membrane strength in the Triaxial test. Geotechnical Testing Journal, 13(4), 361-369.

Lange, G. d. (1991). Experience with the seismic cone penetrometer in offshore site investigations. In J. M. Hovem, M. D. Richardson, & R. D. Stoll (Eds.), Shear Waves in Marine Sediments. (pp. 275-282). La Spezia, Italy: Kluwer Academic Publications.

Lange, G. d., Rawlings, C. G., & Willet, N. (1990). Comparison of shear moduli from offshore seismic cone tests and resonant column and piezoceramic bender element laboratory tests. Underwater Technology, 16(3), 13-20.

Lee, K. L., & Fitton, J. A. (1968). Factors affecting the cyclic loading strength of soil. In E. T. Selig (Eds.), Vibration effects of earthquakes on soils and foundations, ASTM 450 (pp. 71-95). San Francisco, Calif.: ASTM, STP 450.

Lee, K. L., & Focht, J. A. J. (1975). Liquefaction potential at Ekofisk Tank in the North Sea. Journal of the Geotechnical Engineering Division, ASCE, 101(GT1), 1-18.

Luternauer, J. L., & Finn, W. D. L. (1983). Stability of the Fraser River delta front. Canadian Geotechnical Journal, 20, 603-616.

Luternauer, J. L., & Murray, J. W. (1973). Sedimentation on the Western Delta front of the Fraser River, British Columbia. Canadian Journal of Earth Sciences, 10, 1642-1663.

Matthews, W. H., & Shepard, F. D. (1962). Sedimentation of Fraser River Delta, British Columbia. Bulletin of the American Association of Petroleum Geologists, 46(8), 1416-1443.

McDermott, I. R. (1991). A laboratory method to investigate shear waves in a soft soil consolidating under self weight. In J. M. Hovem, M. D. Richardson, & R. D. Stoll (Eds.), Shear Waves in Marine Sediments. (pp. 103-110). La Spezia, Italy: Kluwer Academic Publications.

McKenna, G. T., Luternauer, J. L., & Kostaschuk, R. A. (1992). Large scale mass wasting events on the Fraser River delta front near Sands Heads, British Columbia. Canadian Geotechnical Journal, 29, 151-156.

McRoberts, E. C., & Sladen, J. A. (1992). Observations on the static and cyclic sand-liquefaction methodologies. Canadian Geotechnical Journal, 29, 650-665.

Milne, W., Rogers, G. C., Riddihough, R. P., McMechan, G. A., & Hyndman, R. C. (1978). Seismicity of Western Canada. Canadian Journal of Earth Sciences, 15, 1170-1193.

Monahan, P. A., Luternauer, J. L., & Barrie, J. V. (1993a). A delta topset sheet sand and modern sedimentary processes in the Fraser River Delta, British Columbia. Current Research, Part A, Geological Survey of Canada, 263-272.

Monahan, P. A., Luternauer, J. L., & Barrie, J. V. (1993b). Subsurface mapping of the Fraser River delta: implications for delta front instability. In 4th Canadian Conference on Marine Geotechnical Engineering, 2 (pp. 451-462). St Johns, Newfoundland.

Mosher, D. C., & Barrie, J. V. (1995). Constraints to development in the offshore Fraser River Delta. In Victoria '95 GAC/MAC Annual Meeting, 20 (pp. 73). Victoria, British Columbia.

Moussa, A. A. (1975). Equivalent drained-undrained shearing resistance of sand to cyclic simple shear loading. Geotechnique, 25(3), 485-494.

Nemat-Nasser, G., & Takahashi, K. (1984). Liquefaction and fabric of sand. Journal of Geotechnical Engineering, 110(9), 1291-1306.

Nisho, S., & Tamaoki, K. (1988). Measurement of shear wave velocities in diluvial gravel samples under triaxial conditions. Soils and Foundations, 28(2), 35-48.

Nur, A., Marion, D., & Yin, H. (1991). Wave velocities in sediments. In J. M. Hovem, M. D. Richardson, & R. D. Stoll (Eds.), Shear waves in Marine Sediments (pp. 131-140). La Spezia, Italy: Kluwer Academic Publishers.

O'Rourke (1995). Geotechnical effects. NCEER Response, special supplement to, NCEER Bulletin, 9(1), 6.

Oldham, R. D. (1899). Report on the Great Earthquake of 12th June 1897. Memoirs of the Geological Society of India, 29, 377pp.

Peacock, W. H., & Seed, H. B. (1968). Sand liqueafaction under cyclic loading simple shear conditions. Journal of the Soil Mechanics and Foundation Division; Proceedings of the ASCE, 94(SM3), 689-708.

Poulos, S. J. (1981). The steady state of deformation. Journal of Geotechnical Engineering, 107(GT5), 553-562.

Poulos, S. J., Castro, G., & France, J. (1985). Liquefaction evaluation procedure. Journal of Geotechnical Engineering, 111(6), 772-792.

Robertson, P. K. (1982) In-situ testing of soil with emphasis on its application to liquefaction assessment. PhD, University of British Columbia, Vancouver.

Robertson, P. K. (1995). Personal communication.

Robertson, P. K., & Campanella, R. G. (1983). Interpretation of cone penetration tests. Part 1: Sands. Canadian Geotechnical Journal, 20, 718-733.

Robertson, P. K., & Campanella, R. G. (1985). Liquefaction potential of sands using the CPT. Journal of Geotechnical Engineering, 111(3), 384-403.

Robertson, P. K., Campanella, R. G., Gillespie, D., & Rice, A. (1986). Seismic CPT to measure in-situ shear wave velocity. Journal of Geotechnical Engineering, 112(8), 791-803.

Robertson, P. K., Campanella, R. G., & Wightman, A. (1983). SPT-CPT correlations. Journal of Geotechnical Engineering, 109(11), 1449-1457.

Robertson, P. K., Sasitharan, S., Cunning, J. C., & Sego, D. C. (1995). Shear wave velocity to evaluate in-situ state of Ottowa Sand. Journal of Geotechnical Engineering, 121(3), 262-273.

Robertson, P. K., Woeller, D. J., & Finn, W. D. L. (1992a). Seismic cone penetration for evaluating liquefaction potential under cyclic loading. Canadian Geotechnical Journal, 29(686-695).

Robertson, P. K., Woeller, D. J., Kokan, D. J., Hunter, J., & Luternauer, J. (1992b). Seismic techniques to evaluate liquefaction potential. In 45th Canadian Geotechnical Conference: Innovation, Conservation, & Rennovation, . Toronto, Ontario.

Roesler, S. K. (1979). Anisotropic Shear Modulus due to Stress Anisotropy. Journal of the Geotechnical Engineering Division, ASCE, 105(GT7), 871-880.

Rogers, G. C. (1980). A documentation of soil failure during the British Columbia earthquake of 23 June, 1946. Canadian Geotechnical Journal, 17(122-127).

Rogers, G. C. (1992). The earthquake threat in S.W British Columbia. In Geohazards'92, Geotechnique and Natural Hazards, (pp. 63-69). Vancouver: BiTec Publications Ltd.

Roscoe, K. H., Schofield, A. N., & Wroth, C. P. (1958). On the yielding of soils. Geotechnique, 8(1), 22-53.

Ross, G. A., Seed, H. B., & Migliaccio, R. R. (1969). Bridge foundation behaviour in Alaska earthquake. Journal of the Soil Mechanics and Foundation Division; Proceedings of the ASCE, 95(SM4), 1007-1036.

Sasitharan, S., Robertson, P. K., & Sego, D. C. (1992). Sample disturbance from shear wave velocity measurements. In 45th Canadian Geotechnical Journal: Innovation, Conservation and Renovation, Toronto, Ontario.

Sasitharan, S., Robertson, P. K., Sego, D. C., & Morgenstern, N. R. (1993). Collapse behaviour of sands. Canadian Geotechnical Journal, 30, 569-577.

Schmertmann, J. H. (1978). 'Use the SPT to measure dynamic soil properties? - Yes, but.....!'. Dynamic Geotechnical Testing, ASTM STP 654, 341-355.

Schnaid, F., & Houlsby, G. T. (1992). Measurement of the properties of sand in a calibration chamber by the cone pressuremeter test. Geotechnique, 42(4), 587-601.

Schultheiss, D. J. (1983). The influence of packing structure on seismic wave velocities in sediments No. Marine Geological Report No:- 83/1). University College of North Wales, Bangor.

Seed, H. B. (1979). Soil liquefaction and cyclic mobility evaluation for level ground during earthquakes. Journal of the Geotechnical Engineering Division, ASCE, 105(GT2), 201-255.

Seed, H. B., & Idriss, I. M. (1967). Analysis of soil liquefaction: Niigata earthquake. Journal of the Soil Mechanics and Foundation Division; Proceedings of the ASCE, 93(SM3), 83-108.

Seed, H. B., & Idriss, I. M. (1971). Simplified procedure for evaluating soil liquefaction potential. Journal of the Soil Mechanics and Foundation Division; Proceedings of the ASCE, SM9, 1249-1273.

Seed, H. B., Idriss, I. M., & Arango, I. (1983). Evaluation of liquefaction potential using field performance data. Journal of Geotechnical Engineering, 109(3), 458-482.

Seed, H. B., & Lee, K. L. (1966). Liquefaction of saturated sands during cyclic loading. Journal of the Soil Mechanics and Foundation Division; Proceedings of the ASCE, 92(SM6), 105-134.

Seed, H. B., Tokimatsu, K., Harder, L. F., & Chung, R. M. (1985). Influence of SPT procedures in soil liquefaction resistance evaluations. Journal of Geotechnical Engineering, 111(12), 1425-1445.

Seed, H. H. (1984). Discussion: a note on earthquake induced liquefaction. Geotechnique, 35(3), 369-371.

Shirley, D. J. (1978). An improved shear wave transducer. Journal of the Acoustical Society of America, 63(5), 1643-1645.

Shirley, D. J., & Hampton, L. D. (1978). Shear wave measurements in laboratory sediments. Journal of the Acoustical Society of America, 63(2), 607-613.

Skempton, A. W. (1986). Standard penetration test procedures and the effects in sands of overburden pressure, relative density, particle size, aging and overconsolidation. Geotechnique, 36(3), 425-447.

Sladen, J. A. (1989). Problems with interpretation of sand state from cone penetration test. Geotechnique, 39(2), 323-332.

Sladen, J. A., D'Hollander, R. D., & Krahn, J. (1985). The liquefaction of sands; a collapse surface approach. Canadian Geotechnical Journal, 22, 564-578.

Sladen, J. A., & Handford, G. (1987). A potential systematic error in laboratory testing of very loose sands. Canadian Geotechnical Journal, 24, 462-466.

Sladen, J. A., & Oswell, J. M. (1989). The behaviour of very loose sand in the triaxial compression test. Canadian Geotechnical Journal, 26, 103-113.

Smith, G. N. (1990). Elements of soil mechanics. (6th ed.). Mackays of Chatham.

Stewart, I., & Tassone, B. (1989). The Fraser River Delta : a review of historical sounding charts. No. Environment Canada - Inland waters, Pacific & Yukon Division.

Stokoe II, K. H., Rix, G. L., Sanchez-Salinera, I., Andrus, R. D., & Mok, Y. J. (1988a). Liquefaction of gravelly soils during the 1983 Borah Peak, Idaho, earthquake. In A. A. Balkema (Ed.), Proceedings of the 9th World Conference on Earthquake Engineering, 3 (pp. 183-188). Tokyo-Kyoto.

Stokoe II, K. H., Rosset, J. M., Bierschwale, J. G., & Aovad, M. (1988b). Liquefaction potential of sands from shear wave velocity. In A. A. Balkema (Ed.), Proceedings of the 9th World Conference on Earthquake Engineering, (pp. 213-218). Tokyo-Kyoto.

Stoll, R. D. (1977). Acoustic waves in ocean sediments. Geophysics, 42(4), 715-725.

Stoll, R. D. (1989). Sediment Acoustics. In S. Bhattacharji, G. M. Friedman, H. J. Neugebauer, & A. Seilacher (Eds.), Lecture Notes in Earth Sciences (pp. 155).

Stoll, R. D. (1991). Shear waves in marine sediments - bridging the gap from theory to applications. In J. M. Hovem, M. D. Richardson, & R. D. Stoll (Eds.), Shear Waves in Marine Sediments (pp. 3-12). La Spezia, Italy: Kluwer Acadmeic Publications.

Strachan, P. (1984). Liquefaction prediction in the marine environment. In B. Dennes (Eds.), Seabed Mechanics (pp. 149-157). Newcastle upon Tyne, UK: Graham & Trotman.

Stumpel, H., Kahler, S., Meisner, R., & Milkereit, B. (1984). The use of seismic shear waves and compressional waves for lithological problems of shallow sediments. Geophysical Prospecting, 32, 662-675.

Tang, Z. H., & Clark, J. I. (1993). Laboratory measurement of shear strength and related acoustic properties. In L. Boone, R. Mckenna, M. Paulin, & K. Witney (Ed.), The 4th Canadian Conference on Marine Geotechnical Engineering, 2 (pp. 495-517). St. Johns, Newfoundland.

Tanizawa, F., Iwasaki, K., Zhou, S., & Tatuoki, F. (1988). Evaluation of liquefaction strength of sand by using the cone penetration test. In A. A. Balkema (Ed.), Proceedings of the 9th World Conference on Earthquake Engineering, 3 (pp. 201-206). Tokyo-Kyoto.

Tatsuoka, F., Iwasaki, T., Fukishima, S., & Sudo, H. (1979). Stress conditions and stress histories affecting shear modulus and damping of sand under cyclic loading. Soils and Foundations, 19(2), 29-43.

Taylor-Smith, D. (1993). Geophysical-geotechnical predictions. In N. G. Pace & D. N. Langhorne (Ed.), Acoustic Classification and Mapping of the Seabed, Institute of Acoustics Conference., 15 (pp. 1-14). Bath, UK: University of Bath.

Theilen, F., & Percher, I. A. (1991). Assessment of shear strength of the sea bottom from shear wave velocity measurements on box cores and in-situ. In J. M. Hovem, M. D. Richardson, & R. D. Stoll (Eds.), Shear Waves in Marine Sediments. (pp. 67-74). La Spezia, Italy: Kluwer Academic Publications.

Tiffin, D. L., Murray, J. W., Mayers, I. R., & Garrison, R. E. (1971). Structure and origin of Foreslope Hills, Fraser Delta, British Columbia. Bulletin of Canadian Petroleum Geology, 19(3), 589-600.

Tokimatsu, K., & Uchida, A. (1990). Correlation between liquefaction resistance and shear wave velocity. Soils and Foundations, 30(2), 33-42.

Tokimatsu, K., Yamazaki, T., & Yoshimi, Y. (1986). Soil liquefaction evaluations by elastic shear moduli. Soils and Foundations, 26(1), 25-35.

Tokimatsu, K., & Yoshimi, Y. (1983). Empirical correlation of soil liquefaction based on SPT - N value and fines content. Soils and Foundations, 23(4), 56-74.

Tokimatsu, K., Yoshimi, Y., & Uchida, A. (1988). Evaluation of undrained shear strength of soils with shear wave velocity. In A. A. Balkema (Ed), Proceedings of the 9th World Conference on Earthquake Engineering. (p207-212). Tokyo - Kyoto.

Townsend, F. C. (1978). A review of factors affecting cyclic triaxial tests. Dynamic Geotechnical Testing, ASTM STP 654, 356-383.

Turgut, A., & Yamamoto, T. (1991). Measurements of compressional wave and shear wave speeds, attenuation, permeability and porosity in marine sediments. In J. M. Hovem, M. D. Richardson, & R. D. Stoll (Eds.), Shear Waves in Marine Sediments. (pp. 403-410). La Spezia, Italy: Kluwer Academic Publications.

Viggrani, G., & Atkinson, J. H. (1995). Interpretation of bender element tests. Geotechnique, 45(1), 149-154.

Wang, T. S. (1992). Mapping liquefaction potential based on SPT & SWV data. In A. A. Balkema (Ed.), Proceedings of the 10th World Conference on Earthquake Engineering, (pp. 6133-6138). Rotterdam.

Whitlow, R. (1990). Basic soil mechanics. 528pp. Longman scientific & technical.

Williams, H. F. L., & Roberts, M. C. (1989). Holocene sea-level change and delta growth: Fraser River delta. British Columbia. Canadian Journal of Earth Sciences, 26, 1657-1666.

Wood, D. M. (1994). Soil behaviour and critical state soil mechanics (1st ed.). Cambridge University Press.

Woods, R. D. (1991). Soil properties for shear wave propogation. In J. M. Hovem, M. D. Richardson, & R. D. Stoll (Eds.), Shear Waves in Marine Sediments. (pp. 29-40). La Spezia, Italy: Kluwer Academic Publications.

Xia, H., & Hu, T. (1991). Effects of saturation and back pressure on sand liquefaction. Journal of Geotechnical Engineering, 117(9), 1347-1362.

Yoshimi, Y., Tokimatsu, K., & Ohara, J. (1994). In-situ liquefaction resistance of clean sands over a wide density range. Geotechnique, 44(3), 479-494.

Youd, T. L., & Wieczorek, G. F. (1984). Liquefaction during the 1981 and previous earthquakes near Westmorland, California. (USGS-OFR-84-680). United States Geological Survey.

Yu, H. S. (1994). State parameter from self boring pressuremeter tests in sands. Journal of Geotechnical Engineering, 120(12), 2118-2135.

Yu, P., & Richart, F. E. J. (1984). Stress ratio effects on shear modulus of dry sands. Journal of Geotechnical Engineering, 110(3), 331-345.

Zar, J. H. (1984). Biostatistical analysis (2nd ed.). New Jersey, USA: Prentice Hall, Inc.

Zhou, S. (1980). Evaluation of the liquefaction of sand by the static cone penetration test. In 7th World Conference on Earthquake Engineering., 1 (pp. 156-162). Istanbul, Turkey.